AQUEOUS-PHASE CATALYTIC CONVERSIONS OF RENEWABLE FEEDSTOCKS FOR SUSTAINABLE BIOREFINERIES, 2nd Edition

EDITED BY: Georgios Papadogianakis, Roger Arthur Sheldon, Yulong Wu and Dmitry Yu. Murzin

PUBLISHED IN: Frontiers in Chemistry

frontiers Research Topics

ISSN 1664-8714
ISBN 978-2-8325-5374-9
DOI 10.3389/978-2-8325-5374-9

About Frontiers

Frontiers is more than just an open-access publisher of scholarly articles: it is a pioneering approach to the world of academia, radically improving the way scholarly research is managed. The grand vision of Frontiers is a world where all people have an equal opportunity to seek, share and generate knowledge. Frontiers provides immediate and permanent online open access to all its publications, but this alone is not enough to realize our grand goals.

Frontiers Journal Series

The Frontiers Journal Series is a multi-tier and interdisciplinary set of open-access, online journals, promising a paradigm shift from the current review, selection and dissemination processes in academic publishing. All Frontiers journals are driven by researchers for researchers; therefore, they constitute a service to the scholarly community. At the same time, the Frontiers Journal Series operates on a revolutionary invention, the tiered publishing system, initially addressing specific communities of scholars, and gradually climbing up to broader public understanding, thus serving the interests of the lay society, too.

Dedication to Quality

Each Frontiers article is a landmark of the highest quality, thanks to genuinely collaborative interactions between authors and review editors, who include some of the world's best academicians. Research must be certified by peers before entering a stream of knowledge that may eventually reach the public - and shape society; therefore, Frontiers only applies the most rigorous and unbiased reviews.
Frontiers revolutionizes research publishing by freely delivering the most outstanding research, evaluated with no bias from both the academic and social point of view. By applying the most advanced information technologies, Frontiers is catapulting scholarly publishing into a new generation.

What are Frontiers Research Topics?

Frontiers Research Topics are very popular trademarks of the Frontiers Journals Series: they are collections of at least ten articles, all centered on a particular subject. With their unique mix of varied contributions from Original Research to Review Articles, Frontiers Research Topics unify the most influential researchers, the latest key findings and historical advances in a hot research area! Find out more on how to host your own Frontiers Research Topic or contribute to one as an author by contacting the Frontiers Editorial Office: frontiersin.org/about/contact

AQUEOUS-PHASE CATALYTIC CONVERSIONS OF RENEWABLE FEEDSTOCKS FOR SUSTAINABLE BIOREFINERIES, 2nd Edition

Topic Editors:
Georgios Papadogianakis, National and Kapodistrian University of Athens, Greece
Roger Arthur Sheldon, University of the Witwatersrand, South Africa
Yulong Wu, Tsinghua University, China
Dmitry Yu. Murzin, Åbo Akademi University, Finland

Publisher's note: This is a 2nd edition due to an article retraction.

Citation: Papadogianakis, G., Sheldon, R. A., Wu, Y., Murzin, D. Y., eds. (2024). Aqueous-phase Catalytic Conversions of Renewable Feedstocks for Sustainable Biorefineries, 2nd Edition. Lausanne: Frontiers Media SA.
doi: 10.3389/978-2-8325-5374-9

Table of Contents

frontiers in Chemistry

EDITORIAL
published: 15 December 2020
doi: 10.3389/fchem.2020.629578

Editorial: Aqueous-Phase Catalytic Conversions of Renewable Feedstocks for Sustainable Biorefineries

Georgios Papadogianakis[1]*, *Roger A. Sheldon*[2,3], *Dmitry Yu. Murzin*[4] and *Yulong Wu*[5]

[1] Industrial Chemistry Laboratory, Department of Chemistry, National and Kapodistrian University of Athens, Athens, Greece, [2] Molecular Sciences Institute, School of Chemistry, University of the Witwatersrand, Johannesburg, South Africa, [3] Department of Biotechnology, Delft University of Technology, Delft, Netherlands, [4] Laboratory of Industrial Chemistry and Reaction Engineering, Abo Akademi University, Biskopsgatan, Finland, [5] Laboratory of Advanced Reactor Engineering and Safety of Ministry of Education, Institute of Nuclear and New Energy Technology, Tsinghua University, Beijing, China

Keywords: water, aqueous medium, green and sustainable catalysis, biomass, lignocellulose, biorefinery, biofuels, platform chemicals

Editorial on the Research Topic

Aqueous-Phase Catalytic Conversions of Renewable Feedstocks for Sustainable Biorefineries

Today, a major research field with enormous growth potential is green catalytic conversions of renewable biomass and its downstream products which decisively contributes to the transition from a fossil-based society into a carbon neutral, sustainable, bio-based economy. Especially interesting is the topic of aqueous-phase catalytic conversions of renewable biomass-based feedstocks in biorefineries to manufacture liquid biofuels, commodity chemicals, value added chemicals and new biomaterials. (i) As a polar solvent water is the ideal medium to convert polar biomass and its upgraded products, (ii) it is involved either as a reagent or as a byproduct in biomass valorization, (iii) it could act as a catalyst in liquefaction subcritical reactions, (iv) it has a beneficial effect and boosts rates in several types of reactions such as hydrogenations and aldol condensations, (v) it possesses a large heat capacity which makets it a suitable medium to perform safely large scale exothermic reactions, (vi) it is a non-toxic, non-inflammable, ubiquitous, inexpensive, abundantly available, green, and sustainable solvent.

The conversion of feedstocks in a biorefinery will largely involve different processes to those involved in a petrochemical refinery. In the latter feedstocks are gaseous or liquid hydrocarbons that are oxidized at elevated temperatures, in the vapor or liquid phase, under solvent-free conditions. In contrast, the feedstocks in biorefineries consist of solid, water soluble carbohydrates and their conversion involves, *inter alia*, aerobic oxidations of hydroxyl functional groups, in water as solvent, under relatively mild conditions. This requires the development of environmentally attractive and cost-effective processes, employing both chemo- and biocatalytic technologies as discussed in the review by Sheldon. Biomass platform chemicals build a bridge from the biomass to commodity chemicals as a part of sustainable utilization. These biomass platform chemicals derive from the primary biomass such as lignin and cellulose through different routes and are

Edited and reviewed by:
Valeria Conte,
University of Rome Tor Vergata, Italy

***Correspondence:**
Georgios Papadogianakis
papadogianakis@chem.uoa.gr

Specialty section:
This article was submitted to Green and Sustainable Chemistry, a section of the journal Frontiers in Chemistry

Received: *15 November 2020*
Accepted: *23 November 2020*
Published: *15 December 2020*

Citation:
Papadogianakis G, Sheldon RA, Murzin DY and Wu Y (2020) Editorial: Aqueous-Phase Catalytic Conversions of Renewable Feedstocks for Sustainable Biorefineries. Front. Chem. 8:629578. doi: 10.3389/fchem.2020.629578

converted into more refined chemicals through a variety of pathways. The review article of Wu et al. summarizes the recent research progress on dehydration, hydrogenation, oxidation and other reactions of platform chemicals by heterogeneous catalysts in the aqueous phase. Levulinic acid is classified as a key platform chemical for biorefineries, due to its large spectrum of potential applications and because it is readily available from lignocellulose by low-cost and high-yield production routes. The review article by Papadogianakis et al. focuses on recent advances in ruthenium-catalyzed hydrogenations of levulinic acid in aqueous medium using heterogeneous catalysts on solid supports, water-dispersible catalytic nanoparticles and homogeneous water-soluble catalytic complexes with biphasic catalyst separation, for the manufacture of advanced biofuels, value-added chemicals, sustainable solvents, additives to gasoline and to food. The significance of the aqueous solvent to carry out catalytic hydrogenations of levulinic acid has been highlighted in numerous experimental investigations and several theoretical studies. The utilization process of renewable resources involves a series of transformation processes, and many important intermediate products are produced in these processes. Adipic acid is an example of such an important bulk chemical. Due to the generation of toxic by-products in the existing processes, it has become an urgent problem to find environmentally friendly alternative pathways to the synthesis of adipic acid. The oxidation of glucose, has the potential to be an alternative route to the current oxidation of cyclohexanone/cyclohexanol mixtures in a petrochemical refinery. Jin et al. report in the mini review article on the progress made in the oxidation reactions of the above mentioned route to adipic acid.

Among several key aspects of biomass conversion in the aqueous phase for production of biofuels and chemicals several authors of this special collection of articles considered primary transformations of cellulose and hemicellulose as well as downstream treatment. Depolymerization of cellulose under milder conditions involving hydrolytic hydrogenation with formation of hexitols and hydrogenolysis leading to glycols was reported in the mini review by the late E. Sulman et al. The authors discussed mainly the promising catalytic systems and operation conditions clearly indicating the challenges on the path to industrial implementation of this technology as a part lignocellulose biorefinery to value-added products. The review of Xin et al. besides the synthesis of polyols through hydrolytic hydrogenation and diols by selective hydrogenolysis covers also hydrogenolysis and hydrodeoxygenation to alkanes as well as dehydration of fructose and subsequent oxidation reactions using cellulose as a starting material in aqueous medium. The authors discussed mechanistic aspects of these transformations and listed the remaining challenges and research objectives. In recent years, a variety of solvents mixed with water have been developed for lignocellulose valorization reactions. The H_2O/THF system is one of such commonly mixed solvents. It has shown excellent properties in increasing the solubility and fractionation of lignin, cellulose and hemicellulose. Due to the extraction effect of THF on organic products, it can promote the reactions and the directional selection of products. The review by Hu et al. discusses and summarizes the above characteristics of the H_2O/THF system.

An envisaged key platform chemical for the production of chemicals and liquid fuels in a biorefinery is 5-hydroxymethylfurfural (5-HMF) which can be produced by acid-catalyzed dehydration of fructose or, preferably, glucose. Unfortunately, this process is plagued by relatively low yields and high production costs that are largely a result of the low stability of 5-HMF under the acidic reaction conditions. In the original research article by Tongtummachat et al. substantial improvements were obtained by conducting the reaction in continuous operation in a biphasic methyl isobutyl ketone/water system in a dispersed flow reactor. A 5-HMF yield of 81.7% and a selectivity of 89.8% were obtained at a reaction temperature of 180°C and a residence time of 3 min. In another approach, Held et al. investigated the dehydration of fructose at 50°C in deep eutectic solvents (DES) consisting of mixtures of tetraethylammonium chloride or choline chloride with lactic or levulinic acid and a vanadium-containing heterpoly acid ($H_8PV_5Mo_7O_{40}$) as the catalyst. Using the latter, in combination with tetraethylammonium chloride and levulinic acid, afforded a 5-HMF yield of 57% and a selectivity of ca. 70% after 5 h reaction time.

Srinivasan et al. examined the hydrogenation of sugars such as xylose, glucose, and mannose to obtain quantitative selectivities toward their corresponding sugar alcohols xylitol, sorbitol, and mannitol using hydrous ruthenium oxide catalyst precursors supported on Na-β zeolite in aqueous solvent. Recycling experiments have shown that this catalyst is stable without losing its activity for five successive runs. Luque et al. developed nanocatalysts functionalized by yttrium oxide for the efficient mono-dehydration reaction of sugar alcohols such as sorbitol and mannitol under mild reaction conditions i.e., at room temperature to obtain with high selectivity the mono-dehydration products in aqueous media. Mechanistic studies indicated that the high efficiency for the mono-dehydration reaction is based mainly on the stability of the catalytically active intermediate species during the dehydration reaction.

An alternative to heterogeneous catalytic depolymerisation of lignocellulosic materials to sugars is enzymatic hydrolysis which is known to be impaired by generated sugar inhibition. The original research work of Ottens et al. presents strategies on conducting extractive enzymatic hydrolysis in aqueous two-phase systems paving the way to eventual design of a feasible process. High content of oxygen in lignocellulosic biomass requires not only efficient processes for deoxygenation quite often using hydrogen, but also sustainable routes for production of biohydrogen from renewable sources. One particular aspect of this was considered by Lefferts et al. who in an original research article reported aqueous phase reforming of butanol over rhodium supported on zirconia, specifically addressing the important issue of the influence of internal mass transfer on activity and selectivity. In the original research work of Özşen depolymerisation of lignocellulosic biomass, namely hazelnut shell waste, was discussed through application of hydrothermal liquefaction under supercritical conditions. The main focus of the author was on production of levulinic acid. Another very

interesting aspect of the work was related to a combination of hydrolysis and electrolysis in subcritical water.

AUTHOR CONTRIBUTIONS

All authors listed have made a substantial, direct and intellectual contribution to the work, and approved it for publication.

ACKNOWLEDGMENTS

We would like to thank all authors for their contributions and all reviewers of their thoughtful evaluations. We also wish to thank the Editors and the Publication Team of Frontiers in Chemistry for their efforts regarding this Research Topic collection of articles.

Conflict of Interest: The authors declare that the research was conducted in the absence of any commercial or financial relationships that could be construed as a potential conflict of interest.

frontiers in Chemistry

ORIGINAL RESEARCH
published: 09 October 2019
doi: 10.3389/fchem.2019.00661

Catalytic Low-Temperature Dehydration of Fructose to 5-Hydroxymethylfurfural Using Acidic Deep Eutectic Solvents and Polyoxometalate Catalysts

Sam Körner[1], *Jakob Albert*[2] *and Christoph Held*[1]*

[1] Laboratory of Thermodynamics, TU Dortmund University, Dortmund, Germany, [2] Lehrstuhl für Chemische Reaktionstechnik, Friedrich-Alexander Universität Erlangen-Nürnberg, Erlangen, Germany

HMF synthesis typically requires high temperature and is carried out in aqueous solutions. In this work, the low-temperature dehydration of fructose to HMF in different deep eutectic solvents (DES) was investigated. We found a very active and selective reaction system consisting of the DES tetraethyl ammonium chloride as hydrogen bond acceptor (HBA) and levulinic acid as hydrogen bond donor (HBD) in a molar ratio of 1:2 leading to a maximum HMF yield of 68% after 120 h at 323 K. The DES still contained a low amount of water at the initial reaction, and water was also produced during the reaction. Considering the DES properties, neither the molar ratio in the DES nor the reaction temperature had a significant influence on the overall performance of the reaction system. However, the nature of the HBA as well as the acidity of the HBD play an important role for the maximum achievable HMF yield. This was validated by measured yields in a DES with different combinations of HBD (levulinic acid and lactic acid) and HBA (choline chloride and tetra-n-alkyl ammonium chlorides). Moreover, addition of vanadium containing catalysts, especially the polyoxometalate HPA-5 ($H_8PV_5Mo_7O_{40}$) leads to drastically increased reaction kinetics. Using HPA-5 and the DES tetraethyl ammonium chloride—levulinic acid we could reach a maximum HMF yield of 57% after only 5 h reaction time without decreasing the very high product selectivity.

Keywords: biomass dehydration, carboxylic acid, alkyl ammonium, HMF, reaction equilibrium

OPEN ACCESS

Edited by:
Roger Arthur Sheldon, University of the Witwatersrand, South Africa

Reviewed by:
Matteo Guidotti, Italian National Research Council (CNR), Italy
Francois Jerome, UMR7285 Institut de Chimie des Milieux et des Matériaux de Poitiers (IC2MP), France

***Correspondence:**
Christoph Held
christoph.held@tu-dortmund.de

Specialty section:
This article was submitted to Green and Sustainable Chemistry, a section of the journal Frontiers in Chemistry

Received: *12 July 2019*
Accepted: *17 September 2019*
Published: *09 October 2019*

Citation:
Körner S, Albert J and Held C (2019) Catalytic Low-Temperature Dehydration of Fructose to 5-Hydroxymethylfurfural Using Acidic Deep Eutectic Solvents and Polyoxometalate Catalysts. Front. Chem. 7:661. doi: 10.3389/fchem.2019.00661

INTRODUCTION

The chemical industry of the future will have to move from decades of fossil energy sources, such as coal and oil, to more sustainable organic resources. Biomass has the greatest substitution potential for fossil raw materials among renewable energy sources. Due to the decreasing availability of these resources and important intermediates, interest in cost-effective biomass conversion processes into valuable platform chemicals is growing. In particular, the energy-efficient and economical dehydration of monosaccharides is the focus of attention (Chheda et al., 2007; Liu et al., 2012).

5-Hydroxymethylfurfural (HMF) is a biomass-based key component in the biological pathways of a variety of high-value platform chemicals. Due to its high functionality, HMF represents an ideal building block in the interface between carbohydrate and petrochemicals. Both the

hydroxymethyl group and the aldehyde group open up the possibility of various subsequent reactions to important platform chemicals (Bozell and Petersen, 2010). Within the derivatization of HMF, there is a particular interest in the resulting furan compounds. Especially furan dicarboxylic acid (FDCA) and levulinic acid (LA), which are included in the list of top 12 biomass-based chemicals with high-added-value published by the U.S. Department of Energy (Bozell and Petersen, 2010). FDCA is a promising alternative to petroleum-derived terephthalic acid. In addition to the normal market for polyethylene terephthalate (PET, $1.8 \cdot 10^9$ tons per year), this substitution potential is gaining in importance with regard to increasing research activities in the direction of "bio-PET" (Werpy and Petersen, 2004; Iwata, 2015).

The acid-catalyzed synthesis of HMF occurs under triple elimination of water starting from fructose as a substrate (Tang et al., 2017). A suitable solvent as a reaction medium is essential for the thermodynamic optimum of an overall process. Due to the fact that often more than 80% of all chemicals in a process make up the solvents, the profitability also depends heavily on the choice of solvent. Therefore a wide variety of solvents, such as aqueous media (Vandam et al., 1986; Hansen et al., 2009), dimethyl sulfoxide and methyl isobutyl ketone (Yi et al., 2015) or biphasic reaction media (Chheda et al., 2007; Hu et al., 2008) and even in melts (Ilgen et al., 2009) have been extensively studied so far. However, either high reaction temperatures are required or the solvents are toxic and often also expensive. Further, from the thermodynamic point of view, water must be avoided as reaction solvent as the product of the reaction is also water; thus the latter as solvent strongly limits the yield of HMF. Ionic liquids (ILs) as more recent solvents are interesting in this respect (due in part to the physicochemical properties), but often also disadvantageous because of the high price or toxicity (Thi et al., 2010; Russ and Konig, 2012) or because of slow kinetics. Thus, alternative solvents are required in combination with new catalysts. ILs have already been successfully applied as reaction medium for fructose dehydration (D'Anna et al., 2014; Zhang et al., 2015).

In recent years, research on deep eutectic solvents (DESs) has been intensified. An eutectic mixture is characterized by the lowest melting temperature of all compositions of the same components (see **Figure S3**). At the eutectic point, the melting temperature is significantly lower than that of the pure substances. If mixtures have a very large melting point reduction compared to the pure substances, these are referred to as deep eutectic systems. Accordingly, DESs as the reaction medium allow for reaction temperatures near room temperature. DESs are composed of a hydrogen-bond acceptor (HBA) and a corresponding donor (HBD) (Abbott et al., 2004). Often the DESs consist of a quaternary ammonium salt as HBA and a wide range of HBDs. For the latter typically carboxylic acids, alcohols or amines are used (Russ and Konig, 2012). Moreover, DESs based on an acid can serve both as a solvent and as a catalyst. Additionally, depending on the combination of HBA-HBD, DESs might represent a green solvent that can replace organic solvents in engineering applications in the long term. Several DESs share many of the benefits and overcome some of the disadvantages of ILs. In addition to the simple and cost-effective production, especially a possible low toxicity as well as a possible good biodegradability and biocompatibility with enzymes are among the advantages. Furthermore, DESs are referred to as designer solvents because the properties can be tailored to the specific requirements, depending on the application (Smith et al., 2014). Product separation from the solvent is often possible by crystallization, which allows more energy-intensive processes to be avoided (Francisco et al., 2013). Therefore, in the interests of the eco-efficient health and safety industry, they offer enormous potential for improving ecotoxicity, waste management and process safety (Zhang et al., 2012). DESs have been also used as reaction medium for fructose dehydration to HMF (Istasse et al., 2018). The use of DESs in the synthesis of biomass-based platform chemicals is well in line with the twelve principles of Green Chemistry. DESs are becoming increasingly important due to their biodegradability, biocompatibility and very low toxicity. In addition, DESs allow for a significant lowering of the reaction temperature leading to lower energy consumption. This not only increases energy efficiency but also atomic efficiency, leading to a reduction of derivatives as the formation of by-products increases with increasing temperature (Zakrzewska et al., 2011). Also, the use of catalysts should be optimized as they are superior to stoichiometric reagents. The reader is further referred to review articles on the use of DESs in upstream and downstream processes (Smith et al., 2014; Sheldon, 2016; Vitale et al., 2017; Garcia-Alvarez et al., 2018).

Moreover, the work-up of the catalyst is frequently complicated and time-consuming (Yi et al., 2015). Typical catalysts for this reaction discussed in the literature are metal and organic acids as well as ion exchange resins (Carniti et al., 2011; Zakrzewska et al., 2011). Chromium compounds used as catalysts showed good results. However, their high toxicity associated with high loadings is an obstacle to commercial applications (Zakrzewska et al., 2011). In the future there will be an increased demand for catalysts for the dehydration of fructose to HMF on a large scale. The use of catalysts is closely linked to the reaction time and therefore an important point in terms of process optimization.

Another promising alternative class of catalysts for low-temperature homogeneous biomass transformation reactions is polyoxometalates (POMs). POMs are well-defined metal-oxyanions linked with oxygen bridges of early transition metals at their highest oxidation state (e.g., Mo^{6+}, W^{6+} or V^{5+}). They can also contain a multitude of hetero atoms to improve their chemical and thermal stability (Ammam, 2013). POMs reveal unique physical and chemical properties like tunable acid-base properties, great redox activity based on the fast and reversible multi-electron transfer, high thermal stability and excellent solubility and stability in water and other polar solvents (Albert et al., 2012; Wang and Yang, 2015). Mostly used in homogeneous catalyzed biomass transformation reactions are POMs from the so called Keggin-type $[XM_{12}O_{40}]^{n-}$. They contain a template of various coordinating anions, e.g., oxo-anions, oxometalates, or halides, together with a framework metal which is typically an early, high-valent transition metal (Kozhevnikov, 1998). The catalytic activity is mostly introduced by substituting some of

the framework metals (W, Mo) with easily reducible heteroatoms like vanadium that results in shifting their reactivity from acidic to redox-dominance (Albert et al., 2016). The generated compounds have the composition $H_{3+n}[PV_nMo_{12-n}O_{40}]$ and are called heteropolyacids, abbreviated as HPA-n depending on the content of vanadium atoms (n).

In this contribution, we investigate the low-temperature dehydration of fructose to HMF in different DESs. Therefore, we identified the best HBA:HBD combination leading to high HMF yields. Moreover, we studied the effect of using different vanadium-containing catalysts on the efficiency and the kinetics of the fructose dehydration reaction.

MATERIALS AND METHODS

Materials

Chemicals that have been used in this work are listed in **Table S8**. The quaternary ammonium salts choline chloride, tetrabutyl, and tetraethyl ammonium chloride were dried for 24 h at 298 K in a vacuum oven before use. All other chemicals were used as obtained without further purification. Deionized water from the Millipore system (Merck KGaA, Darmstadt, Germany) was used.

Moreover, three vanadium-containing acid catalysts were used in this study. The vanadium precursor NH_4VO_3 (CAS-Nr. 8037803-55-6) was purchased from Acros Organics with a purity of 99.5%. $VOSO_4$ (CAS-Nr. 123334-20-3) was obtained from Alfa Aesar with a purity of 99.9%. Moreover, we used the heteropolyacid HPA-5 ($H_8PV_5Mo_7O_{40}$) that was synthesized in the Erlangen labs according to the literature (Odyakov and Zhizhina, 2008; Albert et al., 2014). The characterization of the heteropolyacid has been carried out using a Perkin Elmer Plasma 400 ICP-OES device resulting in a P/V/Mo ratio of 1/4.80/6.93 as well as FTIR spectroscopy (Jasco FT/IR-4100 spectrometer equipped with a PIKE GladiATR-accessory) showing the characteristic vibrations at wavenumbers of 1,045 (Mo = O), 948 (P-O), 864 (Mo-Ob-Mo) as well as 725 (Mo-Oc-Mo) cm^{-1}.

All powdered catalysts were finally dried at 10^{-3} mbar by keeping a constant low temperature of max. Two hundred and seventy seven Kelvin in order to adjust a fixed content of hydration water. Thermogravimetric analyses (TGA) were conducted using a SETSYS-1750 CS Evolution from SETARAM Instruments, resulting in water contents of 2 moles for NH_4VO_3, 4 moles for $VOSO_4$, and 12 moles for the HPA-5 catalyst, respectively.

Synthesis of Deep Eutectic Solvents

The various DESs were prepared in a molar ratio of 1:2. For this purpose, two moles of the carboxylic acid per mole of the quaternary ammonium compound were weighed into one 10 ml Falcon tube. The DESs were prepared gravimetrically using a Sartorius laboratory balance Cubis (Sartorius, Goettingen, Germany) with an accuracy of ±10–4 g. The tubes were placed in the ThermoMixer® (Eppendorf, Hamburg, Germany) at 373 K and 1,000 rpm for a few minutes until a homogeneous liquid was obtained.

Solid-Liquid Equilibria of the Deep Eutectic Systems

In order to allow liquid reactions at 323 K, the solvent (in this work: DESs) have to be a homogenous liquid. The phase diagram was measured in this work in order to ensure homogenous liquid phase conditions at the desired reaction temperature of 323 K at 1 bar. For this purpose, solid-liquid equilibria were investigated by means of measurements and validation by thermodynamic modeling. In the experimental work, HBD (levulinic acid) and HBA (choline chloride) were prepared in different molar ratios by weighing HBD and HBA as desired into 10 ml Falcon tubes gravimetrically using a Sartorius laboratory balance Cubis (Sartorius, Goettingen, Germany) with an accuracy of $\pm 10^{-4}$ g. These mixtures were placed in a Thermomixer C at 373 K and shaken at 300 rpm. All considered mixtures were homogenously liquid at 373 K. Afterwards, temperature of the Thermomixer block was reduced by 5 K, and shaken again for another 24 h. In case heterogeneity was observed during this time period the temperature was assumed to be the solubility temperature of the samples at 1 bar and known composition. In any other case the temperature was reduced by another 5 K and the procedure was repeated accordingly. This method is not very accurate, and the uncertainty in the measured solubility temperature is 5 K. Thus, the measured phase diagram was predicted a priori with the thermodynamic model PC-SAFT. All available PC-SAFT parameters of the pure components were taken from literature [choline chloride (Zubeir et al., 2016), lactic acid (Zubeir et al., 2016), and levulinic acid (Altuntepe et al., 2017)]. Binary parameters were not used. Details of the model and the solid-liquid equilibrium condition can be found in (Crespo et al., 2018).

Reaction Equilibrium Experiments and Analysis

In each case 1 g of the different DESs was transferred by syringe into a 10 ml Falcon tube and 2.5 wt.% fructose was added. The amount of fructose was adapted to the lowest experimentally determined fructose solubility in the different DESs. Every initial reaction mixture was prepared twice, so that each experimental reaction equilibrium position was obtained by dual approach. The reaction mixtures were prepared gravimetrically using a Sartorius laboratory balance Cubis (Sartorius, Goettingen, Germany) with an accuracy of ±10–4 g. The tubes were shaken in the ThermoMixer® (Eppendorf, Hamburg, Germany) at 323 K and 1,000 rpm. Thereafter, samples were taken at solvent-specific intervals over an extended period of time and analyzed by HPLC. The length of the period depended on the time required to reach the reaction equilibrium.

Equilibrium concentrations of the reacting agents were analyzed using two different analytical methods. For this purpose, an Agilent series 1,200 HPLC (Agilent, Böblingen, Germany) equipped with a refractive index detector (RID) was used to detect the key components HMF and fructose. Sampling from the vial and subsequent injection of 5 µl of the sample in the chromatography column was fully automatic by a built-in syringe. For the separation a Nucleogel® Sugar 810 H column

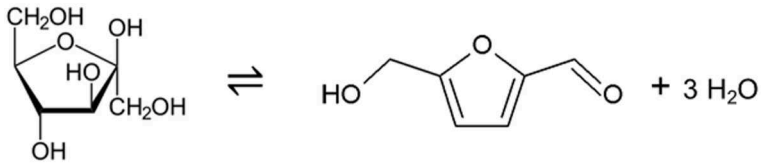

SCHEME 1 | Reaction considered in this work: Dehydration of D-(-)-fructose to 5-hydroxymethylfurfural (HMF) and three water molecules.

(300 × 7.8 mm, Macherey Nagel, Düren, Germany) thermostated at 308.15 K and at a flow rate of 0.6 ml/min was used. The stationary phase was a polymer phase suitable for the separation of a wide range of organic acids, alcohols and sugars. The mobile phase was a mixture of sulfuric acid (5 mmol/l) and water that was used isocratically (sulfuric acid:water = 1:20). The calibration for the key components was carried out for at least three different mass fractions in the range from 0.00 to 13.05 wt.%. Each sample and calibration solution was prepared twice and analyzed at least three times. The experimentally determined retention times are listed in **Table S1**. If the components were solid at room temperature (298 K), they were dissolved in deionized water. Two chromatograms are given as an example in **Figures S1**, **S2**.

The evaluation of the water peak was not possible at the given conditions due to overlays through similar retention times of other substances. Therefore, the equilibrium concentration of water was determined by means of the Karl Fisher titration (KFT) with a Metrohm 915 KF Ti Touch (Metrohm, Herisau, Switzerland). Each sample was measured at least three times and the results were averaged. The results are given in **Table S9**.

If the fructose peak was not evaluable due to overlay, the concentration in the reaction equilibrium was estimated from the molar balance using the initial molalities, the measured molality of HMF and water at equilibrium as well as the stoichiometry of the reaction.

Further, the chemical stability the carboxylic acids at reaction conditions (323 K at 1 bar as well as 343 K at 1 bar) was verified by HPLC-measured peak areas of the carboxylic acids (levulinic acid and lactic acid) after exposure to reaction conditions for up to 300 h (this was the maximally applied reaction time).

Reaction Experiments Using Additional Vanadium-Based Catalyst

Several days may pass before the reaction equilibrium is reached in DESs, which ideally serve both as a solvent and as a catalyst. Because of the slow kinetics, the use of additional catalysts in the most promising DES has been studied. For this purpose, three selected catalysts were used. The powdered catalysts used included NH_4VO_3, $VOSO_4$, and HPA-5. The catalysts were added both in powder form and dissolved in water to the DES. Regardless of whether the catalyst was present as a powder or in solution, the weight of pure catalyst in all batches was 4.0 wt.%. This corresponded to the lowest solubility of any of the undissolved powdered catalysts in the DES used. The time intervals of sampling and analysis were adjusted to the expected higher reaction rate. Otherwise, the experimental procedure was as described in the previous section.

RESULTS AND DISCUSSION

In this work, the reaction of fructose to HMF was studied (**Scheme 1**) using the chemicals as listed in **Table S1**.

Choice of the Reaction Temperature

In order to define a meaningful temperature for fructose dehydration in DESs, the influence of the reaction temperature on the HMF yield was measured in the DES ChCl:LA. Two independent DES samples were synthesized, both in a molar ratio of 1:2. The reaction mixtures were stirred at 323 K as well as at 343 K. These temperatures were chosen as we wanted to have a temperature near to ambient conditions in order to minimize the energy required and to minimize side reactions, as it was found that temperatures higher than 343 K cause losses in selectivity (Assanosi et al., 2014). **Table 1** shows the yields of HMF at these different reaction temperatures.

At a reaction temperature of 323 K, an HMF yield of 18% after 24 h and of 48% after 120 h was observed. At 343 K, the yield of HMF increased from 21% after 24 h to 45% after 120 h. Thus, on the basis of these measurement results, increasing the reaction temperature to 343 K is not beneficial for the HMF yield. It should be noted that this depends also on the nature of the solvent. For the reaction carried out in ILs, a more significant temperature effect on the kinetics of the reaction was observed in the literature (Okano et al., 2013). For the reaction in the DESs under investigation in this work, increasing temperature to 343 K did not lead to the desired improvement in reaction kinetics considering the rather small temperature range (323 K to 343 K). One reason might be a phase separation that was observed after the reaction at 343 K and cooling to

TABLE 1 | 5-Hydroxymethylfurfural (HMF) yields in choline chloride:levulinic acid (ChCl:LA) in a molar ratio of 1:2; reaction temperature: 323 or 343 K; fructose starting concentration: 2.5 wt.%; pressure: 1 bar.

Time [h]	ChCl:LA (323 K)		ChCl:LA (343 K)	
	Y_{HMF} [%]	SD [%]	Y_{HMF} [%]	SD [%]
24	18	–	21	0.3
120	48	3.3	45	4.3

Standard uncertainty: u(T) = 0.5 K; u(Y_{HMF}) = 1.7%.

room temperature, and the brownish color of the sample let assume polymerization of reactants and intermediates as well as production of humins. This might also explain that the yield is more or less the same at 343 K and at 323 K after 120 h of reaction time, in contrast to expectations based on Arrhenius. Therefore, 323 K was selected as the preferred reaction temperature for the following investigations. This decision was especially based on the fact that high selectivity was reached according to the chromatograms in **Figures S1**, **S2**.

Fructose Dehydration to HMF in Various Reaction Media

As to be seen from **Scheme 1**, water as a reaction medium is undesired as it will shift the reaction equilibrium to the left hand side and thus will limit the HMF yield. Consequently, the use of DES as green reaction solvents was studied in this work. Non-aqueous reaction media such as the DESs do not have this shortcoming, and potentially should allow a much higher HMF yield compared to aqueous reaction medium. It should be noted that in the present study fructose was used as reactant at rather low concentration, which will not lead to formation of a DES based on fructose. To further limit the range of DESs that might be suitable as reaction solvent, several criteria were defined: First, the DES should be homogenously liquid at 323 K. Further, systems of low viscosity were preferred to reduce energy required for mixing. In order to avoid addition of acid which might be required as dehydration of fructose to HMF is known to be acid-catalyzed, carboxylic acids were chose as HBDs. Lactic acid can be synthesized by the fermentation of starch and levulinic acid by the hydrolysis of cellulose, thus both of them were tested as biogenic DES constituents. Although the use of salts might be critically seen for a greener chemistry in the future, the reaction of fructose to HMF seems to be favored under the presence of chloride. Thus, choline chloride (ChCl) was chosen as HBA DES constituent due to its biodegradability, biocompatibility and very low toxicity. Choline chloride is technically used in food supplements and feeds. As the DESs based on choline chloride and carboxylic acids are liquid and of extremely low volatility, low reaction temperatures are possible that opens the door for energy-efficient processes. These DESs further have a comparably low viscosity (Zhao et al., 2015; Li et al., 2016).

The studied DESs were chosen at a composition which allows liquefied system conditions at 323 K. The solid-liquid equilibria of the systems under consideration are presented in **Figure S3**. All systems were found to be liquid at the reaction temperature 323 K. The DESs are mixtures of two components. The hypothesis that should be verified in this work is that the combination of the two DES constituents to form a close-to-eutectic mixture yields solvent properties for the reaction that is very different from the solvent composed of only one of the DES constituents. Thus, the DESs as well as the individual constituents of the DESs were used as reaction solvents. The DESs as well as the individual constituents of DES have been studied with focus on HMF yield, and the following reaction solvents were analyzed: ChCl was dissolved in water (ChCl is a solid up to 575 K), pure levulinic acid (LA), and finally the DES consisting of these components (ChCl:LA) in a molar ratio of 1:2. These experiments indicated that the individual DES components are poorly suitable as reaction medium, whereas the DES consisting of these constituents are highly promising. Indeed, this supports the hypothesis that DESs act reaction solvent in a different way than its constituents. The most probable reason behind this is the interactions between reacting agents and the DES, which are different compared to the interactions between reacting agents and a single DES constituent. The yield of HMF over time in these different solvents is shown in **Figure 1**.

Kinetics and yield of chemical and biochemical reactions strongly depend on the reaction solvent (Lemberg and Sadowski, 2017; Voges et al., 2017; Wangler et al., 2019). **Figure 1** shows that this was also observed for the reaction under consideration in the present study. After 48 h, an HMF yield of 14% was achieved in pure LA. This yield remained unchanged even after 328 h and thus corresponds to the maximum yield, which is the value at equilibrium assuming no side reactions or consecutive reactions. However, there was no reaction in the aqueous ChCl solution observable. This shows that neither aqueous ChCl, nor pure LA promote the reaction sufficiently. In comparison, using the DES ChCl:LA in a molar ratio of 1:2, which is already liquid at about 323 K (see **Figure S3**), HMF yields of 23% after 48 h and 57% after 288 h were achieved. The latter corresponds to the yield of HMF in equilibrium. The positive effect on the HMF yield by using the DES compared to the pure substances confirms the hypothesis on the synergetic effect that is the driving force for the reaction. Thus, HMF yields could be achieved, which exceeded those in the pure substances by up to 57%. However, it has to be mentioned that under the mild reaction conditions of 323 K and ambient pressure, the dehydration reaction in the DES is still very slow, as no additional catalyst was used to improve the kinetics. Moreover, HPLC analysis confirmed the very high selectivity of the reaction, as no other byproducts could be detected within

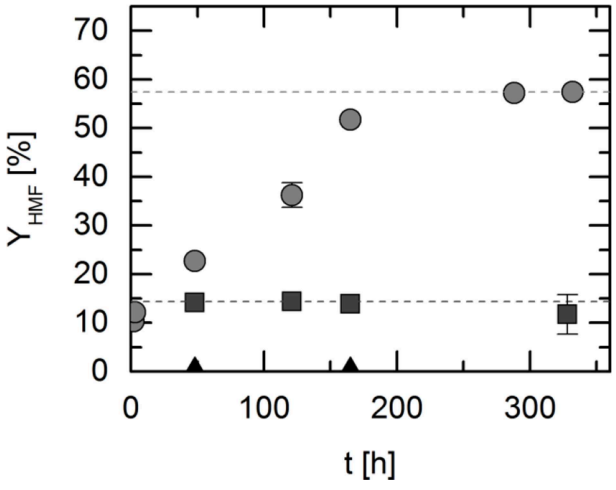

FIGURE 1 | HMF yield over time in choline chloride (ChCl) dissolved in water (triangles), in pure levulinic acid (LA; squares) and in the corresponding deep eutectic system (DES ChCl:LA 1:2; circles); fructose starting concentration: 2.5 wt.%; reaction temperature 323 K; pressure 1 bar. Data listed in **Table S2**.

a retention time of 1 h. Two chromatograms are given as an example in **Figures S1**, **S2**.

Influence of Molar Ratio in the DES

Obviously, a mixture of ChCl and carboxylic acid is superior over using the individual DES constituents with respect to HMF yield. In **Figure 1**, this was demonstrated using the ratio of 1:2 (ChCl:LA). To analyze the influence of the molar ratio of the DESs on the HMF yield, two DES mixtures were synthesized, one in a molar ratio of 1:2 (ChCl:LA) and the other in the ratio 1:3 (ChCl:LA), respectively. **Table 2** shows the experimentally observed yields of HMF at these considered molar ratios of the DES constituents.

In the DES ChCl:LA with a molar ratio of 1:2, the yield of HMF increased from 21% after 24 h to 45% after 120 h. The HMF yield in the DES ChCl:LA with a molar ratio of 1:3 was 24% after 24 h, and 50% after 120 h, respectively. From this it is evident that there is no significant correlation between the molar ratio within the DESs and the HMF yield. Also the viscosities of the pure DESs ChCl:LA 1:3 [viscosity about 134 mPas (Li et al., 2016)] and ChCl:LA 1:2 [viscosity about 119 mPas (Zhao et al., 2015)] are very similar and mass-transport limitations are not expected to have a major influence. As the differences in viscosity and HMF yield as well as in kinetics are not very pronounced, a molar ratio of 1:2 was chosen as DES solvent for the following experiments. This decision was mainly based on the fact that other DESs with a ratio of 1:2 were analyzed as well (see section Influence of the Chemical Nature of the HBA in DESs With Levulinic Acid) and the results will be compared on the basis of a constant molar ratio of the different DESs under consideration.

Influence of Acidity and pH

Dehydration of fructose to HMF is an acid-catalyzed reaction. Thus, by using a carboxylic acid as HBD, the DESs operate in functions of reaction medium as well as of the catalyst by assuring a certain required (low) pH. Previous works have shown that pH alone decides whether the reaction takes place or not. It was found that HMF is not formed at pH $>$ 3.9 (Kuster and van der Baan, 1977), which fits to the observation that LA is a too weak acid for acting as a catalyst. This was found by Carniti et al. (2011), and also within this work. pH of LA was measured to be about pH $=$ 4. ChCl-water mixtures are by far not acidic enough to catalyze the reaction, as at 323 K the pH values of these mixtures are 4 $<$ pH $<$ 6. As we found that pH $<$ 4 is required for the acid-catalyzed reaction, all reaction mixtures with DESs as solvents were chosen that have pH values pH $<$ 4, namely 0.8 $<$ pH $<$ 2.9. This was also the reason why we decided not to investigate standard DES: Aqueous solutions of DESs prepared from ChCl:glycerol (1:2) and ChCl:ethylene glycol (1:2) have rather high pH values of approximately between 4.40 and 4.00, and 4.36 and 4.08, and thus they are not suitable for the fructose dehydration. Given that pH $<$ 4, the solvent decides on the yield, and the pH does not influence the yield any more. Similar observations were found which, however, used extremely acid conditions by toluene sulfonic acid (pKa $=-2.8$) (Assanosi et al., 2014). Thus, given that pH is low enough (pH $<$ 3 is recommended) and the reaction is catalyzed meaningfully, the kind of the solvent determines the equilibrium yield of HMF. In order to validate this hypothesis, the influence of acidity on the HMF yield was investigated in this work. For this purpose, the reaction was carried out in a DES consisting of constant HBA while varying the HBD under equal reaction conditions. The salt tetraethyl ammonium chloride (TEAC) served as HBA in this study combined with the HBDs levulinic acid (LA) or lactic acid (LAA). All DESs were prepared with a molar ratio of TEAC:HBD 1:2. The so-obtained HMF yields and selectivity are illustrated in **Figure 2**.

After 48 h, an HMF yield of 29% was achieved in TEAC:LAA compared to 45% in TEAC:LA. Thus, using levulinic acid as HBD allows faster kinetics. Even more, also the reaction equilibrium (TEAC:LA 68% yield) was found to be favored in levulinic acid based DESs over lactic acid based DESs (TEAC:LAA 57% yield). The results shown in **Figure 2** mean that the DES containing the weaker acid (levulinic acid) allows a faster reaction and even a higher yield of HMF. This is unexpected since it disproves the hypothesis that very acidic conditions are required for the considered reaction (Chheda et al., 2007). Rather, the molecular interactions caused by the solvents are the reason for higher yield and faster kinetics of the reaction. This has been found for diverse

TABLE 2 | 5-Hydroxymethylfurfural (HMF) yields in choline chloride:levulinic acid (ChCl:LA) in a molar ratio of 1:2 and 1:3; reaction temperature: 343 K; fructose starting concentration: 2.5 wt.%; pressure: 1 bar.

Time [h]	ChCl:LA (mr 1:2)		ChCl:LA (mr 1:3)	
	Y_{HMF} [%]	SD [%]	Y_{HMF} [%]	SD [%]
24	21	0.3	24	2.9
120	45	4.3	50	2.1

Standard uncertainty: u(T) = 0.5 K; u(Y_{HMF}) = 1.7%.

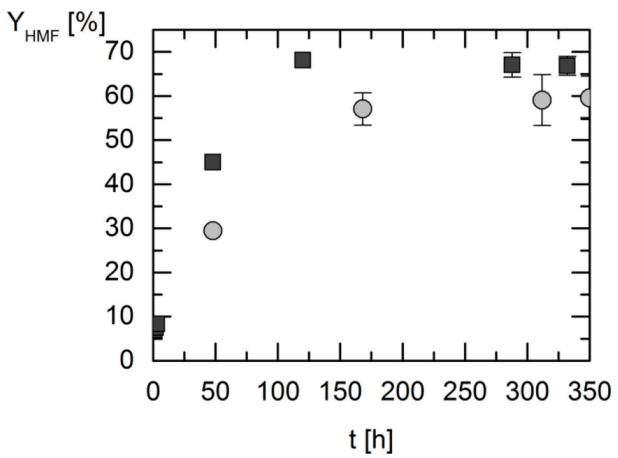

FIGURE 2 | 5-Hydroxymethylfurfural (HMF) yield over time in the different deep eutectic systems based on tetraethyl ammonium chloride (TEAC); reaction temperature: 323 K; $w_{FRU,0}$ = 2.5 wt.%; pressure: 1 bar. Circles: TEAC:lactic acid 1:2; squares: TEAC:levulinic acid 1:2. Data listed in **Table S3**.

TABLE 3 | The pH values of the different DESs at 295 K and 1 bar.

DES	ChCl:LA	TBAC:LA	TEAC:LA	ChCl:LAA	TBAC:LAA	TEAC:LAA
pH [–]	1.62 ± 0.04	1.71 ± 0.04	2.92 ± 0.06	0.48 ± 0.01	0.83 ± 0.02	1.37 ± 0.01

Standard uncertainty: u(T) = 0.5 K; u(pH) = 0.02.

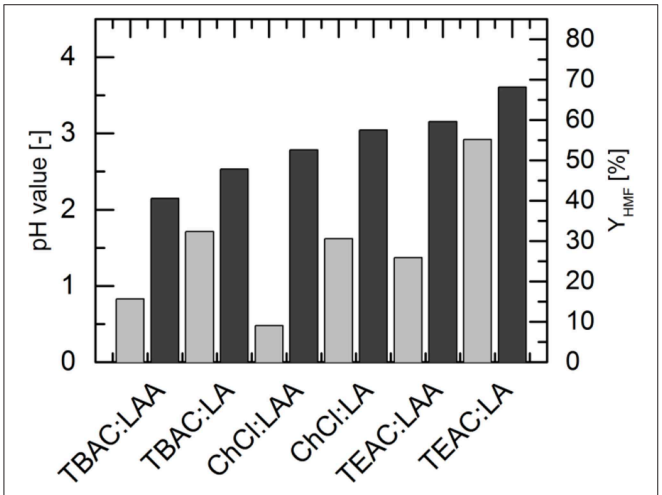

FIGURE 3 | The HMF yields (black bars) as well as the pH-values (gray bars) in the different deep eutectic solvents with molar ratio HBA:HBD 1:2. The HMF yields were achieved in the DESs consisting of the quaternary ammonium salts and levulinic acid or lactic acid. Data listed in **Table S4**.

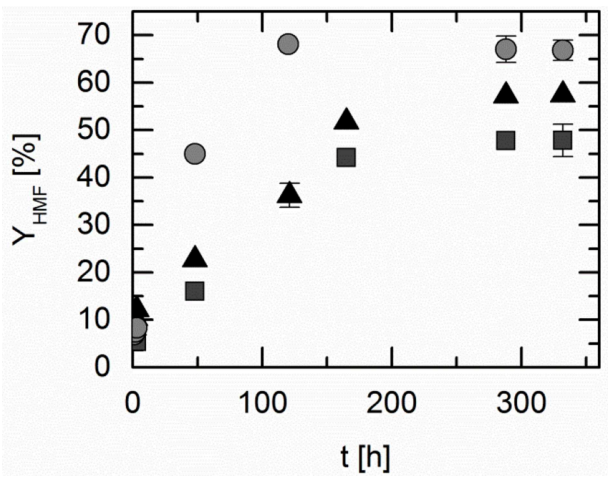

FIGURE 4 | 5-Hydroxymethylfurfural (HMF) yield over time in the different deep eutectic systems based on levulinic acid (LA); reaction temperature 323 K; $w_{FRU,0}$ = 2.5 wt.%; pressure 1 bar. Symbols are yields in different DESs: triangles: choline chloride (ChCl):LA 1:2; squares: tetrabutyl ammonium chloride (TBAC):LA 1:2; circles: tetraethyl ammonium chloride (TEAC):LA 1:2. Data listed in **Table S5**.

reactions in the literature (Lemberg and Sadowski, 2017; Voges et al., 2017; Wangler et al., 2019).

The finding that acidity plays a minor role is further studied by analyzing the relation between pH and HMF yield. pH values in various DESs was measured with the pH meter Qph 70 (VWR International GmbH, Langenfeld, Germany). The measurements were carried out three times at 295 K. These averaged pH values are listed in **Table 3**.

In both the LA-based DESs and in the LAA-based DESs, the pH can be sequenced in the same order of the HBA quaternary ammonium salts: pH(TEAC-based DES) > pH(TBAC-based DES) > pH(ChCl-based DES). Due to the carboxylic acids used, the pH in the DESs with LAA as HBD is comparatively lower than in the DESs with LA as HBD. The HMF yield and the pH obtained in the DESs are plotted in **Figure 3**.

It can be observed from **Figure 3** that pH-value of the DESs does not correlate with the achieved HMF yield. This result was obtained for both LA-based DESs and LAA-based DESs. Thus, it can be concluded that the chemical nature of the HBA itself leads to the different reactivities in the reaction under investigation. This is further investigated in the next set of experiments.

Influence of the Chemical Nature of the HBA in DESs With Levulinic Acid

The experiments in LA-based DESs were performed as described in the section Experiments and Methods. The results of the two independent samples were measured in triplicate and are shown in **Figure 4**, which presents the influence of the HBA constituent on the HMF yield. Three different HBAs were investigated: choline chloride (ChCl), tetrabutyl ammonium chloride (TBAC), and tetraethyl ammonium chloride (TEAC).

In ChCl:LA the HMF yield after 3 h reached 12%, in TBAC:LA 5% and in TEAC:LA 8%. After 120 h, maximum yield (equilibrium) was reached in TEAC: LA of 68%. In both, ChCl:LA and TBAC:LA equilibrium was reached after 312 h with maximum yields of HMF of 57% (ChCl:LA) and of 48% (TBAC:LA). The maximum yield of HMF increased from TBAC as HBA, through ChCl to TEAC, as it was already observed in the LAA-based DESs (**Table S6**). These results indicate a significant influence of hydrophilicity on HMF yield. This again points out the finding that molecular interactions induced by the solvent are responsible for the findings in this work.

Reactivity of Reaction Medium Containing DES and Additional Vanadium Catalyst

Due to the large time span required to reach the reaction equilibrium in the investigated systems, the use of different vanadium catalysts was further investigated. The selection of promising homogeneous vanadium-based catalysts was done based on former investigations carried out by Albert et al. (2019). The influence of the catalysts on the reaction kinetics was

determined using the DES that allowed highest yields of HMF without additional catalyst. In this work this was found to be the DES TEAC:LA in a molar ratio of 1:2 at a reaction temperature of 323 K. The experiments were carried out as described in section Synthesis of Deep Eutectic Solvents. In the following, a sample was taken every hour at the beginning and analyzed immediately. In each case the same amount of catalyst was added as a powder to the standard reaction mixture consisting of 2.5 wt% fructose in of DES. **Figure 5** shows the HMF yields obtained in TEAC:LA with and without additional vanadium catalyst.

The maximum reachable yield for the reaction in the solvent TEAC:LA is illustrated in **Figure 5** yielding $Y_{HMF} = 68\%$. This value is the thermodynamically limited equilibrium yield, reached after about 100 h. Using additional catalysts allows improving the kinetics, which is shown clearly in **Figure 5**. In the solvent TEAC:LA + NH_4VO_3, the yield reached 5% (3%) after 1 h (24 h) of reaction time. Using the solvent TEAC:LA + $VOSO_4$, the HMF yield was found to be 17% (45%) after 1 h (24 h) of reaction time. After 24 h, the yield did not further increase in this solvent. In comparison to the above-used vanadium salts, the addition of HPA-5 as a catalyst to the solvent TEAC:LA allows an HMF yield of 57% after 5 h. This was the maximally achievable yield at the applied conditions. Thus, the heteropolyacid HPA-5 drastically increased reaction kinetics and might be a very promising perspective for future investigations. Furthermore, high HMF selectivities (see **Figure S2**) could be reached demonstrating the beneficial effect of the DES:POM reaction system. Nevertheless, still the yield does not increase higher than $Y_{HMF} = 57\%$, even not after 5 h of time. The yield was measured in HPA-5 + TEAC:LA up to 48 h (see **Figure S5**). The reason behind the difference to the maximum achievable yield ($Y_{HMF} = 68\%$) is probably caused by solvent/catalyst interactions. For samples that contained HPA-5 a color change of the reaction solution was observed turning from yellowish to dark brownish with increasing reaction time (see **Figure S4**). This might be due to side product (mostly humin) formation as described earlier. Obviously, this limits the maximum achievable HMF yield using this catalyst system without product isolation. This underlines the necessity to isolate the product (and especially water as the side product) from the reaction solution as it further decreases the pH value that favors undesired humin formation.

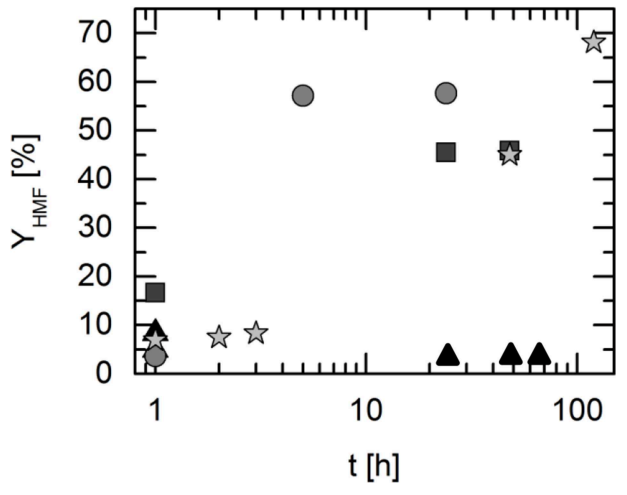

FIGURE 5 | 5-Hydroxymethylfurfural (HMF) yield over time in the deep eutectic systems consisting of tetraethyl ammonium chloride and levulinic acid (TEAC:LA 1:2) with different catalysts. The catalysts were added to the fructose+DES mixture undissolved as a powder. Reaction temperature: 323 K; $w_{FRU,0} = 2.5$ wt.%. Symbols present yields in different reaction medium: triangles: TEAC:LA with NH_4VO_3; squares: TEAC:LA with $VOSO_4$; circles: TEAC:LA with HPA-5; stars: TEAC:LA without catalyst. Data listed in **Table S7**.

As a remark, it shall be stated that the total achievable HMF yield at thermodynamic equilibrium is 57% using the DES consisting of ChCL:LA, while the highest yield was found for the DES TEAC:LA. Even though the reaction conditions used in this study are mild, these yields are still moderate and the reaction time without catalyst is very long especially (cf. more than 300 h in **Figure 1**) to reach the equilibrium yield. In the literature, higher yields were obtained at cost of more toxic conditions and higher energy required (Vandam et al., 1986; Chheda et al., 2007; Hu et al., 2008; Hansen et al., 2009; Ilgen et al., 2009; Thi et al., 2010; Russ and Konig, 2012; D'Anna et al., 2014; Yi et al., 2015; Zhang et al., 2015).

Solvent Recycling

As a final step the solvent recyclability was investigated for the best system, i.e., TEAC-LA (1:2) in combination with 4 wt. % HPA-5 at 323 K. For this step, the initial reaction mixture was prepared once, and after defined times the reactant fructose was added again. It should be mentioned that no new catalyst was added. That is, the DES solvent was used for five subsequent times and after about 5 h of reaction the concentration of HMF was measured prior to adding another 2.5 w% of fructose only. The results are shown in **Figure 6**. It can be observed that a nearly linear increase of HMF weight fraction was obtained. That is, adding fructose at defined reaction time allows similar conversion of fructose independent of the HMF that was subsequently produced during the single reaction steps. To conclude, the solvent could be successfully used for five times in a row without losing its efficiency at the conditions under investigation. Please note that we did not investigate any additional cycle of fructose addition.

The exact procedure we carried out can be described as "Recycling without product isolation," which is standard procedure in chemical reaction engineering. We have recently developed methods to extract HMF from aqueous solutions using hydrophobic solvents such as ketones (Mohammad et al., 2016) or hydrophobic DESs (Dietz et al., 2019). Thus, a meaningful extraction method is to feed the product with hydrophobic solvent (ketone or DES), upon which the HMF will be separated into a second phase, and then to distillate the mixture (in case of ketone as extractant the ketone will be the head product). Further, an increase of the fructose concentration is of course an important step for an upscale of the process. However, the limited fructose solubility in the considered DESs might be a limitation toward concentration increase. We measured experimentally the fructose solubilities in the considered DESs. It can be observed

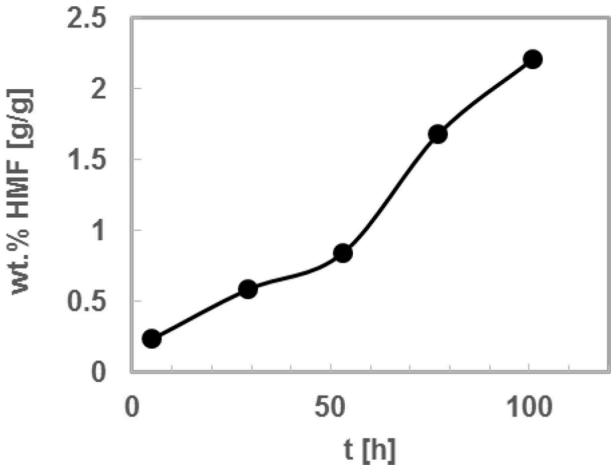

FIGURE 6 | 5-Hydroxymethylfurfural (HMF) weight fraction over time in the deep eutectic systems consisting of tetraethyl ammonium chloride and levulinic acid (TEAC:LA 1:2) with HPA-5 catalyst. Four wt% of the catalyst was added at $t = 0$ to the fructose+DES mixture undissolved as a powder. Reaction temperature: 323 K; $w_{FRU,0} = 2.5$ wt.%. Symbols present data upon addition of 2.5 wt% fructose after each reaction step.

that solubility in LAA– based DESs are higher than in LA-based DESs. However, the HMF yields in the LAA– based DESs are lower than in LA-based DESs. The solubilities are presented in **Table S9**.

CONCLUSIONS

The conversion of biomass to valuable products is of utmost importance to replace petroleum-based chemical syntheses. In this contribution, we studied the reaction from fructose to HMF as a key reaction and as a model reaction in which water is formed as product. From thermodynamic point-of-view, water as reaction medium has to be avoided for high conversion. Nevertheless, the conversion is acid-catalyzed. Thus, we used acidic deep eutectic solvents (DES) as a reaction medium, and due to their low thermal stability we focused on low reaction temperatures of 323 K. The used DESs were chosen to be liquid at this reaction temperature, which we measured and also predicted with thermodynamic models. Further, the used DESs had to behave acidic and thus we studied DESs based on carboxylic acids, in this work the biogenic levulinic acid and lactic acid.

The results showed that the DESs based on the combination of a chloride salt (e.g., choline chloride) and of a carboxylic acid are promising reaction medium for the synthesis of HMF. Maximum yields of about 70% were obtained at 323 K. A detailed study on the influence of the kind of DES revealed that temperature (up to 343 K) and acidity in the reaction mixtures ($0.4 < pH < 3.5$) as well as the composition of the DES (i.e., the ratio between chloride salt and carboxylic acid) do little influence the maximum achieved yield. In contrast, the kind of the DES constituents strongly influenced the measured yield. The use of DESs composed of levulinic acid instead of lactic acid as well as of tetraethyl ammonium chloride instead of choline chloride or tetrabutyl ammonium chloride allowed higher yields. As the reaction reached high yields after long reaction times, the kinetics were increased in this work using different vanadium-based catalysts. The polyoxometalate HPA-5 ($H_8PV_5Mo_7O_{40}$) lead to drastically increased reaction kinetics giving a maximum HMF yield of about 60% after only 5 h reaction time without decreasing the very high product selectivity. The reaction solvent (DES+HPA-5) could be successfully used for five times in a row without losing its efficiency at the conditions under investigation We consider this to be very important step toward sustainable green processing of biomass in the future.

DATA AVAILABILITY STATEMENT

All datasets generated for this study are included in the manuscript/**Supplementary Files**.

AUTHOR CONTRIBUTIONS

CH and JA: conceptualization. CH and JA: methodology. SK: validation. All authors: formal analysis. SK: investigation. CH and JA: resources. SK: data curation. SK: writing—original draft preparation. CH and JA: writing—review and editing. SK: visualization. CH: supervision. CH: project administration. CH: funding acquisition.

FUNDING

Max-Buchner Research Foundation (CH).

ACKNOWLEDGMENTS

JA thanks Natalie Mayer for performing the TGA measurements and Anna Bukowski for measuring FTIR spectra of the HPA-5 catalyst. CH gratefully acknowledges financial support from Max-Buchner Research Foundation with number 3577 and Prof. Dieter Vogt for discussions.

SUPPLEMENTARY MATERIAL

The Supplementary Material for this article can be found online at: https://www.frontiersin.org/articles/10.3389/fchem.2019.00661/full#supplementary-material

REFERENCES

Abbott, A. P., Boothby, D., Capper, G., Davies, D. L., and Rasheed, R. K. (2004). Deep eutectic solvents formed between choline chloride and carboxylic acids: versatile alternatives to ionic liquids. *J. Am. Chem. Soc.* 126, 9142-9147. doi: 10.1021/ja048266j

Albert, J., Luders, D., Bosmann, A., Guldi, D. M., and Wasserscheid, P. (2014). Spectroscopic and electrochemical characterization of heteropoly acids for their

optimized application in selective biomass oxidation to formic acid. *Green Chem.* 16, 226–237. doi: 10.1039/C3GC41320A

Albert, J., Mehler, J., Tucher, J., Kastner, K., and Streb, C. (2016). One-step synthesizable lindqvist-isopolyoxometalates as promising new catalysts for selective conversion of glucose as a model substrate for lignocellulosic biomass to formic acid. *Chem. Select* 1, 2889–2894. doi: 10.1002/slct.201600797

Albert, J., Mendt, M., Mozer, M., and Voss, D. (2019). Explaining the role of vanadium in homogeneous glucose transformation reactions using NMR and EPR spectroscopy. *Appl. Catalysis A General* 570, 262–270. doi: 10.1016/j.apcata.2018.10.030

Albert, J., Wolfel, R., Bosmann, A., and Wasserscheid, P. (2012). Selective oxidation of complex, water-insoluble biomass to formic acid using additives as reaction accelerators. *Energy Environ Sci.* 5, 7956–7962. doi: 10.1039/c2ee21428h

Altuntepe, E., Emel'yanenko, V. N., Forster-Rotgers, M., Sadowski, G., Verevkin, S. P., and Held, C. (2017). Thermodynamics of enzyme-catalyzed esterifications: II. Levulinic acid esterification with short-chain alcohols. *Appl. Microbiol. Biotechnol.* 101, 7509–7521. doi: 10.1007/s00253-017-8481-4

Ammam, M. (2013). Polyoxometalates: formation, structures, principal properties, main deposition methods and application in sensing. *J. Mater. Chem. A* 1, 6291–6312. doi: 10.1039/c3ta01663c

Assanosi, A. A., Farah, M. M., Wood, J., and Al-Duri, B. (2014). A facile acidic choline chloride-p-TSA DES-catalysed dehydration of fructose to 5-hydroxymethylfurfural. *RSC Adv.* 4, 39359–39364. doi: 10.1039/C4RA07065H

Bozell, J. J., and Petersen, G. R. (2010). Technology development for the production of biobased products from biorefinery carbohydrates—the US Department of Energy's "Top 10" revisited. *Green Chem.* 12, 539–554. doi: 10.1039/b922014c

Carniti, P., Gervasini, A., and Marzo, M. (2011). Absence of expected side-reactions in the dehydration reaction of fructose to HMF in water over niobic acid catalyst. *Catalysis Commun.* 12, 1122–1126. doi: 10.1016/j.catcom.2011.03.025

Chheda, J. N., Román-Leshkov, Y., and Dumesic, J. A. (2007). Production of 5-hydroxymethylfurfural and furfural by dehydration of biomass-derived mono- and poly-saccharides. *Green Chem.* 9, 342–350. doi: 10.1039/B611568C

Crespo, E. A., Silva, L. P., Martins, M. A. R., Bulow, M., Ferreira, O., Sadowski, G., et al. (2018). The role of polyfunctionality in the formation of [ch]cl-carboxylic acid-based deep eutectic solvents. *Ind. Eng. Chem. Res.* 57, 11195–11209. doi: 10.1021/acs.iecr.8b01249

D'Anna, F., Marullo, S., Vitale, P., Rizzo, C., Lo Meo, P., and Noto, R. (2014). Ionic liquid binary mixtures: promising reaction media for carbohydrate conversion into 5-hydroxymethylfurfural. *Appl. Catalysis A General* 482, 287–293. doi: 10.1016/j.apcata.2014.05.039

Dietz, C. H. J. T., Gallucci, F., van Sint Annaland, M., Held, C., and Kroon, M. C. (2019). 110th anniversary: distribution coefficients of furfural and 5-hydroxymethylfurfural in hydrophobic deep eutectic solvent + water systems: experiments and perturbed-chain statistical associating fluid theory predictions. *Ind. Eng. Chem. Res.* 58, 4240–4247. doi: 10.1021/acs.iecr.8b06234

Francisco, M., van den Bruinhorst, A., and Kroon, M. C. (2013). Low-transition-temperature mixtures (lttms): a new generation of designer solvents. *Angew. Chem. Int. Ed.* 52, 3074–3085. doi: 10.1002/anie.201207548

Garcia-Alvarez, J., Hevia, E., and Capriati, V. (2018). The future of polar organometallic chemistry written in bio-based solvents and water. *Chemistry* 24, 14854–14863. doi: 10.1002/chem.201802873

Hansen, T. S., Woodley, J. M., and Riisager, A. (2009). Efficient microwave-assisted synthesis of 5-hydroxymethylfurfural from concentrated aqueous fructose. *Carbohydrate Res.* 344, 2568–2572. doi: 10.1016/j.carres.2009.09.036

Hu, S., Zhang, Z., Zhou, Y., Han, B., Fan, H., Li, W., et al. (2008). Conversion of fructose to 5-hydroxymethylfurfural using ionic liquids prepared from renewable materials. *Green Chem.* 10, 1280–1283. doi: 10.1039/b810392e

Ilgen, F., Ott, D., Kralisch, D., Reil, C., Palmberger, A., and König, B. (2009). Conversion of carbohydrates into 5-hydroxymethylfurfural in highly concentrated low melting mixtures. *Green Chem.* 11, 1948–1954. doi: 10.1039/b917548m

Istasse, T., Bockstal, L., and Richel, A. (2018). Production of 5-hydroxymethylfurfural from D-fructose in low-transition-temperature mixtures enhanced by chloride anions and low amounts of organic acids. *ChemPlusChem* 83, 1135–1143. doi: 10.1002/cplu.201800416

Iwata, T. (2015). Biodegradable and bio-based polymers: future prospects of eco-friendly plastics. *Angew. Chem. Int. Ed.* 54, 3210–3215. doi: 10.1002/anie.201410770

Kozhevnikov, I. V. (1998). Catalysis by heteropoly acids and multicomponent polyoxometalates in liquid-phase reactions. *Chem. Rev.* 98, 171–198. doi: 10.1021/cr960400y

Kuster, B. F. M., and van der Baan, S. H. (1977). The influence of the initial and catalyst concentrations on the dehydration of d-fructose. *Carbohydrate Res.* 54, 165–176. doi: 10.1016/S0008-6215(00)84806-5

Lemberg, M., and Sadowski, G. (2017). Predicting the solvent effect on esterification kinetics. *ChemPhysChem* 18, 1977–1980. doi: 10.1002/cphc.201700507

Li, G. B., Jiang, Y. T., Liu, X. B., and Deng, D. S. (2016). New levulinic acid-based deep eutectic solvents: synthesis and physicochemical property determination. *J. Mol. Liquids* 222, 201–207. doi: 10.1016/j.molliq.2016.07.039

Liu, F., Barrault, J., Vigier, K. D., and Jerome, F. (2012). Dehydration of highly concentrated solutions of fructose to 5-hydroxymethylfurfural in a cheap and sustainable choline chloride/carbon dioxide system. *ChemSusChem* 5, 1223–1226. doi: 10.1002/cssc.201200186

Mohammad, S., Held, C., Altuntepe, E., Köse, T., and Sadowski, G. (2016). Influence of salts on the partitioning of 5-hydroxymethylfurfural in water/MIBK. *J. Phys. Chem. B* 120, 3797–3808. doi: 10.1021/acs.jpcb.5b11588

Odyakov, V. F., and Zhizhina, E. G. (2008). A novel method of the synthesis of molybdovanadophosphoric heteropoly acid solutions. *Reaction Kinetics Catalysis Lett.* 95, 21–28. doi: 10.1007/s11144-008-5374-7

Okano, T., Qiao, K., Bao, Q. X., Tomida, D., Hagiwara, H., and Yokoyama, C. (2013). Dehydration of fructose to 5-hydroxymethylfurfural (HMF) in an aqueous acetonitrile biphasic system in the presence of acidic ionic liquids. *Appl. Catalysis A General* 451, 1–5. doi: 10.1016/j.apcata.2012.11.004

Russ, C., and Konig, B. (2012). Low melting mixtures in organic synthesis - an alternative to ionic liquids? *Green Chem.* 14, 2969–2982. doi: 10.1039/c2gc36005e

Sheldon, R. A. (2016). Biocatalysis and biomass conversion in alternative reaction media. *Chemistry* 22, 12983–12998. doi: 10.1002/chem.201601940

Smith, E. L., Abbott, A. P., and Ryder, K. S. (2014). Deep eutectic solvents (DESs) and their applications. *Chem. Rev.* 114, 11060–11082. doi: 10.1021/cr300162p

Tang, X., Zuo, M., Li, Z., Liu, H., Xiong, C. X., Zeng, X. H., et al. (2017). Green processing of lignocellulosic biomass and its derivatives in deep eutectic solvents. *ChemSusChem* 10, 2696–2706. doi: 10.1002/cssc.201700457

Thi, P. T. P., Cho, C. W., and Yun, Y. S. (2010). Environmental fate and toxicity of ionic liquids: a review. *Water Res.* 44, 352–372. doi: 10.1016/j.watres.2009.09.030

Vandam, H. E., Kieboom, A. P. G., and Vanbekkum, H. (1986). The conversion of fructose and glucose in acidic media—formation of hydroxymethylfurfural. *Starch Starke* 38, 95–101. doi: 10.1002/star.19860380308

Vitale, P., Abbinante, V. M., Perna, F. M., Salomone, A., Cardellicchio, C., and Capriati, V. (2017). Unveiling the hidden performance of whole cells in the asymmetric bioreduction of aryl-containing ketones in aqueous deep eutectic solvents. *Adv. Synthesis Catalysis* 359, 1049–1057. doi: 10.1002/adsc.201601064

Voges, M., Fischer, C., Wolff, D., and Held, C. (2017). Influence of natural solutes and ionic liquids on-the yield of enzyme-catalyzed reactions: measurements and predictions. *Organic Process Res. Dev.* 21, 1059–1068. doi: 10.1021/acs.oprd.7b00178

Wang, S. S., and Yang, G. Y. (2015). Recent advances in polyoxometalate-catalyzed reactions. *Chem. Rev.* 115, 4893–4962. doi: 10.1021/cr500390v

Wangler, A., Loll, R., Greinert, T., Sadowski, G., and Held, C. (2019). Predicting the high concentration co-solvent influence on the reaction equilibria of the ADH-catalyzed reduction of acetophenone. *J. Chem. Thermodyn.* 128, 275–282. doi: 10.1016/j.jct.2018.08.021

Werpy, T., and Petersen, G. (2004). *Top Value Added Chemicals from Biomass: Volume I—Results of Screening for Potential Candidates from Sugars and Synthesis Gas*. Springfield, VA: U.S. Department of Energy. doi: 10.2172/15008859

Yi, X. H., Delidovich, I., Sun, Z., Wang, S. T., Wang, X. H., and Palkovits, R. (2015). A heteropoly acid ionic crystal containing Cr as an active catalyst for dehydration of monosaccharides to produce 5-HMF in water. *Catalysis Sci. Technol.* 5, 2496–2502. doi: 10.1039/C4CY01555J

Zakrzewska, M. E., Bogel-Lukasik, E., and Bogel-Lukasik, R. (2011). Ionic liquid-mediated formation of 5-hydroxymethylfurfural-a promising biomass-derived building block. *Chem. Rev.* 111, 397–417. doi: 10.1021/cr100171a

Zhang, J., Yu, X. X., Zou, F. X., Zhong, Y. H., Du, N., and Huang, X. R. (2015). Room-temperature ionic liquid system converting fructose into 5-hydroxymethylfurfural in high efficiency. *ACS Sustain. Chem. Eng.* 3, 3338–3345. doi: 10.1021/acssuschemeng.5b01015

Zhang, Q. H., Vigier, K. D., Royer, S., and Jerome, F. (2012). Deep eutectic solvents: syntheses, properties and applications. *Chem. Soc. Rev.* 41, 7108–7146. doi: 10.1039/c2cs35178a

Zhao, B. Y., Xu, P., Yang, F. X., Wu, H., Zong, M. H., and Lou, W. Y. (2015). Biocompatible deep eutectic solvents based on choline chloride: characterization and application to the extraction of rutin from *Sophora japonica*. *ACS Sustain. Chem. Eng.* 3, 2746–2755. doi: 10.1021/acssuschemeng.5b00619

Zubeir, L. F., Held, C., Sadowski, G., and Kroon, M. C. (2016). PC-SAFT modeling of CO_2 solubilities in deep eutectic solvents. *J. Phys. Chem. B* 120, 2300–2310. doi: 10.1021/acs.jpcb.5b07888

Conflict of Interest: The authors declare that the research was conducted in the absence of any commercial or financial relationships that could be construed as a potential conflict of interest.

frontiers in Chemistry

MINI REVIEW
published: 29 November 2019
doi: 10.3389/fchem.2019.00834

Cellulose Conversion Into Hexitols and Glycols in Water: Recent Advances in Catalyst Development

Oleg V. Manaenkov[1], Olga V. Kislitsa[1], Valentina G. Matveeva[1,2], Ester M. Sulman[1,2], Mikhail G. Sulman[1,3] and Lyudmila M. Bronstein[3,4,5]**

[1] Department of Biotechnology, Chemistry, and Standardization, Tver State Technical University, Tver, Russia, [2] Regional Technological Center, Tver State University, Tver, Russia, [3] A.N. Nesmeyanov Institute of Organoelement Compounds, Russian Academy of Sciences, Moscow, Russia, [4] Department of Chemistry, Indiana University, Bloomington, IN, United States, [5] Department of Physics, Faculty of Science, King Abdulaziz University, Jeddah, Saudi Arabia

Conversion of biomass cellulose to value-added chemicals and fuels is one of the most important advances of green chemistry stimulated by needs of industry. Here we discuss modern trends in the development of catalysts for two processes of cellulose conversion: (i) hydrolytic hydrogenation with the formation of hexitols and (ii) hydrogenolysis, leading to glycols. The promising strategies include the use of subcritical water which facilitates hydrolysis, bifunctional catalysts which catalyze not only hydrogenation, but also hydrolysis, retro-aldol condensation, and isomerization, and pretreatment (milling) of cellulose together with catalysts to allow an intimate contact between the reaction components. An important development is the replacement of noble metals in the catalysts with earth-abundant metals, bringing down the catalyst costs, and improving the environmental impact.

Keywords: cellulose, hydrolytic hydrogenation, hydrogenolysis, sorbitol, mannitol, ethylene glycol, propylene glycol

OPEN ACCESS

Edited by:
Dmitry Yu. Murzin,
Åbo Akademi University, Finland

Reviewed by:
Keiichi Tomishige,
Tohoku University, Japan
Brent Shanks,
Iowa State University, United States

****Correspondence:***
Oleg V. Manaenkov
ovman@yandex.ru
Lyudmila M. Bronstein
lybronst@indiana.edu

Specialty section:
This article was submitted to Green and Sustainable Chemistry, a section of the journal Frontiers in Chemistry

Received: *01 October 2019*
Accepted: *15 November 2019*
Published: *29 November 2019*

Citation:
Manaenkov OV, Kislitsa OV, Matveeva VG, Sulman EM, Sulman MG and Bronstein LM (2019) Cellulose Conversion Into Hexitols and Glycols in Water: Recent Advances in Catalyst Development. Front. Chem. 7:834. doi: 10.3389/fchem.2019.00834

INTRODUCTION

The recent data show that around $1.1 \cdot 10^{11}$ tons of lignocellulose biomass (including both lignin and cellulose) are synthesized in Nature annually, the majority of which (30–55%) is cellulose (Li et al., 2018a). Cellulose is a natural polymer consisting of glucose repeating units and is the most promising alternative for syntheses of value-added chemicals to replace non-renewable resources such as gas and oil (Li et al., 2015b, 2018a). Currently, there are numerous methods for direct catalytic conversion of cellulose to a number of valuable chemicals such as glucose (Shrotri et al., 2016, 2018), hexitols (Li et al., 2015a; Zada et al., 2017; Shrotri et al., 2018), glycols (Li et al., 2015a; Zheng et al., 2017), 5-hydroxymethylfurfural (Li et al., 2018b), methane (Wang et al., 2018), hydrogen (Wen et al., 2010), hexane and hexanols (Liu et al., 2014, 2015; Op De Beeck et al., 2015).

The presence of a large number of hydroxyl groups in the cellulose structure determines the optimal route of its conversion to polyols via hydrolytic hydrogenation or hydrogenolysis (involving C-C cleavage) (Li et al., 2015a). Both processes consist of several reactions but can be carried out in a one-pot procedure. Major products of hydrolytic hydrogenation are hexitols (sorbitol and mannitol, **Figure 1A**), while in hydrogenolysis they are glycols (ethylene glycol, EG, and propylene glycol, PG, **Figure 1B**). From the viewpoint of green chemistry, the best reaction medium for these processes is subcritical water (Rinaldi, 2014; Shitu et al., 2015) due to its availability, low cost, and non-toxicity. In subcritical water the concentration of both hydroxyls and

hydroxonium ions increases by a factor of 35 (compared to r.t. water), which leads to acceleration of the reactions catalyzed by acids or bases, for example, hydrolysis (Gagic et al., 2018; Abaide et al., 2019). Moreover, the efficiency of both processes are strongly dependent on the hydrogenation catalyst activity, i.e., its ability to rapidly and selectively hydrogenate hexoses and induce their decomposition following retro-aldol mechanism.

In this review we discuss most interesting and promising catalytic systems which were proposed for hydrolytic hydrogenation and hydrogenolysis of cellulose in hydrothermal conditions in water in the last 5 years.

CELLULOSE HYDROLYTIC HYDROGENATION

As was demonstrated in a recent review (Makhubela and Darkwa, 2018), among noble metals Ru is the most active and employed in the majority of catalytic systems proposed for hydrolytic hydrogenation of cellulose (Li et al., 2015a; Ribeiro et al., 2015b). In studies of Ru-containing catalysts, the major focus is on various supports and attempts to increase the catalyst efficiency via control of the support structure and properties.

Carbon Based Supports

Carbon based materials are popular catalyst supports for cellulose conversion due to high surface area, porosity, and mechanical and thermal stability (Ribeiro et al., 2017a; Adsuar-Garcia et al., 2018). The Ru-containing catalyst based on commercial carbon black treated with H_2SO_4 to create acidic surface sites displayed comparatively high selectivity to sorbitol (40% at 190°C, 5 MPa, 3 h) and stability upon repeated use (Adsuar-Garcia et al., 2018). Ribeiro et al. compared Ru-containing catalysts based on original multiwall carbon nanotubes (CNT) and those modified by HNO_3 to impart oxygenated groups (Ribeiro et al., 2017b). Although the activity of the catalyst based on original CNT was lower than that for the modified support (due to increased acidity), the maximum selectivity to sorbitol reached 70% (205°C, 5 MPa, 2 h), while for the modified support, it was lower by 20%. Clearly, acidity is important for cellulose hydrolysis, but it should be moderate to maintain a high sorbitol yield. This catalyst showed excellent stability upon four reuses. Micro/mesoporous activated carbon containing sulfonic groups and Pt nanoparticles allowed a total hexitol yield of 69.5% at comparatively mild conditions (180°C, 2 MPa, 24 h) (Lazaridis et al., 2017). It is noteworthy, that Ru on the same support showed a much lower hexitol yield, but allowed for high yields of glycerol and PG due to increased hydrogenolysis of hexitols formed. Both catalysts were stable upon four consecutive reaction, while a decreased number of sulfonic groups did not influence the activity and selectivity to hexitols. Rey-Raap et al. reported glucose-derived carbons obtained in the presence of CNT as a support for Ru nanoparticles (Rey-Raap et al., 2019). These materials possess high surface areas, abundant microporosity and low acidity, which increase Ru dispersion and the sorbitol yield to 64.1% (205°C, 5 MPa, 2 h). This type of catalysts is also cost effective as a significant fraction of CNT is replaced with low-cost biomass generated carbon as well as stable. No deterioration of the cellulose conversion or sorbitol yield was observed after four consecutive reactions, which the authors assign to the unchanged Ru oxidation state (according to XPS). A similar approach to low-cost supports was utilized by Li et al. (2019). Carbonized cassava dregs (formed in the starch production) functionalized with SO_3H groups and containing Ru nanoparticles allowed for a comparable sorbitol yield (63.8%) at 180°C, 4 MPa for 10 h. The catalyst was stable in hydrothermal conditions in at least five consecutive cycles. Ru-Ni bimetallic catalysts based on activated carbon or CNT (Ru-Ni/AC; Ru-Ni/CNT) have been proposed for direct cellulose conversion to sorbitol (Ribeiro et al., 2017c). Independently of the support, Ni in bimetallic nanoparticles had a promoting effect on catalysis, increasing conversion, and selectivity to sorbitol due to intimate interaction of both metals. The sorbitol yield was in the range of 50–60% (205°C, 5 MPa, 5 h), but it could be further increased to more than 70% when cellulose and catalysts were milled together, an important development in the catalyst pretreatment (Ribeiro et al., 2015a; Liu et al., 2016b). These catalysts preserved their activity in at least four consecutive reactions.

Matveeva et al. reported Ru-containing catalysts based on micro/mesoporous hypercrosslinked polystyrene (HPS), allowing for the sorbitol yield of $\sim$ 50% (245°C, 6 MPa, 0.08 h) at cellulose conversion of 85% (Matveeva et al., 2017). High efficiency of the catalyst is believed to be due to the HPS high surface area and a narrow pore size distribution, controlling the formation of 1.4 ± 0.3 nm Ru-containing nanoparticles. The catalyst stability in at least three catalytic cycles was demonstrated.

Metal Oxide Based Supports

The catalyst based on CuO (a catalytic phase) and the CeO_2-ZrO_2 support has showed exceptional efficiency: 99.1% selectivity to sorbitol at 92% of the cellulose conversion (245°C, 5.2 MPa, 4 h) in the neutral medium (Dar et al., 2015). Moreover, the catalyst was stable during five consecutive catalytic reactions. The authors believe that such outstanding properties should be attributed to the mesoporous structure of the support, facilitating mass transfer as well as enhanced ability of the Cu-containing catalyst in promoting hydrogenation.

Ru-containing catalysts based on zeolites were also successfully utilized. Wang et al. obtained 39.4% yield of hexitols using mesoporous Ru/HZSM-5 at 200°C, 5 MPa for 10 h (Wang et al., 2015b). The authors believe that Lewis (LAS) and Brønsted (BAS) acid sites formed during the zeolite treatment promote cellulose hydrolysis. In addition, the mesoporous structure of the support increases the surface area and provides better Ru-containing nanoparticle dispersion, leading to a comparatively high yield of hexitols. A significantly higher yield (up to 63.6%) has been obtained with Ni-containing catalysts based on ZSM-5 (Liang et al., 2015). Formation of electron deficient multiply-twinned Ni particles imbedded in zeolite allows for excellent CO adsorption and activation of glucose carbonyl groups, facilitating its hydrogenation with active hydrogen. This is an especially remarkable development

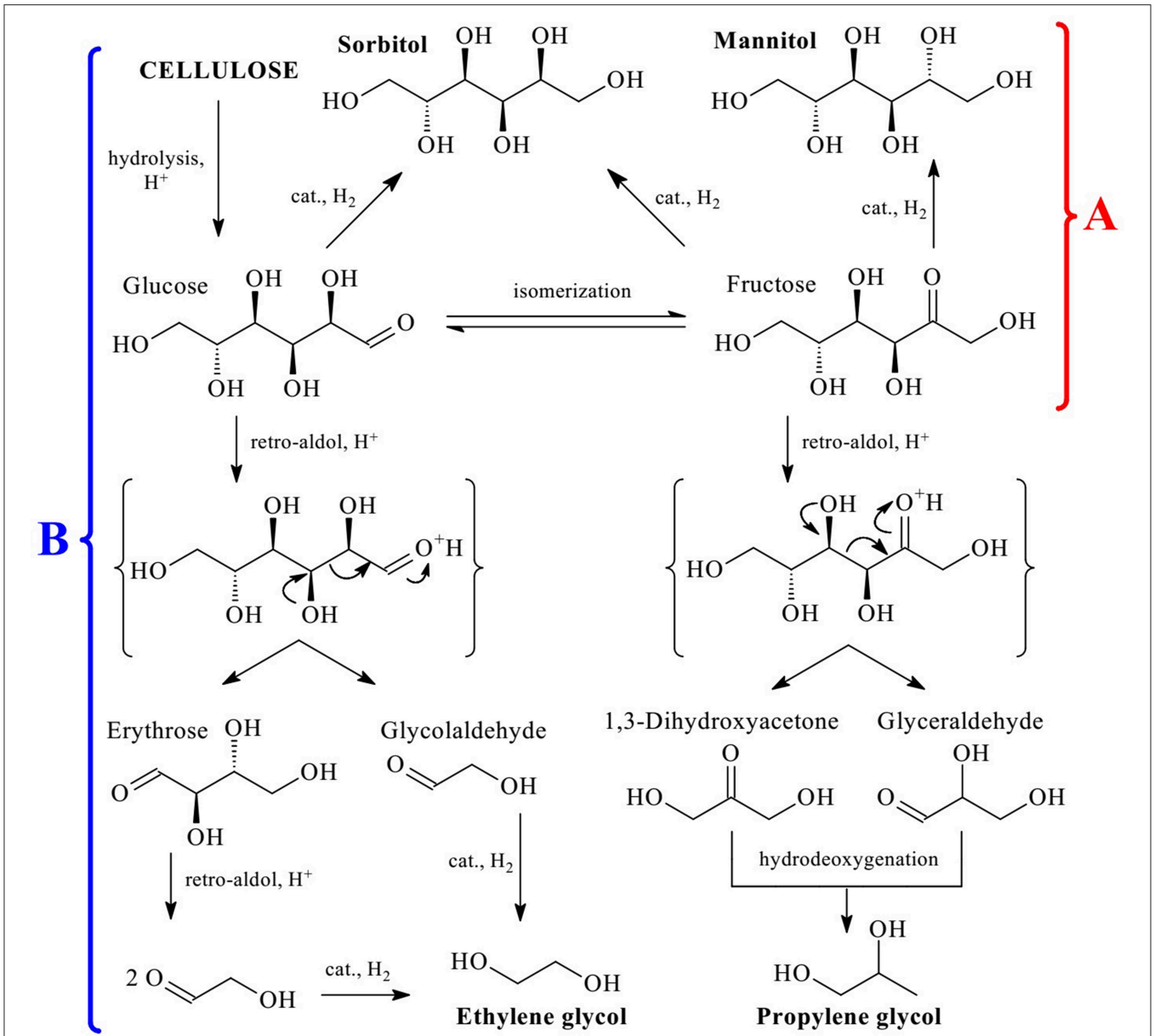

FIGURE 1 | Schematic representation of hydrolytic hydrogenation **(A)** and hydrogenolysis **(B)** of cellulose to hexitols and glycols, respectively.

because a noble metal (Ru) was replaced with an earth-abundant metal, leading to a greener and cheaper catalyst. Approximately similar hexitol yield (60%) was obtained for Ni/mesoporous-ZSM-5 (240°C, 4 MPa, 2.5 h) (Zhang et al., 2016). Here, the ZSM-5 synthesis was carried out using nanocrystalline cellulose as a template, creating mesopores in a simple and inexpensive way. However, the authors recognize that there is room for improvement as the catalyst is unstable in hydrothermal conditions, with a decreasing hexitol yield to 30 and 10% in the second and third uses, respectively. That is believed to be a consequence of the damage of the zeolite mesoporous structure and aggregation of Ni nanoparticles.

CELLULOSE HYDROGENOLYSIS

There is a high demand for EG and PG for various applications. In 2015, 23 million tons of EG and 1.8 million tons of PG were produced, while the growth prognosis for these compounds for the next 10–20 years is on average 5% a year (Pang et al., 2016; Zheng et al., 2017). However, cellulose conversion to EG and PG is very complicated (**Figure 1B**) and includes several reactions: hydrolysis, isomerization, retro-aldol condensation, hydrogenation, and hydrodeoxygenation (Rinaldi, 2014; Zheng et al., 2017). In this respect, the development of highly selective catalytic systems for this process is an important and challenging task.

TABLE 1 | Catalytic properties of W-containing catalysts in conversion of cellulose to glycols[a].

Catalysts	Reaction conditions (substrate, temperature, pressure, time)	*X*, %	η_{EG} (S_{EG}), %	η_{PG} (S_{PG}), %	References
W(0.24)-MA + Ru/C (5%)	MCC; 518 K; 6 MPa H_2; 0.5 h	43.5	S_{EG} 19.4	S_{PG} 3.6	Wang et al., 2015a
6 wt.% WO_3/C + 3 mas.% Ru/C	MCC; 478 K; 6 MPa H_2; 0.5 h	~ 62	S_{EG} 55.8	S_{PG} 12.3	Liu and Liu, 2016
1% Ru/WO_3	MCC; 240°C; 4 MPa H_2; 2 h	100	η_{EG} 76.3	η_{PG} 4.3	Li et al., 2017
1% Ru/h-WO_3	MCC; 240°C; 4 MPa H_2; 2 h	100	η_{EG} 77.5	η_{PG} 4.4	Li et al., 2018b
W/Zr + Ru/C	MCC; 215°C; 5.2 MPa H_2; 1.5 h	90	η_{EG} 58.8	η_{PG} 4.5	Chai et al., 2017
0.8% Ru-30% W/CNT	BMC; 205°C; 50 bar H_2; 3 h	100	η_{EG} 40.0	η_{PG} 7.2	Ribeiro et al., 2018a
5% Ru-30% $W_{18}O_{40}$/graphene	MCC; 245°C; 6 MPa H_2; 1 h	100	η_{EG} 62.5	η_{PG} 5.1	Zhang et al., 2019
Ru/CG_{HNO3} + W/CG	BMC; 205°C; 50 bar H_2; 5 h	100	η_{EG} 48.4	η_{PG} 0.0	Ribeiro et al., 2019
10% Ni-20% W/SBA-15 (1.00)	MCC; 518 K; 5 MPa H_2; 2 h	100	η_{EG} 64.9	η_{PG} 6.5	Xiao et al., 2017b
5% Ni-20% W/SiO_2	MCC; 240°C; 5 MPa H_2; 2 h	100	η_{EG} 63.3	η_{PG} 4.7	Xiao et al., 2018a
15% Ni-20% W/SiO_2-OH	MCC; 240°C; 5 MPa H_2; 2 h	100	η_{EG} 63.1	η_{PG} 1.9	Xiao et al., 2018c
3Ni-15W-3Al	MCC; 503 K; 4 MPa H_2; 1.5 h	100	S_{EG} 76.0	S_{PG} 8.3	Hamdy et al., 2017
30% Cu-30% WO_x/AC + Ni/AC	MCC; 518 K; 4 MPa H_2; 2 h	100	η_{EG} 70.5	η_{PG} 4.5	Chu and Zhao, 2018
30% NiWB (1:1)/CNTs	MCC; 523 K; 6 MPa; 2 h	100	η_{EG} 57.7	η_{PG} 4.6	Liu et al., 2016a
$Ni_{0.3}$-$W_{0.3}$/CNF	MCC; 245°C; 6 MPa H_2; 2 h	95	η_{EG} 33.6	η_{PG} 7.1	Yang et al., 2016

[a] *X is the cellulose conversion; η_{EG} and η_{PG} are the yields of EG and PG, respectively; S_{EG} and S_{PG} are selectivities to EG and PG, respectively; MCC is microcrystalline cellulose; BMC is ball-milled cellulose; CG is glucose based carbon; SBA-15 is ordered silica; AC is activated carbon; CNF is carbon nanofibers, while subscript for Ni and W is weight percentage of each species.*

W-Containing Catalysts

Recent studies showed that the high yield of glycols in cellulose hydrogenolysis occurs in the presence of catalysts containing tungsten compounds (**Table 1**) (Zheng et al., 2017). W-containing catalysts can be used in conjunction with the hydrogenation catalysts or bifunctional catalysts including the hydrogenation catalyst in the W-containing phase can be formed.

Wang et al. synthesized the W-containing catalyst based on ordered mesoporous alumina (MA) which was used together with Ru/C (5 wt.%) in cellulose hydrogenolysis (Wang et al., 2015a). The addition of W(*x*)-MA (*x* is the W fraction) allowed for the EG selectivity increase from 3.2 to 19.4%, while conversion remained the same. The authors concluded that W(*x*)-MA does not participate in cellulose depolymerization (although it contains both LAS and BAS), but influences the final distribution of the reaction products. A more detailed study on the distribution of hydrogenolysis products was presented in (Liu and Liu, 2016). The process was carried out with a mixture of Ru/C and WO_3/C (6%) and the dependence of the product distribution on the catalyst was elucidated using kinetic studies of the three competitive reactions of glucose: hydrogenation, isomerization, and C–C bond cleavage. WO_3 (solid acid) was found to stimulate cellulose hydrolysis and also to promote cleavage of the C–C bonds in C_6 sugars, resulting in EG and PG instead of the sugar hydrogenation to corresponding hexitols on Ru/C. The carbon support with basic properties catalyzed isomerization of glucose to fructose, which again led to the preferential formation of EG and PG. The authors determined that this kinetic analysis allows one to forecast the maximum selectivity ratio of PG to EG (2.5) with the maximum PG yield of ~ 71% (**Table 1**). Li et al. synthesized Ru-containing catalysts based on WO_3 nanocrystals of different shapes: rectangular nanosheets (Li et al., 2017), hexagonal nanorods (h-WO_3), and monoclinic nanosheets (m-WO_3) (Li et al., 2018b). Detailed structural studies showed the crucial importance of surface LAS formed upon adsorption of water on the surface of WO_3 for cellulose conversion to EG. The catalyst based on h-WO_3 crystals and containing the largest number of LAS allows for the highest EG yield (77.5%) (**Table 1**). A 5-fold catalyst reuse did not affect its activity, which could be explained by the unchanged WO_3 structure and Ru dispersion. Similar conclusions were obtained by Chai et al. (2017), who compared a series of catalysts based on WO_3-ZrO_2 (WZr) in conjunction with Ru/C for one-pot cellulose conversion. It was demonstrated that W^{5+}-OH species on the surface of WO_3 are active catalytic sites for cleavage of the C_2-C_3 bond in glucose, while glycolaldehyde formed is hydrogenated to EG on the Ru/C surface.

Ribeiro et al. synthesized Ru- and W-containing mono- and bimetallic catalysts on CNT (Ribeiro et al., 2018a). Incorporation of tungsten in the catalyst along with Ru species shifted the reaction to EG (**Table 1**). The authors demonstrated a synergetic effect when both Ru and W species were present, while the EG yield could be controlled by the weight fraction of metals. Four repeated uses of the catalyst did not decrease its activity. The authors demonstrated that the structure of the catalyst surface remains unchanged and there is no W leaching, explaining the stability of the catalytic performance. In the other publication reduced graphene oxide (called graphene) has been utilized for syntheses of Ru, WO_3, and Ru-$W_{18}O_{49}$ containing catalysts in the one-pot solvothermal synthesis, allowing reduction of Ru ions and graphene oxide as well as the formation of $W_{18}O_{49}$ nanowires (Zhang et al., 2019). The bimetallic catalyst showed the

highest EG yield at the 100% cellulose conversion and stability in three consecutive cycles, after which the EG yield decreased due to dissolution of the tungsten species in the reaction solution. The catalyst support based on the glucose-derived carbons utilized for hydrolytic hydrogenation of cellulose (Rey-Raap et al., 2019) has been also proposed for cellulose hydrogenolysis (**Table 1**) (Ribeiro et al., 2019). In this case, the authors demonstrated similar EG yields as those reported for CNT based catalysts (Ribeiro et al., 2018a), but with the much cheaper support at the similar catalyst stability.

As was discussed above, a replacement of noble metals with earth-abundant alternatives has a huge impact on process sustainability and cost. Xiao et al. synthesized multimetallic catalysts based on mesoporous silica (SBA-15) with the composition M-W/SBA-15 (M = Ni, Pd, Zn, Cu) (Xiao et al., 2017b) as well as on silica nanospheres SiO_2-OH (Ni-W/SiO_2) (Xiao et al., 2018a,c) and demonstrated good EG yields in the range 40–65% (**Table 1**). An exceptionally high EG selectivity (76%) at the 100% cellulose conversion has been achieved using the 3Ni-15W-3Al catalyst based on mesoporous siliceous material (Hamdy et al., 2017). The catalyst was synthesized in a one-pot procedure to incorporate isolated Al^{3+} ions, WO_3 nanoparticles, and Ni^0 nanoparticles with different loadings. The downside of this system is low catalyst stability as leaching of W and Ni after the catalytic reaction was observed (16% of W and 7% of Ni). Nevertheless, we believe this system deserves recognition and further improvement to eliminate leaching. Chu et al. synthesized Cu^0-WO_x ($2<x<3$)/AC which allowed >70% EG yield when combined with Ni/AC (**Table 1**) (Chu and Zhao, 2018). A combination of Cu^0 with WO_x nanoparticles leads to improved adsorption of a C_6 sugar intermediate, followed by its conversion to C_2-hydroxyaldehyde further hydrogenated to EG on the Ni species. It was determined that to balance C-C bond cleavage and hydrogenation, a molar ratio of Ni and W should be in the range 1/5–1/3.

CNT and CNF were also utilized as supports for Ni-W-containing catalysts (**Table 1**) (Liu et al., 2016a; Yang et al., 2016). Both catalysts showed good stability in two-three cycles and an abrupt decrease of the EG yield in further reactions. However, in the case of $Ni_{0.3}$-$W_{0.3}$/CNF, the authors determined that the activity loss is not due to leaching or the nanoparticle size change or carbon deposition, but solely due to retention of reaction products which shield active sites. Thus, the catalyst was easily regenerated with full restoration of its initial activity using simple purging with N_2 for 30 min at 300°C. This makes the $Ni_{0.3}$-$W_{0.3}$/CNF catalyst promising for practical applications despite comparatively low EG yield.

It is noteworthy that the interaction of two types of catalytic species, acidic, and metallic in cellulose hydrogenolysis, is complex and not yet fully understood because of the combination of several processes (see the discussion above). On one hand, it was demonstrated that the reactions of the glucose retro-aldol condensation to glycolaldehyde and its hydrogenation to EG occur independently on different catalytic sites, thus, their intimate contact is not needed (Wiesfeld et al., 2019). On the other hand, the interaction of WO_3 and metallic nanoparticles occurring at the electronic level leads to increase of the number of W^{5+} active sites (Li et al., 2017, 2018b; Chu and Zhao, 2018), which selectively break the C2-C3 bond in glucose (Chai et al., 2017). These data demonstrate the necessity of close contact between acidic and metallic sites. These inconsistencies show that more studies are needed for better understanding of the mechanism of these processes.

Sn- and Co-containing Catalysts

Sun et al. proposed a catalytic system, selectivity of which could be switched from one diol to the other (Sun et al., 2016) using Sn species with different oxidation states in conjunction with Ni catalysts. In the case of combination of Ni/AC with a metallic Sn powder, the main hydrogenolysis product was EG with the yield of 57.6% (245°C, 5 MPa, 1.6 h). When a mixture of Ni/AC and SnO was used, PG with the yield of 32.2% (22.9% for EG) was formed. The authors demonstrated that the Sn species in the NiSn alloy formed *in situ* from Ni and Sn powders are active sites for the EG formation. It is noteworthy that both Sn in the alloy and SnO catalyze the glucose retro-aldol condensation to glycolaldehyde, but only SnO is active in the isomerization of glucose to fructose. These catalysts showed a relative stability in hydrothermal conditions, which according to authors' opinion make them promising for industrial applications. Xiao et al. observed a similar effect of the increasing PG yield upon using nano-Sn species with different oxidation states in combination with Ni catalysts (10%Ni−15%Sn/SBA-15) (Xiao et al., 2017a). Excellent glycol yields (55.2% for EG and 33.9% for PG) were obtained with the weakly basic Co/CeO_x catalyst (Li et al., 2019). The authors demonstrated that the interaction between well-dispersed Co species and the CeO_x support results in the formation of the Co^{n+}-O_x-Ce^{3+} base-acid pairs—main catalytic sites—providing the optimal balance between hydrolysis, retro-aldol condensation, isomerization, and hydrogenation and leading to high diol yields. Unfortunately, the lack of the catalyst stability studies does not allow one to evaluate the promise of these catalysts.

Magnetically Recoverable Catalysts

Magnetically recoverable catalysts received considerable attention in all fields of catalysis including cellulose conversion due to economic and environmental benefits upon easy magnetic separation of catalysts (Li et al., 2015a; Liu and Zhang, 2016; Sudarsanam et al., 2018). To the best of our knowledge, direct conversion of cellulose to EG and PG with magnetically recoverable catalysts was reported only in (Manaenkov et al., 2016), although the utilization of magnetically recoverable catalysts in cellulose hydrolysis (Zhang and Fang, 2012; Li et al., 2015a), direct conversion of cellulose to sorbitol (Kobayashi et al., 2014; Zhang et al., 2014) and hydrogenolysis of sorbitol to glycols (Ye et al., 2012) has been previously described. The authors developed magnetically recoverable catalysts based on Ru-containing nanoparticles formed in the pores of magnetic silica, Fe_3O_4-SiO_2. The highest selectivities to EG and PG were 19 and 20%, respectively, at 100% cellulose conversion (255°C, 6 MPa, 0.83 h) with the addition of 0.195 mol of $Ca(OH)_2$ per 1 mol of cellulose. High stability in at least three consecutive cycles and

easy magnetic separation from the reaction medium make this catalyst promising for applications in biomass conversion.

SUMMARY AND OUTLOOK

In summary, we can identify several major trends in hydrolytic hydrogenation and hydrogenolysis of cellulose:

Cellulose is converted in pure subcritical water, which is cheap, non-toxic and an excellent medium for acid-based catalyzed reactions;

Mineral acids as co-catalysts are replaced by simultaneous ball milling of the catalyst and cellulose to facilitate the process;

The majority of the proposed catalytic systems are bifunctional and could catalyze not only hydrogenation, but also hydrolysis, retro-aldol condensation, and isomerization, giving the best yields of target polyols—a strategy based on a balance of the catalytic efficiency toward the above reactions;

In the most promising catalytic systems, noble metals (Ru, Pt, etc.) are substituted by earth-abundant metals (Ni, Cu, Sn, Co, etc.), although the problem of stability of these systems still needs to be addressed.

Despite some unresolved issues, many reported catalysts possess excellent catalytic properties and stability in hydrothermal conditions, which allowed their successful testing not only in the conversion of pure microcrystalline cellulose, but also for cellulose containing materials such as cotton, cotton wool, paper (Ribeiro et al., 2017a,d, 2018b), wood lignocellulosic biomass (Yamaguchi et al., 2016; Ribeiro et al., 2018b; Xiao et al., 2018b; Pang et al., 2019), corn stalks, millet, sugarcane, etc. (Liu et al., 2017; Li et al., 2018a), which demonstrates a promising outlook for the future development of multi tonnage production of value-added chemicals and fuels from cellulose biomass.

AUTHOR CONTRIBUTIONS

All authors listed have made a substantial, direct and intellectual contribution to the work, and approved it for publication.

FUNDING

This work was supported by the Russian Foundation for Basic Research (projects 18-08-00404, 18-29-06004, and 19-08-00414).

ACKNOWLEDGMENTS

ES, OM, and VM thank Russian Science Foundation (Project 19-19-00490) for the financial support.

REFERENCES

Abaide, E. R., Mortari, S. R., Ugalde, G., Valerio, A., Amorim, S. M., Di Luccio, M., et al. (2019). Subcritical water hydrolysis of rice straw in a semi-continuous mode. *J. Clean. Prod.* 209, 386–397. doi: 10.1016/j.jclepro.2018.10.259

Adsuar-Garcia, M. D., Flores-Lasluisa, J. X., Azar, F. Z., and Roman-Martinez, M. C. (2018). Carbon-black-supported Ru catalysts for the valorization of cellulose through hydrolytic hydrogenation. *Catalysts* 8, 572/571–572/514. doi: 10.3390/catal8120572

Chai, J., Zhu, S., Cen, Y., Guo, J., Wang, J., and Fan, W. (2017). Effect of tungsten surface density of WO3-ZrO2 on its catalytic performance in hydrogenolysis of cellulose to ethylene glycol. *RSC Adv.* 7, 8567–8574. doi: 10.1039/C6RA27524A

Chu, D., and Zhao, C. (2018). Reduced oxygen-deficient CuWO4 with Ni catalyzed selective hydrogenolysis of cellulose to ethylene glycol. *Catal. Today*. doi: 10.1016/j.cattod.2018.10.006

Dar, B. A., Khalid, S., Wani, T. A., Mir, M. A., and Farooqui, M. (2015). Ceria-based mixed oxide supported CuO: an efficient heterogeneous catalyst for conversion of cellulose to sorbitol. *Green Sustain. Chem.* 5, 15–24. doi: 10.4236/gsc.2015.51003

Gagic, T., Perva-Uzunalic, A., Knez, Z., and Skerget, M. (2018). Hydrothermal degradation of cellulose at temperature from 200 to 300°C. *Ind. Eng. Chem. Res.* 57, 6576–6584. doi: 10.1021/acs.iecr.8b00332

Hamdy, M. S., Eissa, M. A., and Keshk, S. M. (2017). New catalyst with multiple active sites for selective hydrogenolysis of cellulose to ethylene glycol. *Green Chem.* 19, 5144–5151. doi: 10.1039/C7GC02122D

Kobayashi, H., Hosaka, Y., Hara, K., Feng, B., Hirosaki, Y., and Fukuoka, A. (2014). Control of selectivity, activity and durability of simple supported nickel catalysts for hydrolytic hydrogenation of cellulose. *Green Chem.* 16, 637–644. doi: 10.1039/C3GC41357H

Lazaridis, P. A., Karakoulia, S. A., Teodorescu, C., Apostol, N., Macovei, D., Panteli, A., et al. (2017). High hexitols selectivity in cellulose hydrolytic hydrogenation over platinum (Pt) vs. ruthenium (Ru) catalysts supported on micro/mesoporous carbon. *Appl. Catal.* 214, 1–14. doi: 10.1016/j.apcatb.2017.05.031

Li, C., Xu, G., Li, K., Wang, C., Zhang, Y., and Fu, Y. (2019). A weakly basic Co/CeOx catalytic system for one-pot conversion of cellulose to diols: Kungfu on eggs. *Chem. Commun.* 55, 7663–7666. doi: 10.1039/C9CC04020J

Li, M.-Q., Ma, Y.-L., Ma, X.-X., Sun, Y.-G., and Song, Z. (2018a). Insight into the efficient catalytic conversion of biomass to EG and 1,2-PG over W-Ni bimetallic catalyst. *RSC Adv.* 8, 10907–10913. doi: 10.1039/C8RA00584B

Li, N., Ji, Z., Wei, L., Zheng, Y., Shen, Q., Ma, Q., et al. (2018b). Effect of the surface acid sites of tungsten trioxide for highly selective hydrogenation of cellulose to ethylene glycol. *Bioresour. Technol.* 264, 58–65. doi: 10.1016/j.biortech.2018.05.026

Li, N., Zheng, Y., Wei, L., Teng, H., and Zhou, J. (2017). Metal nanoparticles supported on WO3 nanosheets for highly selective hydrogenolysis of cellulose to ethylene glycol. *Green Chem.* 19, 682–691. doi: 10.1039/C6GC01327A

Li, X., Li, X., Qi, W., Shi, J., Zhang, J., Xu, Y., et al. (2015a). Preparation of magnetic biomass-based solid acid catalyst and effective catalytic conversion of cellulose into high yields of reducing sugar. *BioResour.* 10, 6720–6729. doi: 10.15376/biores.10.4.6720-6729

Li, Y., Liao, Y., Cao, X., Wang, T., Ma, L., Long, J., et al. (2015b). Advances in hexitol and ethylene glycol production by one-pot hydrolytic hydrogenation and hydrogenolysis of cellulose. *Biomass Bioenergy* 74, 148–161. doi: 10.1016/j.biombioe.2014.12.025

Liang, G., He, L., Cheng, H., Zhang, C., Li, X., Fujita, S.-I., et al. (2015). ZSM-5-supported multiply-twinned nickel particles: Formation, surface properties, and high catalytic performance in hydrolytic hydrogenation of cellulose. *J. Catal.* 325, 79–86. doi: 10.1016/j.jcat.2015.02.014

Liu, B., and Zhang, Z. (2016). Catalytic conversion of biomass into chemicals and fuels over magnetic catalysts. *ACS Catal.* 6, 326–338. doi: 10.1021/acscatal.5b02094

Liu, H., Qin, L., Wang, X., Du, C., Sun, D., and Meng, X. (2016a). Hydrolytic hydro-conversion of cellulose to ethylene glycol over bimetallic CNTs-supported NiWB amorphous alloy catalyst. *Catal. Commun.* 77, 47–51. doi: 10.1016/j.catcom.2016.01.014

Liu, Q., Tan, J., Cai, C., Ma, L., and Wang, T. (2016b). Enhanced sugar alcohol production from cellulose by pretreatment with mixed ball-milling and solid acids. *BioResources* 11, 1843–1854. doi: 10.15376/biores.11.1.1843-1854

Liu, Q., Zhang, T., Liao, Y., Cai, C., Tan, J., Wang, T., et al. (2017). Production of C5/C6 sugar alcohols by hydrolytic hydrogenation of raw lignocellulosic biomass over Zr based solid acids combined with Ru/C. *ACS Sustain. Chem. Eng.* 5, 5940–5950. doi: 10.1021/acssuschemeng.7b00702

Liu, S., Okuyama, Y., Tamura, M., Nakagawa, Y., Imai, A., and Tomishige, K. (2015). Production of renewable hexanols from mechanocatalytically depolymerized cellulose by using Ir-ReOx/SiO2 catalyst. *ChemSusChem* 8, 628–635. doi: 10.1002/cssc.201403010

Liu, S., Tamura, M., Nakagawa, Y., and Tomishige, K. (2014). One-Pot conversion of cellulose into n-Hexane over the Ir-ReOx/SiO2 catalyst combined with HZSM-5. *ACS Sustain. Chem. Eng.* 2, 1819–1827. doi: 10.1021/sc5001463

Liu, Y., and Liu, H. (2016). Kinetic insight into the effect of the catalytic functions on selective conversion of cellulose to polyols on carbon-supported WO3 and Ru catalysts. *Catal. Today* 269, 74–81. doi: 10.1016/j.cattod.2015.09.056

Makhubela, B. C. E., and Darkwa, J. (2018). The role of noble metal catalysts in conversion of biomass and bio-derived intermediates to fuels and chemicals: a review of promising approaches on plant based biomass as a renewable alternative feedstock. *Johnson Matthey Technol. Rev.* 62, 4–31. doi: 10.1595/205651317X696261

Manaenkov, O. V., Mann, J. J., Kislitza, O. V., Losovyj, Y., Stein, B. D., Morgan, D. G., et al. (2016). Ru-containing magnetically recoverable catalysts: a sustainable pathway from cellulose to ethylene and propylene glycols. *ACS Appl. Mater. Interfaces* 8, 21285–21293. doi: 10.1021/acsami.6b05096

Matveeva, V. G., Sulman, E. M., Manaenkov, O. V., Filatova, A. E., Kislitza, O. V., Sidorov, A. I., et al. (2017). Hydrolytic hydrogenation of cellulose in subcritical water with the use of the Ru-containing polymeric catalysts. *Catal. Today* 280, 45–50. doi: 10.1016/j.cattod.2016.09.001

Op De Beeck, B., Dusselier, M., Geboers, J., Holsbeek, J., Morre, E., Oswald, S., et al. (2015). Direct catalytic conversion of cellulose to liquid straight-chain alkanes. *Energy Environ. Sci.* 8, 230–240. doi: 10.1039/C4EE01523A

Pang, J., Zheng, M., Li, X., Sebastian, J., Jiang, Y., Zhao, Y., et al. (2019). Unlock the compact structure of lignocellulosic biomass by mild ball milling for ethylene glycol production. *ACS Sustain. Chem. Eng.* 7, 679–687. doi: 10.1021/acssuschemeng.8b04262

Pang, J., Zheng, M., Sun, R., Wang, A., Wang, X., and Zhang, T. (2016). Synthesis of ethylene glycol and terephthalic acid from biomass for producing PET. *Green Chem.* 18, 342–359. doi: 10.1039/C5GC01771H

Rey-Raap, N., Ribeiro, L. S., Orfao, J. J. D. M., Figueiredo, J. L., and Pereira, M. F. R. (2019). Catalytic conversion of cellulose to sorbitol over Ru supported on biomass-derived carbon-based materials. *Appl. Catal.* 256:117826. doi: 10.1016/j.apcatb.2019.117826

Ribeiro, L., Orfao, J. J. M., and Pereira, M. F. (2015a). Enhanced direct production of sorbitol by cellulose ball-milling. *Green Chem.* 17, 2973–2980. doi: 10.1039/C5GC00039D

Ribeiro, L. S., Delgado, J. J., De Melo Orfao, J. J., and Pereira, M. F. R. (2017a). Direct conversion of cellulose to sorbitol over ruthenium catalysts: influence of the support. *Catal. Today* 279, 244–251. doi: 10.1016/j.cattod.2016.05.028

Ribeiro, L. S., Delgado, J. J., De Melo Orfao, J. J., and Ribeiro Pereira, M. F. (2017b). Influence of the surface chemistry of multiwalled carbon nanotubes on the selective conversion of cellulose into sorbitol. *ChemCatChem* 9, 888–896. doi: 10.1002/cctc.201601224

Ribeiro, L. S., Delgado, J. J., Orfao, J. J. M., and Pereira, M. F. R. (2017c). Carbon supported Ru-Ni bimetallic catalysts for the enhanced one-pot conversion of cellulose to sorbitol. *Appl. Catal.* 217, 265–274. doi: 10.1016/j.apcatb.2017.04.078

Ribeiro, L. S., Orfao, J., De Melo Orfao, J. J., and Pereira, M. F. R. (2018a). Hydrolytic hydrogenation of cellulose to ethylene glycol over carbon nanotubes supported Ru-W bimetallic catalysts. *Cellulose* 25, 2259–2272. doi: 10.1007/s10570-018-1721-7

Ribeiro, L. S., Órfão, J. J. D. M., and Pereira, M. F. R. (2017d). Direct catalytic production of sorbitol from waste cellulosic materials. *Bioresour. Technol.* 232, 152–158. doi: 10.1016/j.biortech.2017.02.008

Ribeiro, L. S., Orfao, J. J. M., and Pereira, M. F. R. (2015b). Comparative study of different catalysts for the direct conversion of cellulose to sorbitol. *Green Process. Synth.* 4, 71–78. doi: 10.1515/gps-2014-0091

Ribeiro, L. S., Órfão, J. J. M., and Pereira, M. F. R. (2018b). Insights into the effect of the catalytic functions on selective production of ethylene glycol from lignocellulosic biomass over carbon supported ruthenium and tungsten catalysts. *Bioresour. Technol.* 263, 402–409. doi: 10.1016/j.biortech.2018.05.034

Ribeiro, L. S., Rey-Raap, N., Figueiredo, J. L., Melo Orfao, J. J., and Pereira, M. F. R. (2019). Glucose-based carbon materials as supports for the efficient catalytic transformation of cellulose directly to ethylene glycol. *Cellulose* 26, 7337–7353. doi: 10.1007/s10570-019-02583-x

Rinaldi, R. (2014). *Catalytic Hydrogenation for Biomass Valorization*. Cambridge: RSC Publishing.

Shitu, A., Izhar, S., and Tahir, T. M. (2015). Sub-critical water as a green solvent for production of valuable materials from agricultural waste biomass: a review of recent work. *Global J. Environ. Sci. Manage.* 1, 255–264.

Shrotri, A., Kobayashi, H., and Fukuoka, A. (2016). Air oxidation of activated carbon to synthesize a biomimetic catalyst for hydrolysis of cellulose. *ChemSusChem* 9, 1299–1303. doi: 10.1002/cssc.201600279

Shrotri, A., Kobayashi, H., and Fukuoka, A. (2018). Cellulose depolymerization over heterogeneous catalysts. *Acc. Chem. Res.* 51, 761–768. doi: 10.1021/acs.accounts.7b00614

Sudarsanam, P., Zhong, R., Van den Bosch, S., Coman, S. M., Parvulescu, V. I., and Sels, B. F. (2018). Functionalised heterogeneous catalysts for sustainable biomass valorisation. *Chem. Soc. Rev.* 47, 8349–8402. doi: 10.1039/C8CS00410B

Sun, R., Zheng, M., Pang, J., Liu, X., Wang, J., Pan, X., et al. (2016). Selectivity-switchable conversion of cellulose to glycols over Ni-Sn catalysts. *ACS Catal.* 6, 191–201. doi: 10.1021/acscatal.5b01807

Wang, H., Guo, Y., Zheng, D., and Han, J. (2015a). Direct incorporation of tungsten into ordered mesoporous alumina and enhanced selectivity for converting cellulose to ethylene glycol. *J. Porous Mater.* 22, 919–925. doi: 10.1007/s10934-015-9965-1

Wang, H., Lv, J., Zhu, X., Liu, X., Han, J., and Ge, Q. (2015b). Efficient hydrolytic hydrogenation of cellulose on mesoporous HZSM-5 supported Ru catalysts. *Top. Catal.* 58, 623–632. doi: 10.1007/s11244-015-0409-6

Wang, H., Zhang, C., Liu, Q., Zhu, C., Chen, L., Wang, C., et al. (2018). Direct hydrogenolysis of cellulose into methane under mild conditions. *Energy Fuels* 32, 11529–11537. doi: 10.1021/acs.energyfuels.8b02235

Wen, G., Xu, Y., Xu, Z., and Tian, Z. (2010). Direct conversion of cellulose into hydrogen by aqueous-phase reforming process. *Catal. Commun.* 11, 522–526. doi: 10.1016/j.catcom.2009.12.008

Wiesfeld, J. J., Persolja, P., Rollier, F. A., Elemans-Mehring, A. M., and Hensen, E. J. M. (2019). Cellulose conversion to ethylene glycol by tungsten oxide-based catalysts. *Mol. Catal.* 473:1104003, doi: 10.1016/j.mcat.2019.110400

Xiao, Z., Fan, Y., Cheng, Y., Zhang, Q., Ge, Q., Sha, R., et al. (2018a). Metal particles supported on SiO2-OH nanosphere: new insight into interactions with metals for cellulose conversion to ethylene glycol. *Fuel* 215, 406–416. doi: 10.1016/j.fuel.2017.11.086

Xiao, Z., Mao, J., Ji, J., Sha, R., Fan, Y., and Xing, C. (2017b). Preparation of nano-scale nickel-tungsten catalysts by pH value control and application in hydrogenolysis of cellulose to polyols. *J. Fuel Chem. Technol.* 45, 641–650. doi: 10.1016/S1872-5813(17)30033-6

Xiao, Z., Mao, J., Jiang, C., Xing, C., Ji, J., and Cheng, Y. (2017a). One-pot selective conversion of cellulose into low carbon polyols on nano-Sn based catalysts. *J. Renew. Sustain. Energy* 9:024703/024701-024703/024712. doi: 10.1063/1.4980158

Xiao, Z., Xu, Y., Fan, Y., Zhang, Q., Mao, J., and Ji, J. (2018b). Plant lignocellulose-based feedstocks hydrogenolysis into polyols over a new efficient nickel-tungsten catalyst. *Asia-Pac. J. Chem. Eng.* 13:e2153. doi: 10.1002/apj.2153

Xiao, Z., Zhang, Q., Chen, T., Wang, X., Fan, Y., Ge, Q., et al. (2018c). Heterobimetallic catalysis for lignocellulose to ethylene glycol on nickel-tungsten catalysts: influenced by hydroxy groups. *Fuel* 230, 332–343. doi: 10.1016/j.fuel.2018.04.115

Yamaguchi, A., Sato, O., Mimura, N., and Shirai, M. (2016). Catalytic production of sugar alcohols from lignocellulosic biomass. *Catal. Today* 265, 199–202. doi: 10.1016/j.cattod.2015.08.026

Yang, Y., Zhang, W., Yang, F., Brown, D. E., Ren, Y., Lee, S., et al. (2016). Versatile nickel-tungsten bimetallics/carbon nanofiber catalysts for direct conversion of cellulose to ethylene glycol. *Green Chem.* 18, 3949–3955. doi: 10.1039/C6GC00703A

Ye, L., Duan, X., Lin, H., and Yuan, Y. (2012). Improved performance of magnetically recoverable Ce-promoted Ni/Al2O3 catalysts for

aqueous-phase hydrogenolysis of sorbitol to glycols. *Catal. Today* 183, 65–71. doi: 10.1016/j.cattod.2011.08.006

Zada, B., Chen, M., Chen, C., Yan, L., Xu, Q., Li, W., et al. (2017). Recent advances in catalytic production of sugar alcohols and their applications. *Sci. China Chem.* 60, 853–869. doi: 10.1007/s11426-017-9067-1

Zhang, B., Li, X., Wu, Q., Zhang, C., Yu, Y., Lan, M., et al. (2016). Synthesis of Ni/mesoporous ZSM-5 for direct catalytic conversion of cellulose to hexitols: modulating the pore structure and acidic sites via a nanocrystalline cellulose template. *Green Chem.* 18, 3315–3323. doi: 10.1039/C5GC03077C

Zhang, F., and Fang, Z. (2012). Hydrolysis of cellulose to glucose at the low temperature of 423 K with CaFe2O4-based solid catalyst. *Bioresour. Technol.* 124, 440–445. doi: 10.1016/j.biortech.2012.08.025

Zhang, J., Wu, S.-B., and Liu, Y. (2014). Direct conversion of cellulose into sorbitol over a magnetic catalyst in an extremely low concentration acid system. *Energy Fuels* 28, 4242–4246. doi: 10.1021/ef500031w

Zhang, K., Yang, G., Lyu, G., Jia, Z., Lucia, L. A., and Chen, J. (2019). One-pot solvothermal synthesis of graphene nanocomposites for catalytic conversion of cellulose to ethylene glycol. *ACS Sustain. Chem. Eng.* 7, 11110–11117. doi: 10.1021/acssuschemeng.9b00006

Zheng, M., Pang, J., Sun, R., Wang, A., and Zhang, T. (2017). Selectivity control for cellulose to diols: dancing on eggs. *ACS Catal.* 7, 1939–1954. doi: 10.1021/acscatal.6b03469

Conflict of Interest: The authors declare that the research was conducted in the absence of any commercial or financial relationships that could be construed as a potential conflict of interest.

frontiers in Chemistry

ORIGINAL RESEARCH
published: 22 January 2020
doi: 10.3389/fchem.2019.00951

Conversion of Glucose to 5-Hydroxymethylfurfural in a Microreactor

*Tiprawee Tongtummachat[1], Nattee Akkarawatkhoosith[1], Amaraporn Kaewchada[2] and Attasak Jaree[3]**

[1] Department of Chemical Engineering, Faculty of Engineering, Mahidol University, Nakhon Pathom, Thailand, [2] Department of Agro-Industrial, Food and Environmental Technology, King Mongkut's University of Technology North Bangkok, Bangkok, Thailand, [3] Department of Chemical Engineering, Faculty of Engineering, Center of Excellence on Petrochemical and Materials Technology, Kasetsart University, Bangkok, Thailand

5-hydroxymethylfurfural (5-HMF) is one of the key bio-based platform chemicals for the production of high-value chemicals and fuels. The conventional production of 5-HMF from biomass is confronted by the relatively low yield and high production cost. In this work, the enhancement of a continuous catalytic synthesis of 5-HMF in a biphasic-dispersed flow reactor was proposed. Glucose, hydrochloric acid, and methyl isobutyl ketone (MIBK) were used as a low-cost raw material, catalyst, and organic solvent, respectively. The main factors (reaction temperature, residence time, solvent amount, and catalyst concentration) affecting the yield and selectivity of 5-HMF were studied. The 5-HMF yield of 81.7% and 5-HMF selectivity of 89.8% were achieved at the residence time of 3 min, reaction temperature of 180°C, the volumetric flow rate of aqueous phase to organic phase of 0.5:1, and catalyst concentration of 0.15 M. The yield and selectivity of 5-HMF obtained from the biphasic system were significantly higher than that obtained from the single phase system. The superior 5-HMF production in our system in terms of operating conditions was presented when compared to the literature data. Furthermore, the continuous process for removing HCl from the aqueous product was also proposed.

Keywords: glucose, 5-hydroxymethylfurfural, microreactor, homogeneous catalyst, dispersed-flow

OPEN ACCESS

Edited by:
Roger Arthur Sheldon, University of the Witwatersrand, South Africa

Reviewed by:
Miguel Angel Centeno, Instituto de Ciencia de Materiales de Sevilla (ICMS), Spain
Zhibao Huo, Shanghai Ocean University, China

***Correspondence:**
Attasak Jaree
fengasj@ku.ac.th

Specialty section:
This article was submitted to Green and Sustainable Chemistry, a section of the journal Frontiers in Chemistry

Received: *28 October 2019*
Accepted: *31 December 2019*
Published: *22 January 2020*

Citation:
Tongtummachat T, Akkarawatkhoosith N, Kaewchada A and Jaree A (2020) Conversion of Glucose to 5-Hydroxymethylfurfural in a Microreactor. Front. Chem. 7:951. doi: 10.3389/fchem.2019.00951

INTRODUCTION

Nowadays, the manufacturing of fuels and chemicals from non-renewable sources has raised growing environmental concerns. This led to research and development promoting the use alternative sources of energy instead of conventional fossil-based sources. One of the promising strategies is to transform biomass into high-value chemical substances. Among the biomass-based materials, 5-Hydroxymethylfurfural (5-HMF) nowadays has received a lot of attention due to the possibility of converting it into various high-value products such as 5-furandicarboxylic acid, 2,5-dimethyltetrahydrofuran, and 2,5-bis(hydroxymethyl)furan (Rosatella et al., 2011).

5-HMF is generally produced through the dehydration reaction of fructose with a presence of catalyst in order to achieve high conversion and selectivity; however, this technique is restricted by the inherent disadvantages posed by the high production cost and limited accessibility of fructose (Agarwal et al., 2018). Recently, many researchers have attempted to find effective substrates for producing 5-HMF such as glucose because of the low production cost and uninterrupted supply (Hu et al., 2013). Unfortunately, using glucose as a substrate to produce 5-HMF normally involves

the isomerization of glucose to fructose and dehydration of fructose to 5-HMF, leading to the catalyst requirement of both Lewis acid and Brønsted acid for isomerization and dehydration, respectively. The relatively low yield and selectivity are the consequence of using this substrate (Rosatella et al., 2011). To overcome the yield issue, many different routes and methods have been proposed. For instance, supercritical conditions was reported to enhance the synthesis of 5-HMF from glucose (Watanabe et al., 2005b). However, the equipment and operating cost are still the major issues for this technique. As an alternative solution, many novel heterogeneous catalysts have been developed (Yang et al., 2015; Xin et al., 2017). Yet, this method requires a complicated catalyst preparation procedure. The synthesis of 5-HMF via the direct dehydration of glucose can be possible with the use of a very high concentration of Brønsted acid (Li et al., 2017). Unfortunately, the slow rate of reaction is one of the major obstacles for this route.

Microreactor technology has emerged as one of the attractive solutions for many applications confronted by the transport phenomena issues (Yao et al., 2015). High productivity with low production costs is another highlight of this technology because it involves a continuous production process. For the production of 5-HMF from glucose, microreactor technology was recently introduced to enhance the yield and selectivity of 5-HMF as reported by Guo et al. (2019) using bifunctional homogeneous catalysts (Lewis and Brønsted acids). High-throughput 5-HMF was successfully achieved through this technique due to efficient extraction of 5-HMF from the aqueous phase compared to the conventional reactors. A slug flow pattern was also observed from their works providing small liquid-liquid interfacial areas for mass transfer compared to the dispersed-flow condition which would conceivably require a shorter contact time (Dore et al., 2012).

Based on the literature, 5-HMF production via the direct dehydration of glucose under dispersed flow conditions has never been investigated. Therefore, in this work, we proposed a simple and effective 5-HMF synthesis through the dehydration of glucose using commercial hydrochloric acid as catalyst by applying the microreactor technology. The effect of operating conditions, including reaction temperature, residence time, catalyst concentration, and organic-to-aqueous volumetric ratio on the 5-HMF yield and selectivity was investigated. The performance of 5-HMF synthesis in both monophasic and biphasic systems was evaluated. The production performance of our method was compared to that of other production techniques. For purification of product, we also developed a continuous method for the removal of HCl from aqueous product.

MATERIALS AND METHODS

Materials

Glucose and fructose (AR grade) were purchased from Fisher Scientific. 37% (w/w) hydrochloric acid (HCl) and methyl isobutyl ketone (MIBK) were obtained from Merck. Analytical standard of 5-HMF was purchased from Sigma-Aldrich. Acetonitrile (HPLC grade) was acquired from Honeywall and was used as a mobile phase for product analyst.

5-HMF Synthesis

Prior to the experiment, glucose, deionized (DI) water, and HCl were uniformly mixed in a beaker at various HCl concentration levels, whereas the glucose concentration was kept constant at 5 g/L for all experiments. MIBK was used as an organic solvent for extraction of 5-HMF during the synthesis. The aqueous phase (glucose and HCl dissolved in water) and the organic phase (MIBK) were separately fed into the T-micromixer via HPLC pumps at different flow rates depending on the residence time and the ratio of organic to aqueous phase investigated. Before entering the micromixer, both liquid streams were preheated to the desired temperature. After mixing, the two-phase mixture entered the microtube reactor (ID: 0.87 mm, 4 mL) where the reactions took place. The micromixer and microreactor were placed in a convection oven to control the reaction temperature. To avoid the vaporization of solvent, a back-pressure regulator was installed at the exit end of the reactor to control the pressure of the system at 80 bar. The outlet stream from the back-pressure regulator was quenched to stop any further reaction. The product, in both organic and aqueous phases, was then collected in order to evaluate the amount of 5-HMF as well as the reaction performance, including conversion, selectivity, and yield. **Figure 1** represents the experimental setup of this work.

Product Analysis

The amount of 5-HMF was determined by HPLC technique with UV detector (UV; model 2550, Varian) at 320 nm. The ACE C_{18} column (4.6 mm × 250 mm, 5 μm particle size, Advanced Chromatography Technologies) was applied as a separation column, which was operated at the temperature of 35°C. The mobile phase solution of water and acetonitrile [90:10 (V/V)] was used at a flow rate of 0.7 mL/min. The identification of peaks was based on the comparison of the retention time between the sample and that of the standard compounds. The external standard was used to quantitate the amount of 5-HMF. The side reaction products including formic acid and levulinic acid were detected under the similar conditions as the analysis of HMF except that the UV wavelength was 295 nm.

The remaining monosaccharides (glucose and fructose) was analyzed by HPLC equipped with RI detector (RI; model YL9170, YL Instrument). The analysis was performed on the APS-2 Hypersil (4.6 mm × 250 mm, 5 μm particle size, Thermo Scientific) at the temperature of 35°C. A stream of 75:25 (v/v) acetonitrile: water was applied as a mobile phase at the flow rate of 0.7 mL/min.

The production performance of our method was designated by several parameters as described below.

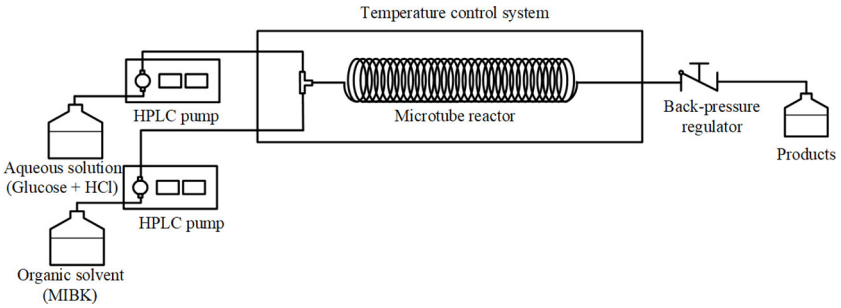

FIGURE 1 | Schematic diagram of the experimental apparatus.

$$Glucose\ \ conversion\ (\%) = \left(1\text{-}\left(\frac{Moles\ of\ glucose\ unreacted}{Moles\ of\ starting\ glucose}\right)\right) \times 100 \quad (1)$$

$$5-HMF\ Yield\ (\%) = \left(\frac{Moles\ of\ HMF\ produced}{Moles\ of\ starting\ glucose}\right) \times 100 \quad (2)$$

$$5-HMF\ selectivity\ (\%) = \left(\frac{5-HMF\ yield}{Glucose\ conversion}\right) \times 100 \quad (3)$$

$$5-HMF\ extraction\ efficiency\ (\%) = \left(\frac{Moles\ of\ HMF\ existed\ in\ organic\ phase}{Moles\ of\ HMF\ produced}\right) \times 100 \quad (4)$$

RESULTS AND DISCUSSION

5-HMF Synthesis in a Monophasic System

First, the monophasic system was used to study the behavior of 5-HMF in a microreactor system. Note that the monophasic synthesis of 5-HMF from glucose in a microreactor has hardly been investigated. The experiments were performed under various reaction temperatures (150–180°C), residence times (3–10 min), and HCl-to-glucose weight ratios (1:1 to 4:1). For the HCl-to-glucose weight ratio, the weight of HCl and glucose were based on the 37% (w/w) HCl and the weight of anhydrous glucose powder, respectively. The results are shown in **Figures 2**, **3**.

Figure 2 shows the effect of reaction temperature on the yield of 5-HMF at a constant HCl-to-glucose weight ratio of 3:1, while the residence time was varied in the range of 3–10 min. The results show that the yield of 5-HMF increased with increasing reaction temperature. For example, at a residence time of 5 min, the 5-HMF yield increased from 9.7 to 36.3% with an increase in reaction temperature from 150 to 180°C, since the dehydration of glucose to 5-HMF is highly endothermic reaction (Assary et al., 2010). This means that an increase in the reaction temperature favors the dehydration reaction that converts glucose into 5-HMF. Note that a further increase in reaction temperature of more than 200°C might cause the decomposition of glucose to undesired products such as anhydroglucose and glyceraldehyde (Matsumura et al., 2006; Souza et al., 2012). The highest yield of 42.5% was achieved at a reaction temperature of 180°C. Therefore, this reaction temperature was selected for further experiments of 5-HMF synthesis in this work, which was in line with many related reports (Zhang et al., 2015; Muranaka et al., 2017). Additionally, at the reaction temperature of 165 and 180°C, the 5-HMF yield decreased with increasing residence time. This was because 5-HMF produced rapidly at the early stage of the reaction was subsequently converted into formic and levulinic acids through the hydration reaction. On the other hand, at the reaction temperature of 150°C, the yield of 5-HMF increased almost linearly as the residence time increased. At this temperature, the system was not greatly affected by the rehydration of 5-HMF because the production rate of 5-HMF was relatively slow.

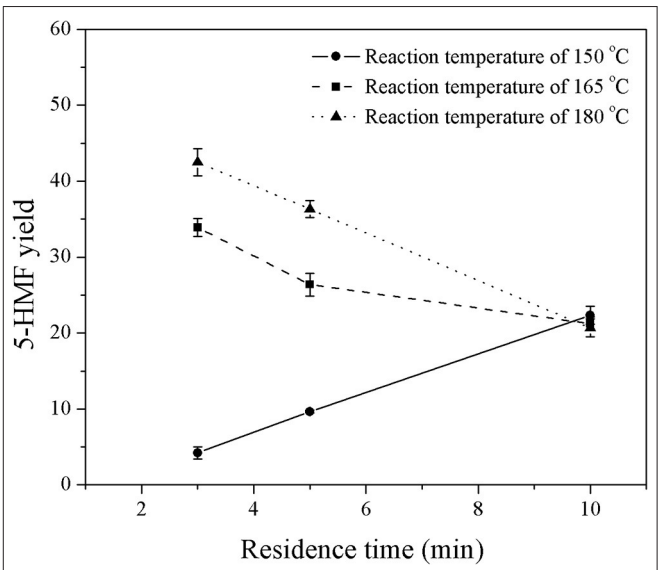

FIGURE 2 | Effect of reaction temperature on the yield of 5-HMF produced in a monophasic system at various residence times.

The effect of residence time on the yield of 5-HMF was further investigated under various HCl-to-glucose weight ratios (represented as a catalyst concentration), as shown in **Figure 3**. To study this effect, the reaction temperature was kept constant

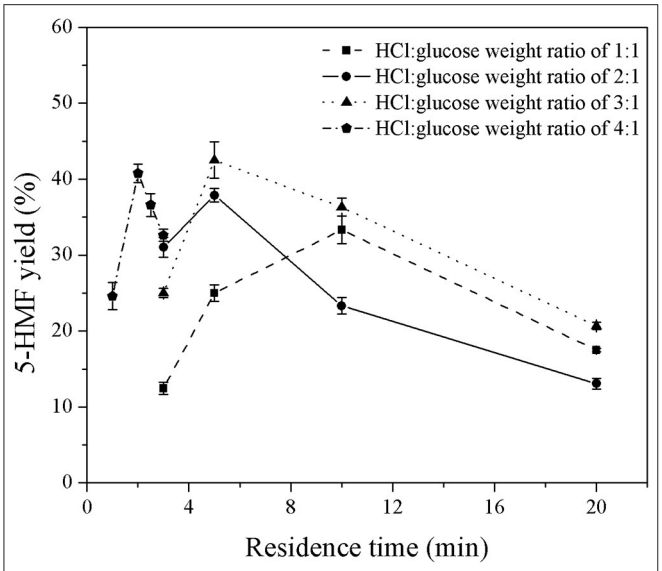

FIGURE 3 | Effect of catalyst concentration on the yield of 5-HMF produced in a monophasic system under various residence times.

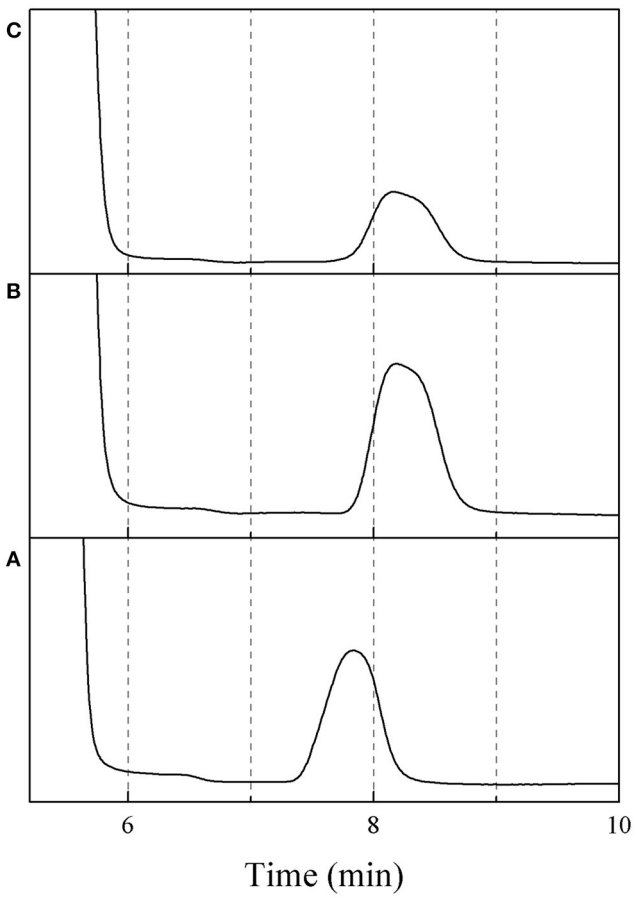

FIGURE 4 | HPLC chromatograms of **(A)** fructose, **(B)** glucose, **(C)** sample (reaction condition: HCl-glucose ratio of 1:1, residence time of 5 min and reaction temperature of 180°C).

at 180°C. For the HCl-to-glucose weight ratio of 1:1, the 5-HMF yield increased from 12.4 to 25.0% when the residence time was changed from 3 to 5 min and then reached the maximum value of 33.3% at the residence time of 10 min. However, the prolonged residence time exceeding 10 min provided a negative impact on the yield of 5-HMF due to the transformation of the 5-HMF into other by-products. This was similar to results obtained using the HCl-to-glucose weight ratio of 2:1, 3:1, and 4:1. Besides, a trace of glucose was detected in the product outlet, as shown in the HPLC chromatogram (see **Figure 4**). This implies that the direct dehydration of glucose to 5-HMF occurred in the system when only the Brønsted acid was applied for 5-HMF synthesis.

Moreover, an increase in catalyst concentration significantly shortened the residence time required to achieve the maximum yield (see **Figure 3**). For example, it took 10 min to reach the maximum yield of 33.3% when using the weight ratio of HCl to glucose of 1:1, while the residence time of only 5 min was sufficient to achieve the maximum yield of 37.8% for the weight ratio of HCl to glucose of 2:1. From this result, at a reaction temperature of 180°C, the highest yield of 42.5% was achieved at the weight ratio of HCl to glucose of 3:1 and residence time of 3 min. It was apparent that our monophasic synthesis in a microreactor provided superior performance compared to the conventional stirred batch reactor carrying out the monophasic synthesis of 5-HMF. For instance, the yield of 5-HMF below 10% was obtained from the conversion of glucose using mineral acid as catalyst operating for the reaction temperature and residence time in the range of 170–200°C and 3–20 min, respectively (Mednick, 1962; Watanabe et al., 2005a; Qi et al., 2008). Nevertheless, the yield of 5-HMF in our system was still too low; therefore, the development of our technique was further extended to the application of a biphasic system.

5-HMF Synthesis in a Biphasic System

In this work, MIBK was applied as solvent to selectively extract 5-HMF from the aqueous phase, preventing further reactions of 5-HMF into undesired products. In order to optimize the operating conditions, several operating variables were investigated as follows; volumetric ratios of organic to aqueous phase (0.2:1 to 5:1), weight ratios of HCl to glucose (1:1 to 3:1), and residence times (2–10 min). The first variable was the weight ratio of HCl to glucose. **Figures 5**, **6** show the effect of catalyst concentration on the yield and selectivity of 5-HMF at different residence times and weight ratios of HCl to glucose, where the volumetric ratio of organic to aqueous phase of 1:1 was kept constant. As expected, a similar behavior was observed as compared to that of the monophasic system. An increase in catalyst concentration promoted both 5-HMF yield and selectivity, indicating that the direct dehydration of glucose into 5-HMF was possible with high concentration of Brønsted acid (HCl). For high HCl-to-glucose weight ratios (high catalyst concentration), a shorter residence time was required to avoid further conversion of 5-HMF to other by-products since large amount of 5-HMF was rapidly produced in the system. This result was in good

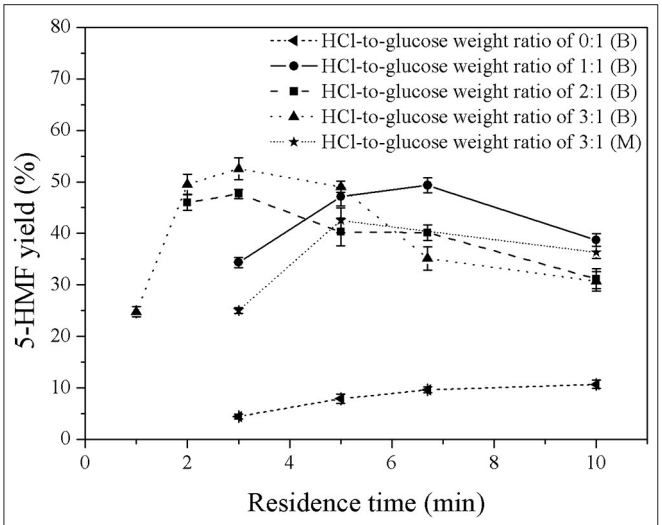

FIGURE 5 | Effect of catalyst concentration on the 5-HMF yield in a biphasic system under various residence times. (B) and (M) represent the biphasic system and monophasic system, respectively.

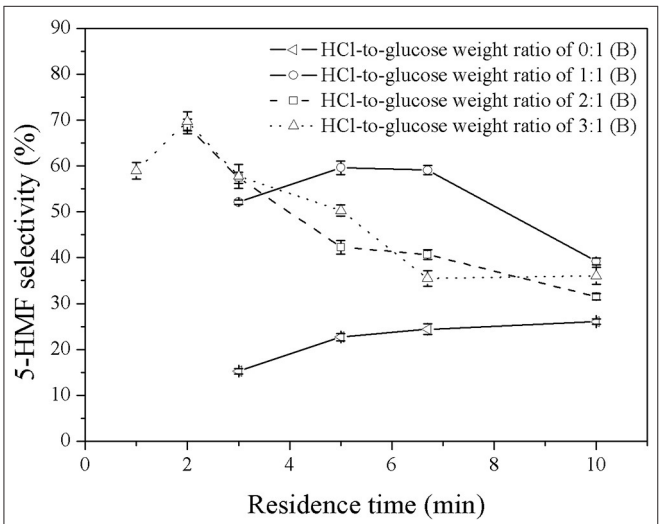

FIGURE 6 | Effect of catalyst concentration on the selectivity of 5-HMF produced in a biphasic system under various residence times.

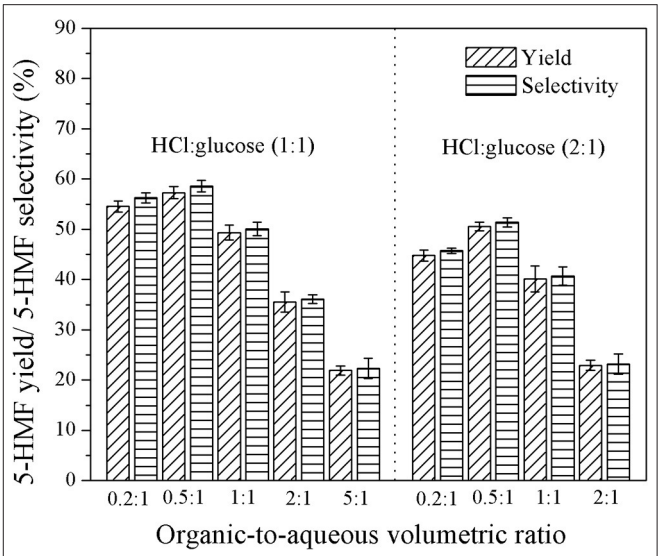

FIGURE 7 | Effect of organic-to-aqueous volumetric ratio on the yield and selectivity of 5-HMF produced in a biphasic system for the residence time of 6.7 min.

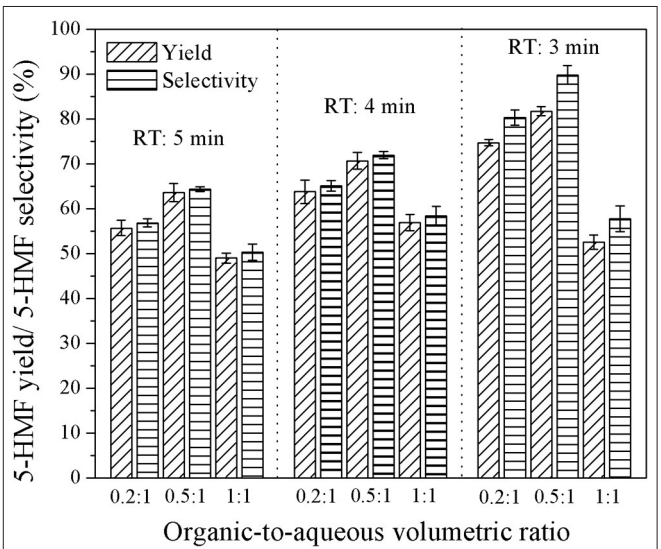

FIGURE 8 | Effect of organic-to-aqueous volumetric ratio on the yield and selectivity of 5-HMF in a biphasic system for the catalyst ratio of 3:1.

agreement with the report of Chheda et al. (2007). An extremely low yield of 5-HMF was obtained in the biphasic catalyst-free system proving that the catalyst is required to obtain reasonably high yield of 5-HMF with relatively short residence time. As shown in **Figure 5**, a significant increase in the yield of 5-HMF produced in the biphasic system was observed when compared to that of the monophasic system (see **Figure 3**). This was owing to the suppression of further conversion of 5-HMF into undesired products as the 5-HMF was efficiently extracted into the organic phase. This also led to the shifting of the equilibrium reaction of glucose toward the formation of 5-HMF through the direct dehydration of glucose. This result verified that the extraction of 5-HMF from the aqueous phase into the organic phase is also one of the major factors to control the yield of 5-HMF. Moreover, a significant increase in the yield and selectivity of 5-HMF from the biphasic system was observed as the concentration of catalyst increased. This was because an increase in the catalyst concentration led to a larger number of acid sites, accelerating the direct dehydration of glucose into 5-HMF. The highest yield of 5-HMF of 52.6% was achieved at the weight ratio of HCl to glucose of 3:1 and the residence time of 3 min (see **Figure 5**).

The effect of organic-to-aqueous volumetric ratio on the yield and selectivity of 5-HMF was investigated in the range of 0.2:1 to 5:1 under various catalyst concentrations and residence

times, whereas the reaction temperature was held constant at 180°C. Results are shown in **Figure 7**. At low organic-to-aqueous volumetric ratios (0.2:1 and 0.5:1) and weight ratio of HCl to glucose of 1:1 (see **Figure 6**), an increase of the organic-to-aqueous volumetric ratio from 0.2:1 to 0.5:1 slightly promoted the yield and selectivity of 5-HMF from 54.6 to 57.3% and from 56.3 to 58.6%, respectively. This was because the larger amount of MIBK in the system transferred 5-HMF from aqueous phase into the organic phase more effectively, preventing the rehydration of 5-HMF into undesired products (Leshkov and Dumesic, 2009; Dalessandro and Pliego, 2018). Higher extraction efficiency was strongly related to the mass transfer rate of 5-HMF into the organic phase (Zhou et al., 2018). However, the negative effect on the yield and selectivity is observed (see **Figure 7**) when the organic-to-aqueous volumetric ratio was higher than 0.5:1. With increasing the amount of MIBK in the system, the possibility that MIBK phase was contaminated with water also increased. As more water was able to dissolve into the MIBK phase, the hydration reaction between 5-HMF and water in the MIBK phase took place to a greater extent leading to the decline in both yield and selectivity of 5-HMF. A similar trend was found when the weight ratios of HCl to glucose of 2:1 (see **Figure 7**) and 3:1 (see **Figure 8**) were applied. Our results were in line with the report of Shimanouchi et al. (2016) who synthesized 5-HMF from fructose in a microtube reactor and found that the yield of 5-HMF decreased the volumetric ratio of organic to aqueous exceeded 1.25:1. Note that the yield and selectivity of 5-HMF decreased with increasing HCl weight ratio. Again, this was due further conversion of 5-HMF to undesired products under the prolonged reaction time (6.7 min).

Figure 8 shows the effect of the organic-to-aqueous volumetric ratio on the yield and selectivity of 5-HMF at various residence times. The highest 5-HMF yield and selectivity of 81.7 and 89.8%, respectively, were achieved when using the organic-to-aqueous volumetric ratio of 0.5:1, reaction temperature of 180°C, and weight ratio of HCl to glucose ratio of 3:1. This was the highest yield reported so far for the synthesis of 5-HMF from glucose, demonstrating the enhancement of

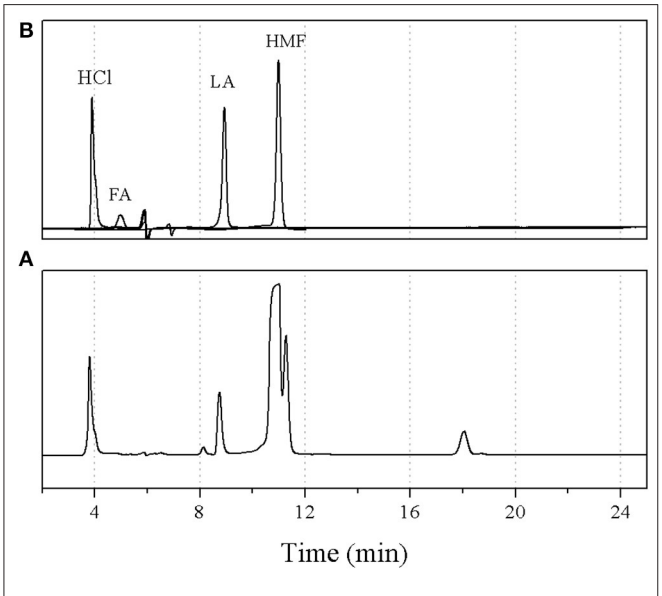

FIGURE 9 | HPLC chromatograms of **(A)** sample at optimal conditions and **(B)** standards; hydrochloric acid (HCl), formic acid (FA), levulinic acid (LA), and hydroxymethylfurfural (HMF).

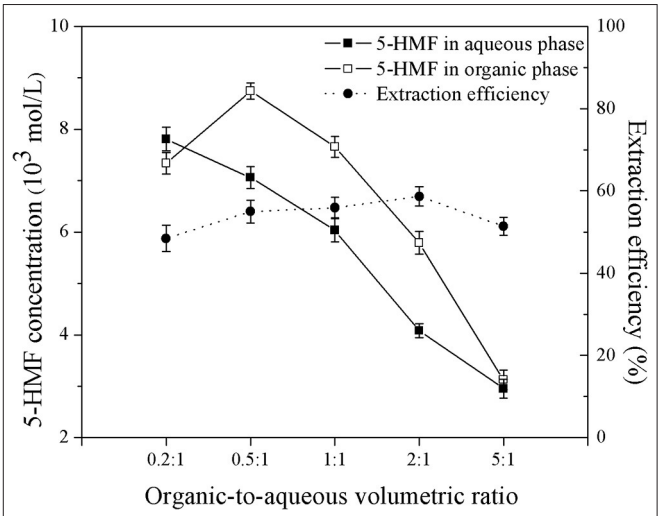

FIGURE 11 | Effect of organic-to-aqueous volumetric ratio on the extraction efficiency.

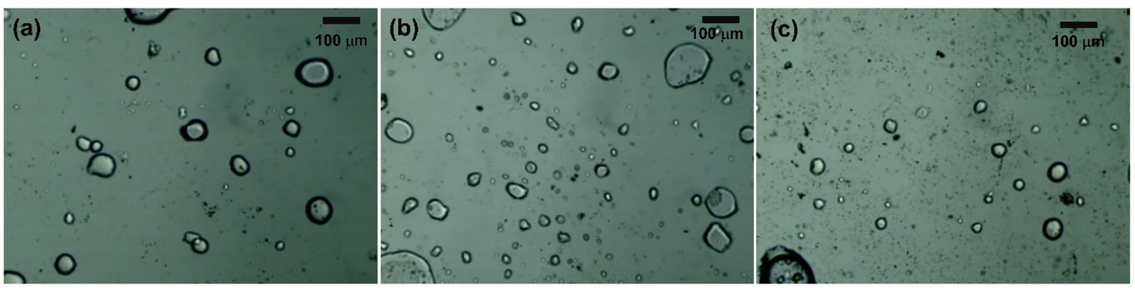

FIGURE 10 | Flow pattern of our reacting mixture at the outlet of micromixer **(a)** O/A of 1:0.5, **(b)** O/A of 1:1, and **(c)** O/A of 1:1.5.

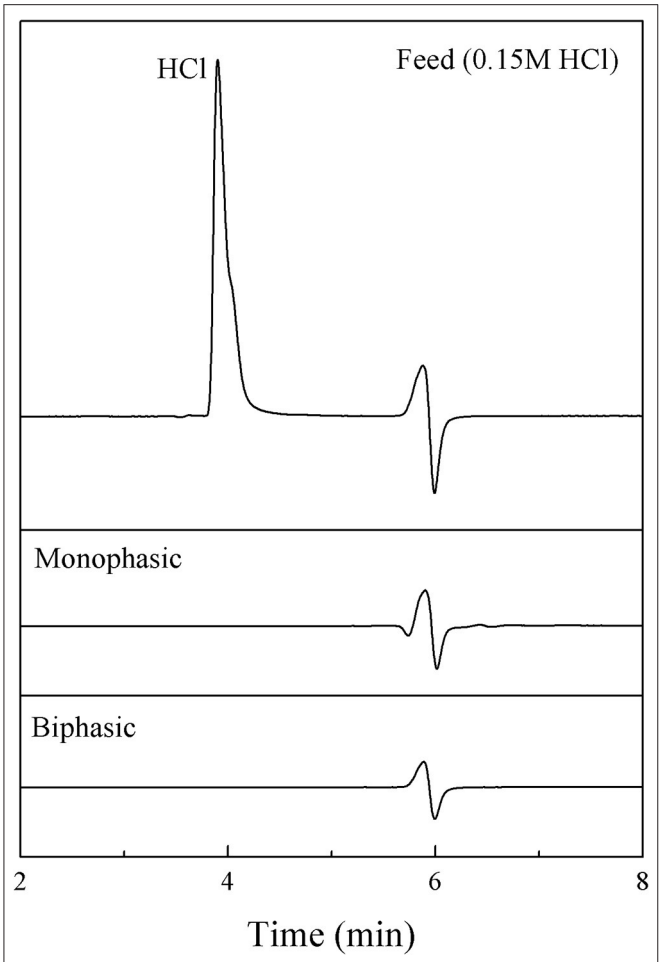

FIGURE 12 | HPLC chromatograms of feed and product from the aqueous phase in both monophasic and biphasic systems.

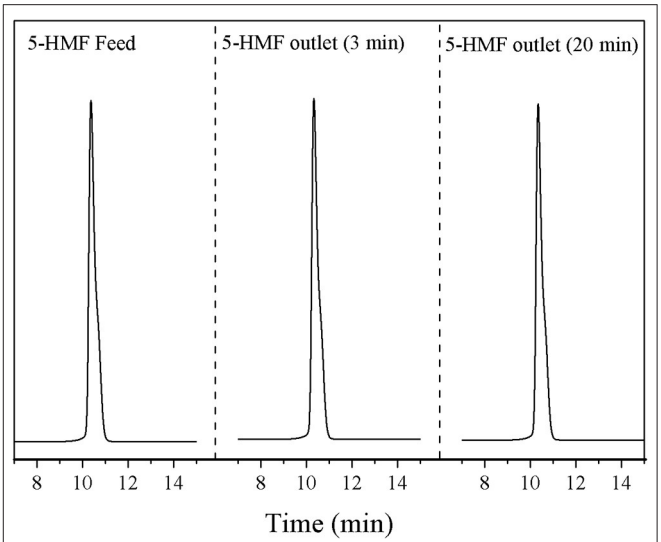

FIGURE 13 | HPLC chromatograms of 5-HMF feed and 5-HMF outlet.

5-HMF synthesis thought our method. The other products were formic acid and levulinic acid, confirmed by comparing with the analytical standards as shown in **Figure 9**.

Furthermore, we compared these findings to the related results from other systems reported in the literature. The superior performance of our synthesis was evident. Only a small amount of MIBK was sufficient to effectively improve the yield and selectivity of 5-HMF. This was quite different to various reports the literature indicating relatively larger amount of MIBK in order to optimize the yield (the MIBK-to-aqueous volumetric is normally between 2:1 and 4:1). For example, in the work of Lueckgen et al. (2018) who applied a microtube reactor to synthesize 5-HMF from fructose, the volumetric ratio of MIBK-to-aqueous phase of 4:1 was necessary to obtain the maximum yield of about 80%. Another example was reported in the work of Delbecq et al. (2017) who studied the conversion of glucose to 5-HMF in a microwave-assisted batch reactor. The yield of 5-HMF of 45% was obtained with the MIBK-to-aqueous volumetric ratio of 3:1. Other related examples can be found elsewhere (Moreno-Recio et al., 2016; Jiang et al., 2018). The superior performance of our process was associated to the efficient extraction of 5-HMF from the aqueous phase due to the dispersed flow of the organic-aqueous mixture in our system. This was confirmed by observing the cloudy liquid product at the outlet of the reactor. This behavior was also investigated through a particular set of experiments to observe the flow pattern at the outlet of the T-micromixer. A stream of glucose solution mixed with green dye (to improve the visibility) and a stream of pure MIBK were used as feed streams. The experiments were carried out under ambient temperature, while the flow rate of aqueous stream and the flow rate of organic stream were the same as those of the reaction test conditions with the residence time of 3 min, and aqueous-to-organic phase of 0.5:1; 1:1; and 1:1.5. As shown in **Figure 10**, the dispersed flow was observed due to the presence of small droplets surrounded by the continuous phase, suggesting that mixing of aqueous and organic streams in our system was efficient.

The effect of organic-to-aqueous volumetric ratio on the yield and selectivity of 5-HMF can be interpreted by the extraction efficiency as shown in **Figure 11**. The results obtained at the residence time of 6.7 min, weight ratio of HCl to glucose of 1:1, and reaction temperature of 180°C showed that, the extraction efficiency was approximately the same throughout the range of organic-to-aqueous volumetric ratio investigated. Again, due to the increased possibility of water to contaminate in the organic phase, the hydration reaction between 5-HMF and water also took place in the organic phase. Consequently, the concentration of 5-HMF in both phases decreased rapidly with increasing the organic-to-aqueous volumetric ratio. These results were in line with the yield and selectivity results shown in **Figure 7**. Similar results were also reported in the work of Lueckgen et al. (2018).

Product Purification

Since the product obtained from the synthesis was contaminated with catalyst, the purification of 5-HMF was required. Note that,

TABLE 1 | Comparison of 5-HMF synthesis from glucose with literature.

Reactor	Catalyst	Organic solvent	Promoter	Ratio[c]	T[d] (°C)	RT[e] (min)	Yield (%)	References
Batch reactor	0.2 M HCl	γ-valerolactone	NaCl	4:1	140	60	62.4	Li et al., 2017
Batch reactor	1 wt% Sn- zeolite/HCl	THF	NaCl	3:1	190	70	53.0	Yang et al., 2015
Batch reactor	4 wt% SnO_2-Al_2O_3	DMSO	–	4:1	150	60	27.5	Marianou et al., 2018
Micro reactor[a]	0.4 M phosphoric acid	2-sec-butyl phenol	Sodium phosphate dihydrate	3:1	180	47	75.7	Muranaka et al., 2017
Micro reactor[a]	$AlCl_3$/HCl	MIBK	NaCl	4:1	160	16	66.2	Guo et al., 2019
Micro reactor[b]	0.15 M HCl	MIBK	–	0.5:1	180	3	81.7	This work

[a] *Synthesized over slug-flow regime.*
[b] *Synthesized over dispersed-flow regime.*
[c] *Organic-to-aqueous volumetric ratio.*
[d] *Reaction temperature.*
[e] *Residence time.*

HCl is not soluble in an organic phase. Hence, we focused on a method for the removal of HCl (catalyst) from the aqueous product. A continuous process was developed by using a ion-exchange resin (Amberlyst A21) in order to selectively adsorb HCl. The amount of 1.5 g of resin was placed in a mini-packed bed (ID: 1/4", 5.7 mL), which was used as a separator. A syringe pump was used to introduce the aqueous product through the bed. To verify our method, 0.15 M HCl in the aqueous phase was used as a model solution. Mini-packed bed reactor packed with ion-exchange resin (Amberlyst A21) with the amount of 1.5 g was used as a separator for both monophasic and biphasic systems. For the monophasic system, Only a stream of hydrochloric solution was fed through the adsorbent. On the other hand, a stream of MIBK was also mixed the stream of HCl solution before passing through the bed. The experiments were carried out at an ambient temperature at various residence times (3–20 min). The amount of HCl (in the aqueous phase) at the outlet of the separator was analyzed by HPLC using the same method as for the analysis of 5-HMF. **Figure 12** shows that the trace of HCl was not detected from the aqueous phase for all residence times studied (3–20 min) for both cases (monophasic and biphasic system with a volumetric ratio of 0.5:1). These results suggested that the separation time of 3 min was sufficient for the removal of HCl from aqueous product. Hence, the product was effectively free of HCl.

Moreover, similar experiments were performed to study the loss of 5-HMF during the separation of HCl. In these experiments, 5-HMF concentration at the optimal condition (81.7% of yield) was used as a feed solution. No significant losses of 5-HMF were observed at the stream outlet for the separation time of 3–20 min (see **Figure 13**). This result suggested that the *in-situ* processes of 5-HMF production and acidic purification is possible. However, further studies for optimizing the separation conditions should be performed. For the removal of solvent from 5-HMF, an evaporator can be used.

Process Performance Comparison

To compare the process performance, 5-HMF yield obtained from our process was compared with those obtained from the related literature that employed different reactor types and operating conditions as summarized in **Table 1**. Apparently, our microreactor system provided an impressive yield of 5-HMF of 81.7% while the residence time was considerably shorter than that of other systems. Our system also offered other advantages such as the use of low catalyst concentration and small amount of organic solvent. This implied a smaller reactor volume required as well as a much reduced cost of solvent separation. Besides, when comparing the different types of reactors, the 5-HMF synthesis in a microreactor was apparently more effective than those performed in a batch reactor. This was due to the effective transfer of 5-HMF through the interface between organic phase and aqueous phase, while the batch reactor was affected by the dilution and small interfacial areas for the transfer of 5-HMF. For the cases of microreactor, the 5-HMF synthesis under a dispersed-flow condition (our method) provided superior performance compared to those performed under a slug-flow condition (Muranaka et al., 2017; Guo et al., 2019). From the results, it was evident that our process would be more economical due to the lower requirement of operating conditions. In addition, the production capacity of the microreactor system would be easily adjusted via the numbering-up method.

CONCLUSION

The synthesis of 5-HMF from glucose using HCl as catalyst was enhanced through the use of microreactor technology performed under the dispersed-flow condition. The biphasic system was found to be an effective means to suppress undesired reaction of 5-HMF and improved the yield and selectivity of 5-HMF. The main effect of operating conditions on the yield and selectivity including reaction temperature, catalyst concentration, organic-to-aqueous volumetric ratio, and residence time was studied. According to the ranges of operating conditions studied in this work, the 5-HMF yield of 81.7% was achieved at the residence time of 3 min, organic-to-aqueous volumetric ratio of 0.5:1, reaction temperature of 180°C, and weight ratio of HCl-glucose of 1:1. Compared to the literature data, this system was considered more efficient in terms of

contact time, catalyst concentration, and the amount of solvent required. The removal of HCl from the aqueous phase was achieved using a mini-packed bed reactor filled with ion-exchange resin.

DATA AVAILABILITY STATEMENT

The datasets generated for this study are available on request to the corresponding author.

AUTHOR CONTRIBUTIONS

TT, NA, AK, and AJ designed and interpreted the experiments and wrote the manuscript. TT and NA set up and performed the experiments under supervision of AK and AJ.

FUNDING

This research project was supported by Mahidol University.

REFERENCES

Agarwal, B., Kailasam, K., Sangwan, R. S., and Elumalai, S. (2018). Traversing the history of solid catalysts for heterogeneous synthesis of 5-hydroxymethylfurfural from carbohydrate sugars: a review. *Renew. Sust. Energ. Rev.* 82, 2408–2425. doi: 10.1016/j.rser.2017.08.088

Assary, R. S., Redfern, P. C., and Hammond, J. R. (2010). Computational studies of the thermochemistry for conversion of glucose to levulinic acid. *J. Phys. Chem. B* 114, 9002–9009. doi: 10.1021/jp101418f

Chheda, J. N., Román-Leshkov, Y., and Dumesic, J. A. (2007). Production of 5-hydroxymethylfurfural and furfural by dehydration of biomass-derived mono- and poly-saccharides. *Green Chem.* 9, 342–350. doi: 10.1039/B611568C

Dalessandro, E. V., and Pliego, J. R. Jr. (2018). Fast screening of solvents for simultaneous extraction of furfural, 5-hydroxymethylfurfural and levulinic acid from aqueous solution using SMD solvation free energies. *J. Braz. Chem. Soc.* 29, 430–434. doi: 10.21577/0103-5053.20170140

Delbecq, F., Wang, Y., and Len, C. (2017). Various carbohydrate precursors dehydration to 5-HMF in an acidic biphasic system under microwave heating using betaine as a co-catalyst. *Mol. Catal.* 434, 80–85. doi: 10.1016/j.mcat.2017.02.037

Dore, V., Tsaoulidis, D., and Angeli, P. (2012). Mixing patterns in water plugs during water/ionic liquid segmented flow in microchannels. *Chem. Eng. Sci.* 80, 334–341. doi: 10.1016/j.ces.2012.06.030

Guo, W., Heeres, H. J., and Yue, J. (2019). Continuous synthesis of 5-hydroxymethylfurfural from glucose using a combination of alcl3 and hcl as catalyst in a biphasic slug flow capillary microreactor. *Chem. Eng. J.* 381:122754. doi: 10.1016/j.cej.2019.122754

Hu, Z., Liu, B., Zhang, Z., and Chen, L. (2013). Conversion of carbohydrates into 5-hydroxymethylfurfural catalyzedby acidic ionic liquids in dimethyl sulfoxide. *Ind. Crop. Prod.* 50, 264–269. doi: 10.1016/j.indcrop.2013.07.014

Jiang, C., Zhu, J., Wang, B., Li, L., and Zhong, H. (2018). One-pot synthesis of 5-hydroxymethylfurfural from glucose over zirconium doped mesoporous KIT-6. *Chinese J. Chem. Eng.* 26, 1270–1277. doi: 10.1016/j.cjche.2018.02.031

Leshkov, Y. R., and Dumesic, J. A. (2009). Solvent effects on fructose dehydration to 5-hydroxymethylfurfural in biphasic systems saturated with inorganic salts. *Top. Catal.* 52, 297–303 doi: 10.1007/s11244-008-9166-0

Li, M., Li, W., Lu, Y., Jameel, H., Chang, H. M., and Ma, L. (2017). High conversion of glucose to 5-hydroxymethylfurfural using hydrochloric acid as a catalyst and sodium chloride as a promoter in a water/γ -valerolactone system. *RSC Adv.* 7, 14330–14336. doi: 10.1039/C7RA00701A

Lueckgen, J., Vanoye, L., Philippe, R., Eternot, M., Fongarland, P., Bellefon, C. D., et al. (2018). Simple and selective conversion of fructose into HMF using extractive-reaction process in microreactor. *J. Flow Chem.* 8, 3–9. doi: 10.1007/s41981-018-0004-7

Marianou, A. A., Michailof, C. M., Pineda, A., Iliopoulou, E. F., Triantafyllidis, K. S., and Lappas, A. A. (2018). Effect of Lewis and Brønsted acidity on glucose conversion to 5-HMF and lactic acid in aqueous and organic media. *Appl. Catal. A General* 555, 75–87. doi: 10.1016/j.apcata.2018.01.029

Matsumura, Y., Yanachi, S., and Takuya, T. (2006). Glucose decomposition kinetics in water at 25 MPa in the temperature range of 448-673 K. *Ind. Eng. Chem. Res.* 45, 1875–1879. doi: 10.1021/ie050830r

Mednick, M. L. (1962). The acid-base-catalyzed conversion of aldohexose into 5-(Hydroxymethyl)-2-furfural. *J. Org. Chem.* 27, 398–403. doi: 10.1021/jo01049a013

Moreno-Recio, M., Santamaría-González, J., and Maireles-Torres, P. (2016). Brønsted and Lewis acid ZSM-5 zeolites for the catalytic dehydration of glucose into 5-hydroxymethylfurfural. *Chem. Eng. J.* 303, 22–30. doi: 10.1016/j.cej.2016.05.120

Muranaka, Y., Nakagawa, H., Masaki, R., Maki, T., and Mae, K. (2017). Continuous 5-hydroxymethylfurfural production from monosaccharides in a microreactor. *Ind. Eng. Chem. Res.* 56, 10998–11005. doi: 10.1021/acs.iecr.7b02017

Qi, X., Watanabe, M., Aida, T. M., and Smith, R. L. Jr. (2008). Catalytical conversion of fructose and glucose into 5-hydroxymethylfurfural in hot compressed water by microwave heating. *Catal. Commun.* 9, 2244–2249. doi: 10.1016/j.catcom.2008.04.025

Rosatella, A. A., Simeonov, S. P., Frade, R. F. M., and Afonso, C. A. M. (2011). 5-Hydroxymethylfurfural (HMF) as a building block platform: biological properties, synthesis and synthetic applications. *Green Chem.* 13, 754–793. doi: 10.1039/c0gc00401d

Shimanouchi, T., Kataoka, Y., Tanifuji, T., and Kimura, Y. (2016). Chemical conversion and liquid-liquid extraction of 5-hydroxymethylfurfural from fructose by slug flow microreactor. *AIChE J.* 62, 2135–2143. doi: 10.1002/aic.15201

Souza, R. L. D., Yu, H., Rataboul, F., and Essayem, N. (2012). 5-Hydroxymethylfurfural (5-HMF) production from hexoses: limits of heterogeneous catalysis in hydrothermal conditions and potential of concentrated aqueous organic acids as reactive solvent system. *Challenges* 3, 212–232. doi: 10.3390/challe3020212

Watanabe, M., Aizawa, Y., Iida, T., Aida, T. M., Levy, C., Sue, K., et al. (2005a). Glucose reactions with acid and base catalysts in hot compressed water at 473K. *Carbohydr. Res.* 340, 1925–1930. doi: 10.1016/j.carres.2005.06.017

Watanabe, M., Aizawa, Y., Iida, T., Levy, C., Aida, T. M., and Inomata, H. (2005b). Glucose reactions within the heating period and the effect of heating rate on the reactions in hot compressed water. *Carbohydr. Res.* 340, 1931–1939. doi: 10.1016/j.carres.2005.05.019

Xin, H., Zhang, T., Li, W., Su, M., Song, L., Shao, Q., et al. (2017). Dehydration of glucose to 5-hydroxymethylfurfural and 5-ethoxymethylfurfural by combining Lewis and Brønsted acid. *RSC Adv.* 7, 41546–41551. doi: 10.1039/C7RA07684C

Yang, G., Wang, C., Lyu, G., Lucia, L. A., and Chen, J. (2015). Catalysis of glucose to 5-hydroxymethylfurfural using Sn-beta zeolites and a Brønsted acid in biphasic systems. *BioResources* 10, 5863–5875. doi: 10.15376/biores.10.3.5863-5875

Yao, X., Zhang, Y., Du, L., Liu, J., and Yao, J. (2015). Review of the applications of microreactors. *Renew. Sust. Energ. Rev.* 47, 519–539. doi: 10.1016/j.rser.2015.03.078

Zhang, X., Hewetson, B. B., and Mosier, N. S. (2015). Kinetics of maleic acid and aluminum chloride catalyzed dehydration and degradation of glucose. *Energy Fuels* 29, 2387–2393. doi: 10.1021/ef502461s

Zhou, C., Shen, C., Ji, K., Yin, J., and Du, L. (2018). Efficient production of 5-hydroxymethylfurfural enhanced by liquid-liquid extraction in a membrane dispersion microreactor. *ACS Sustainable Chem. Eng.* 63, 3992–3999. doi: 10.1021/acssuschemeng.7b04368

Conflict of Interest: The authors declare that the research was conducted in the absence of any commercial or financial relationships that could be construed as a potential conflict of interest.

frontiers in Chemistry

ORIGINAL RESEARCH
published: 28 January 2020
doi: 10.3389/fchem.2020.00017

Influence of the Catalyst Particle Size on the Aqueous Phase Reforming of *n*-Butanol Over Rh/ZrO_2

Heikki Harju[1,2], *Giuseppe Pipitone*[3] *and Leon Lefferts*[1,2]*

[1] Department of Chemical and Metallurgical Engineering, Aalto University, Espoo, Finland, [2] Catalytic Processes and Materials, Department of Science and Technology, MESA+ Institute for Nanotechnology, University of Twente, Enschede, Netherlands, [3] Department of Applied Science and Technology, Politecnico di Torino, Turin, Italy

Butanol is a by-product obtained from biomass that can be valorized through aqueous phase reforming. Rh/ZrO_2 catalysts were prepared and characterized, varying the size of the support particles. The results showed a relatively mild effect of internal mass transport on butanol conversion. However, the influence of internal transport limitations on the product distribution was much stronger, promoting consecutive reactions, i.e., dehydrogenation, hydrogenolysis, and reforming of propane and ethane. Hydrogen consuming reactions, i.e., hydrogenolysis, were more strongly enhanced than hydrogen producing reactions due to internal concentration gradients. Large support particles deactivated faster, attributed to high concentrations of butyraldehyde inside the catalyst particles, enhancing deposit formation via aldol condensation reactions. Consequently, also the local butyric acid concentration was high, decreasing the local pH, enhancing Rh leaching. The influence of internal transfer limitation on product distribution and stability is discussed based on a reaction scheme with three main stages, i.e., (1) formation of liquid intermediates via dehydrogenation, (2) formation of gas via decarbonylation/decarboxylation reactions, and (3) hydrocarbon hydrogenolysis/reforming/dehydrogenation.

Keywords: aqueous phase reforming, hydrogen, mass transfer, reaction pathway, rhodium

OPEN ACCESS

Edited by:
Dmitry Yu. Murzin,
Åbo Akademi University, Finland

Reviewed by:
Benjaram M. Reddy,
Indian Institute of Chemical Technology (CSIR), India
Atte Aho,
Åbo Akademi University, Finland

***Correspondence:**
Leon Lefferts
l.lefferts@utwente.nl

Specialty section:
This article was submitted to Catalysis and Photocatalysis, a section of the journal Frontiers in Chemistry

Received: *29 October 2019*
Accepted: *08 January 2020*
Published: *28 January 2020*

Citation:
Harju H, Pipitone G and Lefferts L (2020) Influence of the Catalyst Particle Size on the Aqueous Phase Reforming of n-Butanol Over Rh/ZrO_2. Front. Chem. 8:17. doi: 10.3389/fchem.2020.00017

INTRODUCTION

The environmental issues and the depletion of conventional sources of energy demand development of alternative and sustainable technologies. Among the several possibilities, biomass is seen as a strategic feedstock for the production of renewable energy and materials. One of the possible products of biomass exploitation is hydrogen, through thermochemical or biological routes (Balat and Kirtay, 2010).

In the last years, a considerable effort has been put on the production of hydrogen from oxygenated hydrocarbons, e.g., via aqueous phase reforming (APR) (Cortright et al., 2002). The Dumesic research group demonstrated that hydrogen can be produced from alcohols in water in the condensed phase, with a noteworthy energetic advantage compared to the conventional steam reforming as evaporation of water is circumvented (Davda et al., 2005).

APR is a promising strategy for valorization of aqueous side-streams. Among the possible reactants for this process, oxygenates with 1 to 1 O to C ratios are preferred for H_2 production,

via reforming and subsequent water gas shift reaction (Cortright et al., 2002; Shabaker et al., 2003a; Davda et al., 2005). Indeed, methanol is the most investigated mono-alcohol, thanks to its optimal carbon/oxygen ratio.

However, little attention has been paid so far to APR of butanol, despite its strategic importance as it can be produced from biomass via fermentation of sugar cane (Kumar et al., 2017). Also, aqueous waste streams of e.g., flash pyrolysis contain butanol, making it an interesting model compound for study. As a matter of fact, butanol has been studied for hydrogen production vis supercritical water reforming for its representativeness of oxygenates present in the bio-oil aqueous phase (Gutiérrez Ortiz et al., 2016; Gutiérrez Ortiz and Campanario, 2018).

Roy et al. investigated for the first time APR of butanol over Ni-based catalysts supported on ceria or alumina (Roy et al., 2011). Successively, the same research group used these catalysts also in harsher conditions, i.e., for steam reforming of butanol, enlarging the range of operating conditions as reaction temperatures, pressure, concentration, and flow rate of the feed (Roy et al., 2014).

In previous work we investigated the steam reforming of butanol over a Rh/ZrO_2 catalyst (Harju et al., 2015, 2016). This catalytic system showed promising results in terms of hydrogen productivity and stability, since coke formation is slower compared to other supports. APR of higher alcohols results in significant formation of hydrocarbons on more conventional metal catalysts (Roy et al., 2011, 2014; Lobo et al., 2012) because of limited C-C cleavage. Rh however is known to be active for C-C cleavage (Sinfelt, 1973; Bond et al., 1996) and low temperature steam reforming (Kolb et al., 2004; Halabi et al., 2010). It has been recently showed that, among several metals (Pd, Ru, Re, Ir, and Cr) Rh was the best promoter in a bimetallic Pt-based catalyst for the APR of glycerol (Larimi and Khorasheh, 2019). Furthermore, ZrO_2 is known as one of the few oxides capable of resisting the harsh hydrothermal conditions of APR (Elliott et al., 1993), unlike more commonly used supports (De Vlieger et al., 2012). Therefore, this study explores the use of Rh/ZrO_2 for the valorization of butanol in APR conditions.

APR is a three phase (G-L-S) system and therefore issues related to mass transfer limitations may arise. Hydrogen mass transfer is of paramount importance in APR as reported by Neira D'Angelo et al. (2013, 2014a,b) reporting that microchannel reactors enhance mass transfer, increasing the hydrogen yield by suppressing sequential reactions consuming H_2.

The goal of this work is to determine the effect of internal mass transfer on aqueous phase reforming of butanol over Rh/ZrO_2 catalyst by varying the dimension of the catalyst particles using a reactor design that increase the sensitivity for internal mass transfer. For example, in contrast to previous works (Neira D'Angelo et al., 2013, 2014a), the reactor was not flushed with inert gas, so that the concentration of gas products outside the catalyst particles was relatively high, retarding diffusion out of gaseous products. The obtained results allow not only to discuss the effect of internal mass transport on product distribution and deactivation, but also to propose a reaction scheme.

MATERIALS AND METHODS

Catalyst Synthesis

The catalysts were prepared by vacuum assisted dry impregnation method followed by calcination at 850°C, described in more detail in earlier work (Harju et al., 2015). To obtain the different catalyst particle sizes, the ZrO_2 support (monoclinic ZrO_2, MEL Chemicals) was crushed and sieved to the desired particle sizes prior to impregnation. The support particles sizes remained unchanged during catalyst preparation.

Catalyst Characterization

The Rh content of both fresh and spent catalyst was determined by X-Ray Fluorescence performed with Malvern Panalytical Axios mAX 3 kW. The 7-point BET surface area of both fresh and spent catalyst was performed with Coulter Omnisorp 100 CX, using methods described elsewhere (Kaila et al., 2007, 2008). Pore volume of both fresh and spent catalyst were determined during the same N_2 physisorption measurement as the BET surface area, using the NLDFT method, assuming spherical and cylindrical pores. Unfortunately, the equipment used for BET measurement did not allow experiments with small particles and only the samples with the largest particle size could be measured. The Rh dispersion on both fresh and spent catalyst was determined using pulsed H_2 chemisorption in Ar (Chemisorb 2750, Micromeritics). The Rh particle size distribution on spent catalyst was determined by scanning tunneling electron microscopy (STEM) using Jeol 2200FS equipped with spherical aberration corrector. Elemental C, H, and O analysis of the deposits on spent catalyst was done using methods described in previous work (Harju et al., 2016). The elemental analysis was also done for fresh catalyst to determine the contribution of hydroxyl and carbonate groups of atmospheric origin.

Reaction Experiments

A schematic representation of the set-up used for APR experiments is reported in **Figure 1**. The reactant solution (5 wt% *n*-butanol in de-ionized water) was pressurized and fed by a setup of dual ISCO D-pumps and pre-heated up to the desired reaction temperature (220°C) before the catalytic bed. The catalytic bed was 7 mm in diameter. The catalyst loading in the reactor was varied (1.5, 1.0 and 0.1 g for the 250–420, 60–100, and 40–60 μm catalysts, respectively, resulting is acceptable bed height), keeping the LHSV constant at 150 h^{-1} for all the experiments by adjusting the volumetric flow rate. The set temperature was reached about 30 min after starting heating, and it was considered in the results as the zero time. Afterwards the effluent was cooled down to room temperature by a water-cooled tubular heat exchanger. The pressure was kept constant at ∼35 bar by a manual back-pressure regulator (TESCOM, model 26-1764-24-090) following the heat exchanger. Prior to phase separation at ambient pressure in a separation vessel, nitrogen sweep gas was introduced to the stream to aid in gas product purging and to keep a steady minimum flow present to improve accuracy of both gas phase analysis and flow rate measurement. The gaseous products were periodically sampled from the top of the de-mister section of the phase separation vessel for analysis in a Varian micro-GC, while

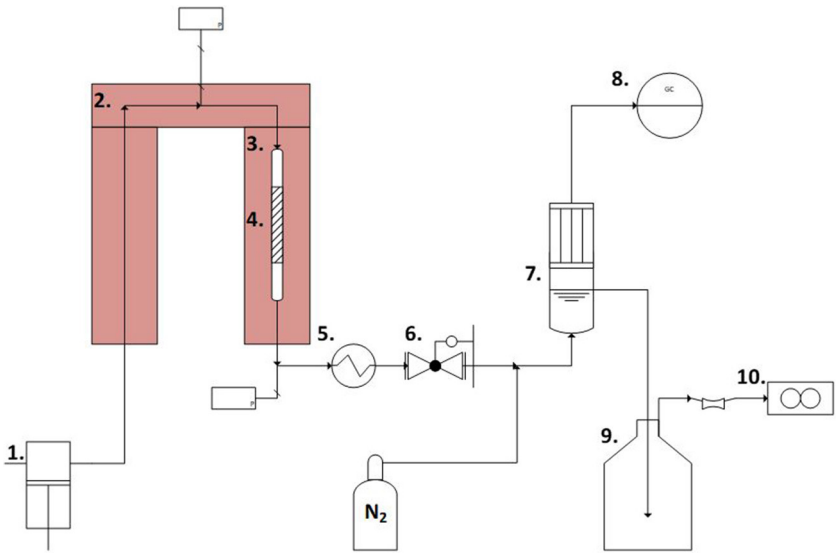

FIGURE 1 | Schematic of the experimental set-up. 1. Piston pumps. 2. Pre-heater. 3. Heater. 4. Catalyst section. 5. Heat exchanger. 6. Back-pressure valve. 7. Gas-liquid separation vessel. 8. Varian Micro-GC. 9. Eluent collection vessel. 10. Gas mass-flow meter.

the gas flowrate was measured by a gas mass flow meter. The liquid flowrate was integrally measured by weighing the eluent collection vessel mounted on a scale.

The time on stream (TOS) was 150 min for the 40–60 and 60–100 μm particles and 210 min for the 250–420 μm particles. After cooling the system overnight, the catalyst was removed from the reactor and dried at 100°C overnight.

Product Analysis and Calculation

The gas products were analyzed with a Varian micro-GC equipped with two columns with a TCD detector to determine the yields. H_2, O_2, N_2, CH_4, and CO were analyzed with a Molsieve 5A column (argon carrier, temperature column 100°C), while CO_2, C_2H_4, C_2H_6, C_3H_6, and C_3H_8 were analyzed over a PoraPLOT U column (helium carrier, temperature column 85°C).

The liquid phase was sampled every 30 min and analyzed with a Shimadzu HPLC (Prominence) equipped with an Aminex HPX-87H column and a refractive index detector (RID). The flow rate of the mobile phase (5 mM H_2SO_4 aqueous solution) was fixed at 0.6 ml/min and the working temperature at 30°C. External calibration curves were used for the quantification. Liquid flow rates were measured according to the variation of the mass in the collecting vessel, assuming density of the liquid product equal to water at room temperature. Gas flow rates were measured with a Brooks gas flow meter; as it was calibrated for nitrogen, the actual value was obtained using conversion factors, knowing the gas composition. The gas flowrate out of the reactor was not constant, coming out in larger bursts, occasionally causing scatter in the micro-GC results and gas mass flow measurement. This problem occurs when gas bubbles form upstream of the backpressure regulator in case of high conversion and high gas-yields. These errors were mitigated by averaging over 30 min periods.

The liquid product yields (C1 based) were calculated according to Equation (1), where $Y_{C_1,\,i}$ is the C_1 based yield of any carbon containing component *i*, F_i is the molar flow rate (mol min^{-1}) of component *i*, N_{Ci} is the carbon number of component *i*. The gas product yields (C1 based) were measured according to Equation (2) as the difference between butanol conversion and liquid yields, based on the fact that the carbon mass balance closed within 10%. The gas selectivity was defined as the ratio between the gas product yield and the butanol conversion. Finally, the selectivity toward a specific component *i* was defined as the ratio between its molar flow and moles of reacted butanol (Equation 4).

$$Y_{C_1,liquid} = \frac{\sum F_{i_{liquid}} N_{C_i}}{F_{butanol_{in}} N_{C_{butanol}}} \quad (1)$$

$$Y_{C_1,\,gas} = X_{butanol} - Y_{C_1,\,liquid} \quad (2)$$

$$S_{C_1,gas} = \frac{Y_{C_1,\,gas}}{X_{butanol}} \quad (3)$$

$$S_i = \frac{F_i}{F_{butanol_{in}} X_{butanol}} \quad (4)$$

Please note that the maximum selectivity depends on the component, i.e., 4 for C_1 compounds, 2 for C_2 compounds, 1 for C_4 compounds as well as C_3 compounds, considering that a butanol molecule can deliver max 1 C_3 molecule, and 12 for H_2.

RESULTS

Catalyst Characterization

XRF, Physisorption and Chemisorption

Table 1 shows the results of N_2 physisorption of both fresh and spent 250–420 μm catalyst. Surface area calculated with the seven-point BET method and the NLDFT model are in agreement, showing a small increase during the experiment. The

TABLE 1 | N_2 physisorption results for the 250–420 μm catalyst.

Sample	Surface area (m^2 g^{-1})		Pore volume (cm^3 g^{-1})			
	7-point BET		NLDFT			
	Fresh	Spent	Fresh	Spent	Fresh	Spent
Rh/ZrO_2 250–420 μm	37.0	42.5	36.6	42.4	0.100	0.121

TABLE 2 | XRF analysis results.

Sample	Time on stream (min)	Rh loading (wt.%)			
		Target	Fresh	Spent	Rh loss (%)
Rh/ZrO_2 40–60 μm	150		0.5	0.43	0.43	0.9
Rh/ZrO_2 60–100 μm	150		0.5	0.42	0.40	5.4
Rh/ZrO_2 250–420 μm	210		0.5	0.50	0.36	27.7

total pore volume is also increased during the experiment and the pore size distribution shifts to slightly larger pores. The catalyst is mesoporous. Surprisingly, application in APR causes a minor but significant increase in surface area and pore volume, despite the fact that ZrO_2 is reported to be stable under APR conditions (Elliott et al., 1993). Also, no significant changes in the morphology of ZrO_2 were observed during preliminary aging experiments in pure water at 200°C for 12 h (not shown).

Table 2 shows the Rh loading in the fresh and spent catalysts, as measured by XRF. The Rh leaching increased significantly with increasing dimension of the catalyst particles. The reduction in Rh content is caused by leaching. Please note that any apparent decrease of Rh loading due to catalyst mass being increased by deposit formation is in all cases much smaller than the observed effects, therefore leaching is the main cause of the decreasing Rh loading.

Table 3 shows the Rh dispersions and metal surface areas in fresh and spent catalysts as measured by H_2 chemisorption as well as the average Rh crystallite size calculated from both Rh surface area and STEM images, shown in **Figure 2**. The fresh catalysts show very good dispersion and small Rh crystallite size. During the reaction, the available Rh surface area is reduced by factor of typically 2, without any significant effect of the zirconia particle. The increase in metal particle sizes according chemisorption are in reasonable agreement with the observed particle sizes observed with STEM, presented below.

STEM Analysis of Spent Catalyst

Figure 2 shows dark field STEM images of the spent 40–60 and 250–420 μm catalysts. The Rh crystallites in the fresh catalysts were oxidized, making it impossible to see them with STEM without a reductive pretreatment. Rh in the spent catalysts is found in mostly round and sometimes also oval particles. The particle size distribution is quite narrow, as seen in **Figure 3** for the 40–60 μm catalyst. Rh particles were considerably harder to locate in the larger catalyst particles, leading to a somewhat limited data set (30 particles as compared to 173 on the 40–60 μm catalyst). However, the distribution in 250–420 μm catalyst (**Supplementary Figure A-1**) reveals no significant difference with the distribution shown in **Figure 3**.

Elemental Analysis

Figure 4 shows the C, H, and O elemental analysis results of spent catalysts; the amount of deposits was calculated by subtracting the amount of C, H, and O detected on fresh catalyst from the amounts detected on spent catalyst. The average rate of deposition (in mg $g_{catalysts^{-1}}$ h^{-1}) is calculated by dividing the amount of deposits by the TOS in order to take into account small differences in the TOS, as also presented in **Figure 4**. Formation of deposits clearly increases with increasing particle size, particularly the amounts of carbon and oxygen as well as the total mass of deposit (mg $g_{catalyst^{-1}}$) and the average rate of deposition.

Catalytic Performance

Conversion and Products Yields

Figure 5 shows conversion and carbon-based selectivity to gaseous product over time. The conversion over the 40–60 and 60–100 μm catalysts is similar, whereas the conversion over the 250–420 μm catalyst is consistently 30–40% lower. Conversion on all catalysts declined at a similar rate over time. Selectivity to gaseous products remained high on 40–60 and 60–100 μm catalysts, declining slowly over time from ca. 99 to 97% in 150 min. On 250–420 μm catalyst, gas selectivity starts similarly high, declining severely over time. The conversion on bare support was too low to enable reliable quantification (**Supplementary Figure A-3A**).

Product Distribution

Figure 6 shows selectivities to butyraldehyde and butyric acid, the main products in liquid phase, over time. In addition, traces of acetic acid and ethanol were detected. On bare support (**Supplementary Figure A-3B**), only butyraldehyde is observed in very low amounts, decreasing with TOS. Clearly, butyraldehyde selectivity is much higher compared to the butyric acid selectivity. The liquid product selectivities over 40–60 and 60–100 μm catalysts are very similar, increasing slowly with time on stream. In contrast, the 250–420 μm catalyst produces much more butyraldehyde and butyric acid, both increasing significantly with time on stream. The molar ratio of aldehyde to acid also increases over time, particularly on the 250–420 μm catalyst, from an initial value 4 to about 14 by the end of the experiment.

Figures 7, **8** show the selectivities to products in the gas phase, i.e., H_2, CO_2, and CH_4 (**Figure 7**) and C_{2-3} hydrocarbons (**Figure 8**). The selectivity to CO was always very low, below 0.05 mol mol^{-1} (**Supplementary Figure A-2**). On the bare support formation of H_2, CO_2, and C_3 was detected at such low concentration that quantification was not possible. H_2 selectivities (**Figure 7A**) were similar on all catalysts, showing no effect of the catalyst particle size. CO_2 selectivities (**Figure 7B**) decreased with decreasing size in the order 250–420 > 60–100 > 40–60. The CO_2 selectivity decreased over time on the 250–420 μm catalyst, whereas such a trend is less clear

TABLE 3 | H_2 chemisorption and particle size determined with STEM; the typical experimental relative error in dispersion and surface area is 10%.

Sample	Rh dispersion		Rh surface area		Average Rh particle size (nm)		
	H_2 chemisorption (%)		H_2 chemisorption ($m^2\ g^{-1}_{catalyst}$)		H_2 chemisorption		STEM
	Fresh	Spent	Fresh	Spent	Fresh	Spent	Spent
Rh/ZrO_2 40–60 μm	78	34	1.5	0.6	1.4	3.3	2.7
Rh/ZrO_2 60–100 μm	110	70	2.1	1.2	1.0	1.6	NA
Rh/ZrO_2 250–420 μm	64	47	1.4	0.75	1.8	2.4	2.6

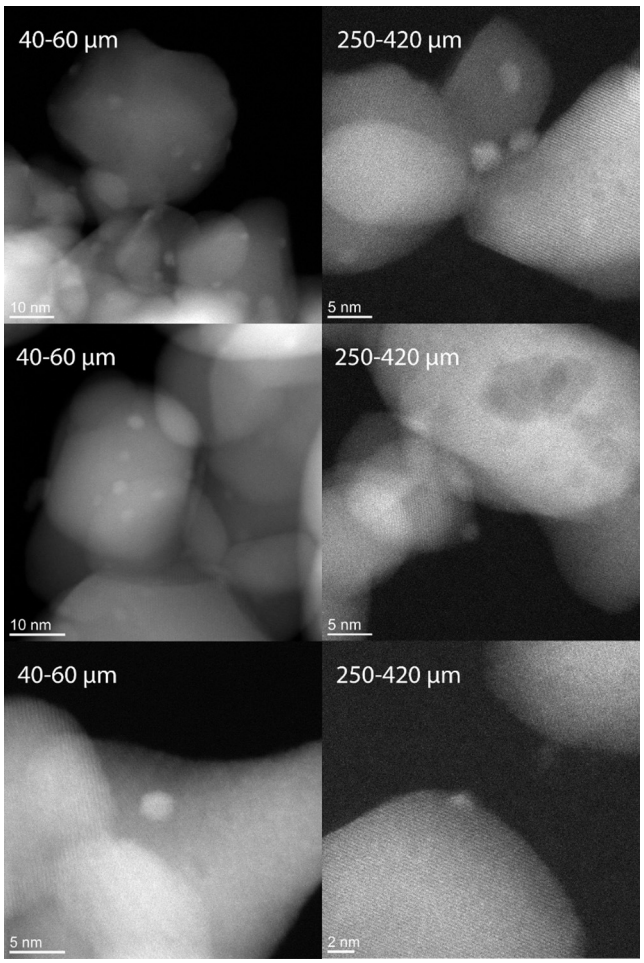

FIGURE 2 | Dark field STEM images of the spent 40–60 and 250–420 μm Rh/ZrO_2 catalysts.

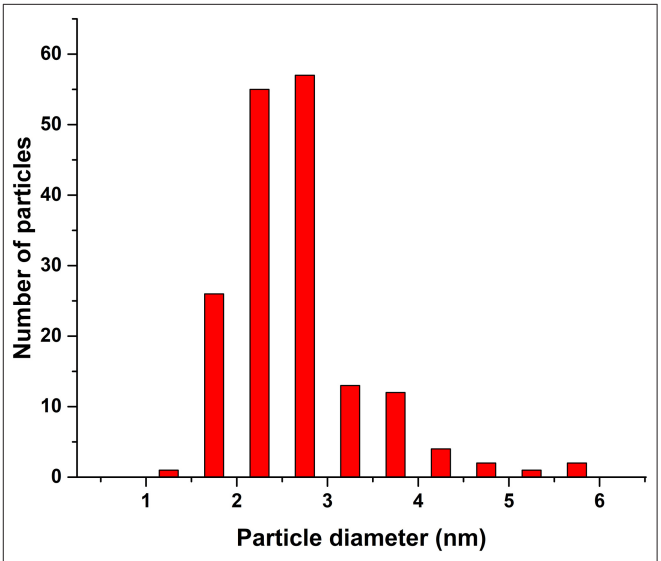

FIGURE 3 | Rh particle size distribution on the 40–60 μm spent catalyst according STEM.

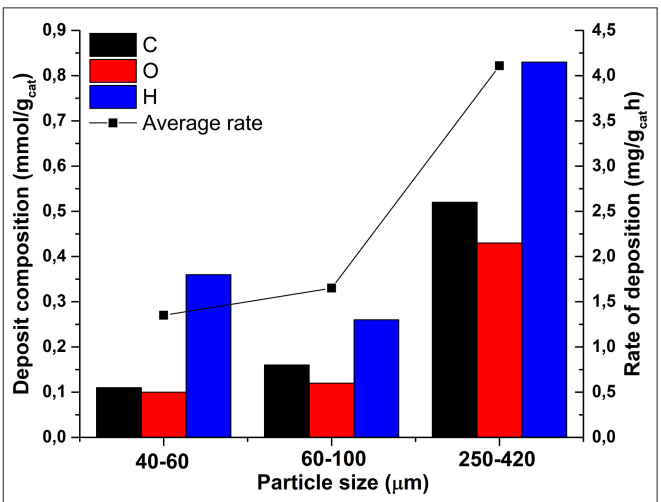

FIGURE 4 | Elemental composition and amounts of deposits as well as averaged rate of formation of deposits in spent catalysts; contamination on fresh catalysts was subtracted.

on the smaller catalysts. Formation of methane (**Figure 7C**) increased with decreasing particle size, opposite to CO_2. In fact, the 250–420 μm catalyst produced hardly any methane. Also selectivity to C_2 compounds (**Figures 8A,B**) increased with decreasing catalyst particle size, similar to methane. Furthermore, ethane (**Figure 8B**) was the main C_2 product over the 40–60 and 60–100 μm catalysts, while the 250–420 μm catalyst produced more ethylene than ethane (**Figure 8A**). Propane (**Figure 8D**) was the main C_3 product on all catalysts, despite the relatively large scatter in the data. Furthermore, large catalyst particles (250–420 μm) produce less C_3 compounds than the 40–60 and 60–100 μm catalysts, showing similar C_3 selectivities.

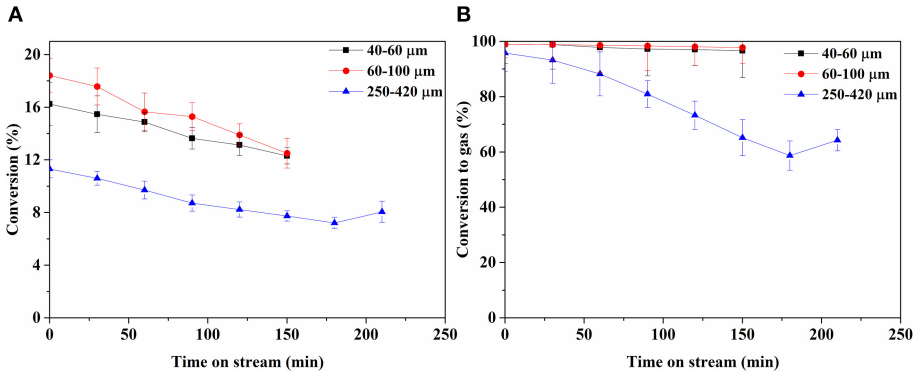

FIGURE 5 | Butanol conversion **(A)** and conversion to gas phase products on C_1-basis over time **(B)**.

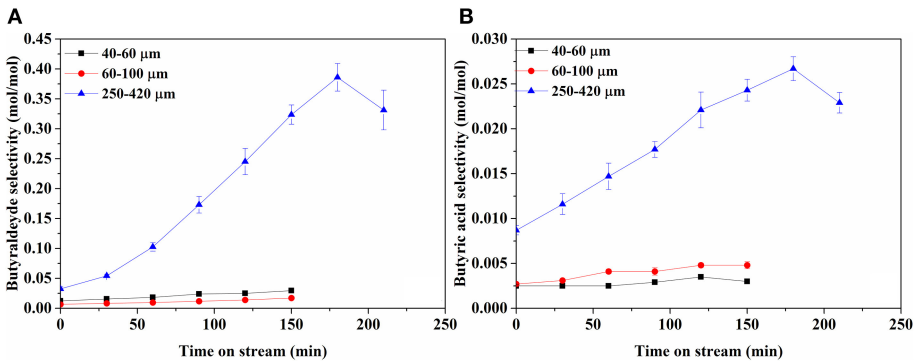

FIGURE 6 | Selectivity of products in liquid phase; **(A)** Butyraldehyde and **(B)** Butyric acid. Note the difference scale between **(A)** and **(B)**.

DISCUSSION

Mass Transfer Criteria

The significance of external mass transfer was evaluated using the Mears' criterion (Equation 5; Mears, 1971):

$$C_M = \frac{r'_A \rho_b R n}{k_c C_{Ab}} < 0.15 \tag{5}$$

The detailed calculation is presented in the **Supplementary Material**. The highest value obtained for the most active and largest catalyst particles was $2.3{*}10^{-3}$, leading to the conclusion that external mass transfer limitations can be disregarded.

The significance of internal mass transfer was estimated using the Weisz-Prater criterion (Equation 6; Weisz and Prater, 1954). Assuming first order reaction, the criterion becomes:

$$C_{WP} = \frac{r'_A R^2 \rho_c}{D_e C_{As}} < 0.25 \tag{6}$$

In which r'_A is the observed reaction rate ($kmol_{butanol}\ kg_{cat^{-1}}\ s^{-1}$), R is the catalyst particle radius (m), ρ_c is the density of the catalyst (kg m^{-3}), C_{As} is the concentration of butanol on the external catalyst surface (kmol m^{-3}) and D_e is the effective diffusion coefficient ($m^2\ s^{-1}$), calculated according to Equation (7):

$$D_e = \frac{D_{AB} \phi_p}{\tau} \tag{7}$$

in which D_{AB} is the binary diffusion coefficient of butanol in water ($m^2\ s^{-1}$), ϕ_p is the catalyst pellet porosity and τ is the tortuosity factor. Catalyst density ρ_c and porosity ϕ_p were estimated using the bulk density of non-porous ZrO_2 and the measured pore volume of the catalyst. As the external mass transfer was considered not limiting, the concentration at the external catalyst surface was assumed to be equal to the bulk concentration, $C_{As} \approx C_{Ab}$. Since the exact value of the tortuosity factor was unknown, the value of C_{WP} was calculated as a function of catalyst particle size with values of τ ranging from 1 to 9, shown in **Figure 9**, using the highest observed reaction rate at time zero. As clearly inferred from the graph, internal diffusion is not limiting for the two smaller particle sizes, but may be limiting for the largest particle size, depending on the value of the tortuosity factor. Therefore, the role of internal diffusion required further experimental evaluation, as will be discussed later. In order to discuss the effect of internal transport on the product distribution, it is necessary to discuss first the main reactions contributing to the overall conversion.

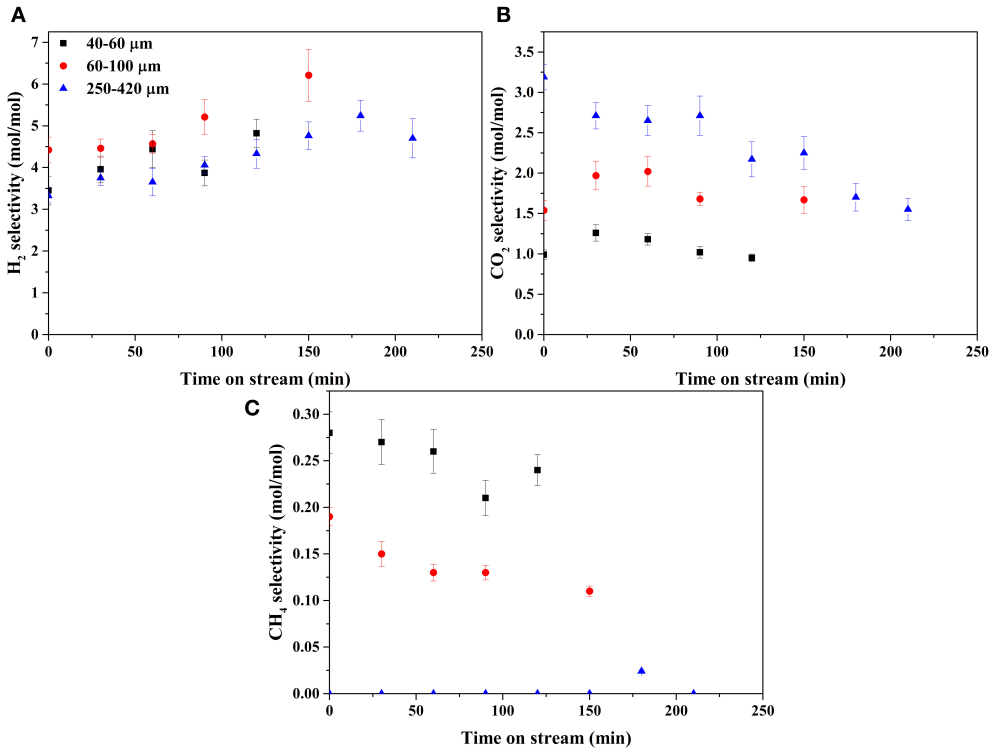

FIGURE 7 | Selectivities of gaseous products: **(A)** H_2, **(B)** CO_2, and **(C)** CH_4.

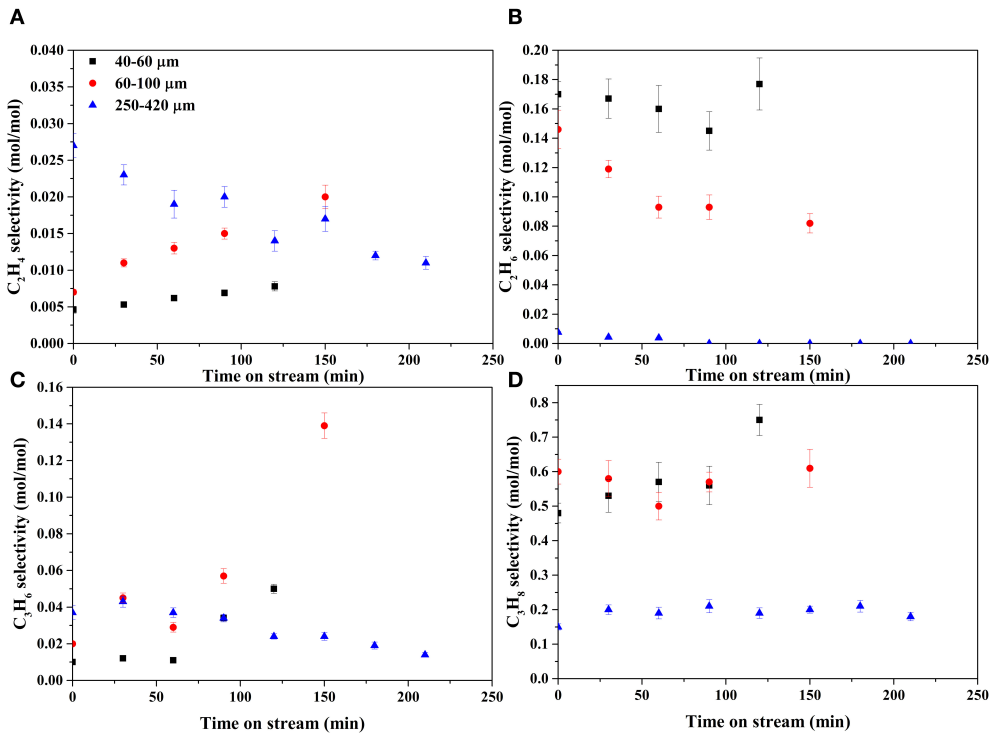

FIGURE 8 | Selectivities of C_{2-3} products. **(A)** ethylene, **(B)** ethane, **(C)** propylene, and **(D)** propane.

Catalyst Performance; Comparison to Literature

APR of alcohols and polyalcohols has been widely investigated, in particular with C-to-O ratio of 1:1 (Shabaker et al., 2003a; Kirilin et al., 2010, 2014). Ethanol, propanol or butanol were typically less studied; the presence of the alkyl groups makes complete reforming less facile and formation of alkanes is reported.

Lobo et al. (2012) studied APR of *n*-propanol over Pt catalysts (5 wt.% propanol solution, 250°C temperature, 69 bar pressure), reporting reaction rates per gram catalyst about one order of magnitude higher. Unfortunately, the Pt loading is not reported. Ethane and carbon dioxide are the main products, with a ratio close to 1, whereas propanal found in the liquid phase.

Godina et al. studied the reforming of alcohols with 3 carbon atoms using Pt-based catalyst on polymer based spherical activated carbons (Godina et al., 2018). Even in this case, exclusively propanal and propionic acid are reported in the liquid phase, whereas ethane was the most formed alkane. On the other hand, methane was not detected, in contrast to our results in the case of the smaller catalyst particles. The presence of propanal and propionic acid from 1-propanol APR was also confirmed by Wawretz and co-workers (Wawrzetz et al., 2010) with an alumina supported Pt catalyst.

Coronado et al. studied the APR of ethanol and propanol with nickel based catalysts on ceria-zirconia supports (Coronado et al., 2018, and literature cited therein), reporting propanal as main liquid product, together with a small amount of propionic acid. On the other hand, methane was found in the gas phase, which was attributed to methanation of CO and CO_2.

Pipitone et al. (2019) studied the aqueous phase reforming of butanol with a Pt-based catalyst in a batch system. The produced gas phase contained hydrogen carbon-dioxide and propane in a 2-1-1 molar ratio, in accordance with the previous works on C3 alcohols (Godina et al., 2018). On the other hand, the nature of the active sites seems to have an effect on the product distribution in the gas phase. Indeed, Roy et al. (2011, 2014) studied APR of *n*-butanol over alumina and ceria supported Ni catalysts (20 wt.% Ni loading, 5 wt.% butanol solution, 185–215°C and 10–31 bar), resulting in reaction rates an order of magnitude lower. The reported product distribution on Ni is similar to the present work, with the exception of somewhat higher selectivity to C_2 hydrocarbons, which the authors attributed to Fischer-Tropsch reactions. The main reaction pathway was proposed to proceed through consecutive dehydrogenation and decarbonylation steps, very similar to the findings of Lobo et al. for APR of propanol with Pt catalysts (Lobo et al., 2012). Tishchenko coupling of propionaldehyde followed by hydrolysis and propionic acid decarboxylation was observed as a side reaction pathway on Pt. Moreover, it was suggested that propane was reformed to hydrogen and carbon monoxide, as likely occurred also in the reaction conditions reported during the present investigation. This result may be explained by the higher activity of nickel toward C-C bond breaking compared to platinum (Sinfelt, 1973).

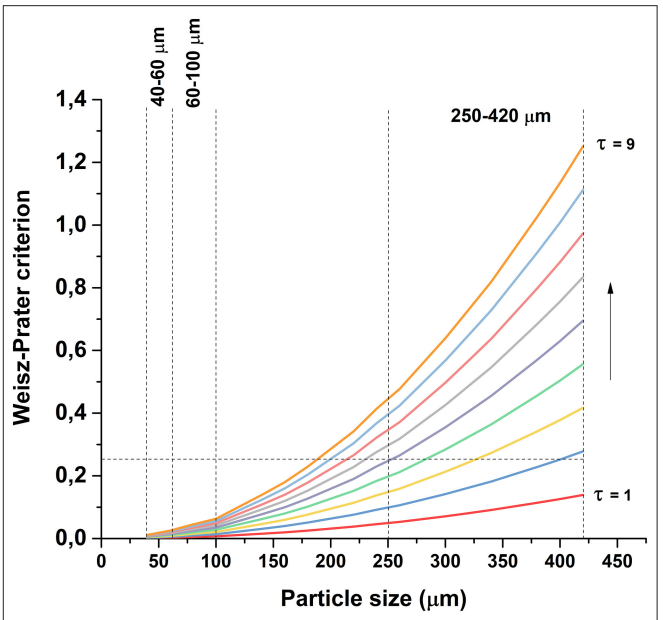

FIGURE 9 | Value of Weisz-Prater criterion as a function of particle size and tortuosity factor.

Reaction Scheme for Rh Catalyst

As no reaction scheme has been reported so far for APR of butanol over Rh catalysts, a proposal for such a scheme is described below (**Figure 10**), based on the observations described above and inspired by literature on APR of butanol on Ni catalysts (Roy et al., 2011, 2014) and of 1-propanol on Pt catalysts (Lobo et al., 2012). Please note this scheme is required for discussing the effect of mass transfer limitations on the product distribution. The scheme is divided in three stages: (I) initial conversion, (II) initial gas formation, and (III) hydrocarbon reactions and reforming.

Stage I is the initial conversion of butanol to liquid intermediates via reactions 1 and 2. Reaction 1, dehydrogenation of butanol into butyraldehyde, mostly takes place on Rh. **Figure 6A** shows a significant yield of butyraldehyde over the Rh catalyst, whereas the yield over plain zirconia (**Supplementary Figure A-3B**) is <0.5 mol% of butanol. This agrees with literature, where dehydrogenation of alcohols is mostly reported on metals (Roy et al., 2011, 2014; Lobo et al., 2012), although it is also reported on zirconia (Sabatier and Mailhe, 1910; Shinohara et al., 1997). Interestingly, the butyraldehyde selectivity (**Figure 6A**) increases over time and the selectivity to gas products (**Figure 5B**) declines simultaneously. This is especially clear over the 250–420 μm catalyst, indicating that the reactions forming gasses deactivate more than the dehydrogenation reaction. Furthermore, no C_3 oxygenates were observed in the liquid phase. Therefore, reactions involving C-C cleavage in butanol are not significant and reaction via butyraldehyde dominates, in agreement with suggestions in literature for Ni and Pt (Roy et al., 2011, 2014; Lobo et al., 2012). Reaction 2 is the formation of butyric acid,

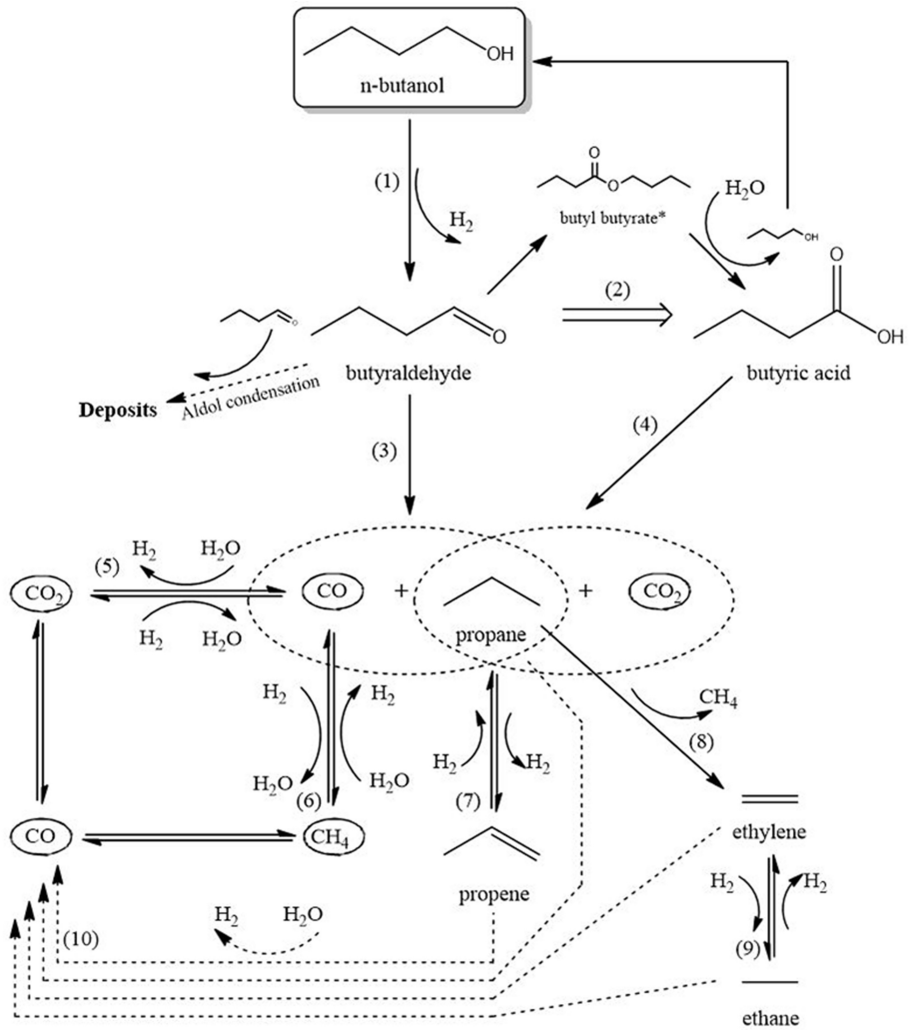

FIGURE 10 | Schematic reaction network. Products marked with *not observed during the experiments.

most likely via Tishchenko esterification on Rh, supported by the fact that butyric acid selectivity closely follows the selectivity for butyraldehyde (**Figures 6A,B**). The intermediate butyl-butyrate was not observed, as would be expected considering that in aqueous medium the equilibrium strongly favors hydrolysis of butyl-butyrate.

Stage II is the formation of CO_x according reactions 3 and 4, respectively, decarbonylation and decarboxylation. The claim that the C-C bond is cleaved via decarbonylation and/or decarboxylation is supported by the observations that propane and C_4 oxygenate products are the dominant products, as well as by the absence of any C_3 oxygenates and the virtual absence of C_2 oxygenates. Decarbonylation of butyraldehyde (reaction 3) is the main reaction forming gaseous products, as much more butyraldehyde than butyric acid is formed (**Figure 6**). The reaction mainly takes place on the metal, but can also be observed on the bare support (**Supplementary Figure A-3A**), in agreement with literature (Bie et al., 2013; Miao et al., 2016). Decarboxylation of butyric acid (reaction 4) requires the presence of an active metal according literature (Bie et al., 2013; Miao et al., 2016).

Stage III consists of the reactions of hydrocarbons (reforming and (de-)hydrogenation) and (R-)WGS (reactions 5–10). The water-gas-shift reaction (WGS, reaction 5) converts virtually all CO to CO_2 and H_2. The aqueous environment is expected to strongly drive WGS toward the products (Shabaker et al., 2003b), causing extremely low CO yields (**Supplementary Figure A-2**).

Propane produced in reactions 3 and 4 can be dehydrogenated over Rh (reaction 7) as indicated by the formation of propylene in **Figure 8C**. The shorter C_{1-2} hydrocarbons are likely formed via propane hydrogenolysis (reaction 8). Although propane hydrogenolysis has not been reported in aqueous phase, it is known to be readily catalyzed by Rh in this temperature range in gas phase (Bond et al., 1996).

Methanation (reaction 6) has been reported on Rh in APR (Davda et al., 2003); however, methanation is slow at the low

temperature of operation (Mutz et al., 2015). We speculate that the dominant pathway to methane is hydrogenolysis of propane based on the observation that the methane selectivity (**Figure 7C**) is very similar to the C_2 selectivity (sum of ethane and ethylene in **Figures 8A,B**), consistent with formation of methane, ethane and ethylene according reactions 8 and 9. Interestingly, selectivity of both methane and C_2 increase when operating with smaller catalyst particles.

Reforming of hydrocarbons (an aggregate reaction 10) probably contributes, possibly via the activation mechanism discussed above, based on three observations. First, on all catalysts the selectivity to CO_2 (**Figure 7B**) is higher than 1 mol/mol butanol, indicating that next to reactions 3 and 4 an additional pathway to CO_2 must exist. Second, H_2 formation via exclusively the sequence dehydrogenation-decarbonylation-WGS (reactions 1, 3, 5) would result in selectivity to hydrogen of 2 mol per mole butanol converted. **Figure 7A** shows that the H_2 selectivity varies between 3 and 6, providing clear evidence that an additional pathway contributes significantly. Third, the combined selectivity of C_{2-3} products (**Figure 8**) is <1 mol per mol butanol converted, clearly indicating that C_{2-3} products are being consumed in a consecutive reaction, most likely reforming. In addition to experimental observations, Rh is more active for steam reforming at low temperature compared to e.g., Pt or Ni (Kolb et al., 2004; Halabi et al., 2010), supporting the suggestion that reforming of alkanes contributes at the temperatures used in the present work. Further research would be needed to confirm this hypothesis.

Effect of Mass Transfer

Internal mass transfer can affect the local concentration of reactants as well as intermediate reaction products, possibly affecting the consecutive reactions and therefore the final product distribution. The data shows several clear trends as discussed below.

Butanol conversion is limited by diffusion in large catalyst particles. **Figure 5A** shows that conversion of butanol over the 250–420 μm catalyst is lower than over the smaller catalyst particles, whereas the conversion is similar over both of the smaller particle sizes. This indicates that diffusion limits the reaction on large catalyst particles, in agreement with the estimated values of Weisz-Prater criterion in **Figure 9**. Possibly, subtle differences in the metal dispersion, metal loading and metal surface area (**Table 3**) cause the relative high activity of the 60–100 μm fraction. On the other hand, difference in performance between the 40–60 μm fraction and the 250–420 μm fraction are clearly due to mass transfer effects.

Butyraldehyde coupling is enhanced on large particles as the selectivity to butyric-acid is higher on the larger particles (**Figure 6B**). The Tishchenko coupling reaction (reaction 2) is 2nd order (Anderson and Peters, 1960) and thus rates are strongly influenced by the butyraldehyde concentration. Slow diffusion increases the local concentration of butyraldehyde in the center of the catalyst particles, thus resulting in high butyric-acid yield.

Conversion of hydrocarbons is enhanced on large catalyst particles, including dehydrogenation (reaction 7), hydrogenolysis (reaction 8), and reforming (reactions 6, 10). This is based on three observations. First, the selectivity to methane (**Figure 7C**) and C_{2-3} hydrocarbons (**Figure 8**) is the lowest on large catalyst particles, suggesting more reforming, attributed to sluggish diffusion of dissolved $C_{1,2,3}$ hydrocarbons. Second, the ratio of olefins to alkanes is at the same time higher on the large catalyst particles, indicative for more dehydrogenation. Third, CO_2 selectivity (**Figure 7B**) is the highest over the large catalyst particles. Furthermore, the CO_2 selectivity is well above 1 mol per mol butanol converted, especially on large catalyst particles (**Figure 7B**), also indicating reforming activity as discussed above. The products of reactions 3 and 4 (i.e., CO, CO_2, and propane) are all gasses and diffusion out of the catalyst particles is controlled by diffusion of these molecules dissolved in water. However, the H_2 selectivity decreases with catalyst particle size (**Figure 7A**) despite reforming activity of large particles, indicating that longer diffusion length increases consecutive reactions consuming hydrogen more than consecutive reactions producing hydrogen.

This argument is analogous to the mechanism proposed by Neira D'Angelo et al. (2013), accounting for decreasing H_2 yield in case of mass transfer limitation because of the lower selectivity, while the conversion is not strongly affected. The difference in the operation of the reactors should be noted. In our case, we do not co-feed any gas, and formation of gas phase can occur only via nucleation of oversaturated solutions. In the case of Neira D'Angelo et al. (2013) as well as most APR studies in continuous operation, inert gas is added to the reactant stream and the reactor operated in trickle-phase mode, resulting in stripping of gaseous components in the reactor. This will enhance internal diffusion by decreasing the concentration at the external surface of the catalyst particles, i.e., in the bulk of the liquid. Therefore, our experiments are more sensitive for effects of internal diffusion of intermediate products.

The particle size affects not only the liquid and gaseous products distribution, but also strongly influences the stability of the catalyst. As reported in **Figure 5B**, the gas selectivity declined slowly for the 40–60 and 60–100 μm catalysts, while decreasing significantly for the 250–420 μm catalyst. This can be understood considering the high butyraldehyde concentration present inside the large catalyst particles. The aldehyde is a precursor of deposits via aldol-condensation reactions enhanced by the acid-base properties of the zirconia support, causing deactivation of the catalyst (Takanabe et al., 2006; Koichumanova et al., 2018). This hypothesis is also supported by the fact that larger particles form more deposits (**Figure 4**) and the high oxygen and hydrogen content of the deposits agrees with formation via butyraldehyde condensation, similar to results with the same catalyst system in gas phase reforming (Harju et al., 2016). Furthermore, it is also clear that larger support particles suffer more from Rh leaching than small particles (**Table 2**) which is in line with the fact that the formation of butyric acid is enhanced, resulting in more acidic conditions inside the larger catalyst particles, enhancing leaching.

Finally, it should be noted that description of internal mass transfer according Thiele modulus and Weisz-Prater criterion can be criticized for the case of APR. These models assume molecular diffusion of dissolved species in pores filled with water. However, APR produces molecules (H_2, CO, CO_2, CH_4, and other light hydrocarbons) that are forming a new phase during the reaction, i.e., gas phase. The critical question is whether bubbles form inside or outside the catalyst particles and at this time this question remains unanswered. Theoretical work of Datsevich (2003a; 2003b; 2004; 2005, Oehmichen et al., 2010) has shown that formation of gas bubbles can influence transfer inside particles dramatically, whereas we have recently demonstrated in a microfluidic device, mimicking pores in a catalyst support, that both retardation as well as enhancement of transport on the pore is possible (Espinosa et al., 2018). Very recently, a simulation using APR of glycerol as model reaction showed the effect of bubbles on the kinetics and transport phenomena in a 2D system (Ripken et al., 2019). This clearly needs further research to decide if such effects experimentally contribute in practical 3D porous catalysts.

CONCLUSIONS

The influence of internal mass transfer in Rh/ZrO_2 catalysts for APR of 1-butanol was studied by varying the support particle size. Larger support particles cause a minor but significant decrease in activity, which can be attributed to internal mass transfer limitations. The effect on selectivity and stability is much stronger though.

A reaction scheme is proposed in order to discuss the effects of internal mass transfer on product distribution and stability. The reaction scheme includes three main stages i.e., (1) formation of liquid intermediates via dehydrogenation, (2) formation of gas via decarbonylation/decarboxylation reactions and (3) hydrocarbon hydrogenolysis/reforming/dehydrogenation. The main pathway to hydrogen involves stages 1 and 2, while methane, ethane, and ethylene are formed via hydrogenolysis of propane.

Internal mass transport limitation of butyraldehyde enhances formation of butyric acid. Slow diffusion of methane, ethane, and propane dissolved in water promotes consecutive reactions, i.e., dehydrogenation, hydrogenolysis, and reforming. Furthermore, large support particles deactivate faster, attributed to high concentrations of butyraldehyde inside the catalyst particles, enhancing deposit formation via aldol condensation reactions, as well as to local high acidity caused by butyric acid.

DATA AVAILABILITY STATEMENT

The datasets generated for this study are available on request to the corresponding author.

AUTHOR CONTRIBUTIONS

HH and LL: conceptualization, methodology, validation, formal analysis, investigation, project administ, and ration. LL: resources, supervision, and funding acquisition. HH, GP, and LL: data curation and writing—review and editing. HH: writing—original draft preparation.

FUNDING

The authors declare that this study received funding from TEKES. The funder was not involved in the study design, collection, analysis, interpretation of data, the writing of this article or the decision to submit it for publication.

ACKNOWLEDGMENTS

The authors thank Ing. B. Geerdink and K. Altena-Schildkamp for technical assistance, Dr. Kaisa Vikla for performing part of the experiments and Ellen de Wit for the preliminary aging experiments. The XRF analyses were made with the assistance of Dr. Esko Ahvenniemi. This work made use of the Aalto University Nanomicroscopy Center (Aalto-NMC) premises. Dr. Hua Jiang is acknowledged for performing the microscopy.

SUPPLEMENTARY MATERIAL

The Supplementary Material for this article can be found online at: https://www.frontiersin.org/articles/10.3389/fchem.2020.00017/full#supplementary-material

REFERENCES

Anderson, J. B., and Peters, M. S. (1960). Acetaldehyde aldol condensation kinetics. *J. Chem. Eng. Data* 5, 359–364. doi: 10.1021/je60007a033

Balat, H., and Kirtay, E. (2010). Hydrogen from biomass - present scenario and future prospects. *Int. J. Hydrogen Energy* 35, 7416–7426. doi: 10.1016/j.ijhydene.2010.04.137

Bie, Y., Gutierrez, A., Viljava, T. R., Kanervo, J. M., and Lehtonen, J. (2013). Hydrodeoxygenation of methyl heptanoate over noble metal catalysts: catalyst screening and reaction network. *Ind. Eng. Chem. Res.* 52, 11544–11551. doi: 10.1021/ie4012485

Bond, G. C., Calhoun, J., and Hooper, A. D. (1996). Hydrogenolysis of propane and n-butane over rhodium catalysts. *J. Chem. Soc. Trans.* 92, 5117–5128. doi: 10.1039/ft9969205117

Coronado, I., Pitínová, M., Karinen, R., Reinikainen, M., Puurunen, R. L., and Lehtonen, J. (2018). Aqueous-phase reforming of Fischer-Tropsch alcohols over nickel-based catalysts to produce hydrogen: Product distribution and reaction pathways. *Appl. Catal. A Gen.* 567, 112–121. doi: 10.1016/j.apcata.2018.09.013

Cortright, R. D., Davda, R. R., and Dumesic, J. A. (2002). Hydrogen from catalytic reforming of biomass-derived hydrocarbons in liquid water. *Nature* 418, 964–967. doi: 10.1038/nature01009

Datsevich, L. B. (2003a). Alternating motion of liquid in catalyst pores in a liquid/liquid-gas reaction with heat or gas production. *Catal. Today* 79–80, 341–348. doi: 10.1016/S0920-5861(03)00061-0

Datsevich, L. B. (2003b). Some theoretical aspects of catalyst behaviour in a catalyst particle at liquid (liquid–gas) reactions with gas production:

oscillation motion in the catalyst pores. *Appl. Catal. A Gen.* 247, 101–111. doi: 10.1016/S0926-860X(03)00091-7

Datsevich, L. B. (2004). Oscillation theory: Part 1. Temperature difference between the center of a catalyst particle and its surface: contradiction to Thiele/Zeldovich model. *Appl. Catal. A Gen.* 262, 149–153. doi: 10.1016/j.apcata.2003.11.023

Datsevich, L. B. (2005). Oscillation theory: Part 4. Some dynamic peculiarities of motion in catalyst pores. *Appl. Catal. A Gen.* 294, 22–33. doi: 10.1016/j.apcata.2005.06.024

Davda, R. R., Shabaker, J. W., Huber, G. W., Cortright, R. D., and Dumesic, J. A. (2003). Aqueous-phase reforming of ethylene glycol on silica-supported metal catalysts. *Appl. Catal. B Environ.* 43, 13–26. doi: 10.1016/S0926-3373(02)00277-1

Davda, R. R., Shabaker, J. W., Huber, G. W., Cortright, R. D., and Dumesic, J. A. (2005). A review of catalytic issues and process conditions for renewable hydrogen and alkanes by aqueous-phase reforming of oxygenated hydrocarbons over supported metal catalysts. *Appl. Catal. B Environ.* 56, 171–186. doi: 10.1016/j.apcatb.2004.04.027

De Vlieger, D. J. M., Mojet, B. L., Lefferts, L., and Seshan, K. (2012). Aqueous phase reforming of ethylene glycol - role of intermediates in catalyst performance. *J. Catal.* 292, 239–245. doi: 10.1016/j.jcat.2012.05.019

Elliott, D. C., Sealock, L. J., and Baker, E. G. (1993). Chemical processing in high-pressure aqueous environments. 2. Development of catalysts for gasification. *Ind. Eng. Chem. Res.* 32, 1542–1548. doi: 10.1021/ie00020a002

Espinosa, R. B., Duits, M. H. G., Wijnperlé, D., Mugele, F., and Lefferts, L. (2018). Bubble formation in catalyst pores; curse or blessing? *React. Chem. Eng.* 3, 826–833. doi: 10.1039/C8RE00110C

Godina, L. I., Tokarev, A. V., Simakova, I. L., Mäki-Arvela, P., Kortesmäki, E., Gläsel, J., et al. (2018). Aqueous-phase reforming of alcohols with three carbon atoms on carbon-supported Pt. *Catal. Today* 301, 78–89. doi: 10.1016/j.cattod.2017.03.042

Gutiérrez Ortiz, F. J., and Campanario, F. J. (2018). Hydrogen production from supercritical water reforming of acetic acid, acetol, 1-butanol and glucose over Ni-based catalyst. *J. Supercrit. Fluids* 138, 259–270. doi: 10.1016/j.supflu.2018.04.023

Gutiérrez Ortiz, F. J., Campanario, F. J., and Ollero, P. (2016). Supercritical water reforming of model compounds of bio-oil aqueous phase: acetic acid, acetol, butanol and glucose. *Chem. Eng. J.* 298, 243–258. doi: 10.1016/j.cej.2016.04.002

Halabi, M. H., De Croon, M. H. J. M., Van Der Schaaf, J., Cobden, P. D., and Schouten, J. C. (2010). Low temperature catalytic methane steam reforming over ceria-zirconia supported rhodium. *Appl. Catal. A Gen.* 389, 68–79. doi: 10.1016/j.apcata.2010.09.004

Harju, H., Lehtonen, J., and Lefferts, L. (2015). Steam- and autothermal-reforming of n-butanol over Rh/ZrO_2 catalyst. *Catal. Today* 244, 47–57. doi: 10.1016/j.cattod.2014.08.013

Harju, H., Lehtonen, J., and Lefferts, L. (2016). Steam reforming of n-butanol over Rh/ZrO_2 catalyst: role of 1-butene and butyraldehyde. *Appl. Catal. B Environ.* 182, 33–46. doi: 10.1016/j.apcatb.2015.09.009

Kaila, R. K., Gutiérrez, A., Korhonen, S. T., and Krause, A. O. I. (2007). Autothermal reforming of n-dodecane, toluene, and their mixture on mono- and bimetallic noble metal zirconia catalysts. *Catal. Lett.* 115, 70–78. doi: 10.1007/s10562-007-9075-z

Kaila, R. K., Gutiérrez, A., Slioor, R., Kemell, M., Leskelä, M., and Krause, A. O. I. (2008). Zirconia-supported bimetallic RhPt catalysts: characterization and testing in autothermal reforming of simulated gasoline. *Appl. Catal. B Environ.* 84, 223–232. doi: 10.1016/j.apcatb.2008.04.001

Kirilin, A. V., Tokarev, A. V., Manyar, H., Hardacre, C., Salmi, T., Mikkola, J. P., et al. (2014). Aqueous phase reforming of xylitol over Pt-Re bimetallic catalyst: effect of the re addition. *Catal. Today* 223, 97–107. doi: 10.1016/j.cattod.2013.09.020

Kirilin, A. V., Tokarev, A. V., Murzina, E. V., Kustov, L. M., Mikkola, J. P., and Murzin, D. Y. (2010). Reaction products and transformations of intermediates in the aqueous-phase reforming of sorbitol. *ChemSusChem* 3, 708–718. doi: 10.1002/cssc.200900254

Koichumanova, K., Vikla, A. K. K., Cortese, R., Ferrante, F., Seshan, K., Duca, D., et al. (2018). *In situ* ATR-IR studies in aqueous phase reforming of hydroxyacetone on Pt/ZrO_2 and Pt/AlO(OH) catalysts: The role of aldol condensation. *Appl. Catal. B Environ.* 232, 454–463. doi: 10.1016/j.apcatb.2018.03.090

Kolb, G., Zapf, R., Hessel, V., and Löwe, H. (2004). Propane steam reforming in micro-channels-results from catalyst screening and optimisation. *Appl. Catal. A Gen.* 277, 155–166. doi: 10.1016/j.apcata.2004.09.007

Kumar, B., Kumar, S., and Kumar, S. (2017). Butanol reforming: An overview on recent developments and future aspects. *Rev. Chem. Eng.* 34, 1–19. doi: 10.1515/revce-2016-0045

Larimi, A., and Khorasheh, F. (2019). Renewable hydrogen production over Pt/Al2O3 nano-catalysts: effect of M-promoting (M=Pd, Rh, Re, Ru, Ir, Cr). *Int. J. Hydrogen Energy* 44, 8243–8251. doi: 10.1016/j.ijhydene.2019.01.251

Lobo, R., Marshall, C. L., Dietrich, P. J., Ribeiro, F. H., Akatay, C., Stach, E. A., et al. (2012). Understanding the chemistry of H2 production for 1-propanol reforming: pathway and support modification effects. *ACS Catal.* 2, 2316–2326. doi: 10.1021/cs300405s

Mears, D. E. (1971). Tests for transport limitations in experimental catalytic reactors. *Ind. Eng. Chem. Process Des. Dev.* 10, 541–547. doi: 10.1021/i260040a020

Miao, C., Marin-Flores, O., Davidson, S. D., Li, T., Dong, T., Gao, D., et al. (2016). Hydrothermal catalytic deoxygenation of palmitic acid over nickel catalyst. *Fuel* 166, 302–308. doi: 10.1016/j.fuel.2015.10.120

Mutz, B., Carvalho, H. W. P., Mangold, S., Kleist, W., and Grunwaldt, J. D. (2015). Methanation of CO_2: structural response of a Ni-based catalyst under fluctuating reaction conditions unraveled by operando spectroscopy. *J. Catal.* 327, 48–53. doi: 10.1016/j.jcat.2015.04.006

Neira D'Angelo, M. F., Ordomsky, V., Van Der Schaaf, J., Schouten, J. C., and Nijhuis, T. A. (2013). Aqueous phase reforming in a microchannel reactor: the effect of mass transfer on hydrogen selectivity. *Catal. Sci. Technol.* 3, 2834–2842. doi: 10.1039/c3cy00577a

Neira D'Angelo, M. F., Ordomsky, V., Van Der Schaaf, J., Schouten, J. C., and Nijhuis, T. A. (2014a). Continuous hydrogen stripping during aqueous phase reforming of sorbitol in a washcoated microchannel reactor with a Pt-Ru bimetallic catalyst. *Int. J. Hydrogen Energy* 39, 18069–18076. doi: 10.1016/j.ijhydene.2014.02.167

Neira D'Angelo, M. F., Schouten, J. C., Van Der Schaaf, J., and Nijhuis, T. A. (2014b). Three-phase reactor model for the aqueous phase reforming of ethylene glycol. *Ind. Eng. Chem. Res.* 53, 13892–13902. doi: 10.1021/ie5007382

Oehmichen, T., Datsevich, L. B., and Jess, A. (2010). Influence of bubble evolution on the effective kinetics of heterogeneously catalyzed gas/liquid reactions. Part I: reactions with gaseous products. *Chem. Eng. Technol.* 33, 911–920. doi: 10.1002/ceat.200900624

Pipitone, G., Zoppi, G., Ansaloni, S., Bocchini, S., Deorsola, F. A., Pirone, R., et al. (2019). Towards the sustainable hydrogen production by catalytic conversion of C-laden biorefinery aqueous streams. *Chem. Eng. J.* 377:120677. doi: 10.1016/j.cej.2018.12.137

Ripken, R. M., Wood, J. A., Gardeniers, J. G. E., and Le Gac, S. (2019). Aqueous-phase reforming in a microreactor: the role of surface bubbles. *Chem. Eng. Technol.* 42, 1–9. doi: 10.1002/ceat.201900142

Roy, B., Sullivan, H., and Leclerc, C. A. (2011). Aqueous-phase reforming of n-BuOH over Ni/Al_2O_3 and Ni/CeO_2 catalysts. *J. Power Sources* 196, 10652–10657. doi: 10.1016/j.jpowsour.2011.08.093

Roy, B., Sullivan, H., and Leclerc, C. A. (2014). Effect of variable conditions on steam reforming and aqueous phase reforming of n-butanol over Ni/CeO_2 and $Ni/Al2O_3$ catalysts. *J. Power Sources* 267, 280–287. doi: 10.1016/j.jpowsour.2014.05.090

Sabatier, P., and Mailhe, A. (1910). Actions des oxydes métalliques sur les alcools pirmaires. *Ann. Chim. Phys.* 20, 289–352.

Shabaker, J. W., Davda, R. R., Huber, G. W., Cortright, R. D., and Dumesic, J. A. (2003a). Aqueous-phase reforming of methanol and ethylene glycol over alumina-supported platinum catalysts. *J. Catal.* 215, 344–352. doi: 10.1016/S0021-9517(03)00032-0

Shabaker, J. W., Huber, G. W., Davda, R. R., Cortright, R. D., and Dumesic, J. A. (2003b). Aqueous-phase reforming of ethylene glycol over supported platinum catalysts. *Catal. Letters.* 88, 1–8. doi: 10.1023/A:1023538917186

Shinohara, Y., Nakajima, T., Suzuki, S., Mishima, S., and Ishikawa, H. (1997). A computational chemical investigation of the dehydration and dehydrogenation of ethanol on oxide catalysts. *J. Chem. Softw.* 4:89. doi: 10.2477/jchemsoft.4.89

Sinfelt, J. H. (1973). Specificity in catalytic hydrogenolysis by metals. *Adv. Catal.* 23, 91–119. doi: 10.1016/S0360-0564(08)60299-0

Takanabe, K., Aika, K., Ken-ichi, A., Seshan, K., and Lefferts, L. (2006). Catalyst deactivation during steam reforming of acetic acid over Pt/ZrO_2. *Chem. Eng. J.* 120, 133–137. doi: 10.1016/j.cej.2006.04.001

Wawrzetz, A., Peng, B., Hrabar, A., Jentys, A., Lemonidou, A. A., and Lercher, J. A. (2010). Towards understanding the bifunctional hydrodeoxygenation and aqueous phase reforming of glycerol. *J. Catal.* 269, 411–420. doi: 10.1016/j.jcat.2009.11.027

Weisz, P. B., and Prater, C. D. (1954). Interpretation of measurements in experimental catalysis. *Adv. Catal.* 6, 143–196. doi: 10.1016/S0360-0564(08)60390-9

Conflict of Interest: The authors declare that the research was conducted in the absence of any commercial or financial relationships that could be construed as a potential conflict of interest.

frontiers in Chemistry

ORIGINAL RESEARCH
published: 29 January 2020
doi: 10.3389/fchem.2020.00024

Conversion of Biomass to Organic Acids by Liquefaction Reactions Under Subcritical Conditions

*Aslı Yüksel Özşen**

Department of Chemical Engineering, Faculty of Engineering, Izmir Institute of Technology, Izmir, Turkey

Recently, liquefaction of biomass in subcritical water to convert it into value-added substances has been broadly attracting attention. However, there is a gap in literature about the levulinic acid, which is a high worth substance, production from biomass using subcritical water. As a green chemistry approach, decomposition of biomass could be obtained using subcritical water effectively. In this case, water uses as a solvent so that it gives a possibility to take place a reaction for the decomposition of biomass. Subcritical water, which liquid water and its temperature is higher than the normal boiling point of water, has higher ion product as well as higher concentrations of H^+ and OH^- ions. Additionally, it has high diffusivity, low viscosity and much lower dielectric constant. For instance, whereas dielectric constant of subcritical water is 80 at 298 K, it is 2 at 673 K. The point of this research paper is to assess the impacts of different reaction parameters on cellulose conversion as the principle segment of lignocellulosic biomasses for the production of value-added chemicals, particularly levulinic acid. Hazelnut shell waste was chosen as model biomass since hazelnut is a standout amongst the most cultivated agricultural crops in Turkey. Besides, Turkey provide 70% of the world's total hazelnut production. It was found that as reaction temperature increases, a considerable improvement on the amount of formed levulinic acid and conversion of hazelnut shell was observed. For instance, when the reaction temperature, time and acid concentration were 280°C, 120 min and 50 mM, respectively, levulinic acid yield and conversion of hazelnut shell were found as 13.05 and 65.40%, respectively. Addition of H_2SO_4 enhanced the production of levulinic acid from waste hazelnut shell. Another method which is hybrid process could be used to produce value-added chemicals from lignocellulosic biomass. Hybrid process basically combines hydrolysis and electrolysis in subcritical water. Subcritical water has much lower dielectric constant than liquid water at ambient temperature. So, it was claimed that if constant current was applied to the reaction medium through specially designed electrodes in subcritical water environment, electrolysis could alter the hydrolysis reaction of cellulose in a way of protonation of intra-and inter-molecular hydrogen bonding around anode and as a result electrolysis in subcritical water could decrease necessary thermal energy to hydrolyze the β(1–4) glycosidic linkage. Therefore, we developed a green hybrid process by combining hydrolysis and electrolysis in subcritical water without using any toxic, organic solvents and catalyst. Effects of especially applied current and temperature on the product distribution and conversions of cellulose were revealed and hydrothermal electrolysis

OPEN ACCESS

Edited by:
Dmitry Yu. Murzin,
Åbo Akademi University, Finland

Reviewed by:
Zhibao Huo,
Shanghai Ocean University, China
Priyanka Sharma,
Stony Brook University, United States

***Correspondence:**
Aslı Yüksel Özşen
asliyuksel@iyte.edu.tr

Specialty section:
This article was submitted to Green and Sustainable Chemistry, a section of the journal Frontiers in Chemistry

Received: *21 October 2019*
Accepted: *09 January 2020*
Published: *29 January 2020*

Citation:
Yüksel Özşen A (2020) Conversion of Biomass to Organic Acids by Liquefaction Reactions Under Subcritical Conditions. Front. Chem. 8:24. doi: 10.3389/fchem.2020.00024

reaction pathway of cellulose was proposed. The significance of the interaction indicated that, applied voltage had major impact on cellulose hydrolysis. Maximum cellulose conversion (82%) was achieved at 230°C and 180 min of reaction time in 25 mM of H_2SO_4. Application of 8.0 V of applied voltage to the reaction medium at reaction temperature of 230°C increased the TOC conversion (50.3%) with acid concentration of 25 mM in comparison with current-free experiments. Thus, the idea of electrochemically generated acid layer due to the dissociation of water around anode is supported. As future perspective, the output of the study gave an idea about converting cellulose and various biomass wastes, which may have high cellulose, content and led the way in obtaining valuable chemicals from no utilized real biomass sources such as hazelnut shell waste. The studies with other biomasses are undergoing.

Keywords: biomass, subcritical water, liquefaction, hydrolysis, electrolysis, levulinic acid

INTRODUCTION

According to BP Energy Outlook 2035 in period from 2013 to 2035 global demand of energy and CO_2 emissions will increase by 37 and 25%, respectively. Biomass is a renewable energy source and the interest for biomass increases day by day. Since 50% of total biomass consists of plant-derived or lignocellulosic biomass and its content made-up from cellulose (38–50%), which is one of the most prevalent organic compounds in the World, hemicelluloses (23–32%), and lignin (15–25%) (Toor et al., 2011).

In this study, microcrystalline cellulose was used as model compound due to its crystalline structure that makes it insoluble and resistant to attack by catalyst. Cellulose has hydrogen bonds which are intra- and intermolecular, so that it has low solubility and high rigid structure (**Figure 1**, arrows). The challenge regarding the solvability of cellulose arises due to the intermolecular hydrogen bonds, which make intermolecular bonds inaccessible to solvent compound. Due to this structure, cellulose does not swell in water as well as it has a resistance against enzymes. However, reported studies showed that hot compressed water can rapidly solubilize cellulose and hydrolyze to its building block as glucose (Sasaki et al., 2004; Knezevic et al., 2009).

Liquefaction of cellulose in subcritical water conditions is one of the most attractive techniques for the production of high value chemicals since water has several advantages against other organic solvents. For instance, water is cheaper than other solvents and it is non-toxic, non-flammable as well as non-explosive. While water becomes a good solvent when its pressure and temperature approach its critical point, it is called as hot-pressurized water. It has a unique characteristic and its thermodynamic properties such as density, dielectric constant, viscosity, ion product, and solvating power could be tuned so that it becomes more effective on decomposition of cellulose (Savage, 1999; Yüksel, 2016).

Cellulose, a model compound, was used for the hydrothermal production of different high-value products. For instance, Saito et al. (2009) investigated the decomposition of cellulose in hot-pressurized water at 200–240°C and 15–20 MPa for 50–120 s. After 120 s, 2-furfural, 5-HMF, glycolic acid, lactic acid, and formic acid formed in high yields. Williams and Onwudili (2006) was studied about the decomposition of model compounds, which are cellulose, glucose, starch, and cassava waste, using sub- and supercritical water. These model compounds decompose to gaseous products carbon dioxide, carbon monoxide, hydrogen, and methane as well as oil and char also formed. Product distribution and gas yield was varied depending on model compound and reaction temperature. For instance, if cellulose is used as a model compound, then high yield of carbon monoxide and char is observed. Additionally, C1 and C4 hydrocarbons were formed (Yüksel, 2016). Ehara and Saka (2005) investigated the treatment of cellulose in three different systems which are sub- and supercritical water and their combined system. In each system, different yields of organics were obtained, however, precipitation was not observed in combined system. Water conditions has more effect over the reaction rate as well as decomposition mechanism of cellulose.

Levulinic acid, furfural and acetic acid are an example for bio-based chemicals and they can form by the decomposition of different types of biomass. It can be said that levulinic acid is a versatile chemical and it is in the list of Top Value-Added Chemicals from Biomass. Pharmaceutical and flavoring agents, resins, herbicides, plasticisers, anti-freeze agents, and biofuel additives can be derived from levulinic acid (Yüksel, 2016). Based on the present knowledge, firstly, hexose sugars dehydrate and the intermediate product 5-hydroxymethylfurfural (5-HMF) forms. After that, 5-HMF hydrates by the addition of water to C2–C3 bond the furan ring so that final products (levulinic and formic acids) form at the same stoichiometric ratio (Horvat et al., 1985; Asghari and Yoshida, 2010).

As model lignocellulosic biomass, waste hazelnut shell was selected since hazelnut is a considerable amount of agricultural crop in Turkey. Hazelnut produces 650,000 tons/year over the World and Turkey supplies 75% of it. During hazelnut processing, waste hazelnut shells form in large quantities and they are mainly used for heating (Guney, 2013). Hence, waste hazelnut shells could utilize to produce value-added chemicals so that they could not only be a natural alternative resource but also contribute in value gaining (Gozaydin and Yuksel, 2017).

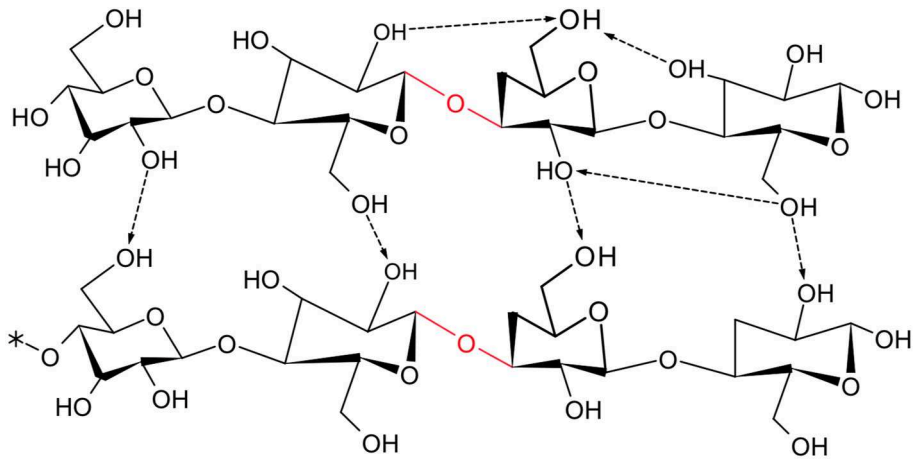

FIGURE 1 | Structure of microcrystalline cellulose with ending and repeating group.

In literature, there are several researches about the natural biomass decomposition in subcritical water. Chan et al. (2014) studied over the comparison of the decomposition of empty fruit bunch, palm mesocarp fiber and palm kernel shell by sub- and supercritical hydrothermal liquefaction. The results show that while phenolic compounds formed from palm mesocarp fiber and palm kernel shell at higher amounts, ester were only produced when palm kernel shell was used. Kruse and Gawlik (2003) investigated to description of possible reaction pathways of degradation of phytomass (mainly consist of cooked carrots and potatoes). According to the results, the degradation of HMF can be observed by two different pathways which are the formation of 1,2,4-benzenetriol and levulinic acid (via acid catalyst). Cheng et al. (2009) studied over the hydrothermal degradation of switchgrass. In this study, the highest conversion, desired product yield (5-HMF and furfural) and 90% of rapid switchgrass conversion were observed when the reaction temperature, pressure and residence time are 250–350°C, 20 MPa and 1–300 s, respectively. Asghari and Yoshida (2010) investigated the effect of dilute phosphate buffer (at pH 2) over the degradation of Japanese red pinewood in subcritical water. It was concluded that the Japanese red pine wood converted into higher amount of sugars within shorter time compared to uncatalyzed conditions. By the help of further treatment, the yield of HMF and furfural were almost doubled. The study of Tymchyshyn and Xu (2010) show that the sawdust and cornstalks was degraded into phenolic compounds at 250–350°C and 2 MPa H_2 in the presence of $Ba(OH)_2$ and $RbCO_3$ catalysts. Bio-oil yield enhanced by the addition of catalysts.

Electrochemical methods such as electrochemical degradation of lignin (Zhang et al., 2014), and electrolysis of corn stover to sugars (Xu et al., 2014) have also been reported. According to the literature, most of the electrochemical reactions were performed in ambient conditions. As novel approach, we developed a hybrid process, which basically combines hydrolysis and electrolysis in subcritical water to produce of high value chemicals from different types of biomass. Subcritical water has much lower dielectric constant than liquid water at ambient temperature. So, it was claimed that if constant current was applied to the reaction medium through specially designed electrodes in subcritical water environment, electrolysis could alter the hydrolysis reaction of cellulose in a way of protonation of intra- and inter-molecular hydrogen bonding around anode and as a result electrolysis in subcritical water could decrease necessary thermal energy to hydrolyze the β(1–4)glycosidic linkage. Therefore, we developed a green hybrid process by combining hydrolysis and electrolysis in subcritical water without using any toxic, organic solvents and catalyst. This hybrid process is applied on cellulose for the first time and synergetic effects of especially applied current and temperature on the product distribution and conversions of cellulose and total organic carbon (TOC) in the liquid product solution were revealed (Akin and Yuksel, 2016, 2017).

This green hybrid process named as hydrothermal electrolysis was conducted in a specially designed batch reactor (450 mL) in which cylindrical type titanium electrode was used as anode and reactor wall was behaved as cathode. In this research activity, effects of different parameters which are direct current, temperature, time and proton donor (sulfuric acid) concentration on the conversion of cellulose were investigated. The conversion of TOC and yields of products (5-HMF, levulinic acid, and furfural) were determined.

After obtaining the optimum conditions, it was proposed when constant voltage is applied, the degradation mechanism of cellulose and hydrolysis product distribution can selectively change. Constant voltage ranges from 4.0 to 8.0 V was applied between anode and cathode. 25 mM of H_2SO_4 was used as an electrolyte and also be a proton source. Hydrothermal electrolysis products of cellulose were investigated. After series of experiments, levulinic acid, 5-HMF and furfural was determined as the main decomposition products of cellulose by hydrothermal electrolysis. Detailed ionic and radical mechanisms of cellulose under constant voltage were revealed.

MATERIALS AND METHODS

Chemicals

All chemicals used in experiments were at analytical grade and all solutions were prepared using de-ionized water. Microcrystalline cellulose (MCC) was purchased from Sigma Aldrich. The standards of reagents used in HPLC analysis are fructose (≥99%), levulinic acid (98%), lactic acid (98%), glycerolaldehyde (99%), glycolaldehyde (99%), 5-HMF (99%), glycolic acid (99%), and pyruvic acid (98%) and they were purchased from Merck. Sulfuric acid (96–98%) was also obtained from Merck. Phosphoric acid (85–90%) were purchased from Fluka. Biomass feedstock, hazelnut shell, was supplied from Ordu, Turkey. Hazelnut shells were dried in an oven at 60°C and then, they ground into small pieces (∼1 mm) using a laboratory type grinder.

Product Analysis

Elemental analysis of hazelnut shell was performed via CHNS-932, Leco, USA branded elemental analyzer. Moisture and ash contents of hazelnut shell (biomass) were determined by Thermal Gravimetric Analysis (TGA-51, Shimadzu, Japan). Hazelnut shell contains cellulose, hemicellulose and lignin and their amount were determined by Van Soest Method (Gozaydin and Yuksel, 2017).

The concentration of liquid products was determined via High Performance Liquid Chromatography (HPLC) and Gas Chromatography with Mass Spectroscopy (GC–MS, Agilent 6890 N/5973 N Network) were used to identify the liquid products which were unidentified in HPLC analyses. In HPLC analysis, sugar column (Shodex, SH1100) was used to separate products clearly and the temperature of column was 40°C. 3.75 mM H_2SO_4 was used as eluent and its flow rate was 0.5 ml/min. Refractive index (RID) was used for detection of aldehydes and organic acids. TOC conversions in the liquid products were determined by TOC analyzer (Shimadzu TOC-VCPH).

Experimental Procedure

Experiments related to liquefaction of cellulose and hazelnut shell waste were performed in a Parr Instrument Company, USA branded 316 stainless steel autoclave (300 mL). The reactor equipped with gas inlet and outlet valves, liquid sampling valve, pressure gage, safety rupture disc, magnetic-driven impeller, internal thermocouple, and cooling loop (Gozaydin and Yuksel, 2017). Firstly, 4 g of biomass feedstock (cellulose, hazelnut shell waste) was placed into the reactor and then, 100 ml of de-ionized water was added to adjust the volume. After all the pins of reactor had been tightened, in order to remove the air inside the autoclave, the reactor was purged with nitrogen.

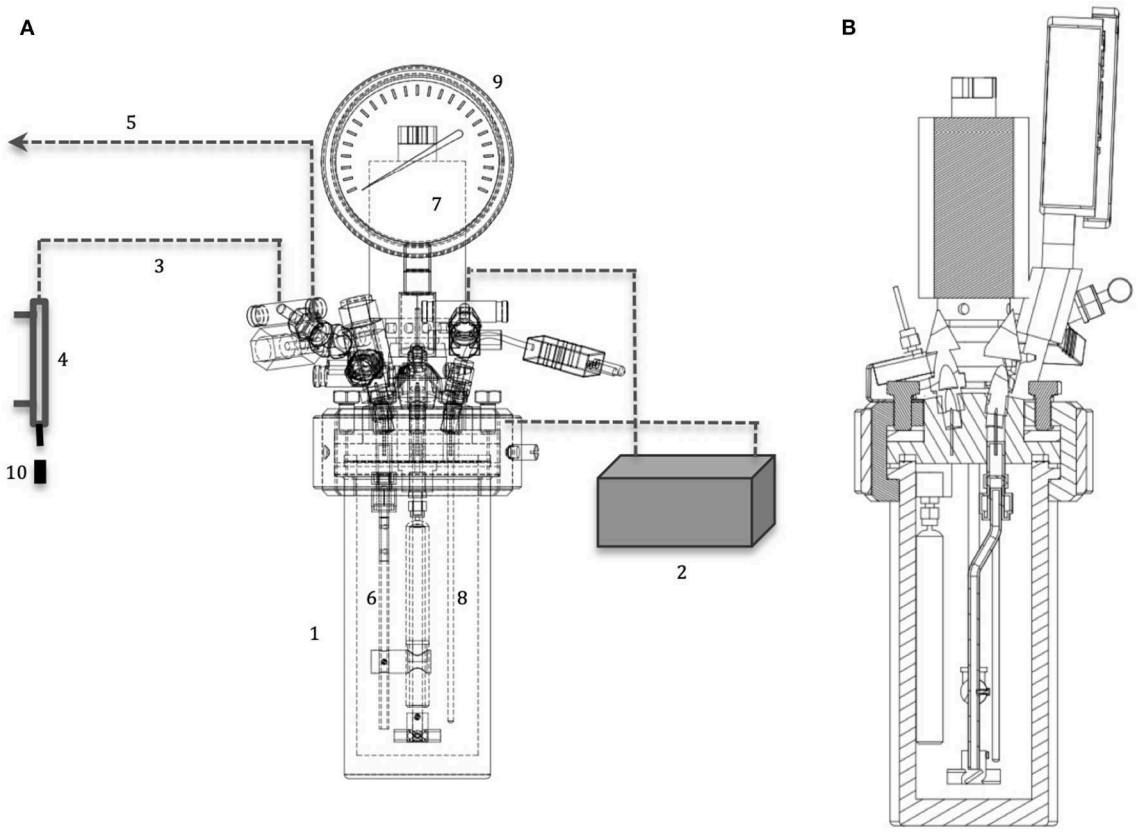

FIGURE 2 | (A) Auxiliary view of hydrothermal electrolysis reactor: (1) electrical heater, (2) dc power controller, (3) liquid sampling tubing, (4) heat exchanger, (5) gas sample collector, (6) anode, (7) rotor, (8) thermocouple, (9) pressure gauge, (10) sample holder; **(B)** section view of hydrothermal electrolysis reactor.

Then, the reaction temperature was set to the desired reaction temperature with stirring rate of 200–250 rpm throughout the experiment. Temperature and pressures were recorded at every 5 min until the temperature reached the desired reaction temperature. The temperature and internal pressure rose until reaching desired reaction temperature and then, the reaction was started for a certain reaction time. At the end of reaction time, the heater was turned off and the system was cooled to 40°C to collect the final products (Gozaydin and Yuksel, 2017).

Hydrothermal electrolysis experiments were performed in a 450 mL of SUS 316 stainless steel batch reactor (Parr 5500 series) with specially designed anode (titanium electrode) and it is illustrated in **Figure 2**.

Hydrothermal electrolysis experiments were carried out at a constant current (0–2 A) passing through the electrodes. Specially designed cylindrical type titanium electrode (D: 12 mm, L: 94 mm) was used as anode and cylindrical reactor wall (D_o: 76 mm, L: 165 mm) was acted as cathode. The experiments were carried out to understand the reaction pathway by using H_2SO_4 solution (25 mM) at 200°C and applying constant voltage (0, 4.0, and 8.0 V) for 180 min. Liquid samples were collected in every 30 min. after the desired reaction temperature was reached. Collected liquid samples were filtered and analyzed immediately without any further treatment (Akin and Yuksel, 2016).

$$\text{Yield of Product } \% = \frac{(\text{Number of carbon of species}) * (\text{Mole of species produced})}{\text{Moles of carbon in cellulose}} * 100 \quad (1)$$

$$\text{Converted Cellulose } \% = \frac{\textit{Initial amount of cellulose (gram)} - \textit{Residual amount at the end (gram)}}{\textit{Initial amount of cellulose (gram)}} * 100 \quad (2)$$

$$\text{Selectivity } \% = \frac{(\text{Number of carbon of species}) * (\text{Mole of species produced})}{\text{Total Moles of carbon (TOC) in liquid}} * 100 \quad (3)$$

RESULTS AND DISCUSSION

Liquefaction of Cellulose and Waste Hazelnut Shell

During this section, in order to investigate the effect of different parameters which are reaction temperature, initial pressure, reaction time, external oxidant concentration, the experiments were performed at 150, 200, 250, and 280°C and 0, 5, 10, and 15 bars for 30, 60, 90, and 120 min using 0, 5, 25, 50, 75, 100, and 125 mM H_2O_2 as an external oxidant. After degradation of microcrystalline cellulose with H_2SO_4 in hot-compressed water, liquid product consists of pyruvic acid, glycolaldehyde, glyceraldehyde, formic acid, glycolic acid, lactic acid, acetic acid, levulinic acid, 5-HMF, glycerol, and furfural was formed. Besides, in liquid product, some oligomers such as cellobiose, cellotriose, etc. and monomers such as glucose, fructose were also formed and they were identified HPLC analysis. HPLC analysis conditions were mentioned previously and HPLC chromatograms of the standard solutions are given in **Figure 3**.

According to the result of TOC analysis, the initial carbon amount of cellulose was determined as 42–45%. The yield of product % was determined using this data and the carbon number of products and the relation is given in Equation 1. Carbon balance was found to be more than 90% in all experiments. The conversion of cellulose and product selectivity were calculated using Equations (2) and (3), respectively.

Cellulose has glycosic bonds so that is show high chemical resistance. In order to break these bonds, subcritical water can be used. Hence, usage of subcritical water provides a favorable environment and reaction medium for degradation of cellulose to desired product (levulinic acid) (Cardenas-Toro et al., 2014). After breakdown of glycosic bonds, de-polymerization of cellulose is occurred and hence, oligosaccharides and monosaccharides (glucose) can formed. After that, hydrolysis and rearrangement/decomposition of glucose and other monomer sugars is occurred and thus, fructose, 5-HMF, furfural, pyruvaldehyde, glyceraldehyde, and glycolaldehyde are formed. Furthermore, hemicellulose is hydrolyzed into oligomers (low and high molecular weight), xylose, furfural, glycolaldehyde, and glyceraldehydes. At higher reaction temperatures, re-polymerization, isomerization and fragmentation of them take place in liquid, gaseous and solid products (Cardenas-Toro et al., 2014). Additionally, organic acids (levulinic acid (desired product), acetic acid, formic acid, etc.) are also formed. Cellulose conversion (%) and product yields (%) were calculated for different reaction temperatures and the results are given in **Figure 4**.

As seen in **Figure 4**, the degradation of cellulose was observed as 70% after 60 min at 280°C. The conversion of cellulose is very low when temperature and pressure 150°C and 5 bar, respectively. At this condition, initial amount of cellulose was 4 g and the remaining amount was 3.61 g. It could be concluded that this reaction temperature (150°C) and pressure (5 bar) was not enough to breakdown of glicosidic bonds of cellulose. However, when temperature was 200°C, whereas yield of desired product (levulinic acid) and degradation of cellulose was suddenly enhanced, the amount of 5-HMF in liquid product decreased to 1.7% (Yüksel, 2016). Thus, it could be concluded that cellulose could be degraded under hydrothermal conditions through two steps so liquid products were formed. Glucose isomerized to fructose at higher reaction temperatures and then, fructose converted to the main intermediate which is 5-HMF (Rosatella et al., 2011). After that, this intermediate leads to form various final compounds. One of the final products is levulinic acid and by-product of it is formic acid which is formed at higher reaction temperatures (Zeng et al., 2010; Rosatella et al., 2011; Cardenas-Toro et al., 2014). This obtained data from literature is matching with our findings. As shown in **Figure 4**, under the conditions with low concentrations of levulinic acid and formic acid were obtained, 5-HMF yield was low that shows the

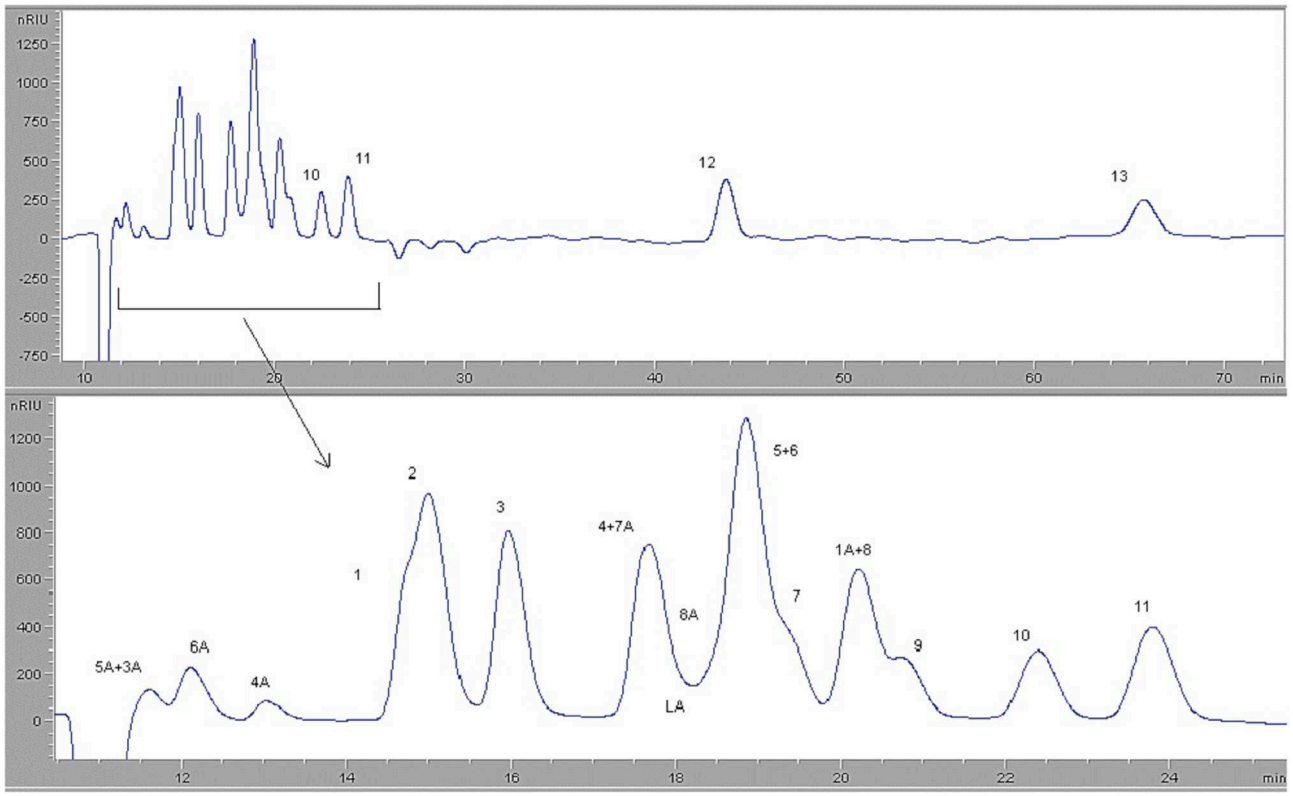

FIGURE 3 | HPLC chromatograms of standard compounds at column temperature of 40°C: (1) pyruvic acid, (2) glucose, (3) fructose, (4) DL-glyceraldehyde, (5) glycolic acid, (6) glycolaldehyde, (7) lactic acid, (8) glycerol, (9) formic acid, (10) acetic acid, (11) levulinic acid, (12) 5-HMF, (13) furfural.

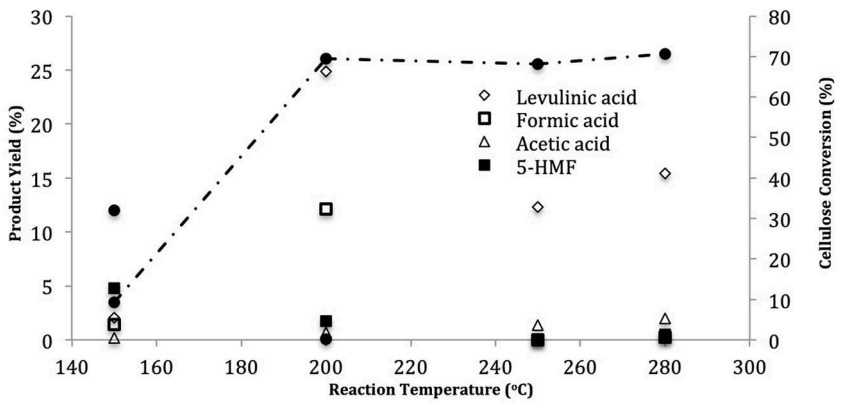

FIGURE 4 | Conversion of cellulose and distribution of the liquid products after 60 min with 50 mM H_2SO_4 at different reaction temperatures (pressure range: 5–64 bar).

dehydration of 5-HMF. According to Kruse and Gawlik (2003), one of the minor organic acids formed from the decomposition of cellulose in subcritical water was acetic acid. In Kruse's study, the concentration of acetic acid was not significantly affected by temperature which is consistent with the results shown in **Figure 4**.

The reaction pathway of cellulose can be separated to three main parts: the first part is about to the hydrolysis of cellulose to oligosaccharides; the second part is related with the hydrolysis of saccharides to glucose (**Figure 5**) and; the last part comprises the glucose isomerization and dehydration to 5-HMF and levulinic acid. In the first part, oligosaccharides and small saccharides such

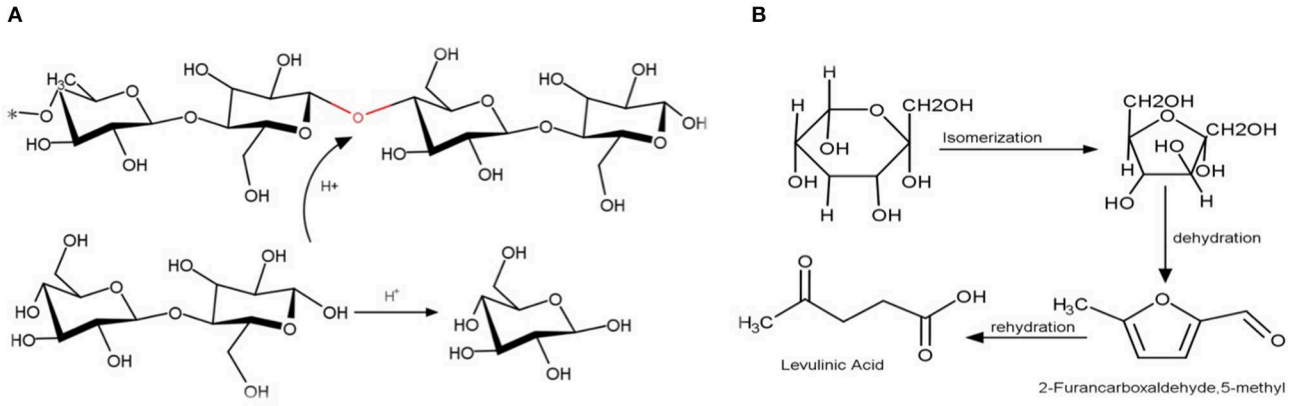

FIGURE 5 | (A) Cellulose hydrolysis to cellobiose and glucose; **(B)** glucose isomerization to fructose, dehydration and rehydration to 5-HMF and levulinic acid.

TABLE 1 | Levulinic acid yield with 50 mM H_2SO_4 from 30 to 120 min at various reaction temperatures of 150, 200, 250, and 280°C.

	Temperature (°C)			
Time (min)	**150**	**200**	**250**	**280**
30	1.49	0.10	25.19	16.76
60	2.04	24.90	12.33	15.42
90	2.40	19.28	18.40	18.69
120	6.07	17.94	14.32	16.20

as cellobiose are formed as the products of cellulose hydrolysis (Cantero et al., 2013).

The effect of temperature on levulinic acid (desired product) yield at different reaction times was investigated and the results are given in **Table 1**. When reaction was carried out at 200°C, whereas levulinic acid was not detected in the liquid product solution during the first 30 min, levulinic acid yield reached to 24.9% at the end of 60 min. Levulinic acid yield raised to 25.2% in the first 30 min when the reaction is carried out at higher reaction temperatures (250°C). However, yield of levulinic acid has decreased to 14.3% for longer reaction times up to 120 min. The opposite case was observed for lower reaction temperature such as 150°C. The yield of levulinic acid increased from 1.5 to 6.1% when the reaction was prolonged, however, it was still lower than the levulinic acid yield at 200°C (Yüksel, 2016). According to Girisuta (2007), the highest levulinic acid yield was obtained at higher reaction temperature in a shorter time. At the same study, it was reported that under the conditions at which high levulinic acid yield was obtained, 5-HMF yield was low in the liquid product solution.

To comprehend the effect of H_2SO_4 concentration (5, 25, 75, 100, and 125 mM) on the product distribution was also investigated. In that case, yield of levulinic acid enhanced with respect to the increasing H_2SO_4 concentration. While the lower yield of levulinic acid was observed as 4.8% using 5 mM H_2SO_4), the highest yield was observed as 38% with the addition of 125 mM H_2SO_4. Similar trend was observed in the yield of formic acid. The yield of formic acid was observed as 2.6 and 21% using 5 and 125 mM H_2SO_4, respectively (Yüksel, 2016). However, the yields of glucose, fructose, and 5-HMF were started to decrease with respect to the increasing acid concentration in the feed and the reaction mechanism of cellulose degradation in hot-compressed water could be lead to decrease in yield of these products. In similar studies in literature, it was found that firstly, cellulose degraded to simple sugars (glucose and fructose). Then, main intermediate (5-HMF) was formed by the conversion of them. Finally, levulinic acid, and formic acid were formed by the decomposition of 5-HMF (Zeng et al., 2010; Rosatella et al., 2011; Cardenas-Toro et al., 2014).

After investigating cellulose behavior in sub-critical water, we used hazelnut shell waste as real lignocellulosic biomass source. Cellulose, hemicellulose and lignin contents of hazelnut shell (**Table 2**) were found by using Van Soest Method (Goering and Van Soest, 1970; Madenoglu et al., 2014).

During the degradation of cellulose in subcritical water, firstly, the dominant mechanism is de-polymerization of cellulose and hence, oligosaccharides, and monosaccharides were formed. After that, hydrolysis and rearrangement/decomposition of glucose and other monomer sugars occur so that various products such as 5-HMF, glyceraldehyde, fructose, furfural, pyruvaldehyde, and glycolaldehyde could form. Besides, hydrolysis of hemicellulose take place to form low and high molecular weight oligomers, xylose, glycolaldehyde, furfural, and glyceraldehydes and the re-polymerization, isomerization and fragmentation of them happen in solid, liquid and gaseous products when the reaction temperature is high (Pavlovic et al., 2013; Cardenas-Toro et al., 2014). Various compounds were formed in liquid product, however, the production of levulinic acid, acetic acid, 5-HMF and furfural had great attention.

Maximum hazelnut shell conversion was found as 65.4% at the following conditions: 280°C, 120 min, 50 mM H_2SO_4. When the reaction temperature increased from 150 to 280°C, hazelnut shell conversion increased considerably. Besides, TOC conversion was also determined solid residues and the results are given in

TABLE 2 | Structural carbohydrate analysis of hazelnut shell.

Ultimate analysis (wt%)	
C	50.44
H	6.76
N	0.76
S	0.11
O	41.92
Proximate analysis (wt%)	
Moisture	8.93
Ash	1.48
Protein	3.11
Structural analysis (wt%)	
Cellulose	36.02
Hemicellulose	12.66
Lignin	40.14
Extractives	7.86

TABLE 3 | The effect of reaction temperature on TOC conversion at different reaction temperature with addition of 50 mM H_2SO_4 concentration.

Temperature (°C)	Time (min)	TOC Conversion (%)
150	15	29.59
	60	38.49
	90	35.01
	120	32.61
200	15	47.73
	60	45.87
	90	46.08
	120	46.96
250	15	46.52
	60	47.30
	90	45.04
	120	47.41
280	15	43.39
	60	49.71
	90	48.26
	120	47.92

Table 3. TOC conversion was found as 49.71% at 280°C and 60 min (Gozaydin and Yuksel, 2017).

In literature (Girisuta, 2007; Toor et al., 2011) various types of acids were described to decompose different biomasses in subcritical water. In our study, as an oxidizing agent sulfuric acid was used. As it seen in **Table 4**, the formation of levulinic acid was not observed for shorter reaction times when the sulfuric acid was not used. However, the degradation of hazelnut shell to form levulinic acid enhanced by the addition of H_2SO_4 for the same reaction conditions. In the light of the studies of Efremov et al. (1997) and Fang and Hanna (2002), it could be deduced

TABLE 4 | The yield of levulinic acid, furfural, and acetic acid in presence and absence of sulfuric acid (50 mM) at different reaction time (150 and 280°C).

Time (min)	150°C without acid	280°C without acid	150°C with acid	280°C with acid
LEVULINIC ACID YIELD (%)				
15	0	0.40	0	8.42
60	0	0.89	0	11.85
90	0	1.22	0.10	13.26
120	2.17	1.05	0.28	13.05
FURFURAL YIELD (%)				
15	0	1.85	1.54	0.25
60	0.08	0.76	5.54	0.18
90	0.389	0.40	6.60	0.07
120	0.77	0.23	11.91	0.04
ACETIC ACID YIELD (%)				
15	1.17	9.30	11.58	8.28
60	2.07	10.64	9.53	8.09
90	1.80	9.51	11.09	8.78
120	1.94	8.65	10.97	8.76

that levulinic acid yield enhanced with respect to the increasing amount of sulfuric acid. The product yields in our study show the same behavior in line with the literature. Moreover, while the addition of sulfuric acid causes an increase in levulinic acid yield (up to 11.91%) at 150°C, it did not affect at 280°C.

Main reaction mechanisms of the liquefaction of waste hazelnut shell were purposed based on those results, and they were illustrated in **Figure 6**. Under subcritical water media, the rate of cellulose hydrolization to oligomers and isomerization of glucose into fructose were rapid at low temperature. The rate of rehydration of 5-HMF into levulinic acid increased when H_2SO_4 (100–125 mM) was used excessively and long reaction time (≥60 min). Two main reaction pathways were possible for hemicellulose. When hydrothermal reaction was performed at low H_2SO_4 concentration (0–5 mM) at 200°C, acetic acid formation was favored by the cleavage of acetyl (Zhu et al., 2014).

Hydrothermal Electrolysis of Cellulose

Hydrothermal electrolysis experiments were carried out in a 450 mL of SUS 316 stainless steel batch reactor (Parr 5500 series), which is illustrated in **Figure 2**. All experiments were carried out using deionized water (200 ml) and cellulose (8 gr). Sulphuric acid was used as an external proton source and it was added to the reaction medium at different concentrations (1–50 mM). Reaction time started when the reaction medium had reached the desired reaction temperature and the first sample (2 mL) was taken for reaction times of 0 and then, other samples were taken at the reaction times of 15, 30, 60, 90, and 120 min. So that, the effect of heating period was investigated.

Experiments of hydrothermal electrolysis were performed at a constant current which are 0 and 2 A passing through the electrodes. In this set-up, anode was specially designed cylindrical type titanium electrode (D: 12 mm, L: 94 mm), cylindrical reactor wall (D_o: 76 mm, L: 165 mm) was used instead of cathode. To

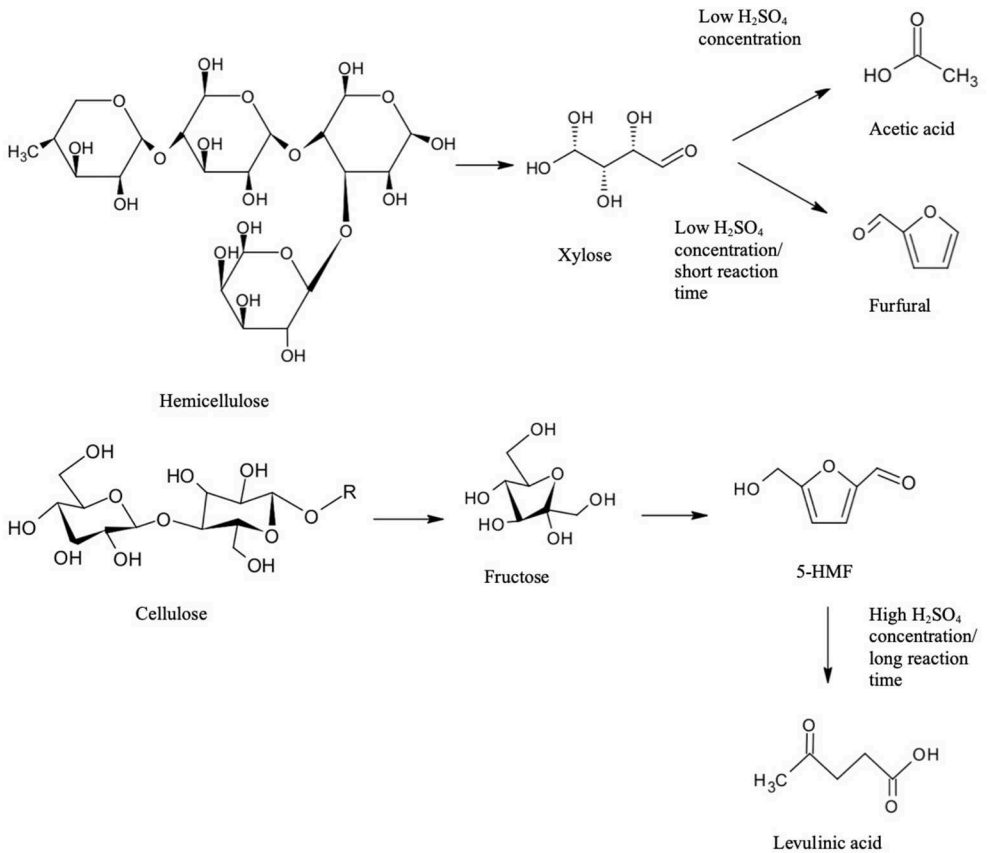

FIGURE 6 | Main proposed reaction pathways for hydrothermal conversion of waste hazelnut shell.

purpose the reaction pathway of degradation of cellulose when current was applied, the reaction conditions were as follows: 25 mM H_2SO_4 solution at 200°C with application of constant voltages (0, 4.0, and 8.0 V) for 180 min.

Sub- and supercritical water have a great attention as a reaction medium because of its versatile properties. For example, this reaction medium has 10^{-11} of ionic product concentration (200–300°C range) and dielectric constant is ≈10 (near critical) (Marshall and Franck, 1981). Water can self-dissociated into hydroxide and hydronium ion and these ions have a critical role for the protonation of β(1–4)glycosidic bond of cellulose so that cellulose could be decomposed. If hydronium ion must access to intra- and inter-molecular hydrogen bonds then, microcrystalline cellulose could be depolymerized. Hence, diffusion of protons with versatile properties such as high diffusivity and low density of near critical water becomes more effective. When ionic product concentration is high, low energy is needed for the migration of electroactive species in electrochemical methods. Thus, electrochemical reactions at near critical conditions become more economically feasible (Asghari and Yoshida, 2008).

The hypothesis of this is that application of direct current into reaction medium under hydrothermal condition would create activated species in terms of ionic and radical molecules due the redox reactions of water and sulfuric acid. Formation of these molecules can alter the decomposition of cellulose as in the postulated reaction mechanism (**Figure 7**). Application of direct current under hydrothermal condition is resulted in the reactions at positive anode (Equations 4, 5) and at negative cathode (Equations 6, 7) Equation (5) yield the formation of H^+ ion which can generate an acid layer around anode that can yield the protonation of β(1–4)glycosidic bond of cellulose.

$$4OH^-_{(aq)} - 4e^- \rightarrow 2H_2O_{(l)} + O_{2(g)} \quad (4)$$

$$2H_2O_{(l)} - 4e^- \rightarrow 4H^+{}_{(aq)} + O_{2(g)} \quad (5)$$

$$4H^+_{(aq)} + 4e^- \rightarrow 2H_{2(g)} \quad (6)$$

$$4H_3O^+_{(aq)} + 4e^- \rightarrow 2H_{2(g)} + 4H_2O_{(l)} \quad (7)$$

A hybrid method comprised of electrochemical oxidation and the production of value added organic species in sub-critical water has gained attraction (Yuksel et al., 2011). Our previous study is related with the decomposition of microcrystalline cellulose in sub-critical water conditions where the reaction temperature varied between 170 and 230°C in the presence of sulfuric acid (1–50 mM) by applying direct constant current (0–2 A). Fractional factorial experimental design was performed to

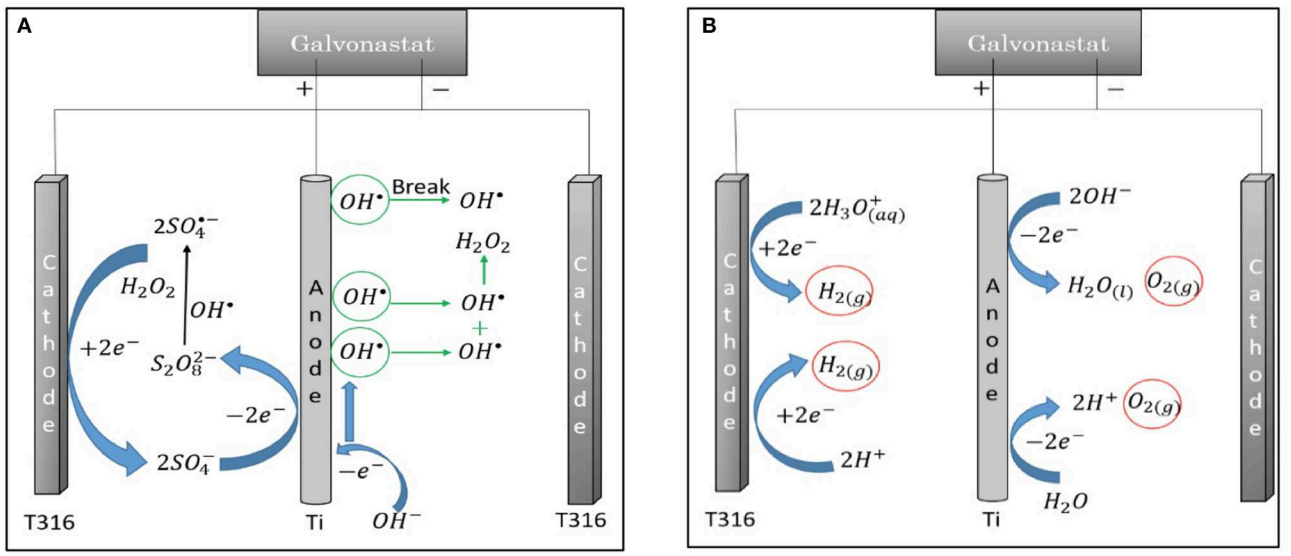

FIGURE 7 | Electrochemical reaction of water and sulfuric acid that yields **(A)** radical, **(B)** ionic products.

determine the coupled and interaction parameters of constant current with sulfuric acid under hydrothermal conditions. According to the results, when 50 mM H_2SO_4 was used and 1 A current was applied to the reaction medium, the required reaction temperature for the maximum cellulose conversion of 82% decreased from 230 to 200°C (Akin and Yuksel, 2016). The application of direct current provides the formation of radicals ($OH^{\cdot -}, SO_4^{\cdot -}$) and ionic products ($OH^-, H_3O^+$), so that TOC conversion enhanced. As current values increased, concentration of radicals in the reaction medium increased. However, TOC conversion decreased when higher current (2 A) was applied. Additionally, the application of direct current (1–2 A) affected the formation yields of 5-HMF and levulinic acid. While the yield of 5-HMF enhanced by direct current, levulinic acid concentration decreased. During the reaction, variable electrode potential was observed because of the application of constant current to reaction medium. Hence, the change in electrode potentials leads to formation of various activated species within the reaction medium. Davis et al. (2014) carried out a study over electrolysis of sulfuric acid solution to form persulfate based on radical mechanism. This study show that the formation of different radical species such as $SO_4^{-\bullet}, HSO_4^{\bullet}, OH^{\bullet}$ and ionic products such as SO_4^{2-}, H_3O^+, OH^- can be observed during electrolysis of sulfuric acid solution at different electrode potentials (Davis et al., 2014). Formation of these products can alter the decomposition mechanism of cellulose to form levulinic acid, furfural and 5-HMF selectively.

Effect of applied voltage (4.0 and 8.0 V) on product selectivity and TOC conversion in hydrothermal reaction medium was investigated in the presence and absence of acid catalyst (H_2SO_4). Selectivity values of cellulose on formation of furfural, 5-HMF and levulinic acid were determined as described in material and methods section. The control reaction was carried out by applying voltage under hydrothermal conditions (200°C) in the absence of acid catalyst. Results are listed on **Table 5**.

TABLE 5 | TOC Yield, conversion of cellulose, and valuable product selectivities at applied voltage values of 0, 4.0, 8.0 V at different electrolyte (H_2SO_4) concentrations as 0 and 25 mM.

		No acid			With 25 mM acid		
In %	**Voltage (V)**	**0 min**	**60 min**	**180 min**	**0 min**	**60 min**	**180 min**
TOC yield	0	2.4	4.1	9.8	10.1	23.8	49.9
	4	2.2	2.6	7.7	9.4	28.7	45.4
	8	2.1	4.0	13.8	10.3	24.6	50.3
Conversion of cellulose	0		9.4	11.3		48.7	77.1
	8		70.6	78.2		30.7	82.0
Levulinic acid selectivity	0	4.3	6.3	1.4	12.4	12.8	10.3
	4	0.2	0.3	0	9.4	10.8	19.1
	8	0.2	0	0	8.8	9.2	23.7
5-HMF selectivity	0	0.8	1.4	9.7	2.7	42.8	26.1
	4	6.9	2.1	3.3	8.1	29.9	21.8
	8	3.9	4.8	15.9	2.2	17.9	9.1
Furfural selectivity	0	7.1	3.7	5.3	2.9	9.6	5.8
	4	2.8	3.2	6.1	6.2	7.6	5.1
	8	2.7	11.3	14.3	5.9	6.3	3.7

When cellulose was degraded under hydrothermal conditions (no current, no electrolyte), TOC was recorded as 13.8%

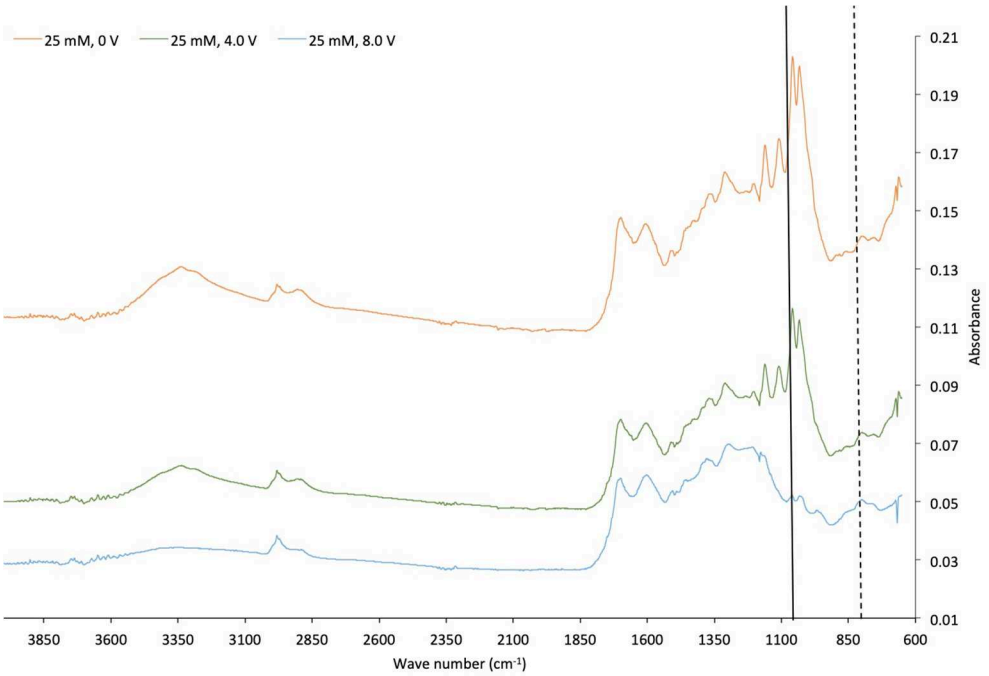

FIGURE 8 | FTIR spectrum of solid residues of applied potential of 0, 4.0, and 8.0 V in 25 mM sulfuric acid medium.

(**Table 5**). Whereas, lower TOC conversions were observed by applying constant voltage (4.0 V) compared to current free experiments, higher TOC values were observed at constant voltage (8.0 V). Rossmeisl et al. (2005) showed that higher potentials could cause to dissociate the water into its ionic products and the formation of radical species such as hydroxyl radical ($OH^{\bullet -}$) could enhance under hydrothermal conditions by applying voltage. Hence, in the light of literature, it is possible to say that higher TOC conversions could be achieved by higher voltage. If concentration of radical species increases, decomposition products could form via radical based mechanism. The coupled effect sulphuric acid (25 mM) and applied voltage can be explained by the oxidation of sulphuric acid to form the sulfate radical ($SO^{\bullet}{}_4{}^-$) near anode (Davis et al., 2014). This synergetic effect causes an increase in the TOC yield to 50.3% (**Table 5**) under hydrothermal conditions (Akin and Yuksel, 2016).

The conversion of fructose to furfural under hydrothermal conditions could be proposed by two reaction pathways (Aida et al., 2007). First one is the removal of formaldehyde from 5-HMF and the second one is the cleavage of C–C bond in fructose so that pentose formation is observed and then dehydration of pentose leads to formation of furfural (Luijkx et al., 1993). The selectivity values of furfural and 5-HMF increased simultaneously. Hence, it could be concluded that furfural might be formed by the cleavage of C–C bond in fructose due to the low yield of fructose (8.0 V) in comparison to hydrothermal reaction (0 V). Rehydration of 5-HMF resulted in formation of levulinic acid (Akin and Yuksel, 2017).

TABLE 6 | Gaseous products (H_2, CO, CH_4, CO_2) of cellulose of degradation under hydrothermal and applied constant current conditions at 230°C and 120 min.

		Concentration of gas products (μg/ml)			
H_2SO_4 (mM)	Current (A)	H_2	CO	CH_4	CO_2
0	0	0.5	52.4	0.21	530.5
0	2	75.3	26.2	0.26	398.7
50	2	98.2	48.7	0.53	418.7

As seen on **Table 5**, in the first 60 min, selectivity of 5-HMF was 42.8% and further reaction time selectivity of levulinic acid was 23.7%. FTIR results (**Figure 8**) showed that S=O Sulfoxide (solid line in **Figure 8**) and S-OR Ester (dashed line in **Figure 8**) groups were formed at solid residuals when voltage (4.0 and 8.0 V) was applied. The activity of sulfonated carbon particles might be hindered due to the high concentrations of sulfone ion radicals which is a reactive species formed at relatively high concentration of sulphuric acid by applying potential (Akin and Yuksel, 2017).

From **Table 6**, it was clearly seen that, when 2 A current was applied for 120 min., there was a dramatic increase in H_2 concentration from 0.5 to 75.3 μg/ml. Under same conditions, CO_2 concentration decreased from 530.5 to 398.7 μg/ml. Under the effect of applied current with the addition of 50 mM H_2SO_4, H_2 concentration increased from 75.3 to 98.2 μg/ml, whereas CO concentration was recorded as 26.2 to 48.7 μg/ml, respectively. This result indicated that water gas shift reaction was favored the

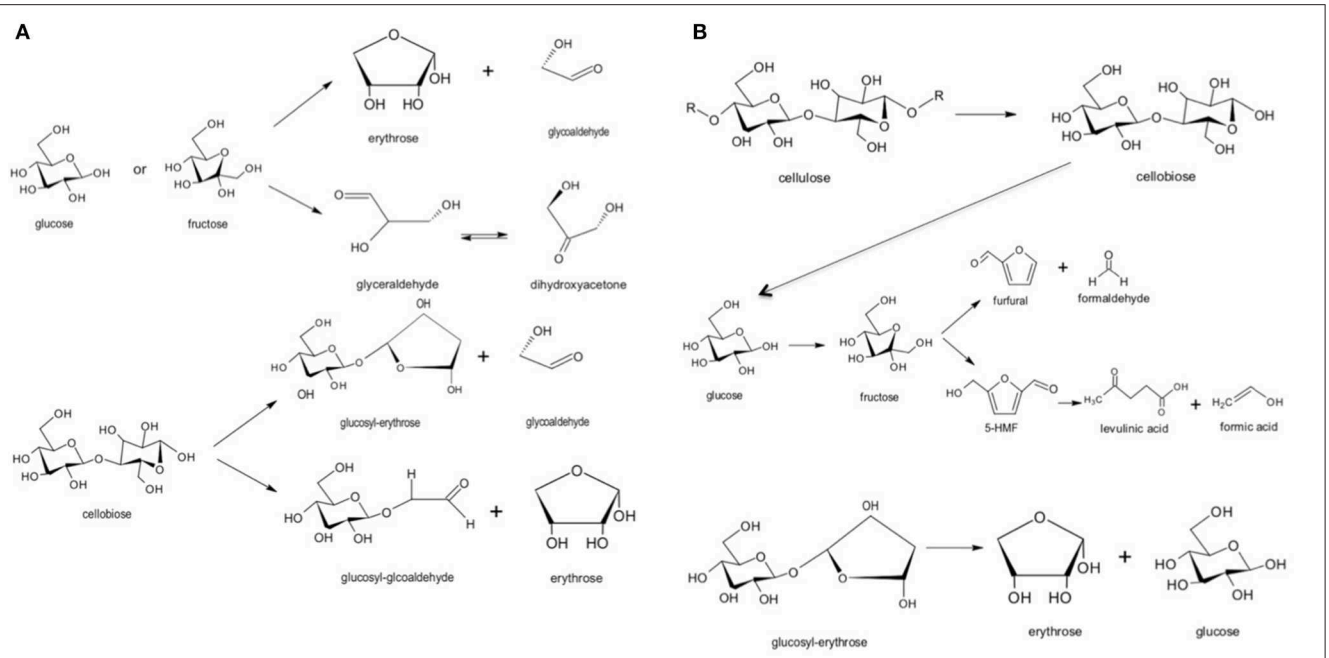

FIGURE 9 | Proposed **(A)** radical and **(B)** ionic reaction pathways for hydrothermal electrolysis of cellulose at constant voltage (8.0 V) with 25 mM H_2SO_4.

carbon monoxide formation with the addition of sulfuric acid as an electrolyte. Methane formation was also observed as gas products and an increase in acid concentration from 0 to 50 mM yields to 0.26 and 0.53 μg/ml, respectively.

The application of constant voltage lead to form radicals and ionic products so that levulinic acid, furfural and 5-HMF can be formed from cellulose selectively. Although it is hard to distinguish the radical and ionic-based mechanism due to common product distribution, under certain potential in the designed hybrid reactor system favors the degradation of cellulose via radical mechanism (Akin and Yuksel, 2019). Proposed ionic and radical reaction pathways for hydrothermal electrolysis of cellulose at constant voltage are given in **Figure 9**.

As the electrode potential (8.0 V) was applied, various activated radical species such as $SO_{-4}{}^{\bullet}$, $HSO^{\bullet}{}_4$, $OH^{\bullet}$ and ionic species such as SO_4^{2-}, $H_3^-O^+$, OH^- could commonly be created when electrolysis was carried out in the presence of H_2SO_4 in sub-critical water. Formation of these products can shift degradation mechanism of cellulose to high value chemicals such as levulinic acid, furfural and 5-HMF (**Figure 9**). Additionally, formation of glucosyl-glycoaldehyde, glucosyl-eryhtrose, and glycoaldehyde was also observed when hydrothermal electrolysis was carried out at 8.0 V so that decomposition mechanism of cellulose via ionic and radical based pathways was revealed (**Figure 9**).

CONCLUSION

Hydrolysis of cellulose in sub-critical water conditions has been widely searched because of the versatile properties (low dielectric constant, high diffusivity, high ion product concentration etc.) of hot compressed water as reaction medium. Thus, high ionic product concentration and its high diffusivity to intra and inter molecular hydrogen bonds enhanced the protonation of β(1–4) glycosidic linkage of cellulose that yield degradation products which are glucose, fructose, 5-HMF, furfural, and levulinic acid.

As model biomass, hazelnut shell waste was converted to value-added chemicals under hot compressed water. In the context of experimental study, the effect of reaction temperature, reaction time and acid (H_2SO_4) concentration was investigated. The main products of hydrothermal acid-treatment were clarified as levulinic acid, furfural and acetic acid by HPLC analysis. As reaction temperature increases, a considerable improvement on the amount of formed levulinic acid and conversion of hazelnut shell was observed. For instance, when the reaction temperature, time and acid concentration were 280°C, 120 min and 50 Mm, respectively, levulinic acid yield and conversion of hazelnut shell were found as 13.05 and 65.40%, respectively. Addition of H_2SO_4 enhanced the production of levulinic acid from waste hazelnut shell.

As alternative novel method to frequently used ones, a novel hybrid system for the conversion of cellulose to high value chemicals was introduced. The application of direct current in constant mode was investigated and was found that applied 1 A of current resulted in higher total organic carbon (TOC) in comparison to current free experiments. The enhancement in TOC was conducted for the formation of an acid layer around anode due to the self-dissociation of water that hydrolyses cellulose. It was proposed that application of constant voltage could selectively change the degradation mechanism of cellulose and hydrolysis product distribution. The detailed product

distribution of decomposition of microcrystalline cellulose under subcritical water condition by application of direct current was investigated and reaction pathway for hydrothermal electrolysis of cellulose was proposed.

DATA AVAILABILITY STATEMENT

All datasets generated for this study are included in the article/supplementary material.

AUTHOR CONTRIBUTIONS

The author confirms being the sole contributor of this work and has approved it for publication.

ACKNOWLEDGMENTS

I would like to thank to my Ph.D. student Ceren Orak for her support in drawing some of the figures.

REFERENCES

Aida, T. M., Sato, Y., Watanabe, M., Tajima, K., Nonaka, T., Hattori, H., et al. (2007). Dehydration Of D-glucose in high temperature water at pressures up to 80 MPa. *J. Supercrit. Fluids* 40, 381–388. doi: 10.1016/j.supflu.2006.07.027

Akin, O., and Yuksel, A. (2016). Novel hybrid process for the conversion of microcrystalline cellulose to value-added chemicals: part 1: process optimization. *Cellulose* 23, 3475–3493. doi: 10.1007/s10570-016-1054-3

Akin, O., and Yuksel, A. (2017). Novel hybrid process for the conversion of microcrystalline cellulose to value-added chemicals: part 2: effect of constant voltage on product selectivity. *Cellulose* 24, 4729–4741. doi: 10.1007/s10570-017-1457-9

Akin, O., and Yuksel, A. (2019). Novel hybrid process for the conversion of microcrystalline cellulose to value-added chemicals: part 3: detailed reaction pathway. *Cellulose* 26, 2999–3008. doi: 10.1007/s10570-019-02291-6

Asghari, F. S., and Yoshida, H. (2008). Electrodecomposition in subcritical water using o-xylene as a model for benzene, toluene, ethylbenzene, and xylene pollutants. *J. Phys. Chem. A* 112, 7402–7410. doi: 10.1021/jp800452s

Asghari, F. S., and Yoshida, H. (2010). Conversion of Japanese red pine wood (*Pinus densiflora*) into valuable chemicals under subcritical water conditions. *Carbohydr. Res.* 345, 124–131. doi: 10.1016/j.carres.2009.10.006

Cantero, D. A., Bermejo, M. D., and Cocero, M. J. (2013). Kinetic analysis of cellulose depolymerization reactions in near critical water. *J. Supercrit. Fluids* 75, 48–57. doi: 10.1016/j.supflu.2012.12.013

Cardenas-Toro, F. P., Alcazar-Alay, S. C., Forster-Carneiro, T., and Meireles, M. A. A. (2014). Obtaining oligo- and monosaccharides from agroindustrial and agricultural residues using hydrothermal treatments. *Food Public Health* 4, 123–139. doi: 10.5923/j.fph.20140403.08

Chan, Y. H., Yusup, S., Quitain, A. T., Uemura, Y., and Sasaki, M. (2014). Bio-oil production from oil palm biomass via subcritical and supercritical hydrothermal liquefaction. *J. Supercrit. Fluids* 95, 407–412. doi: 10.1016/j.supflu.2014.10.014

Cheng, L. M., Ye, X. P., He, R. H., and Liu, S. (2009). Investigation of rapid conversion of switchgrass in subcritical water. *Fuel Process. Technol.* 90, 301–311. doi: 10.1016/j.fuproc.2008.09.009

Davis, J., Baygents, J. C., and Farrell, J. (2014). Understanding persulfate production at boron doped diamond film anodes. *Electrochim. Acta* 150, 68–74. doi: 10.1016/j.electacta.2014.10.104

Efremov, A. A., Pervyshina, G. G., and Kuznetsov, B. N. (1997). Thermocatalytic transformations of wood and cellulose in the presence of HCl, HBr, and H_2SO. *Chem. Nat. Comp.* 33, 107–112. doi: 10.1007/BF02273932

Ehara, K., and Saka, S. (2005). Decomposition behavior of cellulose in supercritical water, subcritical water, and their combined treatments. *J. Wood Sci.* 51, 148–153. doi: 10.1007/s10086-004-0626-2

Fang, Q., and Hanna, M. A. (2002). Experimental studies for levulinic acid production from whole kernel grain sorghum. *Bioresour. Technol.* 81, 187–192. doi: 10.1016/S0960-8524(01)00144-4

Girisuta, B. (2007). *Levulinic acid from lignocellulosic biomass* (Ph.D. dissertation), University of Groningen, Groningen, Netherlands.

Goering, H. K., and Van Soest, P. J. (1970). "Forage fiber analysis (apparatus reagents, procedures and some applications)," in *Agriculture Handbook* (Washington, DC: United States Department of Agriculture).

Gozaydin, G., and Yuksel, A. (2017). Valorization of hazelnut shell waste in hot compressed water. *Fuel Process. Technol.* 166, 96–106. doi: 10.1016/j.fuproc.2017.05.034

Guney, M. S. (2013). Utilization of hazelnut husk as biomass. *Sus. Energy Technol. Assess.* 4, 72–77. doi: 10.1016/j.seta.2013.09.004

Horvat, J., Klaic, B., Metelko, B., and Sunjic, V. (1985). Mechanism of levulinic acid formation. *Tetrahedron Lett.* 26, 2111–2114. doi: 10.1016/S0040-4039(00)94793-2

Knezevic, D., Van Swaaij, W. P. M., and Kersten, S. R. A. (2009). Hydrothermal conversion of biomass: I, glucose conversion in hot compressed water. *Ind. Eng. Chem. Res.* 48, 4731–4743. doi: 10.1021/ie801387v

Kruse, A., and Gawlik, A. (2003). Biomass conversion in water at 330–410 degrees C and 30– 50 MPa. Identification of key compounds for indicating different chemical reaction pathways. *Ind. Eng. Chem. Res.* 42, 267–279. doi: 10.1021/ie0202773

Luijkx, G. C., van Rantwijk, F., and van Bekkum, H. (1993). Hydrothermal formation of 1,2,4-benzenetriol from 5-hydroxymethyl-2-furaldehyde and d-fructose. *Carbohydr. Res.* 242, 131–139. doi: 10.1016/0008-6215(93)80027-C

Madenoglu, T. G., Yildirir, E., Saglam, M., Yuksel, M., and Ballice, L. (2014). Improvement in hydrogen production from hard-shell nut residues by catalytic hydrothermal gasification. *J. Supercrit. Fluids* 95, 339–347. doi: 10.1016/j.supflu.2014.09.033

Marshall, W. L., and Franck, E. U. (1981). Ion product of water substance, O-Degrees-C-1000-Degrees-C, 1–10,000 bars—new international formulation and its background. *J. Phys. Chem. Ref. Data* 10, 295–304. doi: 10.1063/1.555643

Pavlovic, I., Knez, Z., and Skerget, M. (2013). Subcritical water - a perspective reaction media for biomass processing to chemicals: study on cellulose conversion as a model for bio- mass. *Chem. Biochem. Eng. Q.* 27, 73–82.

Rosatella, A. A., Simeonov, S. P., Fradea, R. F. M., and Carlos, A. M. A. (2011). 5 – Hydroxymethylfurfural (HMF) as a building block platform: biological properties, synthesis and synthetic applications. *Green Chem.* 13, 754–793. doi: 10.1039/c0gc00401d

Rossmeisl, J., Logadottir, A., and Norskov, J. K. (2005). Electrolysis of water on (oxidized) metal surfaces. *Chem. Phys.* 319, 178–184. doi: 10.1016/j.chemphys.2005.05.038

Saito, T., Sasaki, M., Kawanabe, H., Yoshino, Y., and Goto, M. (2009). Subcritical water reaction behavior of D-glucose as a model compound for biomass using two different continuous-flow reactor configurations. *Chem. Eng. Technol.* 32, 527–533. doi: 10.1002/ceat.200800537

Sasaki, M., Adschiri, T., and Arai, K. (2004). Kinetics of cellulose conversion at 25 MPa in sub- and supercritical water. *AIChE J.* 50, 192–202. doi: 10.1002/aic.10018

Savage, P. E. (1999). Organic chemical reactions in supercritical water. *Chem. Rev.* 99, 603–621. doi: 10.1021/cr9700989

Toor, S. S., Rosendahl, L., and Rudolf, A. (2011). Hydrothermal liquefaction of biomass: a review of subcritical water technologies. *Energy* 36, 2328–2342. doi: 10.1016/j.energy.2011.03.013

Tymchyshyn, M., and Xu, C. B. (2010). Liquefactionofbio-massinhot-compressedwaterforthe production of phenolic compounds. *Bioresour. Technol.* 101, 2483–2490. doi: 10.1016/j.biortech.2009.11.091

Williams, P. T., and Onwudili, J. (2006). Subcritical and supercritical water gasification of cellulose, starch, glucose, and biomass waste. *Energy Fuels* 20, 1259–1265. doi: 10.1021/ef0503055

Xu, B., Zhang, B. G., Li, M., Huang, W. W., Chen, N., Feng, C. P., et al. (2014). Production of reducing sugars from corn stover by electrolysis. *J. Appl. Electrochem.* 44, 797–806. doi: 10.1007/s10800-014-0696-9

Yüksel, A. (2016). Hydrothermal treatment of cellulose in hot-pressurized water for the production of levulinic acid. *Uludag Univ. J. Fac. Eng.* 21, 415–434. doi: 10.17482/uumfd.278150

Yuksel, A., Sasaki, M., and Goto, M. (2011). A new green technology: hydrothermal electrolysis for the treatment of biodiesel wastewater. *Res. Chem. Intermediates* 37, 131–143. doi: 10.1007/s11164-011-0260-8

Zeng, W., Cheng, D., Zhang, H., Chen, F., and Zhan, X. (2010). Dehydration of glucose to levulinic acid over MFI-type zeolite in subcritical water at moderate conditions. *React. Kinet. Mech. Catal.* 100, 377–384. doi: 10.1007/s11144-010-0187-x

Zhang, Y. M., Peng, Y., Yin, X. L., Liu, Z. H., and Li, G. (2014). Degradation of lignin to BHT by electrochemical catalysis on Pb/PbO_2 anode in alkaline solution. *J. Chem. Technol. Biotechnol.* 89, 1954–1960. doi: 10.1002/jctb.4282

Zhu, G. Y., Zhu, X., Xiao, Z. B., Zhou, R. J., Zhu, Y. L., and Wan, X. L. (2014). Kinetics of peanut shell pyrolysis and hydrolysis in subcritical water. *J. Mater. Cycles Waste Manage.* 16, 546–556. doi: 10.1007/s10163-013-0209-7

Conflict of Interest: The author declares that the research was conducted in the absence of any commercial or financial relationships that could be construed as a potential conflict of interest.

frontiers in Chemistry

REVIEW
published: 07 February 2020
doi: 10.3389/fchem.2020.00070

The Roles of H_2O/Tetrahydrofuran System in Lignocellulose Valorization

*Jianmei Li, Wenyu Zhang, Shuguang Xu and Changwei Hu**

Key Laboratory of Green Chemistry and Technology, Ministry of Education, College of Chemistry, Sichuan University, Chengdu, China

Lignocellulosic biomass as a potential alternative to fossil resource for the production of valuable chemicals and fuels has attracted substantial attention, while reducing the recalcitrance of lignocellulosic biomass is still challenging due to the complex and cross-linking structure of biomass. Solvent system plays important roles in the pretreatment of lignocellulose, enabling the transformation of solid biomass to liquid fluid with better mass and heat transfer, as well as in the selective formation of target products. In particular, H_2O/tetrahydrofuran (H_2O/THF) system has recently been widely applied in lignocellulose valorization, which has been proved to exhibit outstanding efficiency for the conversion of lignocellulose, solubilization of the intermediates and products, and shifting reaction equilibrium, thereby significantly improving the yield and selectivity of target products, as well as the full utilization of lignocellulose. In addition, THF shows low toxicity, and is known as a renewable solvent which can be produced from bio-derived chemicals. Herein, this review concentrates on the advances of H_2O/THF system in lignocellulose valorization in recent years. Several aspects relative to the roles of H_2O/THF system are discussed as follows: the pretreatment of lignin, conversion of hemicellulose and cellulose components in lignocelluloses, and the promoting formation of valuable chemicals like furfural, 5-hydroxymethyl furfural (HMF), levulinic acid, and so on, as well as the inhibiting role in humins formation. This review might provide useful information for the design of effective solvent system in full utilization of lignocellulosic biomass.

Keywords: water, tetrahydrofuran, co-solvent, lignin, hemicellulose, cellulose, value-added chemicals

OPEN ACCESS

Edited by:
Yulong Wu,
Tsinghua University, China

Reviewed by:
Xuebing Zhao,
Tsinghua University, China
Antonio De Lucas Consuegra,
University of Castilla La Mancha, Spain

****Correspondence:***
Changwei Hu
changweihu@scu.edu.cn

Specialty section:
This article was submitted to Green and Sustainable Chemistry, a section of the journal Frontiers in Chemistry

Received: *31 October 2019*
Accepted: *22 January 2020*
Published: *07 February 2020*

Citation:
Li J, Zhang W, Xu S and Hu C (2020) The Roles of H_2O/Tetrahydrofuran System in Lignocellulose Valorization. Front. Chem. 8:70. doi: 10.3389/fchem.2020.00070

INTRODUCTION

The over-exploitation of fossil resources and the resultant environmental concerns have impelled the development of renewable alternative feedstock to replace the depleting fossil resources. In recent years, increasing interests have been focused on the valorization of renewable lignocellulosic biomass instead of the conventional fossil resources for the production of value-added chemicals and biofuels (Lim et al., 2012; Lin et al., 2013). Every year, about 220 billion tons of dry biomass (ca. 45 EJ of energy content) can be obtained, and lignocellulosic biomass occupies about 70–95% of it. Cellulose, as the major component (40–50%) and elementary fibrils of lignocellulosic biomass, is a homopolysaccharide, comprised of D-glucose units via β-1,4-glucosidic bonds (**Figure 1**). It has high degree of crystallinity, polymerization (from 100 to 20,000) with high molecular weight, caused by the abundant hydrogen bonds between different anhydroglucan chains. Hemicellulose, surrounding the cellulose fibrils, bonds with cellulose and forms the gel matrix. Hemicelluloses (occupied 25–35% of the lignocellulose) are amorphous polysaccharides, and are made up of

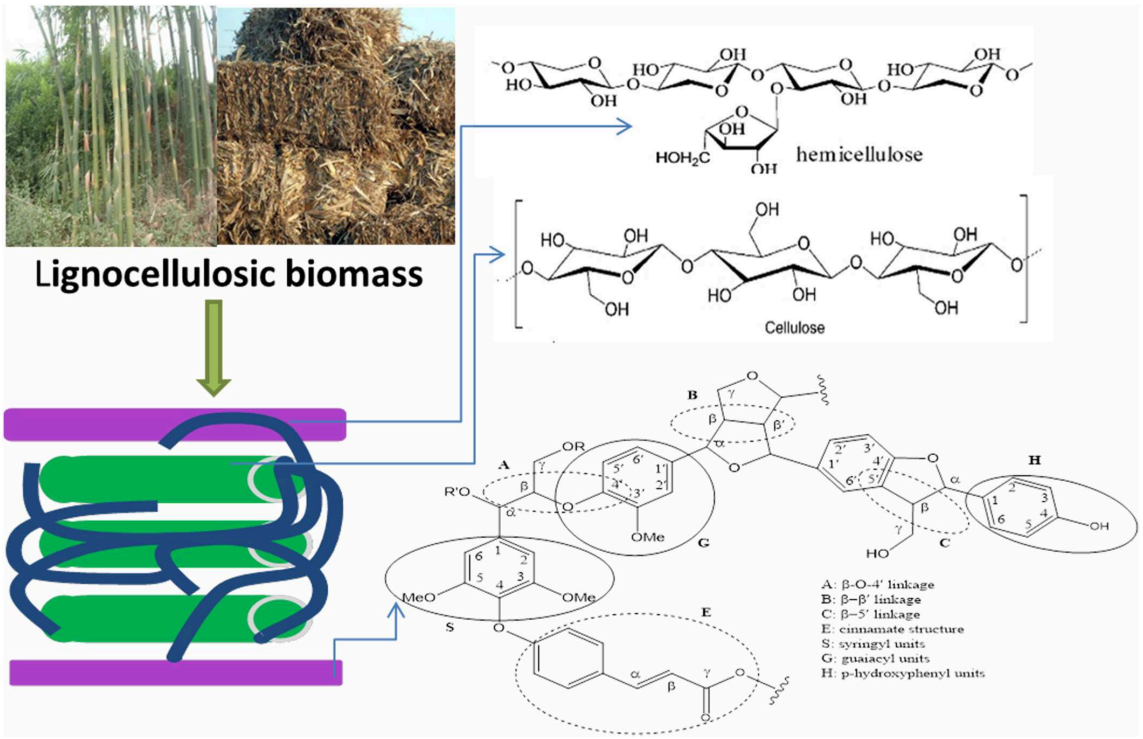

FIGURE 1 | The structure of lignocellulosic biomass.

mainly two pentoses (xylose and arabinose) and three hexoses (galactose, glucose, and mannose). Compared to cellulose, hemicellulose has lower degree of polymerization (80–200). Different from carbohydrate-based cellulose and hemicellulose, lignin (occupied 15–20% of the lignocellulose) with high molecular weights in a range of 600–15,000 kDa, is comprised of three phenyl-propanols linking with each other via C-O linkages (e.g., β-O-4,α-O-4, and so on) and C-C linkages (e.g., β-β′, β-5, and 5–5′ linkages, etc.) (Zhou et al., 2011; Tuck et al., 2012). Via effective utilization of the natural structure of raw lignocellulose, various platform chemicals and fine chemicals can be produced. Typically, xylose, furfural, and acetic acid can be produced from hemicellulose in lignocellulose. Glucose, fructose, sorbitol, ethylene glycol, 5-hydroxymethyl furfural (HMF), levulinic acid (LA) as well as lactic acid, can be obtained from the conversion of cellulose component in lignocellulose (Kunkes et al., 2008). Among these platform chemicals, furfural, HMF, and levulinic acid have been recently defined as the top candidates of future bio-based chemicals (Zakzeski et al., 2010; Cai et al., 2014a). From the degradation of lignin in lignocellulosic biomass, many aromatic compounds, such as guaiacol, 4-ethylphenol, 4-vinylphenol, 2,6-dimethoxylphenol, and so on, can be obtained (Collard and Blin, 2014; Graglia et al., 2015). Most of these aromatic compounds can be used as the feedstock for the synthesis of polymers and materials with novel interesting properties. However, the complex composition and cross-linked structure of these three main components make the degradation of lignocellulose challenging.

Liquefaction in the presence of solvent has been considered as an efficient approach for the production of valuable chemicals or biofuels from lignocellulose, since solvents significantly improve the mass and heat transfer of solid lignocellulosic biomass (Li et al., 2018). Compared to pyrolysis, solvent liquefaction requires relatively moderate reaction temperature. Importantly, it also greatly improves the reaction rates, selectivity and the stability of desired products, as well as the economics of downstream separation. Moreover, solvent liquefaction (usually in H_2O solvent) endures the presence of water in lignocellulose feedstock, thus eliminating the process of drying raw feedstock. Several studies have suggested that the mixture of polar aprotic solvent with water in lignocellulose conversion can promote the solubility of substrate fractions and influence the chemical reaction thermodynamics, thus leading to high reaction rates and improving the selectivity toward target products, where either homogeneous catalysts (acids, alkaline) or heterogeneous catalysts are usually employed (Liu et al., 2015; McCallum et al., 2018; Chen et al., 2019; Maneechakr and Karnjanakom, 2019). The type and properties of solvent not only determines the distribution of products and their yields, but also affects the subsequent separation of target products (Pace et al., 2012; Shuai et al., 2016). Shuai and Luterbacher (2016) divided the solvent effects into two categories: effects on the solubility of biomass components and their derivatives, and effects on chemical thermodynamics, which could be represented by considering the typical kinetic expression of a first-order reaction rate: $r = k \times C$. Here, r represents the reaction rate and k represents

TABLE 1 | The comparison of THF with other solvents.

Organic solvents	Properties			Advantages, disadvantages for biomass conversion
	Density (g cm^{-3})	Boiling point (K)	Solubility in water	
DMSO	1.1	462.1	Miscible	Poor solubility, environmental unfriendly and non-renewable, difficult recycle, high boiling point
Dioxane	1.0	374.0	Miscible	Poor solubility, environmental unfriendly and non-renewable
Water	1.0	373.1	–	Green, safe, abundant, but limited solubility for lignin
THF	0.9	339.0	Miscible	Easy separation and recycle, renewable, but poor solubility for cellulose and hemicellulose
Ethanol	0.79	351.3	Miscible	Safe, renewable, easy separation and recycle, but limited solubility for biomass
GVL	1.05	480.1	Miscible	Safe, renewable, good solubility for lignin, but high boiling point leads to difficult separation and recycle

the rate constant. C is the reactant concentration. Due to the low concentrations (C) of insoluble biomass in solvent, the reaction rates of biomass conversion are often restricted. Therefore, enhancing the biomass solubility can effectively improve the reaction rate of biomass conversion. Besides, increasing the rate constant (k) can also promote biomass conversion, which can be achieved by using a solvent that affects the thermodynamics of the molecules and complexes that participate in the chemical reaction.

Recently, H_2O/tetrahydrofuran (H_2O/THF) mixture has been proved to act as a promising solvent system with multi-functions for the fractionation of lignocellulose and solubilizing the resulted derivatives to obtain valuable chemicals with high yield and selectivity. In addition, THF can be synthesized from biomass-based derivatives, such as furfural, maleic anhydride, or 1,4-butanediol, thus is a promising renewable and green solvent. **Table 1** summarizes the advantages and disadvantages of THF system compared to other solvents for the conversion of biomass. Herein, this review tends to concentrate on the advances and roles of H_2O/THF mixture in lignocellulose valorization in recent years.

THE PROPERTIES OF H_2O/THF CO-SOLVENT

THF has been employed as a solvent and intermediate in industry for decades. THF has low boiling point (66°C) with a high vapor pressure (21.6 kPa at 25°C), which enables it easy recovery. In general, it is known that THF is highly polar and miscible with water, forming an azeotrope with water (Howard, 1990; Kroschwitz et al., 2004). Liu et al. (2019) performed *ab initio* molecular dynamics simulations, and proved that hydrogen bond was formed between the H atom of H_2O and O atom of THF with a 1.694 Å of bond length. However, Matouš et al. (1972) demonstrated that H_2O/THF co-solvent had great positive deviations from Raoult's law to such degree. H_2O/THF co-solvent passed through a temperature regime where THF and H_2O became immiscible, in which a transition from a transparent mixture to opaque medium could be observed. That is to say, H_2O/THF co-solvent exhibits an unusual closed-loop miscibility gap, in which H_2O and THF are mixed when the temperature is both below a certain temperature point and above a second value, while they spontaneously demix between this temperature gap. The region of limited miscibility is close and bounded by the mass fraction $\omega_{THF} \in (0.28, 0.72)$ and by temperature $t \in (71.8, 137.1)$°C (Fowles et al., 2013).

It is also considered that the presence of THF in H_2O/THF co-solvent has potential harm to both human and animal health. To investigate the toxicity of THF, Fowles et al. (2013) presented a detailed review to discuss the toxicological, exposures, risks and environmental hazards of THF. It is indicated that THF is neither a sensitizer nor irritant for skin. THF is non-mutagenic according to the studies both *in vitro* and *in vivo*. In addition, the low $\log K_{ow}$ value (<3) implies that THF has low bioaccumulation. THF is not persistent in environment as it can be biodegraded. Therefore, it is considered that THF shows low acute toxicity, and it is not necessary to pose a concern on its hazards to both human and environment, as it is utilized and managed in current use (Cheng et al., 2007; Chen et al., 2013).

LIGNIN SOLUBILIZATION AND DEPOLYMERIZATION IN H_2O/THF SYSTEM

The extensive covalent cross-linking of lignin with hemicellulose (or cellulose) in lignocelluloses limits the accessibility to carbohydrates and prevents the extraction of polysaccharides. Therefore, lignin removal is usually necessary in many industries, such as paper industry and bio-ethanol production, in which lignin is firstly fractionated and conversion from lignocellulose as a "lignin-first" approach. However, the efficient solubilization of lignin is still challenging. It is reported that the solubility of lignin in solvent is related to the Hildebrand solubility parameter (δ), which is defined as follows (Schuerch, 1952; Ni and Hu, 1995; Meng et al., 2018; Wang et al., 2018).

$$\delta = (E/V)^{1/2}$$

Here V represents the molar volume of solvent. E represents the vaporization energy at free pressure, which is constituted by three parameters corresponding to hydrogen bonding forces, non-polar/dispersion forces, and dipole forces, showing as follows:

$$\delta^2 = \delta_D^2 + \delta_P^2 + \delta_H^2$$

Here, δ_D represents the dispersion interaction and δ_P is polar interaction, while δ_H represents the hydrogen bonding interaction. It is considered that solvent, whose δ-values is approximate to 22.5 $MPa^{1/2}$, shows good solubility for lignin. The δ value of water is 23.4 $(cal/cm^3)^{1/2}$, and the δ value of THF is 9.5 $(cal/cm^3)^{1/2}$. H_2O/THF co-solvent is commonly considered as a good solvent for lignin (Mlynar and Sarkanen, 1996; Hansen, 2007). For example, Xin et al. (2012) used HSP to study the characteristics of several solute–solvent pairs, including three organic solvents (1,4-dioxane, ethyl acetate, and THF) and 1-ethyl-3-methylimidazolium acetate, and proved that THF was the best solvent for lignin among the three investigated solvent systems, followed by dioxane and ethyl acetate. In the process of lignin dissolution in H_2O/THF co-solvent, it is considered that H_2O molecules with smaller molecular size than organic solvent can act as an efficient plasticizer, which favors organic solvent diffusion into the compact lignin complexes, thereby leading to the solubilization of lignin in water-organic solvent mixture (Wang et al., 2018; Meng et al., 2019).

Recently, a "lignin-first" strategy, called as Co-solvent Enhanced Lignocellulosic Fractionation (CELF), has been widely applied in the fractionation of lignin from raw lignocellulose with high efficiency, in which H_2O/THF co-solvent is employed as the solvent system with the help of dilute acid (Nguyen et al., 2015; Smith et al., 2016a,b,c). In H_2O/THF mixture, about 85–90% of lignin in raw lignocellulosic biomass can be fractionated and solubilized. After boiling off the THF solvent, a lignin product without ash and sugar can be obtained by precipitation, which can act as a potential feedstock and be upgraded to high value-added chemicals and fuels in the further bio-refinery (Zhuo et al., 2018). The pretreatment in H_2O/THF system drastically reduces the molecular weight of lignin, and the cross-condensation reactions can be also efficiently minimized. For example, Meng et al. (2018) investigated the CELF lignin structure isolated under different conditions, and revealed that the molecular weight of lignin obtained sharply reduced by up to ∼90% when compared to the native lignin. Moreover, the extensive cleavage of β-O-4 linkages in lignin after pretreatment was also found, in addition to an obvious decrease of aliphatic OH groups resulting from the oxidation of side chains in lignin. However, the amount of phenolic OH groups greatly increased caused by the breakage of inter-unit linkages in lignin (Cai et al., 2013, 2014a,b; Nguyen et al., 2015).

Zhang et al. (2018) compared the performances of several solvents, including THF, 2-methyltetrahydrofuran (MeTHF), γ-valerolactone (GVL), ethyl acetate (EAC), and γ-butyrolactone (GBL), on the solubilization of lignin in corncob residue, and indicated that miscible co-solvents (e.g., H_2O-THF, H_2O-GVL, and H_2O-GBL) generally showed better ability for lignin fractionation than both single solvents and immiscible co-solvents like H_2O–MeTHF and H_2O–EAC under mild temperature. It was revealed that H_2O and organic solvent showed significant synergetic effect which favored the cleavage of linkages between lignin and amorphous cellulose in corncob residue. Organic solvent with different structure and property also influenced the solubilization of lignin with various structure units. For instance, MeTHF, EAC, and GVL preferentially dissolved S- and G-type lignin, while THF solvent showed high selectivity to fractionate and solubilize lignin with G and H units. In H_2O–THF, H_2O–MeTHF, H_2O–EAC, and H_2O–GBL co-solvents, β-γ bond was easier to be broken than β-O-4 bond, thereby giving 4-ethylguaiacol and 4-ethylphenol at higher temperature which occupied ∼70% of the total determined monophenols. In contrast, in H_2O–GVL co-solvent, α-1 bond was firstly broken, yielding guaiacol as the main product which occupied ∼75% of the total determined monophenols. Jiang et al. (2014) investigated the conversion of lignin in corncob residue in H_2O/THF co-solvent, and revealed that H_2O and THF solvents showed a synergistic effect on facilitating the dissolution of lignin, in which the ratio of H_2O to THF played an important role. It was found that the conversion of lignin in corncob residue initially increased with an increasing ratio of H_2O/THF, and got a maximum (89.8%) at the ratio of 3:7 (v/v), then decreased (**Figure 2**). H_2O, as a nucleophile agent, was necessary to break the linkages between lignin and cellulose components, such as hydrogen bonds, ether and ester bonds, ascribing to its high hydrogen bond acceptor ability. Due to the lower hydrogen bond acceptor ability of THF than that of H_2O, THF mainly presented a core effect on dissolving the fragment of dissolved lignin. The fractionated and solubilized lignin existed as oligomers with little monophenolic compound formation. When the solubilized lignin was further converted at higher temperature (300°C) in single THF solvent, the yield of monophenols was significantly enhanced. In particular, the yield of 2,6-dimethoxylphenol, 4-ethylguaiacol and 4-ethylphenol sharply increased to 6.6, 4.0, 10.5 wt%, respectively. The yield of determined monophenols was raised to 24.3 wt% in the absence of extra hydrogen source addition. It was considered that the special properties of THF as a supercritical fluid under the reaction conditions contributed to the great increase of

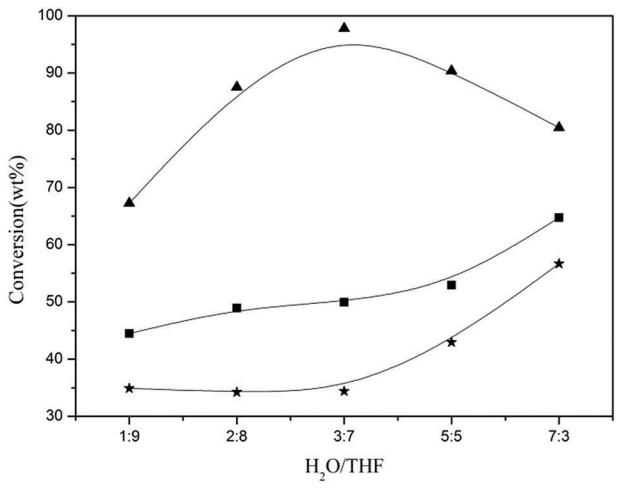

FIGURE 2 | Effect of the ratio of H_2O/THF on the conversion of corncob residue (■ raw material, ★ cellulose converted/cellulose contained, ▲ lignin converted/lignin contained; reaction conditions: corncob residue: 4.0 g, reaction temperature: 220°C, reaction time: 2.0 h). Reproduced from Jiang et al. (2014) with permission from Royal Society of Chemistry.

TABLE 2 | The effect of reaction medium on lignin conversion.

Solvent	Catalyst	Conversion of lignin (%)	Yield of phenolic monomer (%)				References
			Phenol	Guaiacol	Syringol	Others	
CH_3OH[a]	MgO	90.7	0.25	1.36	1.19	6.46	Long et al., 2014
C_2H_5OH[a]	MgO	84.5	0.25	1.42	1.24	5.54	Long et al., 2014
C_2H_5OH/H_2O[a]	MgO	92.5	0.82	1.58	1.32	7.52	Long et al., 2014
THF[a]	MgO	97.5	0.75	2.81	1.45	7.79	Long et al., 2014
H_2O[a]	MgO	42.3	0.23	0.70	0.52	0.74	Long et al., 2014
H_2O/THF[b]	Na_2CO_3	–	7.4	5.2	6.0	4.8	Jiang et al., 2016
H_2O/THF[c]	Na_2CO_3	–	5.6	4.9	12.2	4.2	Jiang et al., 2016
THF	–	–	6.5	2.79	1.01	1.39	Jiang et al., 2014

[a] *Condition: solvent 40 mL, MgO 3.0 mmol, and lignin 0.5 g, 250°C, 30 min.*
[b] *In step-one: Na_2CO_3 was introduced into 100 mL solvent (H_2O/THF: 3:7, v/v), 140°C.*
[c] *In step-one: Na_2CO_3 was introduced to 100 mL solvent (H_2O/THF: 5:5, v/v), 140°C.*

monophenol yield at 300°C. Thus, they proposed that THF solvent significantly favored the depolymerization of resulted lignin oligomers yielding monophenols under severe reaction conditions. Meng also investigated the solubilization of CELF lignin in several solvents. Results showed that 50 mL H_2O/THF co-solvent (40% THF) could solubilize about 2 g of lignin. 30% THF/H_2O co-solvent gave the maximum fraction yield (∼51%), however, there was no obvious relationship between the THF content and the fraction yield (Meng et al., 2019). Both molecular weights of the individual fractions obtained sharply decreased with the decrease of THF concentration from 35 to 20%.

The introduction of catalyst, especially alkaline, into H_2O/THF system could selectively improve the solubility and depolymerization of fractionated lignin (Nakasaka et al., 2017). For instance, it was pointed out that, with the introduction of MgO, much higher phenolic monomer yield (13.2%) was obtained in THF solvent than that without catalyst, attributing to the excellent fractionation and dissolution of lignin and the promoting effect on the catalytic activity of MgO in THF (**Table 2**; Long et al., 2014). Furthermore, it was considered that O atom of THF could coordinate with Lewis acids, thereby increasing the basicity of catalyst. When Na_2CO_3 was introduced into H_2O/THF co-solvent, it was found that almost all hydrogen bonds, ester and ether bonds between the cellulose and lignin components in corncob residue were broken at 140°C, leading to 94.6% removal of lignin (Jiang et al., 2016). In addition, the Cα-Cβ in aliphatic side-chain of lignin as well as β-O-4 linkage could be cleaved, yielding aryl aldehydes. In this work, H_2O was considered to contribute to the breakage of weak inter-linkages between lignin and cellulose components in corncob residue, and THF primarily solubilized the resulted fragments under mild temperature. Higher temperature (300°C) enabled the further cleavage of C_{Ar}-Cα bond, selectively giving monophenols with limited substituted alkyl groups. In the absence of extra hydrogen sources, 26.9 wt% yield of monophenol was achieved.

Given the outstanding lignin solubility in H_2O/THF co-solvent, many efforts have been devoted to reveal the solubilization mechanism of lignin in H_2O/THF co-solvent. Smith et al. (2016a,b) used temperature replica-exchange molecular dynamics to simulate lignin structure in H_2O/THF co-solvent, and revealed that single water media was a bad solvent for lignin, in which polymer–polymer interactions were favored. In this case, the lignin polymer collapsed to "globular" conformation, in which monomers were tightly packed. On the contrary, H_2O/THF co-solvent acted as a "theta" solvent, wherein lignin adopted a random coil state, unlike the collapsed globular conformation in single water medium. Because the interactions between polymer and solvent was preferential to the interactions between polymer and polymer, the self-aggregate of lignin with coil conformation could not happen, thereby resulting in the easy removal of lignin. Since H_2O/THF co-solvent system passed through a temperature gap in which H_2O and THF became immiscible, they also investigated the conformation of lignin in H_2O/THF co-solvent at this temperature regime. At the ratio of H_2O to THF commonly adopted in the process of lignin pretreatment, H_2O and THF became immiscible near 348 K and turned to miscible again above 410 K, which was just lower than the temperature (445–475 K) of lignin pretreatment in CELF approach (Smith et al., 2016b). It was worthy of noting that lignin was still a flexible random coil in H_2O/THF co-solvent for $T \geq 303$ K (Smith et al., 2018). At lower temperature ($T = 283$ K), it was found that lignin did swell in H_2O/THF co-solvent when compared to that in single water, although it did not exist in a random-coil conformation. This indicated that the presence of THF promoted the transform of lignin conformations from crumpled-globules to random-coil states, thereby benefiting to lignin removal. Because this effect was invariant to the temperature, it was proposed that H_2O/THF system was effective to fractionate and solubilize lignin from lignocellulose biomass even at low temperatures (Smith et al., 2016a,b). Three models for the transform from globule lignin to coil lignin were proposed, those are, one-state model, two-state model and three-state model. The free energy ΔG for the transition was obtained from the fitted kinetic constants, in which the slope and intercept of ΔG-temperature function were taken as the ΔS and ΔH values, respectively. The results showed that the best fit among these three models was the two-state model. Due to the negative ΔG, the globule-to-coil transition

TABLE 3 | Effects of reaction systems on the production of furfural from xylose/xylan.

Entry	Feedstock	Solvent system	Catalyst	*T* (°C)	Furfural yield (%)	References
1	Xylose	H_2O	$CrPO_4$	160	18	Xu et al., 2018b
2	Xylose	NaCl-H_2O/*n*-Butanol (10/30,v/v)	$CrPO_4$	160	48	Xu et al., 2018b
3	Xylose	NaCl-H_2O/2-Butanol(10/30,v/v)	$CrPO_4$	160	19	Xu et al., 2018b
4	Xylose	NaCl-H_2O/Toluene(10/30,v/v)	$CrPO_4$	160	71	Xu et al., 2018b
5	Xylose	NaCl-H_2O/MIBK(10/30,v/v)	$CrPO_4$	160	86	Xu et al., 2018b
6	Xylose	NaCl-H_2O/MeTHF(10/30,v/v)	$CrPO_4$	160	82	Xu et al., 2018b
7	Xylose	NaCl-H_2O/THF(10/30,v/v)	$CrPO_4$	160	88	Xu et al., 2018b
8	Xylose	NaCl-H_2O/THF(10/20,v/v)	$CrPO_4$	160	69	Xu et al., 2018b
9	Xylose	NaCl-H_2O/THF(10/40,v/v)	$CrPO_4$	160	43	Xu et al., 2018b
10	Xylose	NaCl-H_2O/THF(1/4,v/v)	$AlCl_3{\cdot}6H_2O$	140	75	Yang et al., 2012b
11	Xylose	H_2O/THF	CO_2	160	53.3	Özbek et al., 2018
12	Hemicellulose hydrolysate	H_2O/THF	CO_2	170	39.6	Özbek et al., 2018
13	Brown seaweed	H_2O/THF (5/95,v/v)	$H_3PW_{12}O_{40}$	180	33.8	Park et al., 2016
14	Wheat straw	H_2O/THF/MIBK(1/1/1, v/v)	CO_2	180	43	Morais et al., 2016

was spontaneous at room temperature, which was also both enthalphically and entropically favorable (Smith et al., 2016a,b).

HEMICELLULOSE FRACTIONATION AND SOLUBILIZATION AND FURTHER CONVERSION TO FURFURAL IN H_2O/THF SYSTEM

Hemicellulose with low degree of polymerization can be fractionated and further converted to furfural. The solubilization of hemicellulose/xylan and the further conversion of the resulted derivatives have also been conducted in H_2O/THF co-solvent. Smith et al. (2018) demonstrated that both H_2O/THF co-solvent and single water solvent acted as "good" solvents for hemicellulose/xylan conversion. In H_2O/THF co-solvent, the temperature-phase behavior determined the constitution of xylan solvation shell. When H_2O and THF were immiscible in the temperature range of 333–418 K, THF was left from the solvation shell of fractionated hemicellulose/xylan. In contrast, both H_2O and THF were present in the solvation shell of fractionated hemicellulose/xylan when the temperature was below and above this temperature regime. This implied that the fractionated hemicellulose/xylan solubilization in single water medium was just similar to that in H_2O/THF co-solvent in a temperature range of 333–418 K, but was greatly different outside this temperature range.

In addition to H_2O/THF single phasic system, it is known that the addition of NaCl to H_2O/THF co-solvent leads to the formation of biphasic NaCl-H_2O/THF system. NaCl-H_2O/THF biphasic system has been proved to show excellent efficiency for furfural formation from hemicellulose/xylan, where the further degradation of furfural produced in aqueous phase to the unwanted by-products like polymer and humins could be significantly inhibited, due to the immediate transfer of furfural from aqueous phase to organic phase. For instance, Xu et al. (2018b) examined the effect of organic solvents [methyl isobutyl ketone (MIBK), toluene, THF, MeTHF, and so on] on the production of furfural from xylose by the catalysis of $CrPO_4$. It was indicated that the addition of organic solvents could obviously promoted xylose conversion when compared to single water medium (**Table 3**). The highest furfural yield was achieved in NaCl-H_2O/THF system, attributing to the highest partition coefficient of THF for furfural among the selected solvent systems, which also efficiently eliminated furfural degradation in the aqueous phase. In addition, it was indicated that the H_2O/THF ratio substantially influenced the furfural yield, and H_2O/THF system with a 10/30 (mL/mL) ratio of H_2O to THF gave much higher furfural yield (88%) than that with 10/20 (mL/mL) and 10/40 (mL/mL) of H_2O/THF ratio. Yang et al. (2012b) also reported the benefits of NaCl-H_2O/THF biphasic system, in which a 75 mol% of furfural yield from xylose conversion was obtained with $AlCl_3{\cdot}6H_2O$ as catalyst under microwave heating.

Besides NaCl, other reagents have also been introduced into H_2O/THF co-solvent, affording a biphasic H_2O/THF system. For example, Özbek et al. (2018) studied the production of furfural in an H_2O/THF system with the addition of high-pressure CO_2. It was found that, in the presence of THF, CO_2 generated biphasic H_2O/THF system, because gaseous CO_2 had low solubility in THF, and was also insoluble in water medium. Consequently, the formed furfural could be continuously transferred from aqueous phase to CO_2/THF phase. Under the optimal pretreatment conditions, the highest furfural yield was up to 53.3 mol% when a model solution (including xylose and acetic acid) was used as starting material. In the case of real hemicellulose hydrolysate as feedstock, the yield of furfural was 39.6 mol% with 40.0 mol% of selectivity. Morais et al. (2016) proposed a two-stage strategy for the production of furfural from raw biomass. The first step involved the production of a water-soluble fraction (including xylose and xylo-oligosaccharide) via extracting hemicellulose component in wheat straw in H_2O system with high-pressure CO_2. In the second step, the resulted liquid fraction was further converted to furfural in H_2O/THF/MIBK-high-pressure CO_2

system, where MIBK was considered as the extracting solvent. However, it was found that the conversion of xylose decreased by 5 mol% in the presence of THF than that in a single water solvent. This was possibly due to the lower dielectric constant of H_2O/THF ($\varepsilon = 40$) than that of pure water ($\varepsilon = 78.5$ at 25°C) which decreased the acidity of reactions system (Critchfield et al., 1953; Muinasmaa et al., 1997). In final, furfural with 56.6 mol% of yield and 62.3 mol% of selectivity was obtained in this H_2O/THF/MIBK-high-pressure CO_2 system (50 bar).

CELLULOSE FRACTIONATION AND SOLUBILIZATION IN H_2O/THF SYSTEM

The presence of substantial hydrogen bonding in cellulose leads to a rigid structure with high crystallinity, which is strongly resistant to fractionation and dissolution and depolymerization in water. Several studies have demonstrated that polar aprotic solvents can simultaneously accelerate cellulose fractionation and dissolution and suppress the further dehydration reaction of monosaccharides, yielding target products with high yield and selectivity (Varhegyi et al., 1994; Ghosh et al., 2018). Typically, Ghosh et al. (2016) investigated the conversion of cellulose in a series of polar aprotic solvents, such as GVL, IMBK, acetonitrile, THF, 1,4-dioxane, ethyl acetate, and acetone. The results demonstrated that all the selected solvent fractionated and solubilized cellulose and gave desired products with high yield within a short time, possibly attributing to the decreased activation energy of cellulose depolymerization in polar aprotic solvents. The maximum yield of solubilized products from cellulose was 72–98% at 350°C. Combing the efficiency of solvents with their properties, it was revealed that the polar solubility parameter of a solvent might be the key factor contributing to its different fractionation and solubilization efficiency for cellulose (Archer, 1991; Su et al., 2009). Levoglucosan was the primary solubilized carbohydrate product, whose yield increased with increasing polar solubility parameter of solvents. The same group then investigated the efficiency of these polar aprotic solvents for the depolymerization of cellulose with the help of acid catalyst, producing water-soluble carbohydrates (Ghosh et al., 2018). The results indicated that acid catalyst significantly weakened the differences of yields in different solvents. In THF solvent, the levoglucosan selectivity at maximum yields reached 80%. Moreover, it was found that low rate of levoglucosan degradation was observed in those polar aprotic solvents with low polarity, thus enhancing the stability and promoting the yield of anhydrosugar.

Among the investigated polar aprotic solvent mixture with H_2O, H_2O/THF co-solvent system has been widely applied in the fractionation and solubilization/decrystallization of cellulose in lignocellulosic biomass (Zhang et al., 2014; Odabas et al., 2016). For instance, Jiang et al. (2016) pointed out that the introduction of THF into H_2O could greatly enhance cellulose conversion from 17.2 to 45.9% with the assistance of heteropolyacid catalysts ($ChH_2PW_{12}O_{40}$), which benefited the formation of HMF whose yield increased from 5.3 to 29.7%. Jiang et al. (2018) deeply investigated the performance

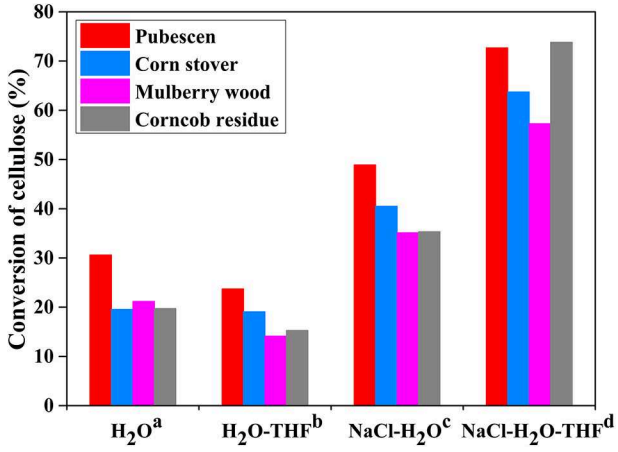

FIGURE 3 | Conversion of cellulose in raw lignocellulose in different reaction systems. Reaction conditions: 4.0 g raw material and (a) 100 mL H_2O; (b) 50 mL H_2O and 50 mL THF; (c) 20 g NaCl and 100 mL H_2O; (d) 20 g NaCl, 50 mL H_2O and 50 mL THF; at 200°C for 2 h. Reproduced from Jiang et al. (2018) with permission from Wiley.

of THF in NaCl-H_2O/THF biphasic system via experimental approaches, and found that the conversion of microcrystalline cellulose (M-cellulose) could reach up to 96.6%, and the cellulose component in actual lignocelluloses could also be completely solubilized (**Figure 3**). In H_2O/THF co-solvent system, it was revealed that THF could promote the cleavage of a half of intermolecular hydrogen bonds (O_6-H···O_3), while the role of H_2O in breaking intra-molecular hydrogen bonds (O_2-H···O_6) was significantly impeded. In NaCl-H_2O/THF biphasic system, THF could significantly improve the performances of both H_2O and NaCl on the cleavage of O_2-H···O_6 and O_3-H···O_5 intra-molecular hydrogen bonds, respectively (**Figure 4**). Moreover, it was indicated that cellulose-derived products could be immediately transferred from aqueous phase to organic phase, ascribing to the formation of hydrogen bonds between O atom of THF and aldehyde group in HMF or H atom in C_4-OH of glucose. This promoted the combination of more NaCl to –OH in M-cellulose, thus further disrupting the hydrogen bonding in M-cellulose and favoring the formation of products with small molecular weight (in particular HMF), which promoted the dissolution of cellulose in turn.

To elucidate the solubilization mechanism of cellulose in H_2O/THF system, Mostofian et al. (2016) employed all-atom molecular dynamic simulation to investigate cellulose structure in H_2O/THF mixture, as well as the interactions between cellulose and solvents. The results showed that H_2O/THF co-solvent afforded different characteristics of both H_2O and THF, resulting in the fractionation and solubilization of single cellulose chains and cellulose fibers via distinct ways. With the addition of THF to a water-only media, the reduction of cellulose hydration, especially for its hydrophobic faces, was observed, demonstrating that THF perturbed the interactions between H_2O molecules and cellulose. In H_2O/THF co-solvent system, H_2O and THF spontaneously phase-separated on the

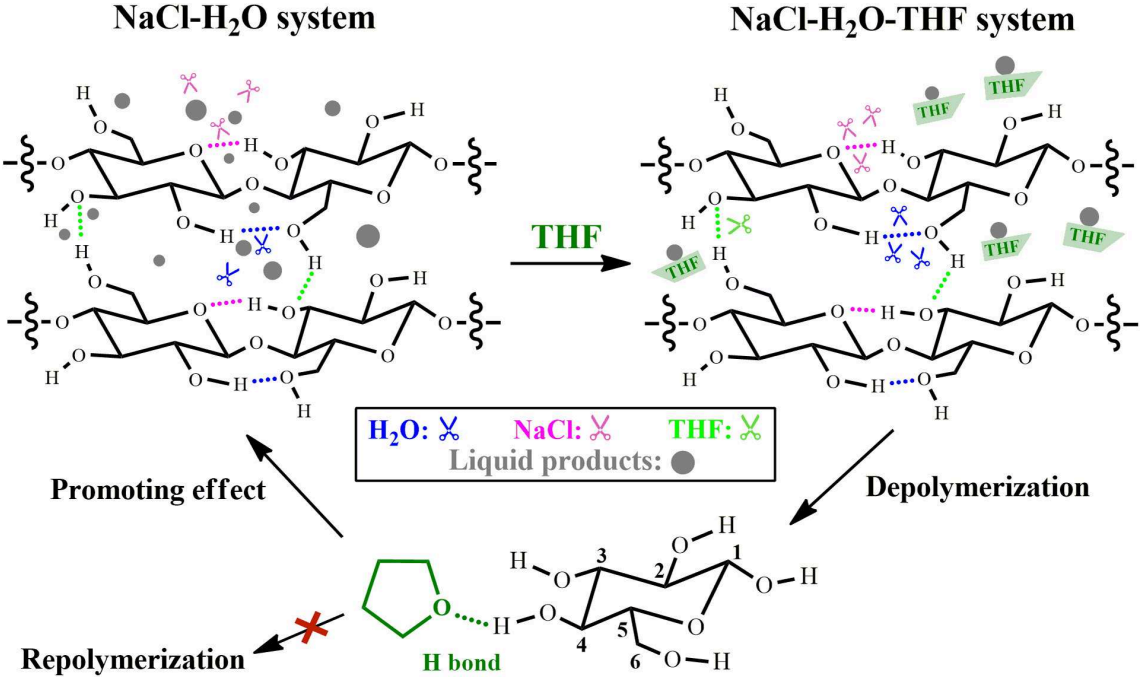

FIGURE 4 | Effect of THF on the dissolution and depolymerization of M-cellulose in NaCl-H_2O-THF system. Reaction conditions: M-cellulose (2.0 g) and NaCl (10 g) in solvent (100 mL, H_2O–organic solvent: 1:1 v/v) at 200°C for 2 h. Reproduced from Jiang et al. (2018) with permission from Wiley.

surface of cellulose fiber, in which H_2O accumulated at the hydrophilic cellulose faces due to the presence of hydrogen bonds between H_2O molecules and cellulose on the hydrophilic faces of cellulose, while THF stacked on the hydrophobic faces of cellulose. In contrast, the cellulose chain with full solvation was preferentially bound by H_2O molecules, indicating the easy hydrolysis of cellulose with the addition of THF. They also employed molecular dynamic simulations to compare the behavior of other H_2O-organosolv co-solvent systems (acetone, ethanol, and GVL) with H_2O/THF system (Smith et al., 2017). It was found that there were only weak differences in the selected solvent systems between the total amounts of hydrogen bonds in cellulose chain/strand-solvent and that of H_2O molecules in the cellulose solvation shell. However, the selected H_2O-organosolv co-solvents showed significantly distinct behavior of phase separation at the interface of co-solvent-cellulose, and the physical process of cellulose deconstruction was also different for these co-solvents. Particularly, in H_2O/THF co-solvent, the fraction of surface water was much slower than that in H_2O/GVL co-solvent, which might be important for promoting the chemical destroying of cellulose structure, since it could increase the reaction of THF-H_2O-cellulose, even when H_2O amount around cellulose was significantly decreased.

PROMOTING CHEMICAL PRODUCTION FROM LIGNOCELLULOSE IN H_2O/THF SYSTEM

THF owns outstanding ability for the extraction of biomass-based chemicals, such as levulinic acid, HMF, and furfural, from water mixtures, thus significantly increasing the yield of target products and minimizing the generation of unwanted by-products like polymers and humins. The investigations of the catalytic conversion of lignocellulose to platform chemicals have shown that chemicals with high yield and selectivity could be achieved in H_2O/THF system. For instance, Cai et al. (2013) reported THF could efficiently "protect" the formed furfural in aqueous phase from further degradation and minimizing furfural loss. In particular, NaCl-H_2O/THF biphasic system significantly enhances the partitioning of target chemicals into organic phase, which has been successfully adopted to increase the yield of products derived from lignocellulosic feedstock (Xie et al., 2019). Saha and Abu-Omar (2014) reviewed the benefits of biphasic solvent system (including H_2O/THF biphasic system) for the production of valuable chemicals (mainly HMF) from lignocellulose. In NaCl-H_2O/THF biphasic solvent system, H_2O is commonly recognized as the reactive phase for polysaccharide hydrolysis. The effects of THF can be classified into physical and chemical effects, wherein chemical effects involved the change of activation energy barriers in the key reaction step induced by the variant dynamics or environment in different solvent systems. The physical effect of THF related to the preferential solvation of the special functional groups in lignocellulosic derivatives, thus inhibiting their further conversion to form undesired by-products, in addition to immediate extracting the produced products from aqueous phase into organic phase once it was formed. Moreover, the extraction of chemicals in THF phase can improve the purity of obtained chemicals and make them be easily separated, thus enabling the treatment of lignocellulose economically and environmentally competitive. In this section,

the roles of H_2O/THF system in promoting the formation of several typical chemicals, including levoglucosan, HMF, levulinic acid, as well as the co-production of furfural and HMF, is attentively reviewed.

Levoglucosan and Fermentable Sugar

Levoglucosenone (LGO), an anhydro-sugar with a double bond combined with a ketone and aldehyde, in addition to two hydroxyl groups (Tang et al., 2017b; Krishna et al., 2018), has shown a huge potential to serve as a bio-based platform chemical (Nguyen et al., 2015; He et al., 2017a; Li et al., 2018). Cao et al. (2015) found that the highest yields of LGO could be obtained in both THF and GVL aqueous co-solvents. However, LGO seemed to be more stable in THF because THF inhibited the further conversion of LGO to HMF. On the contrary, GVL favored the isomerization of LGO to HMF, leading to its degradation. In addition, it was demonstrated that the water content controlled the product distribution derived from cellulose, in which the increase of water content to 5 wt% led to HMF production, and no LGO was produced when using single water as solvent. They also compared the yield of LGO in H_2O/THF with other H_2O-organic co-solvents (such as diglyme, tetraglyme, cyclopentyl methyl ether, 1,4-dioxane, and dimethyl sulfoxide), and found that H_2O/THF(1–2.5 wt% H_2O) afforded the highest yields of HMF and LGO (∼65 carbon%), with sulfuric acid as catalyst (He et al., 2017b). Weingarten et al. (2014) deeply investigated the influence of H_2O/THF ratio on cellulose degradation with dilute sulfuric acid as catalyst, and indicated that higher carbon yield of LGO was obtained in both single THF solvent and H_2O/THF co-solvent with a ratio of 40:1 (H_2O/THF) compared to the other reaction mixtures. As for the TOF value of cellulose conversion, it was more than 20 times in THF higher than that in single water solvent. As for HMF generation in THF solvent, the TOF value was 40 times higher than that in single water medium. The promoting performance of THF under this reaction condition was attributed to the fact that proton catalyst was more stable in THF solvent than in water medium (by 5.7 kcal mol^{-1}), thus resulting in the high reactivity of proton catalyst. Krishna et al. (2017) also showed that THF played a role in LGO stabilization and inhibited its isomerization reaction, thus resulting in the decrease of the yields of HMF and levulinic acid. The yield of xylose, arabinose, and glucose was up to 95% using corn stover as feedstock in H_2O/THF aqueous dilute acid system.

HMF Production

As for HMF production from lignocellulosic biomass, Weingarten et al. (2014) investigated the influence of a series of single organic solvents using H_2SO_4 as catalyst under mild conditions, and demonstrated that the polar aprotic solvents including THF, GVL, and acetone, gave a much higher HMF yield from cellulose when compared with water, ethyl acetate, and ethanol solvents. THF solvent afforded the highest HMF yield among the selected solvents. Compared to single THF solvent, the introduction of DMSO to THF solvent further improved the yield of HMF (98.0%). Wang et al. (2013) pointed out that the introduction of a small amount of water (<2.5 vol%) into THF was also beneficial for HMF production. The highest HMF yield from cellulose was 44%. In H_2O/THF (1:4 v/v) co-solvent, the yields of fructose and HMF from glucose conversion were 61 and 30%, respectively, by the catalysis of a base ($-NH_2$) functionalized mesoporous silica (aminopropyl-FMS) catalyst and a mesoporous silica with $-SO_3H$ (propylsulfonic acid-FMS) (Huang et al., 2014). Tucker et al. (2013) showed that the use of H_2O/THF co-solvent resulted in the significant increase of HMF selectivity (>70%) with a 80% of fructose conversion.

Although HMF yield can be promoted in H_2O/THF monophasic system, wherein the addition of a certain amount of H_2O can favor the dissolution of polysaccharides in addition to promoting the degradation of LGO to produce HMF, HMF degradation to levulinic and formic acids would take place with further increasing H_2O amount. To ensure the complete dissolution of feedstock in water but avoiding the degradation of HMF produced, NaCl–H_2O/THF biphasic system appears to be a promising solution, which has been proved to efficiently inhibit the rehydration of HMF to levulinic acid in water by immediate extraction of HMF to organic phase (**Table 4**; Chen et al., 2016; Zhao et al., 2018a,b). Glucose is a typical feedstock for the production of HMF, with the help of various catalysts. For example, Nikolla et al. (2011) described the conversion of glucose to HMF using Sn-Beta with acid as catalysts in a H_2O/THF biphasic system, and obtained the highest HMF selectivity (72%). Manganese phosphate ($MnPO_4$) also exhibited good efficiency for HMF production from biomass-derived carbohydrates, and the yield of HMF was 59% using glucose as feedstock in H_2O/THF biphasic reaction system (Xu et al., 2018a). Yang et al. (2012a) obtained a 61% yield of HMF from glucose by the catalysis of $AlCl_3{\cdot}6H_2O$ in NaCl-H_2O/THF system at 160°C under microwave heating. They demonstrated that THF inhibited HMF rehydration to generate levulinic acid, and also decreased the yield of lactic acid. Moreover, THF also showed high partitioning coefficient for HMF, and HMF recovery reached up to 94% when using HMF as starting material. The same group next investigated the reaction kinetics of glucose conversion to HMF in water, H_2O/THF, and NaCl–H_2O/THF reaction solvents by the catalysis of $AlCl_3$ (Tang et al., 2017a). Different product distributions were obtained in the three solvent systems, in which NaCl–H_2O/THF biphasic system gave the highest yield and selectivity to HMF. The kinetics of possible reaction pathways in these three solvent systems was investigated. The results demonstrated that the rate constants in the kinetic model were very sensitive to the ratios of solvent compositions. In the H_2O–THF co-solvent, the rates for fructose isomerization to glucose and formic acid formation from glucose and fructose were accelerated. On the contrary, the isomerization of glucose to fructose, fructose dehydration to HMF, and humins formation from fructose was decelerated. These results suggested that THF contributed to the inhibition of the rehydration and polymerization reactions of HMF, decreasing the formation of unwanted byproducts, as well as the dehydration of fructose to HMF and the polymerization of fructose to humins, but improved formic acid formation directly from glucose/fructose degradation without levulinic acid production. The yield of formic acid was therefore higher than that of levulinic acid in these selected solvents. Both in H_2O/THF and NaCl–H_2O/THF

TABLE 4 | The production of HMF from carbohydrates in different reaction systems.

Entry	Feedstock	Catalyst	Solvent system	*T* (°C)	HMF yield (%)	References
1	Glucose	THF	PCP(Cr)-NH_{2-x}	180	4.5	Liang et al., 2019
2	Glucose	H_2O	PCP(Cr)-NH_{2-x}	160	30.7	Liang et al., 2019
3	Glucose	H_2O	PCP(Cr)-NH_{2-x}	180	36.6	Liang et al., 2019
4	Glucose	H_2O	PCP(Cr)-NH_{2-x}	200	30.2	Liang et al., 2019
5	Glucose	H_2O/THF (1:2)	PCP(Cr)-NH_{2-x}	180	58.3	Liang et al., 2019
6	Glucose	H_2O/THF(1:1)	PCP(Cr)-NH_{2-x}	190	56.4	Liang et al., 2019
7	Glucose	H_2O/THF(1:2)	PCP(Cr)-NH_{2-x}	190	65.9	Liang et al., 2019
8	Glucose	H_2O/THF(1:3)	PCP(Cr)-NH_{2-x}	190	64.3	Liang et al., 2019
9	Glucose	H_2O/THF(1:4)	PCP(Cr)-NH_{2-x}	190	52.0	Liang et al., 2019
10	Glucose	H_2O/THF(1:2)	PCP(Cr)-NH_{2-x}	200	60.7	Liang et al., 2019
11	Glucose	H_2O	$AlCl_3{\cdot}6H_2O$	160	22	Yang et al., 2012a
12	Glucose	NaCl-H_2O/THF	$AlCl_3{\cdot}6H_2O$	160	52	Yang et al., 2012a
13	Glucose	NaCl-H_2O	$AlCl_3{\cdot}6H_2O$	160	17	Yang et al., 2012a
14	Glucose	NaCl-H_2O/THF	$AlCl_3{\cdot}6H_2O$	160	61	Yang et al., 2012a
15	Glucose	NaCl-H_2O/THF	HCl	160	12	Yang et al., 2012a
16	Glucose	H_2O	Sn-Beta, HCl	160	2.7	Nikolla et al., 2011
17	Glucose	H_2O/1-butanol	Sn-Beta, HCl	160	20.0	Nikolla et al., 2011
18	Glucose	NaCl-H_2O/1-butanol	Sn-Beta	160	13.5	Nikolla et al., 2011
19	Glucose	NaCl-H_2O/1-butanol	HCl	160	10.4	Nikolla et al., 2011
20	Glucose	NaCl-H_2O/1-butanol	Sn-Beta, HCl	160	41.3	Nikolla et al., 2011
21	Glucose	NaCl-H_2O/THF	Sn-Beta, HCl	180	56.9	Nikolla et al., 2011
22	Glucose	NaCl-H_2O/THF	Ti-Beta, HCl	180	53.2	Nikolla et al., 2011
23	Glucose	H_2O/THF	Aminopropyl-FMS, propylsulfonic acid-FMS	90	30	Huang et al., 2014
24	Glucose	NaCl-H_2O/THF	$MnPO_4$	160	59	Xu et al., 2018a
25	Fructose	NaCl-H_2O/THF	$FePO_4$	140	71.5	Yang et al., 2015
26	Cellobiose	NaCl-H_2O/THF	Sn-Beta, HCl	180	13.0	Nikolla et al., 2011
27	Cellulose	THF	H_2SO_4	190	44	Yang et al., 2015
28	Cellulose	H_2O/THF	$NaHSO_4/ZrO_2$	190	86.5	Fang et al., 2018
29	Bamboo fiber	H_2O	–	180	Trace	Sun et al., 2015
30	Bamboo fiber	H_2O	NH_2SO_3H	180	20.9	Sun et al., 2015
31	Bamboo fiber	H_2O-NaCl	NH_2SO_3H	180	11.6	Sun et al., 2015
32	Bamboo fiber	H_2O/THF(1:3)	NH_2SO_3H	180	30.7	Sun et al., 2015
33	Bamboo fiber	NaCl-H_2O/THF(3:1)	NH_2SO_3H	180	11.3	Sun et al., 2015
34	Bamboo fiber	NaCl-H_2O/THF(1:1)	NH_2SO_3H	180	39.7	Sun et al., 2015
35	Bamboo fiber	NaCl-H_2O/THF(1:3)	NH_2SO_3H	180	52.2	Sun et al., 2015
36	Bamboo fiber	NaCl-H_2O/THF(1:5)	NH_2SO_3H	180	49.2	Sun et al., 2015
37	Starch	NaCl-H_2O/THF	Sn-Beta, HCl	180	51.8	Nikolla et al., 2011

systems, the ratios of formic acid to levulinic acid were higher with lower levulinic acid yield, compared to that in water. Liang et al. (2019) indicated that HMF yield from glucose conversion in NaCl-H_2O/THF biphasic system was higher than that in any single phase solvents by the catalysis of bifunctional porous polymer (PCP) [PCP(Cr)-$NH_{2-x}(CH_3)_x$; $x = 0$, 1, or 2]. They also investigated the influence of H_2O-to-THF ratio, and revealed that the yield of HMF greatly increased with the increase of H_2O-to-THF ratio (from 1:1 to 1:2). In the case of 1:2 H_2O-to-THF ratio, the yield of HMF was 65.9% with 99.9% of glucose conversion. However, the minor decrease of HMF yield was observed above this ratio, possibly ascribing to the reductive performance of catalyst with the addition of excessive THF. When using fructose as feedstock, fructose could transform to furaniod form, which could be converted to HMF more easily (Zhu et al., 2011). For instance, Yang et al. (2015) obtained the highest yield (71.5 mol%) of HMF when using fructose as starting material in biphasic H_2O/THF system with $FePO_4$ as catalyst.

In addition to glucose/fructose, the conversion of cellulose even raw lignocellulosic biomass could yield HMF in H_2O/THF biphasic reaction system (Zhang et al., 2016; Yu et al., 2017). Fang et al. (2018) studied the production of HMF from cellulose in H_2O/THF biphasic system with $NaHSO_4$ and ZrO_2. It was pointed out that the yield of HMF linearly increased when THF dosage was raised to 32 g, and kept stable with more THF addition. Instead, the yield of levulinic acid gave an opposite

tendency to that of HMF with the increase of THF amount. The increasing THF amount also led to the enhancement of HMF extracting capacity. Consequently, the degradation of HMF to levulinic acid could be remarkably inhibited. More importantly, limited humins was formed with the addition of more THF, suggesting the efficient prevention of HMF condensation with glucose due to the transfer of HMF from aqueous phase to THF phase. The highest yield of HMF was up to 86.5%. Xuan et al. (2018) also showed that the volume ratio of H_2O/THF could influence the conversion of M-cellulose to HMF in H_2O/THF biphasic system with 1-(3-sulfonic acid)-propyl-3-methylimidazolium hydrogen sulfate ([PSMIM]HSO_4) and $ZnSO_4{\cdot}7H_2O$ as catalyst, since altering the water content led to a change in catalyst concentration. The yields of HMF exhibited a volcano trend with increasing H_2O volume, and a maximal value (58.8%) was achieved at a H_2O/THF ratio of 2:20 (v/v), in which the side reactions in the aqueous phase was remarkably suppressed. Sun et al. (2015) investigated the production of HMF from lignocellulosic biomass by the catalysis of solid organic acid catalyst NH_2SO_3H (SA) in H_2O/THF biphasic system with microwave heating, and found that THF contributed to suppress HMF rehydration, thus giving the highest HMF yield of 52.2%.

The Co-production of HMF and Furfural

As we know, furfural is unstable and highly reactive, which can be further degraded especially in the presence of dilute acid at high temperature, therefore mild reaction conditions are generally benefited to reducing furfural degradation. On the contrary, the conversion rate of glucan/cellulose to HMF in pure water is much slower because of the slow rate of glucan hydrolysis, thus severer conditions are required to enhance the generation rate for HMF. When raw lignocellulose is employed as feedstock, the loss of furfural usually exceeds the rate of HMF generation. Therefore, the co-production of furfural and HMF is always challenging because the different requirement of activation barrier for HMF and furfural formation. Recently, it has been proved that H_2O/THF co-solvent can overcome the practical barrier, which enables the simultaneous production of furfural and HMF from lignocellulose (**Table 5**). For example, Smith et al. (2018) observed that the formation of furfural was slower in H_2O/THF system, although the rate of disappearance of xylose monomers was faster than that of bulk water. THF seemed to co-catalyze the dehydration reaction of both C5 and C6 sugars via a kinetically favorable pathway.

Tan et al. (2018) investigated the production of furfural and HMF in different organic solvents, and found that THF media gave the highest yield (49.4%) of furfural, HMF and levulinic acid among the selected solvents over Hβ zeolite catalyst, followed by dioxane with the total yield of 43.8%. Due to the formation of char, both sulfolane and DMSO gave low yield of furfural, although the conversion of glucose was high. It was reported that Hβ zeolite catalyst showed a similar activity to a strong Brønsted acid, which depended on the solvation of proton relative to solvent polarity (Mellmer et al., 2014). Dioxane and THF solvents had smaller dipole moments, suggesting their weaker polarity compared with that of other solvents, thus resulting in less proton solvation and decreasing the degradation/polymerization of the generated HMF and furfural (Karinen et al., 2011; Hu et al., 2014). However, further increasing the water content in THF enhanced the rehydration of HMF forming levulinic acid and formic acid. Besides, the formation of by-products, such as polymer and humins resulted from the polymerization of sugars with HMF or levulinic acid could be also promoted owing to the increase of solution polarity. Cai et al. (2013) compared the yields of furfural, HMF, and levulinic acid derived from raw maple wood chips in H_2O/THF co-solvent to that in non-solvent system, and indicated that THF promoted both the hydrolysis of polysaccharides in maple wood as well as the next dehydration reactions of C5 and C6 sugars. The control experiments by varying the H_2O/THF ratio in H_2O/THF co-solvent demonstrated that the highest yield was realized with 1:3 solutions, obtaining 86% furfural, 21% HMF, and 40% levulinic acid. They also achieved the highest total yields of HMF (51%) and furfural (95%) directly from lignocellulosic biomass using $FeCl_3$ as catalyst in H_2O/THF co-solvent, whereas the yield of levulinic acid was very low (6%) (Cai et al., 2014a).

In general, biphasic NaCl-H_2O/THF system is more effective for the simultaneous production of furfural and HMF than miscible co-solvent, with the assistance of catalysts. In H_2O/THF biphasic system, Fang et al. (2019) obtained 76 and 81% yields of HMF and furfural from corn stover, respectively, using H_2SO_4/Na_2SO_4 as catalyst. In combination of Lewis acid with Brønsted acids in NaCl-H_2O/THF biphasic system, the yields of HMF and furfural was 44.0 and 92.2% catalyzed by $AlCl_3$/HCl and 36.5 and 81.4% by the catalysis of $ZnCl_2$/HCl, respectively (Gomes et al., 2018). As high as 71% yield of furfural and 30% yield of HMF could be simultaneously produced from wheat straw in NaCl-H_2O/THF biphasic system catalyzed by $SnCl_2$-PTA/β (Phosphotungstic acid) catalyst (Xu et al., 2019). Over $NbOPO_4$ and Sn-Mont catalyst, the simultaneous production of furfural and HMF from lignocellulose in NaCl-H_2O/THF biphasic system could be further converted to 2,5-dimethylfuran (DMF) and 2-methylfuran over Ru/Co_3O_4 catalyst, both of which could act as the promising liquid biofuels (Wang et al., 2014).

Levulinic Acid

The influence of different solvent systems, including water, THF and toluene solvents, on the production of levulinic acid from typical C6 sugar monomers/oligomers have also been investigated over solid acid catalysts, such as Amberlyst 70 (Hu et al., 2015). It was shown that solvent greatly influenced the yield of levulinic acid, in which the highest yield of levulinic acid was obtained in water, while the lowest yield was obtained in THF with dried A70 in toluene. This was possibly attributed to the different dispersion of sugars, products and catalyst in the solvents. In addition, solvent polarity affected the behaviors of Amberlyst 70, as well as the ability for the transfer of hydrogen ions and changing its dispersion in solvent. Mellmer et al. (2015) investigated the production of levulinic acid from furfuryl alcohol in a series of solvents, and indicated that the maximum levulinic acid yield (>70%) was achieved in monophasic H_2O/THF (1:4, w/w) solvent system using HZSM-5 zeolite as catalyst (**Figure 5**). It was revealed that the hydrophobic feature of ZSM-5 could change the solvent microenvironment within the framework of zeolite, enabling the formation of levulinic acid with high yield, even though the concentration of THF was very low

TABLE 5 | The production of furfural and HMF from lignocellulosic feedstock[a].

Entry	Solvent	Substrate	Catalyst	*T* (°C)	Yields (%)		References
					Furfural	HMF	
1	None	Maple wood[b]	1 wt% H_2SO_4	170	62[a]	2.4[a]	Cai et al., 2013
2	1:3 THF-H_2O	Maple wood[b]	1 wt% H_2SO_4	170	76[a]	4.9[a]	Cai et al., 2013
3	1:1 THF-H_2O	Maple wood[b]	1 wt% H_2SO_4	170	87[a]	13[a]	Cai et al., 2013
4	3:1 THF-H_2O	Maple wood[b]	1 wt% H_2SO_4	170	87[a]	21[a]	Cai et al., 2013
5	3:1 THF-H_2O	Maple wood[b]	1 wt% H_2SO_4	170	86[a]	21[a]	Cai et al., 2013
6	None	Maple wood[b]	1 wt% H_2SO_4	170	39[a]	2.6[a]	Cai et al., 2013
7	1:1 THF-H_2O	Maple wood[b]	1 wt% H_2SO_4	170	69[a]	7.6[a]	Cai et al., 2013
8	None	Maple wood[c]	1.5 wt% H_2SO_4	200	–	–	Cai et al., 2013
9	1:1 THF-H_2O	Maple wood[b]	$FeCl_3$	170	85[a]	16[a]	Cai et al., 2014a
10	1:1 THF-H_2O	Maple wood[b]	$CuCl_2$	170	83[a]	14[a]	Cai et al., 2014a
11	1:1 THF-H_2O	Maple wood[b]	$AlCl_3$	170	58[a]	18[a]	Cai et al., 2014a
12	1:1 THF-H_2O	Maple wood[b]	$CrCl_3$	170	43[a]	15[a]	Cai et al., 2014a
13	1:1 THF-H_2O	Maple wood[b]	$ZrOCl_2$	170	44[a]	14[a]	Cai et al., 2014a
14	1:1 THF-H_2O	Corn stover[b]	H_2SO_4	170	84[a]	16[a]	Cai et al., 2014a
15	1:1 THF-H_2O	Corn stover[b]	$FeCl_3$	170	85[a]	12[a]	Cai et al., 2014a
16	1:1 THF-H_2O	Corn stover[b]	$ZrOCl_2$	170	38[a]	14[a]	Cai et al., 2014a
17	3:1 THF-H_2O	Maple wood[b]	H_2SO_4	170	86[a]	21[a]	Cai et al., 2014a
18	3:1 THF-H_2O	Maple wood[b]	$FeCl_3$	170	97[a]	41[a]	Cai et al., 2014a
19	3:1 THF-H_2O	Maple wood[b]	$CuCl_2$	170	81[a]	22[a]	Cai et al., 2014a
20	3:1 THF-H_2O	Maple wood[b]	$AlCl_3$	170	75[a]	33[a]	Cai et al., 2014a
21	3:1 THF-H_2O	Corn stover[b]	$FeCl_3$	170	97[a]	42[a]	Cai et al., 2014a
22	3:1 THF-H_2O	Corn stover[b]	$CuCl_2$	170	89[a]	22[a]	Cai et al., 2014a
23	3:1 THF-H_2O	Corn stover[b]	$AlCl_3$	170	76[a]	36[a]	Cai et al., 2014a
24	4:1 THF-H_2O	Maple wood[b]	$FeCl_3$	170	95[a]	51[a]	Cai et al., 2014a
25	4:1 THF-H_2O	Corn stover[b]	$FeCl_3$	170	95[a]	45[a]	Cai et al., 2014a
26	NaCl-H_2O/THF (1/3)	Wheat straw	$SnCl_2$-PTA/β	180	71	30	Xu et al., 2019
27	NaCl-H_2O/THF	Cellulose	$AlCl_3$-HCl	180	92.2	44	Gomes et al., 2018
28	NaCl-H_2O/THF	Cellulose	$ZnCl_2$-HCl	180	81.4	36.5	Gomes et al., 2018
29	H_2O/THF	Corn stover	H_2SO_4	190	81	76	Fang et al., 2019

[a]*The yield was based on the theoretical yield.*
[b]*5 wt% solid loading.*
[c]*10% total solid loading.*

(2:1, H_2O/THF, w/w). The reaction kinetic studies demonstrated that the increase of yield was attributed to the fact that the reaction rate could be significantly enhanced in polar aprotic solvents. The obtained levulinic acid could be further converted to GVL in THF medium. For example, 100% yield of GVL could be produced using molecular H_2 over Ni/SA catalyst in THF medium, whereas much lower yield was found in water medium (Gundekari and Srinivasan, 2019).

INHIBITING HUMINS FORMATION

One of the most important contributions of H_2O/THF system for the improvement of both yield and selectivity to target products is relative to its role in inhibiting humins formation, which can also significantly enhance the carbon balance, as well as benefiting to the effective utilization of lignocellulose. This has been proved by substantial experimental results. For instance, Fu et al. (2017) showed that the presence of THF in CO_2-H_2O/THF system (1:1,V_{H2O}/V_{THF}) inhibited the generation of oligomers as well as increasing carbon balance. This suggested the promoting effect of THF on the retro-aldol condensation of fructose and the rehydration reaction of HMF, in addition to the inhibitory performance on the condensation of glucose via retro-aldol reaction (**Figure 6**). To deeply reveal the mechanism of H_2O/THF co-solvent on the inhibition of humins formation, Vasudevan and Mushrif (2015) conducted molecular dynamics simulations to study glucose solvation in H_2O/THF co-solvent. It was demonstrated that the added THF preferentially occupied the first solvation shell of glucose by competing with water molecules, in which most of water molecules were driven away from the first shell and existed in the second shell. Even in the presence of only a few THF, about 50% water molecules could be driven away from the first shell. Although the number of water molecules, which directly coordinated with glucose, became fewer with the addition of THF, the interaction between

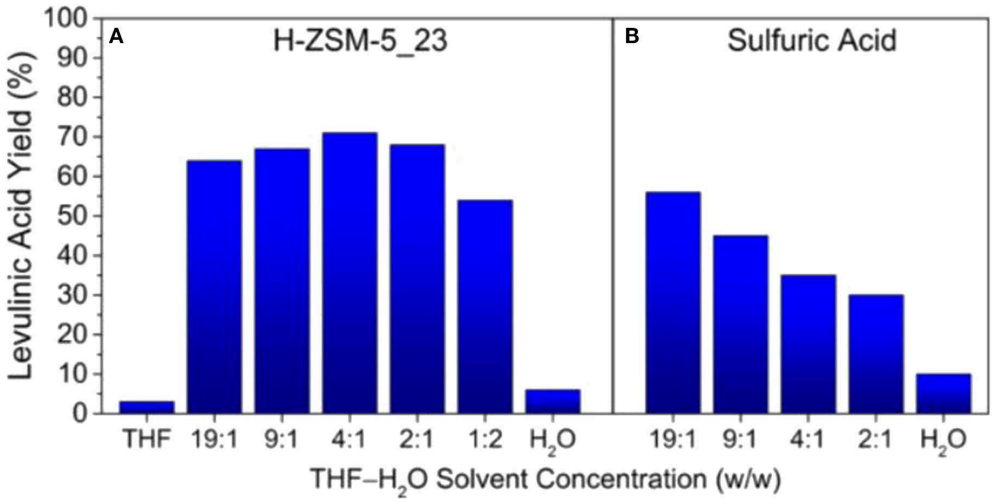

FIGURE 5 | Maximum levulinic acid yields achieved at various H_2O/THF solvent concentrations using **(A)** H-ZSM-5_23 and **(B)** sulfuric acid as catalyst. Reaction conditions: furfuryl alcohol (1 M), solvent (1.5 mL), 393 K, and stirring at 700 rpm. Reactant to solid catalyst ratio (w/w) = 0.6. Sulfuric acid solution = 0.1 M. Reproduced from Mellmer et al. (2015) with permission from American Chemistry Society.

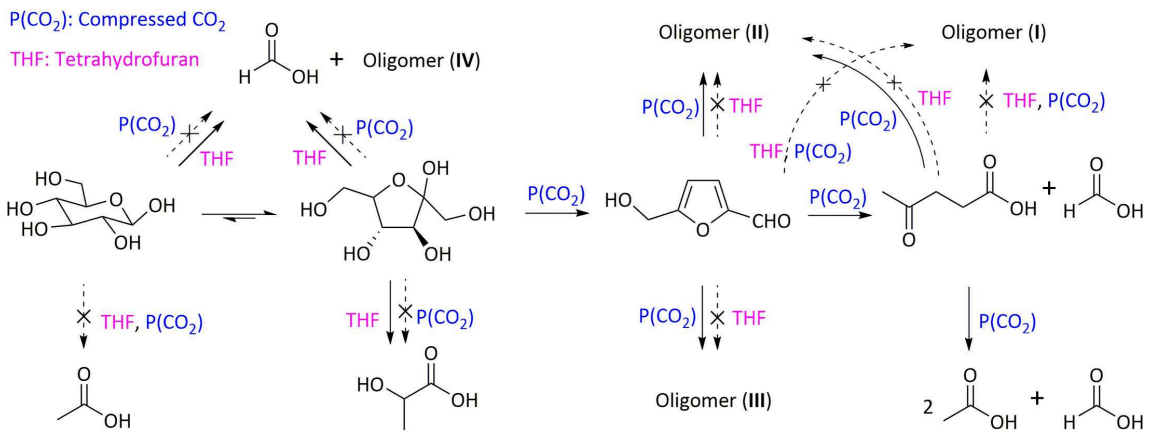

FIGURE 6 | Role of compressed CO_2 and THF in each subreaction of glucose conversion in a compressed CO_2-H_2O/THF solvent system. Reaction conditions: 2.2 mmol glucose, 32 mL solvent (H_2O-THF 1:1), 1.0 MPa CO_2, 190°C, 4 h. Reproduced from Fu et al. (2017) with permission from Royal Society of Chemistry.

water molecules with glucose was indeed strengthened, where THF mainly localized around H atom of -OH in glucose. The preferential arrangement of water molecules and THF molecules around glucose might facilitate the conversion of glucose to HMF or levulinic acid, and also reduce the degradation of glucose to undesired by-products. Increasing the ratio of THF to H_2O could also increase the lifetimes of hydrogen bond between glucose and water, thereby restricting the mobility of glucose in the solvent, thus reducing the formation rate of polymerization/condensation products and humins.

CONCLUDING REMARKS AND PERSPECTIVE

In summary, H_2O/THF co-solvent significantly fractionated and solubilized lignocellulosic biomass, especially for lignin and cellulose components, and lowered the recalcitrance of lignocellulose, affording liquid fluid with better mass and heat transfer, and enabling the adequate contact with catalyst, thereby favoring its further upgrading. In addition, H_2O/THF system also promotes the hydrolysis of fractionated cellulose/hemicellulose to sugars, as well as the next sugar dehydration, thereby achieving high yields of valuable chemicals with high selectivity (e.g., furfural, HMF, and levulinic acid). More importantly, H_2O/THF system, in particular NaCl-H_2O/THF biphasic system, also own extraordinary properties for extracting these chemical compounds from water mixture, thus inhibiting their further conversion and significantly increasing the yield and selectivity of target products, and minimizing the formation of byproducts, such as polymerization products and humins. Therefore, H_2O/THF system is a promising solvent system with multi-functions including not only the pretreatment and fractionation of lignocellulose but also the next conversion

of solubilized oligomers to obtain valuable chemicals with high yield and selectivity. After reaction, THF could be separated and recycled by simple distillation, due to its lower boiling point, which could be reused for the next run. Thus, the valorization of biomass in H_2O/THF system is considered as an economical approach.

There are still several problems which are not clarified and need deep investigation. For instance, the synergetic effect of H_2O and organic solvent (e.g., THF) in the process of fractionated lignin or cellulose/hemicellulose solubilization, as well as the influence of solvent system on the structure and property of resulted liquid fluid which decides the yield and selectivity of downstream product, required further studies. In addition, the recent research has pointed out that co-solvent mixture with various organic solvent structure or different ratios of H_2O to organic solvent exhibited unique selectivity for the solubilization of different components in lignocellulosic biomass. However, it is unknown about the reason and relationship between the properties of solvent system and its selectivity toward different components in lignocellulosic biomass. As for the further conversion of the resulted fluid, more information on the performance of solvent system needs to be revealed, besides the well-known extraction function. The influence of solvent system on the performance of catalyst also needs further clarification. In future work, we think more attention would be focused on the following aspects: (1) the influence of type and properties of solvent system on the selective fractionation and solubilization of one or two components in lignocellulosic biomass, (2) the deep elucidation of fractionation and solubilization in various solvents, (3) the performances of solvent system on the subsequent liquid fluid conversion, (4) mechanistic aspects at molecular level of the above conversion processes.

AUTHOR CONTRIBUTIONS

WZ and SX collaborated the references. JL and CH co-wrote and revised the paper.

FUNDING

This work was financially supported by the National Natural Science Foundation of China (No. 21606155) and Application Foundation Program of Sichuan Province (No. 2016JY0189).

REFERENCES

Archer, W. L. (1991). Determination of Hansen solubility parameters for selected cellulose ether derivatives. *Ind. Eng. Chem. Res.* 30, 2292–2298. doi: 10.1021/ie00058a008

Cai, C. M., Nagane, N., Kumar, R., and Wyman, C. E. (2014a). Coupling metal halides with a co-solvent to produce furfural and 5-HMF at high yields directly from lignocellulosic biomass as an integrated biofuels strategy. *Green Chem.* 16, 3819–3829. doi: 10.1039/c4gc00747f

Cai, C. M., Zhang, T., Kumar, R., and Wyman, C. E. (2013). THF co-solvent enhances hydrocarbon fuel precursor yields from lignocellulosic biomass. *Green Chem.* 15, 3140–3145. doi: 10.1039/c3gc41214h

Cai, C. M., Zhang, T., Kumar, R., and Wyman, C. E. (2014b). Integrated furfural production as a renewable fuel and chemical platform from lignocellulosic biomass. *J. Chem. Technol. Biotechnol.* 89, 2–10. doi: 10.1002/jctb.4168

Cao, F., Schwartz, T. J., McClelland, D. J., Krishna, S. H., Dumesic, J. A., and Huber, G. W. (2015). Dehydration of cellulose to levoglucosenone using polar aprotic solvents. *Energy Environ. Sci.* 8, 1808–1815. doi: 10.1039/c5ee00353a

Chen, B., Xu, G., Zheng, Z., Wang, D., Zou, C., and Chang, C. (2019). Efficient conversion of corn stover into 5-ethoxymethylfurfural catalyzed by zeolite USY in ethanol/THF medium. *Ind. Crop Prod.* 129, 503–511. doi: 10.1016/j.indcrop.2018.12.027

Chen, D.-Z., Fang, J.-Y., Shao, Q., Ye, J.-X., Ouyang, D.-J., and Chen, J.-M. (2013). Biodegradation of tetrahydrofuran by Pseudomonas oleovorans DT4 immobilized in calcium alginate beads impregnated with activated carbon fiber: Mass transfer effect and continuous treatment. *Bioresour. Technol.* 139, 87–93. doi: 10.1016/j.biortech.2013.04.037

Chen, D. W., Liang, F. B., Feng, D. X., Xian, M., Zhang, H. B., Liu, H. Z., et al. (2016). An efficient route from reproducible glucose to 5-hydroxymethylfurfural catalyzed by porous coordination polymer heterogeneous catalysts. *Chem. Eng. J.* 300, 177–184. doi: 10.1016/j.cej.2016.04.039

Cheng, W.-H., Chou, Y.-J., and Lin, H.-P. (2007). Air-water partitioning equilibrium of tetrahydrofuran in an activated sludge system. *J. Environ. Sci. Health Part A* 42, 129–134. doi: 10.1080/10934520601011205

Collard, F.-X., and Blin, J. (2014). A review on pyrolysis of biomass constituents: mechanisms and composition of the products obtained from the conversion of cellulose, hemicelluloses and ligni. *Renew. Sust. Energy Rev.* 38, 594–608. doi: 10.1016/j.rser.2014.06.013

Critchfield, F. E., Gibson, J. A. Jr., and Hall, J. L. (1953). Dielectric constant and refractive index from 20 to 35° and density at 25° for the system tetrahydrofuran—water. *J. Am. Chem. Soc.* 75, 6044–6045. doi: 10.1021/ja01119a509

Fang, X., Wang, Z., Song, W., Li, S., and Lin, W. (2019). Preparation of furans from catalytic conversion of corn stover in H_2O–THF co-solvent system–The effects of acids combined with alkali metal cations. *J. Taiwan Inst. Chem. Eng.* 97, 105–111. doi: 10.1016/j.jtice.2019.02.024

Fang, X., Wang, Z., Yuan, B., Song, W., Li, S., and Lin, W. (2018). Efficient conversion of cellulose to 5-hydroxymethylfurfural in $NaHSO_4/ZrO_2/H_2O$-THF biphasic system. *ChemistrySelect* 3, 1224–12249. doi: 10.1002/slct.201802029

Fowles, J., Boatman, R., Bootman, J., Lewis, C., Morgott, D., Rushton, E., et al. (2013). A review of the toxicological and environmental hazards and risks of tetrahydrofuran. *Crit. Rev. Toxicol.* 43, 811–828. doi: 10.3109/10408444.2013.836155

Fu, X., Dai, J., Guo, X., Tang, J., Zhu, L., and Hu, C. (2017). Suppression of oligomer formation in glucose dehydration by CO_2 and tetrahydrofuran. *Green Chem.* 19, 3334–3343. doi: 10.1039/c7gc01115f

Ghosh, A., Bai, X., and Brown, R. C. (2018). Solubilized carbohydrate production by acid-catalyzed depolymerization of cellulose in polar aprotic solvents. *ChemistrySelect* 3, 477–4785. doi: 10.1002/slct.201800764

Ghosh, A., Brown, R. C., and Bai, X. (2016). Production of solubilized carbohydrate from cellulose using non-catalytic, supercritical depolymerization in polar aprotic solvents. *Green Chem.* 18, 1023–1031. doi: 10.1039/c5gc02071a

Gomes, G. R., Rampon, D. S., and Ramos, L. P. (2018). Production of furan compounds from sugarcane bagasse using a catalytic system containing $ZnCl_2$/HCl or $AlCl_3$/HCl in a biphasic system. *J. Braz. Chem. Soc.* 29, 1115–1122. doi: 10.21577/0103-5053.20180014

Graglia, M., Kanna, N., and Esposito, D. (2015). Lignin refinery: towards the preparation of renewable aromatic building blocks. *Chem. Bio. Eng. Rev.* 2, 377–392. doi: 10.1002/cben.201500019

Gundekari, S., and Srinivasan, K. (2019). Screening of solvents, hydrogen source, and investigation of reaction mechanism for the hydrocyclisation of levulinic

acid to γ-valerolactone using Ni/SiO_2-Al_2O_3 catalyst. *Catal. Lett*. 149, 215–227. doi: 10.1007/s10562-018-2618-7

Hansen, C. M. (2007). *Hansen Solubility Parameters: A Use's Handbook, 2nd Edn.* New York, NY: CRC Press.

He, J., Huang, K., Barnett, K. J., Krishna, S. H., Alonso, D. M., Brentzel, Z. J., et al. (2017a). New catalytic strategies for α,ω-diols production from lignocellulosic biomass. *Faraday Discuss*. 202, 247–267. doi: 10.1039/c7fd00036g

He, J., Liu, M., Huang, K., Walker, T. W., Maravelias, C. T., Dumesic, J. A., et al. (2017b). Production of levoglucosenone and 5-hydroxymethylfurfural from cellulose in polar aprotic solvent–water mixtures. *Green Chem*. 19, 3642–3653. doi: 10.1039/c7gc01688c

Howard, P. H. (1990). *Handbook of Environmental Fate and Exposure Data for Organic Chemicals: Solvent v2*. Boca Raton, FL; London; New York, NY: CRC Press.

Hu, X., Wang, S., Westerhof, R. J. M., Wu, L., Song, Y., Dong, D., et al. (2015). Acid-catalyzed conversion of C6 sugar monomer/oligomers to levulinic acid in water, tetrahydrofuran and toluene: importance of the solvent polarity. *Fuel* 14, 56–63. doi: 10.1016/j.fuel.2014.10.034

Hu, X., Westerhof, R., Dong, D., Wu, L., and Li, C. Z. (2014). Acid-catalyzed conversion of xylose in 20 solvents: insight into interactions of the solvents with xylose, furfural, and the acid catalyst. *ACS Sustain. Chem. Eng*. 2, 2562–2257. doi: 10.1021/sc5004659

Huang, H., Denard, C. A., Alamillo, R., Crisci, A. J., Miao, Y., Dumesic, J. A., et al. (2014). Tandem catalytic conversion of glucose to 5-hydroxymethylfurfural with an immobilized enzyme and a solid acid. *ACS Catal*. 4, 2165–2168. doi: 10.1021/cs500591f

Jiang, Z., He, T., Li, J., and Hu, C. (2014). Selective conversion of lignin in corncob residue to monophenols with high yield and selectivity. *Green Chem*. 16, 4257–4265. doi: 10.1039/c4gc00620h

Jiang, Z., Zhang, H., He, T., Lv, X., Yi, J., Li, J., et al. (2016). Understanding the cleavage of inter- and intramolecular linkages in corncob residue for utilization of lignin to produce monophenols. *Green Chem*. 18, 4109–4115. doi: 10.1039/c6gc00798h

Jiang, Z., Zhao, P., Li, J., Liu, X., and Hu, C. (2018). Effect of tetrahydrofuran on the solubilization and depolymerization of cellulose in a biphasic system. *ChemSusChem* 11, 397–405. doi: 10.1002/cssc.201701861

Karinen, R., Vilonen, K., and Niemelä, M. (2011). Biorefining: heterogeneously catalyzed reactions of carbohydrates for the production of furfural and hydroxymethylfurfural. *ChemSusChem* 4, 1002–1016. doi: 10.1002/cssc.201000375

Krishna, S. H., Assary, R. S., Rashke, Q. A., Schmidt, Z. R., Curtiss, L. A., Dumesic, J. A., et al. (2018). Mechanistic insights into the hydrogenolysis of levoglucosanol over bifunctional platinum silica–alumina catalysts. *ACS Catal*. 8, 3743–3753. doi: 10.1021/acscatal.7b03764

Krishna, S. H., Walker, T. W., Dumesic, J. A., and Huber, G. W. (2017). Kinetics of levoglucosenone isomerization. *ChemSusChem* 10, 129–138. doi: 10.1002/cssc.201601308

Kroschwitz, J., Kirk, R. E., and Othmer, D. F. (2004). *Kirk-Othmer Concise Encyclopedia of Chemical Technology, 5th Edn*. New York, NY: John Wiley & Sons.

Kunkes, E. L., Simonetti, D. A., West, R. M., Serrano-Ruiz, J. C., Gärtner, C. A., and Dumesic, J. A. (2008). Catalytic conversion of biomass to monofunctional hydrocarbons and targeted liquid-fuel classes. *Science* 322, 417–421. doi: 10.1126/science.1159210

Li, W., Ghosh, A., Bbosa, D., Brown, R., and Wright, M. M. (2018). Comparative techno-economic, uncertainty and life cycle analysis of lignocellulosic biomass solvent liquefaction and sugar fermentation to ethanol. *ACS Sustain. Chem. Eng*. 6, 16515–11652. doi: 10.1021/acssuschemeng.8b03622

Liang, F., Chen, D., Liu, H., Liu, W., Xian, M., and Feng, D. (2019). One-pot synthesis of 5-hydroxymethylfurfural from glucose by Brønsted acid-free bifunctional porous coordination polymers in water. *ACS Omega* 4, 9316–9323. doi: 10.1021/acsomega.9b00882

Lim, J. S., Manan, Z. A., Alwi, S. R. W., and Hashim, H. (2012). A review on utilisation of biomass from rice industry as a source of renewable energy. *Renew. Sust. Energy Rev*. 16, 3084–3094. doi: 10.1016/j.rser.2012.02.051

Lin, C. S., Pfaltzgraff, L. A., Herrero-Davila, L., Mubofu, E. B., Abderrahim, S., Clark, J. H., et al. (2013). Food waste as a valuable resource for the production of chemicals, materials and fuels. Current situation and global perspective. *Energy Environ. Sci*. 6, 426–464. doi: 10.1039/c2ee23440h

Liu, J., Yan, Y., Yan, Y., and Zhang, J. (2019). Tetrahydrofuran (THF)-mediated structure of $THF(H_2O)_{n=1-10}$: a computational study on the formation of the THF hydrate. *Crystals* 9:73. doi: 10.3390/cryst9020073

Liu, Y., Mellmer, M. A., Alonso, D. M., and Dumesic, J. A. (2015). Effects of water on the copper-catalyzed conversion of hydroxymethylfurfural in tetrahydrofuran. *ChemSusChem* 8, 3983–3986. doi: 10.1002/cssc.201501122

Long, J., Zhang, Q., Wang, T., Zhang, X., Xu, Y., and Ma, L. (2014). An efficient and economical process for lignin depolymerization in biomass-derived solvent tetrahydrofuran. *Bioresour. Technol*. 154, 10–17. doi: 10.1016/j.biortech.2013.12.020

Maneechakr, P., and Karnjanakom, S. (2019). Selective conversion of fructose into 5-ethoxymethylfurfural over green catalyst. *Res. Chem. Intermediate* 45, 743–756. doi: 10.1007/s11164-018-3640-5

Matouš, J., Novák, J. P., Šobr, J., and Pick, J. (1972). Phase equilibria in the system tetrahydrofuran (1)–water (2). *Chem. Commun*. 37, 2653–2663. doi: 10.1135/cccc19722653

McCallum, C. S., Strachan, N., Bennett, S. C., Graham Forsythe, W., Garrett, M. D., Hardacre, C., et al. (2018). Catalytic depolymerisation of suberin rich biomass with precious metal catalysts. *Green Chem*. 20, 2702–2705. doi: 10.1039/C8GC00605A

Mellmer, M. A., Gallo, J. M. R., Alonso, D. M., and Dumesic, J. A. (2015). Selective production of levulinic acid from furfuryl alcohol in THF solvent systems over H-ZSM-5. *ACS Catal*. 5, 3354–3359. doi: 10.1021/acscatal.5b00274

Mellmer, M. A., Sener, C., Gallo, J. M., Luterbacher, J. S., Alonso, D. M., and Dumesic, J. A. (2014). Solvent effects in acid-catalyzed biomass conversion reactions. *Angew. Chem. Int. Ed*. 53, 11872–11875. doi: 10.1002/anie.201408359

Meng, X., Parikh, A., Seemala, B., Kumar, R., Pu, Y., Christopher, P., et al. (2018). Chemical transformations of poplar lignin during cosolvent enhanced lignocellulosic fractionation process. *ACS Sustain. Chem. Eng*. 6, 8711–8787. doi: 10.1021/acssuschemeng.8b01028

Meng, X., Parikh, A., Seemala, B., Kumar, R., Pu, Y., Wyman, C. E., et al. (2019). Characterization of fractional cuts of co-solvent enhanced lignocellulosic fractionation lignin isolated by sequential precipitation. *Bioresour. Technol*. 272, 202–208. doi: 10.1016/j.biortech.2018.09.130

Mlynar, J., and Sarkanen, S. (1996). Renaissance in ultracentrifugal sedimentation equilibrium calibrations of size exclusion chromatographic elution profiles. *ACS Symp. Ser*. 635, 379–400. doi: 10.1021/bk-1996-0635.ch021

Morais, A. R. C., Matuchaki, M. D. D. J., Andreaus, J., and Bogel-Lukasik, R. (2016). A green and efficient approach to selective conversion of xylose and biomass hemicellulose into furfural in aqueous media using high-pressure CO_2 as a sustainable catalyst. *Green Chem*. 18, 2985–2994. doi: 10.1039/C6GC00043F

Mostofian, B., Cai, C. M., Smith, M. D., Petridis, L., Cheng, X., Wyman, C. E., et al. (2016). Local phase separation of co-solvents enhances pretreatment of biomass for bioenergy applications. *J. Am. Chem. Soc*. 138, 10869–10878. doi: 10.1021/jacs.6b03285

Muinasmaa, U., Råfols, C., Bosch, E., and Rosés, M. (1997). Ionic equilibria in aqueous organic solvent mixtures the dissociation constants of acids and salts in tetrahydrofuran/water mixtures. *Anal. Chim. Acta* 340, 133–141. doi: 10.1016/s0003-2670(96)00516-8

Nakasaka, Y., Yoshikawa, T., Kawamata, Y., Tago, T., Sato, S., Takanohashi, T., et al. (2017). Fractionation of degraded lignin by using a water/1-butanol mixture with a solid-acid catalyst: a potential source of phenolic compounds. *ChemCatChem* 9, 2875–2880. doi: 10.1002/cctc.201700104

Nguyen, T. Y., Cai, C. M., Kumar, R., and Wyman, C. E. (2015). Co-solvent pretreatment reduces costly enzyme requirements for high sugar and ethanol yields from lignocellulosic biomass. *ChemSusChem* 8, 1716–1725. doi: 10.1002/cssc.201403045

Ni, Y., and Hu, Q. (1995). Alcell® lignin solubility in ethanol–water mixtures. *J. Appl. Polym. Sci*. 57, 1441–1446. doi: 10.1002/app.1995.070571203

Nikolla, E., Roman-Leshkov, Y., Moliner, M., and Davis, M. E. (2011). "One-Pot" synthesis of 5-(Hydroxymethyl)furfural from carbohydrates using tin-beta zeolite. *ACS Catal*. 1, 408–410. doi: 10.1021/cs2000544

Odabas, N., Amer, H., Bacher, M., Henniges, U., Potthast, A., and Rosenau, T. (2016). Properties of cellulosic material after cationization in different solvents. *ACS Sustain. Chem. Eng*. 4, 2295–2301. doi: 10.1021/acssuschemeng.5b01752

Özbek, H. N., Fockink, D. H., Yanik, D. K., Gögüs, F., and Łukasik, R. M. (2018). The green biorefinery concept for the valorisation of pistachio shell by high-pressure CO_2/H_2O system. *J. Clean. Prod.* 196, 842–848. doi: 10.1016/j.jclepro.2018.06.062

Pace, V., Hoyos, P., Castoldi, L., Domínguez de María, P., and Alcántara, A. R. (2012). 2-Methyltetrahydrofuran (2-MeTHF): a biomass-derived solvent with broad application in organic chemistry. *ChemSusChem* 5, 1369–1379. doi: 10.1002/cssc.201100780

Park, G., Jeon, W., Ban, C., Woo, H. C., and Kim, D. H. (2016). Direct catalytic conversion of brown seaweed-derived alginic acid to furfural using 12-tungstophosphoric acid catalyst in tetrahydrofuran/water co-solve. *Energy Convers. Manage.* 118, 135–141. doi: 10.1016/j.enconman.2016.03.091

Saha, B., and Abu-Omar, M. M. (2014). Advances in 5-hydroxymethylfurfural production from biomass in biphasic solvents. *Green Chem.* 16, 24–38. doi: 10.1039/c3gc41324a

Schuerch, C. (1952). The solvent properties of liquids and their relation to the solubility, swelling, isolation, and fractionation of lignin. *J. Am. Chem. Soc.* 74, 5061–5067. doi: 10.1021/ja01140a020

Shuai, L., and Luterbacher, J. (2016). Organic solvent effects in biomass conversion reactions. *ChemSusChem* 9, 133–155. doi: 10.1002/cssc.201501148

Shuai, L., Questell-Santiago, Y. M., and Luterbacher, J. S. (2016). A mild biomass pretreatment using γ-valerolactone for concentrated sugar production. *Green Chem.* 18, 937–943. doi: 10.1039/c5gc02489g

Smith, M. D., Cai, C. M., Cheng, X., Petridisa, L., and Smith, J. C. (2018). Temperature-dependent phase behavior of tetrahydrofuran–water alters solubilization of xylan to improve co-production of furfurals from lignocellulosic biomass. *Green Chem.* 20, 1612–1620. doi: 10.1039/c7gc03608f

Smith, M. D., Cheng, X., Petridis, L., Mostofian, B., and Smith, J. C. (2017). Organosolv-water cosolvent phase separation on cellulose and its influence on the physical deconstruction of cellulose: a molecular dynamics analysis. *Sci. Rep.* 7:14494. doi: 10.1038/s41598-017-15048-7

Smith, M. D., Mostofian, B., Cheng, X., Petridis, L., Cai, C. M., Wymanc, C. E., et al. (2016a). Cosolvent pretreatment in cellulosic biofuel production: effect of tetrahydrofuran-water on lignin structure and dynamics. *Green Chem.* 18, 1268–1277. doi: 10.1039/C5GC01952D

Smith, M. D., Mostofian, B., Petridis, L., Cheng, X., and Smith, J. C. (2016b). Molecular driving forces behind the tetrahydrofuran-water miscibility gap. *J. Phys. Chem. B* 120, 740–747. doi: 10.1021/acs.jpcb.5b09770

Smith, M. D., Petridis, L., Cheng, X., Mostofianacd, B., and Smith, J. C. (2016c). Enhanced sampling simulation analysis of the structure of lignin in the THF–water miscibility gap. *Phys. Chem. Chem. Phys.* 18, 6394–6398. doi: 10.1039/c5cp07088k

Su, Y., Brown, H. M., Huang, X., Zhou, X., Amonette, J. E., and Zhang, Z. C. (2009). Single-step conversion of cellulose to 5-hydroxymethylfurfural (HMF), a versatile platform chemical. *Appl. Catal. A* 361, 117–122. doi: 10.1016/j.apcata.2009.04.002

Sun, J., Yuan, X., Shen, Y., Yi, Y., Wang, B., Xu, F., et al. (2015). Conversion of bamboo fiber into 5-hydroxymethylfurfural catalyzed by sulfamic acid with microwave assistance in biphasic system. *Ind. Crop Prod.* 70, 266–271. doi: 10.1016/j.indcrop.2015.03.044

Tan, J., Wang, H., Ma, L., Wang, C., Liu, Q., Zhang, Q., et al. (2018). Selective yields of furfural and hydroxymethylfurfural from glucose in tetrahydrofuran over Hb zeolite. *RSC Adv.* 8, 24534–24540. doi: 10.1039/c8ra04060e

Tang, J., Zhu, L., Fu, X., Dai, J., Guo, X., and Hu, C. (2017a). Insights into the kinetics and reaction network of aluminum chloride-catalyzed conversion of glucose in NaCl–H_2O/THF biphasic system. *ACS Catal.* 7, 256–266. doi: 10.1021/acscatal.6b02515

Tang, X., Wei, J., Ding, N., Sun, Y., Zeng, X., Hu, L., et al. (2017b). Chemoselective hydrogenation of biomass derived 5-hydroxymethylfurfural to diols: Key intermediates for sustainable chemicals, materials and fuels. *Renew. Sust. Energy Rev.* 77, 287–296. doi: 10.1016/j.rser.2017.04.013

Tuck, C. O., Pérez, E., Horváth, I. T., Sheldon, R. A., and Poliakoff, M. (2012). Valorization of biomass: deriving more value from waste. *Science* 337, 695–699. doi: 10.1126/science.1218930

Tucker, M. H., Alamillo, R., Crisci, A. J., Gonzalez, G. M., Scott, S. L., and Dumesic, J. A. (2013). Sustainable solvent systems for use in tandem carbohydrate dehydration hydrogenation. *ACS Sustain. Chem. Eng.* 1, 554–560. doi: 10.1021/sc400044d

Varhegyi, G., Jakab, E., and Antal, M. J. (1994). Is the broido-shafizadeh model for cellulose pyrolysis true? *Energy Fuel* 8, 1345–1352. doi: 10.1021/ef00048a025

Vasudevan, V., and Mushrif, S. H. (2015). Insights into the solvation of glucose in water, dimethyl sulfoxide (DMSO), tetrahydrofuran (THF) and N,N-dimethylformamide (DMF) and its possible implications on the conversion of glucose to platform chemicals. *RSC Adv.* 5, 20756–20763. doi: 10.1039/c4ra15123b

Wang, J., Liu, X., Hu, B., Lu, G., and Wang, Y. (2014). Efficient catalytic conversion of lignocellulosic biomass into renewable liquid biofuels via furan derivatives. *RSC Adv.* 4, 31101–31103. doi: 10.1039/c4ra04900d

Wang, J., Ren, J., Liu, X., Lu, G., and Wang, Y. (2013). High yield production and purification of 5-hydroxymethylfurfural. *AIChE J.* 59, 2558–2566. doi: 10.1002/aic.14019

Wang, Y.-Y., Li, M., Wyman, C. E., Cai, C. M., and Ragauskas, A. J. (2018). Fast fractionation of technical lignins by organic cosolvents. *ACS Sustain. Chem. Eng.* 6, 6064–6072. doi: 10.1021/acssuschemeng.7b04546

Weingarten, R., Rodriguez-Beuerman, A., Cao, F., Luterbacher, J. S., Alonso, D. M., Dumesic, J. A., et al. (2014). Selective conversion of cellulose to hydroxymethylfurfural in polar aprotic solvents. *ChemCatChem* 6, 2229–2234. doi: 10.1002/cctc.201402299

Xie, Y., Yu, F., Wang, Y., He, X., Zhou, S., and Cui, H. (2019). Salt effect on liquideliquid equilibria of tetrahydrofuran/water/5-hydroxymethylfurfural system. *Fluid Phase Equilibr.* 493, 137–143. doi: 10.1016/j.fluid. 2019.04.018

Xin, Q., Pfeiffer, K., Prausnitz, J. M., Clark, D. S., and Blanch, H. W. (2012). Extraction of lignins from aqueous–ionic liquid mixtures by organic solvents. *Biotechnol. Bioeng.* 109, 346–352. doi: 10.1002/bit.24337

Xu, S., Pan, D., Li, W., Shen, P., Wu, Y., Song, X., et al. (2018a). Direct conversion of biomass-derived carbohydrates to 5- hydroxymethylfurfural using an efficient and inexpensive manganese phosphate catalyst. *Fuel Process Technol.* 181, 199–206. doi: 10.1016/j.fuproc.2018.09.027

Xu, S., Pan, D., Wu, Y., Song, X., Gao, L., Li, W., et al. (2018b). Efficient production of furfural from xylose and wheat straw by bifunctional chromium phosphate catalyst in biphasic systems. *Fuel Process Technol.* 175, 90–96. doi: 10.1016/j.fuproc.2018.04.005

Xu, S., Pan, D., Wu, Y., Xu, N., Yang, H., Gao, L., et al. (2019). Direct conversion of wheat straw components into furan compounds using a highly efficient and reusable $SnCl_2$-PTA/β zeolite catalyst. *Ind. Eng. Chem. Res.* 58, 9276–9285. doi: 10.1021/acs.iecr.9b00984

Xuan, Y., He, R., Han, B., Wu, T., and Wu, Y. (2018). Catalytic conversion of cellulose into 5-hydroxymethylfurfural using [PSMIM]HSO_4 and $ZnSO_4 \cdot 7H_2O$ Co-catalyst in biphasic system. *Waste Biomass Valor.* 9, 401–408. doi: 10.1007/s12649-016-9752-5

Yang, L., Yan, X., Xu, S., Chen, H., Xia, H., and Zuo, S. (2015). One-pot synthesis of 5-hydroxymethylfurfural from carbohydrates using an inexpensive $FePO_4$ catalyst. *RSC Adv.* 5, 19900–19906. doi: 10.1039/C4RA16145A

Yang, Y., Hu, C., and Abu-Omar, M. M. (2012a). Conversion of carbohydrates and lignocellulosic biomass into 5-hydroxymethylfurfural using $AlCl_3 \cdot 6H_2O$ catalyst in a biphasic solvent System. *Green Chem.* 14, 509–513. doi: 10.1039/c1gc15972k

Yang, Y., Hu, C.-W., and Abu-Omar, M. M. (2012b). Synthesis of furfural from xylose, xylan, and biomass using $AlCl_3 \cdot 6H_2O$ in biphasic media via xylose isomerization to xylulose. *ChemSusChem* 5, 405–410. doi: 10.1002/cssc.201100688

Yu, I. K. M., Tsang, D. C. W., Chen, S. S., Wang, L., Hunt, A. J., Sherwood, J., et al. (2017). Polar aprotic solvent-water mixture as the medium for catalytic production of hydroxymethylfurfural (HMF) from bread waste. *Bioresour. Technol.* 245, 456–462. doi: 10.1016/j.biortech.2017.08.170

Zakzeski, J., Bruijnincx, P. C., Jongerius, A. L., and Weckhuysen, B. M. (2010). The catalytic valorization of lignin for the production of renewable chemicals. *Chem. Rev.* 110, 3552–3599. doi: 10.1021/cr900354u

Zhang, H., Liu, X., Li, J., Jiang, Z., and Hu, C. (2018). Performances of several solvents on the cleavage of inter and intramolecular linkages of lignin in corncob residue. *ChemSusChem* 11, 1494–1504. doi: 10.1002/cssc.201800309

Zhang, W., Zhao, W., and Dai, Y. (2014). The effect of different methods to pretreat reed pulp on the crystallinity of microcrystalline cellulose. *Adv. Mater. Res.* 1056, 12–15. doi: 10.4028/www.scientific.net/amr.1056.12

Zhang, X., Zhang, D., Sun, Z., Xue, L., Wang, X., and Jiang, Z. (2016). Highly efficient preparation of HMF from cellulose using temperature-responsive

heteropolyacid catalysts in cascade reaction. *Appl. Catal. B* 196, 50–56. doi: 10.1016/j.apcatb.2016.05.019

Zhao, P., Cui, H., Zhang, Y., Zhang, Y., Wang, Y., Zhang, Y., et al. (2018a). Synergetic effect of Bronsted/Lewis acid sites and water on the catalytic dehydration of glucose to 5-hydroxymethylfurfural by heteropolyacid-based ionic hybrids. *ChemistryOpen* 7, 824–832. doi: 10.1002/open.201800138

Zhao, Y., Wang, S. R., Lin, H. Z., Chen, J. P., and Xu, H. (2018b). Influence of a Lewis acid and a Bronsted acid on the conversion of microcrystalline cellulose into 5-hydroxymethylfurfural in a single phase reaction system of water and 1,2-dimethoxyethane. *RSC Adv*. 8, 7235–7242. doi: 10.1039/c7ra13387a

Zhou, C.-H., Xia, X., Lin, C.-X., Tong, D.-S., and Beltramini, J. (2011). Catalytic conversion of lignocellulosic biomass to fine chemicals and fuels. *Chem. Soc. Rev*. 40, 5588–5617. doi: 10.1039/c1cs15124j

Zhu, H., Cao, Q., Li, C. H., and Mu, X. D. (2011). Acidic resin-catalyzed conversion of fructose into furan derivatives in low boiling point solvents. *Carbohyd. Res.* 346, 2016–2018. doi: 10.1016/j.carres.2011.05.026

Zhuo, S., Peng, B., Yan, X., Zhang, K., Si, M., Liu, M., et al. (2018). Conquering lignin recalcitrance by *Pandoraea* sp. B-6 to improve co-solvent pretreatment of corn stover. *Process Biochem*. 75, 187–193. doi: 10.1016/j.procbio.2018.09.012

Conflict of Interest: The authors declare that the research was conducted in the absence of any commercial or financial relationships that could be construed as a potential conflict of interest.

frontiers in Chemistry

REVIEW
published: 07 February 2020
doi: 10.3389/fchem.2019.00948

Recent Advances in Aqueous-Phase Catalytic Conversions of Biomass Platform Chemicals Over Heterogeneous Catalysts

Xiaoxian Li[1], *Lilong Zhang*[1], *Shanshan Wang*[1] *and Yulong Wu*[1,2]*

[1] *Institute of Nuclear and New Energy Technology, Tsinghua University, Beijing, China,* [2] *Laboratory of Advanced Reactor Engineering and Safety of Ministry of Education, Institute of Nuclear and New Energy Technology, Tsinghua University, Beijing, China*

A series of biomass-derived platform molecules, such as glucose, furans, levulinic acid, 5-hydroxymethylfurfural, and acetic acids, can be converted into a variety of value-added chemicals through catalytic transformations that include dehydration, hydrogenation, oxidation, isomerization, reforming, ketonization, and aldol condensation over heterogeneous catalysts. Aqueous-phase processing is an important issue and a great challenge for the heterogeneous catalytic conversion of biobased chemicals due to the high water content of the biomass and the formation of water during the transformation process. In this paper, heterogeneous catalysts that are applicable to the aqueous-phase conversion process of biomass platform chemicals, including noble metal catalysts, non-noble metal catalysts, bimetallic catalysts, metal oxides, and zeolite, are introduced, and a comprehensive evaluation of the catalyst performance, including the catalytic activity, stability, and regeneration performance of different kinds of heterogeneous catalysts, are made. Besides, we highlighted the effect of water on heterogeneous catalysts and the deactivation mechanism in the aqueous phase. Beyond this, several catalytic mechanisms of aqueous-phase conversion over heterogeneous catalysts are summarized in order to help understand the reaction process on the surface of catalysts in the aqueous phase, so as to design targeted catalysts. At last, a prospect of biobased chemicals and fuels is forecasted.

Keywords: biomass, aqueous phase, heterogeneous catalysis, dehydration, hydrogenation, oxidation, isomerization, ketonization

OPEN ACCESS

Edited by:
Yasushi Sekine,
Waseda University, Japan

Reviewed by:
Miguel Angel Centeno,
Instituto de Ciencia de Materiales de Sevilla (ICMS), Spain
Zhibao Huo,
Shanghai Ocean University, China

***Correspondence:**
Yulong Wu
wylong@tsinghua.edu.cn

Specialty section:
This article was submitted to Green and Sustainable Chemistry, a section of the journal Frontiers in Chemistry

Received: *30 October 2019*
Accepted: *31 December 2019*
Published: *07 February 2020*

Citation:
Li X, Zhang L, Wang S and Wu Y (2020) Recent Advances in Aqueous-Phase Catalytic Conversions of Biomass Platform Chemicals Over Heterogeneous Catalysts. Front. Chem. 7:948. doi: 10.3389/fchem.2019.00948

INTRODUCTION

With the depletion of traditional fossil energy and its environmental adverse impact, alternative energy sources that have good renewability and environment friendliness are needed (Tang et al., 2017). Among all of the alternative resources, biomass is considered to be one of the most potential competitors not only as fuels but also as chemical intermediates (Dusselier et al., 2013) because of the rich abundant and good sustainability. There is no doubt that biofuels are promising products of the utilization of biomass, which have a huge market demand; however, the discussion on the conversion of biomass into biofuels is not within the scope of this work. Despite the fact that simple edible starting materials like starch and sugars can easily be converted into valuable

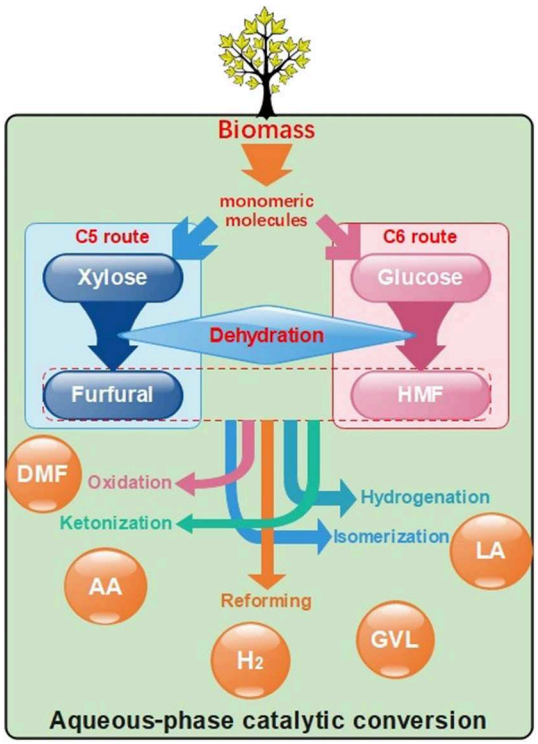

FIGURE 1 | A general conversion route of biomass.

products (Binder and Raines, 2009), this pathway is not perceived as a promising approach because it competes with food production, directly, or indirectly (Sheldon, 2014). In contrast, lignocellulose, which is composed of cellulose, hemicellulose, and lignin (Luterbacher et al., 2014), is edible, although relatively difficult to process. Similar to the petrifaction industry, the biomass-based industry can achieve economic feasibility by producing chemical platform molecules via several routes as shown in **Figure 1**, and then further converting them into valuable chemicals through biorefinery (Serrano-Ruiz et al., 2011). These platform compounds often contain a high degree of oxygenated groups, which can exert negative effects while converting them into fuels. On the other hand, the high oxygen content makes them water-soluble; therefore, it is possible to convert those chemicals through aqueous-phase processes at mild temperature and pressure. Besides, waters are produced either by biomass itself or by the process of reducing the oxygen content; this also provides a beneficial effect on the aqueous-phase conversion of biomass compounds.

During a general conversion route of lignocellulose, monomeric molecules such as xylose and glucose are firstly produced through the fermentation process (Menon and Rao, 2012). Subsequently, the key intermediate products, furfural, and 5-hydroxymethylfurfural (HMF), can be produced through dehydration of pentoses and hexoses, respectively (Chheda et al., 2007). These chemicals can be further processed into a variety of useful platform chemicals like levulinic acid (LA) or 2,5-dimethylfuran (DMF) (Gallezot, 2012) by hydrogenation or oxidation. These substances can be subsequently processed into desired products by isomerization (Roman-Leshkov et al., 2010), reforming (Cortright et al., 2002), ketonization (Pham et al., 2013), esterification (Fernandes et al., 2012), and aldol condensation (Patil and Lund, 2011). In the aqueous phase, the produced water has a lower effect on the conversion process. Heterogeneous catalysts, because of their excellent separation, are of good prospects for development. Obviously, the activity and stability of catalysts play a significant role in the process. For heterogeneous catalysts, properties like activity and selectivity depend on the surface area, pore structures, and acid sites, and stability and recyclability depend on water tolerance and hydrophobicity. Many reactions have been achieved in the gas phase or the organic solvent phase before; however, most catalysts cannot play full catalytic ability in the aqueous phase; the most common is deactivated rapidly, because of the degradation of catalysts caused by the corrosive effects of H^+ or OH^- ions and dissolved organic carbon in water (Han Y. L. et al., 2016). Thus, it is necessary to improve the stability of heterogeneous catalysts in the aqueous phase by improving their surface hydrophobicity through doping of the support with heteroatoms, surface modification, thin-film coatings, or other ways (Ravenelle et al., 2011). In that case, increasing the hydrophobic character of catalysts through the increase in the Si/Al ratio of zeolites (Xiong et al., 2014), or using appropriate hydrophobic supports, such as metal oxide and carbon materials, can be used to improve the activity and hydrothermal stability (Ravenelle et al., 2011).

Several reviews have been published about reactions of biomass platform chemicals (Irshad et al., 2019; Liu et al., 2019; Luo W. H. et al., 2019). This field has broad prospects because of the demand for renewable energy resources. Furthermore, water can act not only as a solvent but also as a reactant, hydrogen source, or catalyst, which is quite different from the relatively inert organic solvents such as toluene and dioxane. Thus, catalysts show completely different activities and stabilities in the aqueous phase, organic phase, or gas phase, so that the aqueous-phase conversions are worth to be discussed in detail. The purpose of this review is to discuss the heterogeneous catalytic conversion in the aqueous phase of biomass platform chemicals, expect to provide a general understanding of this field, and give possible direction for developing novel catalysts or methods to the reactions. The following explanation starts from three aspects: species of biomass platform chemicals, advantages, and challenges of aqueous-phase conversion, and the characteristics of heterogeneous catalysts.

Biomass Platform Chemicals

First of all, the types of biomass platform chemicals should be identified. These platform molecules were initially selected by the US Department of Energy (DOE) in 2004 (Werpy and Petersen, 2004) and revisited by Bozell and Petersen (2010). The original list includes carbon 1,4-diacids, 2,5-furan dicarboxylic acid (FDCA), 3-hydroxy propionic acid (3-HPA),

aspartic acid, glucaric acid, glutamic acid, itaconic acid, LA, 3-hydroxybutyrolactone, glycerol, sorbitol, and xylitol/arabinitol. In the course of further research and development, some compounds, such as organic acids like aspartic acid, glucaric acid, glutamic acid, and itaconic acid, had been neglected and gradually faded out of sight (Bozell and Petersen, 2010); in contrast, some other compounds were carried out because of the demand arising from the progress of transformation technology. In recent years, research on biomass platform molecules includes the following: ethanol, furans (including furfural and HMF), glycerol, lactic acid, succinic acid, LA, sorbitol, and xylitol. Some of these molecules are produced by fermentation; some of them are converted from C_5 or C_6 sugars (Climent et al., 2014). The similar point of these chemicals is that they all have a large source and a variety of transformation methods.

Advantages and Challenges of the Aqueous-Phase Conversion of Biomass Platform Chemicals

As previously mentioned, the aqueous-phase conversion is a feasible strategy for biomass utilization, because of the high dissolvability, easiness of separation, and green color and nontoxicity (Climent et al., 2014) of water as the solvent. Despite water being not the only option as a green solvent, it can be one of the most promising and competitive solvents because of its widespread presence in biomass sources. Moreover, water can also participate in the reaction through multiple ways, such as a hydrogen donor in the hydrogenation process (Hu et al., 2014) or as one of the reactors in ring opening and isomerization reaction (Choudhary et al., 2013). The most noteworthy is the effect of hydrogen bonds; water as a solvent can significantly accelerate the transformation of H atoms from the bulk phase to the catalyst surface through a hydrogen bond network composed of water, which is called the Grotthuss mechanism (Agmon, 1995). However, the hydrothermal stability of heterogeneous catalysts has been one of the critical factors restricting the development of biomass aqueous-phase transformation technology (Huo et al., 2018). Although this stability can be improved through particular treatments, such as modification with metals, coating, or silanization (Gayubo et al., 2010), these treatments are often observed to affect other properties of catalysts. Therefore, it is necessary to expand the development of the transformation of biomass resources and the efficient utilization technology in the aqueous phase.

Heterogeneous Catalysts in the Aqueous Phase

According to the different physical and chemical properties of the reactants, different kinds of catalysts are required. In general, these catalysts can be divided into homogeneous and heterogeneous catalysts. Homogeneous catalysts have the advantage of high solubility, which makes them better to contact with the reactants, to show higher activity or milder reaction conditions (Shylesh et al., 2010). However, homogeneous catalysts faced difficulty in catalyst recovery and separation with the products, which increases their cost, and that becomes one of the bottlenecks of the industry. On the other hand, with the increasing environmental and economic demands for sustainability (Shylesh et al., 2010), heterogeneous catalysts, with the advantages of environment friendliness, easy separation, and great reusability, are more in line with the needs of technological development in recent days. The heterogeneous catalysts that are applied for the aqueous-phase conversion of biomass platform chemicals are usually porous materials with high surface activity and specific surface areas, such as alumina, silica, carbon materials, and metal oxides (Wu K. J. et al., 2016). Because of the foundation of the petrochemical industry, traditional heterogeneous catalysts are mainly used in the conversion of hydrocarbons in the gas phase, which enables them to be stable at high temperatures and to adapt to non-polar compounds (Rinaldi and Schuth, 2009). As highlighted above, however, the aqueous-phase conversions are quite different, and that places new requirements for heterogeneous catalysts.

To date, biomass platform chemicals' heterogeneous catalytic reactions in the aqueous phase, such as dehydration, hydrogenation, oxidation, isomerization, reforming, ketonization, and aldol condensation, have been studied. In the following sections, we will highlight the recent advances of heterogeneous catalysts for these reactions in the aqueous phase.

Production of Biomass Platform Chemicals From Biomass

As described above, biomass platform chemicals could be various in different types. A common way of classification is through the carbon number, which is closely related to its biomass source. Therefore, compared with the conversion and utilization of biomass, the production process of biomass is also worthy of attention. Because of the limitation of the focus and length of this paper, too much discussion may not be added here, but the most basic discussion is necessary.

Biomass platform chemicals are originally produced by wood or algae through thermochemical conversion processes. Wood generally contains cellulose (40–50%), hemicellulose (10–30%), and methyl cellulose (20–30%). According to different components, different biomass platform chemicals can be produced. Cellulose, which is formed by the D-glucose units, can be converted to glucose by the hydrolysis of β-1,4 glucan (Suganuma et al., 2008), and then goes through the C_6 pathway to other platform chemicals such as sorbitol (Rey-Raap et al., 2019), 5-HMF (Yu and Tsang, 2017), or LA (Kang et al., 2018). In contrast, hemicellulose is not a single carbohydrate polymer. The hardwood hemicelluloses contain mostly xylans (Saha, 2003), which is the major source of xylose and C_5 platform chemicals such as furfural (Luo Y. P. et al., 2019). Furans are a promising and important platform chemical because they are precursors of many other platforms as mentioned above. Therefore, the platform chemical system constructed by cellulose and hemicellulose has been widely studied.

The case of algae is quite different. The main components of algae are fat, polysaccharide, and protein (Khoo et al., 2019), which makes the problem more complicated. Though the current conventional way of utilization is to make it into bio-oil, the

complex composition of algae also provides a possible way to separate each component and produce value-added chemicals (Harun et al., 2010); the most common are acetone, glycerol (Karimi et al., 2015), bioethanol (Dave et al., 2019), or other alcohols. In general, algae are not the main battlefield for the production of biomass platform chemicals.

DEHYDRATION

High-valued products of furan compounds such as furfural and HMF, generated from dehydration of renewable biomass platform chemicals of six-carbon ketose and pentose, have been identified as a primary and versatile renewable biomass feedstock. Dehydration reactions play vital roles in aqueous-phase catalytic processing to produce fine chemicals and liquid fuels from biomass-derived oxygenated hydrocarbons (Huber et al., 2004).

Xylose, glucose, and sorbitol as the most abundant renewable biomass platform chemicals can be transformed to several molecules such as HMF, furfural, levulinic ester, furfuryl alcohol, and isosorbide. Because of the rehydration and polymerization reactions, many by-products, such as organic acids and humins, were synthesized in glucose dehydration to HMF in the water phase (Delidovich et al., 2014).

In this part, we summarize recent advances in the heterogeneous reaction system for the catalytic production of furan compounds from dehydration of biomass platform chemicals (Wang et al., 2017). Solid acid catalysts are advantageous due to their economic promise, environmental viability, and recyclability for aqueous-phase dehydration. Thus, solid acid catalysts such as phosphate, nanosized mixed oxides, and zeolites have been investigated (Kobayashi et al., 2015).

Phosphates

A great deal of effort was focused on the development of efficient, inexpensive, simple structure and easily separated heterogeneous solid acid phosphate catalysts, in order to solve the shortcomings of restricted large-scale use and complex preparation process. What's more, a phosphate catalyst containing both Lewis and Brønsted acidic sites and the synergistic effect of Lewis and Brønsted acid sites in the phosphate catalyst were demonstrated to be an efficient conversion of xylose to furfural. Typically, the catalyzed dehydration of xylose to furfural involved the isomerization of xylose to xylulose or lyxose, followed by dehydration to produce furfural. Lewis acid plays a critical role in the xylose-to-xylulose isomerization, while Brønsted acid is active for xylulose dehydration. On the other hand, for the dehydration of xylose to HMF or furfural, lots of studies have also confirmed that the conversion rate of xylose and the yield of HMF or furfural were greatly improved in the water/organic biphasic system by using the solid phosphate catalysts. For xylose dehydration to furfural, it is desirable to have a high ratio of Brønsted to Lewis acid sites to design efficient aqueous-phase dehydration catalysts. Lewis acid sites decrease furfural selectivity by catalyzing a side reaction between xylose and furfural to form humins. Fang et al. (2017) demonstrated that a high furfural yield of 54.9 mol% and a complete conversion (100%) of xylose were obtained at 180°C for 3 h in the aqueous phase by a bifunctional $NbOPO_3$ catalyst. In the work reported by Xu et al. (2018), a furfural yield could reach 18% from the xylose at 160°C for 60 min under a $CrPO_4$ catalyst in the aqueous phase. However, an excellent furfural yield is up to 88% at the same condition by $CrPO_4$ catalysis in the water/tetrahydrofuran biphasic system. Moreover, after four catalytic cycles, a desired 47% furfural yield was still obtained.

Nanosized Metal Oxides

In recent years, production of nanosized metal oxide catalysis material led to new innovations and improvements in science and industry. It has been confirmed that metal oxide nanoparticles with a large surface area such as CuO, ZnO, Ga_2O_3, and MgO exhibit good activity and selectivity for the dehydration of xylose to furfural (Kumar et al., 2015).

Zn doped CuO nanoparticles ($Cu_{0.89}Zn_{0.11}O$) synthesized by Gedanken group (Mishra et al., 2019) exhibit good activity and selectivity for the conversion of xylose to furfural, which enhances its catalytic activity and enables it to completely convert xylose and the 86% yield of furfural at 150°C within 12 h. The incorporation of Zn into CuO lattice resulted in a highly defective structure of the Zn doped CuO NPs, which provide more active sites for xylose to dehydrate. The Zn doped CuO NPs catalyst on the mechanism of dehydration of xylose to furfural is provided in **Figure 2**. In this mechanism, the reaction is in the forward direction via xylose isomerization with a 1,2-hydride shift. Then, xylulose is converted into an oxicarbenium ion by Zn and Cu, which act as Lewis acids. The subsequent deprotonation of these species produces an enol and further yields furfural by losing three molecules of water.

The catalytic activity of β-Ga_2O_3 nanorods was examined during the dehydration reaction of xylose to furfural, and results showed that β-Ga_2O_3 exhibits good activity and selectivity. The 94% yield of furfural is obtained at 150°C within 12 h (Kumar et al., 2016). The inherent characteristics of the stimuli and thermoresponsiveness for gallium-based oxide nanoparticles catalyst might be key factors leading to higher production of furfural from xylose.

Sn-based catalysts have demonstrated high activity for dehydration of glucose to platform chemicals, such as HMF and lactic acid. The catalytic results obtained by Sn supported on γ-Al_2O_3 (Sn/γ-Al_2O_3) catalyst concluded that the Lewis acidity offered by Sn oxides promotes the retro-aldol reaction pathway toward lactic acid, while the Lewis acidity offered by γ-Al_2O_3 enhances the synthesis of both HMF and lactic acid (Marianou et al., 2018). HMF yields of 12 and 88% glucose conversion were obtained in the aqueous phase at 150°C, 60 min, by Sn/γ-Al_2O_3. The highest HMF molar yield of 27.5% (at complete glucose conversion) was achieved. Lewis acid was used as a catalyst for the dehydration of glucose to produce versatile high value-added biochemicals and liquid biofuels.

Zeolites

Zeolites with well-defined pores between 5 and 13Å are usually highly structured crystalline inorganic aluminosilicates, which show excellent thermal and chemical stability and mostly present

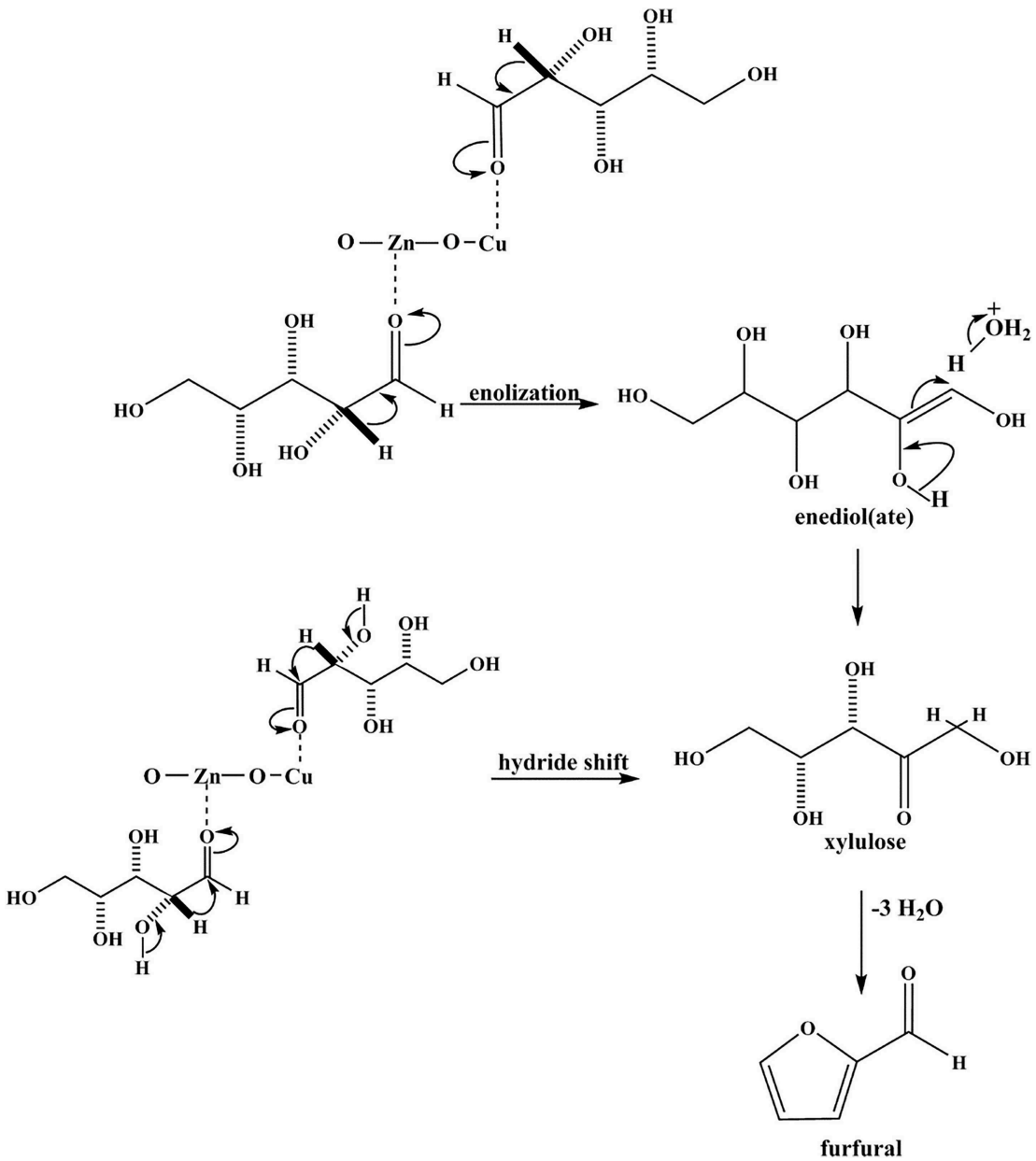

FIGURE 2 | Possible reaction mechanism for the dehydration of xylose to furfural on Zn doped CuO catalyst. Reprinted from Mishra et al. (2019), with permission from Elsevier.

Brønsted acidity giving them the ability to transform substrates into products, for instance, sorbitol dehydration into isosorbide, and glucose dehydration to prepare HMF (Kruger et al., 2012).

Sorbitol is one of the top 10 platform chemicals in biorefinery proposed by US DOE (Bozell and Petersen, 2010), and the most promising derivative of sorbitol is isosorbide. Isosorbide is used for treating glaucoma, brain hypertension, and Ménière's disease (Yemi and Mazza, 2019). The most common zeolites used in the dehydration of sorbitol into isosorbide are H-beta zeolites. Kobayashi et al. (2015) revealed that conversion of sorbitol to isosorbide by H-beta zeolites with a drastically high Si/Al ratio of 75 gives isosorbide in up to 76% yield at 127°C for 2 h.

In the comparison study of the catalytic performance for dehydration of D-xylose into furfural obtained with H-zeolites, Kim et al. (2011) carried out some contrast experiments by H-Y, H-mordenite, H-Ferrierite, H-ZSM, and H-beta. The highest furfural yield of 21.9% was obtained with H-Y in the presence of the aqueous solvent. They concluded that the D-xylose conversion and furfural yield generally decreased with an increasing Si/Al ratio of the H-zeolites.

Researchers have demonstrated that the zeolites are active in the glucose dehydration to prepare HMF. Mercedes revealed a glucose conversion of 57% and an HMF yield of 1.6% in the aqueous phase at 195°C, 30 min, using H-ZSM-5 zeolites with

a Lewis/Brønsted molar ratio of 0.25. However, a conversion of 80% and an HMF yield of 42% were achieved by using a biphasic NaCl (20 wt%) aqueous solution/methyl isobutyl ketone system (Moreno-Recio et al., 2016). They corroborated that the catalytic activity is enhanced with the H-ZSM-5 zeolite introducing inorganic salt NaCl solution in the biphasic reaction medium.

The dehydration of xylose to furfural in aqueous solutions by a ZSM-5 zeolite catalyst was studied by O'Neill et al. (2009). They demonstrated that 46% furfural yield was produced at 200°C in an aqueous medium by H-ZSM-5 with a pore size of 1.2 nm. Therefore, a zeolite with a pore size around 0.8 nm, which ideally is close to xylose and furfural molecular sizes, would be more effective for the dehydration of xylose to furfural, as it would allow enough room for xylose to thread in and dehydrate to furfural.

Compared with microporous zeolites, mesoporous zeolites can provide excellent support because they are free from kinetic diffusion limitations in the case of larger molecules. Mesoporous zeolites, due to their good structural feature, high surface area, and relatively large pore size, have been widely studied for the dehydration of biomass platform chemicals, such as glucose dehydration to HMF. The most widely described reaction route of glucose to HMF consists of two steps: (1) isomerization of glucose to fructose in which Lewis acid sites play a significant role, and (2) dehydration of fructose to HMF; appropriate Brønsted acid sites are beneficial to the production of higher HMF yield. Jiang et al. designed and synthesized a zirconium doped mesoporous KIT-6 catalyst (Zr-KIT-6) for the dehydration of glucose into HMF. The maximum glucose conversion of 54.8% and HMF yield of 19.5% are obtained at 170°C after 3 h in an aqueous phase. In the biphasic MIBK–water system, 79.0% conversion of glucose and 34.5% HMF yield were optimally obtained (Jiang et al., 2018). This excellent result is mainly attributed to the highly distributed ZrO_2 nanoparticles and multicoordinated Zr^{4+} species in Zr-KIT-6 samples.

Mesoporous SBA-15 materials, because of their unique surface, pore structure with tunable uniform hexagonal channels, and hydrothermal stabilities, are a good candidate as a support for the dispersion of active centers. Wu's group (Shi et al., 2011a; Hua et al., 2013) designed synthesis SBA-15-SO_3H and AAO/SBA-15-SO_3H catalysts containing active centers of sulfoacid, a support of SBA-15 and substrate of porous alumina membrane (AAO). The conversion of xylose and selectivity of furfural were 90 and 70%, respectively, at 160°C for 4 h in a water/toluene two-phase system on both catalysts. A high reaction rate, mass transfer, and heterogeneous distribution of the active site of the AAO/SBA-15-SO_3H catalyst are shown in **Figure 3** (Hua et al., 2013).

Besides, Wu prepared a metal oxide loaded on the support of SBA-15 as Al-promoted SO_4^{2-}/ZrO_2/SBA-15 catalysts (Shi et al., 2011b). The introduction of the Al stabilizes the tetragonal phase of the ZrO_2 and thus increases the number and intensity of acid sites. The catalytic activity for dehydration of xylose to furfural was investigated. With increasing Al loading to 12%, the 98.7% xylose conversion and 53.4% furfural selectivity can be obtained at 160°C for 4 h in a H_2O/toluene biphasic system.

In addition to the above catalysts, the relatively cheap and environmentally friendly ion-exchange resin was reported for the conversion of xylose to furfural. The result for the reaction of the xylose conversion rate is 71.8% and the furfural yield is 28.8% in water at 150°C for 16 h with Amberlyst 70 (specific surface area 36 $m^2\ g^{-1}$ concentration of acid sites 2.65 mmol-$H^+\ g^{-1}$, average pore diameter 22 nm) as the catalyst (Sato et al., 2019).

Summary

Referring to the recently published literatures on the dehydration of biomass platform chemicals in the aqueous phase, the heterogeneous catalysts have been widely investigated. In this part, we have summarized the heterogeneous catalysts that have been relatively well studied in recent years including phosphate,

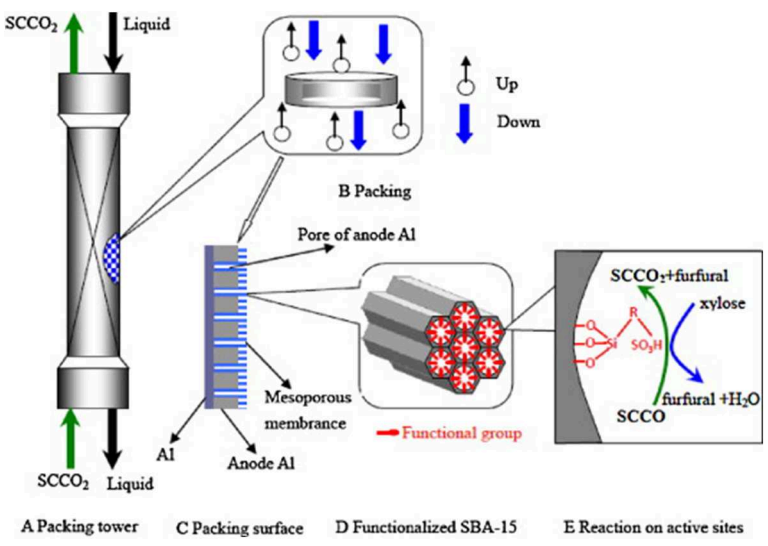

FIGURE 3 | The scheme of solid acid catalyst packing and dehydration of xylose to furfural. Reprinted from Hua et al. (2013), with permission from Elsevier.

nanosized metal oxides, and zeolites, which are mostly used for the dehydration of glucose, xylose, and sorbitol to furfural and isosorbide. For phosphate catalyst and zeolites, they have the common characteristic that the synergistic effect of Lewis and Brønsted acid sites with a high ratio of Brønsted to Lewis acid sites was demonstrated to be efficient and has superior activity to transform xylose and glucose into furfural. Nanosized metal oxides exhibit good activity and selectivity for the dehydration of xylose to furfural. From the current results, the highest conversion rate can reach ∼100% by the phosphate of $NbOPO_3$ and the mesoporous SBA-15 catalyst on the dehydration of xylose. On the other hand, the highest yield of furfural (94%) dehydration from xylose is obtained by the metal oxide of β-Ga_2O_3 nanorod. To sum up, the design and synthesis of a catalyst, which not only can convert reactants to 100% and achieve 100% yield but also has good hydrothermal stability, will be a difficult problem that we urgently need to solve.

HYDROGENATION

Most of the biomass platform chemicals, such as furfural or HMF, contain unsaturated bonds. Hydrogenation is needed in the process of the conversion to fine chemicals or bio-oil. The essence of hydrogenation, hydrogenolysis, and hydrodeoxygenation is the hydrogenation of C=O, C=C, or C–O bonds; generally, C=O bonds are more easily activated. In recent research of hydrogenation, VIII group metal catalysts, especially Ni, Pt, Pd, or Ru, are mostly studied; noble metal catalysts usually show higher catalytic activity; however, more works are demanded to stop the conversion at target products, instead of excessive hydrogenation. In this section, recent advances in heterogeneous catalysts for aqueous-phase hydrogenation of biomass platform chemicals are discussed in order to provide ideas for the design of new catalysts.

Noble Metal Catalysts

Because of outstanding activity, selectivity, and stability, noble metal catalysts are considered to be one of the best hydrogenation catalysts. The high activity can be attributed to the special electron and band structure. The adsorption capacity of the substrate depends on the percentage of d orbital (d%) in the *spd* hybrid bonding orbit. In noble metals such as Ru, Pd, and Pt, the d% can be over 40% or even 50%.

Noble metal supported catalysts received the most extensive research because of the excellent hydrogenation activity in the aqueous phase. Under the existence of noble metal catalysts, the hydrogenation of furfural (Taylor et al., 2016) and LA (Dhanalaxmi et al., 2017) can reach nearly 100% conversion and selectivity. Li et al. (2016) compared the reaction mechanisms between Cu and group VIII metals of the conversion of furfural to furfural alcohol, showing that the different binding mode and lower activation barrier interpreted the higher activity of group VIII metal. Zhao et al. (2019) explained the effect of water of the same conversion through free energy calculations, illustrating that water helps surface charge separation to form solvated protons in water and electrons left in the metal reservoir, both of which reach the adsorbed reactants simultaneously (Zhao et al., 2019). The activation barrier of hydrogenation can be significantly reduced by the transformation of the proton through a hydrogen-bonded water network. Thus, it can be seen that the advantages of using the aqueous phase on hydrogenation are mainly manifested in hydrogen bonds. On the one hand, the binding energy of substrates can be decreased through hydrogen bonds with water. On the other hand, the proton transfers through hydrogen bonds between water molecules can accelerate the protonation of the carbonyl group.

The effect of support should not be neglected. Li S. P. et al. (2019) decorated Ru on the ultrathin anatase TiO_2 nanosheets with exposed (001) facets, which proved that the different electronic and surface properties of support can strongly affect the activity of the catalysts. Ru/TiO_2-n, which contains most (001) planes, showed the highest activity because of the presence of more Ru (0) on the surface. Abdelrahman et al. (2014) studied the mechanism of this reaction. LA firstly hydrogenated in the Ru sites, and then acid-catalyzed dehydration occurs homogeneously catalyzed by acid. Therefore, it is necessary to regulate acidity and alkalinity according to the reaction.

A characteristic of aqueous-phase hydrogenation is that it is a gas–liquid reaction that occurs at the liquid–solid interface, so the mass transfer restriction can be one of the major influencing factors. Under that influence, overcoming the mass transfer limitation can speed up the reaction process. Bagnato et al. (2018) synthesized a series of catalytic membranes to increase the phase interface for the selective hydrogenation of furfural to furfural alcohol. The use of Ru-based catalytic membrane reactor significantly reduced the H_2 requirement and increased the turnover frequency. The furfural alcohol selectivity reached >99% under 70°C and 7 bar. However, it was observed that some of Ru clusters were lost after the reaction; it is necessary to find some more resistant metal support.

As reported by Yakabi et al. (2018), Pd/Al_2O_3 catalysts were synthesized for the hydrogenation of succinic acid to γ-butyrolactone (GBL). Among catalysts with different loads, 2 wt% Pd/Al_2O_3 prepared by co-precipitation achieved optimal performance. Transmission electron microscope (TME) images and particle size distributions show that this catalyst possessed a smaller mean particle size and a narrower particle size distribution. The particle size and dispersion of metal clusters can affect the catalytic activity, which are also reported by Upare et al. (2011); the Ru/C catalyst showed the best catalytic activity attributed to the higher dispersion.

In summary, not only particle size and dispersion of the metal active sites but also structure or even orientation of the support can affect the activity, selectivity, and stability of catalysts. The different impact of water on noble metals is also noticeable. Besides, the high price of noble metals is still a problem; using bimetallic catalysts or designing a new reactor with higher availability might be a way out.

Non-noble Metal Catalysts

Because of the high price of noble metal catalysts, some of the non-noble metals that have similar chemical properties

and catalytic activity, such as Fe, Co, Ni, or Cu, also received great attention.

Dutta et al. (2019) summarized Ni, Cu, and Zr supported catalysts for the conversion of LA to gamma-valerolactone (GVL) reported in the last 5 years. Some of them, such as Ni/Al_2O_3, Cu/ZrO_2, or Cu/Al_2O_3, showed 100% conversion and >99% selectivity at harsh conditions (about 200°C, >30 bar H_2 pressure). However, further research on catalyst stability and recyclability is still needed. The leach of metal can be attributed to the weak interplay between metals and supports, but stronger interplay may sacrifice dispersion and reduce the catalytic activity.

Cerium also showed fair activity in the hydrogenation reaction. Feng et al. (2019) reported a $(CePO_4)_{0.16}/Co_2P$ catalyst, which achieved 98.2% LA conversion and 97.1% GVL yield at 90°C, 4.0 MPa H_2 in 1.5 h. Moreover, the catalyst continued to have high performance in at least five cycles, which proved that it can maintain long-term activity and stability under strongly acidic conditions.

In contrast, non-noble catalysts are used in the hydrogenation of furfural more frequently. Gong et al. (2018) reported two N-doped carbon nanotube-encapsulated metal nanoparticles called Ni@NCNTs-600-800 and Co@NCNTs-600-800, which showed excellent catalytic performance in the hydrogenation of furfural. The yield of furfural alcohol reached as high as 100% at 80°C and still active after six cycles. The high yield of deep hydrogenation products, tetrahydrofurfuryl alcohol or cyclopentanone, indicated that the catalyst has greater catalytic potential at higher temperature and pressure.

In summary, non-noble metal catalysts can reduce the cost of catalysts but faces the predicament of metal leaching for a long time. With the research in-depth, this problem is gradually being solved to a certain extent. Nevertheless, the superiority of noble metal catalysts is still reflected in terms of conversion, selectivity, or reaction conditions, such as temperature and pressure. In order to give full play to the advantages of high activity of noble metal catalysts and low cost of non-noble metal catalysts, a possible way to achieve that is to use bimetallic catalysts.

Bimetallic Catalysts

In the directional selection of products, catalysts with appropriate activity are required frequently. In recent years, some bimetallic catalysts are reported. Some of them are non-noble metal catalysts modified with noble metals, and some of them are alloy metal catalysts. These kinds of catalysts are designed based on the structural and catalytic characteristics of different metals, thus improving the catalytic efficiency through synergism.

Qiu et al. (2019) reported a Ru prompted MoO_{3-x}/C catalyst in the conversion of sorbitol into C_5-C_6 alkane, which showed the excellent activity of 87.3% yield. The production of alkanes depends on the relative rates on C–C and C–O bond cleavage (Li and Huber, 2010), so the concentration of metal to acid sites is the key to control the product distribution. The addition of Ru promoted the reduction of Mo to strengthen the hydrogenation capacity of it.

Putro et al. (2017) synthesized a Ni–Fe alloy catalyst by using a hydrothermal method that achieved high selectivity in the hydrogenation of furfural. The result suggested that the electron-deficient Fe can weaken and activate the C=O bonds through a side bonding interaction of the lone pair of oxygen in the

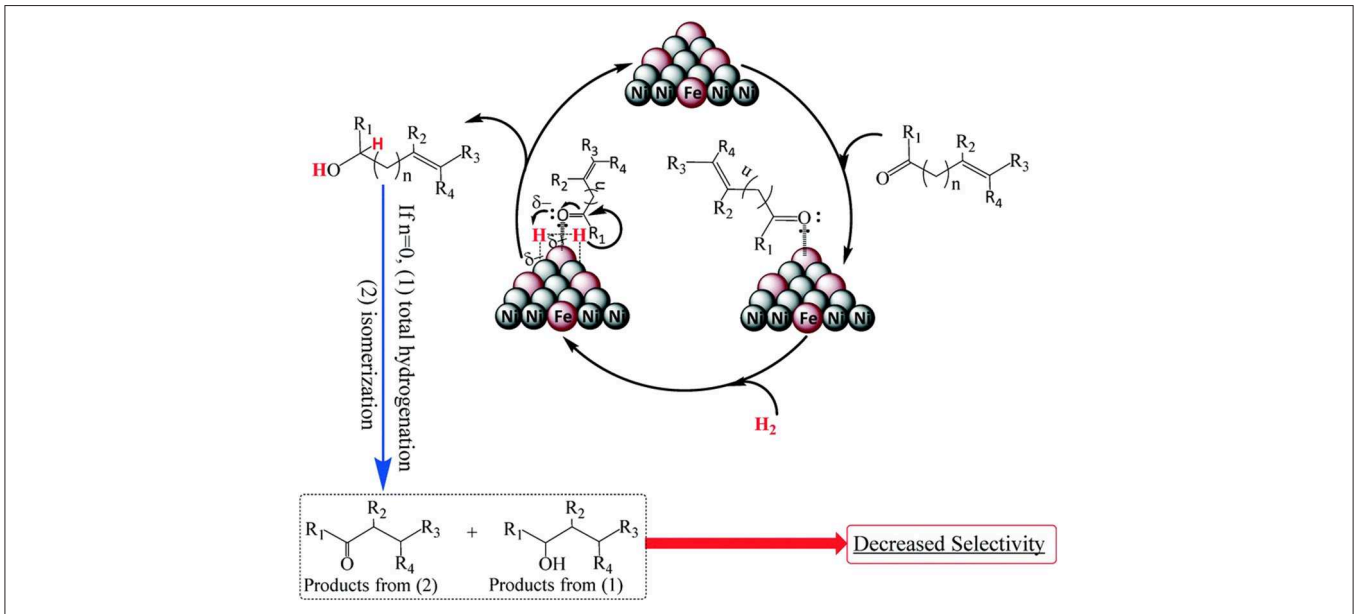

FIGURE 4 | Plausible mechanism for the selective hydrogenation of unsaturated alcohols over Ni–Fe-based alloy. Used with permission of Royal Society of Chemistry, from Putro et al. (2017); permission conveyed through Copyright Clearance Center, Inc.

carbonyl group, making π-complexing occur between the C=O bonds and the Ni atoms, as shown in **Figure 4**.

Using non-noble metal catalysts can reduce the cost, and the promotion of noble metal or other effective metals can optimize the performance of the catalyst. Hence, it can be a feasible technique of aqueous-phase conversion of biomass platform chemicals.

Summary

Hydrogenation, which can reduce the unsaturation and oxygen content, is a very important conversion of biomass platform chemicals. The advantages of aqueous-phase hydrogenation are manifested in hydrogen bond, which can decrease the binding energy of substrates and accelerate the process of carbonyl group protonation. As far as the catalytic effects are concerned, noble metal catalysts present the best activity, stability, and recyclability, but they will cost more. Because many noble metal catalysts can achieve nearly 100% conversion, the higher activity cannot be reflected. Hence, more temperate reaction conditions and better stability are the current research direction. On the other hand, this also provides an opportunity for non-noble metal catalysts. Because of the congenital advantage in price, non-noble metal catalysts gained a lot of attention, especially in the study of the catalytic stability and recyclability to prevent the loss of metal, which is the dominant issue at present.

With the in-depth studies of the active sites of metal catalysts, the effects of the support structure and the interaction with metals are attracting more attention. The surface morphology and defects of support can strongly affect the dispersion and the stability of the combination of metal active sites. Moreover, the acid sites on the surface of support also play an important role in the conversion process. Different calcination temperature and acid or base treatment can affect the surface topography of support, but the effect on the activity and stability of catalysts is complicated. In general, treatment of acid or base brings the increase in active sites, which can enhance the catalytic activity but reduce the stability at the same time.

OXIDATION

In the traditional petrochemical industry, a wide range of commodity chemicals are produced via selective oxidation of petroleum-derived feedstock (Zope et al., 2010; Lanzafame et al., 2014; Kwon et al., 2016). Lignocellulose typically contains 40–45% (weight in dry base) oxygen content, which outclassed that of petroleum (He et al., 2014). These value-added molecules could potentially be more economical to produce platform chemicals containing oxygen elements from biomass rather than petroleum. So, catalytic oxidation of biomass into platform chemicals widely attracts scholars' attention.

Recently, many reports have been published about oxidation of biomass-derived compounds into value-added platform chemicals (Albonetti et al., 2015; Elliott et al., 2015; Huang et al., 2018; Zhang and Huber, 2018). **Figure 5** shows that a wide variety of commodity platform chemicals can be produced from the catalytic oxidation of cellulose or carbohydrate-derived compounds.

Direct Catalytic Conversion of Cellulose Into HFM

The necessary path of conversion from biomass into platform chemicals is cellulose hydrolysis and monosaccharide oxidation (Deng et al., 2014). It basically requires two steps: the acid-catalyzed hydrolysis of carbohydrates (cellulose or lignocellulose) into monosaccharides (glucose or xylose) and the oxidative cleavage of C–C bonds in monosaccharides into organic acid (Wang et al., 2018).

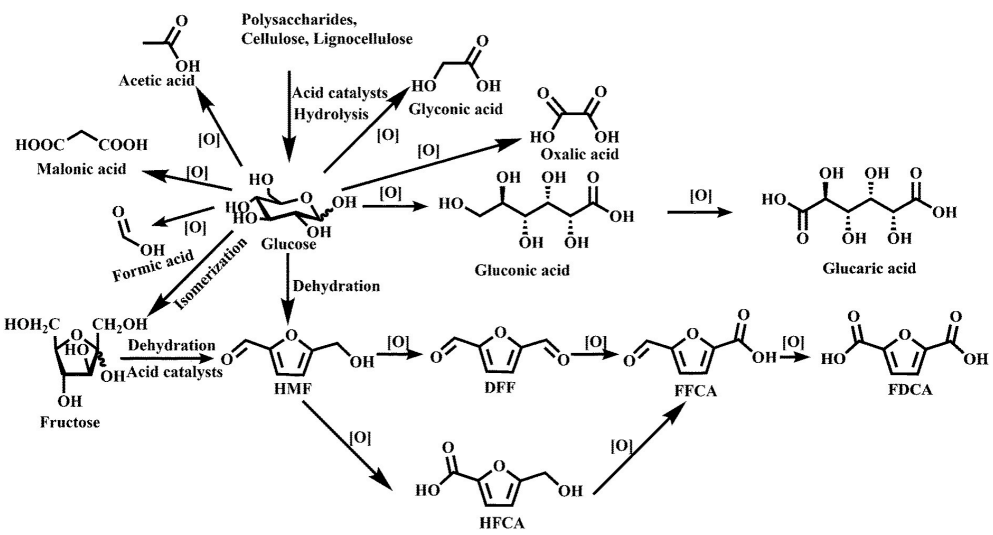

FIGURE 5 | Chemicals produced by oxidation of glucose and glucose-derived molecules. Used with permission of Royal Society of Chemistry, from Zhang and Huber (2018); permission conveyed through Copyright Clearance Center, Inc.

For the first step, liquid acid like sulfuric acid and hydrochloric acid was widely applied in the hydrolysis conversion of cellulose due to its high catalytic activity, acid strength, hydrogen ion releasing efficiency, and lower cost (Liu et al., 2013; Su et al., 2018). However, compared with liquid acid, solid acid has many advantages: (1) easy in separation and purification of the products; (2) stable catalysis effect under high temperature; and (3) aerobic oxidation can be controlled by the modified surface functional group of solid acid (Zhang and Zhao, 2009; Rinaldi et al., 2010). Yang and Pan (2016) found that a functional mesoporous polymeric catalyst bearing boronic acid as cellulose-binding groups and sulfonic acid as cellulose-hydrolytic groups was prepared, resulting in an excellent hydrolysis performance.

For monosaccharide oxidation, different oxidation degree has an essential influence on oxidation productions. Over-oxidation of glucose and xylose will lead to the complete combustion of monosaccharide to water and CO_2, which are the thermodynamically favored products (Gliozzi et al., 2014). Thus, it is of critical importance that the selected catalyst systems control the degree of the reaction oxidation.

Hence, suitably functional catalysts combining both metal and acidic sites are necessary to combine the hydrolysis with oxidation steps into a one-pot reaction that converted polysaccharides into platform chemicals. The oxidative cleavage of C–C bonds is usually activated by metal catalysts. Polyoxometalates (POMs) with a formula of $H_{3n}PV_nMo_{12n}O_{40}$ (HPA) contains Vanadium(V), which has acid sites that are considered as one effective catalysis for organic acid production from biomass with O_2 (Wolfel et al., 2011). Zhang investigated a temperature-responsive heteropolyacid ($H_2PW_{12}O_{40}$) catalyst. It was prepared by $H_3PW_{12}O_{40}$ and choline chloride (ChCl) as catalysis-based material. And 75.0% HMF yield and 87.0% cellulose conversion were achieved under the condition of 140°C for 8 h in biphasic solvent system H_2O and methyl isobutyl ketone (MIBK) (H_2O/MIBK=1) in the one-pot transformation of cellulose to HMF (Teong et al., 2014). By contrast, with the homogeneous $H_3PW_{12}O_{40}$, the excellent HMF yield may result from the higher Brønsted acidity (Choudhary et al., 2012). Li reported an Nb/carbon catalyst (Nb/C-50, 50 wt% of Nb_2O_5) prepared from niobium tartrate (Nb_2O_5) and glucose as raw materials via carbonization. The conversion of cellulose into HMF would increase by 77.8% from 53.3% in the THF/H_2O system at 170°C for 8 h (Li et al., 2012).

Selective Oxidation of HMF Into FDCA

HMF is regarded as a versatile platform compound and an intermediary that connects biomass resources and petrochemical industry (Zhang et al., 2015). It is a renewable furan chemical, which is produced from the dehydration of C_6 carbohydrates. Except for its high value, HMF can be further transformed into diverse high-quality fuels such as C_9-C_{15} alkanes and many oxidized furan chemicals (Wu et al., 2014; Zhang and Deng, 2015; Kang et al., 2019). For example, FDCA can take the place of the fossil resource (p-xylene), which was used for producing the polyesters. Currently, 98% of p-xylene produced was used as a raw material for the production of terephthalic acid, a monomer for polyethylene terephthalate (PET). PET is the fundamental material for the production of fibers, films, containers, packaging materials, molded articles, and household consumable goods (Zakrzewska et al., 2010; Fang et al., 2016).

Noble Metal Catalysts

Metal is favored for the conversion of HMF to FDCA during the catalysis reaction. Noble metal catalysts offer an empty electron orbital, narrow level spacing, and diversity of coordination modes that can receive an electron pair from the reactants. The transfer of an electron pair results in bond weakening. These are the active sites for the reaction that is conducive to the adsorption of reactants on the catalysts. Gold-based catalysts were widely studied with different supports, and their reactivity was described as depending on the structure of the catalyst and the ratio of the gold nanoparticles with other metals or support (Jeong et al., 2015; Carrillo et al., 2018).

Oxidation of HMF in the presence of Ru catalysts and in the absence of base was found to be quantitative under moderate conditions. Different Ru catalysts were introduced with different supports, though some of them were not of much use because of metal leaching problems (Romero et al., 2016).

The oxidation conversion of HMF into FDCA has mainly performed over noble metal (Pd, Pt, and Au) catalysts in an alkaline solution (**Table 1**). Single gold metal, though has an effective increase in the ratio of conversion, cannot totally convert HMF into FDCA. As **Figure 6** shows, catalyst support was regarded as one oxygen pump by releasing and adsorbing the oxidizing species through the change of valence states during the redox process. And the molecular O_2 was activated by the Au and promoted the formation of the carboxyl by releasing OH^- (Chen et al., 2013).

The Au/C catalysts can increase the yield of FDCA by 72% (**Table 1**, No. 1) (Davis et al., 2011). A different shape of the supporter has different catalysis efficiency. When TiO_2 was used for supporting the Au as the catalyst, the yield of FDCA can reach up to 79% (**Table 1**, No. 2) (Cai et al., 2013). When gold metal added another kind of metal, the conversion ratio and yield reached above 94% (Davis et al., 2012). When support was changed by CeO_2, the 90% yield was obtained after 4 h at 443 K under 20 bar O_2, 4 equiv. (Li Q. Q. et al., 2019), NaOH condition (**Table 1**, No. 4). Adjustment of the molar ratio Au/Cu=1 in the Au-Cu/TiO_2 catalyst is done by the immersion method. This kind of doping metal catalysis showed the highest catalytic activity, which has achieved a 99% FDCA yield at 368 K and 10 bar O_2 (**Table 1**, No. 5) (Wan et al., 2014). This catalyst was stable without treating the leaching and aggregation for the metal nanoparticles. Two kinds of noble metal can be one step closer to increasing catalysis efficiency. Supported bimetallic Au–Pd catalysts appeared to have better catalytic performance than single Au catalysts (Villa et al., 2013). For example, an FDCA yield of 99% was produced after 4 h at 333 K over the Au_8-Pd_2/C catalyst (**Table 1**, No. 6). The Au_8-Pd_2/C catalyst could be reused for five runs with the FDCA yield remaining at 99% (Villa et al., 2013). In most cases, the oxidation of HMF into FDCA over Au catalysts was performed by the use of an excessive base.

TABLE 1 | Several catalysts for the oxidation of HMF into FDCA.

No.	Catalyst	Catalyst ratio[a*]	Oxidant	NaOH dosage[b*]	T (K)	Time (h)	Con. (%)	Yield (%)	References
1	Au/C	150	6.9 bar O_2	2 equiv.	296	6	100	7	Davis et al., 2011
		150	20 bar O_2	20 equiv.	296	22	100	72	Davis et al., 2011
2	Au/TiO_2	150	20 bar Air	20 equiv.	295	22	100	79	Cai et al., 2013
3	Au-Pd/CNT	100	5 bar O_2	No	373	12	100	94	Davis et al., 2012
4	Au/CeO_2	400	50 bar Air	4 equiv.	443	4	100	90	Li Q. Q. et al., 2019
5	Au-Cu/TiO_2	100	10 bar O_2	4 equiv.	368	4	100	99	Wan et al., 2014
6	Au_8-Pd_2/C	200	10 bar O_2	2 equiv.	333	6	>99	>99	Villa et al., 2013; Wan et al., 2014
7	Pt/C	100	6.9 bar O_2	2 equiv.	296	6	100	79	Davis et al., 2011
8	Pt/C-EDA-4.1	100	10 bar O_2	1.25 M	373	12	100	96	Han X. W. et al., 2016
9	Pt-Pd/C	100	10 bar O_2	1.25 M	298	2	100	99	Davis et al., 2012
10	Pt/RGO	39	10 bar O_2	5 equiv.	298	24	100	84	Negoi et al., 2014
11	Pd/C	150	6.9 bar O_2	2 equiv.	296	6	100	71	Davis et al., 2011
12	Pd/TiO_2	100	1 bar O_2, 35 mL min^{-1}	1.25 equiv.	363	8	>99	53	Davis et al., 2011
13	Pd/HT	21.2	1 bar O_2, 35 mL min^{-1}	1.25 equiv.	373	7	>99	99	Davis et al., 2011; Niu et al., 2014

[a*] *The catalyst ratio was defined as the molar ratio of HMF to the metals.*
[b*] *Equivalent calculated based on the molar ratio of NaOH to HMF.*

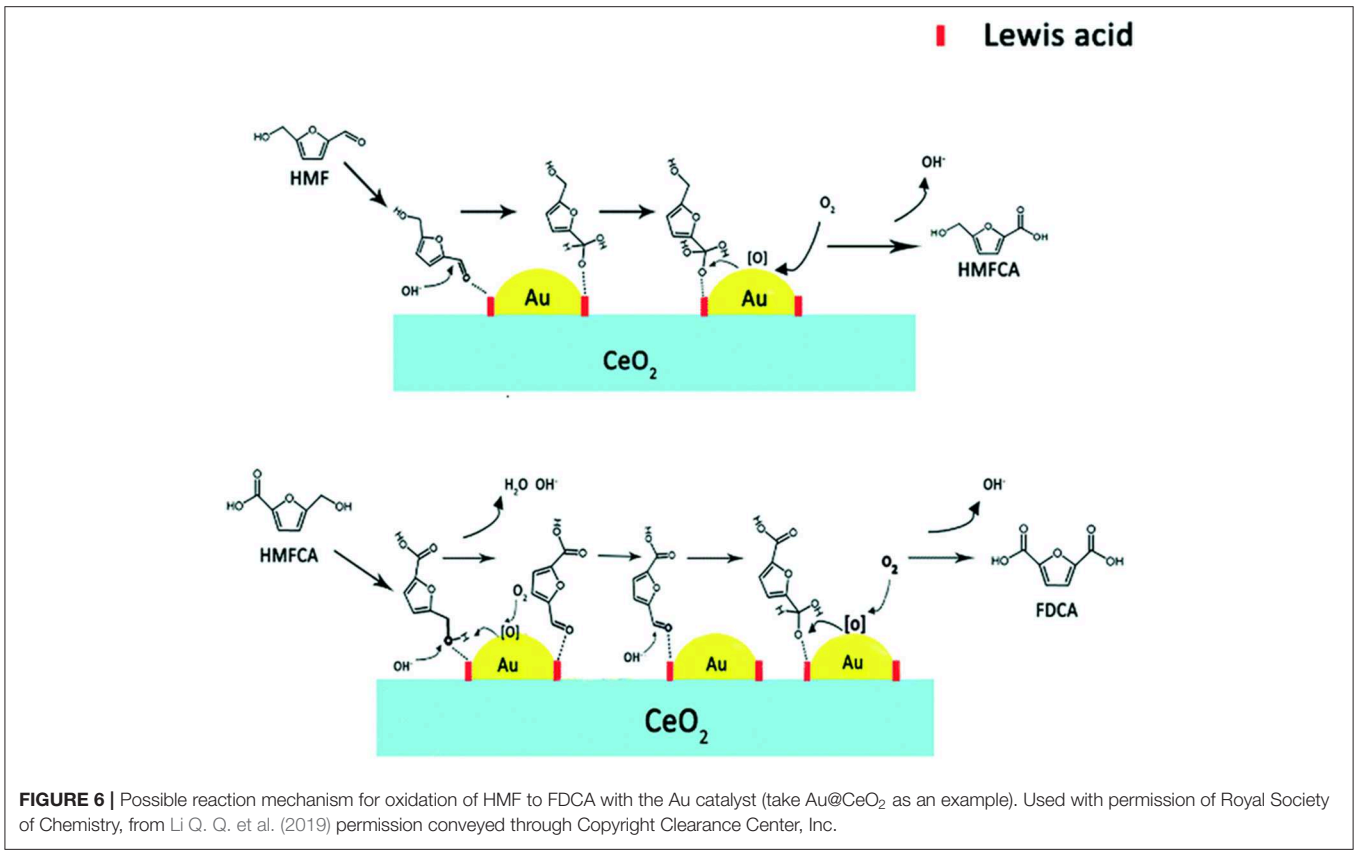

FIGURE 6 | Possible reaction mechanism for oxidation of HMF to FDCA with the Au catalyst (take Au@CeO_2 as an example). Used with permission of Royal Society of Chemistry, from Li Q. Q. et al. (2019) permission conveyed through Copyright Clearance Center, Inc.

The other important noble metal is Pt, and its catalysts are the subject of many theoretical, experimental, and industrial oxidation studies. Compared with Au, Pt has a higher yield of FDCA with the same C catalysis supporter under the same reaction condition. Verdeguer et al. (1994) studied Pt/C catalysts and the yield of FDCA was increased by 81% with full HMF conversion after 2 h at 25°C (**Table 1**, No. 7). The FDCA yield increased to 99% over a Pt-Pb/C catalyst. Kinetic studies showed that the first step was the oxidation of the formyl group, and then the hydroxymethyl group followed up. After 2 h at 25°C under

10 bar O_2, the HMF was fully converted by Pt-Pd/C catalysts. However, the FDCA yield was 99% for Pt-Pd/C catalysts (Davis et al., 2012; Han X. W. et al., 2016). It means that the addition of Pd largely increased the catalysis reaction. Davis et al. (2011) reported the catalytic performance of Pt/C, Pd/C, and Au/C catalysts for HMF oxidation in 0.3 M NaOH solution at 23°C and 6.90 bar O_2 pressure. The HMF conversion reached 100% after 6 h for these catalysts with FDCA and 5-hydroxymethylfuran-2-carboxylic acid (HFCA) as the oxidation products. The yields of FDCA were 79% and 71% for Pt/C and Pd/C catalysts, respectively (**Table 1**, No. 7 and No. 11) (Han X. W. et al., 2016). However, because of the different reaction mechanisms, Au/C only has a 7% yield (**Table 1**, No. 1). Han X. W. et al. (2016) also investigated the Pt/C catalyst, with N doping in the Pt/C-EDA-4.1 catalyst showing the highest activity in the oxidation of HMF to FDCA, and as high as 96% FDCA was obtained under optimal reaction conditions (110 °C, 1.0 MPa O_2, 12 h). With the addition of other noble metal, the yield of FDCA can be further increased by 99% for the Pt-Pd/C catalyst (**Table 1**, No. 8) (Davis et al., 2012). Besides the C catalyst supporter, reduced graphene oxide (RGO) was also used to stabilize Pt nanoparticles (Pt/RGO) for the oxidation of HMF at 25°C (**Table 1**, No. 10). FDCA was produced with a yield of 84%, while HFCA was produced with a yield of 16% by the Pt/RGO catalyst after 24 h under 10 bar O_2 pressure (Negoi et al., 2014). The Pt/RGO catalyst efficiency was reused with 100% HMF conversion in each run. However, the FDCA yield showed a slight decrease with a slight increase in the HFCA yield. Several kinds of Pd catalysts were also active for the oxidation of HMF into FDCA. There was full HMF conversion in each run, but the FDCA yield decreased by 53% for Pd/TiO_2 catalysis (**Table 1**, No.1 2) (Siyo et al., 2014). The Pd/HT catalyst also has a bond between Mg and metal with basic support, which was also active for the oxidation reaction of HMF into FDCA (**Table 1**, No. 13) (Liu et al., 2000). The yield of FDCA could reach up to 99% in water after 7 h at 100°C. And it has stable catalysis efficiency after the fourth run. There was only a slight decrease in the FDCA yield after the fifth run, while there was full HMF conversion over the Pd/HT catalyst.

Non-noble Metal Catalysts

Non-noble metallic oxides (such as Mn, Fe, Co, and Ni) (Jiang et al., 2016; You et al., 2016, 2017; Schade et al., 2018) have been developed to produce FDCA. A 90% FDCA yield, nearly 100% faradaic efficiency, and robust stability were achieved for $NiCo_2O_4$ nanowires (Gao et al., 2018). The non-noble metal (Fe–Zr–O) as a catalyst was used in [Bmim]Cl solvent for the conversion of fructose into HMF. And the formed HMF in the same reactor was further oxidized into FDCA. Under the one-pot conditions, an FDCA yield of 46.4% was obtained with fructose conversion of 100%. The potassium ferrate (K_2FeO_4) catalysis was employed, and a maximum of FDCA yield (48.3%) could be obtained under optimal reaction conditions (Zhang et al., 2015). Photocatalysis processes were usually used for improving the catalytic oxidation; CoPz/g-C_3N_4 is a highly efficient photocatalyst for the aerobic oxidation of HMF to FDCA under sunlight using air as an oxidant. As **Figure 7** shows, the photocatalyst mechanism significantly enhanced the catalytic performance by activating O_2 to $^1O_2$ on the surface of CoPz and then selectively oxidized HMF into FDCA by the release of energy. Mn/N co-doped carbon supported Co catalysts from Co/Mn-lignin complexes, which exhibited excellent performance for aerobic oxidation of HMF to FDCA in water. After six times of use, the HMF conversion and FDCA yield are still 99.5 and 92.7% (Xu et al., 2017; Zhou et al., 2019).

Although many catalysts were developed, some internal disadvantages include high cost of noble metal catalysts, high energy consumption (because of the high reaction temperatures), and high oxygen pressures, and the requirement for the excessive base has been made up. Therefore, developing routes for the selective oxidation of HMF into FDCA under mild conditions is an important challenge. The design of effective, inexpensive, and nonprecious metal-based heterogeneous catalysts for selective HMF oxidation is still a challenge and is of enormous demand.

OTHER REACTIONS

Although the most studied conversions of biomass platform chemicals are the focus on the above reactions, there are other several important reactions of biomass platform chemicals to fine chemicals. Depending on the different types of products, various processes, involving the precise cutting of different C–C bonds, are needed. Common types of reactions include isomerization, reforming, ketonization, or aldol condensation. In this section, recent advances of those reactions in the aqueous phase are discussed.

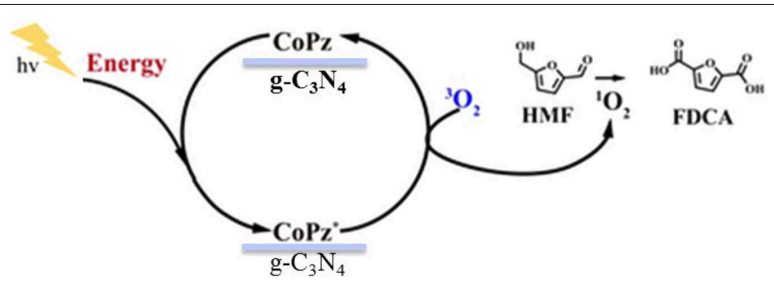

FIGURE 7 | Possible mechanism of the photocatalytic oxidation of HMF into FDCA with the CoPz/g-C_3N_4 catalyst. Reprinted with permission from Xu et al. (2017) American Chemical Society.

Isomerization

Because of the outstanding dehydration performance and subsequent utilization of ketose, the isomerization between aldose and ketose is an important research direction in the aqueous-phase conversion of biomass platform chemicals. In the production process of HMF or LA from cellulose, it has been proved that the dehydration of fructose (**Figure 8**) is much easier than the dehydration of glucose (Kang et al., 2018), and the isomerization is considered as the limiting step (Garces et al., 2019); therefore, improving the conversion and selectivity of the isomerization of glucose to fructose is a very important case for the utilization of these kinds of biobased chemicals.

The isomerization process of glucose to fructose can be accelerated by three types of catalysts, i.e., enzyme, base, and Lewis acid (Garces et al., 2019). Cordon et al. (2019) synthesized several hydrophobic Sn-Beta-F and hydrophilic Sn-Beta-OH catalysts and suggested that Sn-Beta-F can be activated first upon water exposure and then deactivated after 24 h. The characterization showed that the conversion of hydrophobic siloxane linkages into hydrophilic silanol defects within microporous voids led to the deactivation of Sn-Beta-F. They also suggested that the hydrogen-bonded networks formed by waters can confer the stability of the transition states and increase the conversion rates. Besides, they also suggested that the hydrolysis of the catalyst framework will lead to an increase in the hydrophilicity of its surface, which can decrease the isomerization conversion and the catalytic lifetime of the catalyst.

Relatively, Souzanchi et al. (2019) studied a series of solid base catalysts. The most active catalyst, MgO, showed 36.3% conversion of glucose and 22.8% yield of fructose at 100°C. Olson et al. (2019) using imogolite nanotubes, a naturally occurring aluminosilicate nanotube, as an isomerization catalyst achieved the highest conversion of 30% and selectivity of 45%. It can be seen that heterogeneous catalysts applied for the isomerization of glucose to fructose have obtained no perfect results and still need further research. To solve this, Garces et al. (2019) combined homogeneous and heterogeneous catalysts; the existence of Brønsted acids promoted the dehydration of fructose. That set up another approach since fructose is not the final product, and there is no need to be confined to the isomerization; combining several steps might have a better effect.

Reforming

The aqueous-phase reforming (APR) reaction is an environmentally green process to convert polyols into H_2 and alkanes or CO_2 (Bastan et al., 2017). As a by-product of biodiesel production, the APR of glycerol is now an active area of research (Bastan et al., 2017); the main product is hydrogen. The APR process includes two main reactions: C–C cleavage (1) and water–gas shift (WGS) (2) (Guo et al., 2012).

$$C_3H_8O_3 \rightarrow 3CO + 4H_2 \quad (1)$$

$$CO + H_2O \rightarrow CO_2 + H_2 \quad (2)$$

An ideal catalyst should be active both for these two reactions and should prevent the cleavage of C–O. VIII group metal catalysts, like Ni, Pd, and Pt, are commonly used. In recent studies, it has been shown that Pt-based catalysts have a high effect of hydrogen production (Callison et al., 2018), and γ-Al_2O_3 support showed a higher H_2 producing rate than SiO_2, TiO_2, and CeO_2 (Guo et al., 2012). Callison et al. (2018) used a Pt/Al_2O_3 catalyst to produce hydrogen or 1,2-propanediol. They discovered that the Pt particle size and the catalytic sites, such as the edge or the facet sites of Pt particles, can greatly affect the activity and selectivity of APR reaction. With Pt particle size in the range of 2–3.6 nm, even a slight change of Pt particle size can significantly affect the activity and selectivity of products. This phenomenon can be explained by surface chemistry: the edge sites like Pt (100), which are responsible for the dehydrogenation of glycerol, exist more on small Pt particles, and with the reaction proceeding, the edge sites decreased. In comparison, facet sites, such as Pt (111), are responsible for the dehydration of glycerol and tend to produce liquid products. This discovery suggests that the APR reaction or the competition between APR and dehydration not only depends on the species of the catalyst but also is very sensitive to the surface morphology and the particle size.

Besides, Ni-based catalysts have attracted attention because of the low price and high activity in C–C scission (Morales-Marin et al., 2019). Morales-Marin et al. (2019) synthesized a nickel aluminate spinel by co-precipitation, and the reduction temperature of calcination was investigated, which indicated that the spinel structure is very stable. However, it was also found that hydrogen treatment could increase the density of medium-strength acid and basic sites, but could reduce the weak and strong sites that are both acid and basic. The reaction network comprises two routes as shown in **Figure 9** (Morales-Marin et al., 2019), dehydrogenation (route A) and dehydration (route B), corresponding to the cleavage of C–C or C–O, respectively. Dehydrogenation requires metal sites, and dehydration requires acid sites. Analysis of the products indicated that the selectivity

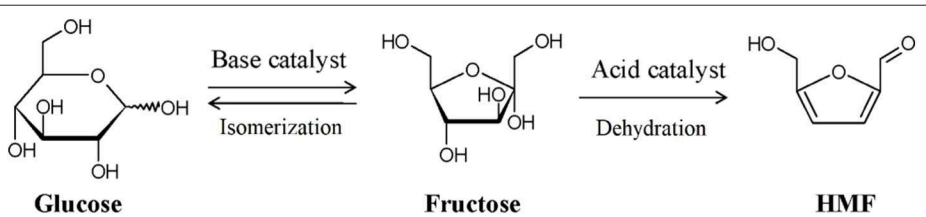

FIGURE 8 | General process of LA production from cellulose. Used with permission of Royal Society of Chemistry, from Takagaki et al. (2009); permission conveyed through Copyright Clearance Center, Inc.

depended on the partial pressure of hydrogen, including the *in situ* formation of H_2 by route A. The result showed that catalysts reduced at the highest temperatures produced the largest yield of H_2, because of the preponderance of the activity of metal sites with respect to the activity of acid sites.

As shown in **Figure 9**, the APR process can also produce small chain alkanes, like methane or ethane. These products also have application foreground and research value. Bastan et al. (2017) used $Ni/Ce_xZr_{1-x}O_2$ to produce alkane. The XRD results showed that the support exists in a mixed-oxide form, and catalytic tests showed the catalytic performance of the catalyst related to the Ce/Zr atomic ratio. For the best performance achieved by 10% $Ni/Ce_{0.3}Zr_{0.7}O_2$, it can produce 99% gas-phase production, with the selectivity of H_2 and alkanes by 45 and 40%, respectively. This catalyst changes CO_2 into alkanes while maintaining the H_2 yield; further research might also focus on the conversion of other valuable chemicals.

Ketonization

Biobased chemicals are mostly composed of oxygenated compounds like alcohols, aldehydes, ketones, carboxylic acids, and aromatics. Take the hydrothermal liquefaction products of algae as an example; nearly 35% of total energy of the raw biomass and many other organic carbons have remained in the aqueous-phase product (Wu et al., 2017a). Acetic acid accounts for a large proportion, about 50% of the organic compounds in the aqueous phase. There is also a large amount of acetic acid that remained in the product of other biomass through thermochemical conversion (Wu et al., 2017a). Therefore, it is necessary to transform the biological acetic acid in the aqueous phase, which can significantly improve the utilization efficiency of algae, lignocellulosic, or other biomass resources. These molecules can be converted to ketones through ketonization and produce hydrocarbons that have a longer chain in the subsequent reaction. As reviewed by Kumar et al. (2018), the ketonization activity of carboxylic acid, aldehydes, alcohols, and esters was compared and sorted: carboxylic acid > aldehyde > alcohol > ester. The kinetically favored mechanism of carboxylic acid ketonization is the β-ketoacid route in **Figure 10**. The ketonization mechanism of other oxygenated compounds is not clear, but it was accepted that surface carboxylate intermediates are formed through an oxidation process under most conditions.

Among ketonization of various oxygenated biomass chemicals, acetic acid is one of the most studied, and Zr-based catalysts are considered to be the most efficient. Wu et al. (2017a) synthesized a $ZrMn_{0.5}O_x$ catalyst, which showed the highest ketonization activity of 88.27% yield of acetone. It was found that Mn can easily form manganese carboxylate with the acetic acid, thus stabilizing the adsorption of acetic acid on the catalyst surface (**Figure 11**). The acid sites strongly affect the catalytic performance, so that the tetragonal ZrO_2 phase, which was always accompanied by high acid property, was the main active phase. They also suggested two different mechanisms of deactivation, the leaching of Mn and the transformation from tetragonal ZrO_2 to monoclinic ZrO_2 (**Figure 11**).

Cai et al. (2018) studied the ketonization of acetic acid over a monoclinic ZrO_2 catalyst by *ab initio* molecular dynamics (AIMD) simulations and density functional theory (DFT) calculations. Compared with vapor phase ketonization, water molecules showed both positive and negative effects on the reaction. On the one hand, water molecules hindered the reaction by blocking active sites or keeping acetic acid solvated through hydrogen bonds. On the other hand, it accelerated the proton transfer through the hydrogen-bonded water network and enhanced the protonation process. They identified an alternative mechanism that was more energetically favorable for the C–C bond formation; however, the α-hydrogen abstraction elementary step had high activation energy.

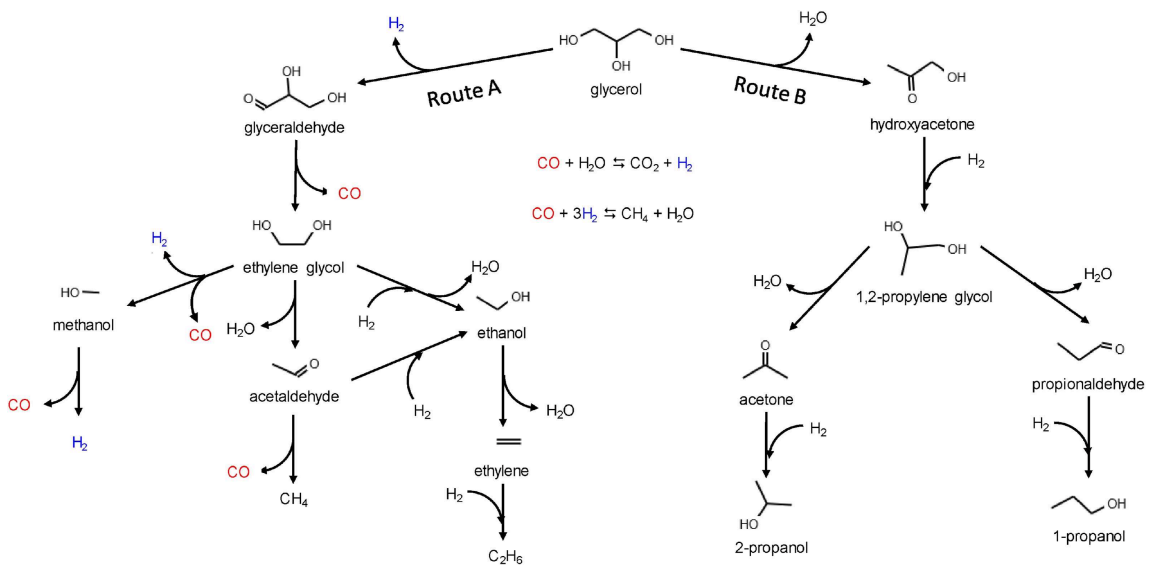

FIGURE 9 | Reaction network for the glycerol APR on nickel catalysts. Reprinted from Morales-Marin et al. (2019), with permission from Elsevier.

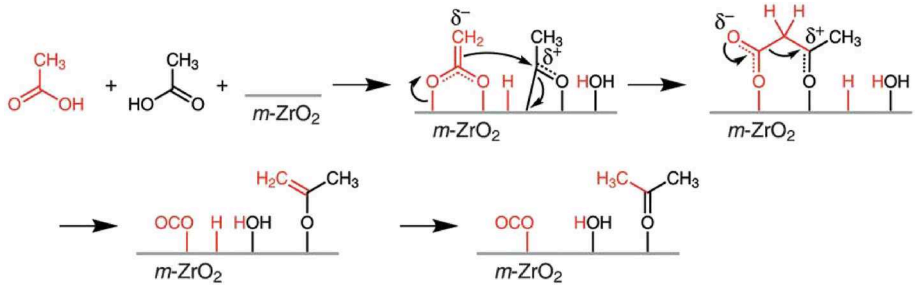

FIGURE 10 | β-ketoacid route of acetic acid ketonization. Reprinted from Kumar et al. (2018), with permission from Elsevier.

FIGURE 11 | Aqueous-phase ketonization and deactivation process on tetragonal (011) facet of **(A)** $ZrMn_yO_x$ ($y \geq 0.2$) and **(B)** $ZrMn_0O_x$ catalysts. Reprinted from Wu et al. (2017a), with permission from Wiley.

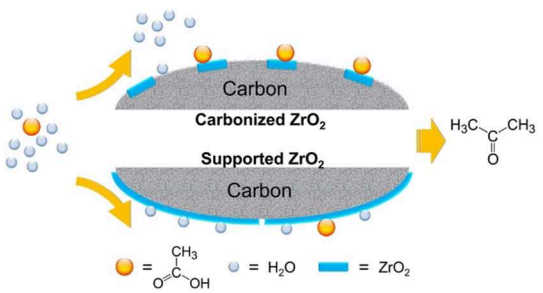

FIGURE 12 | Comparison between the surface of high carbonized ZrO_2 catalysts and conventional catalysts. Reprinted with permission from Wu et al. (2017b); American Chemical Society.

Because water has a blocking effect on the active site of the catalysts, the hydrophobic treatment of the catalyst surface can reduce the negative effect of water to a certain extent. Wu et al. (2017b) synthesized a series of highly carbonized ZrO_2 catalysts. As shown in **Figure 12**, the carbon species in carbonized catalysts reduced the crystallite size of ZrO_2 and improved the surface hydrophobicity, which can enrich the acetic acid on the catalyst surface and weaken the water adsorption, resulting in high ketonization activity. The leaching of carbon and the transformation of the crystal phase of ZrO_2 are still the key factors of the catalyst deactivation, which is the direction of the improvement of heterogeneous catalysts for aqueous-phase ketonization.

In summary, there have been studies on the mechanism of oxygenated biomass chemical ketonization and some mechanisms have been widely accepted, but decisive evidence is still needed. Water phase transformation has been proved to have certain advantages; research on this has long-term significance for the utilization of biobased chemicals.

Aldol Condensation

As mentioned above, ketonization and subsequent aldol condensation are a possible pathway to convert short-chain biomass platform chemicals into long-chain liquid hydrocarbon fuels or value-added chemicals. Although there are several ways to upgrade the primary biomass, the advantage of condensation is low carbon loss and by-product generation. As an important part of C–C bond formation and carbon chain growth, aldol condensation is usually catalyzed by alkaline catalysts (Chheda and Dumesic, 2007), ion-exchanged resins, or zeolites, and because of the high reactivity of aldehydes and ketones, the fractional aldol condensation is not easy to achieve, which makes the aldol condensation of stable platform chemicals very unique (Wu L. P. et al., 2016). Because of this, the aldol condensation of ketones with furfural or HMF has been extensively studied. Faba et al. (2012) studied the aldol condensation of HMF and acetone using MgAl and MgZr mixed oxide catalysts. The results showed that the ratio of medium-strength acid and basic sites can strongly affect the catalytic activity. The results suggested that C_9 and C_{15} products are observed, and the selectivity of the C_{15} product decreased with the rise of conversion.

The aldol condensation mechanism of acetone and 5-HMF using MgAl and MgZr mixed oxide catalysts in the aqueous phase is studied by Cueto et al. (2017). As shown in **Figure 13**, a proton from acetone is first abstracted, and then attacks the carbonyl group of the HMF molecule (Cueto et al., 2017). The

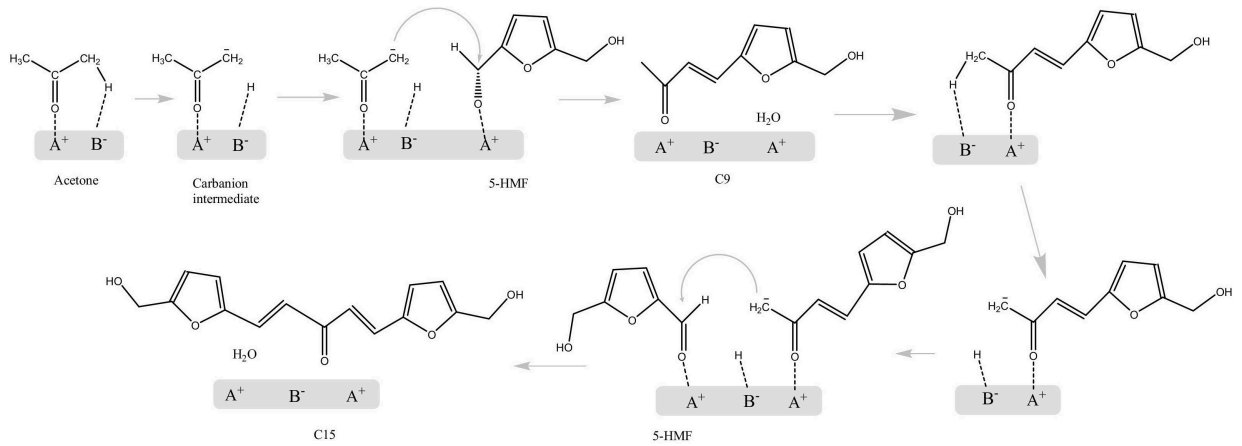

FIGURE 13 | The aldol condensation mechanism of HMF and acetone. Reprinted from Cueto et al. (2017), with permission from Elsevier.

results also explained the selectivity of C_9 and C_{15} varying with the conversion. A second aldolization of the C_9 adduct can occur, as the C_9 adduct still has an α-proton, but the large difference of activation energies between C_6-, C_9-, and C_{15}-based reactions led to the selectivity difference with temperature and the total conversion.

Because C_5 or C_6 alkanes are difficult to be used as fuels due to the short carbon chain, the aqueous-phase aldol condensation is a promising route to convert C_5 or C_6 sugars that are directly produced from cellulose and hemicellulose as usable biofuels. However, there are not many studies about the application of these compounds in fuel manufacturing, which may be related to the relative value between fuels and chemicals. Though the direct pyrolysis or hydrothermal liquefaction of raw biomass as biofuels may be more competitive at present, it is undeniable that the aldol condensation of C_5 or C_6 platform chemicals has opened up a potential application route of upgrading the value of biomass and producing specific chemicals from biomass.

SUMMARY AND OUTLOOK

The aqueous-phase conversion of biomass platform chemicals over heterogeneous catalysts offers economic and environmental benefits to produce valuable chemicals from biomass. Besides, with water as a solvent, the principles of green chemistry are better embodied in terms of the reaction and separation processes. In this review, typical reactions such as dehydration, hydrogenation, oxidation, isomerization, reforming, ketonization, and aldol condensation have been introduced for a general conversion process of biomass. However, aqueous-phase catalytic conversion of biomass still faces many problems to be solved, and advances in the catalysts or the reactions themselves are still developing.

Reaction Mechanisms and Kinetics

In the research of improving the conversion processes and catalysts, the reaction mechanisms are fundamentally needed. Compared with the complicated reaction system of the thermochemical conversion process of biomass to bio-oil, such as hydrothermal liquefaction or pyrolysis of the macromolecular biomass, the reaction mechanisms of conversions of biomass platform chemicals are quite simple. Despite this, catalysts with the same function may produce different products under different conditions. Taking the hydrogenation of furfural as an example, because of its high unsaturation, precise hydrogenation is not so easy to achieve, which makes it difficult to obtain a desirable product with high selectivity. Therefore, the precise regulation of products requires a better understanding of reaction mechanisms and kinetics. In recent years, in combination with the developing technical means, some breakthroughs have been made in the mechanism of many reactions. The common method is to combine kinetic studies with DFT calculation or isotopic labeling (Gilkey et al., 2015). The reaction order can be calculated by controlling the reaction time in a short time, which can reflect the participation level of various species in the reaction system and is helpful in inferring the reaction mechanism. DFT calculation can be used to calculate the energy of each transition state, judge the adsorption mode, and determine the pathway of the reaction process. Isotopic labeling can determine the transfer pathway of a certain kind of atom; e.g., using labeled hydrogen donor can track the hydrogen transfer during the hydrogenation step. In particular, the formation and fracture of chemical bonds and the sequence of competitive reactions can also be observed by labeling the atom in a specific site. However, the case in the aqueous phase is complicated, especially the influence of hydrogen bond and the fast proton exchange; studies are still needed at present, and further research on the mechanisms and kinetics of the reaction pathways will contribute to the development of this field.

Catalysts Development

Hydrothermal stability is an eternal topic of heterogeneous catalysts in aqueous-phase conversion. The deactivation caused

by structural damage or leaching of active components of catalyst pores is the main problem restricting the lifetime of catalysts. Previous efforts have been made in the past few years so that some catalysts with high hydrothermal stability have been formed. The treatment that has been reported to increase the hydrothermal stability of the heterogeneous catalysts includes doping heteroatoms, surface modification, and coating. In recent researches, most catalysts can be recycled, and no significant decrease in activity was observed in more than five times. This is a preliminary attempt at industrial application; the development of water-resistant catalysts with high activity and long-life cycle can be anticipated in the future. In addition, noble metal catalysts once had overwhelming efficiency advantages, but with the general increase in the yield led by the development of new catalysts, this advantage is no longer so obvious in some reactions. On the contrary, the expensive price is more prominent. Therefore, how to show its superiority in other aspects is important. The advantage may be reflected in a lower load and more mild reaction conditions. There is no doubt that all kinds of catalysts are still developing, and the criteria for evaluating the quality of catalysts are also diversified. It will be more and more difficult to make progress on the catalyst that is much better than the existing catalysts in all aspects. In the future, it might be a better way to select catalysts based on appropriate objectives.

Economic Performance

Despite the fact that research on biomass aqueous-phase conversion to high value-added chemicals has shown environmental advantages, the economic feasibility is also one of the factors that ultimately affect the industrialization of it. In other words, if the existing technology cannot reflect economic advantages, its implementation will not be easy. Considering that higher heat capacity and more corrosiveness of water in contrast with traditional non-polar organic solvents like dioxane mean higher heating and equipment costs are needed, more researches of economic feasibility are still needed. In fact, that is not just a matter of cost and benefit; considering the transformation from the traditional petroleum-based industry, more social backgrounds need to be considered, which involves the formulation of relevant standards or the implementation of policies. It is not a chemistry or chemical engineering problem, but a socioeconomic problem. To solve this, research from a wider field is needed.

Product Selection

Although the conversion of biomass as bio-oil is not covered in this article, bio-oil is also widely expected as a promising alternative energy. In fact, compared with the demand for high value-added chemicals, the demand for fuel is ever greater in human society. In other words, some biobased products will have a greater market and strategic significance as fuels. But on the other hand, because the petroleum industry has already had a very mature production process, the price of biobased fuels maybe not as high as that of chemicals at present. The combination of the production of high value-added chemicals with biobased fuels that have a large market and strategy can better reflect the value of biomass in both economic and strategic aspects. For these reasons, some more macroanalysis needs to be made in order to give a better guiding significance for the selection of utilizing route for biomass resources.

In this work, a series of aqueous-phase heterogeneous catalytic conversions of biomass platform molecules have been introduced, and the reaction mechanisms and signs of progress of catalysts have been highlighted. We hope readers can have a broad understanding of this promising field and be able to get guidance and technical support.

AUTHOR CONTRIBUTIONS

XL performed critical reviews and contributed to the section of Introduction, Hydrogenation, and Other Reactions. LZ and SW contributed to the preparation of the sections Oxidation and Dehydration, respectively. YW designed the structure of the manuscript and is responsible for the work. All authors discussed the results, wrote, and commented on the manuscript.

FUNDING

The authors are grateful for the financial support from the Natural Science Foundation of China (Nos. 21838006, 21576155, and 21776159) and National Key Research and Development Program of China (No. 2018YFC1902101).

REFERENCES

Abdelrahman, O. A., Heyden, A., and Bond, J. Q. (2014). Analysis of kinetics and reaction pathways in the aqueous-phase hydrogenation of levulinic acid to form gamma-valerolactone over Ru/C. *ACS Catal.* 4, 1171–1181. doi: 10.1021/cs401177p

Agmon, N. (1995). The grotthuss mechanism. *Chem. Phys. Lett.* 244, 456–462. doi: 10.1016/0009-2614(95)00905-J

Albonetti, S., Lolli, A., Morandi, V., Migliori, A., Lucarelli, C., and Cavani, F. (2015). Conversion of 5-hydroxymethylfurfural to 2,5-furandicarboxylic acid over au-based catalysts: optimization of active phase and metal-support interaction. *Appl. Catal. B* 163, 520–530. doi: 10.1016/j.apcatb.2014.08.026

Bagnato, G., Figoli, A., Ursino, C., Galiano, F., and Sanna, A. (2018). A novel Ru-polyethersulfone (PES) catalytic membrane for highly efficient and selective hydrogenation of furfural to furfuryl alcohol. *J. Mater. Chem. A.* 6, 4955–4965. doi: 10.1039/C7TA10575D

Bastan, F., Kazemeini, M., and Larimi, A. S. (2017). Aqueous-phase reforming of glycerol for production of alkanes over $Ni/Ce_xZr_{1-x}O_2$ nano-catalyst: Effects of the support's composition. *Renew. Energy* 108, 417–424. doi: 10.1016/j.renene.2017.02.076

Binder, J. B., and Raines, R. T. (2009). Simple chemical transformation of lignocellulosic biomass into furans for fuels and chemicals. *J. Am. Chem. Soc.* 131, 1979–1985. doi: 10.1021/ja808537j

Bozell, J. J., and Petersen, G. R. (2010). Technology development for the production of biobased products from biorefinery carbohydrates-the US Department of Energy's "Top 10" revisited. *Green Chem*. 12, 539–554. doi: 10.1039/b922014c

Cai, J. Y., Ma, H., Zhang, J. J., Song, Q., Du, Z. T., Huang, Y. Z., et al. (2013). Gold nanoclusters confined in a supercage of Y zeolite for aerobic oxidation of HMF under mild conditions. *Chem. Eur. J*. 19, 14215–14223. doi: 10.1002/chem.201301735

Cai, Q. X., Lopez-Ruiz, J. A., Cooper, A. R., Wang, J. G., Albrecht, K. O., and Mei, D. H. (2018). Aqueous-phase acetic acid ketonization over monoclinic zirconia. *ACS Catal*. 8, 488–502. doi: 10.1021/acscatal.7b03298

Callison, J., Subramanian, N. D., Rogers, S. M., Chutia, A., Gianolio, D., Catlow, C. R. A., et al. (2018). Directed aqueous-phase reforming of glycerol through tailored platinum nanoparticles. *Appl. Catal. B*. 238, 618–628. doi: 10.1016/j.apcatb.2018.07.008

Carrillo, A. I., Llanes, P., and Pericas, M. A. (2018). A versatile, immobilized gold catalyst for the reductive amination of aldehydes in batch and flow. *React. Chem. Eng*. 3, 714–721. doi: 10.1039/C8RE00101D

Chen, J. Z., Wang, S. P., Huang, J., Chen, L. M., Ma, L. L., and Huang, X. (2013). Conversion of cellulose and cellobiose into sorbitol catalyzed by ruthenium supported on a polyoxometalate/metal-organic framework hybrid. *ChemSusChem*. 6, 1545–1555. doi: 10.1002/cssc.201200914

Chheda, J. N., and Dumesic, J. A. (2007). An overview of dehydration, aldol-condensation and hydrogenation processes for production of liquid alkanes from biomass-derived carbohydrates. *Catal. Today*. 123, 59–70. doi: 10.1016/j.cattod.2006.12.006

Chheda, J. N., Roman-Leshkov, Y., and Dumesic, J. A. (2007). Production of 5-hydroxymethylfurfural and furfural by dehydration of biomass-derived mono- and poly-saccharides. *Green Chem*. 9, 342–350. doi: 10.1039/B611568C

Choudhary, V., Mushrif, S. H., Ho, C., Anderko, A., Nikolakis, V., Marinkovic, N. S., et al. (2013). Insights into the interplay of lewis and brønsted acid catalysts in glucose and fructose conversion to 5-(Hydroxymethyl)furfural and levulinic acid in aqueous media. *J. Am. Chem. Soc*. 135, 3997–4006. doi: 10.1021/ja3122763

Choudhary, V., Sandler, S. I., and Vlachos, D. G. (2012). Conversion of xylose to furfural using lewis and brønsted acid catalysts in aqueous media. *ACS Catal*. 2, 2022–2028. doi: 10.1021/cs300265d

Climent, M. J., Corma, A., and Iborra, S. (2014). Conversion of biomass platform molecules into fuel additives and liquid hydrocarbon fuels. *Green Chem*. 16, 516–547. doi: 10.1039/c3gc41492b

Cordon, M. J., Hall, J. N., Harris, J. W., Bates, J. S., Hwang, S. J., and Gounder, R. (2019). Deactivation of Sn-Beta zeolites caused by structural transformation of hydrophobic to hydrophilic micropores during aqueous-phase glucose isomerization. *Catal. Sci. Technol*. 9, 1654–1668. doi: 10.1039/C8CY02589D

Cortright, R. D., Davda, R. R., and Dumesic, J. A. (2002). Hydrogen from catalytic reforming of biomass-derived hydrocarbons in liquid water. *Nature* 418, 964–967. doi: 10.1038/nature01009

Cueto, J., Faba, L., Diaz, E., and Ordonez, S. (2017). Performance of basic mixed oxides for aqueous-phase 5-hydroxymethylfurfural-acetone aldol condensation. *Appl. Catal. B*. 201, 221–231. doi: 10.1016/j.apcatb.2016.08.013

Dave, N., Selvaraj, R., Varadavenkatesan, T., and Vinayagam, R. (2019). A critical review on production of bioethanol from macroalgal biomass. *Algal Res*. 42:101606. doi: 10.1016/j.algal.2019.101606

Davis, S. E., Houk, L. R., Tamargo, E. C., Datye, A. K., and Davis, R. J. (2011). Oxidation of 5-hydroxymethylfurfural over supported Pt, Pd and Au catalysts. *Catal. Today* 160, 55–60. doi: 10.1016/j.cattod.2010.06.004

Davis, S. E., Zope, B. N., and Davis, R. J. (2012). On the mechanism of selective oxidation of 5-hydroxymethylfurfural to 2,5-furandicarboxylic acid over supported Pt and Au catalysts. *Green Chem*. 14, 143–147. doi: 10.1039/C1GC16074E

Delidovich, I., Leonhard, K., and Palkovits, R. (2014). Cellulose and hemicellulose valorisation: an integrated challenge of catalysis and reaction engineering. *Energy Environ. Sci*. 7, 2803–2830. doi: 10.1039/C4EE01067A

Deng, W. P., Zhang, Q. H., and Wang, Y. (2014). Catalytic transformations of cellulose and cellulose-derived carbohydrates into organic acids. *Catal. Today* 234, 31–41. doi: 10.1016/j.cattod.2013.12.041

Dhanalaxmi, K., Singuru, R., Mandal, S., Bai, L. Y., Reddy, B. M., Bhaumik, A., et al. (2017). Magnetic nanohybrid decorated porous organic polymer: synergistic catalyst for high performance levulinic acid hydrogenation. *ACS Sust. Chem. Eng*. 5, 1033–1045. doi: 10.1021/acssuschemeng.6b02338

Dusselier, M., Van Wouwe, P., Dewaele, A., Makshina, E., and Sels, B. F. (2013). Lactic acid as a platform chemical in the biobased economy: the role of chemocatalysis. *Energy Environ. Sci*. 6, 1415–1442. doi: 10.1039/c3ee00069a

Dutta, S., Yu, I. K. M., Tsang, D. C. W., Ng, Y. H., Ok, Y. S., Sherwood, J., et al. (2019). Green synthesis of gamma-valerolactone (GVL) through hydrogenation of biomass-derived levulinic acid using non-noble metal catalysts: a critical review. *Chem. Eng. J*. 372, 992–1006. doi: 10.1016/j.cej.2019.04.199

Elliott, D. C., Biller, P., Ross, A. B., Schmidt, A. J., and Jones, S. B. (2015). Hydrothermal liquefaction of biomass: Developments from batch to continuous process. *Bioresour. Technol*. 178, 147–156. doi: 10.1016/j.biortech.2014.09.132

Faba, L., Diaz, E., and Ordonez, S. (2012). Aqueous-phase furfural-acetone aldol condensation over basic mixed oxides. *Appl. Catal. B*. 113, 201–221. doi: 10.1016/j.apcatb.2011.11.039

Fang, C. J., Wu, W. B., Li, H., Yang, T. T., Zhao, W. F., Wang, Z. W., et al. (2017). Production of bio-based furfural from xylose over a recyclable niobium phosphate ($NbOPO_3$) catalyst. *Energy Sources Part A*. 39, 2072–2077. doi: 10.1080/15567036.2017.1402103

Fang, R. Q., Luque, R., and Li, Y. W. (2016). Efficient one-pot fructose to DFF conversion using sulfonated magnetically separable MOF-derived Fe_3O_4 (111) catalysts. *Green Chem*. 19, 647–655. doi: 10.1039/C6GC02018F

Feng, H. J., Li, X. C., Qian, H., Zhang, Y. F., Zhang, D. H., Zhao, D., et al. (2019). Efficient and sustainable hydrogenation of levulinic-acid to gamma-valerolactone in aqueous solution over acid-resistant $CePO_4/Co_2P$ catalysts. *Green Chem*. 21, 1743–1756. doi: 10.1039/C9GC00482C

Fernandes, D. R., Rocha, A. S., Mai, E. F., Mota, C. J. A., and da Silva, V. T. (2012). Levulinic acid esterification with ethanol to ethyl levulinate production over solid acid catalysts. *Appl. Catal. A*. 425, 199–204. doi: 10.1016/j.apcata.2012.03.020

Gallezot, P. (2012). Conversion of biomass to selected chemical products. *Chem. Soc. Rev*. 41, 1538–1558. doi: 10.1039/C1CS15147A

Gao, L. F., Bao, Y., Gan, S. Y., Sun, Z. H., Song, Z. Q., Han, D. X., et al. (2018). Hierarchical nickel-cobalt-based transition metal oxide catalysts for the electrochemical conversion of biomass into valuable chemicals. *ChemSusChem* 11, 2547–2553. doi: 10.1002/cssc.201800695

Garces, D., Faba, L., Diaz, E., and Ordonez, S. (2019). Aqueous-phase transformation of glucose into hydroxymethylfurfural and levulinic acid by combining homogeneous and heterogeneous catalysis. *ChemSusChem*. 12, 924–934. doi: 10.1002/cssc.201802315

Gayubo, A. G., Alonso, A., Valle, B., Aguayo, A. T., Olazar, M., and Bilbao, J. (2010). Hydrothermal stability of HZSM-5 catalysts modified with Ni for the transformation of bioethanol into hydrocarbons. *Fuel* 89, 3365–3372. doi: 10.1016/j.fuel.2010.03.002

Gilkey, M. J., Panagiotopoulou, P., Mironenko, A. V., Jenness, G. R., Vlachos, D. G., and Xu, B. J. (2015). Mechanistic insights into metal lewis acid-mediated catalytic transfer hydrogenation of furfural to 2-methylfuran. *ACS Catal*. 5, 3988–3994. doi: 10.1021/acscatal.5b00586

Gliozzi, G., Innorta, A., Mancini, A., Bortolo, R., Perego, C., Ricci, M., et al. (2014). Zr/P/O catalyst for the direct acid chemo-hydrolysis of non-pretreated microcrystalline cellulose and softwood sawdust. *Appl. Catal. B*. 145, 24–33. doi: 10.1016/j.apcatb.2012.12.035

Gong, W. B., Chen, C., Zhang, H. M., Wang, G. Z., and Zhao, H. J. (2018). Highly dispersed Co and Ni nanoparticles encapsulated in N-doped carbon nanotubes as efficient catalysts for the reduction of unsaturated oxygen compounds in aqueous phase. *Catal. Sci. Technol*. 8, 5506–5514. doi: 10.1039/C8CY01488D

Guo, Y., Azmat, M. U., Liu, X. H., Wang, Y. Q., and Lu, G. Z. (2012). Effect of support's basic properties on hydrogen production in aqueous-phase reforming of glycerol and correlation between WGS and APR. *Appl. Energy*. 92, 218–223. doi: 10.1016/j.apenergy.2011.10.020

Han, X. W., Li, C. Q., Guo, Y., Liu, X. H., Zhang, Y. G., and Wang, Y. Q. (2016). N-doped carbon supported Pt catalyst for base-free oxidation of 5-hydroxymethylfurfural to 2,5-furandicarboxylic acid. *Appl. Catal. A*. 526, 1–8. doi: 10.1016/j.apcata.2016.07.011

Han, Y. L., Liu, C. J., Horita, J., and Yan, W. L. (2016). Trichloroethene hydrodechlorination by Pd-Fe bimetallic nanoparticles: Solute-induced catalyst

deactivation analyzed by carbon isotope fractionation. *Appl. Catal. B*. 188, 77–86. doi: 10.1016/j.apcatb.2016.01.047

Harun, R., Singh, M., Forde, G. M., and Danquah, M. K. (2010). Bioprocess engineering of microalgae to produce a variety of consumer products. *Renew. Sust. Energy Rev*. 14, 1037–1047. doi: 10.1016/j.rser.2009.11.004

He, C., Chen, C. L., Giannis, A., Yang, Y. H., and Wang, J. Y. (2014). Hydrothermal gasification of sewage sludge and model compounds for renewable hydrogen production: a review. *Renew. Sust. Energy Rev*. 39, 1127–1142. doi: 10.1016/j.rser.2014.07.141

Hu, L., Lin, L., and Liu, S. J. (2014). Chemoselective hydrogenation of biomass-derived 5-hydroxymethylfurfural into the liquid biofuel 2,5-dimethylfuran. *Ind. Eng. Chem. Res*. 53, 9969–9978. doi: 10.1021/ie5013807

Hua, D. R., Li, P. P., Wu, Y. L., Chen, Y., Yang, M. D., Dang, J., et al. (2013). Preparation of solid acid catalyst packing AAO/SBA-15-SO_3H and application for dehydration of xylose to furfural. *J. Ind. Eng. Chem*. 19, 1395–1399. doi: 10.1016/j.jiec.2013.01.002

Huang, Y. B., Yang, T., Lin, Y. T., Zhu, Y. Z., Li, L. C., and Pan, H. (2018). Facile and high-yield synthesis of methyl levulinate from cellulose. *Green Chem*. 20,1323–1334. doi: 10.1039/C7GC02883K

Huber, G. W., Cortright, R. D., and Dumesic, J. A. (2004). Renewable alkanes by aqueous-phase reforming of biomass-derived oxygenates. *Angew. Chem. Int. Edit*. 43, 1549–1551. doi: 10.1002/anie.200353050

Huo, J. J., Johnson, R. L., Duan, P., Pham, H. N., Mendivelso-Perez, D., Smith, E. A., et al. (2018). Stability of Pd nanoparticles on carbon-coated supports under hydrothermal conditions. *Catal. Sci. Technol*. 8, 1151–1160. doi: 10.1039/C7CY02098H

Irshad, M., Lee, S., Choi, E., and Kim, J. W. (2019). Efficient synthetic routes of biomass-derived platform chemicals. *Appl. Chem. Eng*. 30, 280–289. doi: 10.14478/ace.2019.1036

Jeong, G. Y., Singh, A. K., Sharma, S., Gyak, K. W., Maurya, R. A., and Kim, D. P. (2015). One-flow syntheses of diverse heterocyclic furan chemicals directly from fructose via tandem transformation platform. *NPG Asia Mater*. 7:e173. doi: 10.1038/am.2015.21

Jiang, C. W., Zhu, J. D., Wang, B., Li, L., and Zhong, H. (2018). One-pot synthesis of 5-hydroxymethylfurfural from glucose over zirconium doped mesoporous KIT-6. *Chinese J. Chem. Eng*. 26, 1270–1277. doi: 10.1016/j.cjche.2018.02.031

Jiang, N., You, B., Boonstra, R., Rodriguez, I. M. T., and Sun, Y. (2016). Integrating electrocatalytic 5-hydroxymethylfurfural oxidation and hydrogen production via co-P-derived electrocatalysts. *ACS Energy Lett*. 1, 386–390. doi: 10.1021/acsenergylett.6b00214

Kang, M. J., Park, H., Jegal, J., Hwang, S. Y., Kang, Y. S., and Cha, H. G. (2019). Electrocatalysis of 5-hydroxymethylfurfural at cobalt based spinel catalysts with filamentous nanoarchitecture in alkaline media. *Appl. Catal. B*. 242, 85–91. doi: 10.1016/j.apcatb.2018.09.087

Kang, S. M., Fu, J. X., and Zhang, G. (2018). From lignocellulosic biomass to levulinic acid: A review on acid-catalyzed hydrolysis. *Renew. Sust. Energy Rev*. 94, 340–362. doi: 10.1016/j.rser.2018.06.016

Karimi, K., Tabatabaei, M., Horvath, I. S., and Kumar, R. (2015). Recent trends in acetone, butanol, and ethanol (ABE) production. *Biofuel Res. J*. 2, 301–308. doi: 10.18331/BRJ2015.2.4.4

Khoo, C. G., Dasan, Y. K., Lam, M. K., and Lee, K. T. (2019). Algae biorefinery: review on a broad spectrum of downstream processes and products. *Bioresour. Technol*. 292:121964. doi: 10.1016/j.biortech.2019.121964

Kim, S. B., You, S. J., Kim, Y. T., Lee, S. M., Lee, H., Park, K., et al. (2011). Dehydration of D-xylose into furfural over H-zeolites. *Korean J. Chem. Eng*. 28, 710–716. doi: 10.1007/s11814-010-0417-y

Kobayashi, H., Yokoyama, H., Feng, B., and Fukuoka, A. (2015). Dehydration of sorbitol to isosorbide over H-beta zeolites with high Si/Al ratios. *Green Chem*. 17, 2732–2735. doi: 10.1039/C5GC00319A

Kruger, J. S., Nikolakis, V., and Vlachos, D. G. (2012). Carbohydrate dehydration using porous catalysts. *Curr. Opin. Chem. Eng*. 1, 312–320. doi: 10.1016/j.coche.2012.06.003

Kumar, N., Stephanidis, B., Zenobi, R., Wain, A. J., and Roy, D. (2015). Nanoscale mapping of catalytic activity using tip-enhanced Raman spectroscopy. *Nanoscale* 7, 7133–7137. doi: 10.1039/C4NR07441F

Kumar, R., Enjamuri, N., Shah, S., Al-Fatesh, A. S., Bravo-Suarez, J. J., and Chowdhury, B. (2018). Ketonization of oxygenated hydrocarbons on metal oxide based catalysts. *Catal. Today* 302, 16–49. doi: 10.1016/j.cattod.2017.09.044

Kumar, V. B., Mishra, R. K., Pulidindi, I. N., Porat, Z., Luong, J. H. T., and Gedanken, A. (2016). Preparation and catalytic activity of thermosensitive Ga_2O_3 nanorods. *Energy Fuels* 30, 7419–7427. doi: 10.1021/acs.energyfuels.6b01568

Kwon, Y., Schouten, K. J. P., van der Waal, J. C., de Jong, E., and Koper, M. T. M. (2016). Electrocatalytic conversion of furanic compounds. *ACS Catal*. 6, 6704–6717. doi: 10.1021/acscatal.6b01861

Lanzafame, P., Centi, G., and Perathoner, S. (2014). Catalysis for biomass and CO_2 use through solar energy: opening new scenarios for a sustainable and low-carbon chemical production. *Chem. Soc. Rev*. 43, 7562–7580. doi: 10.1039/C3CS60396B

Li, J., Ding, D. J., Deng, L., Guo, Q. X., and Fu, Y. (2012). Catalytic air oxidation of biomass-derived carbohydrates to formic acid. *ChemSusChem* 5, 1313–1318. doi: 10.1002/cssc.201100466

Li, N., and Huber, G. W. (2010). Aqueous-phase hydrodeoxygenation of sorbitol with Pt/SiO_2-Al_2O_3: identification of reaction intermediates. *J. Catal*. 270, 48–59. doi: 10.1016/j.jcat.2009.12.006

Li, Q. Q., Wang, H. Y., Tian, Z. P., Weng, Y. J., Wang, C. G., Ma, J. R., et al. (2019). Selective oxidation of 5-hydroxymethylfurfural to 2, 5-furandicarboxylic acid over Au/CeO_2 catalysts: the morphology effect of CeO_2. *Catal. Sci. Technol*. 9, 1570–1580. doi: 10.1039/C9CY00211A

Li, S. P., Wang, Y. Y., Yang, Y. D., Chen, B. F., Tai, J., Liu, H. Z., et al. (2019). Conversion of levulinic acid to gamma-valerolactone over ultra-thin TiO_2 nanosheets decorated with ultrasmall Ru nanoparticle catalysts under mild conditions. *Green Chem*. 21, 770–774. doi: 10.1039/C8GC03529F

Li, X. D., Jia, P., and Wang, T. F. (2016). Furfural: a promising platform compound for sustainable production of C-4 and C-5 chemicals. *ACS Catal*. 6, 7621–7640. doi: 10.1021/acscatal.6b01838

Liu, C., Wu, S. L., Zhang, H. Y., and Xiao, R. (2019). Catalytic oxidation of lignin to valuable biomass-based platform chemicals: a review. *Fuel Process. Technol*. 191, 181–201. doi: 10.1016/j.fuproc.2019.04.007

Liu, M., Jia, S. G., Gong, Y. Y., Song, C. S., and Guo, X. W. (2013). Effective hydrolysis of cellulose into glucose over sulfonated sugar-derived carbon in an ionic liquid. *Ind. Eng. Chem. Res*. 52, 8167–8173. doi: 10.1021/ie400571e

Liu, Y. Y., Suzuki, K., Hamakawa, S., Hayakawa, T., Murata, K., Ishii, T., et al. (2000). Highly active methanol decomposition catalyst derived from Pd-hydrotalcite dispersed on mesoporous silica. *Catal. Lett*. 66, 205–213. doi: 10.1023/A:1019088732045

Luo, W. H., Cao, W. X., Bruijnincx, P. C. A., Lin, L., Wang, A. Q., and Zhang, T. (2019). Zeolite-supported metal catalysts for selective hydrodeoxygenation of biomass-derived platform molecules. *Green Chem*. 21, 3744–3768. doi: 10.1039/C9GC01216H

Luo, Y. P., Li, Z., Li, X. L., Liu, X. F., Fan, J., Clark, J. H., et al. (2019). The production of furfural directly from hemicellulose in lignocellulosic biomass: a review. *Catal. Today* 319, 14–24. doi: 10.1016/j.cattod.2018.06.042

Luterbacher, J. S., Alonso, D. M., and Dumesic, J. A. (2014). Targeted chemical upgrading of lignocellulosic biomass to platform molecules. *Green Chem*. 16, 4816–4838. doi: 10.1039/c4gc01160k

Marianou, A. A., Michailof, C. M., Pineda, A., Iliopoulou, E. F., Triantafyllidis, K. S., and Lappas, A. A. (2018). Effect of Lewis and Brønsted acidity on glucose conversion to 5-HMF and lactic acid in aqueous and organic media. *Appl. Catal. A Gen*. 555, 75–87. doi: 10.1016/j.apcata.2018.01.029

Menon, V., and Rao, M. (2012). Trends in bioconversion of lignocellulose: biofuels, platform chemicals and biorefinery concept. *Prog. Energy Combust. Sci*. 38, 522–550. doi: 10.1016/j.pecs.2012.02.002

Mishra, R. K., Kumar, V. B., Victor, A., Pulidindi, I. N., and Gedanken, A. (2019). Selective production of furfural from the dehydration of xylose using Zn doped CuO catalyst. *Ultrason. Sonochem*. 56, 55–62. doi: 10.1016/j.ultsonch.2019.03.015

Morales-Marin, A., Ayastuy, J. L., Iriarte-Velasco, U., and Gutierrez-Ortiz, M. A. (2019). Nickel aluminate spinel-derived catalysts for the aqueous phase reforming of glycerol: Effect of reduction temperature. *Appl. Catal. B*. 244, 931–945. doi: 10.1016/j.apcatb.2018.12.020

Moreno-Recio, M., Santamaría-González, J., and Maireles-Torres, P. (2016). Brønsted and Lewis acid ZSM-5 zeolites for the catalytic dehydration

of glucose into 5-hydroxymethylfurfural. *Chem. Eng. J.* 303, 22–30. doi: 10.1016/j.cej.2016.05.120

Negoi, A., Triantafyllidis, K., Parvulescu, V. I., and Coman, S. M. (2014). The hydrolytic hydrogenation of cellulose to sorbitol over M (Ru, Ir, Pd, Rh)-BEA-zeolite catalysts. *Catal. Today* 223, 122–128. doi: 10.1016/j.cattod.2013.07.007

Niu, W. Q., Wang, D., Yang, G. H., Sun, J., Wu, M. B., Yoneyama, Y., et al. (2014). Pt nanoparticles loaded on reduced graphene oxide as an effective catalyst for the direct oxidation of 5-hydroxymethylfurfural (HMF) to produce 2,5-furandicarboxylic acid (FDCA) under mild conditions. *Bull. Chem. Soc. Jpn.* 87, 1124–1129. doi: 10.1246/bcsj.20140096

Olson, N., Deshpande, N., Gunduz, S., Ozkan, U. S., and Brunelli, N. A. (2019). Utilizing imogolite nanotubes as a tunable catalytic material for the selective isomerization of glucose to fructose. *Catal. Today* 323, 69–75. doi: 10.1016/j.cattod.2018.07.059

O'Neill, R., Ahmad, M. N., Vanoye, L., and Aiouache, F. (2009). Kinetics of aqueous phase dehydration of xylose into furfural catalyzed by ZSM-5 zeolite. *Ind. Eng. Chem. Res.* 48, 4300–4306. doi: 10.1021/ie801599k

Patil, S. K. R., and Lund, C. R. F. (2011). Formation and growth of humins via aldol addition and condensation during acid-catalyzed conversion of 5-hydroxymethylfurfural. *Energy Fuels* 25, 4745–4755. doi: 10.1021/ef2010157

Pham, T. N., Sooknoi, T., Crossley, S. P., and Resasco, D. E. (2013). Ketonization of carboxylic acids: mechanisms, catalysts, and implications for biomass conversion. *ACS Catal.* 3, 2456–2473. doi: 10.1021/cs400501h

Putro, W. S., Kojima, T., Hara, T., Ichikuni, N., and Shimazu, S. (2017). Selective hydrogenation of unsaturated carbonyls by Ni-Fe-based alloy catalysts. *Catal. Sci. Technol.* 7, 3736–3646. doi: 10.1039/C7CY00945C

Qiu, S. B., Wang, T. J., and Fang, Y. X. (2019). High-efficient preparation of gasoline-ranged C5-C6 alkanes from biomass-derived sugar polyols of sorbitol over Ru-MoO_{3-x}/C catalyst. *Fuel Process. Technol.* 183, 19–26. doi: 10.1016/j.fuproc.2018.11.002

Ravenelle, R. M., Copeland, J. R., Kim, W. G., Crittenden, J. C., and Sievers, C. (2011). Structural changes of gamma-Al2O3-supported catalysts in hot liquid water. *ACS Catal.* 1, 552–561. doi: 10.1021/cs1001515

Rey-Raap, N., Ribeiro, L. S., Orfao, J. J. D., Figueiredo, J. L., and Pereira, M. F. R. (2019). Catalytic conversion of cellulose to sorbitol over Ru supported on biomass-derived carbon-based materials. *Appl. Catal. B.* 256:117826. doi: 10.1016/j.apcatb.2019.117826

Rinaldi, R., Meine, N., Stein, J., Palkovits, R., and Schüth, F. (2010). Which controls the depolymerization of cellulose in ionic liquids: the solid acid catalyst or cellulose? *ChemSusChem*. 3, 266–276. doi: 10.1002/cssc.200900281

Rinaldi, R., and Schuth, F. (2009). Design of solid catalysts for the conversion of biomass. *Energy Environ. Sci.* 2, 610–626. doi: 10.1039/b902668a

Roman-Leshkov, Y., Moliner, M., Labinger, J. A., and Davis, M. E. (2010). Mechanism of glucose isomerization using a solid lewis acid catalyst in water. *Angew. Chem. Int. Ed.* 49, 8954–8957. doi: 10.1002/anie.201004689

Romero, A., Cantero, D. A., Nieto-Marquez, A., Martinez, C., Alonso, E., and Cocero, M. J. (2016). Supercritical water hydrolysis of cellulosic biomass as effective pretreatment to catalytic production of hexitols and ethylene glycol over Ru/MCM-48. *Green Chem.* 18, 4051–4062. doi: 10.1039/C6GC00374E

Saha, B. C. (2003). Hemicellulose bioconversion. *J. Ind. Microbiol. Biotechnol.* 30, 279–291. doi: 10.1007/s10295-003-0049-x

Sato, O., Mimura, N., Masuda, Y., Shirai, M., and Yamaguchi, A. (2019). Effect of extraction on furfural production by solid acid-catalyzed xylose dehydration in water. *J. Supercrit. Fluid.* 144, 14–18. doi: 10.1016/j.supflu.2018.10.004

Schade, O. R., Kalz, K. F., Neukum, D., Kleist, W., and Grunwaldt, J. D. (2018). Supported gold- and silver-based catalysts for the selective aerobic oxidation of 5-(hydroxymethyl) furfural to 2,5-furandicarboxylic acid and 5-hydroxymethyl-2-furancarboxylic acid. *Green Chem.* 20, 3530–3541. doi: 10.1039/C8GC01340C

Serrano-Ruiz, J. C., Luque, R., and Sepulveda-Escribano, A. (2011). Transformations of biomass-derived platform molecules: from high added-value chemicals to fuels via aqueous-phase processing. *Chem. Soc. Rev.* 40, 5266–5281. doi: 10.1039/c1cs15131b

Sheldon, R. A. (2014). Green and sustainable manufacture of chemicals from biomass: state of the art. *Green Chem.* 16, 950–963. doi: 10.1039/C3GC41935E

Shi, X. J., Wu, Y. L., Li, P. P., Yi, H. F., Yang, M. D., and Wang, G. H. (2011b). Catalytic conversion of xylose to furfural over the solid acid SO_4^{2-}/ZrO_2-Al_2O_3/SBA-15 catalysts. *Carbohyd. Res.* 346, 480–487. doi: 10.1016/j.carres.2011.01.001

Shi, X. J., Wu, Y. L., Yi, H. F., Rui, G., Li, P. P., Yang, M. D., et al. (2011a). Selective preparation of furfural from xylose over sulfonic acid functionalized mesoporous sba-15 materials. *Energies* 4, 669–684. doi: 10.3390/en4040669

Shylesh, S., Schunemann, V., and Thiel, W. R. (2010). Magnetically separable nanocatalysts: bridges between homogeneous and heterogeneous catalysis. *Angew. Chem. Int. Ed.* 49, 3428–3459. doi: 10.1002/anie.200905684

Siyo, B., Schneider, M., Radnik, J., Pohl, M. M., Langer, P., and Steinfeldt, N. (2014). Influence of support on the aerobic oxidation of hmf into FDCA over preformed Pd nanoparticle based materials. *Appl. Catal. A.* 478, 107–116. doi: 10.1016/j.apcata.2014.03.020

Souzanchi, S., Nazari, L., Rao, K. T. V., Yuan, Z. S., Tan, Z. C., and Xu, C. B. (2019). Catalytic isomerization of glucose to fructose using heterogeneous solid Base catalysts in a continuous-flow tubular reactor: Catalyst screening study. *Catal. Today* 319, 76–83. doi: 10.1016/j.cattod.2018.03.056

Su, J. L., Qiu, M., Shen, F., and Qi, X. H. (2018). Efficient hydrolysis of cellulose to glucose in water by agricultural residue-derived solid acid catalyst. *Cellulose* 25, 17–22. doi: 10.1007/s10570-017-1603-4

Suganuma, S., Nakajima, K., Kitano, M., Yamaguchi, D., Kato, H., Hayashi, S., et al. (2008). Hydrolysis of cellulose by amorphous carbon bearing SO_3H, COOH, and OH groups. *J. Am. Chem. Soc.* 130, 12787–12793. doi: 10.1021/ja803983h

Takagaki, A., Ohara, M., Nishimura, S., and Ebitani, K. (2009). A one-pot reaction for biorefinery: combination of solid acid and base catalysts for direct production of 5-hydroxymethylfurfural from saccharides. *Chem. Commun.* 41, 6276–6278. doi: 10.1039/b914087e

Tang, X., Wei, J. N., Ding, N., Sun, Y., Zeng, X. H., Hu, L., et al. (2017). Chemoselective hydrogenation of biomass derived 5-hydroxymethylfurfural to diols: key intermediates for sustainable chemicals, materials and fuels. *Renew. Sust. Energy Rev.* 77, 287–296. doi: 10.1016/j.rser.2017.04.013

Taylor, M. J., Durndell, L. J., Isaacs, M. A., Parlett, C. M. A., Wilson, K., Lee, A. F., et al. (2016). Highly selective hydrogenation of furfural over supported Pt nanoparticles under mild conditions. *Appl. Catal. B.* 180, 580–585. doi: 10.1016/j.apcatb.2015.07.006

Teong, S. P., Yi, G. S., and Zhang, Y. G. (2014). Hydroxymethylfurfural production from bioresources: past, present and future. *Green Chem.* 16, 2015–2026. doi: 10.1039/c3gc42018c

Upare, P. P., Lee, J. M., Hwang, D. W., Halligudi, S. B., Hwang, Y. K., and Chang, J. S. (2011). Selective hydrogenation of levulinic acid to gamma-valerolactone over carbon-supported noble metal catalysts. *Ind. Eng. Chem.* 17, 287–292. doi: 10.1016/j.jiec.2011.02.025

Verdeguer, P., Merat, N., Rigal, L., and Gaset, A. (1994). Optimization of experimental conditions for the catalytic-oxidation of furfural to furoic acid. *J. Chem. Technol. Biotechnol.* 61, 97–102. doi: 10.1002/jctb.280610203

Villa, A., Schiavoni, M., Campisi, S., Veith, G. M., and Prati, L. (2013). Pd-modified Au on carbon as an effective and durable catalyst for the direct oxidation of HMF to 2,5-furandicarboxylic acid. *ChemSusChem* 6, 609–612. doi: 10.1002/cssc.201200778

Wan, X. Y., Zhou, C. M., Chen, J. S., Deng, W. P., Zhang, Q. H., Yang, Y. H., et al. (2014). Base-free aerobic oxidation of 5-hydroxymethyl-furfural to 2,5-furandicarboxylic acid in water catalyzed by functionalized carbon nanotube-supported Au-Pd alloy nanoparticles. *ACS Catal.* 4, 2175–2185. doi: 10.1021/cs5003096

Wang, J. J., Xi, J. X., Xia, Q. N., Liu, X. H., and Wang, Y. Q. (2017). Recent advances in heterogeneous catalytic conversion of glucose to 5-hydroxymethylfurfural via green routes. *Sci. China: Chem.* 60, 870–886. doi: 10.1007/s11426-016-9035-1

Wang, M., Ma, J. P., Liu, H. F., Luo, N. C., Zhao, Z. T., and Wang, F. (2018). Sustainable productions of organic acids and their derivatives from biomass via selective oxidative cleavage of C-C bond. *ACS Catal.* 8, 2129–2165. doi: 10.1021/acscatal.7b03790

Werpy, T. A., and Petersen, G. (2004). *Top Value Added Chemicals From Biomass. Volume I: Results of Screening for Potential Candidates from Sugars and Synthesis Gas.* U. S. Dep. Energy. doi: 10.2172/15008859

Wolfel, R., Taccardi, N., Bosmann, A., and Wasserscheid, P. (2011). Selective catalytic conversion of biobased carbohydrates to formic acid using molecular oxygen. *Green Chem.* 13, 2759–2763. doi: 10.1039/c1gc15434f

Wu, K. J., Wu, Y. L., Chen, Y., Chen, H., Wang, J. L., and Yang, M. D. (2016). Heterogeneous catalytic conversion of biobased chemicals into liquid fuels in the aqueous phase. *ChemSusChem* 9, 1355–1385. doi: 10.1002/cssc.201600013

Wu, K. J., Yang, M. D., Chen, Y., Pu, W. H., Hu, H. S., and Wu, Y. L. (2017a). Aqueous-phase ketonization of acetic acid over Zr/Mn mixed oxides. *AIChE J.* 63, 2958–2967. doi: 10.1002/aic.15687

Wu, K. J., Yang, M. D., Pu, W. H., Wu, Y. L., Shi, Y. C., and Hu, H. S. (2017b). Carbon promoted ZrO_2 catalysts for aqueous-phase ketonization of acetic acid. *ACS Sust. Chem. Eng.* 5, 3509–3516. doi: 10.1021/acssuschemeng.7b00226

Wu, L. P., Moteki, T., Gokhale, A. A., Flaherty, D. W., and Toste, F. D. (2016). Production of fuels and chemicals from biomass: condensation reactions and beyond. *Chem* 1, 32–58. doi: 10.1016/j.chempr.2016.05.002

Wu, L. Q., Song, J. L., Zhang, B. B., Zhou, B. W., Zhou, H. C., Fan, H. L., et al. (2014). Very efficient conversion of glucose to 5-hydroxymethylfurfural in DBU-based ionic Liquids with benzenesulfonate anion. *Green Chem.* 16, 3935–3941. doi: 10.1039/C4GC00311J

Xiong, H. F., Pham, H. N., and Datye, A. K. (2014). Hydrothermally stable heterogeneous catalysts for conversion of biorenewables. *Green Chem.* 16, 4627–4643. doi: 10.1039/C4GC01152J

Xu, S., Zhou, P., Zhang, Z. H., Yang, C. J., Zhang, B. G., Deng, K. J., et al. (2017). Selective oxidation of 5-hydroxymethylfurfural to 2,5-furandicarboxylic acid using o_2 and a photocatalyst of co-thioporphyrazine bonded to g-C_3N_4. *J. Am. Chem. Soc.* 139, 14775–14782. doi: 10.1021/jacs.7b08861

Xu, S. Q., Pan, D. H., Wu, Y. F., Song, X. H., Gao, L. J., Li, W. Q., et al. (2018). Efficient production of furfural from xylose and wheat straw by bifunctional chromium phosphate catalyst in biphasic systems. *Fuel Process. Technol.* 175, 90–96. doi: 10.1016/j.fuproc.2018.04.005

Yakabi, K., Jones, A., Buchard, A., Roldan, A., and Hammond, C. (2018). Chemoselective lactonization of renewable succinic acid with heterogeneous nanoparticle catalysts. *ACS Sust. Chem. Eng.* 6, 16341–16351. doi: 10.1021/acssuschemeng.8b03346

Yang, Q., and Pan, X. J. (2016). Bifunctional porous polymers bearing boronic and sulfonic acids for hydrolysis of cellulose. *ACS Sust. Chem. Eng.* 4, 4824–4830. doi: 10.1021/acssuschemeng.6b01102

Yemi,ş, O., and Mazza, G. (2019). Catalytic performances of various solid catalysts and metal halides for microwave-assisted hydrothermal conversion of xylose, xylan, and straw to furfural. *Waste Biomass Valori.* 10, 1343–1353. doi: 10.1007/s12649-017-0144-2

You, B., Jiang, N., Liu, X., and Sun, Y. J. (2016). Simultaneous H-2 generation and biomass upgrading in water by an efficient noble-metal-free bifunctional electrocatalyst. *Angew. Chem.* 55, 9913–9917. doi: 10.1002/anie.201603798

You, B., Liu, X., Liu, X., and Sun, Y. (2017). Efficient H-2 evolution coupled with oxidative refining of alcohols via a hierarchically porous nickel bifunctional electrocatalyst. *ACS Catal.* 7, 4564–4570. doi: 10.1021/acscatal.7b00876

Yu, I. K. M., and Tsang, D. C. W. (2017). Conversion of biomass to hydroxymethylfurfural: A review of catalytic systems and underlying mechanisms. *Bioresour. Technol.* 238, 716–732. doi: 10.1016/j.biortech.2017.04.026

Zakrzewska, M. E., Bogel-Lukasik, E., and Bogel-Lukasik, R. (2010). Solubility of carbohydrates in ionic liquids. *Energy Fuels* 24, 737–745. doi: 10.1021/ef901215m

Zhang, J. H., Li, J. K., Tang, Y. J., Lin, L., Long, M. N., and Yang, F. (2015). Selective conversion of biomass-derived precursor 5-hydroxymethylfurfural to 2,5-furandicarboxylic acid by ferrate (VI) oxidation. *J. Biobased Mater. Bioenergy*. 9, 1547–1552. doi: 10.1166/jbmb.2015.1547

Zhang, Z. H., and Deng, K. J. (2015). Recent advances in the catalytic synthesis of 2,5-furandicarboxylic acid and its derivatives. *ACS Catal.* 5, 6529–6544. doi: 10.1021/acscatal.5b01491

Zhang, Z. H., and Huber, G. W. (2018). Catalytic oxidation of carbohydrates into organic acids and furan chemicals. *Chem. Soc. Rev.* 47, 1351–1390. doi: 10.1039/C7CS00213K

Zhang, Z. H., and Zhao, Z. B. K. (2009). Solid acid and microwave-assisted hydrolysis of cellulose in ionic liquid. *Carbohydr. Res.* 344, 2069–2072. doi: 10.1016/j.carres.2009.07.011

Zhao, Z., Bababrik, R., Xue, W. H., Li, Y. P., Briggs, N. M., Nguyen, D. T., et al. (2019). Solvent-mediated charge separation drives alternative hydrogenation path of furanics in liquid water. *Nat. Catal.* 2, 431–436. doi: 10.1038/s41929-019-0257-z

Zhou, H., Xu, H. H., and Liu, Y. (2019). Aerobic oxidation of 5-hydroxymethylfurfural to 2,5-furandicarboxylic acid over Co/Mn-lignin coordination complexes-derived catalysts. *Appl. Catal. B.* 244, 965–973. doi: 10.1016/j.apcatb.2018.12.046

Zope, B. N., Hibbitts, D. D., Neurock, M., and Davis, R. J. (2010). Reactivity of the gold/water interface during selective oxidation catalysis. *Science* 330, 74–78. doi: 10.1126/science.1195055

Conflict of Interest: The authors declare that the research was conducted in the absence of any commercial or financial relationships that could be construed as a potential conflict of interest.

frontiers in Chemistry

REVIEW
published: 28 February 2020
doi: 10.3389/fchem.2020.00132

Catalytic Oxidations in a Bio-Based Economy

Roger A. Sheldon [1,2]*

[1] School of Chemistry, Molecular Sciences Institute, University of the Witwatersrand, Johannesburg, South Africa,
[2] Department of Biotechnology, Delft University of Technology, Delft, Netherlands

The role of bio- and chemo-catalytic aerobic oxidations in the production of commodity chemicals in a bio-refinery is reviewed. The situation is fundamentally different to that in a petrochemicals refinery where the feedstocks are gaseous or liquid hydrocarbons that are oxidized at elevated temperatures in the vapor or liquid phase under solvent-free conditions. In contrast, the feedstocks in a biorefinery are carbohydrates that are water soluble solids and their conversion will largely involve aerobic oxidations of hydroxyl functional groups in water as the solvent under relatively mild conditions of temperature and pressure. This will require the development and use of cost-effective and environmentally attractive processes using both chemo- and biocatalytic methods for alcohols and polyols.

Keywords: bio-based economy, biomass, biocatalysis, catalytic oxidation, alcohol oxidases, carbohydrates, waste valorization

OPEN ACCESS

Edited by:
Vasile I. Parvulescu, University of Bucharest, Romania

Reviewed by:
Valeria Conte, University of Rome Tor Vergata, Italy
Konstantinos Triantafyllidis, Aristotle University of Thessaloniki, Greece

***Correspondence:**
Roger A. Sheldon
roger.sheldon@wits.ac.za

Specialty section:
This article was submitted to Green and Sustainable Chemistry, a section of the journal Frontiers in Chemistry

Received: *18 December 2019*
Accepted: *13 February 2020*
Published: *28 February 2020*

Citation:
Sheldon RA (2020) Catalytic Oxidations in a Bio-Based Economy. Front. Chem. 8:132. doi: 10.3389/fchem.2020.00132

INTRODUCTION

One of the grand challenges of the twenty-first century is the implementation of the transition from an unsustainable economy based on fossil resources–oil, coal, and natural gas—to a sustainable, carbon-neutral economy based on the use of renewable biomass. This switch to a so-called bio-based economy is urgently required in order to mitigate global warming caused by increasing carbon dioxide emissions to the atmosphere. First generation (1G) renewable raw materials, exemplified by corn starch, sugar cane, and sugar beet, are not perceived as sustainable options in the long term as their utilization involves, directly, or indirectly, competition with food production. In contrast, the use of second generation (2G) renewable biomass, in the form of waste polysaccharides, such as lignocellulose (Liguori and Faraco, 2016; Zhang et al., 2017) and pectin, from agricultural and forestry residues and food supply chain waste (Dahiya et al., 2018), is perceived as a sustainable long term option for producing biofuels and commodity chemicals (Sheldon, 2014, 2016, 2018; Horváth et al., 2017). Looking further afield, third generation (3G) aquatic biomass, such as micro- and macro-algae and cyanobacteria, has additional advantages (John et al., 2011; Al Abdallah et al., 2016; Shuba and Kifle, 2018). For example, there is no requirement for arable land and fresh water for their production and they have much higher growth rates than terrestrial plants. On the other hand, there are substantial technical problems associated with their production and conversion which, in the short term, represent a significant hurdle to be overcome for commercial viability.

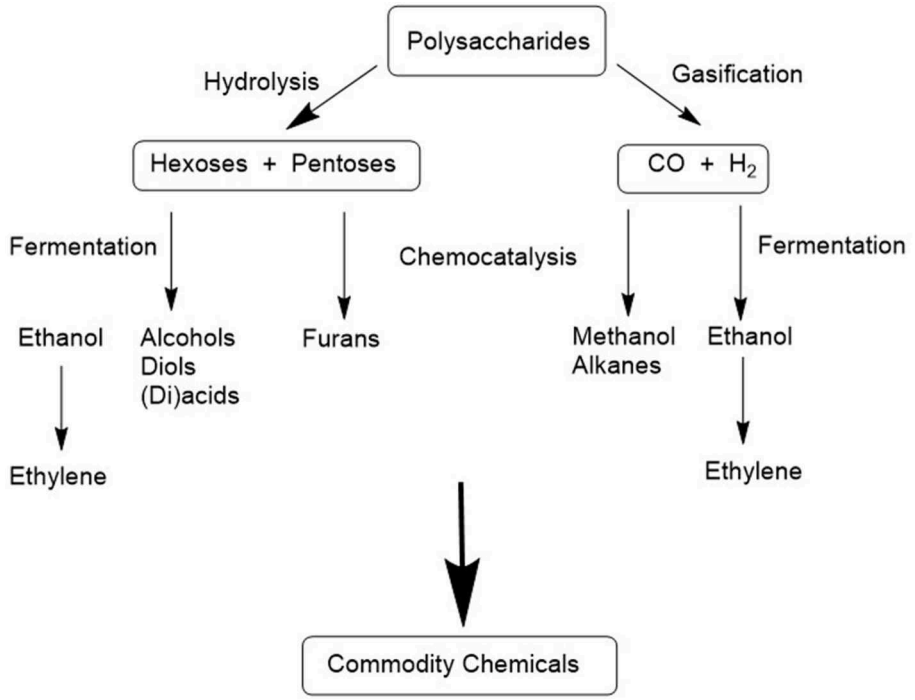

FIGURE 1 | Conversion of polysaccharides to biofuels and commodity chemicals in a biorefinery.

CARBOHYDRATES TO COMMODITY CHEMICALS IN A BIOREFINERY

In a petrochemical refinery the basic chemicals are lower olefins (ethylene, propylene, and butenes) and aromatics (BTX: benzene, toluene, and xylenes), together with carbon monoxide and hydrogen (syn gas). The hydrocarbons are gases or hydrophobic liquids. They are converted with petrochemical catalytic technologies, particularly catalytic oxidation with dioxygen, to a variety of commodity chemicals, usually in solvent-free systems. In contrast, the basic chemicals in a biorefinery will be C_6 and C_5 sugars produced by hydrolysis of polysaccharide feedstocks, and/or syn gas produced by their gasification. The carbohydrates are hydrophilic, water soluble solids. Several scenarios can be envisaged for further conversion to commodity chemicals (**Figure 1**):

(i) Syn gas could be converted to commodity chemicals by applying existing catalytic technologies used in petrochemical refineries or by fermentation (Phillips et al., 2017; Asimakopoulos et al., 2018).
(ii) Monosaccharides such as glucose could be converted to a variety of lower alcohols, diols, carboxylic acids, and dicarboxylic acids by fermentation. Indeed, fermentation is already the commercially most viable route to many of these products with lactic acid, 1,3-propane diol and 1,4-butane diol as prominent examples.
(iii) Bioethanol, produced as a carbon neutral fuel, could be converted to ethylene and a variety of other products using established technologies (see **Figure 1**), including catalytic aerobic oxidations.
(iv) Chemo- or bio-catalytic conversion of monosaccharides, such as glucose, to commodity chemicals will require in many cases removal of oxygen, by hydrogenolysis and/or dehydration. Catalytic oxidations in a biorefinery involve oxidation of alcoholic OH groups in monosaccharides, or even the polysaccharide precursors, or their downstream products and further oxidation of the resulting carbonyl compounds.

CATALYTIC OXIDATIONS

A key reaction in organic synthesis is the oxidation of primary and secondary alcohols to give the corresponding aldehydes or carboxylic acids and ketones, respectively. Traditionally these transformations were performed with stoichiometric quantities of inorganic oxidants, notably chromium (VI) compounds such as the Jones reagent (CrO_3 and sulfuric acid). However, such procedures are not atom efficient and lead to the formation of copious amounts of toxic, chromium-containing waste, i.e., high E factors and problematic waste disposal issues. Consequently, in the last two decades such methods have been increasingly replaced by atom efficient catalytic alternatives involving dioxygen or hydrogen peroxide as the terminal oxidant.

Interestingly, the history of catalytic oxidations of carbohydrates (Arts et al., 1997) predates the oxidations of lower olefins and aromatics that form the basis of the

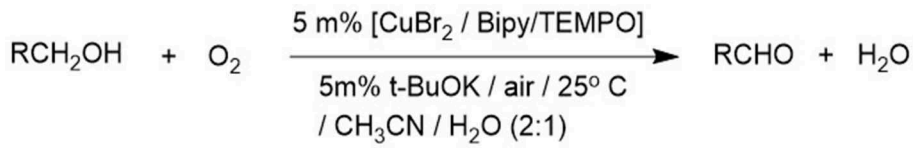

Alcohol	Time (h)	Conversion (%)
Benzyl alcohol	2.5	100
1-Phenylethanol	5	no reaction
Geraniol	5	100
Octan-1-ol	24	95
Octan-2-ol	5	no reaction
Benzyl alcohol + 1-phenylethanol	1.5	63 / 0

FIGURE 2 | Aerobic oxidation of primary alcohols catalyzed by Cu/TEMPO.

petrochemical industry. The aerobic oxidation of mannose over a platinum black catalyst, for example, dates from 1861 (von Gorup-Besanez, 1861) and many supported noble metal catalyzed aerobic oxidations of carbohydrates were developed in the first half of the last century. At the turn of the century, we developed an aqueous biphasic system for the aerobic oxidation of primary and secondary alcohols to the corresponding aldehydes and ketones, respectively, in a solvent free system using a water-soluble palladium complex of bathophenanthroline (ten Brink et al., 2000). This system could also be effective in the aerobic oxidation of water soluble alcohols, including carbohydrates. Indeed, there are many examples of the aerobic oxidation of alcohols catalyzed by precious metals such as palladium, platinum and gold (Stahl, 2004; Parmaggiani and Cardona, 2012). However, in the context of the conversion of carbohydrates to large volume, low-priced commodity chemicals, precious metals such as palladium have the disadvantage that the future availability of these scarce, "endangered elements" at cost-effective prices is rather unpredictable. Indeed, in contrast to most materials, their price tends to increase with increasing usage. Another disadvantage of noble metal catalyzed oxidations is their functional group intolerance. First row, more earth abundant metals tend to be more functional group tolerant.

Consequently, alternative methods have been developed that use "earth abundant" metals, such as copper and iron, as catalysts. One method with broad applications in the selective oxidation of primary alcohols to aldehydes, even in the presence of secondary alcohols, involves the combination of a Cu(II)-bipyridine (Cu-bpy) complex with a base, such as potassium hydroxide, a stable nitroxyl radical, exemplified by 2,2,6,6-tetramethyl-1-piperidine-N-oxyl (TEMPO) and its derivatives, at ambient temperature with air in aqueous acetonitrile (**Figure 2**; Gamez et al., 2003; Sheldon and Arends, 2004; Marais and Swarts, 2019). The generally accepted mechanism involves as the key, rate determining step, abstraction of a hydrogen atom from an alkoxide ligand by a coordinated nitroxyl radical analogous to that involved in the aerobic oxidation of primary alcohols catalyzed by the copper-dependent oxidase, galactose oxidase (Dijksman et al., 2003). An improved procedure, using Cu(I) salts with TEMPO and bipy in combination with N-methylimidazole as a base in acetonitrile as solvent was subsequently described by Stahl and coworkers (Hoover and Stahl, 2011). Furthermore, extensive mechanistic studies confirmed the copper-centered galactose oxidase-like mechanism for these systems (Geiβlmeir et al., 2005; Hoover et al., 2013).

The lack of reactivity of secondary alcohols was attributed to steric hindrance in the abstraction of an α-hydrogen atom from a coordinated alkoxide by a coordinated TEMPO ligand. Consequently, the use of sterically less hindered nitroxyl radicals such as AZADO and ABNO, respectively, in combination with Cu(I) complexes, were developed by the groups of Iwabuchi (Shibuya et al., 2006, 2011; Iwabuchi, 2013) and Stahl (Steves and Stahl, 2013), for the aerobic oxidation of secondary alcohols (**Figure 3**), including sterically demanding alcohols such as menthol and a variety of unprotected amino alcohols (Sasano et al., 2014).

More recently, Ma and coworkers reported the use of an Fe(III)/4-hydroxyTEMPO/NaCl combination as a catalyst for the aerobic oxidation of both primary and secondary alcohols (Jiang et al., 2016, 2019). Other metals, including manganese, cobalt and vanadium, have also been used in combination with nitroxyl radicals (Cao et al., 2014) Transition metal free nitroxyl systems have also been described, usually involving nitrogen dioxide as the active co-catalyst. The commercially most attractive source of the NO_2 cocatalyst is nitric acid (Kuang et al., 2010). For example, nitric acid or $NaNO_2$ or a mixture of both was used, in combination with ABNO or keto-ABNO, for the selective aerobic oxidation of secondary alcohols (**Figure 4**; Lauber and Stahl, 2013). Interestingly, the combination of nitric acid and $NaNO_2$ catalyzes the aerobic oxidation of alcohols even in the absence of a stable nitroxyl radical. The reaction involves an alkyl nitrite intermediate which decomposes to the carbonyl

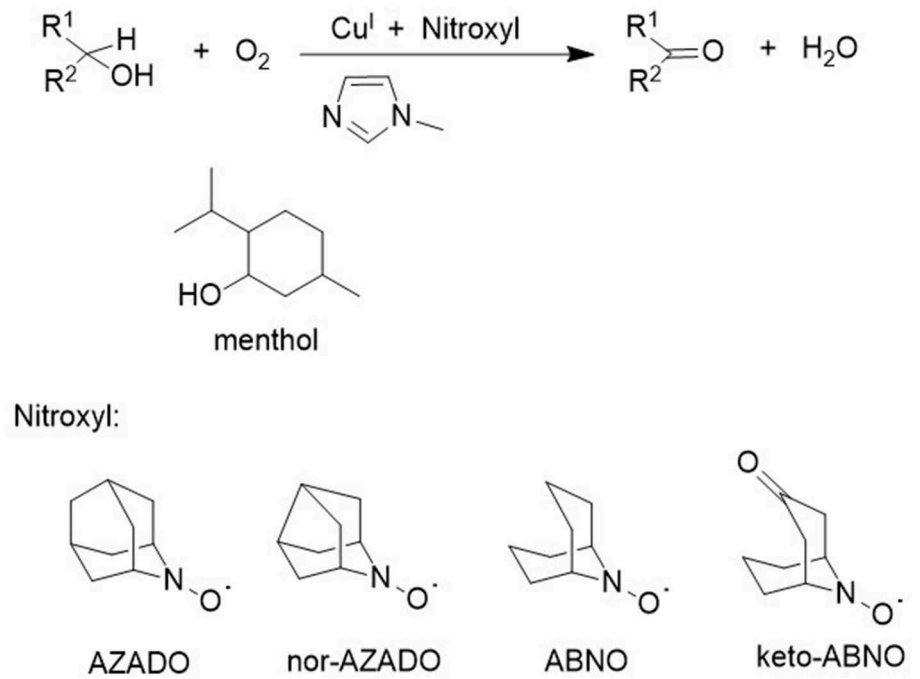

FIGURE 3 | Catalytic aerobic oxidation of secondary alcohols with Cu (I)/nitroxyl catalysts.

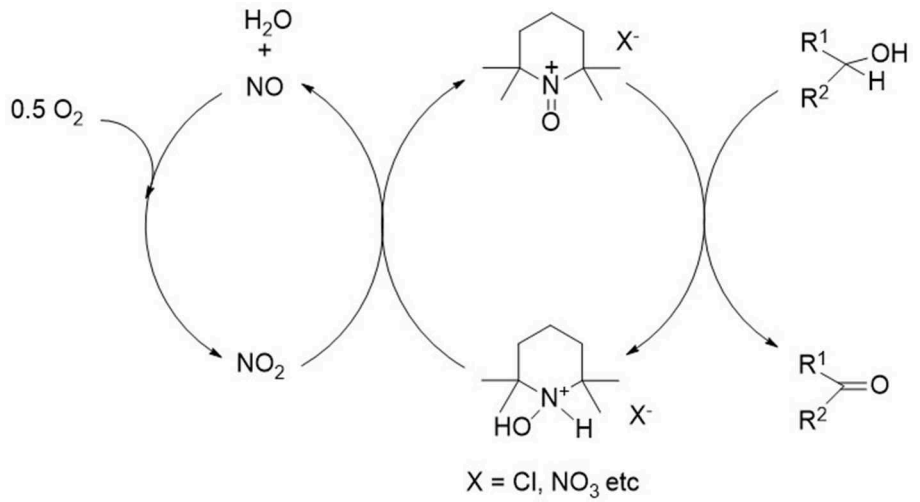

FIGURE 4 | Nitric acid catalyzed aerobic oxidation of alcohols.

compound and HNO which is reoxidized by dioxygen (Aellig et al., 2011). Unfortunately, the greenhouse gas, nitrous oxide (N_2O), can be irreversibly formed as a byproduct.

CATALYTIC OXIDATIONS IN A BIO-BASED ECONOMY

Although these various nitroxyl radical-based catalysts have been widely used in the aerobic oxidations of alcohols they have generally involved relatively simple primary and secondary alcohols in organic solvents, sometimes mixed with water. This was done with the development of green syntheses of, for example, active pharmaceutical ingredients (APIs) and flavors and fragrances, in mind. However, in a bio-based economy it is of interest to use these methodologies in the selective oxidation of renewable carbohydrates or key alcohols, diols, and polyols derived from them, and this involves in many cases aqueous solutions of solid substrates.

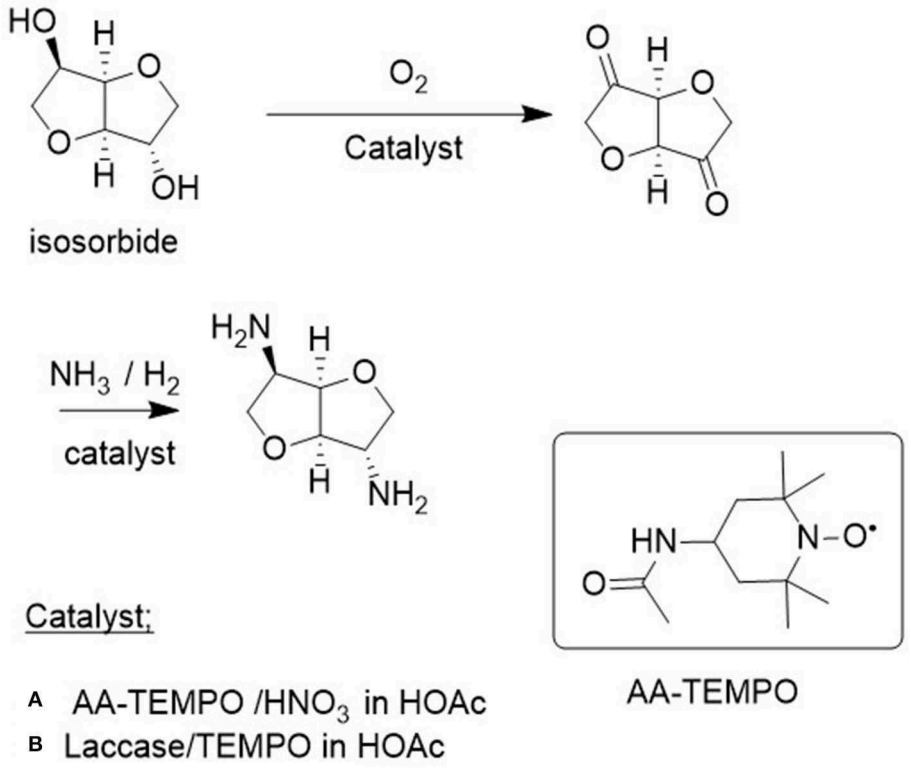

FIGURE 5 | Aerobic oxidation of isosorbide to the corresponding diketone. **(A)** AA-TEMPO/HNO_3 in HOAc. **(B)** Laccase/Tempo in HOAc.

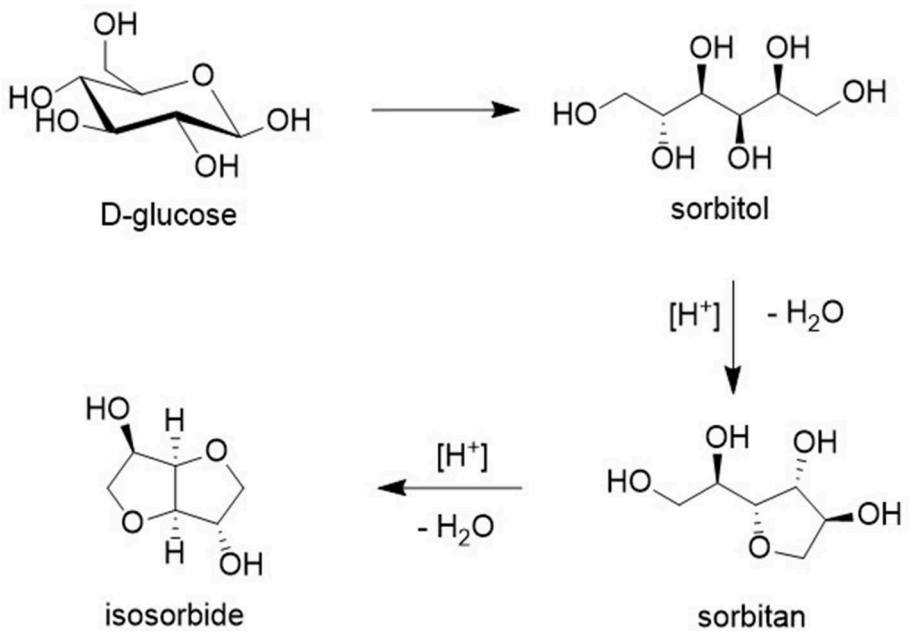

FIGURE 6 | Isosorbide as a platform chemical.

Water has both advantages and limitations as a solvent for aerobic oxidations. For example, oxidations with oxygen are much safer as there is no formation of explosive mixtures of oxygen with volatile organic solvents in the gas phase. In a typical process oxygen is supplied by bubbling air through the solution. However, the transfer of oxygen from the gas to the liquid phase is notoriously slow owing to its low solubility in water under typical operating conditions (0.268 mM at 25°C and 1 bar air) which limits the maximum space time yield to 200 mmol/L/h (Pedersen et al., 2015). This problem was alleviated in the Cu/TEMPO system by using air-microbubble techniques to facilitate gas absorption into the liquid phase (Mase et al., 2011). Alternatively, the rates of enzymatic aerobic oxidations were increased by a factor of 100 in continuous flow operation compared to the conventional batch operation (Chapman et al., 2018; Hone and Kappe, 2019). Another disadvantage of water as a solvent is that its relatively high heat capacity, compared to volatile organic solvents, translates to high energy costs for its removal by distillation.

A pertinent example, from the viewpoint of the bio-based economy, is the use of acetylamino-TEMPO (AA-TEMPO) together with nitric acid as the cocatalyst for the aerobic oxidation of primary and secondary alcohols to the corresponding aldehydes and ketones, respectively, in acetic acid or water as the solvent (Dingerdissen et al., 2011). The method was particularly useful for the oxidation of the key biomass-derived diol, isosorbide, to the corresponding diketone (**Figure 5**; Klasovsky et al., 2015). This is particularly surprising because of the low reactivity of the shielded *endo* OH group in isosorbide.

Isosorbide is a commercially interesting platform chemical produced by hydrogenation of glucose to sorbitol followed by dehydration (**Figure 6**). It has interesting features as an industrial monomer based on its rigidity, chirality, and non-toxicity (Fenouillot et al., 2010). For example, reaction with dicarboxylic acids (or esters) affords polyesters. Alternatively, oxidation to the corresponding diketones, followed by reductive amination, affords the corresponding bis-primary amine (**Figure 5**) which can be converted to polyamides by reaction with dicarboxylic acids (esters).

BIOCATALYSIS *IN AQUA*: THE NATURAL SOLUTION

As was noted elsewhere, biocatalysis is green and sustainable (Hollmann et al., 2011; Sheldon and Woodley, 2018), conforming to 10 of the 12 principles of green chemistry, and the catalyst is non-toxic, biocompatible and biodegradable. Moreover, enzymatic reactions are generally performed in water, a particularly suitable medium for conversions of polysaccharides in a bio-based economy. Furthermore, carbohydrates tend to be ideal substrates and generally have a stabilizing effect on enzymes. In contrast with precious metal catalysts, the long term availability and price stability of enzymes is assured since they are produced from inexpensive, readily available biomass. Moreover, industrial scale oxidations employing precious metal catalysts often involve a costly purification step to remove traces of the metal in the product. In contrast, no costly removal of trace amounts of enzymes are needed in enzymatic oxidations and any enzyme ending up in aqueous effluent undergoes facile biodegradation.

Laccase/Nitroxyl Radical Combinations

Laccases (EC 1.10. 3.2) are a diverse group of extracellular, copper-dependent oxidases. They are produced, for example,

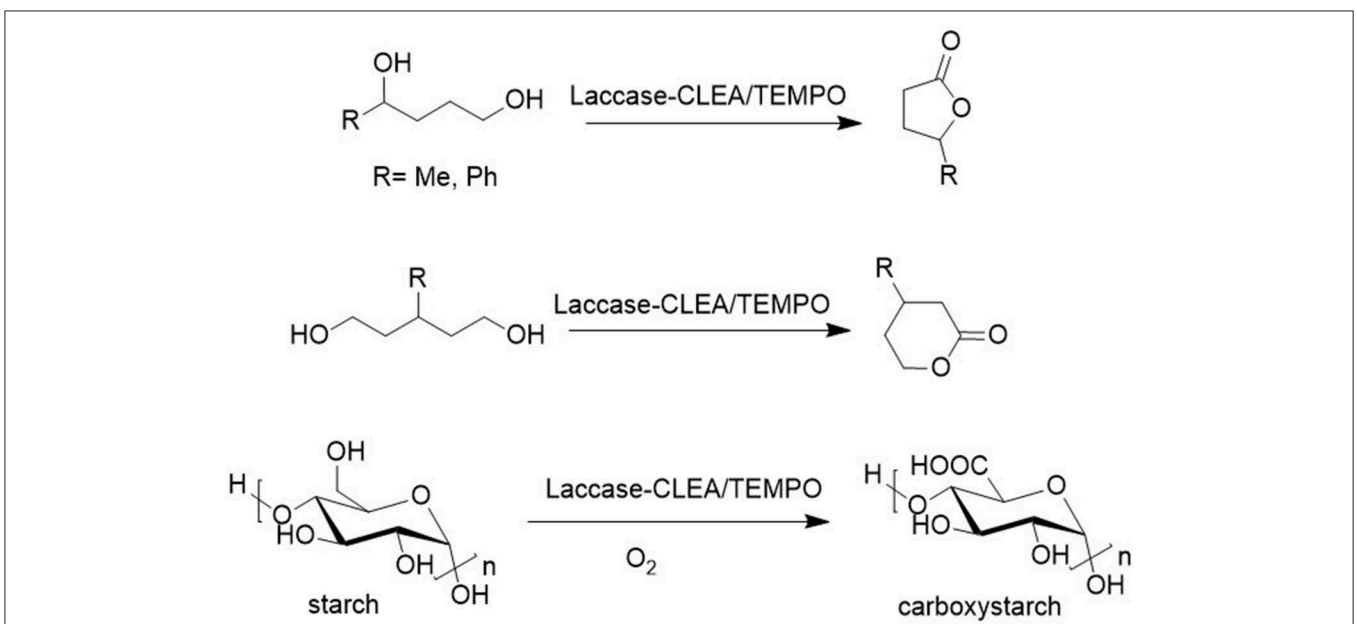

FIGURE 7 | Laccase/TEMPO catalyzed oxidation of diols and polyols.

by white rot fungi, and play a key role in the delignification of lignocellulose *in vivo* (Rochefort et al., 2004). There is considerable commercial interest in the use of laccases in the pulp and paper industry and in waste water remediation in general (Gasser et al., 2014; Singh et al., 2018; Unuofin et al., 2019). They have broad substrate specificity and use dioxygen to oxidize a wide variety of, *inter alia*, phenols and aromatic amines *in vivo*. In combination with so-called mediators, notably TEMPO, they are able oxidize alcohols as was first shown by Fabbrini et al. (2001). These reactions involve one-electron oxidation of the TEMPO by the laccase to give the oxoammonium cation which is the active oxidant (Arends et al., 2006a). The reduced form of laccase is then reoxidized by dioxygen.

The laccase/TEMPO system was shown to catalyze the aerobic oxidation of primary and secondary aliphatic alcohols and 10 mol% was sufficient to give good conversions and excellent selectivities (Arends et al., 2006b). Interestingly, Ying and coworkers (Zhu et al., 2014) obtained superior results with 5 mol% laccase/AZADO, especially in the aerobic oxidation of complex and highly functionalized alcohols. Suicide inactivation is a problem with laccases since at high substrate conversions the oxoammonium cation can oxidize reactive groups in the protein or in the associated glycosyl moieties on the periphery of the enzyme (laccases are glycosylated enzymes). The stability of laccases under the reaction conditions can be significantly increased by immobilization as cross-linked enzyme aggregates (CLEAs) (Matijosyte et al., 2010).

The laccase/TEMPO system also catalyzed the aerobic oxidation of the renewable diol, isosorbide to the corresponding diketone (see section Catalytic Oxidations and **Figure 5B**) in >99% yield (Gross et al., 2014). Similarly, 1,4 and 1,5-diols were oxidized to the corresponding lactones (**Figure 7**, Diaz-Rodriguez et al., 2012) and immobilization of the laccase as cross-linked enzyme aggregates (CLEAs) enabled multiple recycling (Sheldon et al., 2013).

Copper and Flavin Dependent Alcohol Oxidases

As shown in **Figure 8**, there are two types of alcohol oxidases: Cu-dependent and flavin adenine dinucleotide (FAD). Both generate an equivalent of hydrogen peroxide as the coproduct and catalase is added to decompose it back to oxygen and water. Alternatively, catalase can be used to generate oxygen *in situ*. A major shortcoming of wild-type oxidases is their substrate specificity. For example, galactose oxidase (GOase) and glucose

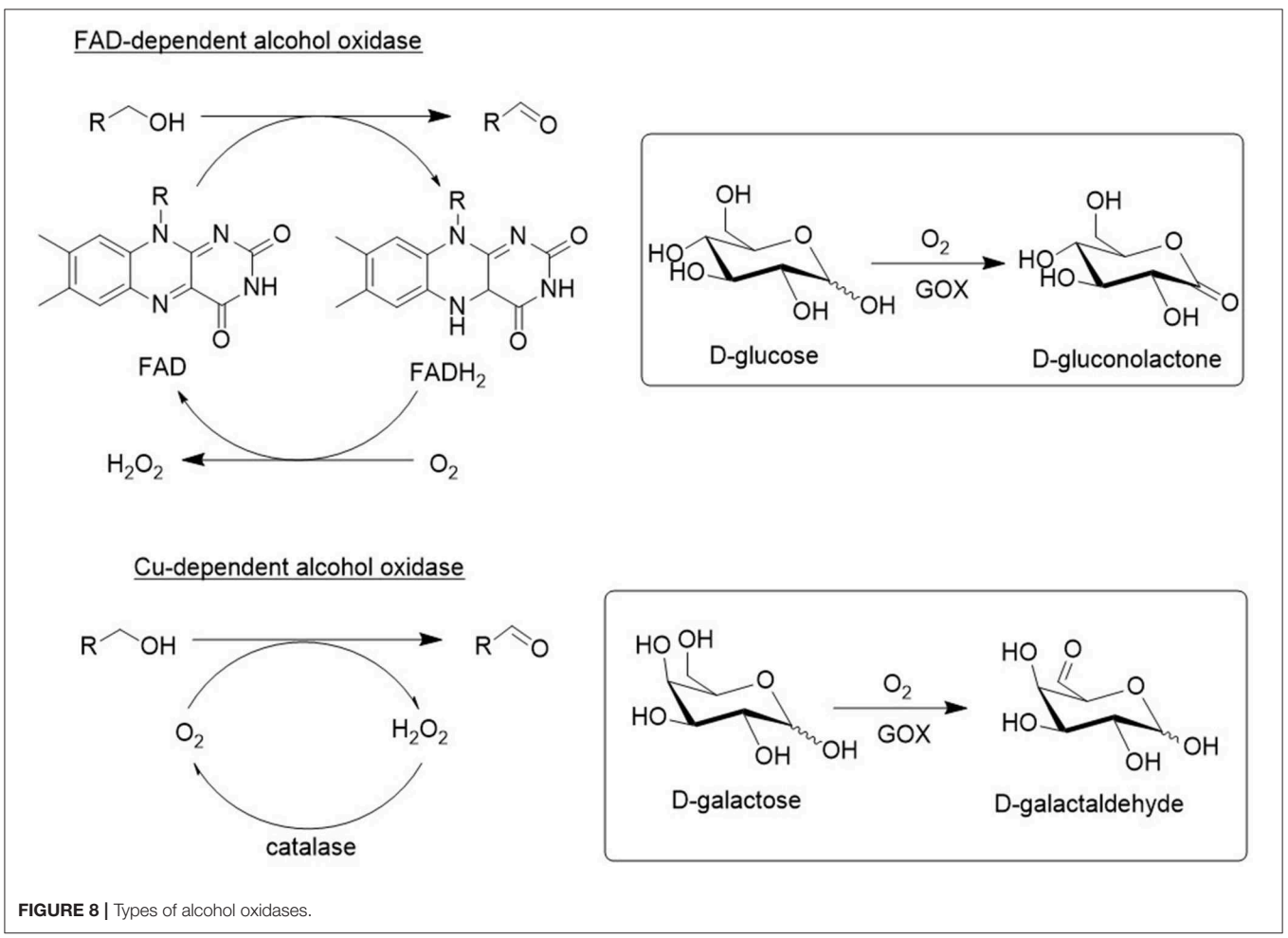

FIGURE 8 | Types of alcohol oxidases.

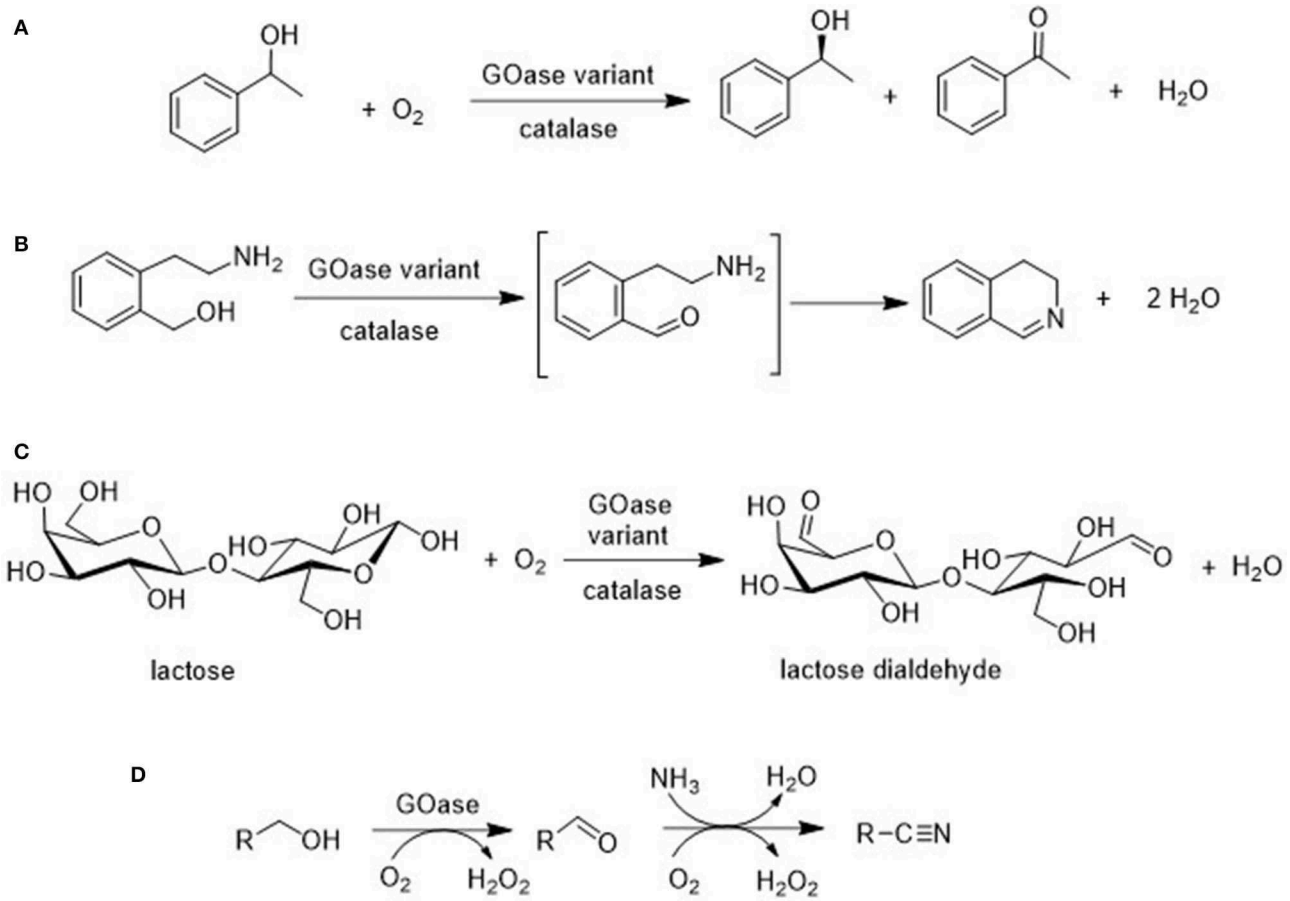

FIGURE 9 | Biocatalytic aerobic oxidation of **(A)** 1-phenylethanol, **(B)** an amino alcohol, **(C)** lactose, and **(D)** ammoxidation of a primary alcohol.

oxidase (GOX) and are very specific for galactose and glucose, respectively. Indeed, these enzymes have evolved *in vivo* to be very efficient in converting their natural substrate. However, in order to be useful in organic synthesis they need to be active and selective with a variety of alcohol substrates, particularly highly functionalized alcohols. Fortunately, this can be achieved with protein engineering using *in vitro* evolution.

For example, Turner and coworkers used directed evolution techniques to produce GOase variants that catalyze the oxidation of secondary alcohols (**Figure 9A**; Escaletters and Turner, 2008) and amino alcohols (Herter et al., 2015; **Figure 9B**). Similarly, a GOase variant catalyzed the aerobic oxidation of lactose, a disaccharide formed as a waste stream (whey) in cheese manufacture, to form the dialdehyde (**Figure 9C**; Cosgrove et al., 2019). The latter is of interest as a raw material for polymers. Interestingly, a GOase variant was also shown to catalyze the synthesis of nitriles by ammoxidation of primary alcohols (**Figure 9D**; Vilim et al., 2018).

Structure directed evolution was also used to develop variants of the FAD-dependent choline oxidase that catalyze the aerobic oxidation of a broad range of primary alcohols to the corresponding aldehydes (**Figure 10**; Heath et al., 2019). Similarly, FAD-dependent HMF oxidase was engineered to effectively catalyze all three oxidation steps in the conversion of HMF to FDCA (see later).

Another reaction of industrial interest is the aerobic oxidation of glucose to glucaric acid. A hypothetical process involving two steps with a mixture of GOX and a GOase variant which is able to accept gluconolactone as a substrate is shown in **Figure 11**. Alternatively, it can be produced by aerobic oxidation of glucuronic acid, a building block derived from (waste) pectin (see section Acid-Catalyzed Dehydration of Carbohydrates to Furan Derivatives). Glucaric acid is of interest as an industrial monomer in itself (Wu et al., 2019) and can also be hydrogenated to adipic acid, the raw material for Nylon 6.

Alcohol Dehydrogenases

Alcohol dehydrogenases (ADHs) catalyze the oxidation of alcohols by utilizing a nicotinamide cofactor which has to be regenerated *in situ* using an excess of a co-substrate (Kroutil et al., 2004a; Weckbecker et al., 2010). Alternatively, NAD(P)H oxidase (NOx) can be employed to catalyze reoxidation of the cofactor by oxygen (Kroutil et al., 2004b; Zhang et al., 2016). Yet another possibility is to couple the oxidation step with a reduction step,

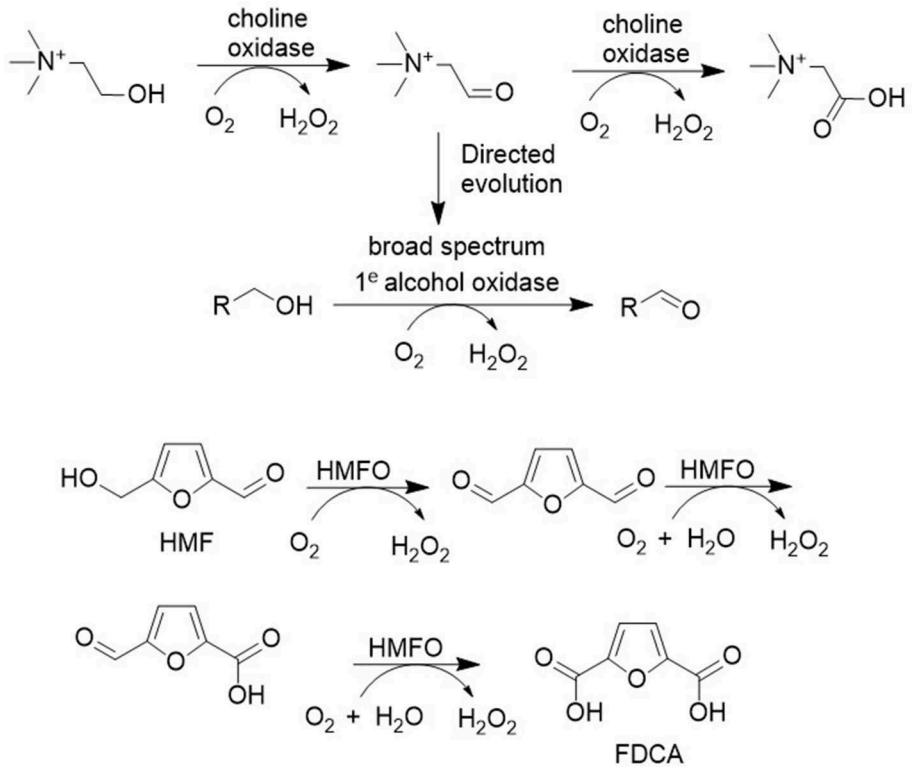

FIGURE 10 | Aerobic oxidations catalyzed by FAD-dependent alcohol oxidase variants.

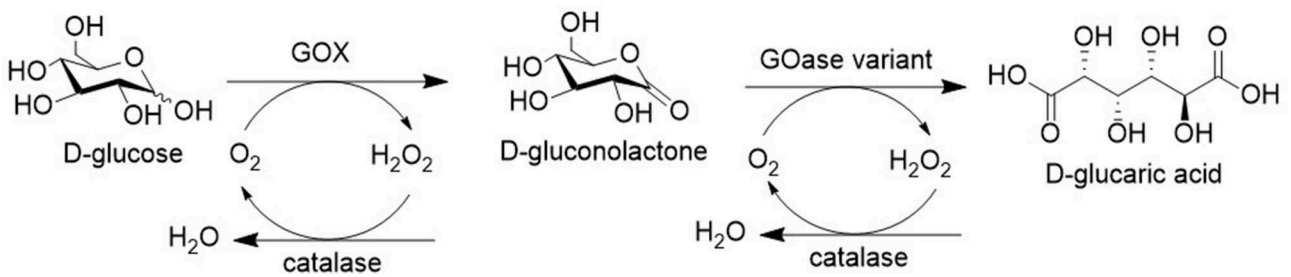

FIGURE 11 | Hypothetical biocatalytic oxidation of glucose to glucaric acid.

to afford an overall redox neutral process by employing so-called hydrogen borrowing, a concept which itself was borrowed from chemocatalysis literature (Hamid et al., 2007). For example, combination of an ADH with an amine dehydrogenase (AmDH) affords a redox-neutral conversion of a racemic alcohol to a single enantiomer of the corresponding amine (**Figure 12**; Mutti et al., 2015). Ironically, it requires the use of an aselective ADH (Thompson and Turner, 2017) because it has to catalyze the oxidation of both alcohol enantiomers, which is not a simple task as most ADHs are highly enantioselective. The overall efficiency of the process, which constitutes a conversion of an OH to an NH_2 group, was improved by co-immobilization of the ADH and AmDH (Böhmer et al., 2018). When the alcohol, or polyol, is readily available this would be an industrially attractive way to produce the corresponding (poly)amine. A pertinent example is the conversion of isosorbide to the diamine discussed in section Catalytic Oxidations.

Direct Oxidation of Polysaccharides

It is also of commercial interest to oxidize polysaccharides, e.g., starch and cellulose, directly to the corresponding polycarboxylic acids. Carboxystarch, for example, has potential applications as a biodegradable water super absorbent. Polysaccharides can be readily oxidized using NaOCl as the stoichiometric oxidant and TEMPO or derivatives as the catalyst (Ponedel'kina et al., 2010). However, for a commercially and environmentally attractive process it should preferably use oxygen as the stoichiometric oxidant. The laccase/TEMPO system (see above) catalyzes the

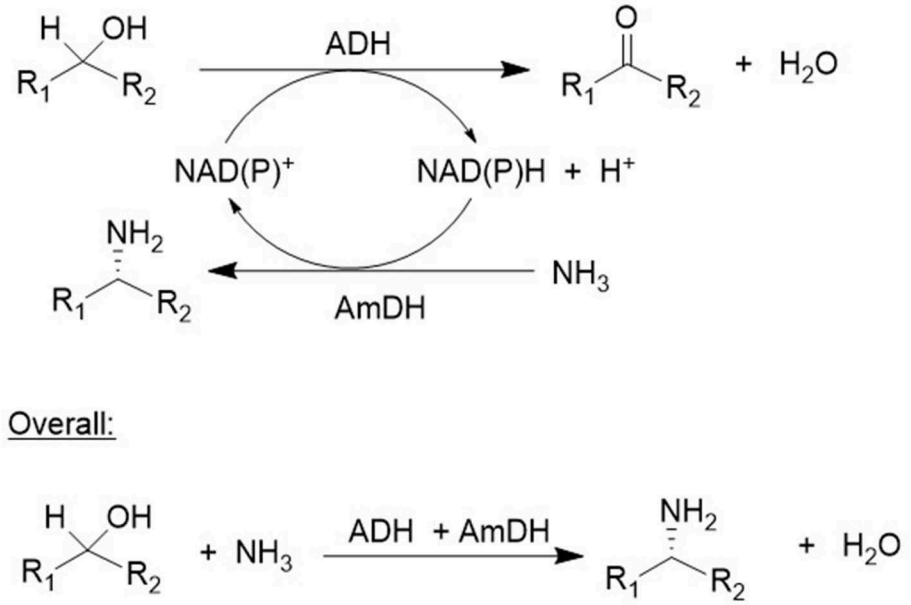

FIGURE 12 | Enzymatic conversion of an alcohol to an amine.

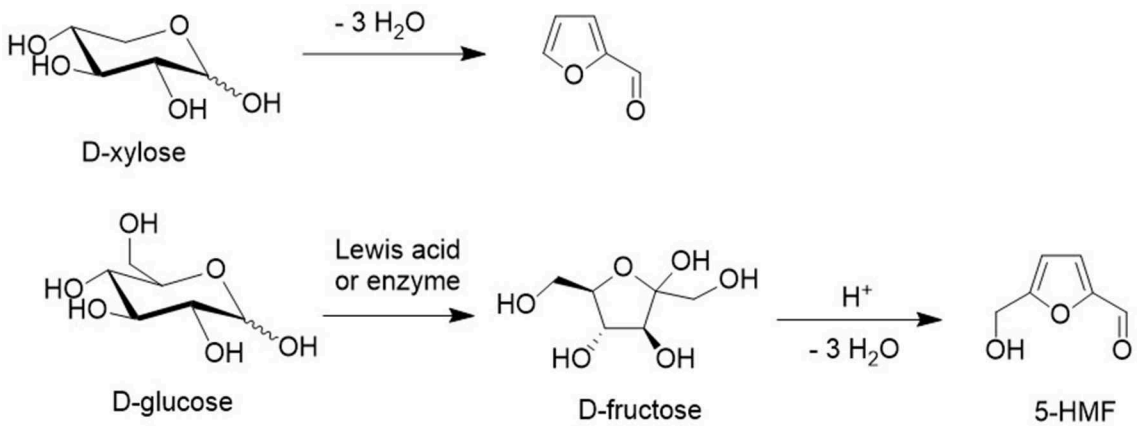

FIGURE 13 | Acid catalyzed dehydration of xylose and glucose.

aerobic oxidation of the primary alcohol moieties in starch affording carboxystarch (Viikari et al., 1999) but the relatively high enzyme costs, owing to its instability under the oxidizing reaction conditions, form an obstacle to commercialization. The stability was improved by immobilization as a cross-linked enzyme aggregate (CLEA) (Matijosyte et al., 2010).

ACID-CATALYZED DEHYDRATION OF CARBOHYDRATES TO FURAN DERIVATIVES

Acid catalyzed dehydration of pentoses and hexoses produces furfural and 5-hydroxymethylfurfural (HMF) (Tong et al., 2010), respectively. Furfural is an important commodity chemical (Lange et al., 2012) and HMF has the potential to become one (van Putten et al., 2013; Kucherov et al., 2018). Initial isomerization of D-glucose to D-fructose is followed by acid catalyzed dehydration (**Figure 13**) but in yields that are not conducive to commercial viability owing to the limited stability of HMF in the acidic reaction medium (Wang et al., 2017). However, according to a recent report HMF can be obtained in 95% yield by conducting the reaction with D-fructose under continuous flow conditions (Galaverna et al., 2018).

Polyethylene furandicarboxylate (PEF), which was developed by Avantium[1] is produced from furan-2,5-dicarboxylic acid

[1]https://www.avantium.com/blog/pef-the-polymer-for-the-future/

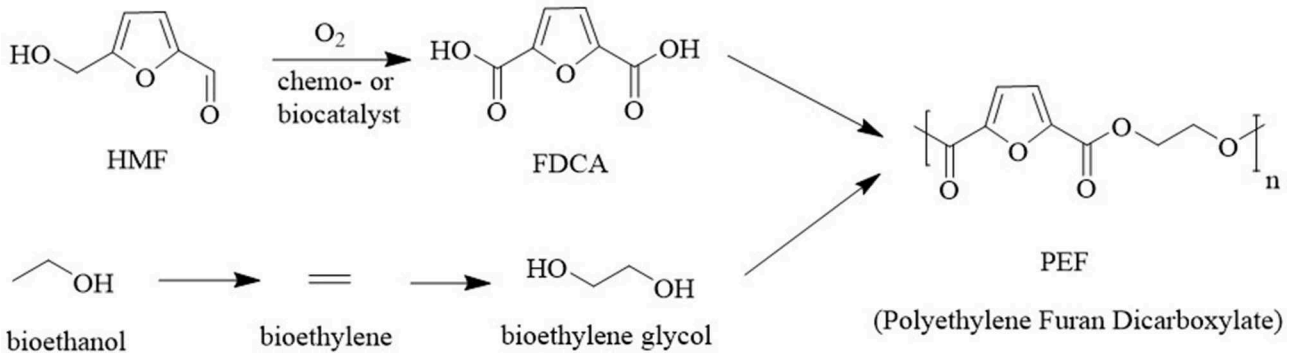

FIGURE 14 | Catalytic aerobic oxidation of HMF to FDCA.

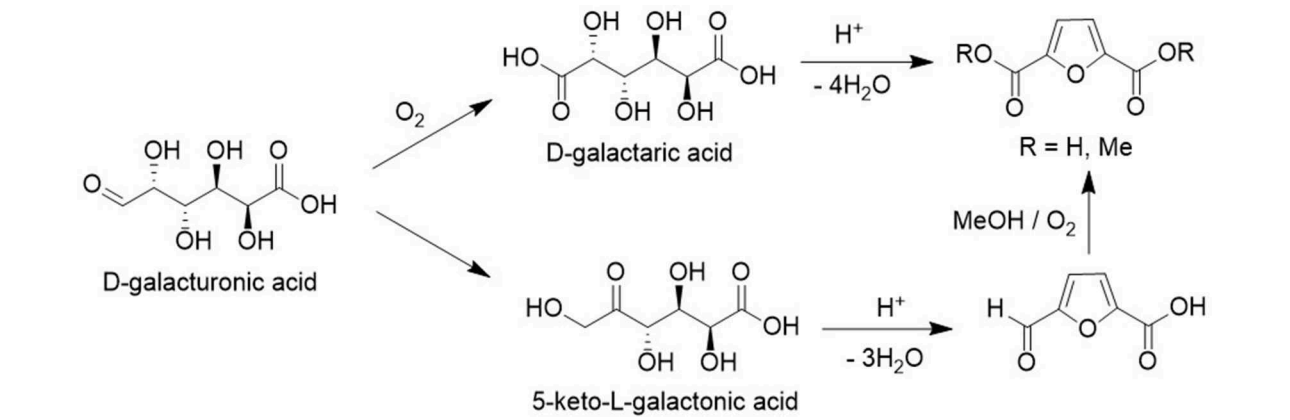

FIGURE 15 | Alternative routes to FDCA.

(FDCA) and ethylene glycol It is seen as a renewable alternative for fossil-based polyethylene terephthalate (PET). In addition to reducing CO_2 emissions, PEF has superior mechanical, thermal, and gas barrier properties to PET. The key raw material, FDCA, can be produced in excellent yields by aerobic oxidation of HMF using supported precious metal catalysts (Liu et al., 2015; Zhang and Deng, 2015; Zheng et al., 2017; Motagamwala et al., 2018) or an engineered flavin-dependent alcohol oxidase (Dijkman et al., 2015) or whole cell biocatalysts (Koopman et al., 2010) in aqueous media (**Figure 14**).

FDCA can also be produced from uronic acids present in various agricultural residues. D-galacturonic acid, for example, is available in large quantities from the pectin in sugar beet pulp (Leijdeckers et al., 2013) and D-glucuronic acid is one of the main constituents of pectin in certain soft- and hardwoods. Aerobic oxidation of uronic acids over gold catalysts (van Es et al., 2013) affords the corresponding aldaric acids that can subsequently be dehydrated to FDCA (**Figure 15**; Miller et al., 2017). Alternatively, uronic acids can be isomerized to the corresponding 5-keto aldonic acids which can be converted to FDCA dimethyl ester by acid catalyzed cyclodehydration to the methyl ester of 5-formyl-2-furoic acid in methanol followed by Au/C catalyzed aerobic oxidation (van der Klis et al., 2017).

Finally, we note that this review is focused on the conversion of the carbohydrate fractions of feedstocks to commodity chemicals in a biorefinery. In practice, for commercial viability both the carbohydrate and the lignin fractions will be converted to both commodity chemicals and biofuels and this will involve both chemo- and biocatalytic methods in water (Rinaldi et al., 2016; Bugg et al., 2019).

CONCLUSIONS AND PROSPECTS

Remarkable progress has been made in the last two decades in the development of green and sustainable catalytic methodologies for the aerobic oxidations of primary and secondary alcohols to aldehydes and ketones, respectively. However, a cursory perusal of the literature reveals that we have hardly scratched the surface with regard to the application of such catalytic methodologies to the valorization of bio-based feedstocks and key platform chemicals in biorefineries. Recent developments in the engineering of oxidative enzymes, such as copper- and flavin-dependent alcohol oxidases, using directed evolution techniques, strongly suggest that industrially viable methods for catalytic oxidations relevant to a bio-based economy will be forthcoming in the near future.

One could say that glucose is the new ethylene, and possibly propylene and butenes all rolled into one. In the words of Primo Levi: "It is the destiny of wine to be drunk and it is the destiny of glucose to be oxidized."

AUTHOR CONTRIBUTIONS

The author confirms being the sole contributor of this work and has approved it for publication.

REFERENCES

Aellig, C., Girard, C., and Hermans, I. (2011). Aerobic alcohol oxidations mediated by nitric acid. *Angew. Chem. Int. Ed.* 50, 12355–12360. doi: 10.1002/anie.201105620

Al Abdallah, Q. A., Nixon, B. T., and Fortwender, J. R. (2016). The enzymatic conversion of major algal and cyanobacterial carbohydrates to bioethanol. *Front. Energy Res.* 4:36. doi: 10.3389/fenrg.2016.00036

Arends, I. W. C. E., Li, Y. X., Ausan, R., and Sheldon, R. A. (2006a). Comparison of TEMPO and its derivatives as mediators in laccase catalysed oxidation of alcohols. *Tetrahedron* 62, 6659–6665. doi: 10.1016/j.tet.2005.12.076

Arends, I. W. C. E., Li, Y. X., and Sheldon, R. A. (2006b). Stabilities and rates in the laccase/TEMPO-catalyzed oxidation of alcohols. *Biocat. Biotransform.* 24, 443–448. doi: 10.1080/10242420601040683

Arts, S. J. H. F., Mombarg, E. J. M., van Bekkum, H., and Sheldon, R. A. (1997). Hydrogen peroxide and oxygen in catalytic oxidation of carbohydrates and related compounds. *Synthesis* 597–613. doi: 10.1055/s-1997-1406

Asimakopoulos, K., Gavala, H. N., and Skiadis, I. V. (2018). Reactor systems for syngas fermentation processes: A review. *Chem. Eng. J.* 348, 732–744. doi: 10.1016/j.cej.2018.05.003

Böhmer, W., Kraus, T., and Mutti, F. (2018). Hydrogen-borrowing alcohol bioamination with coimmobilized *dehydrogenases. ChemCatChem.* 10, 731–735. doi: 10.1002/cctc.201701366

Bugg, T. D. H., Williamson, J. J., and Rashid, G. M. M. (2019). Bacterial enzymes for lignin depolymerisation: new catalysts for generation of renewable chemicals from biomass. *Curr. Opin. Chem. Biol.* 55, 26–33. doi: 10.1016/j.cbpa.2019.11.007

Cao, Q., Dornan, L. M., Rogan, L., Hughes, N. L., and Muldoon, M. J. (2014). Aerobic oxidation catalysis with stable radicals. *Chem. Commun.* 50, 4524–4543. doi: 10.1039/C3CC47081D

Chapman, M. R., Cosgrove, S. C., Turner, N. J., Kapur, N., and Blacker, N. J. (2018). Highly productive oxidative biocatalysis in continuous flow by enhancing the aqueous equilibrium solubility of oxygen. *Angew. Chem. Int. Ed.* 57,10535–10539. doi: 10.1002/anie.201803675

Cosgrove, S. C., Mattey, A. P., Riese, S., Chapman, M. R., Birmingham, W. R., Blacker, J. A., et al. (2019). Biocatalytic oxidation in continuous flow for the generation of carbohydrate dialdehydes. *ACS Catal.* 9, 11658–11662. doi: 10.1021/acscatal.9b04819

Dahiya, S., Kumar, A. N., Sravan, J. S., Chatterjee, S., and Sarkar, O. (2018). Food waste biorefinery: sustainable strategy for circular economy. *Bioresour. Technol.* 248, 2–12. doi: 10.1016/j.biortech.2017.07.176

Diaz-Rodriguez, A., Lavandera, I., Kanbak-Aksu, S., Sheldon, R. A., Gotor, V., and Gotor-Fernandez, V. (2012). From diols to lactones under aerobic conditions using a laccase/TEMPO catalytic system in aqueous medium. *Adv. Synth. Catal.* 354, 3405–3408. doi: 10.1002/adsc.201200892

Dijkman, W. P., Binda, C., Fraaije, M. W., and Mattevi, A. (2015). Structure-based enzyme tailoring of 5-hydroxymethylfurfural oxidase. *ACS Catalysis* 5, 1833–1839. doi: 10.1021/acscatal.5b00031

Dijksman, A., Arends, I. W. C. E., and Sheldon, R. A. (2003). Cu(II)-Nitroxyl radicals as catalytic galactose oxidase mimics. *Org. Biomol. Chem.* 1, 3232–3237. doi: 10.1039/b305941c

Dingerdissen, U., Pfeffer, J., Tacke, T., Haas, T., Schmidt, H., Klasovsky, F., et al. (2011). *Method for Producing Aldehydes and Ketones From Primary and Secondary Alcohols*. US 2011/0251399 A1. Essen: Evonik Degussa GmbH.

Escaletters, F., and Turner, N. J. (2008). Directed evolution of galactose oxidase: generation of enantioselective secondary alcohol oxidases. *ChemBioChem.* 9, 857–860. doi: 10.1002/cbic.200700689

Fabbrini, M., Galli, C., Gentili, P., and Machitella, D. (2001). An oxidation of alcohols by oxygen with the enzyme laccase and mediation by TEMPO. *Tetrahedron Lett.* 42, 7551–7553. doi: 10.1016/S0040-4039(01)01463-0

Fenouillot, F., Rousseau, A., Colomines, G., Saint-Loup, R., and Pascault, J. P. (2010). Polymers from renewable 1,4:3,6-dianhydrohexitols (isosorbide, isomannide and isoidide): a review. *Progr. Polym. Sci.* 35, 578–622. doi: 10.1016/j.progpolymsci.2009.10.001

Galaverna, R., Breitkreitz, M. C., and Pastre, J. C. (2018). Conversion of D-fructose to 5-(hydroxymethyl)furfural: evaluating batch and continuous flow conditions by design of experiments and in-line FTIR monitoring. *ACS Sust. Chem. Eng.* 6, 4220–4230. doi: 10.1021/acssuschemeng.7b04643

Gamez, P., Arends, I. W. C. E., Reedijk, J., and Sheldon, R. A. (2003). Copper(II)- catalysed oxidation of primary alcohols. *Chem. Commun.* 2414–2415. doi: 10.1039/b308668b

Gasser, C. A., Ammann, E. M., Shahgaldian, P., and Corvini, P. F. X. (2014). Laccases to take on the challenge of emerging organic contaminants in wastewater. *Appl. Microbiol. Biotechnol.* 98, 9931–9952. doi: 10.1007/s00253-014-6177-6

Geiβlmeir, D., Jary, W. G., and Falk, H. (2005). The TEMPO/copper catalyzed oxidation of primary alcohols to aldehydes using oxygen as stoichiometric oxidant. *Monatsh Chem.* 136, 1591–1599. doi: 10.1007/s00706-005-0349-0

Gross, J., Tauber, K., Fuchs, M., Schmidt, N. G., Rajagopalan, A., Faber, K., et al. (2014). Aerobic oxidation of isosorbide and isomannide employing TEMPO/Laccase. *Green Chem.* 16, 2117–2121. doi: 10.1039/C3GC41855C

Hamid, M. H. S. A., Slatford, P. A., and Williams, J. M. J. (2007). Borrowing hydrogen in the activation of alcohols. *Adv. Synth. Catal.* 349, 1555–1575. doi: 10.1002/adsc.200600638

Heath, R. S., Birmingham, W. R., Thompson, M. P., Taglieber, A., Daviet, L., and Turner, N. J. (2019). An engineered alcohol oxidase for the oxidation of primary alcohols. *ChemBioChem.* 20, 276–281. doi: 10.1002/cbic.201800556

Herter, S., McKenna, S. M., Frazer, A. R., Lehmkαhler, S., Carnell, A. J., and Turner, N. J. (2015). Galactose oxidase variants for the oxidation of amino alcohols in enzyme cascade synthesis. *ChemCatChem.* 7, 2313–2317. doi: 10.1002/cctc.201500218

Hollmann, F., Arends, I. W. C. E., Buehler, K., Schallmey, A., and Bühler, B. (2011). Enzyme-mediated oxidations for the chemist. *Green Chem.* 13, 226–265. doi: 10.1039/C0GC00595A

Hone, C. A., and Kappe, C. O. (2019). The use of molecular oxygen for liquid phase aerobic oxidations in continuous flow. *Top. Curr. Chem.* 377:2. doi: 10.1007/s41061-019-0233-8

Hoover, J. M., Ryland, B. L., and Stahl, S. S. (2013). Copper/TEMPO- catalyzed aerobic oxidation of alcohols: mechanistic assessment of different catalyst systems. *ACS Catal.* 3, 2599–2605. doi: 10.1021/cs400689a

Hoover, J. M., and Stahl, S. S. (2011). Highly practical copper(I)/TEMPO catalyst system for chemoselective aerobic oxidation of primary alcohols. *J Am Chem Soc.* 133, 16901–16910. doi: 10.1021/ja206230h

Horváth, I. T., Cséfalvay, E., Mika, L. T., and Debreczeni, M. (2017). Sustainability metrics for biomass-based carbon chemicals. *ACS Sustainable Chem. Eng.* 5, 2734–2740. doi: 10.1021/acssuschemeng.6b03074

Iwabuchi, Y. (2013). Discovery and exploitation of AZADO: the highly active catalyst for alcohol oxidation. *Chem. Pharm. Bull.* 61, 1197–1213. doi: 10.1248/cpb.c13-00456

Jiang, X., Liu, J., and Ma, S. (2019). Iron-catalyzed aerobic oxidation of alcohols: lower cost and improved selectivity. *Org. Proc. Res. Dev.* 23, 825–835. doi: 10.1021/acs.oprd.8b00374

Jiang, X., Zhang, J., and Ma, S. (2016). Iron catalysis for room-temperature aerobic oxidation of alcohols to carboxylic acids. *J. Am. Chem. Soc.* 138, 8344–8347. doi: 10.1021/jacs.6b03948

John, R. P., Anisha, G. S., Nampoothiri, K. M., and Pandey, A. (2011). Micro and macroalgal biomass: a renewable source for bioethanol. *Bioresour. Technol.* 102, 186–193. doi: 10.1016/j.biortech.2010.06.139

Klasovsky, F., Haas, T., Tacke, T., Pfeffer, J. C., Rimbach, M., Volland, M., et al. (2015). *Continuously Operable Method for Producing Carbonyl Compounds by*

Means of a Catalyst Containing a Nitroxyl Radical. US 8,981,159 B2. Essen: Evonik Degussa GmbH.

Koopman, F., Wiercxk, N., de Winde, J. H., and Ruijssenaaars, H. J. (2010). Efficient whole-cell biotransformation of 5-(hydroxymethyl)furfural into FDCA, 2,5-furandicarboxylic acid. *Bioresour. Technol.* 101, 6291–6296. doi: 10.1016/j.biortech.2010.03.050

Kroutil, W., Mang, H., Edegger, K., and Faber, K. (2004a). Biocatalytic oxidation of primary and secondary alcohols. *Adv. Synth. Catal.* 346, 125–142. doi: 10.1002/adsc.200303177

Kroutil, W., Mang, H., Edegger, K., and Faber, K. (2004b). Recent advances in the biocatalytic reduction of ketones and oxidation of sec-alcohols. *Curr. Opin. Chem. Biol.* 8, 120–126. doi: 10.1016/j.cbpa.2004.02.005

Kuang, Y., Rokubuichi, H., Nabae, Y., Hayakawa, T., and Kakimoto, M. (2010). A nitric acid assisted carbon-catalyzed oxidation system with nitroxide radical cocatalysts as an efficient and green protocol for selective aerobic oxidation of alcohols. *Adv. Synth. Catal.* 352, 2635–2642. doi: 10.1002/adsc.201000366

Kucherov, F. A., Romashov, L. V., Galkin, K. I., and Ananikov, V. P. (2018). Chemical transformations of biomass-derived C6-furanic platform chemicals for sustainable energy research, materials science and synthetic building blocks. *ACS Sust. Chem. Eng.* 6, 8064–8092. doi: 10.1021/acssuschemeng.8b00971

Lange, J. P., van der Heide, E., van Buijtenen, J., and Price, R. (2012). Furfural - a promising platform for lignocellulosic biofuels. *ChemSusChem*. 5, 150–166. doi: 10.1002/cssc.201100648

Lauber, M. B., and Stahl, S. S. (2013). Efficient aerobic oxidation of secondary alcohols at ambient temperature with an ABNO/NO_x catalyst system. *ACS Catal.* 3, 2612–2616. doi: 10.1021/cs400746m

Leijdeckers, A. G. M., Bink, J. P. M., Geutjes, S., Schols, H. A., and Gruppen,. H. (2013). Enzymatic saccharification of sugar beet pulp for the production of galacturonic acid and arabinose; a study on the impact of the formation of recalcitrant oligosaccharides. *Bioresour. Technol.* 128, 518–525. doi: 10.1016/j.biortech.2012.10.126

Liguori, R., and Faraco, V. (2016). Biological processes for advancing lignocellulosic waste biorefinery by advocating circular economy. *Bioresour. Technol.* 215, 13–20. doi: 10.1016/j.biortech.2016.04.054

Liu, B., Ren, Y., and Zhang, Z. (2015). Aerobic oxidation of 5-hydroxymethylfurfural into 2,5-furandicarboxylic acid in water under mild conditions. *Green Chem*. 17, 1610–1617. doi: 10.1039/C4GC02019G

Marais, L., and Swarts, A. J. (2019). Biomimetic Cu/Nitroxyl catalyst systems for selective alcohol oxidation. *Catalysts* 9, 1–28. doi: 10.3390/catal9050395

Mase, N., Mizumori, T., and Tatemoto, Y. (2011). Aerobic copper/TEMPO-catalyzed oxidation of primary alcohols to aldehydes using a microbubble strategy to increase gas concentration in liquid phase reactions. *Chem. Commun*. 47, 2086–2088. doi: 10.1039/c0cc04377j

Matijosyte, I., Arends, I. W. C. E., de Vries, S., and Sheldon, R. A. (2010). Preparation and use of cross-linked enzyme aggregates (CLEAs) of laccases. *J. Mol. Catal. B* 62, 142–148. doi: 10.1016/j.molcatb.2009.09.019

Miller, D. J., Peereboom,. L., and Wegener, E., Gattinger, M. (2017). *Formation of 2,5-Furandicarboxylic Acid From Aldaric Acids*. US 9701652 B1 2017. Board of Trustees of Michigan State University.

Motagamwala, A. H., Won, W., Sener, C., Alonso, D. M., Marvelias, C. T., and Dumesic, J. A. (2018). Toward biomass-derived renewable plastics: production of 2,5-furandicarboxylic acid from fructose. *Sci Adv*. 4, 1–8. doi: 10.1126/sciadv.aap9722

Mutti, F. G., Knaus, T., Scrutton, N. S., Breuer, M., and Turner, N. J. (2015). Conversion of alcohols to enantiopure amines through dual-enzyme hydrogen-borrowing cascades. *Science* 349, 1525–1529. doi: 10.1126/science.aac9283

Parmaggiani, C., and Cardona, F. (2012). Transition metal based catalysts in the aerobic oxidation of alcohols. *Green Chem*. 14, 547–564. doi: 10.1039/c2gc16344f

Pedersen, A. T., Birmingham, W. R., Rehn, G., Charnock, S. J., Turner, N. J., and Woodley, J. M. (2015). Process requirements of galactose oxidase catalyzed oxidation of alcohols. *Org. Proc. Res. Dev.* 19, 1580–1589. doi: 10.1021/acs.oprd.5b00278

Phillips, J. R., Huhnke, R. L., and Atiyeh, H. K. (2017). Syngas fermentation: a microbial conversion process of gaseous substrates to various products. *Fermentation* 3:28. doi: 10.3390/fermentation3020028

Ponedel'kina, I. Y., Khaibrakhmanova, E. A., and Odinokov, V. N. (2010). Nitroxide-catalyzed selective oxidation of alcohols and polysaccharides. *Russ. Chem. Rev*. 79, 63–75. doi: 10.1070/RC2010v079n01ABEH004074

Rinaldi, R., Jastrzebski, R., Clough, M. T., Ralph, J., Kennema, M., Bruijnincx, P. C. A., and Weckhuysen, B. M. (2016). Paving the way for lignin valorization: recent advances in bioengineering, biorefining and catalysis. *Angew. Chem. Int. Ed.* 55, 8164–8215. doi: 10.1002/anie.201510351

Rochefort, D., Leech, D., and Bourbonnais,. R. (2004). Electron transfer mediator systems for bleaching of paper pulp. *Green Chem.* 6, 614–624. doi: 10.1039/b311898n

Sasano, Y., Nagasawa, S., Yamazaki, M., Shibuya, M., Park, J., and Iwabuchi, Y. (2014). Highly chemoselective aerobic oxidation of amino alcohols into amino carbonyl compounds. *Angew. Chem. Int. Ed.* 53, 3236–3240. doi: 10.1002/anie.201309634

Sheldon, R. A. (2014). Green and sustainable manufacture of chemicals from biomass: state of the art. *Green Chem*. 16, 950–963. doi: 10.1039/C3GC41935E

Sheldon, R. A. (2016). Green chemistry, catalysis and valorization of waste biomass *J. Mol. Catal. A* 422, 3–12. doi: 10.1016/j.molcata.2016.01.013

Sheldon, R. A. (2018). The road to biorenewables: carbohydrates to commodity chemicals. *ACS Sustain. Chem. Eng.* 6, 4464–4480. doi: 10.1021/acssuschemeng.8b00376

Sheldon, R. A., and Arends, I. W. C. E. (2004). Organocatalytic oxidations mediated by nitroxyl radicals *Adv. Synth. Catal.* 346, 1051–1071. doi: 10.1002/adsc.200404110

Sheldon, R. A., van Pelt, S., Kanbak-Aksu, S., Rasmussen, J., and Janssen, M. H. A. (2013). Cross-linked enzyme aggregates in organic synthesis. *Aldrichimica Acta*, 46, 81–93.

Sheldon, R. A., and Woodley, J. M. (2018). Role of biocatalysis in sustainability. *Chem. Rev*.118, 801–838. doi: 10.1021/acs.chemrev.7b00203

Shibuya, M., Osada, Y., Sasano, Y., Tomizawa, M., and Iwabuchi, Y. (2011). Highly efficient, organocatalytic aerobic alcohol oxidation. *J. Am. Chem. Soc.* 133, 6497–6500. doi: 10.1021/ja110940c

Shibuya, M., Tomizawa, M., Suzuki, I., and Iwabuchi, Y. (2006). 2-Azaadamantane *N*-Oxyl (AZADO) and 1-Me-AZADO: highly efficient organocatalysts for oxidation of alcohols. *J. Am. Chem. Soc.* 128, 8412–8413. doi: 10.1021/ja0620336

Shuba, E. S., and Kifle, D. (2018). Microalgae to biofuels: 'Promising' alternative and renewable energy, review. *Renew Sust. Energy Rev.* 81, 743–755. doi: 10.1016/j.rser.2017.08.042

Singh, J., Saharan, V., Kumar, S., Gulati, P., and Kapoor, R. K. (2018). Laccase grafted membranes for advanced water filtration systems: a green approach to water purification technology. *Crit. Rev. Biotechnol.* 38, 883–901. doi: 10.1080/07388551.2017.1417234

Stahl, S. S. (2004). Selective oxidation of organic compounds by direct dioxygen-coupled turnover. *Angew. Chem. Int. Ed.* 43, 3400–3420. doi: 10.1002/anie.200300630

Steves, J. E., and Stahl, S. S. (2013). Copper/ABNO catalyzed aerobic alcohol oxidation. Alleviating steric and electronic constraints of Cu/tempo catalyst systems. *J. Am. Chem. Soc.* 135, 15742–15745. doi: 10.1021/ja409241h

ten Brink, G. J., Arends, I. C. W. E., and Sheldon, R. A. (2000). Green, catalytic oxidation of alcohols in water. *Science* 287,1636–1639. doi: 10.1126/science.287.5458.1636

Thompson, M. P., and Turner, N. J. (2017). Two-enzyme hydrogen-borrowing amination of alcohols enabled by a cofactor-switched alcohol dehydrogenase. *ChemCatChem*. 23, 3833–3836. doi: 10.1002/cctc.201701092

Tong, X., Ma, Y., and Li, Y. (2010). Biomass into chemicals: conversion of sugars to furan derivatives by catalytic processes. *Appl. Catal. A* 385, 1–13. doi: 10.1016/j.apcata.2010.06.049

Unuofin, J. O., Okoh, A. I., and Nwodo, U. U. (2019). Aptitude of oxidative enzymes for treatment of wastewater pollutants: a laccase perspective. *Molecules*, 24:2064. doi: 10.3390/molecules24112064

van der Klis, F., van Haveren, J., van Es, D. S., and Bitter, J. H. (2017). Synthesis of furan dicarboxylic acid esters from nonfood feedstocks without concomitant levulinic acid formation. *ChemSusChem*, 10, 1460–1468. doi: 10.1002/cssc.201700051

van Es, D. S., van Haveren, J., Raaijmakers, H. W. C., van der Klis, F., and van Engelen, G. P. F. M. (2013). *Catalytic Oxidation of Uronic Acids to Aldaric Acids*. WO 2013/151428 A1. Wageningen: Stichting Dienst Landbouwkundig Onderzoek.

van Putten, R. J., van der Waal, J. C., de Jong, E., Rasrendra, C. B., Heeres, H. J., and de Vries, J. G. (2013). Hydroxymethylfurfural, a versatile platform chemical made from renewable resources. *Chem. Rev.* 113, 1499–1597. doi: 10.1021/cr300182k

Viikari, L., Niku-Paavola, M. I., Buchert, J., Forssell, P. Teleman, A., and Kruus, K. (1999). *Method of Producing Oxidized Starch.* Helsinki: Valtion Teknillinen Tutkimuskeskus, WO 99/23240.

Vilim, J., Kraus, T., and Mutti, F. (2018). Catalytic Promiscuity of galactose oxidase. a mild synthesis of nitriles from alcohols, air and ammonia. *Angew. Chem. Int. Ed.* 57, 14240–14244. doi: 10.1002/anie.201809411

von Gorup-Besanez, E. F. (1861). Ueber die producte der einwirkung des platinmohrs auf mannit. *Ann Chem.* 118:257. doi: 10.1002/jlac.18611180302

Wang, J., Xi, J., Xia, Q., Liu, X., and Wang, Y. (2017). Recent advances in heterogeneous catalytic conversion of glucose to 5-hydroxymethylfurfural via green routes. *Sci. China Chem.* 60, 870–886. doi: 10.1007/s11426-016-9035-1

Weckbecker, A., Gröger, H., and Hummel, W. (2010). Regeneration of nicotinamide coenzymes: principles and applications for the synthesis of chiral compounds. *Adv. Biochem. Eng. Biotechnol.* 120, 195–242. doi: 10.1007/10_2009_55

Wu, Y., Enomoto, Y., Masaki, H., and Iwata, T. (2019). Synthesis of polyamides from sugar derived D-glucaric acid and xylylenediamines. *J. Appl. Polym. Sci.* 136, 1–6. doi: 10.1002/app.47255

Zhang, J. D., Cui, Z. M., Fan, X. J., Wu, H. L., and Chang, H. H. (2016). Cloning and characterization of two distinct water-forming NADH oxidases from *Lactobacillus pentosus* for the regeneration of NAD. *Bioprocess Biosyst. Eng.* 39, 603–611. doi: 10.1007/s00449-016-1542-8

Zhang, Z., and Deng, K. (2015). Recent advances in the catalytic synthesis of 2,5-furandicarboxylic acid and its derivatives. *ACS Catal.* 5, 6529–6544. doi: 10.1021/acscatal.5b01491

Zhang, Z., Song, J., and Han, B. (2017). Catalytic transformation of lignocellulose into chemicals and fuel products in ionic liquids. *Chem. Rev.* 117, 6834–6880. doi: 10.1021/acs.chemrev.6b00457

Zheng, L., Zhao, J., Du, Z., Zong, B., and Liu, H. (2017). Efficient aerobic oxidation of 5-hydroxymethylfufural to 2,5-furandicarboxylic acid on Ru/C catalysts. *Chem. Sci. China* 60, 950–957. doi: 10.1007/s11426-016-0489-3

Zhu, C., Zhang, Z., Ding, W., Xie, J., Chen, Y., Wu, J., et al. (2014). A mild and highly efficient laccase-mediator system for aerobic oxidation of alcohols. *Green Chem.* 16, 1131–1138. doi: 10.1039/C3GC42124D

Conflict of Interest: The author declares that the research was conducted in the absence of any commercial or financial relationships that could be construed as a potential conflict of interest.

frontiers in Chemistry

MINI REVIEW
published: 31 March 2020
doi: 10.3389/fchem.2020.00185

Recent Progress in Adipic Acid Synthesis Over Heterogeneous Catalysts

*Wenjuan Yan[1], Guangyu Zhang[1], Jinyao Wang[1], Mengyuan Liu[1], Yu Sun[1], Ziqi Zhou[1], Wenxiang Zhang[1], Shuxia Zhang[1], Xiaoqiang Xu[2], Jian Shen[3] and Xin Jin[1]**

[1] State Key Laboratory of Heavy Oil Processing, Center for Chemical Engineering Experimental Teaching, China University of Petroleum, Qingdao, China, [2] Oil Production Group#2, Huabei Oil Field Company at PetroChina, Langfang, China, [3] College of Environment and Resources, Xiangtan University, Xiangtan, China

Adipic acid is one of the most important feedstocks for producing resins, nylons, lubricants, plasticizers. Current industrial petrochemical process, producing adipic acid from KA oil, catalyzed by nitric acid, has a serious pollution to the environment, due to the formation of waste nitrous oxide. Hence, developing cleaner methods to produce adipic acid has attracted much attention of both industry and academia. This mini-review article discussed advances on adipic acid synthesis from bio-renewable feedstocks, as well as most recent progress on cleaner technology from fossil fuels over novel catalytic materials. This work on recent advances in green adipic acid production will provide insights and guidance to further study of various other industrial processes for producing nylon precursors.

Keywords: nanostructured catalyst, glucose, glucaric acid, adipic acid, cyclohexanone, polyoxometalates

OPEN ACCESS

Edited by:
Yulong Wu,
Tsinghua University, China

Reviewed by:
Kannan Srinivasan,
Central Salt and Marine Chemicals Research Institute (CSIR), India
Huijuan Wei,
Zhengzhou University, China

****Correspondence:***
Xin Jin
jamesjinxin@upc.edu.cn

Specialty section:
This article was submitted to Green and Sustainable Chemistry, a section of the journal Frontiers in Chemistry

Received: *01 November 2019*
Accepted: *28 February 2020*
Published: *31 March 2020*

Citation:
Yan W, Zhang G, Wang J, Liu M, Sun Y, Zhou Z, Zhang W, Zhang S, Xu X, Shen J and Jin X (2020) Recent Progress in Adipic Acid Synthesis Over Heterogeneous Catalysts. Front. Chem. 8:185. doi: 10.3389/fchem.2020.00185

INTRODUCTION

Adipic acid (AA) has immense practical use in industrial for the production of nylon-66, nylon-6, lubricant and plasticizer (Feng et al., 2019; Perkel and Voronina, 2019; Pisk et al., 2019; Yang B. et al., 2019; Yang J. et al., 2019). In current industrial processes, AA is synthesized mainly by oxidation of KA oil using 50–60% nitric acid as oxidant and copper/ammonium metavanadate as the catalyst (Van de Vyver and Roman-Leshkov, 2013; Deng et al., 2016; Rahman et al., 2016). However, this process emits nitrous oxide which can cause ozone depletion, acid rain, and global warming. Furthermore, the applicability of the phase-transfer catalyst in industrial scale is expensive. Obviously, we need to develop more sustainable AA manufacturing process which can avoid the use of toxic reagents and tedious products separation (Dugal et al., 2000; Cheng et al., 2007; Fujitani et al., 2009; Jin et al., 2011; Indulkar et al., 2012; Lu et al., 2012; Vafaeezadeh et al., 2012).

Cyclohexane, cyclohexanol, cyclohexanone can be oxidized to produce AA without formation of any greenhouse gases (Sato et al., 1998; Chatterjee et al., 2018; Luo et al., 2018; Mazzi et al., 2018; Mouheb et al., 2018; Wang et al., 2018). Oxygen, air, hydrogen peroxide (H_2O_2) are regarded as clean oxidant since they give water as the only byproduct. It is essential to use separable and reusable inexpensive catalysts for development of sustainable protocols (Baig and Varma, 2012). Various of solid supported catalysts, such as metal oxides, (Hereijgers and Weckhuysen, 2010; Makgwane and Ray, 2014) hollow structure silicates, (Dai et al., 2016; Xia et al., 2018) carbon nanotubes (CNTs), (Machado et al., 2014; Yang et al., 2016) and polyoxometalates (POMs), (Luo et al., 2018)

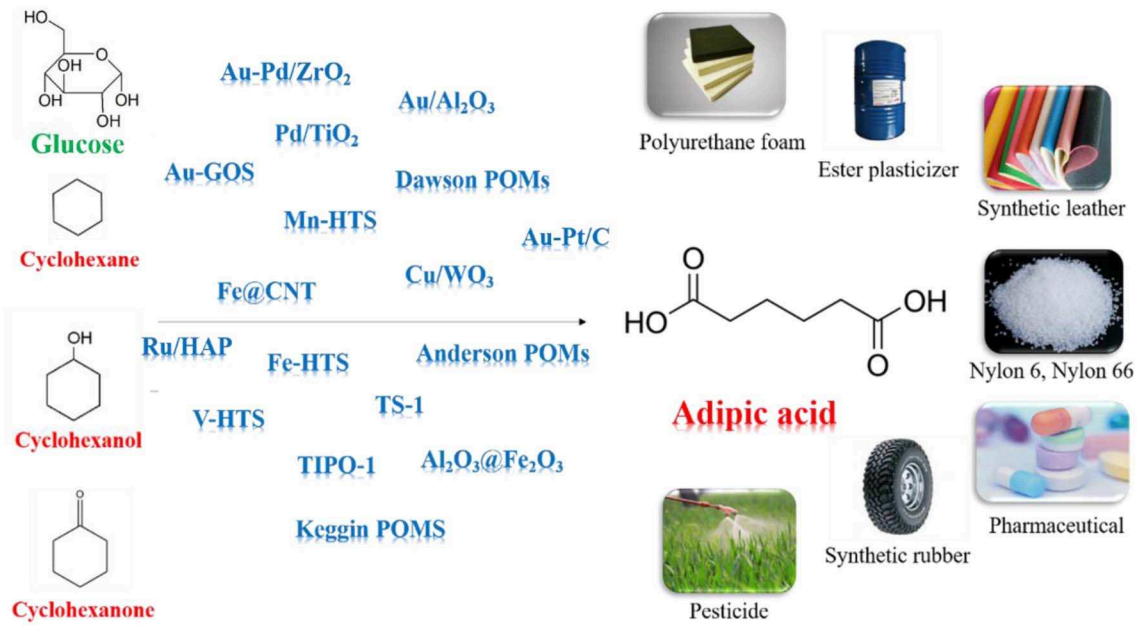

GRAPHICAL ABSTRACT | Heterogeneous Catalysts for Adipic Acid Synthesis.

show remarkable performances in AA synthesis, due to the inherent adsorptive properties and tunable acidity.

Some alternative bio-derived AA processes have been extensively reported for synthesizing AA by oxidizing lignocellulosic biomass derived chemicals, e.g., hemicellulose, cellulose, and lignin (Vardon et al., 2015; Han, 2016). Different processes including glucose to glucaric acid process, hydroxymethylfurfural (HMF) to furan dicarboxylic acid (FDCA) process, γ -valerolactone process, lignin and lignin-derived oils process, were reported for AA synthesis from biomass feedstocks (Deng et al., 2016; Gunukula and Anex, 2017; Skoog et al., 2018). In the glucose conversion route, glucaric acid was formed as intermediate by oxidizing the glucose and further undergo hydrogenolysis to form AA (Zhang and Deng, 2015; Zhang and Huber, 2018). This reaction can be achieved in the presence of Au, Pt, and Pd catalysts (Ibert et al., 2002; Merbouh et al., 2002). In the FDCA process, FDCA were formed as intermediates by oxidizing the HMF and was further hydrogeneolyzed to form AA (Gilkey et al., 2018). Noble Pt and Au metals-based catalysts were reported most effective for this reaction (Kong et al., 2018).

Most recent review articles on the synthesis of AA have been listed in this section. Van de Vyver and Roman-Leshkov (2013), Deng et al. (2016), and Rahman et al. (2016) summarized the performances of various catalysts for AA production, with specific focus on metal catalyst design and reaction mechanism. The progress of the metabolic pathways for AA production has been reviewed (Polen et al., 2013; Alonso et al., 2015; Deng et al., 2016; Kruyer and Peralta-Yahya, 2017; Skoog et al., 2018). In 2018, Li et al. (2018) summarized the conversion of cellulose and its derivatives to various organic acids. In this mini review, the glucose and HMF processes will be reviewed systematically. We will particularly focus on the advances of the performances of metallic solid catalysts and POM catalysts for synthesis of AA from both glucose and HMF routes in past 5 years, including mechanistic insights and catalysts stability. The opportunities and challenges in the green process of AA production will be discussed.

HETEROGENEOUS METALLIC CATALYST FOR GLUCSOE AND DERIVATIVES OXIDATION

The transformation of bio-based glucose and its derivatives into AA is green and sustainable. In the first step, the glucose was oxidized to form glucaric acid which was further converted to AA by a catalytic hydrodeoxygenation (HDO) process (**Figure 1A**). A patent disclosed a yield of 89% of AA in the HDO process over Pt/Rh metallic catalysts in acidic condition using acetic acid and HBr as solvent (Boussie et al., 2014). Lin et al. (2019) reported the deoxydehydration of cellulose-derived D-glucaric acid to AA ester over ReO_x/ZrO_2-Pd/C catalysts (Y = 82%). In this part, we summarized the most recent progress of glucaric acid synthesis from glucose.

In the industry, this process can be achieved in the presence of homogeneous catalysts and toxic oxidants under harsh conditions (Smith et al., 2012). The difficulty of separation and the hazardous byproducts hampered the further development of this process. Literatures have widely demonstrated the synthesis of glucaric acid over the supported noble metal catalysts, e.g., Pd, (Jin et al., 2016) Pt, (Bellardita et al., 2016; Shi et al., 2018) and Au (Wojcieszak et al., 2016; Derrien et al., 2017; Solmi et al., 2017) catalysts. Au nanoparticles were immobilized on

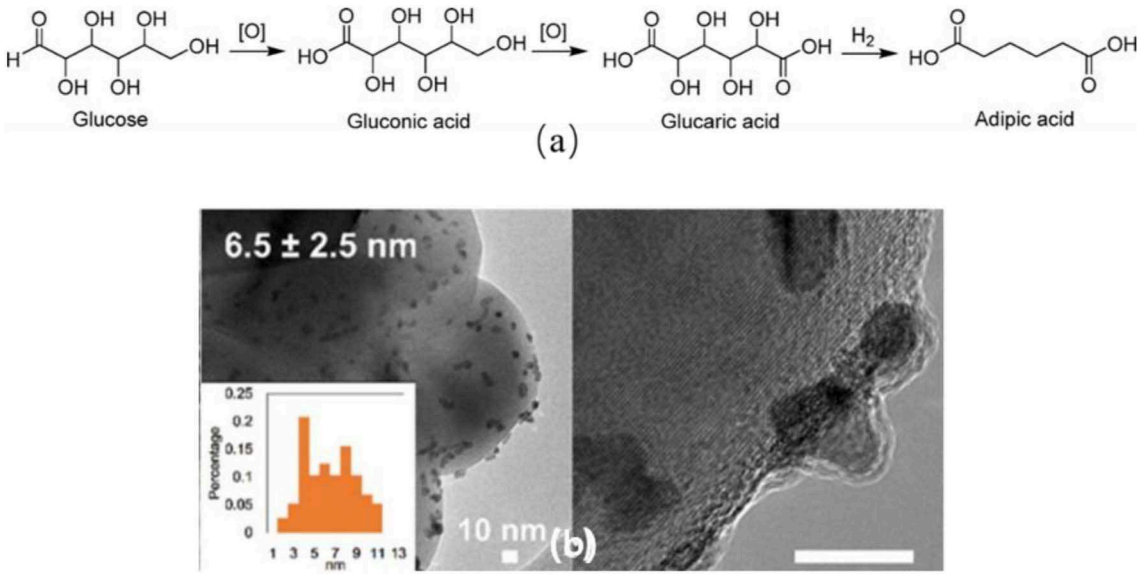

FIGURE 1 | (A) Glucose oxidation to produce AA, (Jin et al., 2016). **(B)** TEM images of $PtPd/TiO_2$ (Jin et al., 2016).

active carbon (**Table 1**, #1) (Solmi et al., 2017). After adding Bi additives, AuBi/AC catalyst showed higher glucaric acid yield (**Table 1**, #2). They claimed that Au particle size affected the ratio between the parallel reactions of gluconic and glucaric acid formation. The reuse study showed a little decline of the activity due to the agglomeration of nanoparticles and the deposition of organic residues (Solmi et al., 2017). Au-Pt and Au-Pd catalysts were supported on various metal oxides (**Table 1**, #3) (Derrien et al., 2017). The catalytic performance of these catalysts was significantly influenced by the nature of the support. The best glucaric acid yield (44%) was obtained in the presence of ZrO_2 supported Au-Pt catalyst under base-free conditions (Derrien et al., 2017) CeO_2 supported Au-Pt catalyst showed the lowest activity. They also noticed that Au-Pd showed higher ability to convert glucose to gluconic acid, but lower ability to further convert gluconic acid to glucaric acid comparing to the Au-Pt catalysts (Derrien et al., 2017). The recycled $Au\text{-}Pt/ZrO_2$ catalyst was stable in three successive runs, but displayed lower glucaric acid selectivity in the fourth to sixth runs. The TEM images showed the particles' morphology did not change after 24 h reaction. ICP results showed there was no trace of Au or Pt presented in the reaction solution. Hence, they concluded that the activity decline was caused by the multiple handling and washing of the catalyst. The same group synthesized Pt/C catalyst and obtained a yield of 54% of glucarate under alkaline conditions (**Table 1**, #4) (Derrien et al., 2016). Lee et al. (2016) get a maximum yield of 74% of glucaric acid with Pt/C in aqueous solution with pH of 7.2 using air as oxidant. They found that the selectivity to gluconic acid was higher in acidic conditions due to C-C bond cleavage to short chain carboxylic acids (**Table 1**, #5) (Lee et al., 2016). The Pt/C catalyst showed good stability in at least five consecutive runs and had no Pt leaching and morphology changing during the reaction. Bimetallic $PtPd/TiO_2$ (TOF = 2404 h^{-1}) catalyst was synthesized via a simple *in situ* reduction method and displayed much higher activity compared to monometallic catalysts (TOF = 248 h^{-1}) due to the existence of PtPd alloy structure as confirmed by the TEM image (**Figure 1B**, **Table 1**, #6) (Jin et al., 2016). The $PtPd/TiO_2$ catalyst was stable in three consecutive runs with no activity loss, but about 4% Pt and Pd leaching was observed. It is highly possible that the leached metal species may be inactive in this reaction. The same group prepared $Pt\text{-}Cu/TiO_2$ catalyst using $NaBH_4$ as reducing agent and demonstrated a satisfactory activity for glucaric acid (X = 92%, S = 60%) under base-free conditions (**Table 1**, #7) (Jin et al., 2015; Shi et al., 2018). They observed strong metal-support interaction between Pt and TiO_2 support. The stability study showed that the catalyst exhibited same conversion of glucose and marginal change of selectivity to glucaric acid after three runs. This work demonstrated that it is practicable to replace the second noble metal with inexpensive Cu metal for the glucose oxidation process (Shi et al., 2018).

HMF is an important platform chemical which can be converted to AA by two steps. HMF was oxidized to form FDCA which undergo deoxygenation to form AA. Wei et al. (2019) reported one-step conversion of FDCA to AA in water over niobic acid-supported Pt catalyst 38% AA yield was obtained at 200°C in 8 h over Pt/Nb_2O_5 catalyst which was proved to be stable in at least five repeated runs. The hydrodeoxygenation of FDCA was also conducted in the presence of $Pt\text{-}MoO_x/TiO_2$ catalyst with AA yield of 21% at 200°C in 4 h (Asano et al., 2016). The low solubility of FDCA in water may cause the low AA yield. Gilkey et al. (2017) studied the metal-free hydrogenolysis of tetrahydrofuran-2,5-dicarboxylic acid (THFDCA) to produce AA. A 99% THFDCA conversion and 89% yield of AA were obtained at 160°C in 2 h. The literatures about this step was rare, but FDCA synthesis from HMF oxidation has been widely reported as one of the key steps of biomass conversion to AA (**Figure 2A**) (Zhang et al., 2015, 2018; Zhou et al., 2016; Diamond

TABLE 1 | Heterogeneous metallic catalyst for glucose and derivatives oxidation.

#	Catalyst	Reaction conditions	Conversion, selectivity
1	Au/C	Glucose, 60°C, 3 h, 1MPa, O_2	Y = 24%
2	AuBi/C	Glucose, 60°C, 3 h, 1MPa, O_2	Y = 31%
3	Au-Pt/ZrO_2	Glucose, 100°C, 4 h, 4MPa, air	Y = 44%
4	Pt/C	Glucose, 60°C, 24 h, 0.1MPa, air	Y = 54%
5	Pt/C	Glucose, 80°C, 10 h, 1.4MPa, O_2	X = 99%, S = 74%
6	PtPd/TiO_2	Glucose, 45°C, 24 h, 0.1MPa, O_2	X = 100%, *S* = 40.4%
7	PtCu/TiO_2	Glucose, 90°C, 12 h, 1.5MPa, O_2	X = 92%, *S* = 60%
8	AuPd/AER	HMF, 100°C, 4 h, 1MPa, O_2	X = 100%, S = 93.2%,
9	AuPd/CaMgAl	HMF, 100°C, 6 h, 0.5MPa, O_2	X = 96.1%, S = 89.4%
10	PdNi/$Mg(OH)_2$	HMF, 100°C, 10 h, 0.1MPa, air	X = 99%, S = 76%
11	PdCo/$Mg(OH)_2$	HMF, 100°C, 10 h, 0.1MPa, air	X = 94%, S = 46%
12	PdCu/$Mg(OH)_2$	HMF, 100°C, 10 h, 0.1MPa, air	X = 81%, S = 41%
13	Pt-Ni/AC	HMF, 100°C, 6 h, 0.4MPa, O_2	X = 100%, S = 43.1%
14	Pt/C	HMF, 110°C, 12 h, 1MPa, O_2	X = 99%, S = 96%
15	Ru/$MnCo_2O_4$	HMF, 120°C, 10 h, 2.4MPa, air	X = 100%, *S* = 99.1%
16	Ru/HAP	HMF, 120°C, 24 h, 2MPa, air	X = 100%, S = 99.6%

et al., 2018; Li et al., 2018; Rathod and Jadhav, 2018; Ventura et al., 2018). Au-Pd alloy nanoparticles were immobilized on basic anion-exchange resin and catalyzed the HMF to FDCA reaction with a yield of 93.2% (**Table 1**, #8) (Antonyraj et al., 2017). The physical mixture of Au and Pd nanoparticles showed only 52% FDCA yield. This confirmed the major role of the AuPd alloy as active species as evidenced by the XPS study (Antonyraj et al., 2017). This catalyst had no metal leaching and activity decreasing after six cycles. Au-Pd alloy was also supported on La-doped CaMgAl layered double hydroxide (LDH) (Gao et al., 2017). TEM images showed that small nanoparticles with 3–4 nm particle size were well-dispersed on the LDH support (**Figure 2B**) (Gao et al., 2017). A yield more than 99% of FDCA was obtained ascribing to the high surface basicity of the support and the synergy between Au-Pd nanoparticles (**Table 1**, #9). They also observed that the La_2O_3 on the surface of the LDH support can form carboxylic acid products and prevent the deterioration of the LDH support, thus enhance the catalyst stability (Gao et al., 2017). This catalyst maintained good activity after four runs with only 2% decreasing of the yield. No leaching of Au or Pd was detected. However, there were 0.8% of Mg and 0.3% of Ca lost after the reaction.

Ni, Co, and Cu metals were selected to synthesis bimetallic Pd catalysts. Gupta et al. (2017a,b) found that PdNi/$Mg(OH)_2$ catalyst displayed higher catalytic performance than Co and Cu based Pd/$Mg(OH)_2$ catalyst due to the synergistic cooperation between Pd and Ni species (**Table 1**, #10–12). This catalyst can be reused for three consecutive reactions without significant activity loss, Pd/Ni metal leaching, or particle size changing. Ni and Pt bimetallic nanoparticles were supported on active carbon by atomic layer deposition method (**Table 1**, #13) (Shen et al., 2018). The TEM images showed that the metal were uniformly dispersed on the support (**Figure 2C**). A 97.5% yield of FDCA (TOF= 35.8 h^{-1}) was obtained in 15 h reaction. They claimed that the presence of Ni species enhanced the ability of Pt to adsorb and oxidize C = O bond (Shen et al., 2018). The catalysts recycled after four runs showed 86.3% FDCA yield which is lower than the fresh catalysts (97.5%). However, the reasons for the activity loss was not discussed in this work. Pt supported on carbon displayed 96% yield of FDCA in the absence of base (**Table 1**, #14) (Han et al., 2016). The introduction of N atom brought more medium strength basic sits to the catalyst and thus elevated the catalytic activity (Han et al., 2016). Ru immobilized on $MnCo_2O_4$ was reported highly active (Y = 99.1%) for HMF oxidation under base-free condition (**Table 1**, #15) (Mishra et al., 2017). The existence of both Lewis and BrØnsted acid sites facilitated the HMF oxidation to FDCA (Mishra et al., 2017). The reusability study showed that there was no significant change in the rate of HMF conversion in at least five successive runs. The TEM images of both fresh and used catalysts indicated that there was no discernible change of the structure. No Ru metal leaching was detected by ICP analysis.

Gao et al. (2018) supported Ru on hydroxyapatite. The TEM image showed a typical rod-shape agglomerates with the mean size of Ru nanoparticles about 1.8 nm (**Figure 2D**). Hundred percentage of conversion of HMF and 99.6% selectivity to FDCA were obtained in the presence of oxygen and water. The acidic-basic sites on hydroxyapatite support were essential for good catalytic performance (**Table 1**, #16) (Gao et al., 2018). There was about 10% loss of the FDCA yield after the fifth runs. ICP results revealed there was no leaching of Ru and Ca species from the catalyst. No aggregation of Ru nanoparticles was noticed from the TEM images. The adsorption of impurities and the partial oxidation of Ru nanoparticles were the main reason of the catalyst deactivation.

CYCLOHEXANE, AND CYCLOHEXANONE/CYCLOHEXANOL OXIDATION TO AA

Cyclohexane and cyclohexanone/cyclohexanol are the most selected chemicals as the model substrates for oxidation reaction to produce AA over various of catalysts, such as metal oxides, carbon nano tubes (CNTs), and TS-1 catalysts (Cavani et al., 2011; Alshammari et al., 2012; Dai et al., 2016; Chen et al., 2017; Nale et al., 2017).

Cyclohexane Oxidation to AA

Metal oxides are widely studied for oxidation reaction (Fang et al., 2013; Hao et al., 2013; Zhang et al., 2013; Li et al., 2014; Qadir et al., 2014; Gui et al., 2015; Imanaka et al., 2015; Wang et al., 2016; Shiraishi et al., 2017). The nature of the metal oxides as support or as active species influenced the catalytic performance of the catalysts significantly (Unnarkat et al., 2016; Ribeiro de Sousa Martins et al., 2017; Yang et al., 2017; Feliciano Miranda et al., 2018). Acharyya et al. (2015) synthesized Cr_2O_3 supported Cu nanoclusters with hydrothermal method which converted cyclohexane to cyclohexanone with high yield, but failed to produce any AA. Whereas, WO_3 supported Cu converted cyclohexane with 88% conversion and 75% selectivity to AA (**Table 2**, #1) (Acharyya et al., 2015). Most probably, the activation energy was lowered in the case of Cu-WO3

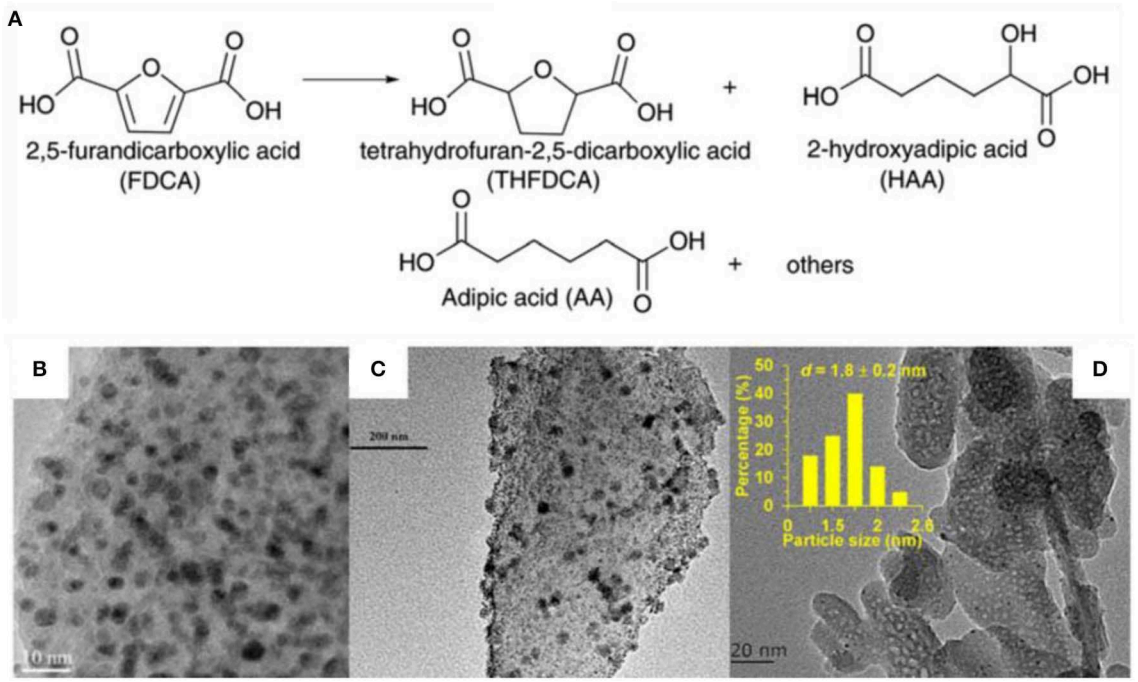

FIGURE 2 | (A) HMF to AA, (Lee et al., 2016) TEM images of **(B)** AuPd/CaMgAl, (Gao et al., 2017) **(C)** Pt-Ni/AC, (Shen et al., 2018) **(D)** Ru/HAP (Gao et al., 2018).

catalysts due to the flexibility property of the Cu-framework. The impregnated CuO/WO_3 catalyst was inactive for cyclohexane oxidation to AA. It seems that the synergistic interaction between the Cu and W species is the main reason of the oxidation activity. Recycled $Cu\text{-}WO_3$ catalysts have no metal leaching in at least four consecutive runs without any decreasing of catalytic performance. Comparing to Cu, Au has the same outermost electronic configurations but far higher activity in oxidation reactions. Liu et al. (2016) coated Au on the wall of the stainless steel microcapillary. A conversion of 2.1% and selectivity of 18.9% to AA were obtained for cyclohexane oxidation in 4 min (**Table 2**, #2). The stability of the catalyst was not reported in this work. Alshammari et al. (2015, 2016) incorporated Au, Pd, and Ag on TiO_2 using sol-gel methods. Bimetallic catalysts $AuPd/TiO_2$ showed higher selectivity compared to monometallic Pd/TiO_2 toward AA (**Table 2**, #3) due to smaller particle size as observed by TEM images. Au as a second metal is important for enhancing the AA selectivity due to the synergistic effects between Au and Pd metals. The bimetallic catalyst was observed deactivated after consecutive runs due to the formation of $Pd^{\delta-}$ species with lower binding energy, metal leaching and coke formation (Alshammari et al., 2016). Chen et al. (2017) confined Au nanoparticles in hybrid shells of organic linker-assisted silica nanospheres (GOS) using amino function groups for anchoring Au precursor. TEM images showed that GOS has uniformed nanospheres with 120–150 nm diameter. The AuNPs (<2 nm) were highly dispersed on the shells of silica. FTIR and Raman results indicated that the incorporation of AuNPs didn't alter the structure of GOS. The obtained catalyst oxidized cyclohexane with 45% selectivity to AA under solvent-free conditions using O_2 as oxidant (TOF = 59,307 h^{-1}, **Table 2**, #4). It seems that the AuNPs confined in silica shell is more active than that in the inner cores. Besides, C-H bonds in silica shell improved the hydrophobicity and the adsorption of cyclohexane.

Hollow structure silicates (HTS) with large intraparticle voids were more active than TS-1 catalyst for cyclohexane oxidation reaction as reported (Shi et al., 2011). This special structure can aggravate the movement of products and reactants in and out of the channels. Zou et al. (2015b) evaluated various of HTS catalysts and found Mn-HTS gave the highest selectivity toward AA due to the nature of Mn metal (**Table 2**, #5). The stability of Mn-HTS catalysts maintained in four runs. The stability was confirmed by comparing the FT-IR and UV-Vis spectra of the fresh and recycled catalysts. This reaction proceeded via radical intermediates with Ti(IV)-O• or Ti(IV)-OO• species as active centers and Mn^{3+} as promoters. W based HTS bifunctional catalysts showed higher activity compared to H_2WO_4/TS-1 for the oxidation of cyclohexane (**Table 2**, #6) due to higher accessibility of Ti species, large intraparticle voids and the bifunctional catalytic sites (Dai et al., 2016).

Carbon nanotubes (CNTs) have been widely used as catalysts support because they are insoluble in the most solvents (Coleman et al., 2006; Moniruzzaman and Winey, 2006; Tangestaninejad et al., 2008, 2009; Moghadam et al., 2010a,b). On the other hand, CNT can create confined spaces for metals to prevent the aggregation and to act as a template for metal seed growth (Moghadam et al., 2010a). Yang et al. (2016) prepared Fe-, Ni-, and FeNi- based CNT catalysts with controllable wall

TABLE 2 | Cyclohexane, cyclohexanol, and cyclohexanone oxidation to AA.

#	Catalyst	Reaction conditions	Conversion, selectivity
1	Cu-WO_3	Cyclohexane, 70°C, 12 h, H_2O_2	X = 75%, S = 88%, TON = 119
2	Au-Al_2O_3	Cyclohexane, 180°C, 0.25 h, 3MPa, O_2	X = 2.1%, S = 18.9%
3	Au/TiO_2	Cyclohexane, 150°C, 4 h, TBHP, 1MPa, O_2	X = 25%, S = 26%, TON=237
4	AuNPs(GOS)	Cyclohexane, 150°C, 3 h, TBHP	X = 34%, S = 45.1%, TON = 59307
5	Mn-HTS	Cyclohexane, 140°C, 6 h, 1MPa, O_2	X = 8.6%, S = 57.7%, TON = 324
6	W/HTS	Cyclohexane, 90°C, 14 h, H_2O_2	X = 31.4%, S = 78.5%, TON = 31
7	Fe@CNT-100	Cyclohexane, 125°C, 8 h, 1.5MPa O_2	X = 39.7%, S = 49.7%, TON = 299
8	M-$PW_{12}O_{40}$	Cyclohexene, 100°C, 72 h, H_2O_2	X = 75%, Y = 61%
9	Al_2O_3@Fe_2O_3	Cyclohexanone, 80°C, 24 h, H_2O_2	TON = 71
10	Mn-HTS	Cyclohexanone, 90°C, 9 h, 0.6Mpa, O_2	X = 68%, S = 93%, TON = 713
11	Mn- HMTS	Cyclohexanone, 90°C, 8 h, 0.6Mpa, O_2	X = 64%, S = 94%, TON = 887
12	TS-1	Cyclohexanone, 80°C, 8 h, H_2O_2	X = 53%, S = 33%, TON = 34
13	FePO-1-2	Cyclohexanone, 75°C, 10 h, 0.1Mpa, O_2	X = 72%, S = 96%, TON = 42
14	TIPO-1	Cyclohexanone, 80°C, 8 h, H_2O_2	X = 92%, S = 66%, TON = 49
15	MnAPO-5	Cyclohexanone, 85°C,72 h, TBHP	X = 100%, S = 100%, TON = 566
16	$NH_4SnPMo_{12}O_{40}$	Cyclohexanone, 90°C, 20 h, H_2O_2	X = 100%, S = 56
17	$HNi_{1.5}PMo_{12}$	Cyclohexanone, 90°C, 20 h, H_2O_2	Y = 31%
18	$CoPMo_{12}O_{40}$	Cyclohexanone, 90°C, 20 h, H_2O_2	Y = 75.5%
19	$H_{3+x}PMo_{12-x}V_xO_{40}$	Cyclohexanone, 70°C, 12 h, 0.41MPa, air	X = 16%, S = 42%,
20	$K_6P_2Mo_6W_{12}O_{62}$	Cyclohexanol, 90°C, 20 h, H_2O_2	Y = 59%

thickness and evaluated for cyclohexane oxidation. They found that Fe@CNT showed highest catalytic performance (**Table 2**, #7) ascribing to the thin walls of CNTs and confined electron-donating metals, which will help the electron transfer on the CNTs surfaces (Yang et al., 2016). Besides, the Fe filling can enhance the electronic property of the graphene sheets. Ni@CNT has lower activity due to the weaker interaction with carbon.

POMs were reported highly active for oxidation reaction to synthesize AA with a TON values as high as 29,550 (Luo et al., 2018) The exceptional performance of POMs was possibly due to the fact that POMs played the roles of co-catalysts, active metal sites stabilizer and electronic structure regulator in the oxidation process (Banerjee et al., 2012; Tahar et al., 2015). Keggin type POMs, were the most studied type POMs for liquid phase oxidation, due to their high resistance to oxygen donors and strong oxidizing power (Wang et al., 2015; He et al., 2016; Yu et al., 2017). Pisk et al. (2019) reported Merrifield resins supported Mo- or W- based Keggin POMs as catalysts to oxidize cyclohexene to AA with 46 and 61% yield (**Table 2**, #8). They found the W based POMs are more active than Mo based catalysts. They proposed Baeyer-Villiger oxidation type of mechanism for this process (**Figure 3A**).

Cyclohexanone Oxidation to AA

Patra et al. (2013) developed a method to encapsulate γ-Al_2O_3 nanoparticles by a thin shell of α-Fe_2O_3. The resulting material showed high surface area and meso-porosity due to self-aggregation of tiny spherical nanocrystals as confirming by SEM images. These catalysts displayed low TON for the oxidation of cyclohexanone to AA in water (**Table 2**, #9), because only the surface Fe center took part in the reaction. A single layer of Fe center on the surface of the core was believed to enhance the performance of the catalysts.

Mn-HTS catalysts displayed the good performance with 68% cyclohexanone conversion, 93% AA selectivity (**Table 2**, #10) (Zou et al., 2015a). Mn-HTS, with high oxidation states, had less BrØnsted acid sites than Lewis acid sites which favored the formation of enolate from the keto-form of cyclohexanone (Zou et al., 2015a). The recycled catalysts were shown to maintain the same Mn and Ti content in about 15 cycles of reuse. They also noticed that the use of acetic acid as the co-solvent can form CH_3COOOH as oxidizing species and thus improve the reaction rate and AA selectivity. Some other groups also noticed the same phenomenon and claimed that the reaction proceed via a radical-chain autoxidation mechanism, rather than a redox mechanism in the presence of acetic acid (Shimizu et al., 2003; Cavani et al., 2011). On the other hand, acetic acid can stabilize the H_2O_2 and prevent the decomposition (Chavan et al., 2002; Shimizu et al., 2003). Gao's group prepared Mn-HMTS catalyst by a one-step hydrothermal approach with tunable textural properties (**Table 2**, #11, TON = 887) (Gao et al., 2019). They noticed that the textural and physicochemical properties of Mn-HMTS can be easily tuned by modifying the amounts of the template agent. Free-radical mechanism was proposed, since Mn species acted as a promoter for both radical intermediates and enol formation from cyclohexanone (Gao et al., 2019). Xia's group also studied TS-1 catalysts for cyclohexanone oxidation reaction by combining density function theory (DFT) calculation with experimental studies (**Table 2**, #12) (Xia et al., 2015). DFT calculations indicated that H_2O_2 molecule was absorbed and activated at the tetrahedral Ti sites.

Phosphonate based metal catalysts have immense potential to be used as ecofriendly catalysts due to the high durability and thermal stability (Zhao et al., 2006; Deng et al., 2011; Dutta et al., 2012; Mahdavi and Hasheminasab, 2015; Xiao et al., 2016; Rezaei et al., 2017). Bhanja et al. (2016) synthesized an organic-inorganic hybrid iron phosphonate materials (FePO-1-2) via a hydrothermal synthesis route. This material displayed high activity for the cyclohexanone oxidation due to the high surface acidity as well as the framework redox $Fe^{II/III}$ sites (**Table 2**, #13). They also observed that water show more remarkable

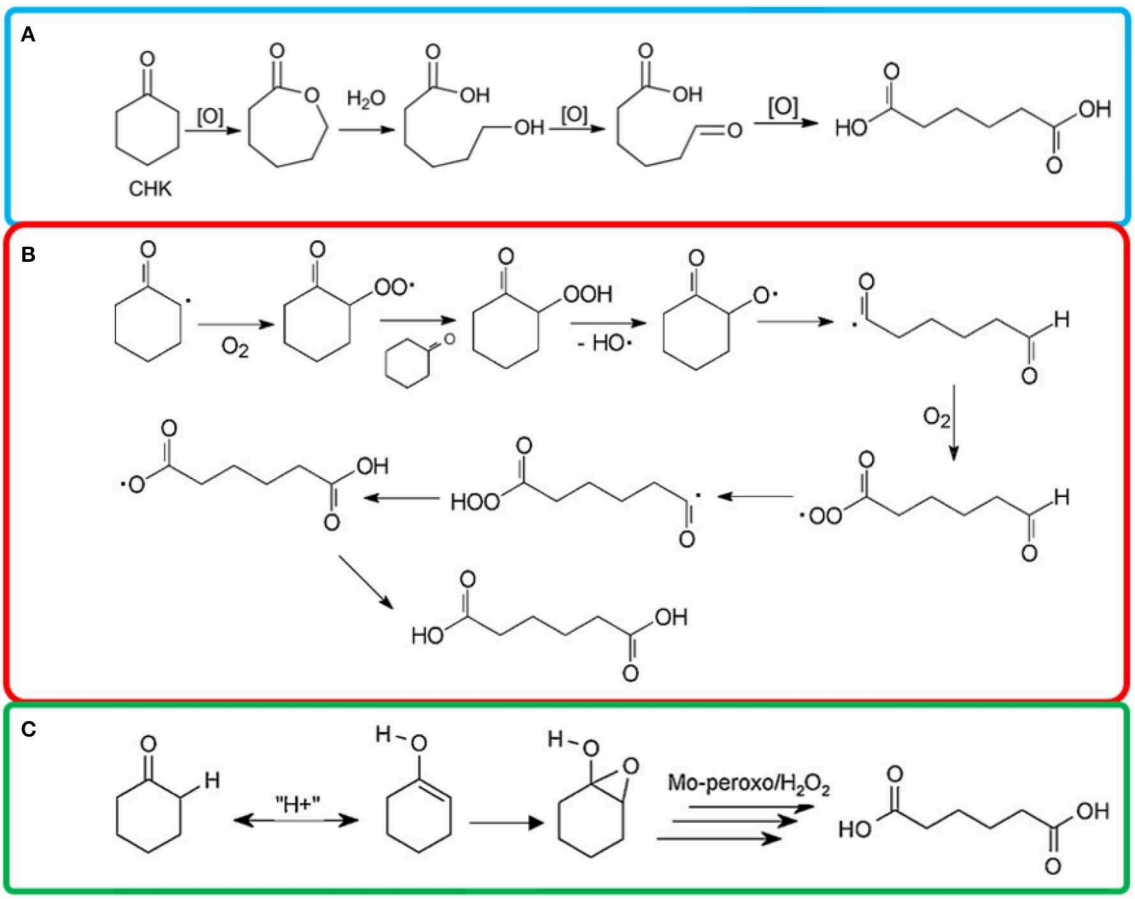

FIGURE 3 | Proposed **(A)** Baeyer-Villiger oxidation type of mechanism, (Pisk et al., 2019) **(B)** radical chain autoxidation mechanism, (Cavani et al., 2011) **(C)** redox mechanism (Amitouche et al., 2018) of cyclohexanone oxidation to AA.

promotion effect and good AA selectivity due to the higher polarity than other solvents (Bhanja et al., 2016). There was only very slight decrease of the AA yield after six consecutive reactions. The XRD results suggested there was only minor decrease in the crystallinity and BET surface area. There was no detectable Fe leaching from the catalyst. Later, the same group developed a oxyfluorinated titanium phosphate material (TIPO-1, **Table 2**, #14) (Bhanja et al., 2018). This material showed a 92% cyclohexanone conversion and 66% selectivity to AA. A Mn incorporating aluminophosphate material (MnAPO-5) was synthesized by Chatterjee's group (Chatterjee et al., 2018). A complete conversion of cyclohexanone and AA selectivity were obtained (**Table 2**, #15). The detected ε-caprolactone as intermediate by ^{1}H NMR. They proposed a reaction pathway that ε-caprolactone formed by Baeyer-Villiger oxidation and then the ring undergoes oxidative C-C bound cleavage to give AA. No leaching of Mn was detected at the end of each run.

Mouheb et al. (2018) synthesized Keggin-type POMs (**Table 2**, #16) and revealed that the active species for cyclohexanone oxidation might be the peroxo-polyoxometalates (Mouheb et al., 2018). On the other hand, more unidentified products formed when cyclohexanol was used as substrate. This catalyst can be reused at least 3 times without regeneration. Amitouche et al. (2018) synthesized Keggin heteropolyacid catalyst. They disclosed the pathways to different $H_3PMo_{12}O_{40}$ reduced state and the transformation into peroxomolybdate complexes (Amitouche et al., 2018). As shown in **Figure 3B**, the H-abstraction at the carbon next to the oxygen in cyclohexanone can be promoted in the presence of active species, and the production of radical reacted with oxygen and formed cyclohexyl hydroperoxide (Zou et al., 2015a). The ketonyl radical underwent ring opening via C–C cleavage and formed OHC–$(CH_2)_4$-C(O) radical species (Amitouche et al., 2018). The last step was oxidation that lead to the formation of AA. $H_{3-2x}Ni_xPMo_{12}O_{40}$ catalysts showed AA yield of 31% (**Table 2**, #17) (Tahar et al., 2015). The results showed that the AA yield was sensitive to the chemical composition and the x value. $H_{3-2x}Co_xPMo_{12}O_{40}$ (x: 0–1.5) catalysts were prepared using the cationic exchange method (Benadji et al., 2013). The cobalt salts were more effective than parent acid to oxidize cyclohexanone (X = 76%) and cyclohexanol (X = 53%) because the Co-based POMs acted as acidifying and oxidizing agent (**Table 2**, #18). $H_{3+x}PMo_{12-x}V_xO_{40}$ catalyzed cyclohexanone oxidation via a redox mechanism and the reoxidation of the reduced POM

was the rate-limiting step (**Table 2**, #19) (Cavani et al., 2011). However, when an acetic acid was used as additive, a radical chain autoxidation mechanism prevailed. The metal composition of the POMs affected the relative importance of the two mechanism (**Figures 3B,C**). The radical chain autoxidation mechanism was more selective to AA than the redox mechanism, because in the radical chain autoxidation mechanism there was no intermediate of partially oxidized products (lighter acids and CO_2) formed (Cavani et al., 2011).

Anderson and Dawson type POMs were also reported active for oxidation reactions. Luo et al. (2018) synthesized a POMs nanoclusters with butterfly-shaped β isomer. This catalyst displayed good activity (TON: 29,550) toward AA in solvent free condition. When cyclohexanol was used as substrate, the AA yield was lower than the cyclohexanone. The recycle ability study indicated that there was an appreciable loss of AA yield after three runs. Dawson-type POMs (P_2M_{18}) have potential to have oxidation properties since they have more elements with a high oxidation state than that of the Keggin anion (Moudjahed et al., 2016). Moudjahed et al. (2016) prepared Dawson-type POMs which showed an AA yield of 69% in the KA oil oxidation reaction (**Table 2**, #20). ^{31}P NMR spectroscopy of used POMs confirmed the formation of "peroxo-POMox" as active intermediate species.

CONCLUSION

Based on the critical review, biomass-based AA provides important and alternative routes for future development of nylon industry. At present, selective oxidation of sugars and derivatives to relevant aldaric acids is the key challenge in this area. Future work should be focused on finding more effective and inexpensive materials to achieve this chemistry. The progress and potential significance of nanostructured solid catalysts and POMs catalysts for oxidation of cyclohexane, cyclohexene, cyclohexanol and cyclohexanone to produce AA with green oxidants have been critically revised in this paper. This work summarized and discussed catalysts synthesis and structural characterization, the oxidation reaction mechanism, as well as catalyst durability. The POMs with dual redox and acidity properties display high catalytic activity and selectivity for cyclohexane/cyclohexene/cyclohexanone/cyclohexanol oxidation. Important accomplishments in this research area could be further achieved by the efficient catalyst design, and a deep understanding of both redox and radical based oxidation mechanisms.

Fundamental understanding of catalysts deactivation and oxidant utilization efficiency improvement should be the focusing efforts in the future study. The economic and environment analysis of the new green processes are needed to systematically study to see if the green processes has the potential to replace in the current industrial process. This work provides guidance for further investigation on metal nano catalysts for the efficient, green, safe, sustainable, ecofriendly and economical route of AA production and oxidation processes for many other value-added fine chemicals production.

AUTHOR CONTRIBUTIONS

WY drafted the manuscript. XJ conceived the concept of the review. GZ, JW, and ML conducted literature survey. YS, ZZ, WZ, and SZ organized figures and revised the manuscript. XX and JS provided comments.

FUNDING

This work was supported by the National Natural Science Foundation (21706290), Natural Science Foundation of Shandong Province (ZR2017BB007 and ZR2017MB004), Postdoctoral Research Funding of Shandong Province (201703016), Qingdao Postdoctoral Research Funding (BY20170210), Fundamental Research Funding of Qingdao (17-1-1-67-jch and 17-1-1-80-jch), the Fundamental Research Funds for the Central Universities (18CX02145A and 17CX02017A), and new faculty start-up funding from China University of Petroleum (YJ201601058).

REFERENCES

Acharyya, S. S., Ghosh, S., and Bal, R. (2015). Nanoclusters of Cu(II) supported on nanocrystalline W(VI) oxide: a potential catalyst for single-step conversion of cyclohexane to adipic acid. *Green Chem.* 17, 3490–3499. doi: 10.1039/C5GC00379B

Alonso, S., Rendueles, M., and Diaz, M. (2015). Microbial production of specialty organic acids from renewable and waste materials. *Crit. Rev. Biotechnol.* 35, 497–513. doi: 10.3109/07388551.2014.904269

Alshammari, A., Kalevaru, V. N., and Martin, A. (2016). Bimetallic catalysts containing gold and palladium for environmentally important reactions. *Catalysts* 6:24. doi: 10.3390/catal6070097

Alshammari, A., Koeckritz, A., Kalevaru, V. N., Bagabas, A., and Martin, A. (2012). Significant formation of adipic acid by direct oxidation of cyclohexane using supported nano-gold catalysts. *Chemcatchem* 4, 1330–1336. doi: 10.1002/cctc.201200008

Alshammari, A., Koeckritz, A., Kalevaru, V. N., Bagabas, A., and Martin, A. (2015). Potential of supported gold bimetallic catalysts for green synthesis of adipic acid from cyclohexane. *Top. Catal.* 58, 1069–1076. doi: 10.1007/s11244-015-0475-9

Amitouche, D., Haouas, M., Mazari, T., Mouanni, S., Canioni, R., Rabia, C., et al. (2018). The primary stages of polyoxomolybdate catalyzed cyclohexanone oxidation by hydrogen peroxide as investigated by *in situ* NMR. Substrate activation and evolution of the working catalyst. *Appl. Catal. A* 561, 104–116. doi: 10.1016/j.apcata.2018.05.017

Antonyraj, C. A., Huynh, N. T. T., Park, S. K., Shin, S., Kim, Y. J., Kim, S., et al. (2017). Basic anion-exchange resin (AER)-supported Au-Pd alloy nanoparticles for the oxidation of 5-hydroxymethyl-2-furfural (HMF) into 2,5-furan dicarboxylic acid (FDCA). *Appl. Catal. A* 547, 230–236. doi: 10.1016/j.apcata.2017.09.012

Asano, T., Tamura, M., Nakagawa, Y., and Tomishige, K. (2016). Selective hydrodeoxygenation of 2-furancarboxylic acid to valeric acid over molybdenum-oxide-modified platinum catalyst. *ACS Sustain. Chem. Eng.* 4, 6253–6257. doi: 10.1021/acssuschemeng.6b01640

Baig, R. B. N., and Varma, R. S. (2012). Alternative energy input: mechanochemical, microwave and ultrasound-assisted organic synthesis. *Chem. Soc. Rev.* 41, 1559–1584. doi: 10.1039/C1CS15204A

Banerjee, A., Bassil, B. S., Röschenthaler, G. V., and Kortz, U. (2012). Diphosphates and diphosphonates in polyoxometalate chemistry. *Chem. Soc. Rev.* 41, 7590–7604. doi: 10.1039/c2cs35153f

Bellardita, M., Garcia-Lopez, E. I., Marci, G., and Palmisano, L. (2016). Photocatalytic formation of H_2 and value-added chemicals in aqueous glucose (Pt)-TiO_2 suspension. *Int. J. Hydrogen Energy* 41, 5934–5947. doi: 10.1016/j.ijhydene.2016.02.103

Benadji, S., Mazari, T., Dermeche, L., Salhi, N., Cadot, E., and Rabia, C. (2013). Clean alternative for adipic acid synthesis via liquid-phase oxidation of cyclohexanone and cyclohexanol over H3-2xCoxPMo12O40 catalysts with hydrogen peroxide. *Catal. Lett.* 143, 749–755. doi: 10.1007/s10562-013-1025-3

Bhanja, P., Chatterjee, S., Patra, A. K., and Bhaumik, A. (2018). A new microporous oxyfluorinated titanium(IV) phosphate as an efficient heterogeneous catalyst for the selective oxidation of cyclohexanone. *J. Colloid Interfaces Sci.* 511, 92–100. doi: 10.1016/j.jcis.2017.09.115

Bhanja, P., Ghosh, K., Islam, S. S., Patra, A. K., Islam, S. M., and Bhaumik, A. (2016). New hybrid iron phosphonate material as an efficient catalyst for the synthesis of adipic acid in air and water. *ACS Sustain. Chem. Eng.* 4, 7147–7157. doi: 10.1021/acssuschemeng.6b02023

Boussie, T. R., Dias, E. L., Fresco, Z. M., Murphy, V. J., Shoemaker, J., Archer, R., et al. (2014). *Production of Adipic Acid and Dericatives From Carbotydrate-Containing Materials*. U.S. Patent No: US8669397B2.

Cavani, F., Ferroni, L., Frattini, A., Lucarelli, C., Mazzini, A., Raabova, K., et al. (2011). Evidence for the presence of alternative mechanisms in the oxidation of cyclohexanone to adipic acid with oxygen, catalysed by Keggin polyoxometalates. *Appl. Catal. A* 391, 118–124. doi: 10.1016/j.apcata.2010.04.032

Chatterjee, S., Bhanja, P., Paul, L., Ali, M., and Bhaumik, A. (2018). MnAPO-5 as an efficient heterogeneous catalyst for selective liquid phase partial oxidation reactions. *Dalton Trans.* 47, 791–798. doi: 10.1039/C7DT03897F

Chavan, S. A., Srinivas, D., and Ratnasamy, P. (2002). Oxidation of cyclohexane, cyclohexanone, and cyclohexanol to adipic acid by a non-HNO3 route over Co/Mn cluster complexes. *J. Catal.* 212, 39–45. doi: 10.1006/jcat.2002.3756

Chen, L., Zhou, Y., Gui, Z., Cheng, H., and Qi, Z. (2017). Au nanoparticles confined in hybrid shells of silica nanospheres for solvent-free aerobic cyclohexane oxidation. *J. Mater. Sci.* 52, 7186–7198. doi: 10.1007/s10853-017-0954-4

Cheng, C. Y., Lin, K. J., Prasad, M. R., Fu, S. J., Chang, S. Y., Shyu, S. G., et al. (2007). Synthesis of a reusable oxotungsten-containing SBA-15 mesoporous catalyst for the organic solvent-free conversion of cyclohexene to adipic acid. *Catal. Commun.* 8, 1060–1064. doi: 10.1016/j.catcom.2006.10.027

Coleman, J. N., Khan, U., Blau, W. J., and Gun'ko, Y. K. (2006). Small but strong: a review of the mechanical properties of carbon nanotube-polymer composites. *Carbon* 44, 1624–1652. doi: 10.1016/j.carbon.2006.02.038

Dai, J., Zhong, W., Yi, W., Liu, M., Mao, L., Xu, Q., et al. (2016). Bifunctional H_2WO_4/TS-1 catalysts for direct conversion of cyclohexane to adipic acid: active sites and reaction steps. *Appl. Catal. B* 192, 325–341. doi: 10.1016/j.apcatb.2016.04.005

Deng, Y., Chen, B., Wu, J., Yuan, X., and Luo, H. (2011). Effect of calcination atmosphere on the catalytic performance of MNAPO−36 molecular sieve. *Petrochem. Technol.* 40, 247–250.

Deng, Y., Ma, L., and Mao, Y. (2016). Biological production of adipic acid from renewable substrates: current and future methods. *Chem. Eng. J.* 105, 16–26. doi: 10.1016/j.bej.2015.08.015

Derrien, E., Marion, P., Pinel, C., and Besson, M. (2016). Influence of residues contained in softwood hemicellulose hydrolysates on the catalytic oxidation of glucose to glucarate in alkaline aqueous solution. *Org. Process Res. Dev.* 20, 1265–1275. doi: 10.1021/acs.oprd.6b00095

Derrien, E., Mounguengui-Diallo, M., Perret, N., Marion, P., Pinel, C., and Besson, M. (2017). Aerobic oxidation of glucose to glucaric acid under alkaline-free conditions: au-based bimetallic catalysts and the effect of residues in a hemicellulose hydrolysate. *Ind. Eng. Chem. Res.* 56, 13176–13190. doi: 10.1021/acs.iecr.7b01571

Diamond, G., Hagemeyer, A., Murphy, V., and Sokolovskii, V. (2018). Catalytic conversion of biorenewable sugar feedstocks into market chemicals. *Comb. Chem. High Throughput Screen.* 21, 616–630. doi: 10.2174/1386207322666181219155050

Dugal, M., Sankar, G., Raja, R., and Thomas, J. M. (2000). Designing a heterogeneous catalyst for the production of adipic acid by aerial oxidation of cyclohexane. *Angew. Chem. Int. Ed.* 39, 2310–2313. doi: 10.1002/1521-3773(20000703)39:13<2310::AID-ANIE2310>3.0.CO;2-G

Dutta, A., Pramanik, M., Patra, A. K., Nandi, M., Uyama, H., and Bhaumik, A. (2012). Hybrid porous tin(IV) phosphonate: an efficient catalyst for adipic acid synthesis and a very good adsorbent for CO2 uptake. *Chem. Commun.* 48, 6738–6740. doi: 10.1039/c2cc32298f

Fang, X., Li, X., Hao, Z., He, J., and Chen, D. (2013). Preparation of complex oxide WO_3-SNO_2 for catalytic synthesis of adipic acid. *Chem. World* 54, 328–331.

Feliciano Miranda, J., Cuesta Zapata, P. M., Gonzo, E. E., Parentis, M. L., Davies, L. E., and Bonini, N. A. (2018). Amorphous Cr/SiO2 materials hydrothermally treated: liquid phase cyclohexanol oxidation. *Catal. Lett.* 148, 2082–2094. doi: 10.1007/s10562-018-2422-4

Feng, J., Li, M., and Meng, X. (2019). Green oxidation of cyclohexanone to adipic acid over phosphotungstic acid encapsulated in UiO-66. *Catal. Lett.* 149, 1504–1512. doi: 10.1007/s10562-019-02764-0

Fujitani, K., Mizutani, T., Oida, T., and Kawase, T. (2009). Oxidative cleavage with hydrogen peroxide: preparation of polycarboxylic acids from cyclic olefins. *J. Oleo Sci.* 58, 37–42. doi: 10.5650/jos.58.37

Gao, T., Yin, Y., Fang, W., and Cao, Q. (2018). Highly dispersed ruthenium nanoparticles on hydroxyapatite as selective and reusable catalyst for aerobic oxidation of 5-hydroxymethylfurfural to 2, 5-furandicarboxylic acid under base-free conditions. *Mol. Catal.* 450, 55–64. doi: 10.1016/j.mcat.2018.03.006

Gao, X., Zhou, Y., Gu, J., Li, L., and Li, Y. (2019). Facile synthesis of hierarchical manganese-containing TS-1 and its application on the oxidation of cyclohexanone with molecular oxygen. *Microporous Mesoporous Mater.* 275, 263–269. doi: 10.1016/j.micromeso.2018.08.037

Gao, Z., Xie, R., Fan, G., Yang, L., and Li, F. (2017). Highly efficient and stable bimetallic aupd over la-doped ca-mg-al layered double hydroxide for base-free aerobic oxidation of 5-hydroxymethylfurfural in water. *ACS Sustain. Chem. Eng.* 5, 5852–5861. doi: 10.1021/acssuschemeng.7b00573

Gilkey, M. J., Balakumar, R., Vlachos, D. G., and Xu, B. (2018). Adipic acid production catalyzed by a combination of a solid acid and an iodide salt from biomass-derived tetrahydrofuran-2,5-dicarboxylic acid. *Catal. Sci. Technol.* 8, 2661–2671. doi: 10.1039/C8CY00379C

Gilkey, M. J., Mironenko, A. V., Vlachos, D. G., and Xu, B. (2017). Adipic acid production via metal-free selective hydrogenolysis of biomass-derived tetrahydrofuran-2,5-dicarboxylic acid. *ACS Catal.* 7, 6619–6634. doi: 10.1021/acscatal.7b01753

Gui, Z., Cao, W., Chen, L., and Qi, Z. (2015). Propene carbonate intensified cyclohexane oxidation over Au/SiO2 catalyst. *Catal. Commun.* 64, 58–61. doi: 10.1016/j.catcom.2015.02.001

Gunukula, S., and Anex, R. P. (2017). Techno-economic analysis of multiple bio-based routes to adipic acid. *Biofuel. Bioprod. Biorefin* 11, 897–907. doi: 10.1002/bbb.1797

Gupta, K., Rai, R. K., Dwivedi, A. D., and Singh, S. K. (2017a). Catalytic aerial oxidation of biomass-derived furans to furan carboxylic acids in water over bimetallic nickel-palladium alloy nanoparticles. *Chemcatchem* 9, 2760–2767. doi: 10.1002/cctc.201600942

Gupta, K., Rai, R. K., and Singh, S. K. (2017b). Catalytic aerial oxidation of 5-hydroxymethyl-2-furfural to furan-2,5-dicarboxylic acid over Ni-Pd nanoparticles supported on Mg(OH)(2) nanoflakes for the synthesis of furan diesters. *Inorg. Chem. Front.* 4, 871–880. doi: 10.1039/C7QI00026J

Han, J. (2016). A bio-based 'green' process for catalytic adipic acid production from lignocellulosic biomass using cellulose and hemicellulose derived gamma-valerolactone. *Energy Convers. Manage.* 129, 75–80. doi: 10.1016/j.enconman.2016.10.019

Han, X., Li, C., Guo, Y., Liu, X., Zhang, Y., and Wang, Y. (2016). N-doped carbon supported Pt catalyst for base-free oxidation of 5-hydroxymethylfurfural to 2,5-furandicarboxylic acid. *Appl. Catal. A* 526, 1–8. doi: 10.1016/j.apcata.2016.07.011

Hao, Z., Yang, H., He, J., and Chen, D. (2013). Preparation of WO3/SiO2 catalyst for green oxidation of cyclohexanone to adipic acid with H_2O_2. *Appl. Chem. Ind.* 42, 245–247.

He, P., Xu, B., Xu, X., Song, L., and Wang, X. (2016). Surfactant encapsulated palladium-polyoxometalates: controlled assembly and their application as single-atom catalysts. *Chem. Sci.* 7, 1011–1015. doi: 10.1039/C5SC03554F

Hereijgers, B. P. C., and Weckhuysen, B. M. (2010). Aerobic oxidation of cyclohexane by gold-based catalysts: new mechanistic insight by thorough product analysis. *J. Catal.* 270, 16–25. doi: 10.1016/j.jcat.2009.12.003

Ibert, M., Marsais, F., Merbouh, N., and Bruckner, C. (2002). Determination of the side-products formed during the nitroxide-mediated bleach oxidation of glucose to glucaric acid. *Carbohydr. Res.* 337, 1059–1063. doi: 10.1016/S0008-6215(02)00072-1

Imanaka, N., Masui, T., and Jyoko, K. (2015). Selective liquid phase oxidation of cyclohexane over Pt/CeO_2-ZrO_2-SnO_2/SiO_2 catalysts with molecular oxygen. *J. Adv. Ceram.* 4, 111–117. doi: 10.1007/s40145-015-0138-0

Indulkar, U. U., Kale, S. R., Gawande, M. B., and Jayaram, R. V. (2012). Ecofriendly and facile nano ZnO catalyzed solvent-free enamination of 1,3-dicarbonyls. *Tetrahedron Lett.* 53, 3857–3860. doi: 10.1016/j.tetlet.2012.05.048

Jin, P., Zhao, Z., Dai, Z., Wei, D., Tang, M., and Wang, X. (2011). Influence of reaction conditions on product distribution in the green oxidation of cyclohexene to adipic acid with hydrogen peroxide. *Catal. Today* 175, 619–624. doi: 10.1016/j.cattod.2011.04.041

Jin, X., Zhao, M., Shen, J., Yan, W., He, L., Thapa, P. S., et al. (2015). Exceptional performance of bimetallic Pt_1Cu_3/TiO_2 nanocatalysts for oxidation of gluconic acid and glucose with O_2 to glucaric acid. *J. Catal.* 330, 323–329. doi: 10.1016/j.jcat.2015.05.018

Jin, X., Zhao, M., Vora, M., Shen, J., Zeng, C., Yan, W., et al. (2016). Synergistic effects of bimetallic $PtPd/TiO_2$ nanocatalysts in oxidation of glucose to glucaric acid: structure dependent activity and selectivity. *Ind. Eng. Chem. Res.* 55, 2932–2945. doi: 10.1021/acs.iecr.5b04841

Kong, X., Zhu, Y., Fang, Z., Kozinski, J. A., Butler, I. S., Xu, L., et al. (2018). Catalytic conversion of 5-hydroxymethylfurfural to some value-added derivatives. *Green Chem.* 20, 3657–3682. doi: 10.1039/C8GC00234G

Kruyer, N. S., and Peralta-Yahya, P. (2017). Metabolic engineering strategies to bio-adipic acid production. *Curr. Opin. Biotechnol.* 45, 136–143. doi: 10.1016/j.copbio.2017.03.006

Lee, J., Saha, B., and Vlachos, D. G. (2016). Pt catalysts for efficient aerobic oxidation of glucose to glucaric acid in water. *Green Chem.* 18, 3815–3822. doi: 10.1039/C6GC00460A

Li, S., Deng, W., Wang, S., Wang, P., An, D., Li, Y., et al. (2018). Catalytic transformation of cellulose and its derivatives into functionalized organic acids. *Chemsuschem* 11, 1995–2028. doi: 10.1002/cssc.201800440

Li, X., Tian, Y., Li, J., Chen, D., and Li, M. (2014). Hydrothermal preparation of tungsten-based catalyst Sn-dopedfor catalytic synthesis of adipic acid. *Appl. Chem. Ind.* 43, 1050–1053.

Lin, J., Song, H., Shen, X., Wang, B., Xie, S., Deng, W., et al. (2019). Zirconia-supported rhenium oxide as an efficient catalyst for the synthesis of biomass-based adipic acid ester. *Chem. Commun.* 55, 11017–11020. doi: 10.1039/C9CC05413H

Liu, Y., Zhu, M. Q., Chen, X. Z., Jameel, U., and Lu, J. G. (2016). Coating of Au-Al_2O_3 catalyst in the wall of microcapillary and its application in cyclohexane oxidation. *J. Flow Chem.* 6, 110–116. doi: 10.1556/1846.2015.00007

Lu, X. H., Yuan, H. X., Lei, J., Zhang, J. L., Yu, A. A., Zhou, D., et al. (2012). Selective oxidation of cyclohexane to KA-oil with oxygen over active Co 3O 4 in a solvent-free system. *Indian J. Chem. Sect. A* 51, 420–427.

Luo, J., Huang, Y., Ding, B., Wang, P., Geng, X., Zhang, J., et al. (2018). Single-atom MN active site in a triol-stabilized beta-anderson manganohexamolybdate for enhanced catalytic activity towards adipic acid production. *Catalysts* 8:121. doi: 10.3390/catal8030121

Machado, K., Mishra, J., Suzuki, S., and Mishra, G. S. (2014). Synthesis of superparamagnetic carbon nanotubes immobilized Pt and Pd pincer complexes: highly active and selective catalysts towards cyclohexane oxidation with dioxygen. *Dalton Trans.* 43, 17475–17482. doi: 10.1039/C4DT02099E

Mahdavi, V., and Hasheminasab, H. R. (2015). Liquid-phase efficient oxidation of cyclohexane over cobalt promoted VPO catalyst using *tert*-butylhydroperoxide. *J. Taiwan Inst. Chem. Eng.* 51, 53–62. doi: 10.1016/j.jtice.2015.01.020

Makgwane, P. R., and Ray, S. S. (2014). Efficient room temperature oxidation of cyclohexane over highly active hetero-mixed WO_3/V_2O_5 oxide catalyst. *Catal. Commun.* 54, 118–123. doi: 10.1016/j.catcom.2014.05.031

Mazzi, A., Paul, S., Cavani, F., and Wojcieszak, R. (2018). Cyclohexane oxidation to adipic acid under green conditions: a scalable and sustainable process. *Chemcatchem* 10, 3680–3682. doi: 10.1002/cctc.201800419

Merbouh, N., Bobbitt, J. M., and Bruckner, C. (2002). 4-AcNH-TEMPO-catalyzed oxidation of aldoses to aldaric acids using chlorine or bromine as terminal oxidants. *J. Carbohydr. Chem.* 21, 65–77. doi: 10.1081/CAR-120003738

Mishra, D. K., Lee, H. J., Kim, J., Lee, H. S., Cho, J. K., Suh, Y.-W., et al. (2017). $MnCo_2O_4$ spinel supported ruthenium catalyst for air-oxidation of HMF to FDCA under aqueous phase and base-free conditions. *Green Chem.* 19, 1619–1623. doi: 10.1039/C7GC00027H

Moghadam, M., Tangestaninejad, S., Mirkhani, V., Mohammadpoor-Baltork, I., and Mirbagheri, N. S. (2010a). Molybdenum hexacarbonyl supported on functionalized multi-wall carbon nanotubes: efficient and highly reusable catalysts for epoxidation of alkenes with *tert*-butyl hydroperoxide. *J. Organomet. Chem.* 695, 2014–2021. doi: 10.1016/j.jorganchem.2010.05.008

Moghadam, M., Tangestaninejad, S., Mirkhani, V., Mohammadpoor-Baltork, I., Mirjafari, A., and Mirbagheri, N. S. (2010b). Multi-wall carbon nanotubes supported molybdenum hexacarbonyl: an efficient and highly reusable catalyst for epoxidation of alkenes with tert-butyl hydroperoxide. *J. Mol. Catal. A Chem.* 329, 44–49. doi: 10.1016/j.molcata.2010.06.016

Moniruzzaman, M., and Winey, K. I. (2006). Polymer nanocomposites containing carbon nanotubes. *Macromolecules* 39, 5194–5205. doi: 10.1021/ma060733p

Moudjahed, M., Dermeche, L., Benadji, S., Mazari, T., and Rabia, C. (2016). Dawson-type polyoxometalates as green catalysts for adipic acid synthesis. *J. Mol. Catal. A Chem.* 414, 72–77. doi: 10.1016/j.molcata.2015.12.014

Mouheb, L., Dermeche, L., Mazari, T., Benadji, S., Essayem, N., and Rabia, C. (2018). Clean adipic acid synthesis from liquid-phase oxidation of cyclohexanone and cyclohexanol using (NH4)(x)A(y)PMo(12)O(40) (A: Sb, Sn, Bi) mixed heteropolysalts and hydrogen peroxide in free solvent. *Catal. Lett.* 148, 612–620. doi: 10.1007/s10562-017-2263-6

Nale, S. D., Rathod, P. V., and Jadhav, V. H. (2017). Manganese incorporated on glucose as an efficient catalyst for the synthesis of adipic acid using molecular O_2 in aqueous medium. *Appl. Catal. A* 546, 122–125. doi: 10.1016/j.apcata.2017.08.008

Patra, A. K., Dutta, A., and Bhaumik, A. (2013). Mesoporous core-shell fenton nanocatalyst: a mild, operationally simple approach to the synthesis of adipic acid. *Chem. Eur. J.* 19, 12388–12395. doi: 10.1002/chem.201301498

Perkel, A. L., and Voronina, S. G. (2019). Liquid-phase oxidation of cyclohexane. Cyclohexyl hydroperoxide, cyclohexanol, and cyclohexanone, mechanisms of formation and transformation. *Russ. Chem. Bull.* 68, 480–492. doi: 10.1007/s11172-019-2443-1

Pisk, J., Agustin, D., and Poli, R. (2019). Organic salts and merrifield resin supported PM12O40 (3-) (M = Mo or W) as catalysts for adipic acid synthesis. *Molecules* 24:783. doi: 10.3390/molecules24040783

Polen, T., Spelberg, M., and Bott, M. (2013). Toward biotechnological production of adipic acid and precursors from biorenewables. *J. Biotechnol.* 167, 75–84. doi: 10.1016/j.jbiotec.2012.07.008

Qadir, M. I., Scholten, J. D., and Dupont, J. (2014). TiO_2 nanomaterials: highly active catalysts for the oxidation of hydrocarbons. *J. Mol. Catal. A Chem.* 383, 225–230. doi: 10.1016/j.molcata.2013.12.012

Rahman, A., Mupa, M., and Mahamadi, C. (2016). A mini review on new emerging trends for the synthesis of adipic acid from metal-nano heterogeneous catalysts. *Catal. Lett.* 146, 788–799. doi: 10.1007/s10562-015-1682-5

Rathod, P. V., and Jadhav, V. H. (2018). Efficient method for synthesis of 2,5-furandicarboxylic acid from 5-hydroxymethylfurfural and fructose using Pd/CC catalyst under aqueous conditions. *ACS Sustain. Chem. Eng.* 6, 5766–5771. doi: 10.1021/acssuschemeng.7b03124

Rezaei, M., Chermahini, A. N., and Dabbagh, H. A. (2017). Green and selective oxidation of cyclohexane over vanadium pyrophosphate supported on mesoporous KIT-6. *Chem. Eng. J.* 314, 515–525. doi: 10.1016/j.cej.2016.12.009

Ribeiro de Sousa Martins, L. M. D., Correia Carabineiro, S. A., Wang, J., Martins Rocha, B. G., Jose Maldonado-Hodar, F., and Latourrette de Oliveira Pombeiro, A. J. (2017). Supported gold nanoparticles as reusable catalysts for oxidation reactions of industrial significance. *Chemcatchem* 9, 1211–1221. doi: 10.1002/cctc.201601442

Sato, K., Aoki, M., and Noyori, R. (1998). A "green" route to adipic acid: direct oxidation of cyclohexenes with 30 percent hydrogen peroxide. *Science* 281, 1646–1647. doi: 10.1126/science.281.5383.1646

Shen, J., Chen, H., Chen, K., Qin, Y., Lu, X., Ouyang, P., et al. (2018). Atomic layer deposition of a pt-skin catalyst for base-free aerobic oxidation of 5-hydroxymethylfurfural to 2,5-furandicarboxylic acid. *Ind. Eng. Chem. Res.* 57, 2811–2818. doi: 10.1021/acs.iecr.7b05101

Shi, C., Zhu, B., Lin, M., Long, J., and Wang, R. (2011). Cyclohexane mild oxidation catalyzed by new titanosilicate with hollow structure. *Catal. Today* 175, 398–403. doi: 10.1016/j.cattod.2011.05.012

Shi, H., Thapa, P. S., Subramaniam, B., and Chaudhari, R. V. (2018). Oxidation of glucose using mono- and bimetallic catalysts under base-free conditions. *Org. Process Res. Dev.* 22, 1653–1662. doi: 10.1021/acs.oprd.8b00302

Shimizu, A., Tanaka, K., Ogawa, H., Matsuoka, Y., Fujimori, M., Nagamori, Y., et al. (2003). An industrial process for adipic acid production by the liquid-phase oxidation of cyclohexanone with molecular oxygen. *Bull. Chem. Soc. Jpn.* 76, 1993–2001. doi: 10.1246/bcsj.76.1993

Shiraishi, Y., Shiota, S., Hirakawa, H., Tanaka, S., Ichikawa, S., and Hirai, T. (2017). Titanium dioxide/reduced graphene oxide hybrid photocatalysts for efficient and selective partial oxidation of cyclohexane. *ACS Catal.* 7, 293–300. doi: 10.1021/acscatal.6b02611

Skoog, E., Shin, J. H., Saez-Jimenez, V., Mapelli, V., and Olsson, L. (2018). Biobased adipic acid - the challenge of developing the production host. *Biotechnol. Adv.* 36, 2248–2263. doi: 10.1016/j.biotechadv.2018.10.012

Smith, T. N., Hash, K., Davey, C. L., Mills, H., Williams, H., and Kiely, D. E. (2012). Modifications in the nitric acid oxidation of D-glucose. *Carbohydr. Res.* 350, 6–13. doi: 10.1016/j.carres.2011.12.024

Solmi, S., Morreale, C., Ospitali, F., Agnoli, S., and Cavani, F. (2017). Oxidation of d-glucose to glucaric acid using Au/C catalysts. *Chemcatchem* 9, 2797–2806. doi: 10.1002/cctc.201700089

Tahar, A., Benadji, S., Mazari, T., Dermeche, L., Marchal-Roch, C., and Rabia, C. (2015). Preparation, characterization and reactivity of keggin type phosphomolybdates, H_{3-2x} Ni_x $PMo_{12}O_{40}$ and $(NH_4)_{3-2x}$ Ni_x $PMo_{12}O_{40}$, for adipic acid synthesis. *Catal. Lett.* 145, 569–575. doi: 10.1007/s10562-014-1373-7

Tangestaninejad, S., Moghadam, M., Mirkhani, V., Mohammadpoor-Baltork, I., and Ghani, K. (2008). $MoO_2(acac)_2$ supported on MCM-41: an efficient and reusable catalyst for alkene epoxidation with tert-BuOOH. *J. Iran. Chem. Soc.* 5, 71–79. doi: 10.1007/BF03246492

Tangestaninejad, S., Moghadam, M., Mirkhani, V., Mohammadpoor-Baltork, I., and Ghani, K. (2009). Alkene epoxidation catalyzed by molybdenum supported on functionalized MCM-41 containing N–S chelating schiff base ligand. *Catal. Commun.* 10, 853–858. doi: 10.1016/j.catcom.2008.12.010

Unnarkat, A. P., Sridhar, T., Wang, H., Mahajani, S., and Suresh, A. K. (2016). Cobalt molybdenum oxide catalysts for selective oxidation of cyclohexane. *Aiche J.* 62, 4384–4402. doi: 10.1002/aic.15335

Vafaeezadeh, M., Hashemi, M. M., and Shakourian-Fard, M. (2012). Design of silica supported task-specific ionic liquid catalyst system for oxidation of cyclohexene to adipic acid with 30% H_2O_2. *Catal. Commun.* 26, 54–57. doi: 10.1016/j.catcom.2012.04.031

Van de Vyver, S., and Roman-Leshkov, Y. (2013). Emerging catalytic processes for the production of adipic acid. *Catal. Sci. Technol.* 3, 1465–1479. doi: 10.1039/C3CY20728E

Vardon, D. R., Franden, M. A., Johnson, C. W., Karp, E. M., Guarnieri, M. T., Linger, J. G., et al. (2015). Adipic acid production from lignin. *Energy Environ. Sci.* 8, 617–628. doi: 10.1039/C4EE03230F

Ventura, M., Lobefaro, F., de Giglio, E., Distaso, M., Nocito, F., and Dibenedetto, A. (2018). Selective aerobic oxidation of 5-hydroxymethylfurfural to 2,5-diformylfuran or 2-formyl-5-furancarboxylic acid in water by using MgO center dot CeO_2 mixed oxides as catalysts. *Chemsuschem* 11, 1305–1315. doi: 10.1002/cssc.201800334

Wang, B., Zhang, Z., Zhang, X., Sun, S., Wu, L., and Xing, R. (2018). Efficient and convenient oxidation of cyclohexene to adipic acid with H_2O_2 catalyzed by H_2WO_4 in acidic ionic liquids. *Chem. Pap.* 72, 643–649. doi: 10.1007/s11696-017-0303-8

Wang, L., Chen, Z., Huang, M., Yang, Z., Sun, P., Wang, K., et al. (2016). A green route to cyclohexanone: selective oxidation of cyclohexanol promoted by non-precious catalyst of h-WO_3 nanorods. *Catal. Lett.* 146, 1283–1290. doi: 10.1007/s10562-016-1751-4

Wang, X., Zhang, X., He, X., Ma, A., Le, L., and Lin, S. (2015). Facile electrodeposition of flower-like PMo_{12}-Pt/rGO composite with enhanced electrocatalytic activity towards methanol oxidation. *Catalysts* 5, 1275–1288. doi: 10.3390/catal5031275

Wei, L., Zhang, J., Deng, W., Xie, S., Zhang, Q., and Wang, Y. (2019). Catalytic transformation of 2,5-furandicarboxylic acid to adipic acid over niobic acid-supported Pt nanoparticles. *Chem. Commun.* 55, 8013–8016. doi: 10.1039/C9CC02877C

Wojcieszak, R., Cuccovia, I. M., Silva, M. A., and Rossi, L. M. (2016). Selective oxidation of glucose to glucuronic acid by cesium-promoted gold nanoparticle catalyst. *J. Mol. Catal. A Chem.* 422, 35–42. doi: 10.1016/j.molcata.2016.02.008

Xia, C., Ju, L., Zhao, Y., Xu, H., Zhu, B., Gao, F., et al. (2015). Heterogeneous oxidation of cyclohexanone catalyzed by TS-1: combined experimental and DFT studies. *Chinese J. Catal.* 36, 845–854. doi: 10.1016/S1872-2067(15)60859-2

Xia, C., Zhao, Y., Zhu, B., Lin, M., Peng, X., Dai, Z., et al. (2018). Environmentally-friendly catalytic oxidation of cyclohexanone with 30% H2O2 solution: a comparison study between hollow titanium silicate and dealuminated HBEA zeolites. *China Pet. Process. Petrochem. Technol.* 20, 8–19.

Xiao, Z., Zhan, W., Guo, Y., Guo, Y., Gong, X., and Lu, G. (2016). The synthesis of Co-doped SAPO-5 molecular sieve and its performance in the oxidation of cyclohexane with molecular oxygen. *Chinese J. Catal.* 37, 273–280. doi: 10.1016/S1872-2067(15)61014-2

Yang, B., Leclercq, L., Schmitt, V., Pera-Titus, M., and Nardello-Rataj, V. (2019). Colloidal tectonics for tandem synergistic pickering interfacial catalysis: oxidative cleavage of cyclohexene oxide into adipic acid. *Chem. Sci.* 10, 501–507. doi: 10.1039/C8SC03345E

Yang, D., Wu, T., Chen, C., Guo, W., Liu, H., and Han, B. (2017). The highly selective aerobic oxidation of cyclohexane to cyclohexanone and cyclohexanol over V_2O_5@TiO_2 under simulated solar light irradiation. *Green Chem.* 19, 311–318. doi: 10.1039/C6GC02748B

Yang, J., Lu, Y., Zhao, Y., Bai, Z., Ma, Z., and Deng, Y. (2019). Site-directed mutation to improve the enzymatic activity of 5-carboxy-2-pentenoyl-CoA reductase for enhancing adipic acid biosynthesis. *Enzyme Microb. Technol.* 125, 6–12. doi: 10.1016/j.enzmictec.2019.02.006

Yang, X., Li, Y., Yu, H., Gui, X., Wang, H., Huang, H., et al. (2016). Enhanced catalytic activity of carbon nanotubes for the oxidation of cyclohexane by filling with Fe, Ni, and FeNi alloy Nanowires. *Aust. J. Chem.* 69, 689–695. doi: 10.1071/CH15516

Yu, H., Ru, S., Dai, G., Zhai, Y., Lin, H., Han, S., et al. (2017). An efficient Iron(III)-catalyzed aerobic oxidation of aldehydes in water for the green preparation of carboxylic acids. *Angew. Chem. Int. Ed.* 56, 3867–3871. doi: 10.1002/anie.201612225

Zhang, F., Yang, H., He, J., and Chen, D. (2013). Preparation of lanthanum modified solid catalyst SnO2 - WO3/La2O3 and its catalytic performance for synthesis of adipic acid. *J. Chinese Rare Earth Soc.* 34, 46–49. doi: 10.16533/j.cnki.15-1099/tf.2013.04.018

Zhang, J., Li, J., Tang, Y., Lin, L., and Long, M. (2015). Advances in catalytic production of bio-based polyester monomer 2,5-furandicarboxylic acid derived from lignocellulosic biomass. *Carbohydr. Polym.* 130, 420–428. doi: 10.1016/j.carbpol.2015.05.028

Zhang, S., Sun, X., Zheng, Z., and Zhang, L. (2018). Nanoscale center-hollowed hexagon MnCo2O4 spinet catalyzed aerobic oxidation of 5-hydroxymethylfurfural to 2,5-furandicarboxylic acid. *Catal. Commun.* 113, 19–22. doi: 10.1016/j.catcom.2018.05.004

Zhang, Z., and Deng, K. (2015). Recent advances in the catalytic synthesis of 2,5-furandicarboxylic acid and its derivatives. *ACS Catal.* 5, 6529–6544. doi: 10.1021/acscatal.5b01491

Zhang, Z., and Huber, G. W. (2018). Catalytic oxidation of carbohydrates into organic acids and furan chemicals. *Chem. Soc. Rev.* 47, 1351–1390. doi: 10.1039/C7CS00213K

Zhao, R., Wang, Y. Q., Guo, Y. L., Guo, Y., Liu, X. H., Zhang, Z. G., et al. (2006). A novel Ce/AlPO-5 catalyst for solvent-free liquid phase oxidation of cyclohexane by oxygen. *Green Chem.* 8, 459–466. doi: 10.1039/b517656e

Zhou, J. D., Cao, F., Yu, Z. L., Wen, B. B., Cui, L. Y., Tang, Z. Q., et al. (2016). Research progress in preparation and application of bio-based 2,5-furandicarboxylic acid as polyester monomer. *Acta Polym. Sin.* 1, 1–13. doi: 10.11777/jissn1000-3304.2016.15142

Zou, G., Zhong, W., Mao, L., Xu, Q., Xiao, J., Yin, D., et al. (2015a). A non-nitric acid method of adipic acid synthesis: organic solvent- and promoter-free oxidation of cyclohexanone with oxygen over hollow-structured Mn/TS-1 catalysts. *Green Chem.* 17, 1884–1892. doi: 10.1039/C4GC02333A

Zou, G., Zhong, W., Xu, Q., Xiao, J., Liu, C., Li, Y., et al. (2015b). Oxidation of cyclohexane to adipic acid catalyzed by Mn-doped titanosilicate with hollow structure. *Catal. Commun.* 58, 46–52. doi: 10.1016/j.catcom.2014.08.026

Conflict of Interest: XX was employed by the company Huabei Oil Field Company at PetroChina.

The remaining authors declare that the research was conducted in the absence of any commercial or financial relationships that could be construed as a potential conflict of interest.

frontiers in Chemistry

REVIEW
published: 21 April 2020
doi: 10.3389/fchem.2020.00221

Recent Advances in Ruthenium-Catalyzed Hydrogenation Reactions of Renewable Biomass-Derived Levulinic Acid in Aqueous Media

*Aristeidis Seretis, Perikleia Diamantopoulou, Ioanna Thanou, Panagiotis Tzevelekidis, Christos Fakas, Panagiotis Lilas and Georgios Papadogianakis**

Industrial Chemistry Laboratory, Department of Chemistry, National and Kapodistrian University of Athens, Athens, Greece

OPEN ACCESS

Edited by:
Manoj B. Gawande, Palacky University Olomouc, Czechia

Reviewed by:
Benjaram M. Reddy, Indian Institute of Chemical Technology (CSIR), India
Anna Maria Raspolli Galletti, University of Pisa, Italy

***Correspondence:**
Georgios Papadogianakis
papadogianakis@chem.uoa.gr

Specialty section:
This article was submitted to Green and Sustainable Chemistry, a section of the journal Frontiers in Chemistry

Received: *04 February 2020*
Accepted: *09 March 2020*
Published: *21 April 2020*

Citation:
Seretis A, Diamantopoulou P, Thanou I, Tzevelekidis P, Fakas C, Lilas P and Papadogianakis G (2020) Recent Advances in Ruthenium-Catalyzed Hydrogenation Reactions of Renewable Biomass-Derived Levulinic Acid in Aqueous Media. Front. Chem. 8:221. doi: 10.3389/fchem.2020.00221

Levulinic acid (LA) is classified as a key platform chemical for the development of future biorefineries, owing to its broad spectrum of potential applications and because it is simply available from lignocellulosic biomass through inexpensive and high-yield production routes. Catalytic hydrogenation reactions of LA into the pivotal intermediate compound γ-valerolactone (GVL), and beyond GVL to yield valeric acid (VA), 1,4-pentanediol (1,4-PDO), and 2-methyltetrahydrofuran (2-MTHF) have gained considerable attention in the last decade. Among the various transition metals used as catalysts in LA hydrogenation reactions, ruthenium-based catalytic systems have been the most extensively applied by far, due to the inherent ability of ruthenium under mild conditions to hydrogenate the keto functionality of LA selectively into an alcohol group to form 4-hydroxyvaleric acid intermediate, which yields GVL spontaneously after dehydration and cyclization. This review focuses on recent advances in the field of aqueous-phase ruthenium-catalyzed hydrogenation reactions of LA toward GVL, VA, 1,4-PDO, 2-MTHF, 2-pentanol, and 2-butanol. It employs heterogeneous catalysts on solid supports, and heterogeneous water-dispersible catalytic nanoparticles or homogeneous water-soluble catalytic complexes with biphasic catalyst separation, for the *inter alia* production of advanced biofuels such as valeric biofuels and other classes of liquid transportation biofuels, value-added fine chemicals, solvents, additives to gasoline, and to food as well. The significance of the aqueous solvent to carry out catalytic hydrogenations of LA has been highlighted because the presence of water combines several advantages: (i) it is highly polar and thus an ideal medium to convert polar and hydrophilic substrates such as LA; (ii) water is involved as a byproduct; (iii) the presence of the aqueous solvent has a beneficial effect and enormously boosts hydrogenation rates. In sharp contrast, the use of various organic solvents gives rise to a dramatic drop in catalytic activities. The promotional effect of water was proven by numerous experimental investigations and several theoretical studies employing various

types of catalytic systems; (iv) the large heat capacity of water renders it an excellent medium to perform large scale exothermic hydrogenations more safely and selectively; and (v) water is a non-toxic, safe, non-inflammable, abundantly available, ubiquitous, inexpensive, and green/sustainable solvent.

Keywords: hydrogenation, renewable, platform chemical, levulinic acid, γ-valerolactone, water, biofuels, biorefinery

INTRODUCTION

Currently, renewable biomass as a raw material is considered to be the grand challenge in the development of Green-Sustainable chemistry which decisively contributes to the transition from a fossil-based society to a bio-resources based economy. Biomass possesses a high potential as a raw material that sustainable biorefineries can use to manufacture biofuels, bio-based chemicals, solvents, materials, energy, power, pharmaceuticals, and food. The use of biomass as an industrial feedstock also combines environmental benefits because it mitigates local air pollution and the global warming problems caused by greenhouse gas emissions. Moreover, the use of biomass is associated with further economic, environmental, social, health and safety benefits which are based, *inter alia*, on the renewable nature of biomass, contrasted to the nature of fossil raw materials which possess a limited capacity in the domestic production of biofuels, and thus on the country's independence from fossil feedstocks, on the profits of local agriculture, on the implementations of financial incentives, and on biodegradability and biocompatibility, as well as on the mechanical and physicochemical properties of biomass-based products. The high potential of biomass is even more remarkable when one considers that the nature's global biomass production capacity is huge, namely about $2.0 \cdot 10^{11}$ t/a compared to only $7 \cdot 10^{9}$ t/a of all extracted fossil fuels, and furthermore that only 3.3% of the annual biomass production capacity is used for food, feed, and non-food applications (Van Bekkum and Gallezot, 2004; Sheldon, 2014; Li et al., 2018; Badgujar et al., 2020). Biomass consists of about 75% carbohydrates, 20% lignin, and 5% triglycerides, i.e., fats and oils, terpenes and proteins (Sheldon, 2014). Storage carbohydrates include the polysaccharides starch and inulin and the disaccharide sucrose. However, the most abundant biomass is lignocellulose, the constituent of plant cell walls, which is not edible and therefore without competition in food and consists of 40–50% cellulose, 25–35% hemicellulose, and 15–20% lignin (Climent et al., 2014). Cellulose is a linear biopolymer consisting entirely of glucose units linked by β-1,4-glycosidic bonds. The presence of extensive hydrogen bonding of both types inter- and intra-chain bonds imparts crystallinity to cellulose and strength to the structure of the plant, which makes cellulose recalcitrant to chemical or enzymatic hydrolysis. Cellulose is the organic compound with the largest capacity in the world. Hemicellulose is an amorphous branched biopolymer composed of C_5 and C_6 sugars with the major compound being xylose. Lignin is a cross-linked polyphenolic amorphous biopolymer surrounding hemicellulose and cellulose. The rigidity and complexity of the lignin structure gives recalcitrance to the cell walls of the plant, which makes difficult the pretreatment of lignocellulosic biomass for the liberation of cellulose and hemicellulose to be applied as feedstocks for the production of fuels, platform chemicals and materials.

One of the most promising platform chemicals obtained from lignocellulose is levulinic acid (LA, **Figure 1**), which was selected by the US Department of Energy (DOE) as one of the top twelve platform chemicals according to its report released in 2004 (Werpy and Petersen, 2004), as well as to the updated, revised and extended DOE's report in 2010 (Bozell and Petersen, 2010). LA is classified as a key platform chemical for the development of future biorefineries because of its broad spectrum of potential applications and because it is simply available with inexpensive and high yield production routes from lignocellulose biomass (Tang et al., 2014; Ye et al., 2020). The first industrial continuous process for the production of LA was developed by BioMetics Inc. in the earlies 1990's, which was well-known as the Biofine process, and proceeds in a proprietary two-reactor system using lignocellulose biomass as feedstock together with a sulfuric acid solution as a reagent. After the deconstruction of lignocellulose, sulfuric acid-catalyzed hydrolysis of cellulose and hemicellulose to yield C_6 and C_5 carbohydrates such as glucose and xylose takes place in the first reactor (**Figure 1**). Glucose is further isomerized into fructose and after dehydration of fructose the 5-hydroxymethylfurfural intermediate (HMF, **Figure 1**) is obtained under conditions to minimize polymerization side reactions, which yield undesired insoluble side products called humins. HMF is continuously removed and subsequently introduced as feedstock in the second reactor where, after hydration reactions, LA is produced with formic acid (**Figure 1**). The solid humins are separated from the solution of levulinic acid and burnt to generate heat and electricity for the process. From dehydration reactions of C_5 carbohydrates e.g., xylose, furfural is produced. This is separately collected and acts as an intermediate after hydrogenation to furfuryl alcohol and hydration to also produce LA (**Figure 1**). The route of hemicellulose to LA possesses the advantage of milder acidic conditions and therefore of lower formation of undesired humins, because of the easier hydrolysis step of amorphous hemicellulose into C_5 and C_6 carbohydrates compared to the hydrolysis step of crystalline and recalcitrant cellulose into glucose intermediate, which is further isomerized into fructose and in the acid-catalyzed dehydration step to HMF unavoidable higher amounts of humins are obtained. The process engineering of Biofine was revised and redesigned by the GFBiochemicals company, which developed an acid catalyzed

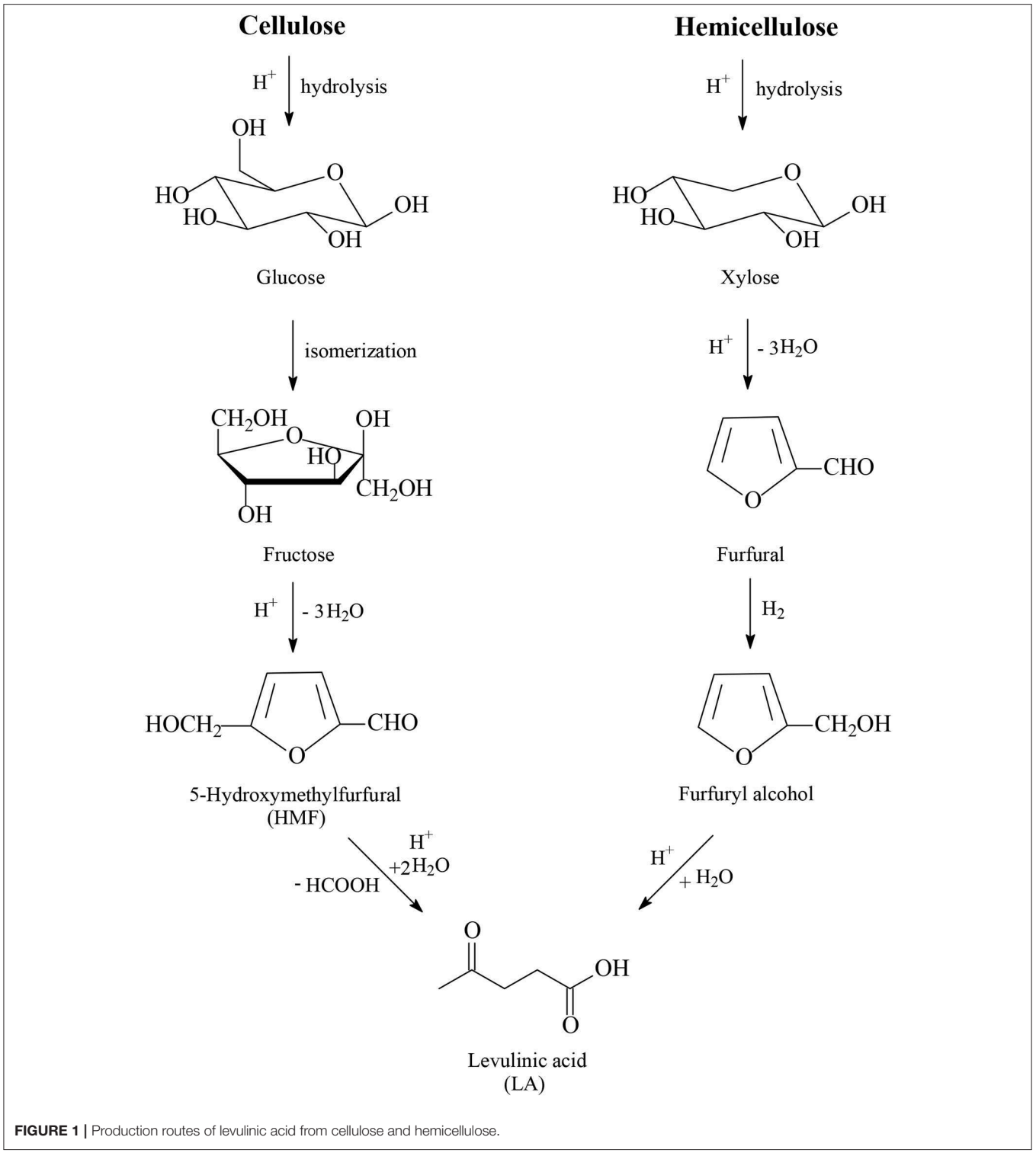

FIGURE 1 | Production routes of levulinic acid from cellulose and hemicellulose.

industrial process (Atlas Technology™) for the manufacture of LA from lignocellulose biomass with a production capacity of 10,000 t/a. Several other industrial companies produce LA worldwide using lignocellulosic biomass as feedstock (Huber et al., 2006; Bozell and Petersen, 2010; Serrano-Ruiz et al., 2012; Bond et al., 2014; Climent et al., 2014; Leitner et al., 2017; Makhubela and Darkwa, 2018; Home page of GFBiochemicals company., 2019).

Among the various routes for the valorization of LA, the catalytic hydrogenation route has been considered as an important pathway that is gaining more interest in recent years because of the wide range of potential applications of

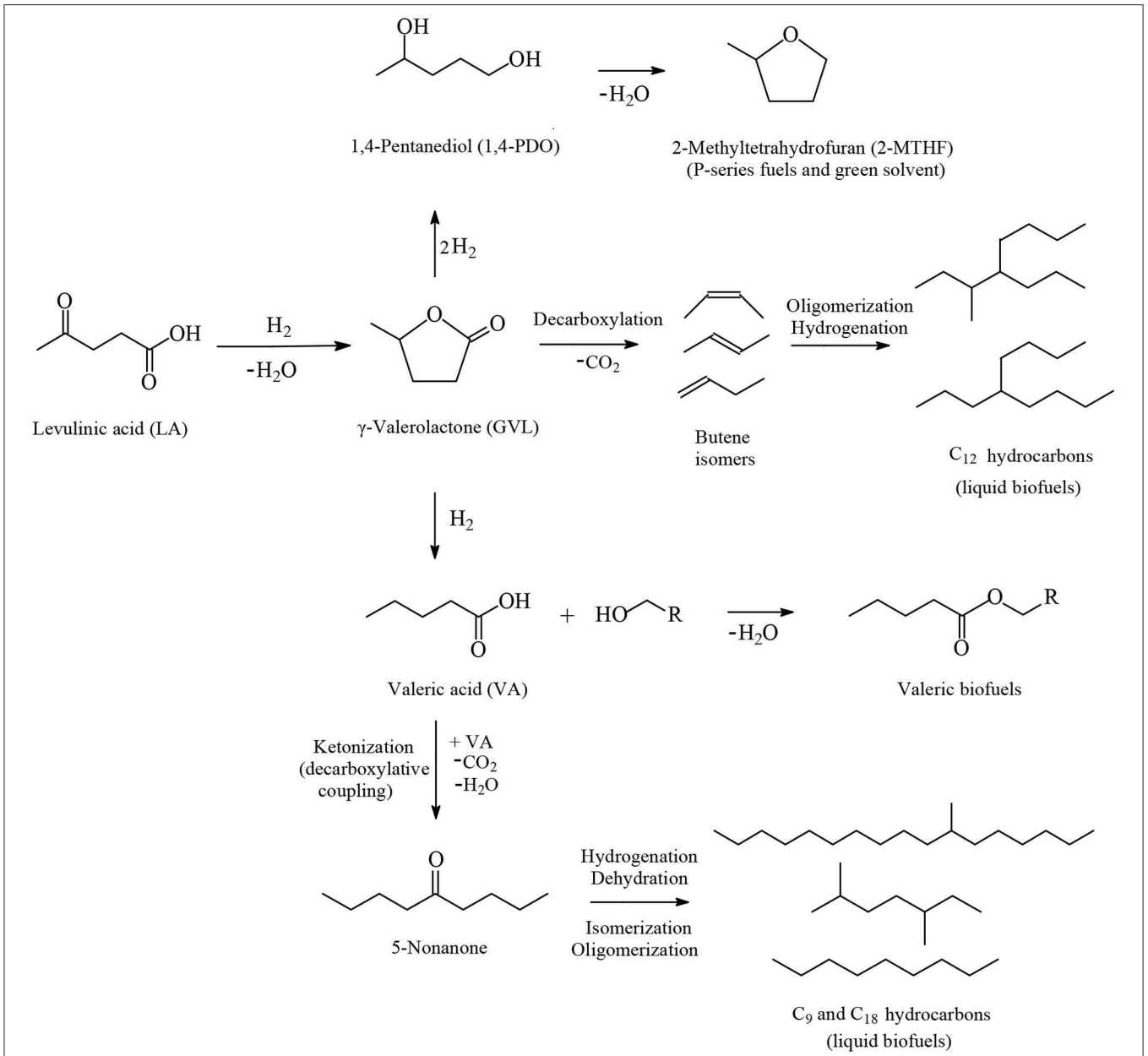

FIGURE 2 | Routes based on the catalytic hydrogenation of LA to obtain advanced biofuels, chemicals and solvents.

the LA's hydrogenation products, which include, *inter alia*, advanced biofuels such as valeric biofuels and other classes of liquid transportation biofuels, fine chemicals, solvents, additives to gasoline as well as additives to food. In the last decade, the hydrogenation reactions of LA into γ-valerolactone (GVL, **Figure 2**), which is a key intermediate compound, and beyond GVL to yield 1,4-pentanediol (1,4-PDO, **Figure 2**) and valeric acid (VA, **Figure 2**), have gained considerable attention. Numerous heterogeneous catalytic systems based on precious and non-noble metals and water-soluble transition metal catalytic complexes have been developed in the absence and presence of organic or aqueous solvents (Serrano-Ruiz et al., 2011, 2012; Tang et al., 2014; Yan et al., 2015a,b; Omoruyi et al., 2016; Pileidis and Titirici, 2016; Osatiashtiani et al., 2017; Makhubela and Darkwa, 2018; Xue et al., 2018; Dutta et al., 2019; Yu et al., 2019; Ye et al., 2020). The catalytic hydrogenation reaction of LA in the aqueous solvent is a more attractive and promising processing mode because the use of water combines several advantages: (i) the highly polar nature of the aqueous solvent makes it an ideal medium to convert polar, with high oxygen content, and hydrophilic platform chemicals such as the water-soluble starting material LA; (ii) water is involved as a byproduct to obtain the GVL intermediate, which is further hydrogenated into 1,4-PDO in the aqueous medium and, after

dehydration and cyclization reactions 2-methyltetrahydrofuran (2-MTHF, **Figure 2**), is formed creating an aqueous/organic two-phase system which provides for the easy separation of the polar aqueous reaction medium from a polar organic product 2-MTHF by a simple phase separation. The same procedure could also be applied in the aqueous/organic biphasic system created with alkyl valerates obtained from LA hydrogenation product valeric acid (VA, **Figure 2**) after esterification with alcohols. This biphasic processing mode results in substantial energy savings, lower emissions and economic benefits; (iii) novel types of catalytic reactivities have been observed in water: in the hydrogenation reaction of LA into GVL, and beyond in the aqueous solvent employing conventional heterogeneous catalytic systems, catalytic nanoparticles, and water-soluble transition metal catalytic complexes, the presence of water has a beneficial effect and accelerates reaction rates, whereas in organic solvents much lower activities were observed. This promotional effect of water in the hydrogenation reaction of LA was proved by several experimental and theoretical studies using various types of catalytic systems; (iv) the large heat capacity of water makes it an excellent medium to perform exothermic reactions, such as the catalytic hydrogenation reaction of LA, more safely and selectively—which is especially important in large scale industrially-applied catalytic hydrogenation processes of LA; (v) water is a non-toxic, non-inflammable, abundantly available, inexpensive, ubiquitous, green and sustainable solvent.

In the LA hydrogenation reaction, ruthenium-based catalytic systems have been by far more extensively applied by than their catalytic counterparts based on other transition metals. This is because of the inherent and unique ability of ruthenium under mild reaction conditions to effectively hydrogenate the keto moiety of LA into an alcohol functionality to form the 4-hydroxyvaleric acid intermediate which spontaneously after dehydration and cyclization yields GVL. This review focuses on recent advances in the field of aqueous-phase ruthenium-catalyzed hydrogenation reactions of LA into GVL and beyond, to obtain VA, 1,4-PDO and 2-MTHF as well as 2-pentanol and 2-butanol employing heterogeneous catalytic systems on solid supports, heterogeneous water-dispersible catalytic nanoparticles and homogeneous water-soluble catalytic complexes for the production, *inter alia*, of advanced biofuels such as valeric biofuels and other classes of liquid transportation biofuels, value-added fine chemicals, solvents, additives to gasoline and to food as well. The significance of the aqueous solvent in such catalytic hydrogenation reactions has been also highlighted.

HYDROGENATION OF LA INTO VALUE-ADDED CHEMICALS AND ADVANCED BIOFUELS

The catalytic hydrogenation reaction of LA yields GVL (**Figure 2**), which is an important C_5 platform chemical and pivotal intermediate compound for the efficient conversion of LA to advanced biofuels of various classes, chemicals and solvents by several different routes as depicted in **Figure 2**. GVL is also used as an aprotic, polar, and sustainable solvent, as an additive to gasoline and suitable for use as a food additive. Hydrogenation and ring-opening reactions of GVL afford 1,4-PDO and VA intermediates (**Figure 2**). 1,4-PDO tends to undergo dehydration and cyclization reactions to yield 2-methyltetrahydrofuran (2-MTHF, **Figure 2**) which is considered as a green solvent (Yan et al., 2010, 2015a,b; Serrano-Ruiz et al., 2012) with a polarity placed between tetrahydrofuran and diethyl ether possessing, however, a potential to form explosive peroxides under air (Aycock, 2007; Fábos et al., 2009; Byrne et al., 2017). 2-MTHF is one of the three components of an alternative type of fuel, namely P-series fuels, that are approved by DOE as fuels that can substitute gasoline. Furthermore, 2-MTHF could be blended up to 70% in conventional gasoline fuels (Yan et al., 2010, 2015a,b; Serrano-Ruiz et al., 2012). Esterification reactions of VA with alcohols produce alkyl valerate advanced biofuels well-known as valeric biofuels, which are suitable to be blended with gasoline or diesel fuels depending on the length of the alkyl chain of added alcohol (**Figure 2**). When shorter chain alcohols such as methanol and ethanol are used in the esterification of VA the methyl and ethyl valerate products are suitable as gasoline fuel, whereas with longer chain alcohols such as butanol and pentanol, the butyl and pentyl valerates are more appropriate as diesel fuel with excellent energy density as well as volatility and ignition properties (Lange et al., 2010; Yan et al., 2010, 2015a,b; Serrano-Ruiz et al., 2012). VA could alternatively be used as starting material in decarboxylative coupling reactions i.e., ketonization reactions to produce 5-nonanone, which is an interesting platform to be applied as starting material in hydrogenation, dehydration, isomerization, and oligomerization reactions for the manufacture of C_9 and C_{18} linear and branched hydrocarbons which are gasoline, diesel, and jet biofuels (**Figure 2**) (Serrano-Ruiz et al., 2012; Simakova and Murzin, 2016). Another route for the production of jet biofuels is based on GVL, which in the first step undergoes decarboxylation into butenes, followed by oligomerization to form higher alkenes which after hydrogenation are suitable as aviation biofuels (**Figure 2**) (Bond et al., 2010, 2014).

Hydrogenation of LA Into GVL

GVL is a water-soluble, non-toxic liquid that is stable at neutral pH in aqueous solvent and air without any formation of a measurable amount of peroxides when in a glass flask exposed to the air for several weeks, making it safe for industrial scale use. Furthermore, GVL does not form an azeotropic mixture with the aqueous solvent and therefore the manufacture of GVL constitutes a less energy demanding process compared to that for the production of absolute ethanol. Two possible reaction pathways were proposed for the synthesis of GVL from LA which are shown in **Figure 3**. According to the first pathway the keto functionality of LA is hydrogenated probably by heterolytic H_2 cleavage into an alcohol group to form the 4-hydroxyvaleric acid intermediate, which then readily undergoes dehydration to give, by favorable intramolecular esterification, the cyclic ester product GVL (**Figures 3**, **4**). The heterolytic dihydrogen cleavage mechanism may be facilitated by heterogenous catalytic systems comprising a transition metal and an oxide as support, such as Ru/TiO_2, Ru/Al_2O_3, by the interaction between the metal with the support in the way

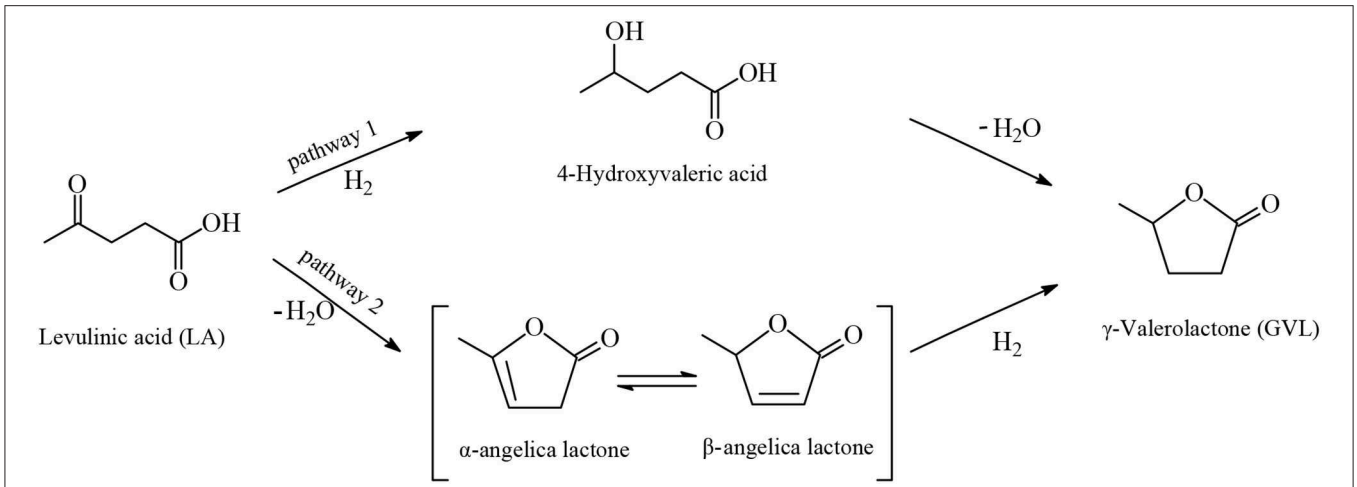

FIGURE 3 | Possible reaction mechanisms for the synthesis of GVL from LA.

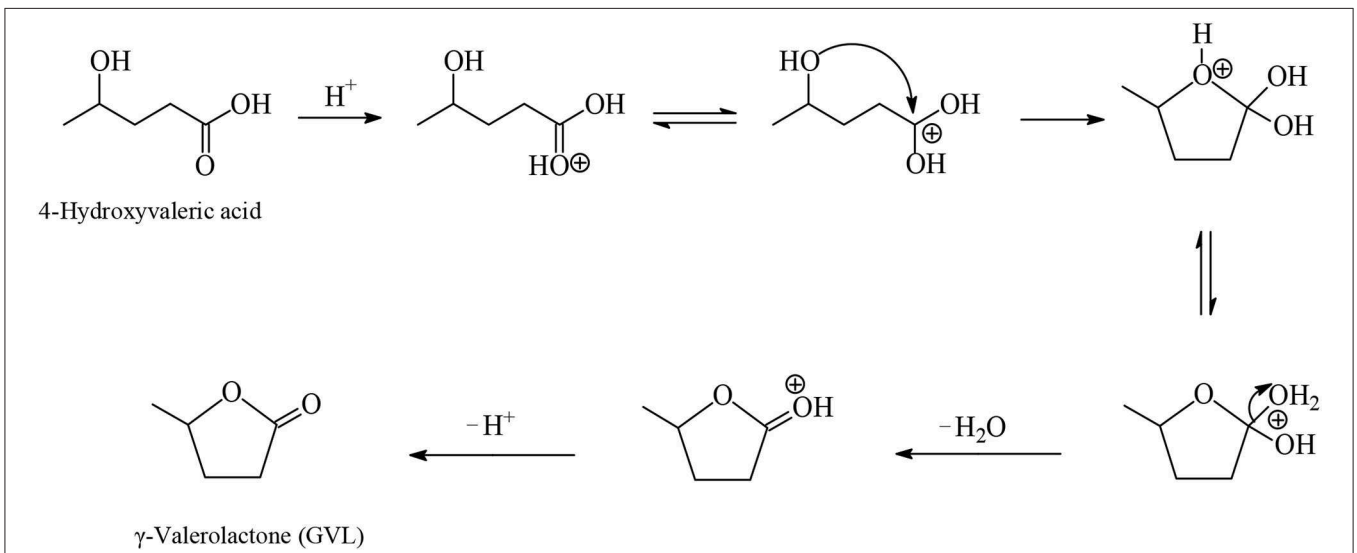

FIGURE 4 | Proposed mechanism for the dehydration of 4-hydroxyvaleric acid intermediate to yield by intramolecular esterification GVL (Ruppert et al., 2015).

that on the surface of transition metal is formed the H^- moiety of dihydrogen and on the oxygen atom of the support the H^+ moiety (Kubas, 2005). The second possible pathway of **Figure 3** involves acid-catalyzed endothermic dehydration of LA at reaction temperatures higher than 180°C to form α-angelica lactone by intramolecular esterification, which is subsequently hydrogenated to yield GVL. In both mechanisms depicted in **Figure 3** the hydrogenation steps are influenced by the nature and activity of the transition metal of the catalysts, whereas the dehydration steps depend on the acidity of the catalysts and of the medium. At elevated temperatures and/or in the presence of acidic heterogeneous catalytic systems the dehydration reaction of LA is promoted to give α-angelica lactone, which easily polymerizes on acidic surfaces to form coke, resulting in a severe deactivation of the heterogeneous catalytic system.

Heterogeneous Catalysts on Solid Supports

Numerous heterogeneous ruthenium-based catalytic systems have been successfully applied in the hydrogenation reaction of LA into GVL usually employing relatively more forcing conditions, i.e., higher temperatures and dihydrogen pressures in aqueous media. The use of heterogeneous catalysts combines the easy catalyst separation from reaction products and catalyst recycling with the possibility to operate easily in a continuous process.

Tan et al. (2015) synthesized ruthenium-supported catalysts with low 0.5 wt.%, moderate 1 wt.% and higher 2 wt.% ruthenium loading on various oxides such as Al_2O_3, SiO_2, ZrO_2, and TiO_2 and investigated their catalytic activity and selectivity on the hydrogenation reaction of LA into GVL at molar ratios of LA/Ru between 8,707 and 2,177, reaction temperatures of 130 and 70°C under 40 bar of dihydrogen

pressure in aqueous and organic media. With a higher ruthenium loading of 2 wt.% all supported catalysts at 130°C exhibited a TOF value of 4,353 per hour with quantitative conversions of LA. At a low ruthenium loading of 0.5 wt.% the Ru/TiO_2 catalytic system exhibited at 130°C within 3 h reaction time the highest catalytic activity of TOF = 2,769 h^{-1} with a conversion of LA of 95.4 mol%, compared with the other ruthenium-supported catalysts under the same conditions which have shown lower activities with e.g., 0.5 wt.% Ru/Al_2O_3 the catalytic activity has been dropped down to 401 TOF's per hour and the conversion of LA to 13.8 mol% (**Table 1**). A much higher catalytic activity of TOF = 7,662 h^{-1} has been obtained with Ru/TiO_2 catalysts with a moderate ruthenium loading of 1 wt.% even at a lower temperature of 70°C within a 15 min reaction time in the aqueous solvent. The higher catalytic activity of Ru/TiO_2 could be explained by both the small size of ruthenium nanoparticles and the better dispersion of the metal on the support, which was proven by TEM analysis in showing average size of ruthenium nanoparticles on the TiO_2 support were smaller, namely 2.0 nm, and more uniform compared with their counterparts on the ZrO_2 support. Furthermore, the nature of the support plays a crucial role in the heterogeneously ruthenium-catalyzed LA hydrogenation reaction, because the support activates the C=O functionality of LA and ruthenium nanoparticles dissociates dihydrogen. It is highly probable that a strong interaction between small ruthenium particles and TiO_2 support takes place which, after activation of the carbonyl moiety on TiO_2, generates highly active sites on the coordination sphere of the metal by catalytic relevant ruthenium species for efficient H_2 dissociation. With all ruthenium-supported catalysts under various reaction conditions in aqueous medium, the only product obtained was GVL with

TABLE 1 | Ruthenium-based heterogeneous catalysts on solid supports and water-dispersible catalytic nanoparticles for the hydrogenation of LA toward GVL.

Catalysts	Molar ratio LA/M	T (°C)	P_{H2} (bar)	t (h)	Solvent	Conversion LA (mol%)	Selectivity GVL (mol%)	TOF[a] (h^{-1})	References
0.5% Ru/Al_2O_3	8,707	130	40	3	Water	13.8	99.9	401	Tan et al., 2015
0.5% Ru/SiO_2	8,707	130	40	3	Water	80.1	99.8	2,325	
0.5% Ru/ZrO_2	8,707	130	40	3	Water	80.3	99.9	2,331	
0.5% Ru/TiO_2	8,707	130	40	3	Water	95.4	99.9	2,769	
1% Ru/TiO_2	4,353	70	40	0.25	Water	44	99.9	7,662	
1% Ru/TiO_2	4,353	130	40	0.5	Water	100	99.9	8,707	
1% Ru/TiO_2	4,353	130	40	1	Ethanol	74.9	47.7	3,261	
1% Ru/TiO_2	4,353	130	40	1	1,4-Dioxane	30.7	99.9	1,337	
1% Ru/OMS	3,831	100	30	1	Water	99.9	99.8	3,420	Molleti et al., 2018
$RuCl_3{\cdot}3H_2O/TiO_2$	4,350	90	45	4	Water	86	92	1,152	Piskun et al., 2018
$RuNO(NO_3)_3/TiO_2$	4,350	90	45	4	Water	77	94	824	
5% Ru/ZrO_2	2,100	170	27	7	Water	99.0	99.9	297	Filiz et al., 2017
2% Ru/FLG	1,460	20	40	8	Water	99.3	97.7	184	Xiao et al., 2016
5% Ru/C	359	130	12	2.7	Water	99.5	86.6	133	Al-Shaal et al., 2012
0.64% Ru/TiO_2	247	150	35	5	Water	100	93	49	Primo et al., 2011
5% Ru/TiO_2	106	150	35	5	Water	100	90	21	
0.83% Ru/TiO_2 ultrathin	4,878	100	40	1.5	Water	100	99.1	19,045[b]	Gao et al., 2019
Ru/NCS	10,000	70	40	1	Water	51	100	9,858	Liu et al., 2019
Ru/CS	10,000	70	40	1	Water	32	100	6,985	
Ru/TiO_2	505	150	20	5	Water	100	94.8[c]	101	Ndolomingo and Meijboom, 2019
$RuCl_3{\cdot}3H_2O$/PEG400	40	130	20	1	PEG/Water	99	99	40	Patil and Bhanage, 2016
$Ru_3(CO)_{12}$	1,720	130	5	12	Water	100	100	143	Ortiz-Cervantes and García, 2013
RuNHC	1,000	130	12	2.7	Water	99	96	361	Tay et al., 2016
RuNHC	1,000	130	12	2.7	THF	1	1	3	
Ru@PEG-CD	1,300	80	40	4	Water	97	99	315	Chen et al., 2017
Ru@PVP	1,300	80	40	4	Water	93	99	302	

[a] *Defined as mole of hydrogenated LA per mole of ruthenium per hour.*

[b] *Defined as mole of hydrogenated LA per number of surface ruthenium atoms per hour.*

[c] *Selectivity toward 2-MTHF: 5.2 mol%.*

essentially quantitative selectivity. A remarkable solvent effect has been observed in the LA hydrogenation reaction with 1 wt.% Ru/TiO_2 catalysts at 130°C and 40 bar in the presence of aqueous and organic solvents. When water was used as a solvent in the LA hydrogenation the catalytic activity was exceptionally high and reached a value of TOF = 8,707 h^{-1}, whereas with organic solvents such as ethanol and 1,4-dioxane, the catalytic activity dramatically drops down to 3,261 and 1,337 TOF's per hour, respectively, under the same reaction conditions (**Table 1**). The promotional effect of water was rationalized by assuming that water acts not only as a solvent but also participates as a reactant after dissociation in this aqueous-phase catalytic hydrogenation reaction. To verify this assumption, Tan et al. carried out the LA hydrogenation reaction in D_2O and found by NMR and GC/MS analysis of the products that a D atom was bonded to the γ-C atom of the GVL product, which originates not from the dihydrogen reactant but from D_2O solvent (**Figure 5**). Furthermore, the authors mixed GVL with D_2O without a D atom to be detected on γ-C atom of GVL, and ruled out an alternative pathway of the incorporation of the D atom in GVL during the hydrogenation reaction of LA in D_2O, which might be due to an H/D exchange between D_2O and GVL. Thus, is proven that the promotional effect of the aqueous solvent in the LA hydrogenation is based on the involvement of water after dissociation as a reactant in the mechanism of this aqueous-phase catalytic reaction. Michel et al. (2014) applied Ru/TiO_2, Pt/TiO_2, and Pd/TiO_2 catalysts possessing a similar metal particle size between 2.1 and 3.2 nm with an uniform distribution of each metal on the titania support in the LA hydrogenation reaction to GVL, under mild reaction conditions of 70°C and 50 bar dihydrogen pressure, using water and tetrahydrofuran as solvents. The catalytic activity of Ru/TiO_2 is strongly influenced by the nature of reaction solvent. In the aqueous medium Ru/TiO_2 catalysts exhibited the highest catalytic activity to obtain essentially quantitative conversions of LA with a yield of 95 mol% of GVL, whereas in organic solvents such as tetrahydrofuran the Ru/TiO_2 system shows no catalytic activity in this hydrogenation reaction. In sharp contrast, the solvent did not influence the catalytic activities of Pt/TiO_2 and Pd/TiO_2 to obtain with Pt/TiO_2 catalysts in both aqueous and organic medium low conversions of LA in the range of 20 up to 30 mol % and yields of GVL between 15 and 20 mol%. A very low catalytic activity has been observed with Pd/TiO_2 catalysts under these mild reaction conditions. To explain the obtained experimental results, the authors performed Density Functional Theory (DFT) calculations using acetone as a model substrate containing a C=O functionality chemisorbed on Ru(0001) surface, and proved that the nature of the aqueous solvent is the reason for the higher activity of Ru/TiO_2 catalysts in water, because the hydrogen bond of a chemisorbed water molecule on Ru-surface formed with the oxygen atom of an adjacent chemisorbed alkoxy intermediate involved in the reaction mechanism enormously lowers the activation energy barrier of the reaction pathway, resulting in enhanced reaction rates among Ru/TiO_2-catalyzed hydrogenation reactions in aqueous media. It should be mentioned that in these DFT calculations the higher activity of ruthenium catalysts in the hydrogenation of acetone in aqueous media was attributed to the formation of hydrogen bonds between chemisorbed water and carbonyl intermediate compounds, and in these calculations the possibility that water may also act as a reactant after dissociation on the ruthenium surface has not been considered. Michel and Gallezot (2015) pointed out that in order to be able to understand the high catalytic activity of ruthenium compared with other transition metals in hydrogenation reactions of starting materials bearing C=O functionalities in water where two mechanisms are operative (the first one includes chemisorbed water molecules which, by hydrogen bonding, lower the energetic span of the reaction pathway to yield the $–CH_2OH$ functionality by dissociation of hydrogen, and the second one involves dissociation of water to produce hydrogen atoms to participate in the hydrogenation reaction of the C=O group into a $–CH_2OH$ moiety), it is necessary to carry out more isotope labeling experiments and also to perform further improved theoretical investigations including both of these mechanisms. Continuous aqueous-phase hydrogenation reactions of LA in a fixed-bed reactor have been carried out over Ru/C, Ru/Al_2O_3 and Ru/MgO catalysts at a high temperature of 275°C under atmospheric pressure of dihydrogen, and the results revealed that Ru/C catalysts exhibited higher conversion of LA with higher selectivity toward GVL compared with Ru/Al_2O_3 and Ru/MgO catalytic systems (Velisoju et al., 2018). The authors further investigated the role of water on the activity over Ru/C catalysts in the continuous hydrogenation of LA toward GVL using various concentrations of LA in water from 70 wt.% down to 5 wt.%, and found that with increasing amounts of water increased both the conversion of LA and the selectivity to GVL, employing probe-adsorbed diffuse reflectance infrared Fourier transform (DRIFT) spectroscopy. Velisoju et al. found that -OH groups were generated in the presence of water on the surface of ruthenium of Ru/C catalyst. According to their proposed mechanism such hydroxyl groups initiate the dehydration step of the enol form of LA to yield α-angelica lactone intermediate, and after isomerization to β-angelica lactone surface ruthenium metal hydride species are responsible for the hydrogenation step of the -C=C- functionality of β-angelica lactone to form GVL (**Figure 6**). Therefore, the higher catalytic activity of Ru/C catalysts in the presence of water in the vapor phase is because of the easier generation of –OH groups on the surface of ruthenium, and also due to the presence of a larger active ruthenium metal surface area in comparison to the other Ru/Al_2O_3 and Ru/MgO catalysts. Mamun et al. (2019) studied solvent effects on the reaction kinetics of the hydrogenation reaction of LA into GVL over Ru(0001) catalysts under various conditions, using three media of different polarity—namely water, methanol, and 1,4-dioxane. The presence of the aqueous solvent enormously facilitated the hydrogenation reaction kinetics and this solvent effect is much stronger at temperatures lower than 100°C. For example, at the low reaction temperature of 50°C, a rate increase of 4 orders of magnitude was obtained due to the solvation effect of water. The strongest solvent effect has been observed in the highly polar solvent water and this effect decreases with decreasing polarity of the solvent, i.e., in the order: water > methanol > 1,4-dioxane. Various transition metals such as ruthenium, palladium, platinum, and nickel supported on

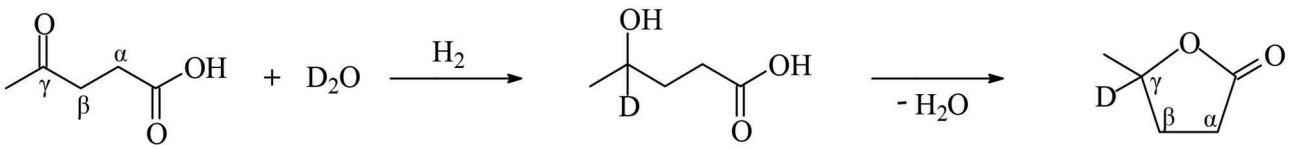

FIGURE 5 | Hydrogenation reaction of LA in D_2O.

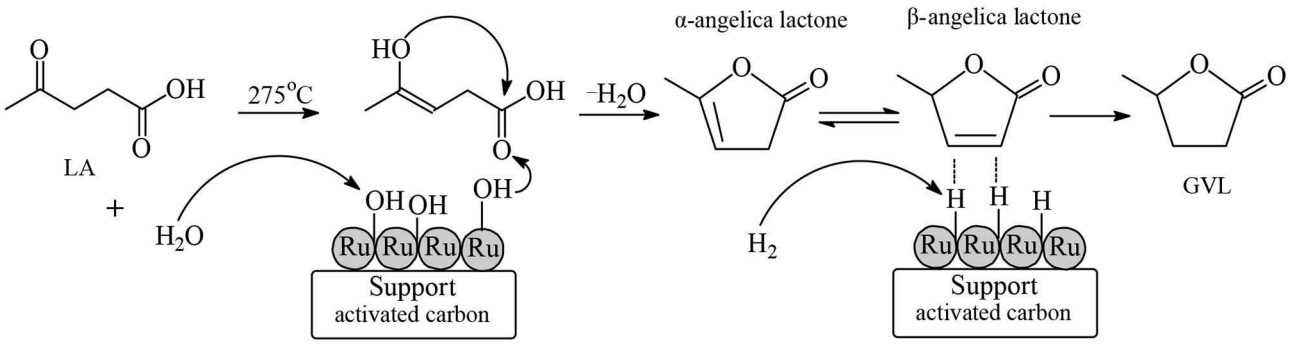

FIGURE 6 | Proposed mechanism for the hydrogenation of LA to GVL at 275°C on the surface of Ru/C catalyst in aqueous media.

hydroxyapatite (HAP) have been applied as catalysts in the liquid phase hydrogenation reaction of LA to GVL at 70°C under 5 bar H_2 pressure in various solvents such as water, ethanol, and toluene (Sudhakar et al., 2014). The highest catalytic activity exhibited ruthenium catalysts and the rates decrease in the order: Ru > Pt > Pd > Ni. With Ru/HAP catalysts the highest activity has been found to be in the aqueous solvent and the catalytic activity decreased with decreasing polarity of the solvent: water > ethanol > toluene. Sudhakar et al. (2016) further examined the activity of ruthenium, palladium, platinum copper, and nickel catalysts supported on HAP in the vapor phase hydrogenation of LA in the presence of water. The obtained rates with such catalysts have the following order: Ru > Pt > Cu > Pd > Ni. At the reaction temperature of 275°C in the Ru/HAP-catalyzed hydrogenation in the presence of water the LA conversion was 65.1 mol% and the selectivity toward GVL 99.8 mol%. In sharp contrast in the absence of water under the same conditions the conversion of LA gives rise to a dramatic drop to 4.0 mol%, and the only product observed was α-angelica lactone. At the higher temperature of 425°C in the presence of water with Ru/HAP catalysts, the conversion of LA increased to 94.0 mol% with the selectivity to GVL to decrease to 80.5 mol% with concomitant formation of α-angelica lactone (13.0 mol%) and β-angelica lactone (5.5 mol%). Ru/HAP catalysts showed a better activity in the presence of water in comparison to organic solvents such as ethanol and methanol. Gundekari and Srinivasan (2019) prepared α novel hydrous ruthenium oxide (HRO) catalyst precursor by a precipitation method using an aqueous solution of $RuCl_3{\cdot}3H_2O$ with $CaCO_3$ and applied HRO systems in the hydrogenation reaction of LA under mild conditions of 50°C and 10 bar dihydrogen pressure to obtain quantitative conversions of LA and yields toward GVL within 30 min in the aqueous solvent. The HRO precursor which possess water molecules strongly bonded to RuO_x surface was reduced to catalytic active Ru(0) species under hydrogenation reaction conditions. Quantitative conversions of LA by HRO catalysts precursors were obtained only in the presence of the aqueous solvent, whereas in organic solvents such as THF and methanol the conversions of LA were very low, i.e., between 2 and 5 mol% at 100°C, 10 bar dihydrogen within 15 min reaction time. HRO catalyst precursors supported on H-β zeolite could be recycled in five consecutive runs with the Ru-HRO/H-β catalyst to retain its activity. Guo et al. (2016) investigated the catalytic properties of Ru@MIL-101(Cr) and Ru@MIL-100(Cr) Metal-Organic Frameworks as well as of Ru@HY-zeolite (Si/Al ≥ 5.2) in the hydrogenation of LA into GVL in aqueous media. The highest catalytic activity was exhibited by the Ru@MIL-101(Cr) system to obtain quantitative conversion of LA with an essentially quantitative selectivity toward GVL under mild reaction conditions at 70°C under 10 bar dihydrogen pressure within 5 h reaction time in water. The authors investigated the catalytic behavior of Ru@MIL-101(Cr) in the presence of water and various organic solvents. The strongest solvent effect, i.e., the highest catalytic activity, has been observed in the highly polar aqueous solvent. This effect decreases with decreasing polarity of the solvent, in the order: water > methanol > ethanol > 2-propanol > 1,4-dioxane. Ultrafinely dispersed ruthenium nanoparticles with a mean size of 2.1 nm have been supported on N-doped hierarchically-porous carbon (Ru/NHPC) with the support to be prepared from cellulose, and applied as catalysts in the aqueous-phase hydrogenation of LA to obtain higher activities, selectivity toward GVL, and (especially) stabilities compared with conventional Ru/C catalytic systems (Wei et al., 2018). Recycling experiments have shown

that the Ru/NHPC catalytic system could be reused in thirteen consecutive hydrogenation runs at 50°C, 10 bar H_2 pressure within 3 h in aqueous media without any obvious deactivation, whereas the Ru/C catalyst under identical conditions was severely deactivated already in the 3rd recycling consecutive run. The authors further compared the catalytic activity of Ru/NHPC systems in water and different organic solvents such as DMF, 1,4-dioxane, cyclohexane, methanol, and ethanol, and found that the highest yields toward GVL were obtained in water in comparison to all used organic solvents.

In studies of ruthenium-based catalytic systems a main focus is on the supports, with the aim to improve the efficiency of the catalyst via pre-treatment methods, modification of the nature and control of the properties, and the structure of the support material. Novel ruthenium supported on manganese oxide octahedral molecular sieve (Ru/OMS) systems have been synthesized and applied as catalysts in the hydrogenation of LA at 100°C under 30 bar dihydrogen pressure and a molar ratio of LA/Ru = 3,831 within 1 h in aqueous media (Molleti et al., 2018). Under these conditions the catalytic activity exhibited Ru/OMS catalyst was high (TOF = 3,420 h^{-1}) to give near quantitative conversion of LA and selectivity toward GVL with retained catalytic activity in four recycling consecutive experiments (**Table 1**). This high catalytic activity exhibited Ru/OMS catalysts could be explained by the moderate acidity of the novel supported system and the high dispersion of ruthenium nanoparticles on the surface. The apparent activation energy of Ru/OMS catalyst in the aqueous-phase hydrogenation of LA was calculated and amounts to only 49.16 kJ/mol. Piskun et al. (2018) have shown that the performance of Ru/TiO_2 (anatase) catalysts applied in the aqueous-phase hydrogenation of LA to GVL strongly depends on the synthesis protocol of the catalytic system by varying the nature of the ruthenium precursor, the calcination and/or reduction step, and the amount of dihydrogen in the gas during the reduction step. The highest initial reaction rates in the aqueous-phase hydrogenation of LA to GVL at 90°C and 45 bar dihydrogen pressure were obtained with $RuCl_3{\cdot}3H_2O$ catalysts precursors compared to $RuNO(NO_3)_3$ precursors (**Table 1**) without an intermediate calcination step using only 10% H_2 in the reduction gas, whereas a calcination step and the presence of a H_2 rich reduction gas gives rise to a drop in catalytic activity. The influence of different phases of titania supports, i.e., rutile and anatase on ruthenium and platinum catalysts, has been investigated in the hydrogenation of LA into GVL at 30°C or 70°C under 50 bar of H_2 pressure in aqueous media (Ruppert et al., 2015). It has been surprisingly found that the influence of the type of support was not the same for ruthenium and platinum catalysts. The highest catalytic activity was exhibited by ruthenium on TiO_2 support, consisting of 10% rutile and 90% anatase to obtain at 70°C quantitative conversion of LA and yield to GVL within 1 h, whereas with Ru on TiO_2 support consisting of 100% anatase the conversion of LA was only 38 mol% and the yield to GVL of only 31 mol% under the same conditions. Microscopy studies showed that the ruthenium particles were exclusively located on the less rutile crystallites and could be understood due to a higher adhesion of ruthenium on rutile compared to anatase. In contrast, with platinum on TiO_2 support consisting of 10% rutile and 90% anatase, the conversion of LA was 22 mol% and the yield to GVL of 18 mol%, whereas a higher conversion of LA of 54 mol% and a higher yield to GVL of 50 mol% were obtained by platinum catalysts on TiO_2 support consisting of 100% of anatase. Novel Ru/TiO_2 systems have been synthesized by photoassisted controlled modification of the TiO_2 support by addition of calcium and applied as catalysts in the transfer hydrogenation of LA using formic acid as an internal hydrogen source in aqueous media (Wojciechowska et al., 2019). The Ca-modification of Ru/TiO_2 catalysts enhanced the performance of both catalytic steps, the transfer hydrogenation of LA into GVL, and also the dehydrogenation of formic acid to yield the dihydrogen reactant. The Ca-modification caused both a decreased size of the anatase crystallite and the formation of a new phase of calcium titanate, resulting in smaller ruthenium metal particles stabilized on the support. The superior catalytic activity of Ca-modified Ru/TiO_2 systems could be further understood probably due to the strong interaction between the smaller ruthenium particles with the Ca-modified TiO_2 support. Gao et al. (2018) disclosed results on the stability of 2.5 wt.% Ru/ZrO_2 catalysts applied in the transfer hydrogenation reaction of LA to GVL with a mixture of formic acid/formate at 150°C in aqueous media, and found that the incorporation of 0.1 wt.% SiO_2 to the support enormously stabilized the system and the catalyst Ru/ZrO_2-SiO_2 retained its activity after recycling in three consecutive runs, whereas the activity of Ru/ZrO_2 catalyst significantly decreased after recycling already in the first consecutive run. The catalytic properties of four different Ru/ZrO_2 systems have been evaluated in the hydrogenation of LA to GVL in aqueous media; catalytic activity is strongly influenced by the pre-treatment method and the most active catalyst was obtained after impregnation of $RuCl_3{\cdot}3H_2O$ on pre-calcined zirconia support, followed by reduction with dihydrogen to give ruthenium metal particles of a size between 3.0 and 4.0 nm with an uniform dispersion (Filiz et al., 2017). Using this Ru/ZrO_2 catalyst in the aqueous phase hydrogenation of LA at 170°C under 27 bar of H_2 within 7 h at a molar ratio of LA/Ru = 2100, the catalytic activity obtained was 297 TOFs per hour with a conversion of LA of 99.0 mol% and a selectivity toward GVL of 99.9 mol% (**Table 1**). Stability studies of Ru/TiO_2, Ru/ZrO_2, and Ru/C catalytic systems have been reported on the hydrogenation reaction of LA to GVL at 150°C under 30 bar dihydrogen pressure in 1,4-dioxane and found that the Ru/TiO_2 benchmark catalyst was deactivated just after the first recycling run, whereas the Ru/ZrO_2 catalyst maintained its activity even after five recycling consecutive runs (Ftouni et al., 2016). The authors have clearly shown that the presence of the aqueous solvent has a promotional effect in the Ru/ZrO_2-catalyzed hydrogenation reaction of LA to GVL. Thus, in a solvent mixture of 1 wt.% water with 99 wt.% 1,4-dioxane an increase in the GVL yield of 25 mol% was observed compared to anhydrous 1,4-dioxane solvent and in a mixture of 10 wt.% water with 90 wt.% 1,4-dioxane the catalytic activity further increased to obtain quantitative GVL yields. Ren et al. (2019) studied a cascade process for the direct conversion of carbohydrates fructose and glucose, and of storage or structural polysaccharides starch or cellulose

toward GVL catalyzed by a system comprising the heteropoly acid-based ionic liquid 1-methyl-3-(3-sulfopropylimidazolium) silicotungstate and Ru/ZrO_2 in aqueous media. Using this catalytic system at 180°C under argon for 3 h for the dehydration step and then under 40 bar dihydrogen pressure within 10 h for the hydrogenation step, the GVL yields obtained from fructose, glucose, starch, and cellulose were 63, 68, 60, and 60mol%, respectively. Recycling experiments with four consecutive runs have shown deactivation of Ru/ZrO_2 catalyst component due to massive coke deposition formed probably from decomposition of humins and α-angelica lactone obtained as side products and intermediates at the reaction temperature of 180°C under acidic conditions. Raspolli Galletti et al. (2013) investigated the one pot approach for the conversion of giant reed (*Arundo donax L.*) directly to GVL by a combination process of acid catalyzed dehydration and catalytic hydrogenation reactions employing a bifunctional catalyst comprising of Ru/C and niobium phosphate or niobium oxide at a low temperature of 70°C and low dihydrogen pressure, i.e., 5 bar, to yield up to 16.6 mol% GVL, based on dry biomass with an essentially quantitative conversion of the LA intermediate in aqueous media. Xiao et al. (2016) synthesized few-layered graphene (FLG)-supported ruthenium nanoparticles and applied as them catalysts in the hydrogenation of LA in aqueous media to obtain at room temperature under 40 bar of H_2 within 8 h a conversion of LA of 99.3 mol% and selectivity toward GVL of 97.7 mol% (**Table 1**). In five recycling experiments the 2.0% Ru/FLG catalyst retained its activity and exhibited four times higher activity compared with ruthenium catalysts on conventional support of activated carbon (Ru/C). Various ruthenium supported catalysts such as Ru/C, Ru/SiO_2, and Ru/Al_2O_3 have been screened in the hydrogenation of LA into GVL under mild reaction conditions (25°C, 12 bar H_2) in the absence of solvents with the Ru/C catalyst to show the highest catalytic activity, whereas Ru/SiO_2 and Ru/Al_2O_3 exhibited significantly lower yields toward GVL (Al-Shaal et al., 2012). The commercial 5 wt.% Ru/C catalytic system has been further applied in the aqueous-phase hydrogenation of LA at 130°C under 12 bar of dihydrogen pressure within 2.7 h reaction time, and exhibited a moderate catalytic activity of 133 TOFs per hour (**Table 1**). It should be mentioned that conventional Ru/C catalysts suffer from enormous deactivation even at low temperatures and pressures, probably because of the suppressed mass transport of LA through the small-sized micropores resulting in a pore blocking of the carbon material. Primo et al. (2011) investigated the activity of 5 wt.% Ru/TiO_2 and 0.64 wt.% Ru/TiO_2 catalysts in the aqueous-phase hydrogenation of LA into GVL and found that the activity of 0.64 wt.% Ru/TiO_2 is about two times higher compared with the activity of 5 wt.% Ru/TiO_2 catalyst (**Table 1**), and could be explained due to the synergism between the small size of ruthenium nanoparticles and the activation of the carbonyl functionality of LA on the TiO_2 support. Highly active ruthenium nanoparticles of a mean size of 1.4 nm supported on ultrathin TiO_2 nanosheets with an unique two dimensional (2D) structure have been applied as catalysts in the hydrogenation of LA toward GVL (**Table 1**) to obtain impressively higher intrinsic catalytic activities (TOF = 19,045 h^{-1}) under relative mild reaction conditions of 100°C and 40 bar dihydrogen pressure within 90 min reaction time, compared with those of conventional Ru/SiO_2, Ru/MoS_2, and Ru/C catalytic systems, which exhibited 7,089, 693, and 1,909 TOFs per hour, respectively, under identical conditions in aqueous media. It is relevant to point out that the calculation of TOF values in this work (**Table 1**) is based on surface ruthenium atoms and not on the bulk ruthenium loading (Gao et al., 2019). Recycling experiments have shown that the Ru/TiO_2 ultrathin nanosheets catalyst could be reused in six consecutive hydrogenation runs without any deactivation. The apparent activation energy of the Ru/TiO_2 ultrathin nanosheets catalyst in the aqueous-phase hydrogenation of LA was calculated and amounts to only 43.4 kJ/mol, which is much lower than that of Ru/C catalyst (E_{app} = 87.66 kJ/mol), indicating a different nature of catalytically active sites. Employing high-resolution transmission electron microscopy (HRTEM), X-ray photoelectron spectroscopy (XPS), and temperature programmed reduction of hydrogen (H_2-TPR) techniques has been revealed that in the Ru/TiO_2 ultrathin nanosheets catalyst the ruthenium atoms are chemically bonded to oxygen atoms of TiO_2 support to form Ru-O-Ti bonds, which cause a strong interfacial interaction. Whereas, in Ru/SiO_2 and Ru/MoS_2 catalysts the ruthenium atoms interact weakly with their supports, although a strong coordination has been observed between each ruthenium with their neighboring ruthenium atoms. The authors performed DFT calculations using a Ru/TiO_2 modeled interface or a model of the most exposed Ru (0002) surface for the hydrogenation of LA, and have shown that the preferential mechanistic pathway is hydrogenation of the keto functionality with formation of $CH_3CH(O)CH_2CH_2COOH^*$, cyclization to GVL-OH and dehydroxylation to give GVL, independent of the structure of the surface. Interestingly, with the Ru/TiO_2 interfacial structure, the rate determining step changes from hydrogenation to cyclization compared to Ru (002) surface, where the rate determining step is the hydrogenation one. In addition, to rationalize the results of exceptionally high catalytic activities exhibited by Ru/TiO_2 ultrathin nanosheets catalysts where a strong interfacial interaction takes place due to the presence of Ru-O-Ti chemical bonds, we assume that such a system enormously facilitates both the heterolytic dihydrogen cleavage mechanism necessary for the easy hydrogenation of the keto functionality of LA into an alcohol group to yield the 4-hydroxyvaleric acid intermediate (*vide supra*, Unit 2.1 Hydrogenation of LA into GVL) and the dehydration step, as well to yield GVL. Van Nguyen et al. (2019) prepared via *de novo* synthesis a $RuCl_3$@MIL-53-NH_2 Metal-Organic Framework which was reduced at 500°C under H_2/N_2 gas flow to obtain the Ru@C-Al_2O_3 catalyst which consists of ruthenium nanoparticles confined in the C-Al_2O_3 honeycomb system. Ru@C-Al_2O_3 catalysts have been applied in the hydrogenation of LA under very mild conditions, i.e., at room temperature and atmospheric pressure of dihydrogen, to obtain a quantitative conversion of LA and a GVL yield of 99.9 mol% within 6 h of reaction time in the aqueous medium. Recycling experiments at 60°C showed that Ru@C-Al_2O_3 catalyst in aqueous media retained its activity in seven consecutive runs, indicating a stable catalytic system. The apparent activation energy of Ru@C-Al_2O_3

catalyst was calculated and amounts to 34.66 kJ/mol. Ru/γ-Al_2O_3 catalysts in the aqueous-phase hydrogenation of LA suffer from mediocre activities and stabilities mainly due to the non-uniform distribution of ruthenium on the support and because γ-Al_2O_3 is unstable in water (due to the existence of surface hydroxyl moieties) and tends after rehydration to form γ-AlOOH, i.e., boehmite. Tan et al. (2016) prepared functionalized γ-alumina supports such as NH_2-γ-Al_2O_3 to obtain highly dispersed ruthenium nanoparticles (**Figure 7**) and applied them as catalytic systems in the hydrogenation reaction of LA selectively to GVL in aqueous media. Ru/NH_2-γ-Al_2O_3 catalysts exhibited superior activity and stability compared with their Ru/γ-Al_2O_3 counterparts. For example, at 70°C with Ru/NH_2-γ-Al_2O_3 catalysts, a TOF value of 3,355 per hour was obtained in the aqueous-phase hydrogenation of LA, whereas with Ru/γ-Al_2O_3 catalysts the activity was very lower, namely 432 TOFs per hour under the same reaction conditions. In ten recycling experiments the Ru/NH_2-γ-Al_2O_3 catalyst retained its activity albeit the reaction temperature was high i.e., 130°C. Raspolli Galletti et al. (2012) investigated the hydrogenation of LA to GVL catalyzed by commercial 5 wt.% Ru/Al_2O_3 or 5 wt.% Ru/C catalysts combined with an acid co-catalyst such as the ion exchange resins of the type Amberlyst A70 and Amberlyst A15, niobium phosphate, and niobium oxide in aqueous media. The catalytic system 5 wt.% Ru/C-Amberlyst A70 exhibited the highest catalytic activity (TOF = 558 h^{-1}) at 70°C under 5 bar dihydrogen pressure within 3 h, whereas with the 5 wt.% Ru/C catalyst in the absence of the acid co-catalyst the activity was rather low (TOF = 74 h^{-1}) under the same reaction conditions. Piskun et al. (2016) have screened a series of 1 wt.% ruthenium catalysts supported on carbon, carbon nanotubes, Al_2O_3, SiO_2, TiO_2, ZrO_2, Nb_2O_5, and zeolite β-12.5 at 90°C, 45 bar dihydrogen in aqueous media. Ru/β-12.5 catalysts exhibited by far higher catalytic activities even with a factor of 5 in comparison to the other ruthenium-supported catalysts, to obtain a conversion of LA of 94 mol% and selectivity to GVL, and 4-hydroxyvaleric acid of 66 and 34 mol%, respectively, within 2 h of reaction time in water. Zhang et al. (2017) applied highly stable Ru/ZSM-5 catalysts in the aqueous-phase hydrogenation of LA to GVL at a low reaction temperature of 70°C and performed recycling experiments with 10 consecutive runs without any loss of catalytic activity indicating no deactivation of the catalyst which is mainly caused by ruthenium aggregation, leaching and carbon deposition on the catalytically active sites. It has been found that a strong ruthenium-support interaction takes place at a higher tetrahedral–coordinated framework Al content, which minimizes the ruthenium aggregation and leaching under the acidic reaction conditions. Highly dispersed ruthenium nanoparticles consisting of Ru(0) to 59% and of RuO_2 to 41%, with an average particle size of 2.3 nm on N-doped carbon nanospheres (Ru/NCS), were used as highly active catalysts (TOF= 9,858 h^{-1}) in the hydrogenation of LA to GVL (**Table 1**) in aqueous media (Liu et al., 2019). The incorporation of N-dopant in the carbon matrix of the support plays a crucial role in the high dispersion of ruthenium nanoparticles because ruthenium nanoparticle catalysts in the absence of N-doping on carbon nanospheres (Ru/CS) were less active (TOF = 6,985 h^{-1}) and displayed a clear sintering of ruthenium nanoparticles in the aqueous solvent (**Table 1**). Ndolomingo and Meijboom (2019) immobilized ruthenium, palladium, copper, and chromium nanoparticles with a mean particle size of 2–6 nm on mesoporous metal oxides such as TiO_2, MnO_2, and NiO, and applied them as catalysts in the LA hydrogenation reaction in aqueous media. At a reaction temperature of 150°C under 20 bar H_2 within 5 h, the highest activity (TOF = 101 h^{-1}) was obtained by Ru/TiO_2 or Ru/MnO_2 catalysts (**Table 1**) compared to Ru/NiO systems. Under the same conditions the reactivity exhibited Cu/TiO_2 catalyst was rather low (TOF = 64 h^{-1}). The catalytic activity of immobilized metal nanoparticles follows the order: Ru ≈ Pd

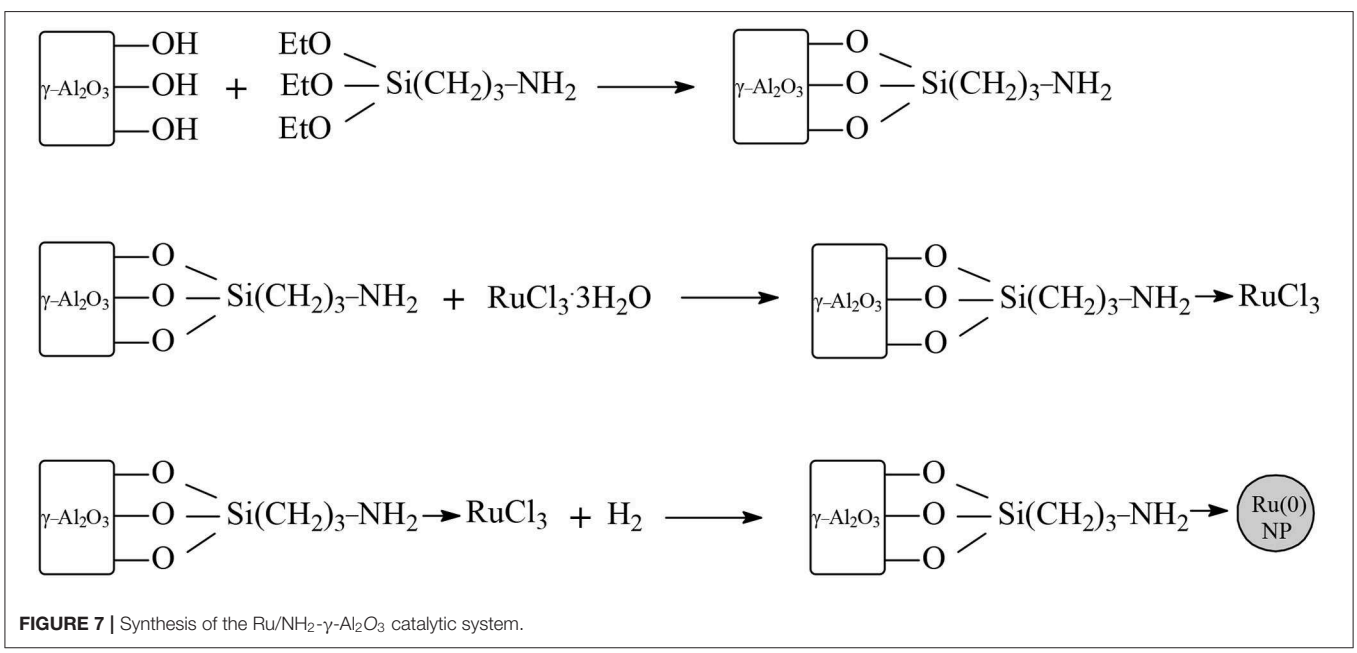

FIGURE 7 | Synthesis of the Ru/NH_2-γ-Al_2O_3 catalytic system.

> Cu > Cr and was revealed to be higher in water compared to the solvent-free system. Ruthenium nanoparticles with a mean size of 1.4 nm were embedded on dendrimers, followed by immobilization of the whole system on mesoporous TiO_2 supports and then applied as catalysts in the LA hydrogenation reaction in the aqueous solvent in order to obtain LA conversions of 92 mol% with selectivities toward GVL and 2-MTHF of 98 and 2 mol%, respectively, and in organic solvents such as 1,4-dioxane where the conversion of LA was slightly higher (98 mol%) with selectivities to GVL and 2-MTHF of 99 and 1 mol%, respectively, at a reaction temperature of 150°C under 10 bar H_2 pressure within 5 h of reaction duration (Nenamashi et al., 2018). Alginates which are polysaccharides in cell walls of macro algae were used to synthesize high surface area TiO_2 and binary TiO_2/ZrO_2 supports for the immobilization of ruthenium nanoparticles applied as catalysts in the hydrogenation of LA toward GVL in aqueous media (Ruppert et al., 2019). The best catalytic performance was obtained with ruthenium nanoparticles possessing a bi-modal particle size distribution consisting of a mean particle size of 1.9 nm and an average size of 3.7 nm on bare TiO_2 support, to achieve a conversion of LA of 79 mol% with a yield to GVL of 76 mol% under mild reaction conditions namely 30°C, and 50 bar of dihydrogen within 1 h of reaction time. Ruthenium nanoparticles with an average size of 2.8 nm diameter were encapsulated in sulfonated exchange resins such as DOWEX, and applied as bifunctional catalysts in the aqueous phase hydrogenation of LA to GVL under batch conditions to obtain an activity in the order of 102 TOF's per hour, with a conversion of LA of 98.3 mol% at 70°C, 10 bar H_2 within 4 h of reaction time, and under continuous conditions at 70°C with dihydrogen pressures between 48 and 70 bar and contact times of 62–211s to observe conversions of LA between 89 and 100 mol% and excellent durability of the bifunctional Ru@ DOWEX catalyst (Moreno-Marrodan and Barbaro, 2014). The surfactant hexadecyl(2-hydroxyethyl)dimethylammonium dihydrogen phosphate (HHDMA) was used as a water-soluble ligand to modify ruthenium nanoparticles with an average diameter of 1.3 nm on $TiSi_2O_6$ support and applied as catalyst in the continuous hydrogenation of LA in water at 100–150°C, under pressures between atmospheric and up to 60 bar of H_2 with contact times of 4–16s to obtain selectivities toward GVL higher than 95 mol%, with the selectivity to 1,4-PDO to be in the range of 5 mol% without any deactivation of the catalyst for a period of 15 h (Albani et al., 2017). A comparison to a conventional Ru/C catalyst with an average ruthenium particle diameter of 1.5 nm has shown that the $Ru/HHDMA/TiSi_2O_6$ catalytic system exhibited four times higher activity compared with the benchmark Ru/C catalyst which even suffers from severe deactivation due to formation of RuO_2. Energy dispersive X-ray (EDX) maps of ruthenium and phosphorus in the $Ru/HHDMA/TiSi_2O_6$ system have shown that P is located in the areas where also Ru appears, and therefore it is highly probable that the HHDMA ligand is bounded to ruthenium nanoparticles with the phosphate moiety and to the $TiSi_2O_6$ carrier by the NCH_2CH_2OH functionality. The authors rationalized the results regarding the difference in stability of 0.24wt.% $Ru/HHDMA/TiSi_2O_6$ and 5wt% Ru/C catalysts by assuming that in the 0.24wt.% $Ru/HHDMA/TiSi_2O_6$ catalyst the phosphate groups of the ligands (ratio of HHDMA/RuNP ∼ 250) shield the ruthenium nanoparticles and make difficult the oxygen approach, and also that the ligand-ruthenium interfacial acidity protects ruthenium nanoparticles from the oxidation reaction to form RuO_2. Furthermore, DFT calculations revealed that these HHDMA ligand-ruthenium interfacial acidic properties in the highly polar aqueous solvent make it possible that the $Ru/HHDMA/TiSi_2O_6$-catalyzed reaction follows a mechanistic path with low energy barriers, resulting in a fourfold increase in catalytic activity.

Heterogeneous Water-Dispersible Catalytic Nanoparticles

Compared to the widely applied heterogeneous transition metal(0) catalytic nanoparticles (NPs) immobilized on the surface of various solid supports, the application of heterogeneous water-dispersible NPs catalysts constitutes a relatively novel but emerging approach in the field of aqueous-phase catalytic conversions of renewable biomass-derived platform chemicals. The aqueous solvent provides for a higher dispersion of the water-dispersible NPs able to exhibit great catalytic activities and impressive stabilities depending on the nature of the transition metal and especially on the choice of an appropriate stabilizer which plays a key role in keeping NPs with small particle size diameters avoiding aggregation under the reaction conditions, and thus keeping a large surface area due to the high ratio of surface metal atoms to bulk metal loading, which makes available a large number of catalytic active sites to convert the starting material. Consequently, a broad spectrum of various types of NPs stabilizers have been applied in different catalytic reactions which include, *inter alia*, surfactants, polymers, dendrimers, and also phosphines or nitrogen-containing ligands which are typically applied to modify homogeneous catalytic complexes (Roucoux et al., 2002; Yan et al., 2010; Dykeman et al., 2012; Yuan et al., 2012; Bouriazos et al., 2014; Bulut et al., 2015; Duan et al., 2015). Similar to the homogeneous water-soluble catalytic molecular complexes, the cumbersome separation and recycling of water-dispersible catalytic NPs in the aqueous solvent could be achieved by extraction after external addition of an organic solvent to create a biphasic system, followed by separation of the two phases.

In 2016, Patil and Bhanage studied the hydrogenation reaction of LA catalyzed by water-dispersible Ru(0) nanoparticles (RuNPs) formed *in situ* from $RuCl_3{\cdot}3H_2O$ precursor and polyethylene glycol (PEG) 400, used both as solvent and stabilizer at 110°C within 4 h reaction time in a solvent mixture PEG400/Water of a volume ratio 70/30. They reported a catalytic activity of TOF= 10 h^{-1} with a conversion of LA and selectivity to GVL of 99 mol%. At a higher temperature of 130°C the catalytic activity increased up to TOF= 40 h^{-1} with 99 mol% of both conversion of LA and selectivity toward GVL (**Table 1**). The formation of ruthenium nanoparticles was confirmed by TEM analysis and found nanoparticles of a very large size, i.e., 100–200 nm. Recycling experiments of the $RuCl_3{\cdot}3H_2O/PEG400/H_2O$ system from the monophasic

hydrogenation reaction mixture, followed by recovery of the catalyst by extraction and phase separation of a biphasic system created after addition of diethyl ether, have shown that the catalyst is stable without losing its activity and selectivity for six successive runs. Lower catalytic activities have been obtained in the absence of water using PEG400 alone or various organic solvents such as toluene, 1,4-dioxane, and ethanol. In, 2013 Ortiz-Cervantes and García applied water-dispersible RuNPs with a mean size of 2.4 nm as catalysts in the hydrogenation of LA prepared *in situ* from $Ru_3(CO)_{12}$ precursors in the absence of stabilizers. This exhibited a catalytic activity of TOF = 143 h^{-1} with a quantitative conversion of LA and selectivity to GVL at 130°C in aqueous media (**Table 1**). The 1,4-PDO product was obtained with a selectivity of 4 mol% at a higher temperature and pressure (150°C, 35 bar H_2) and longer reaction time (24 h), with the selectivity of GVL to remain 96 mol% at a quantitative conversion of LA. Using RuNPs in organic solvents such as THF, the catalytic activities were lower with those obtained in water, and in the presence of alcohols such as methanol and propanol the main products were their corresponding levulinate esters. Tay et al. (2016) investigated hydrogenation reaction of LA to GVL catalyzed by water-dispersible RuNPs obtained *in situ* from both monodentate and bidentate *p*-cymene ruthenium(II) N-heterocyclic carbene (RuNHC) complexes as catalyst precursors in aqueous media. *p*-cymene RuNHC catalyst precursors with monodentate N-heterocyclic carbene ligands form RuNPS in both water and organic solvents and exhibited much higher catalytic activities in water (TOF = 361 h^{-1}) compared with those obtained in organic solvents such as THF (TOF= 3 h^{-1}), methanol, and isopropanol (**Table 1**). However, in organic solvents, *p*-cymene RuNHC catalyst precursors with bidentate N-heterocyclic carbene ligands form stable homogeneous complexes without any formation of RuNPs under hydrogenation reaction conditions and showed moderate catalytic activities. In 2017, Chen et al. synthesized water-dispersible RuNPs on cross-linked β-cyclodextrin with polyethylene glycol diglycidyl ether (PEG-CD) stabilizers and applied them as catalysts in the hydrogenation of LA to GVL in aqueous media. Ru@PEG-CD catalysts with an average particle size of 1.7 nm exhibited slightly higher activity compared to RuNPs with polyvinyl pyrrolidone (PVP), one of the most applied stabilizers, with a mean size of 2.3 nm at 80°C in water (**Table 1**). However, the Ru@PEG-CD catalytic system could be recycled in four consecutive runs without losing its activity, whereas the Ru@PVP catalyst already suffered from serious deactivation in the second recycling run. Protsenko et al. (2016, 2017, 2018) prepared RuO_2 nanoparticles on hypercrosslinked polystyrene stabilizers containing amino groups (5% Ru/MN100) and on stabilizers without functionalities (5% Ru/MN270), and systematically studied the influence of operating reaction parameters on the catalytic activity of both systems applied in the hydrogenation reaction of LA selectively to GVL under mild conditions in aqueous media. It was found that 5 wt.% Ru/MN100 catalysts exhibited the highest activity (conversion of LA: 85 mol%), which was even superior to the activities obtained with commercial 5 wt.% Ru/C catalysts (conversion of LA: 64 mol%) under the same conditions (90°C, 20 bar H_2, 50 min) in aqueous media, albeit the surface of Ru/C catalyst consists to 12.5% of Ru(0) and to 87.5% of RuO_2 with a different degree of hydration, whereas the composition of the surface of Ru/MN100 catalyst consists to 100% of RuO_2 with different degrees of hydration. This is remarkable because Ru(0) catalysts usually exhibit much higher activities compared to RuO_2 in the LA hydrogenation reaction in aqueous media. Kubo et al. (2016) prepared water-dispersible boronate nanoparticles coated by polyethyleneimine (BNP) with an average diameter of 121 nm and used as support materials for ruthenium, palladium, and platinum nanoparticles with mean diameters < 1 nm to catalyze the hydrogenation reaction of LA in aqueous media under mild conditions (100°C, 8 bar H_2, 4 h). The highest conversion of LA (94.6 mol%) was obtained with Ru/BNP catalyst, which was stable in four recycling runs, whereas Pt/BNP and Pd/BNP catalysts exhibited lower activities to give conversions of LA of 46.9 and 24.4 mol%, respectively, with essentially quantitative selectivity toward GVL with all three catalysts. The authors further applied Ru/BNP catalysts in the LA hydrogenation reaction in organic media such as ethanol and toluene with however much lower activities in both solvents in comparison to water. RuNPs with an average size of 3.0 nm randomly distributed on the surface of a cross-linked sulfonated polyethersulfone (SPES) support were used as catalysts for the hydrogenation of LA to afford GVL in quantitative selectivity with a conversion of LA up to 87.9 mol% at 70°C under 30 bar H_2 within 2 h in aqueous medium (Yao et al., 2014). The swelling properties of SPES support in water facilitated both the adsorption of LA to ruthenium catalytic active sites for its hydrogenation to yield 4-hydroxyvaleric acid intermediate, and to access easily the $–SO_3H$ acid sites for its dehydration reaction to give by intramolecular esterification the GVL product.

Homogeneous Water-Soluble Catalytic Complexes

The use of homogeneous water-soluble transition metal catalytic complexes in aqueous media is of great interest, particularly in the aqueous/organic biphasic mode, owing to the possibility for the heterogenization of homogeneous catalysis, which combines many advantages: (i) high activities and selectivities even under mild conditions by fine tuning of the coordination sphere of the transition metal employing a wide spectrum of water-soluble ligands in the aqueous solvent (Papadogianakis and Sheldon, 1996), (ii) easy and quantitative recovery of the catalyst in active form from organic reaction products by simple phase separation of the biphasic system and facile catalyst recycling. Consequently, numerous steps in classical homogeneous industrial processes are rendered superfluous and process engineering is enormously simplified, resulting in substantial energy savings and lower emissions (Papadogianakis and Sheldon, 1997) and (iii) new types of catalytic reactivities have been observed in the aqueous medium. The catalytic activities were much higher in water compared to organic solvents in various and different types of catalytic reactions such as hydrogenation (Moustani et al., 2018), hydrocarboxylation (Papadogianakis et al., 1997), and hydroformylation reactions (Fremy et al., 1995), which contrasts with the general perception that aqueous-phase

catalysis normally exhibits lower rates compared to analogous catalytic reactions in organic solvents. Water-soluble rhodium catalytic complexes with trisulfonated triphenylphosphine ligands (TPPTS, **Figure 8**) have found important industrial applications such as in the Ruhrchemie/Rhône-Poulenc process for the hydroformylation of the lower olefins propylene and 1-butene, which is rich in the raffinate II mixture [raffinate II consists of 1-butene, 2-butenes (*cis*/*trans*) and butanes (*n*-/*iso*-) obtained from C_4-stream of naphtha crackers] and in the Rhône-Poulenc process for the synthesis of vitamin E and A intermediates in aqueous/organic two-phase systems. Moreover, water-soluble palladium and rhodium complexes with monosulfonated triphenylphosphine ligands (TPPMS, **Figure 8**) have been used as catalysts in the aqueous/organic biphasic system in the Kuraray process, which is a four step process for the hydrodimerization of 1,3-butadiene to produce 1,9-non-anediol and 1-octanol as well (Papadogianakis et al., 1997). The hydrogenation reaction of LA in the aqueous solvent catalyzed by water-soluble ruthenium complexes proceeds in a monophasic system mode because LA is a polar and hydrophilic starting material. Therefore, the separation of water-soluble ruthenium catalytic complexes from aqueous one-phase LA hydrogenation reaction mixture proceeds with biphasic recovery of the catalyst in active form from organic reaction products by extraction and simple phase separation of an aqueous/organic two-phase system created after external addition of an organic solvent such as ethyl acetate or diethyl ether, which finally results in a facile recycling of the water-soluble catalyst.

The advent of aqueous-phase LA hydrogenation reactions catalyzed by homogeneous water-soluble ruthenium complexes could be traced back to 1977 with the pioneering work of F. Joó on hydrogenate keto carboxylic acids, such as pyruvic acid and LA by water-soluble Ru/TPPMS catalytic complexes in aqueous monophasic systems (Joó et al., 1977). Mehdi et al. (2008) reported the aqueous monophasic hydrogenation of LA catalyzed by water-soluble $Ru(acac)_3$/TPPTS complexes at 140°C under 69 bar hydrogen pressure at molar ratios of LA/Ru = 600 and TPPTS/Ru = 10 within 12 h to yield 95% GVL, which was isolated after extraction by means of a biphasic system created by external addition of ethyl acetate (Mika et al., 2015). In Chalid et al. (2011) studied the biphasic hydrogenation of LA to GVL catalyzed by water-soluble $RuCl_3{\cdot}3H_2O$/TPPTS systems at molar ratios of LA/Ru= 100 and TPPTS/Ru = 1, a pH value of 7, a reaction temperature of 90°C under 45 bar hydrogen pressure within 1 h to observe a conversion of 82% of LA in a dichloromethane/water (volume ratio = 100/25) two-phase system which could allow recovery and recycling of the catalyst. In a recycling experiment, however, the $RuCl_3{\cdot}3H_2O$/TPPTS catalyst was partially deactivated because in the first run the conversion of LA was 81% and in the followed catalyst recycling experiment only 55% of LA was converted. Tukacs et al. (2012) described the hydrogenation of LA catalyzed by $Ru(acac)_3$ modified with several water-soluble sulfonated alkylphenylphosphines under solvent-free conditions and found that the $Ru(acac)_3$ precursor modified with the disulfonated diphenylbutylphosphine ligand (BDPPDS, **Figure 8**) exhibited the highest catalytic activity of 3,540 TOFs per hour under 100 bar hydrogen pressure at 140°C and molar ratios of LA/Ru = 6,370 and P/Ru = 10 within 1.8 h reaction time to yield 99.9% GVL. Recycling experiments of the Ru/BDPPDS catalyst were carried out using the technique of separation by distillation of volatile compounds under reduced pressure from homogeneous catalyst and addition of a new portion of LA without a significant decrease in catalytic activity for six consecutive runs. Delhomme et al. (2013) disclosed the hydrogenation reaction of LA in aqueous monophasic systems using $RuCl_3{\cdot}3H_2O$ and $Ru(acac)_3$ catalyst precursors modified with water-soluble phosphine ligands such as TPPTS, TPPMS, trisulfonated tris(2,4-dimethylphenyl)phosphine (TDMPPTS), 1,3,5-triaza-7-phosphaadamantane (PTA) and tris(2-carboxyethyl)phosphine (TCEP) (**Figure 8**) at 140°C under 50 bar of dihydrogen pressure, molar ratios of LA/Ru = 100–600 and of P/Ru = 3.25–10 within 5 h reaction time. The highest activity of TOF = 210 h^{-1} was exhibited by the $RuCl_3{\cdot}3H_2O$/TPPTS catalytic system, whereas with the $Ru(acac)_3$/TPPTS system the activity was lower to achieve 202 TOF's per hour, and the conversion of LA and selectivity to GVL were 99 and 97 mol%, respectively. Moustani et al. (2018) investigated the hydrogenation reaction of LA using $RuCl_3{\cdot}3H_2O$, $Ru(NO)(OAc)_3$, $Ru(NO)(NO_3)_3$, $Ru(acac)_3$, $[Ru(NO)]_2(SO_4)_3$, and $RuO_2{\cdot}H_2O$ catalyst precursors modified with water-soluble phosphine and especially with nitrogen-containinig ligands such as TPPTS, PTA, bathophenanthrolinedisulfonic acid disodium salt (BPhDS), bathocuproinedisulfonic acid disodium salt (BCDS), 2-aminoethanesulfonic acid (taurine), nitrilotriacetic acid trisodium salt ($NTA{\cdot}Na_3$), ethylenediaminetetraacetic acid tetrasodium salt ($EDTA{\cdot}Na_4$), 2,2'-biquinoline-4,4'dicarboxylic acid dipotassium salt (BQC), tris(2-pyridyl)phosphine (T_2PyP), N,N'-2,2'-bipyridine-4,4'-dicarboxylic acid (BPyDCA), diethylenetriaminepentakis(methylphosphonic acid) (DTPPA), diethylenetriaminepentaacetic acid pentasodium salt ($DTPA{\cdot}Na_5$) and 3-pyridinesulfonic acid (3-PSA) (**Figure 8**) in the aqueous monophasic system. The highest activity of TOF = 3,000 h^{-1} was obtained with $RuCl_3{\cdot}3H_2O$/BPhDS catalysts at 140°C, 80 bar H_2 pressure within 1 h and molar ratios of LA/Ru = 3,000 and BPhDS/Ru=1 with addition of 5 ml of aqueous solvent by a ruthenium concentration of 75 ppm and pH value of 2.43 where the conversion of LA was quantitative with essentially quantitative selectivity to GVL of 99.9 mol% and formation of only 0.1 mol % of the 1,4-PDO byproduct. The apparent activation energy of the Ru/BPhDS catalytic system amounts a relative low value of 53.3 kJ/mol, which is remarkable when one considers that this catalyst reduces a less reactive keto functionality into an alcohol group. Recycling experiments of the Ru/BPhDS catalyst from the aqueous monophasic LA hydrogenation reaction mixture, followed by biphasic recovery of the catalyst in active form from organic reaction products by extraction and simple phase separation of an aqueous/organic two-phase system created after external addition of diethyl ether, has shown that the catalyst is stable without loss of activity and selectivity in a consecutive run. The presence of organic solvents gives rise to a dramatic drop in catalytic activities which was obvious during the recycling experiments of the

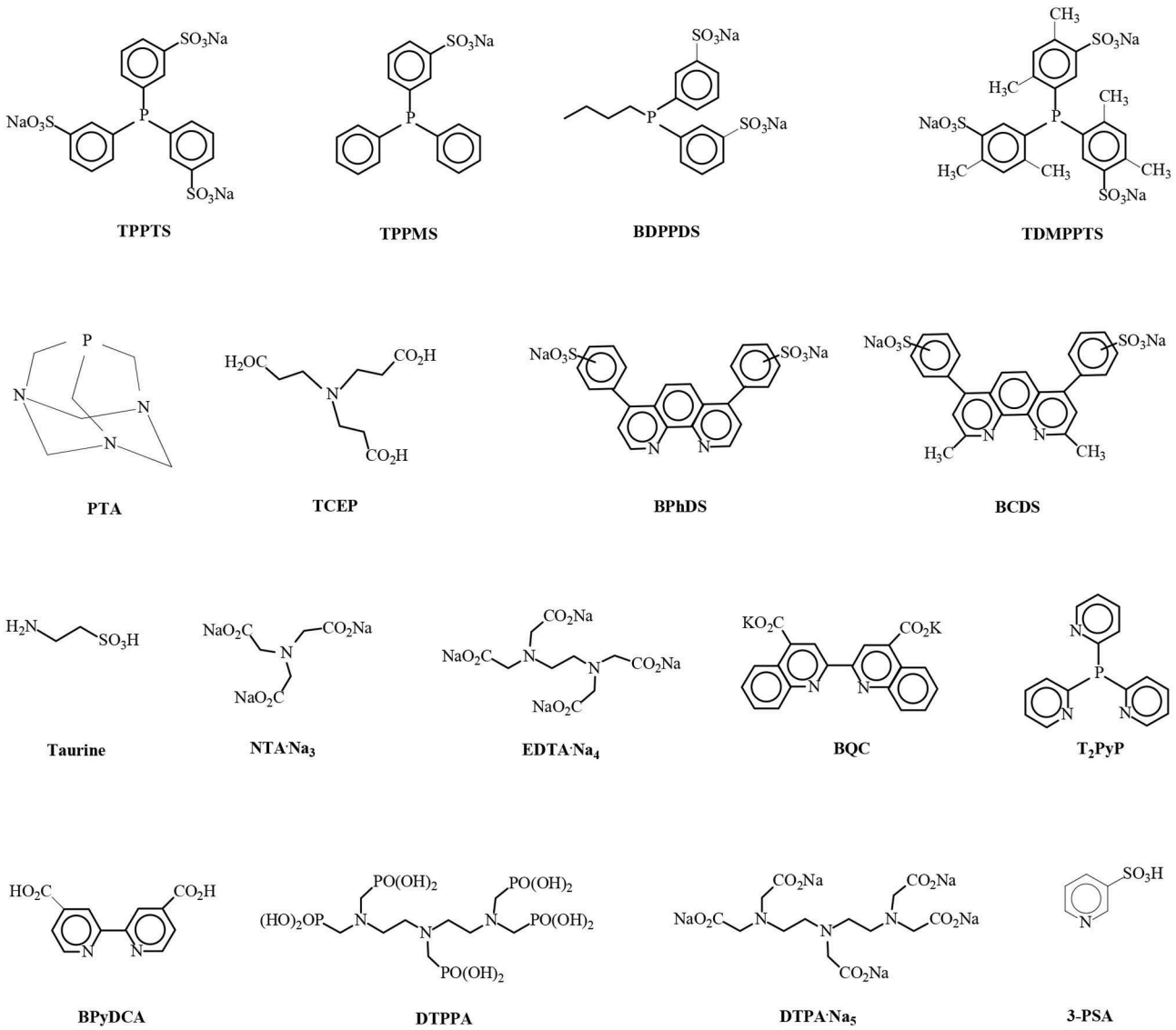

FIGURE 8 | Structures of the water-soluble ligands triphenylphosphinetrisulfonic acid trisodium salt (TPPTS), triphenylphosphinemonosulfonic acid monosodium salt (TPPMS), *n*-butyldiphenylphosphinedisulfonic acid disodium salt (BDPPDS), tris(2,4-dimethylphenyl)phosphinetrisulfonic acid trisodium salt (TDMPPTS), 1,3,5-triaza-7-phosphaadamantane (PTA), tris(2-carboxyethyl)phosphine (TCEP), bathophenanthrolinedisulfonic acid disodium salt (BPhDS), bathocuproinedisulfonic acid disodium salt (BCDS), 2-aminoethanesulfonic acid (Taurine), nitrilotriacetic acid trisodium salt (NTA·Na_3), ethylenediaminetetraacetic acid tetrasodium salt (EDTA·Na_4), 2,2′-biquinoline-4,4′dicarboxylic acid dipotassium salt (BQC), tris(2-pyridyl)phosphine (T_2PyP), N,N′-2,2′-bipyridine-4,4′-dicarboxylic acid (BPyDCA), diethylenetriaminepentakis(methylphosphonic acid) (DTPPA), diethylenetriaminepentaacetic acid pentasodium salt (DTPA·Na_5) and 3-pyridinesulfonic acid (3-PSA).

Ru/BPhDS catalytic system. After the hydrogenation run it is crucial to add small amounts of the organic solvent, i.e., only up to 10 ml of diethyl ether to the aqueous monophasic reaction mixture (10 ml), to form a biphasic system for the recovery and recycling of the Ru/BPhDS catalyst. In the case that higher quantities of diethyl ether were added for the extraction, the catalytic activity exponentially decreased in the consecutive LA hydrogenation run due to the minor amount of diethyl ether which was inevitably dissolved in the aqueous catalyst solution.

One-Pot Hydrogenation of LA Into VA, 1,4-PDO, 2-MTHF, 2-Pentanol and 2-Butanol

The catalytic hydrogenation of LA beyond GVL to yield VA, which in the presence of alcohols under acidic conditions forms alkyl valerate biofuels and 1,4-PDO followed by dehydration to obtain 2-MTHF (**Figure 9**), is a difficult reaction which usually takes place in the gas-phase often in the presence of platinum-based heterogeneous catalysts under severe conditions i.e., high temperatures and/or high dihydrogen pressures. For example,

Kon et al. (2014) described how the one-pot hydrogenation of LA catalyzed by Pt/H-ZSM-5 at 200°C under solvent-free conditions yielded up to 99 mol% VA. Whereas, with methanol up to 87 mol% methyl valerate, Lange et al. (2010) disclosed the one-step conversion of GVL into valeric esters over Pt/TiO_2 catalysts with a selectivity of 20–50 mol% pentyl valerate at higher temperatures of 275–300°C. Ruthenium-catalyzed one-pot hydrogenation reactions of LA into VA and 1,4-PDO are rare probably because ruthenium-based catalysts in the gas-phase suffer from drawbacks such as poor hydrogenation activity compared to analogous platinum and other transition metals-based counterparts applied in the gas-phase. The first example of one-pot hydrogenation reaction of LA into VA was reported by Luo et al. (2013), and deals with the application of the Ru/H-ZSM catalyst which contains strongly acidic sites able to catalyze the most difficult step in that sequence which is considered to be the rate-limiting step, namely the ring-opening reaction of GVL to yield at 200°C under 40 bar of dihydrogen pressure up to 45.8 mol% VA together with alkyl valerate co-products. The Ru/H-ZSM catalyst suffers from gradual deactivation, which could be attributed to dealumination resulting in a loss of catalytically active acid sites. At the higher temperature of 200°C the acid-catalyzed dehydration reaction of LA takes place with formation of α-angelica lactone, which polymerizes on the acidic sites to yield coke that after deposition also deactivates the Ru/H-ZSM catalyst. Bababrik et al. (2017) disclosed DFT calculations to present in detail the reaction mechanism of GVL conversion on Ru(0001) surfaces. The authors have shown that the GVL ring-opening step through breaking the C(1)-O(2) bond (**Figure 10**) proceeds rather easily with an activation energy of 25 kJ/mol and exothermicity (-31 kJ/mol), and the rate-limiting step is the hydrogenation step of the formed acyl intermediate $CH_3CH(O^*)$-$(CH_2)_2$-C^*-O^* with an activation barrier of 146 kJ/mol and endothermicity (+74 kJ/mol) to yield 1,4-PDO. In contrast, the alternative pathway of GVL ring-opening through breaking the C(4)-O(2) bond (**Figure 10**) proceeds with more difficulty with a much higher energy barrier of 122 kJ/mol, which leads to VA (Rozenblit et al., 2016). Aqueous-phase hydrogenations of GVL catalyzed by 5 wt.% Ru/C were carried out by Rozenblit et al. (2016) at 200°C under 69 bar dihydrogen pressure to obtain a conversion of GVL of 10.3 mol% and a spectrum of products with a yield of 4.95 mol% 2-butanol, formed after C-C bond cleavage in a decarbonylation step of the surface acyl intermediate $CH_3CH(O^*)$-$(CH_2)_2$-C^*-O^* obtained after GVL ring-opening, and further 4.63 mol% 1,4-PDO after hydrogenation of the acyl intermediate, 0.64 mol% 2-MTHF after dehydration of 1,4-PDO and cyclization, and 0.08 mol% 2-pentanol obtained after deoxygenation and further hydrogenation of the surface $CH_3CH(O^*)$-$(CH_2)_2$-C^*-O^* acyl intermediate. Cui et al. (2018) studied the continuous one-pot aqueous-phase hydrogenation reaction of LA catalyzed by molybdenum-modified Ru/C catalysts to obtain almost quantitative conversion of LA and selectivities of 96.7 mol% 1,4-PDO, 0.2 mol% 2-MTHF, 0.5 mol% GVL, 0.6 mol% 2-butanol and 2.0 mol% 2-pentanol using an atomic ratio of Mo/Ru= 0.25 under mild conditions at 70° C and 40 bar dihydrogen pressure. *In situ* FTIR investigations revealed that RuNPs are responsible for the activation and dissociation of the dihydrogen reactant and on Mo catalytically active species the absorption and activation of the keto functionality of LA starting material takes place. The Ru-MoO_x/C catalyst remained stable for a period of 200 h continuous one-pot LA hydrogenation

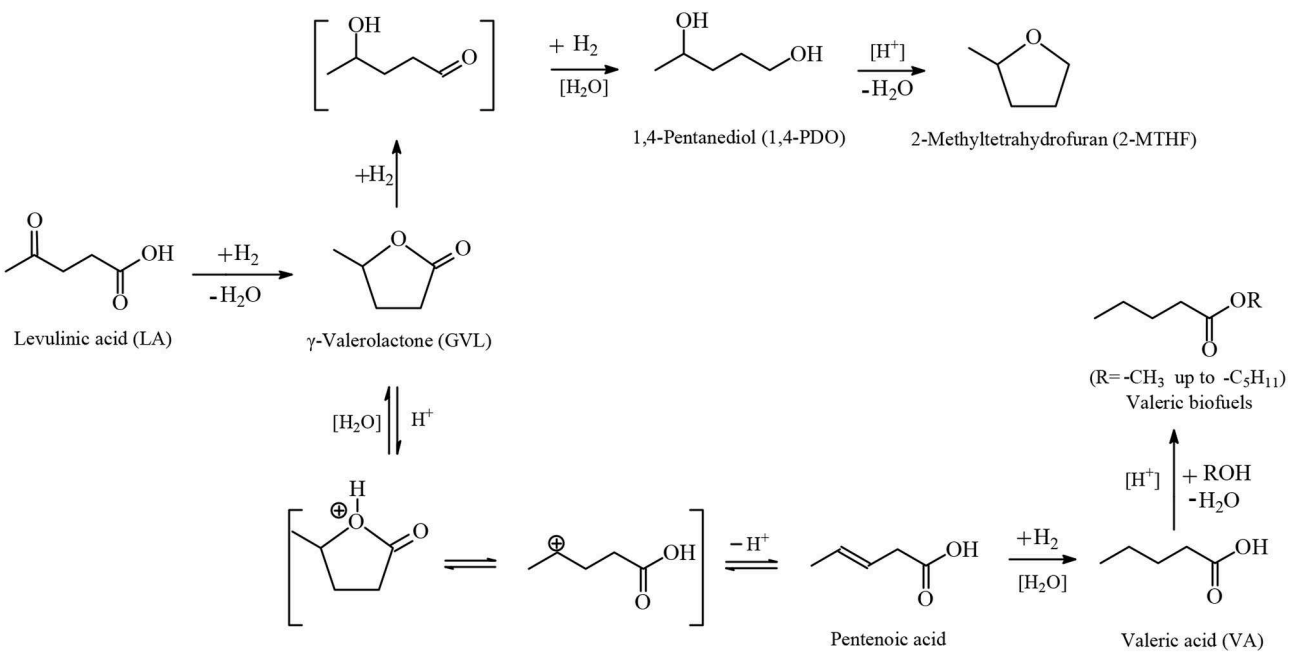

FIGURE 9 | Hydrogenation of LA beyond GVL to yield VA for the production of valeric biofuels and 1,4-PDO followed by dehydration to form 2-MTHF.

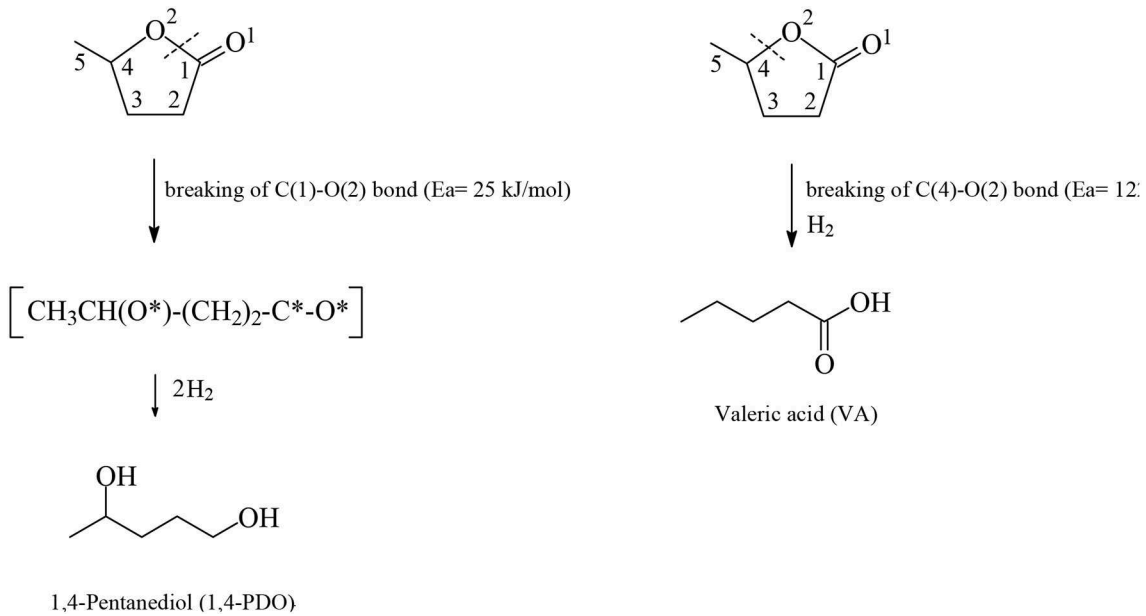

FIGURE 10 | Ring-opening pathways of GVL through breaking the C(1)-(O)2 bond which after hydrogenation eventually leads into 1,4-PDO and through C(4)-(O)2 bond breaking into VA.

reaction toward 1,4-PDO without any deactivation. Lv et al. (2018) reported the one-pot aqueous-phase hydrogenation of LA catalyzed by nanoporous ruthenium-based catalysts to obtain at 100°C under 60 bar H_2 within 6 h reaction time a yield of 74.6 mol% 1,4-PDO, 1.9 mol% 2-MTHF, 4.6 mol% GVL, 10.4 mol% 2-butanol and 5.0 mol% 2-pentanol. At a higher temperature of 140°C the yields of both 2-butanol and 2-pentanol were increased to 63.6 and 15.2 mol%, respectively, with, however, a low yield of 1,4-PDO of 0.9 mol%. Mizugaki et al. (2017) and Mizugaki and Kaneda (2019) investigated the one-pot hydrogenative C-C bond cleavage reaction of LA catalyzed by RuNPs with an average particle diameter of 3 nm supported on CeO_2 to achieve almost an quantitative conversion of LA and a yield of 85 mol% 2-butanol and of 5 mol% 2-pentanol at 150°C under 30 bar dihydrogen pressure within 12 h reaction time in aqueous media. The presence of the aqueous solvent is indispensable in the Ru/CeO_2-catalyzed hydrogenative C-C cleavage reaction of LA toward 2-butanol, because in organic solvents such as 2-propanol, THF or dimethoxyethane the yield to 2-butanol was only up to 5 mol% and the major products were GVL of 70 mol% and 1,2-PDO of 23 mol%. Licursi et al. (2018) studied a cascade process for the direct conversion of LA or GVL into 2-MTHF or 2-butanol and 2-pentanol, employing commercially available catalysts in the aqueous solvent. The authors used for the first time a catalyst combination of Ru/C along with Re/C, together with niobium phosphate to obtain selectivities toward 2-MTHF of 28 mol% or 65 mol % from LA or GVL substrates, respectively. In sharp contrast employing a catalyst combination comprising of Ru/C and HY zeolite at 200°C under 30 bar dihydrogen pressure, the reaction takes another course and yields a mixture of 2-butanol with 2-pentanol of 88.8 mol% and 100 mol% from LA and GVL starting materials, respectively, in aqueous media.

SUMMARY AND OUTLOOK

The catalytic hydrogenation route for the valorization of LA has received considerable interest recent years because of the wide range of potential applications of LA's hydrogenation products which include, *inter alia*, advanced biofuels, fine chemicals, solvents and additives to gasoline or to food. In the last decade the hydrogenation reactions of LA into GVL, which is a key intermediate compound, and beyond GVL to yield VA, 1,4-PDO, 2-MTHF, 2-pentanol, and 2-butanol have gained a lot of attention and various transition metal catalytic systems have been developed in the absence and presence of organic or aqueous solvents. Remarkable progress has been made, however, in the application of ruthenium-based catalytic systems which have been used extensively due to the inherent ability of ruthenium under mild conditions to hydrogenate the carbonyl functionality of levulinic acid selectively into an alcohol group to form 4-hydroxyvaleric acid intermediate, which spontaneously after dehydration and cyclization yields GVL. This critical review has summarized and discussed the progress made in the last decade in the field of aqueous-phase ruthenium-catalyzed hydrogenation reactions of LA employing heterogeneous catalysts on solid supports and heterogeneous water-dispersible catalytic nanoparticles or homogeneous water-soluble catalytic

complexes with biphasic catalyst separation. The significance of the aqueous solvent to carry out catalytic hydrogenation reactions of LA has been highlighted because the presence of water combines many environmental and economic benefits. Therefore, this review constitutes a guidance for the development of novel efficient ruthenium-based catalytic systems which would be more active and especially capable for the one-pot hydrogenation of LA toward VA, 1,4-PDO, 2-MTHF, 2-pentanol and 2-butanol. At the same time it offers guidance on more stable and recyclable systems suitable as catalysts for industrial-scale LA hydrogenation reaction in green and sustainable aqueous solvents to be integrated into biorefineries of the future.

AUTHOR CONTRIBUTIONS

GP has written this review. All other authors have equally contributed and approved it for publication.

FUNDING

Financial support of this work by the Postgraduate Studies Programme on Catalysis and its Applications in the Industry of Greek Ministry of Education and by the Special Account for Research Grants of the Research Committee of the National and Kapodistrian University of Athens under contract 70/4/7568 are gratefully acknowledged.

REFERENCES

Albani, D., Li, Q., Vilé, G., Mitchell, S., Almora-Barrios, N., Witte, P. T., et al. (2017). Interfacial acidity in ligand-modified ruthenium nanoparticles boosts thehydrogenation of levulinic acid to gamma-valerolactone. *Green Chem.* 19, 2361–2370. doi: 10.1039/C6GC02586B

Al-Shaal, M. G., Wright, W. R. H., and Palkovits, R. (2012). Exploring the ruthenium catalyzedsynthesis of γ-valerolactone in alcohols and utilisation of mild solvent-free reactionconditions. *Green Chem.* 14, 1260–1263. doi: 10.1039/c2gc16631c

Aycock, D. F. (2007). Solvent applications of 2-methyltetrahydrofuran in organometallic and biphasic reactions. *Org. Process Res. Rev.* 11, 156–159. doi: 10.1021/op060155c

Bababrik, R. M., Wang, B., and Resasco, D. (2017). Reaction mechanism for the conversion of γ-valerolactone (GVL) over a Ru catalyst: a first-principles study. *Ind. Eng. Chem. Res.* 56, 3217–3222. doi: 10.1021/acs.iecr.7b00196

Badgujar, K. C., Badgujar, V. C., and Bhanage, B. M. (2020). A review on catalytic synthesis ofenergy rich fuel additive levulinate compounds from biomass derived levulinic acid. *Fuel Process. Technol.* 197:106213. doi: 10.1016/j.fuproc.2019.106213

Bond, J. Q., Alonso, D. M., Wang, D., West, R. M., and Dumesic, J. A. (2010). Intergrated catalyticconversion of γ-valerolactone to liquid alkenes for transportation fuels. *Science* 327, 1110–1114. doi: 10.1126/science.1184362

Bond, J. Q., Upadhye, A. A., Olcay, H., Tompsett, G. A., Jae, J., Xing, R., et al. (2014). Production of renewable jet fuel range alkanes and commodity chemicals from integrated catalytic processing of biomass. *Energy Environ. Sci.* 7, 1500–1523. doi: 10.1039/C3EE43846E

Bouriazos, A., Sotiriou, S., Stathis, P., and Papadogianakis, G. (2014). Superior aqueous-phasecatalytic hydrogenation activity of palladium modified with nitrogen-containing ligands compared with the TPPTS benchmark modifier in micellar nanoreactors. *Appl. Catal. B: Environ.* 150–151, 345–353. doi: 10.1016/j.apcatb.2013.12.032

Bozell, J. J., and Petersen, G. R. (2010). Technology development for the production of biobased products from biorefinery carbohydrates - the US Department of Energy's "Top 10" revisited. *Green Chem.* 12, 539–554. doi: 10.1039/b922014c

Bulut, S., Fei, Z., Siankevich, S., Zhang, J., Yan, N., and Dyson, P. J. (2015). Aqueous-phase hydrogenation of alkenes and arenes: The growing role of nanoscale catalysts. *Catal. Today* 247, 96–103. doi: 10.1016/j.cattod.2014.09.002

Byrne, F., Forier, B., Bossaert, G., Hoebers, C., Farmer, T. J., Clark, J. J., et al. (2017). 2,2,5,5-Tetramethyltetrahydrofuran (TMTHF): a non-polar, non-peroxide forming ether replacement for hazardous hydrocarbon solvents. *Green Chem.* 19, 3671–3678. doi: 10.1039/C7GC01392B

Chalid, M., Broekhuis, A. A., and Heeres, H. J. (2011). Experimental and kinetic modeling studies on the biphasic hydrogenation of levulinic acid to γ-valerolactone using a homogeneous water-soluble Ru-(TPPTS) catalyst. *J. Mol. Catal. A: Chem.* 341, 14–21. doi: 10.1016/j.molcata.2011.04.004

Chen, M., Dong, Q., Ni, W., Zhao, X., Gu, Q., Tang, G., et al. (2017). Cyclodextrin-based polymer-assisted Ru nanoparticles for the aqueous hydrogenation of biomass-deriver platform molecules. *ChemistrySelect* 2, 10537–10545. doi: 10.1002/slct.201702229

Climent, M. A., Corma, A., and Iborra, S. (2014). Conversion of biomass platform molecules into fuel additives and liquid hydrocarbon fuels. *Green Chem.* 16, 516–547. doi: 10.1039/c3gc41492b

Cui, J., Tan, J., Zhu, Y., and Cheng, F. (2018). Aqueous hydrogenation of levulinic Acid to 1,4-pentanediol over Mo-modified Ru/activated carbon catalyst. *ChemSusChem.* 11, 1316–1320. doi: 10.1002/cssc.201800038

Delhomme, C., Schaper, L.-A., Zhang-Preße, M., Raudaschl-Sieber, G., Weuster-Botz, D., and Kühn, F. E. (2013). Catalytic hydrogenation of levulinic acid in aqueous phase. *J. Organomet. Chem.* 724, 297–299. doi: 10.1016/j.jorganchem.2012.10.030

Duan, H., Wang, D., and Li, Y. (2015). Green chemistry for nanoparticle synthesis. *Chem. Soc. Rev.* 44, 5778–5792. doi: 10.1039/C4CS00363B

Dutta, S., Yu, I. K. M., Tsang, D. C. W., Ng, Y. H., Ok, Y. S., Sherwood, J., et al. (2019). Green synthesis of gamma-valerolactone (GVL) through hydrogenation of biomass-derived levulinic acid using non-noble metal catalysts: a critical review. *Chem. Eng. J.* 372, 992–1006. doi: 10.1016/j.cej.2019.04.199

Dykeman, R. R., Yuan, Y., Yan, N., Asakura, H., Teramura, K., Tanaka, T., et al. (2012). Rational design of a molecular nanocatalyst-stabilizer that enhances both catalytic activity and nanoparticle stability. *ChemCatChem* 4, 1907–1910. doi: 10.1002/cctc.201200552

Fábos, V., Koczó, G., Mehdi, H., Boda, L., and Horváth, I. T. (2009). Bio-oxygenates and the peroxide number: a safety issue alert. *Energy Environ. Sci.* 2, 767–769. doi: 10.1039/b900229b

Filiz, B. C., Gnanakumar, E. S., Martínez-Arias, A., Gengler, R., Rudolf, P., Rothenberg, G., et al. (2017). Highly selective hydrogenation of levulinic acid to γ-valerolactone over Ru/ZrO_2 catalysts. *Catal. Lett.* 147, 1744–1753. doi: 10.1007/s10562-017-2049-x

Fremy, G., Monflier, E., Carpentier, J.-F., Castanet, Y., and Mortreux, A. (1995). Enhancement of catalytic activity for hydroformylation of methyl acrylate by using biphasic and "supported aqueous phase" systems. *Angew. Chem. Int. Ed Engl.* 34, 1474–1476. doi: 10.1002/anie.199514741

Ftouni, J., Murillo, A. M., Goryachev, A. E., Hofmann, J. P., Hensen, E. J. M., Lu, L., et al. (2016). ZrO_2 is preferred over TiO_2 as support for the Ru-catalyzed hydrogenation of levulinic acid to γ-valerolactone. *ACS Catal.* 6, 5462–5472. doi: 10.1021/acscatal.6b00730

Gao, X., Zhu, S., Dong, M., Wang, J., and Fan, W. (2019). Ru nanoparticles deposited on ultrathin TiO_2 nanosheets as highly active catalyst for levulinic acid hydrogenation to γ-valerolactone. *Appl. Catal. B: Environ.* 259:118076. doi: 10.1016/j.apcatb.2019.118076

Gao, Y., Zhang, H., Han, A., Wang, J., Tan, H.-R., Tok, E.-S., et al. (2018). Ru/ZrO_2 catalysts for transfer hydrogenation of levulinic acid with formic acid/formate mixtures: importance of support stability. *Chem. Select* 3, 1343–1351. doi: 10.1002/slct.201702152

Gundekari, S., and Srinivasan, K. (2019). Hydrous ruthenium oxide: a new generation remarkable catalyst precursor for energy efficient and sustainable production of γ-valerolactone from levulinic acid in aqueous medium. *Appl. Catal. A Gen.* 569, 117–125. doi: 10.1016/j.apcata.2018.10.018

Guo, Y., Li, Y., Chen, J., and Chen, L. (2016). Hydrogenation of levulinic acid into γ-valerolactone over ruthenium catalysts supported on Metal-Organic Frameworks in aqueous medium. *Catal Lett.* 146, 2041–2052. doi: 10.1007/s10562-016-1819-1

Home page of GFBiochemicals company. (2019). Available online at: http://www.gfbiochemicals.com/company/ (accessed January 20, 2020)

Huber, G. W., Iborra, S., and Corma, A. (2006). Synthesis of transportation fuels from biomass: chemistry, catalysts, and engineering. *Chem. Rev.* 106, 4044–4098. doi: 10.1021/cr068360d

Joó, F., Tóth, Z., and Beck, M. T. (1977). Homogeneous hydrogenations in aqueous solutions catalyzed by transition metal phosphine complexes. *Inorg. Chim. Acta* 25, L61–L62 doi: 10.1016/S0020-1693(00)95645-7

Kon, K., Onodera, W., and Shimizu, K.-I. (2014). Selective hydrogenation of levulinic acid to valeric acid and valeric biofuels by a Pt/HMFI catalyst. *Catal. Sci. Technol.* 4, 3227–3234. doi: 10.1039/C4CY00504J

Kubas, G. J. (2005). Catalytic processes involving dihydrogen complexes and other sigma-bond Complexes. *Catal. Lett.* 104, 79–101. doi: 10.1007/s10562-005-7440-3

Kubo, Y., Kakizaki, D., Kogo, M., and Magatani, Y. (2016). Water-dispersible boronate nanoparticles as support materials for noble metals in the hydrogenation of levulinic acid to γ-valerolactone. *Supramol. Chem.* 28, 91–97. doi: 10.1080/10610278.2015.1086764

Lange, J. P., Price, R., Ayoub, P. M., Louis, J., Petrus, L., Clarke, L., et al. (2010). Valeric biofuels: a platform of cellulosic transportation fuels. *Angew. Chem. Int. Ed.* 49, 4479–4483. doi: 10.1002/anie.201000655

Leitner, W., Klankermayer, J., Pischinger, S., Pitsch, H., and Kohse-Höinghaus, K. (2017). Advanced biofuels and beyond: chemistry solutions for propulsion and production. *Angew. Chem. Int. Ed.* 56, 5412–5452. doi: 10.1002/anie.201607257

Li, G., Liu, W., Ye, C, Li, X., and Si, C. L., (2018). Chemocatalytic conversion of cellulose into key platform chemicals. *Int. J. Polym. Sci.* 2018:21. doi: 10.1155/2018/4723573

Licursi, D., Antonetti, C., Fulignati, S., Giannoni, N., and Raspolli Galletti, A. M. (2018). Cascade strategy for the tunable catalytic valorization of levulinic acid and γ-valerolactone to 2-methyltetrahydrofuran and alcohols. *Catalysts* 8:277. doi: 10.3390/catal8070277

Liu, X., Lan, G., Boyjoo, Y., Qian, L., Gu, S., Price, C. A. H., et al. (2019). N-doped carbon spheres impregnated with highly monodispersed ruthenium nanoparticles as a hydrogenation catalyst. *Chem. Eng. J.* 374, 895–903. doi: 10.1016/j.cej.2019.05.213

Luo, W., Deka, U., Beale, A. M., Van Eck, E. R. H., Bruijnincx, P. C. A., and Weckhuysen, B. M. (2013). Ruthenium-catalyzed hydrogenation of levulinic acid: Influence of the support and solvent on catalyst selectivity and stability. *J. Catal.* 301, 175–186. doi: 10.1016/j.jcat.2013.02.003

Lv, J., Rong, Z., Sun, L., Liu, C., Lu, A.-H., Wang, Y., et al. (2018). Catalytic conversion of biomass-derived levulinic acid into alcohols over nanoporous Ru catalyst. *Catal. Sci. Technol.* 8, 975–979. doi: 10.1039/C7CY01838J

Makhubela, B. C. E., and Darkwa, J. (2018). The role of noble metal catalysts in conversion of biomass and bio-derived intermediates to fuels and chemicals. *Johnson Matthey Technol. Rev.* 62, 4–31. doi: 10.1595/205651317X696261

Mamun, O., Saleheen, M., Bond, J. Q., and Heyden, A. (2019). Investigation of solvent effects in the hydrodeoxygenation of levulinic acid to γ-valerolactone over Ru catalysts. *J. Catal.* 379, 164–179. doi: 10.1016/j.jcat.2019.09.026

Mehdi, H., Fábos, V., Tuba, R., Bodor, A., Mika, L. T., and Horváth, I. T. (2008). Integration of homogeneous and heterogeneous catalytic processes for a multi-step conversion of biomass: from sucrose to levulinic acid, γ-valerolactone, 1,4-pentanediol, 2-methyl-tetrahydrofuran, and alkanes. *Top. Catal.* 48, 49–54. doi: 10.1007/s11244-008-9047-6

Michel, C., and Gallezot, P. (2015). Why is ruthenium an efficient catalyst for the aqueous-phase hydrogenation of bio-sourced carbonyl compounds? *ACS Catal* 5, 4130–4132. doi: 10.1021/acscatal.5b00707

Michel, C., Zaffran, J., Ruppert, A. M., Matras-Michalska, J., Jedrzejczyk, M., Grams, J., et al. (2014). Role of water in metal catalyst performance for ketone hydrogenation: a joint experimental and theoretical study on levulinic acid conversion into gamma-valerolactone. *Chem. Commun.* 50, 12450–12453. doi: 10.1039/C4CC04401K

Mika, L. T., Cséfalvay, E., and Horváth, I. T. (2015). The role of water in catalytic biomass-based technologies to produce chemicals and fuels. *Catal. Today* 247, 33–46. doi: 10.1016/j.cattod.2014.10.043

Mizugaki, T., and Kaneda, K. (2019). Development of high performance heterogeneous catalysts for selective cleavage of C-O and C-C bonds of biomass-derived oxygenates. *Chem. Rec.* 19, 1179–1198. doi: 10.1002/tcr.201800075

Mizugaki, T., Togo, K., Maeno, Z., Mitsudome, T., Jitsukawa, K., and Kaneda, K. (2017). New routes for refinery of biogenic platform chemicals catalyzed by cerium oxide-supported ruthenium nanoparticles in water. *Sci. Rep* 7:14007. doi: 10.1038/s41598-017-14373-1

Molleti, J., Tiwari, M. S., and Yadav, G. D. (2018). Novel synthesis of Ru/OMS catalyst by solvent-free method: Selective hydrogenation of Levulinic acid to γ-valerolactone in aqueous medium and kinetic modelling. *Chem. Eng. J.* 334, 2488–2499. doi: 10.1016/j.cej.2017.11.125

Moreno-Marrodan, C., and Barbaro, P. (2014). Energy efficient continuous production of γ-valerolactone by bifunctional metal/acid catalysis in one pot. *Green Chem.* 16, 3434–3438. doi: 10.1039/c4gc00298a

Moustani, C., Anagnostopoulou, E., Krommyda, K., Panopoulou, C., Koukoulakis, K. G., Bakeas, E. B., et al. (2018). Novel aqueous-phase hydrogenation reaction of the key biorefinery platform chemical levulinic acid into γ-valerolactone employing highly active, selective and stable water-soluble ruthenium catalysts modified with nitrogen-containing ligands. *Appl. Catal. B: Environ.* 238, 82–92. doi: 10.1016/j.apcatb.2018.07.009

Ndolomingo, M. J., and Meijboom, R. (2019). Noble and base-metal nanoparticles supported on mesoporous metal oxides: efficient catalysts for the selective hydrogenation of levulinic acid to γ-valerolactone. *Catal. Lett.* 149, 2807–2822. doi: 10.1007/s10562-019-02790-y

Nenamashi, M., Noh, J.-H., and Meijboom, R. (2018). Hydrogenation of biomass-derived levulinic acid to γ-valerolactone catalyzed by mesoporous supported dendrimer-derived Ru and Pt catalysts: an alternative method for the production of renewable biofuels. *Appl. Catal. A Gen.* 550, 77–89. doi: 10.1016/j.apcata.2017.10.015

Omoruyi, U., Page, S., Hallett, J., and Miller, P. W. (2016). Homogeneous catalyzed reactions of levulinic acid: to γ-valerolactone and beyond. *ChemSusChem* 9, 2037–2047. doi: 10.1002/cssc.201600517

Ortiz-Cervantes, C., and García, J. J. (2013). Hydrogenation of levulinic acid to γ-valerolactone using ruthenium nanoparticles. *Inorg. Chimica Acta* 397, 124–128. doi: 10.1016/j.ica.2012.11.031

Osatiashtiani, A., Lee, A. F., and Wilson, K. (2017). Recent advances in the production of γ- valerolactone from biomass-derived feedstocks via heterogeneous catalytic transfer hydrogenation. *J. Chem. Technol. Biotechnol.* 92, 1125–1135. doi: 10.1002/jctb.5213

Papadogianakis, G., and Sheldon, R. A. (1996). Catalytic conversions in water: environmentally attractive processes employing water soluble transition metal complexes. *New J. Chem.* 20, 175–185

Papadogianakis, G., and Sheldon, R. A. (1997). Catalytic conversions in water. Part 7: An environmentally benign concept for heterogenization of homogeneous catalysis. *Catalysis*, *Specialist Periodical Reports, Royal Soc. Chem.* 13, 114–193. doi: 10.1039/9781847553256-00114

Papadogianakis, G., Verspui, G., Maat, L., and Sheldon, R. A. (1997). Catalytic conversions in water. Part 6. A novel biphasic hydrocarboxylation of olefins catalyzed by palladium TPPTS complexes (TPPTS= $P(C_6H_4\text{-}m\text{-}SO_3Na)_3$). *Catal. Lett.* 47, 43–46.

Patil, N. M., and Bhanage, B. M. (2016). Greener, recyclable, and reusable ruthenium(III) chloride/ polyethylene glycol/water system for the selective hydrogenation of biomass-derived levulinic acid to γ-valerolactone. *ChemCatChem* 8, 3458–3462. doi: 10.1002/cctc.201600872

Pileidis, F. D., and Titirici, M.-M. (2016). Levulinic acid biorefineries: new challenges for efficient utilization of biomass. *ChemSusChem* 9, 562–582. doi: 10.1002/cssc.201501405

Piskun, A., Winkelman, J. G. M., Tang, Z., and Heeres, H. J. (2016). Support screening studies on the hydrogenation of levulinic acid to γ-valerolactone in water using Ru catalysts. *Catalysts* 6:131. doi: 10.3390/catal6090131

Piskun, A. S., Ftouni, J., Tang, Z., Weckhuysen, B. M., Bruijnincx, P. C. A., and Heeres, H. J. (2018). Hydrogenation of levulinic acid to γ-valerolactone over anatase-supported Ru catalysts: effect of catalyst synthesis protocols on activity. *Appl. Catal. A Gen.* 549, 197–206. doi: 10.1016/j.apcata.2017.09.032

Primo, A., Concepción, P., and Corma, A. (2011). Synergy between the metal nanoparticles and the support for the hydrogenation of functionalized carboxylic acids to diols on Ru/TiO_2. *Chem. Commun.* 47, 3613–3615. doi: 10.1039/c0cc05206j

Protsenko, I. I., Abusuek, D. A., Nikoshvili, L. Z., Bykov, A. V., Matveeva, V. G., and Sulman, E. M. (2018). The use of the Ru-containing catalyst based on hypercrosslinked polystyrene in the hydrogenation of levulinic acid to γ-valerolactone. *Catal. Ind.* 10, 301–312. doi: 10.1134/S2070050418040128

Protsenko, I. I., Nikoshvili, L. Z., Bykov, A. V., Matveeva, V. G., Sulman, A., Sulman, E. M., et al. (2017). Hydrogenation of levulinic acid using Ru-containing catalysts based on hypercrosslinked polystyrene. *Green Process. Synth.* 6, 281–286. doi: 10.1515/gps-2016-0189

Protsenko, I. I., Nikoshvili, L. Z., Matveeva, V. G., Sulman, E. M., and Rebrov, E. (2016). Selective hydrogenation of levulinic acid to gamma-valerolactone using polymer-based Ru-containing catalysts. *Chem. Eng. Trans.* 52, 679–684. doi: 10.3303/CET1652114

Raspolli Galletti, A. M., Antonetti, C., De Luise, V., and Martinelli, M. (2012). A sustainable process for the production of γ-valerolactone by hydrogenation of biomass-derived levulinic acid. *Green Chem.* 14, 688–694. doi: 10.1039/c2gc15872h

Raspolli Galletti, A. M., Antonetti, C., Ribechini, E., Colombini, M. P., Di Nasso, N. N., and Bonari, E. (2013). From giant reed to levulinic acid and gamma-valerolactone: a high yield catalytic route to valeric biofuels. *Appl. Energy* 102, 157–162. doi: 10.1016/j.apenergy.2012.05.061

Ren, H.-F., Zhu, D., Li, J.-F., Liu, C.-L., Yang, R.-Z., and Dong, W.-S. (2019). One-pot conversion of carbohydrates into γ-valerolactone under the coordination of heteropoly acid based ionic liquid and Ru/ZrO_2 in water media. *J. Chem. Technol. Biotechnol.* 94, 2355–2363. doi: 10.1002/jctb.6031

Roucoux, A., Schulz, J., and Patin, H. (2002). Reduced transition metal colloids: a novel family of reusable catalysts? *Chem. Rev.* 102, 3757–3778. doi: 10.1021/cr010350j

Rozenblit, A., Avoian, A. J., Tan, Q., Sooknoi, T., and Resasco, D. E. (2016). Reaction mechanism of aqueous-phase conversion of γ-valerolactone (GVL) over a Ru/C catalyst. *J. Energy Chem.* 25, 1008–1014. doi: 10.1016/j.jechem.2016.11.010

Ruppert, A. M., Agulhon, P., Grams, J., Wachała, M., Wojciechowska, J., Swierczynski, D., et al. (2019). Synthesis of TiO_2-ZrO_2 mixed oxides via the alginate route: application in the Ru catalytic hydrogenation of levulinic acid to gamma-valerolactone. *Energies* 12:4706. doi: 10.3390/en12244706

Ruppert, A. M., Grams, J., Jedrzejczyk, M., Matras-Michalska, J., Keller, N., Ostojska, K., et al. (2015). Titania-supported catalysts for levulinic acid hydrogenation: influence of support and its impact on γ-valerolactone yield. *ChemSusChem* 8, 1538–1547. doi: 10.1002/cssc.201403332

Serrano-Ruiz, J. C., Luque, R., and Sepúlveda-Escribano, A. (2011). Transformations of biomass-derived platform molecules: from high added-value chemicals to fuels via aqueous-phase processing. *Chem. Soc. Rev.* 40, 5266–5281. doi: 10.1039/c1cs15131b

Serrano-Ruiz, J. C., Pineda, A., Balu, A. M., Luque, R., Campelo, J. M., Romero, A. A., et al. (2012). Catalytic transformations of biomass-derived acids into advanced biofuels. *Catal. Today* 195, 162–168. doi: 10.1016/j.cattod.2012.01.009

Sheldon, R. A. (2014). Green and sustainable manufacture of chemicals from biomass: state of the art. *Green Chem.* 16, 950–963. doi: 10.1039/C3GC41935E

Simakova, I. L., and Murzin, D. Y. (2016). Transformation of bio-derived acids into fuel-like alkanes via ketonic decarboxylation and hydrodeoxygenation: design of multifunctional catalyst, kinetic and mechanistic aspects. *J. Energy Chem.* 25, 208–224. doi: 10.1016/j.jechem.2016.01.004

Sudhakar, M., Kantam, M. L., Jaya, V. S., Kishore, R., Ramanujachary, K. V., and Venugopal, A. (2014). Hydroxyapatite as a novel support for Ru in the hydrogenation of levulinic acid to γ-valerolactone. *Catal. Commun.* 50, 101–104. doi: 10.1016/j.catcom.2014.03.005

Sudhakar, M., Kumar, V. V., Naresh, G., Kantam, M. L., Bhargava, S. K., and Venugopal, A. (2016). Vapor phase hydrogenation of aqueous levulinic acid over hydroxyapatite supported metal (M= Pd, Pt, Ru, Cu, Ni) catalysts. *Appl. Catal. B: Environ.* 180, 113–120. doi: 10.1016/j.apcatb.2015.05.050

Tan, J., Cui, J., Deng, T., Cui, X., Ding, G., Zhu, Y., et al. (2015). Water-promoted hydrogenation of levunilic acid to γ-valerolactone on supported ruthenium catalyst. *ChemCatChem* 7, 508–512. doi: 10.1002/cctc.201402834

Tan, J., Cui, J., Ding, G., Deng, T., Zhu, Y., and Li, Y.-W. (2016). Efficient aqueous hydrogenation of levulinic acid to γ-valerolactone over highly active and stable ruthenium catalyst. *Catal. Sci. Technol.* 6, 1469–1475. doi: 10.1039/C5CY01374G

Tang, X., Zeng, X., Li, Z., Hu, L., Sun, Y., Liu, S., et al. (2014). Production of γ-valerolactone from lignocellulosic biomass for sustainable fuels and chemicals supply. *Renew. Sustain. Energy Rev.* 40, 608–620. doi: 10.1016/j.rser.2014.07.209

Tay, B. Y., Wang, C., Phua, P. H., Stubbs, L. P., and Huynh, H. V. (2016). Selective hydrogenation of levulinic acid to γ-valerolactone using in-situ generated ruthenium nanoparticles derived from Ru-NHC complexes. *Dalton Trans.* 45, 3558–3563. doi: 10.1039/C5DT03366G

Tukacs, J. M., Király, D., Strádi, A., Novodarszki, G., Eke, Z., Dibó, G., et al. (2012). Efficient catalytic hydrogenation of levulinic acid: a key step in biomass conversion *Green Chem.* 14:2057–2065. doi: 10.1039/c2gc35503e

Van Bekkum, H., and Gallezot, P. (2004). Preface on the special issue "catalytic conversion of renewables". *Top Catal.* 27, 1–2. doi: 10.1023/B:TOCA.0000013637.57340.ab

Van Nguyen, C., Matsagar, B. M., Yeh, J.-Y., Chiang, W.-H., and Wu, K. C.-W. (2019). MIL-53-NH_2-derived carbon-Al_2O_3 composites supported Ru catalyst for effective hydrogenation of levulinic acid to γ-valerolactone under ambient conditions. *Mol. Catal.* 475:110478. doi: 10.1016/j.mcat.2019.110478

Velisoju, V. K., Peddakasu, G. B., Gutta, N., Boosa, V., Kandula, M., Chary, K. V. R., et al. (2018). Influence of support for Ru and water role on product selectivity in the vapour phase hydrogenation of levulinic acid to γ-valerolactone: investigation by probe adsorbed FT-IR spectroscopy. *J. Phys. Chem. C* 122, 19670–19677. doi: 10.1021/acs.jpcc.8b06003

Wei, Z., Li, Z., Deng, J., Wang, J., Li, H., and Wang, Y. (2018). Improved catalytic activity and stability for hydrogenation of levulinic acid by Ru/N-doped hierarchically porous carbon. *Mol. Catal.* 448, 100–107. doi: 10.1016/j.mcat.2018.01.024

Werpy, T., and Petersen, G. (2004). *Top Value Added Chemicals From Biomass. Vol. I: Results of Screening for Potential Candidates From Sugars and Synthesis Gas.* NREL/TP-510-35523, U.S. Department of Energy, National Renewable Energy Laboratory, Golden, CO. Avaliable online at: https://www.nrel.gov/docs/fy04osti/35523.pdf (accessed November 30, 2019)

Wojciechowska, J., Jedrzejczyk, M., Grams, J., Keller, N., and Ruppert, A. M. (2019). Enhanced production of γ-valerolactone with an internal source of hydrogen on Ca-modified TiO_2 supported Ru catalysts, *ChemSusChem* 12, 639–650. doi: 10.1002/cssc.201801974

Xiao, C., Goh, T.-W., Qi, Z., Goes, S., Brashler, K., Perez, C., et al. (2016). Conversion of levulinic acid to gamma-valerolactone over few-layer graphene-supported ruthenium catalysts. *ACS Catal.* 6, 593–596. doi: 10.1021/acscatal.5b02673

Xue, Z., Liu, Q., Wang, J., and Mu, T. (2018). Valorization of levulinic acid over non-noble metal catalysts: challenges and opportunities. *Green Chem.* 20, 4391–4408. doi: 10.1039/C8GC02001A

Yan, K., Jarvis, C., Gu, J., and Yan, Y. (2015b). Production and catalytic transformation of levulinic acid: a platform for specialty chemicals and fuels. *Renew. Sustain. Energy Rev.* 51, 986–997. doi: 10.1016/j.rser.2015.07.021

Yan, K., Yang, Y., Chai, J., and Lu, Y. (2015a). Catalytic reactions of gamma-valerolactone: a platform to fuels and value-added chemicals. *Appl. Catal. B: Environ.* 179, 292–304. doi: 10.1016/j.apcatb.2015.04.030

Yan, N., Xiao, C., and Kou, Y. (2010). Transition metal nanoparticle catalysis in green solvents. *Coord. Chem. Rev.* 254, 1179–1218. doi: 10.1016/j.ccr.2010.02.015

Yao, Y., Wang, Z., Zhao, S., Wang, D., Wu, Z., and Zhang, M. (2014). A stable and efficient Ru/polyethersufone catalyst for levulinic acid hydrogenation to γ-valerolactone in aqueous solution. *Catal. Today* 234, 245–250. doi: 10.1016/j.cattod.2014.01.020

Ye, L., Han, Y., Feng, J., and Lu, X. (2020). A review about GVL production from lignocellulose: Focusing on the full components utilization. *Ind. Crops Prod.* 144:112031. doi: 10.1016/j.indcrop.2019.112031

Yu, Z., Lu, X., Liu, C., Han, Y., and Ji, N. (2019). Synthesis of γ-valerolactone from different biomass-derived feedstocks: recent advances on reaction mechanisms and catalytic systems. *Renew. Sustain. Energy Rev.* 112, 140–157. doi: 10.1016/j.rser.2019.05.039

Yuan, Y., Yan, N., and Dyson, P. J. (2012). Advances in the rational design of rhodium nanoparticle catalysts: control via manipulation of the nanoparticle core and stabilizer. *ACS Catal.* 2, 1057–1069. doi: 10.1021/cs300142u

Zhang, B., Wu, Q., Zhang, C., Su, X., Shi, R., Lin, W., et al. (2017). A robust Ru/ZSM-5 hydrogenation catalyst: Insights into the resistances to ruthenium aggregation and carbon deposition. *ChemCatChem* 9, 3646–3654. doi: 10.1002/cctc.201700664

Conflict of Interest: The authors declare that the research was conducted in the absence of any commercial or financial relationships that could be construed as a potential conflict of interest.

frontiers in Chemistry

REVIEW
published: 05 May 2020
doi: 10.3389/fchem.2020.00333

Catalytic Production of Oxygenated and Hydrocarbon Chemicals From Cellulose Hydrogenolysis in Aqueous Phase

Haosheng Xin [1,2,3,4], Xiaohong Hu [1,2,3,4], Chiliu Cai [1,2,3], Haiyong Wang [1,2,3], Changhui Zhu [1,2,3,4], Song Li [1,2,3,4], Zhongxun Xiu [5], Xinghua Zhang [1,2,3], Qiying Liu [1,2,3,6] and Longlong Ma [1,2,3]*

[1] Guangzhou Institute of Energy Conversion, Chinese Academy of Sciences, Guangzhou, China, [2] CAS Key Laboratory of Renewable Energy, Guangzhou, China, [3] Guangdong Provincial Key Laboratory of New and Renewable Energy Research and Development, Guangzhou, China, [4] University of Chinese Academy of Sciences, Beijing, China, [5] Nano Science and Technology Institute, University of Science and Technology of China, Suzhou, China, [6] Dalian National Laboratory for Clean Energy, Dalian, China

OPEN ACCESS

Edited by:
Dmitry Yu. Murzin, Åbo Akademi University, Finland

Reviewed by:
Alessandro Pellis, University of Natural Resources and Life Sciences, Austria
Mohammad Boshir Ahmed, Gwangju Institute of Science and Technology, South Korea

***Correspondence:**
Qiying Liu
liuqy@ms.giec.ac.cn

Specialty section:
This article was submitted to Green and Sustainable Chemistry, a section of the journal Frontiers in Chemistry

Received: *04 December 2019*
Accepted: *31 March 2020*
Published: *05 May 2020*

Citation:
Xin H, Hu X, Cai C, Wang H, Zhu C, Li S, Xiu Z, Zhang X, Liu Q and Ma L (2020) Catalytic Production of Oxygenated and Hydrocarbon Chemicals From Cellulose Hydrogenolysis in Aqueous Phase. Front. Chem. 8:333. doi: 10.3389/fchem.2020.00333

As the most abundant polysaccharide in lignocellulosic biomass, a clean and renewable carbon resource, cellulose shows huge capacity and roused much attention on the methodologies of its conversion to downstream products, mainly including platform chemicals and fuel additives. Without appropriate treatments in the processes of cellulose decompose, there are some by-products that may not be chemically valuable or even truly harmful. Therefore, higher selectivity and more economical and greener processes would be favored and serve as criteria in a correlational study. Aqueous phase, an economically accessible and immensely potential reaction system, has been widely studied in the preparation of downstream products of cellulose. Accordingly, this mini-review aims at making a related summary about several conversion pathways of cellulose to target products in aqueous phase. Mainly, there are four categories about the conversion of cellulose to downstream products in the following: (i) cellulose hydrolysis hydrogenation to saccharides and sugar alcohols, like glucose, sorbitol, mannose, etc.; (ii) selective hydrogenolysis leads to the cleavage of the corresponding glucose C-C and C-O bond, like ethylene glycol (EG), 1,2-propylene glycol (PG), etc.; (iii) dehydration of fructose and further oxidation, like 5-hydroxymethylfurfural (HMF), 2,5-furandicarboxylic acid (FDCA), etc.; and (iv) production of liquid alkanes *via* hydrogenolysis and hydrodeoxygenation, like pentane, hexane, etc. The representative products were enumerated, and the mechanism and pathway of mentioned reaction are also summarized in a brief description. Ultimately, the remaining challenges and possible further research objects are proposed in perspective to provide researchers with a lucid research direction.

Keywords: cellulose, hydrolysis, hydrogenolysis, biorefinery, catalysis, aqueous phase

INTRODUCTION

To alleviate the adverse impact caused by excessive consumption of traditional fossil fuels, finding a green-renewable-sustainable resource on Earth that could be regarded as a replacement of fossil has aroused much attention nowadays. Meanwhile, this resource that we are striving to find could not only meet the global growing energy needs but also demonstrate the potential of promising block for application in the fields of crucial medicines, high value-added chemicals, and functional materials, etc. (Delbecq et al., 2018). Lignocellulosic biomass, the most promising renewable resource on the planet, has already been integrated into the blueprint of energy system for its high economic and practical application value (Den et al., 2018). In common, lignocellulosic biomass consists of 10–25% lignin, 20–35% hemicellulose, and 35–50% cellulose. Serving as the most abundant component of lignocellulosic biomass, cellulose plays a vital role not only in the field of utilizing of renewable resource but also in providing more possibilities for the production of a battery of high value-added chemicals (Wang et al., 2019). Therefore, how to efficiently catalyze the conversion of cellulose to desirable products by hydrolysis and subsequent reactions is challengeable and has become the meritorious object pursued by researchers.

Well-known that the cellulose molecules in biomass are formed by the glucose units linked by β-1,4 glycosidic bonds and the molecular chains are connected to each other through numerous hydrogen bonds (Singh et al., 2016). Therefore, the primary premise of being able to take full advantage of cellulose is to break those β-1,4 glycosidic bonds and hydrogen bonds. At the outset, direct pyrolysis of cellulose has been paramount considered as an efficient means to obtain target fuels and chemicals (Atalla and Vanderhart, 1984). The degree of polymerization of cellulose begins to decrease with the increase of pyrolysis temperature; meanwhile, hydrogen bonds (Xin et al., 2015) and β-1,4 glycosidic bonds (Yu et al., 2012) are successively broken. In view of the effect of β-1,4 glycosidic linkage, multiformity of end-products and complexity of reactions in the research of cellulose pyrolysis, cellulose model compounds (including cellotriose, cellobiose, glucose, etc.) are usually adopted as selection objects (Paine et al., 2007; Mayes et al., 2014; Zhang et al., 2015a; Zhang M. et al., 2015; Gao Z. et al., 2019). Moreover, the degree of polymerization and positions and orientation of glycosidic linkages about organic product speciation were also investigated among different model compounds when comparing to the elementary products distribution after pyrolysis of glucose and its oligomers (Patwardhan et al., 2009). Researchers found that the positions and orientation of glycosidic linkages caused an insignificant effect on elementary products distribution except for the case of dextran, the elementary product—levoglucosane yield trend follows the order: monosaccharide < disaccharides < oligosaccharides < polysaccharides. Although pyrolysis is a capable method in the field of directly converting cellulose, it is limited to its single conversion means and more complicated uncontrollable reactions, making it difficult to obtain a specific target product directly through a specified reaction path. Therefore, researchers are also promoted to explore other effective ways to convert cellulose to the target products.

In the past few decades, researchers have endeavored to overcome the obstacles in the process of cellulose biorefinery, such as intrinsic robust, complex, and heterogeneous structure of cellulose, so as to depolymerize cellulose into intermediary monosaccharide and further transformation to other high value-added chemicals. Pursuing the philosophy of efficient conversion of cellulose and hydrolyzed monosaccharide, organic solvent, biphasic solvent, ionic liquid, and aqueous-phase solvent systems were adopted and confirmed that high selectivity and yield of downstream products could be obtained (Ji et al., 2008; Van Putten et al., 2013; Wang et al., 2015; Mariscal et al., 2016; Zhang Z. et al., 2017). For instance, a biphasic system made up of water and biomass-derived γ-valerolactone (GVL) has achieved a great progress in the hydrolysis of lignocellulosic biomass into various carbohydrates by disrupting the hydrogen-bond network or decreasing the transparent activation energy (Mellmer et al., 2014a; Li W. et al., 2017; Xin et al., 2017; Zhang T. et al., 2017; Zhang et al., 2019). It is also demonstrated that 5-hydroxymethylfurfural (HMF) is inclined to be steady due to the existence of GVL–water biphasic solvent system and reduce the occurrence of side reactions, thereby promoting the reaction toward the target product. In addition, not confined to monosaccharide, cellulose can also be directly converted into HMF with higher yield in tetrahydrofuran (THF)/H_2O-NaCl biphasic system using Sn-Mont catalyst and THF–seawater biphasic system even without any acid added (Wang et al., 2012; Li et al., 2018). In essence, the yield could be enhanced because HMF can be simultaneously extracted into organic phase after formation in a biphasic system, which could maintain HMF in a steady state and avoid the occurrence of some side reactions. And further studies also confirmed that the reaction kinetics can be influenced by aprotic organic solvents (e.g., GVL, THF) in the way of transforming the stabilization of the acidic proton vs. the protonated transition state, resulting in enormous increases of reaction rates and product selectivity in acid-catalyzed systems (Mellmer et al., 2014b, 2018). Moreover, ionic liquids as novel catalysts have shown its giant potential in the conversion of various raw biomass materials and their derivatives that could accord with the demand of green chemistry (Zhang et al., 2005; Li and Zhao, 2007; Li et al., 2008; Zavrel et al., 2009). For example, an ionic liquid for cellulose hydrolysis named 1-butyl-3-methylimidazolium chloride [(C_4mim)Cl] has been verified to accelerate reaction rates so that facilitating the hydrolysis of cellulose dramatically under atmospheric pressure. In [C_4mim]Cl solvent, cellulose could completely dissolve and then form a homogeneous solution, which made the H^+ more accessible to the β-1,4 glycosidic bonds so as to promote the reaction process (Li and Zhao, 2007). In addition, two Brønsted acidic ionic liquid catalysts [1-(3-proylsulfonic)-3-methylimidazolium chloride and 1-(4-butylsulfonic)-3-methylimidazolium chloride] were successfully applied to the further conversion to furanic biocrude products including HMF after cellulose hydrolysis, and several products formed from aldol condensation of HMF with

one to three acetone molecules and some other HMF ether products (Amarasekara and Reyes, 2019).

Even a series of organic solvents and ionic liquids reported previously has exhibited a certain level of activity in the conversion of biomass raw materials and derived model compounds, aqueous-phase solvent has the most practical application value especially in economics to obtain downstream products in view of the difficulty of separation recovering the organic solvents after reaction and expensive price of ionic liquids.

CATEGORIES OF CELLULOSE CONVERSION

Cellulose conversion includes both conversion between different cellulose forms (such as microcrystalline cellulose, cellulose nanocrystals, cellulose acetate, cellulose nitrate could be obtained) and deep cellulose degradation to small-molecule chemicals. This review would focus on the deep cellulose degradation to representative small molecular chemicals in aqueous phase, which is also different from those reviews about introducing cellulose conversion in the field of catalyst, reaction pathway, or organic solvent effects (Shuai and Luterbacher, 2016; Jing et al., 2019; Pang et al., 2019). Cellulose can be catalytically converted into various chemicals as the established reaction paths under aqueous-phase reaction atmosphere, sugars (glucose, fructose, sorbitol, mannitol, etc.), furan compounds [HMF, N,N-dimethylformamide (DMF), 2,5-furandicarboxylic acid (FDCA), etc.], alcohols [ethylene glycol (EG), ethanol, erythritol, 1,2-propanediol, etc.], liquid hydrocarbons (pentane, hexane, methylcyclopentanone, etc.), phenols and other pharma [hydroxyacetone (HA), 1-hydroxy-2-butanone (HB), etc.], or polymer building blocks are available.

In summary, there are mainly four categories of reactions during biorefinery and catalytic process of cellulose degradation in aqueous phase are summed up hereinafter (**Scheme 1**): (i) cellulose hydrolysis and hydrogenation to sugar alcohols; (ii) selective hydrogenolysis of glucose to alcohols by fracturing the corresponding C-C and C-O bond; (iii) further dehydration and hydrogenation of fructose (glucose isomerization) to HMF and its derivatives; (iv) *via* hydrogenolysis and hydrodeoxygenation to liquid alkanes. Some other reaction types may be also referred, including but not limited to isomerization, epimerization, oxidation, aldol condensation, or hydration, and all the reaction types abovementioned are carried out in aqueous phase. In addition to those abovementioned, a very hot topic about using enzymes as green and sustainable catalysts for the processing of cellulose conversion and the production of derived green solvents would also be introduced, such as bioethanol, levoglucosenone, and dihydrolevoglucosenone (cyrene).

Cellulose Hydrolysis Hydrogenation to Saccharides and Sugar Alcohols

Polysaccharides

For a better understanding of the cellulose hydrolysis process, high degree of polymerization of cellulose is hydrolyzed to cello-oligosaccharides firstly, which are biologically important molecules that can be directly used in agricultural and food industries that are made up of 10 or less glucose units linked by β-1,4 glycosidic bonds and could be degraded to a single glucose unit fleetly. Homogeneous catalysts could dissolve and hydrolyze cellulose. Eighty-five percent H_3PO_4 solution and 3.8% HF/SbF_5 were tested for the synthesis of cello-oligosaccharides from cellulose (Liebert et al., 2008; Martin-Mingot et al., 2012). Although acceptable activities were achieved, the difficulty for catalysts recycling, water pollution problems, and certain operational risk limited the application of such catalysts. Subsequently, carbon materials containing oxygenated functional groups as heterogeneous catalysts are stabilized under the hydrothermal and high-pressure conditions requested for cellulose hydrolysis (Kobayashi et al., 2013; Charmot et al., 2014; Zhao et al., 2014). Reaction mechanisms reveal that cellulose adsorbed on the carbon material surface primarily relies on CH-π and hydrophobic interactions, and then the acidic functional group designed on the catalyst surface acting on the β-1,4 glycosidic bonds resulting in the hydrolysis of cellulose to cello-oligosaccharides (Yabushita et al., 2014; Kobayashi et al., 2015). Food-grade activated carbon with weak acidity after being oxidized in air shows a good ability in the field of cellulose conversion to cello-oligosaccharides, 56% yield of target product were obtained in batch reactor with 40 ml distilled water under 453 K after 20 min (Chen et al., 2019). Consistent with the literatures abovementioned, with good adsorption of catalyst to cellulose, acidic functional groups on activated carbon surface and high space velocity are essential to make a contribution to maximize the product yield.

Glucose

Besides polysaccharides, glucose is the target product during the conversion of cellulose as it is a significant precursor to all kinds of valuable chemicals and fuels (Alonso et al., 2010). Hence, the efficient hydrolysis of cellulose to glucose is one of the most important subjects with low environmental impact in green and sustainable chemistry. Homogeneous sulfuric acid catalyst (Rinaldi and Schüth, 2009), cellulase enzymes (Kim and Hong, 2001), sub- or supercritical water (Adschiri et al., 1993), and heterogeneous solid catalysts (Rinaldi and Schüth, 2009) were successfully applied to the hydrolysis of cellulose, but homogeneous acid catalyst is highly corrosive and neutralizing treatment is required after reaction in order to avoid environmental problems; cellulose enzymes show a low reaction rate with high costs, and it is difficult to recover the enzyme from the mixtures after reaction; reaction apparatuses with high quality are desired due to the harsh conditions under sub- or supercritical water, and the thermal instability of glucose at high temperature caused the low selectivity of this method. Thereby, heterogeneous solid catalysts are gaining increasing attention and would be favorable for cellulose hydrolysis because solid catalysts not only can be applied under a wide range of reaction conditions and pH tolerance but also can be easily separated from the mixture after reaction with good cycle performance (Jun et al., 2000; Kitano et al., 2009; Yamaguchi et al., 2009). In the

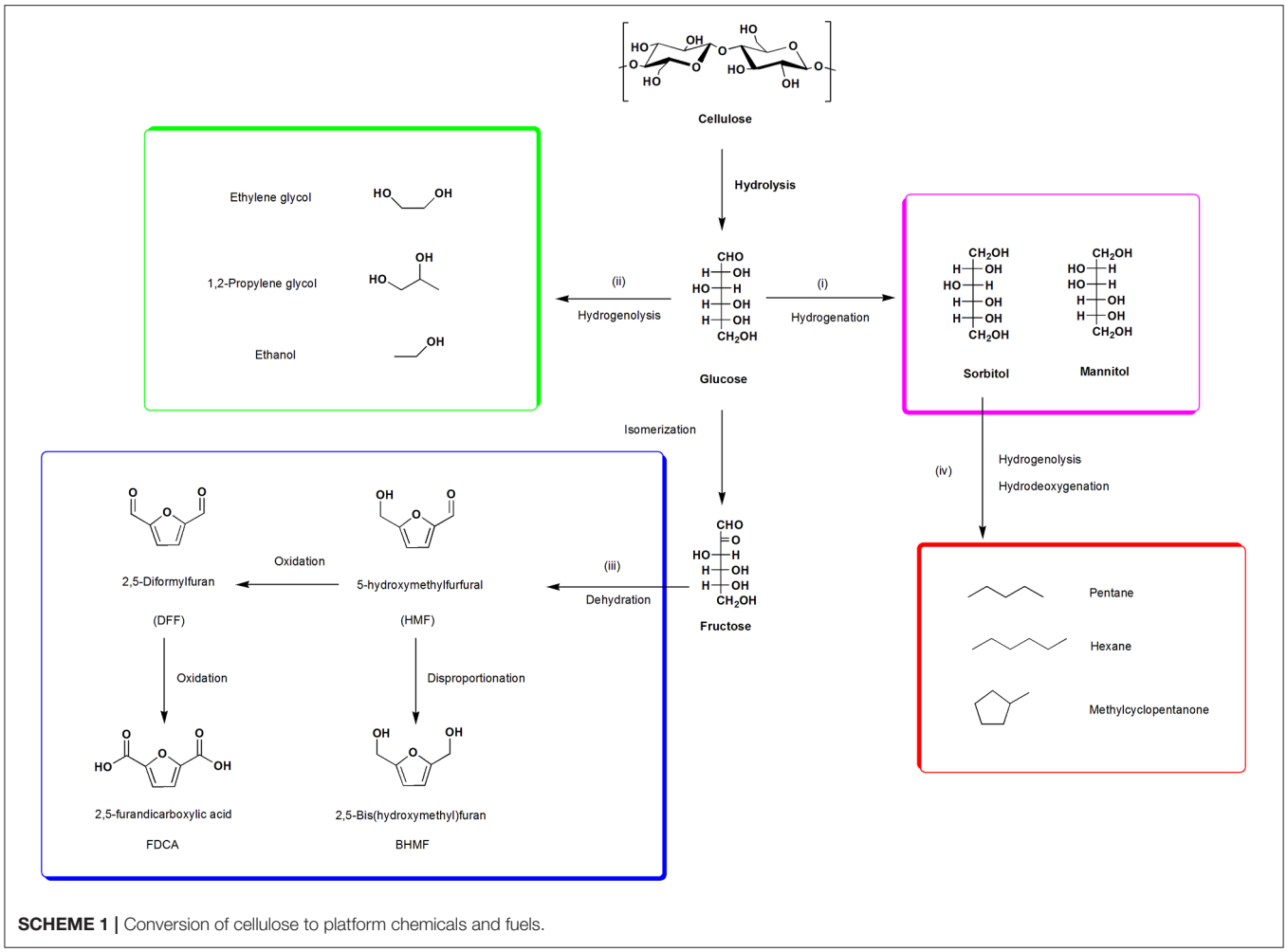

SCHEME 1 | Conversion of cellulose to platform chemicals and fuels.

selective hydrolysis of cellulose to glucose, a sulfonated activated-carbon catalyst (AC-SO_3H) was synthesized and showed an excellent catalytic activity and high selectivity (over 90%) of glucose compared with H-morderite, H-ZSM5, AC, sulfated zircoria, Amberlyst 15, and other solid materials, which turns out that the high hydrothermal stability and the prominent catalytic property are attributed to the surface acid sites of SO_3H functional groups and the intrinsic hydrophobic planes (Onda et al., 2008). Sulfonic groups might become unstable and leach into the water under high temperature and pressure that are required in case of further conversion to target chemicals and fuels, which may lead to a decrease in catalyst activity and the yield of the target products. In the meantime, solid materials supported various metal (Pt, Ru, Ni, etc.) catalysts were also investigated with respect to the degradation of cellulose (Fukuoka and Dhepe, 2006; Luo et al., 2007; Deng et al., 2009). A water-tolerant solid catalyst Ru/CMK-3 was successfully synthesized by combining mesoporous carbon material (CMK-3) and metal Ru, which provided high glucose yields and turnover numbers (TONs) for the hydrolysis of cellulose in pure aqueous phase (Kobayashi et al., 2010). The results of X-ray diffraction (XRD) and transmission electron microscopy (TEM) indicate that Ru is uniformly dispersed on the surface of CMK-3 and not reduced to form zero-valent nanoparticles thoroughly, without cramming the CMK-3 pores. There is a synergistic effect between CMK-3 and Ru, in which CMK-3 plays a vital role for the hydrolysis of cellulose to intermediate oligosaccharides while Ru promotes the further conversion of oligosaccharides into glucose.

Fructose

Generally, fructose is derived from the isomerization of glucose obtained after the hydrolysis of cellulose in the presence of enzymes, homogeneous acids, bases, or Lewis acidic sites, which plays a key role in the way of producing platform chemicals and fuels (Lee and Hong, 2000; Tanase et al., 2001; Moliner et al., 2010; Liu C. et al., 2014). Recently, the catalytic performance of macroporous niobium phosphate (NbP) supported by MgO catalysts for isomerization of glucose to fructose was investigated and shows high efficiency in water and air atmosphere (Gao D. et al., 2019). The TON (defined as the number of moles of fructose formed per mole of basic sites on the fresh catalyst when the yield of fructose reached maximum value) values increased with the increase of MgO content from 20 to 60 wt%. And the surface characteristics of MgO were obviously improved

while loading on the synthesized porous niobium phosphate, the distribution and amounts of basic sites and the resistance to water are comprised. However, noting that the yield of fructose was obviously decreased because of the mediocre cycle performance of MgO/NbP after first reaction without regeneration, thus the practical application value is limited. A heterogeneous bifunctional solid catalyst (UiO-66-MSBDC, substituted the organic linker of the zirconium organic framework UiO-66 with 2-monosulfo-benzene-1,4-dicarboxylate partially) with Brønsted and Lewis acid sites was successfully prepared and shows good stability and selectivity for glucose isomerization to fructose in deionized water (Oozeerally et al., 2018). The Lewis acidity can be affected while modification. UiO-66 was modified by MSBDC, attributed to the formation of more defective materials, and the nearby electron-withdrawing groups are enhanced in the presence of Zr^{4+}, consistent with previous literature reports (Degirmenci et al., 2011). Some representative works abovementioned on the preparation of saccharides and sugar alcohols are summarized in **Table 1**.

Sorbitol and Mannitol

When some metal catalysts with hydrogenation effect is added to the reaction, during the hydrolytic process of cellulose, the glucose-derived downstream products such as sorbitol and mannitol are generated. Sorbitol and mannitol are produced by the hydrogenation of glucose that are used not only as sweeteners but also as precursors to isosorbide, lactic acid, 1,4-sorbitan, and other useful chemical compounds (Huber et al., 2003; Davda and Dumesic, 2004). It is first reported that supported metal catalysts can work on cellulose conversion into sorbitol and mannitol by a green environmental process, in the presence of Pt/γ-Al_2O_3, 31% yield of sugar alcohols (sorbitol: 25%, mannitol: 6%) were obtained in water solvent under 5 MPa H_2 atmosphere at 463 K after 24 h (Fukuoka and Dhepe, 2006). Among the supported metal catalysts, Pt and Ru catalysts gave the higher yields of the sorbitol and mannitol, while Ir, Pd, and Ni catalysts showed lower activity. The reaction mechanism suggested that H_2 is adsorbed on the Pt surface dissociatively and the hydrogen species spill over onto the γ-Al_2O_3 surface reversibly. Hence, the acid sites for the hydrolysis of cellulose are not only due to the acidic surface sites intrinsic in the γ-Al_2O_3 but also generated *in situ* from H_2. The acidic sites play a decisive role in the first of cellulose hydrolysis to glucose, and then the sorbitol formed by means of reducing the C=O group in glucose with Pt and H_2. Currently, bifunctional catalysts which contain acid sites and metal sites show excellent activity on direct conversion of cellulose into sorbitol have become the focus of researchers (Han and Lee, 2012; Zhu et al., 2014; Romero et al., 2016, 2017). A bifunctional catalyst Ru/CCD-SO_3H (sulfonic acid-functionalized carbonized cassava dregs supported ruthenium) was prepared and successfully employed for the hydrolysis of cellulose to sorbitol in a neutral aqueous solution (Li Z. et al., 2019). More than double yield of sorbitol 63.8% can be achieved under the optimal conditions at lower temperature 180°C and shorter time 10 h compared with Pt/γ-Al_2O_3 catalyst abovementioned. Meanwhile, there exists a strong synergistic effect between -SO_3H and Ru nanoparticles, acid sites are necessary in the depolymerization of cellulose to glucose and the hydrogenation sites of Ru could promote the formation of sorbitol from glucose. Furthermore, except supported metal catalysts and bifunctional catalysts, emerging catalysts like Ru-Ni bimetallic catalysts (supported by mesoporous carbon, activated carbon, and carbon nanotubes) also already show their potential for enhance one-pot hydrolytic hydrogenation of cellulose to sugar alcohols (Alonso et al., 2012; Pang et al., 2012; Sankar et al., 2012; Ribeiro et al., 2017). The result reveals that there is an interaction between both metals, and the presence of Ni improved the catalytic performance of the Ru monometallic catalysts both in terms of activity and selectivity. Furthermore, the yield of sorbitol is over 70% in a very short time (1 h) if the catalyst and cellulose are ball milled together. In addition, mannose can be obtained from glucose epimerization in the presence of acid through an intramolecular carbon shift as the Bilik reaction claimed. Another possible way to form mannose is from a reverse 1,2-hydride transfer from fructose, and further hydrogenation leads to the formation of mannitol (Gunther et al., 2012). When sodium tetraborate is incorporated into the active site of Sn-Beta zeolite, the selective epimerization of glucose to products would be promoted in aqueous media. The reaction proceeds by means of a 1,2 carbon shift of aldose wherein the bond is cleaved between C-2 and C-3 and a corresponding new bond is formed between C-1 and C-3, resulting in an inverted configuration by moving C-1 to the C-2 position.

Concisely, saccharides and sugar alcohols have always been considered as the link between the preceding cellulose and following platform chemicals; therefore, finding more efficient ways to prepare saccharides and sugar alcohols in aqueous phase has great significance for the utilization of cellulose.

Scheme 2 shows the pathway of cellulose conversion to saccharides and sugar alcohols.

Selective Hydrogenolysis of Glucose to Small Molecular Alcohols

Various small molecular alcohols have been widely used as solvents, fuel additives, and chemical synthesis intermediate; hence, efficient preparation of small molecular alcohols with ingenious catalysts design from direct hydrolysis and hydrogenolysis of cellulose has become the goal pursued by researchers.

Ethylene Glycol

In an earlier pioneering report, the process of EG production from cellulose in one-pot is significantly promoted by using a nickel-modified tungsten carbide catalyst (Ni-W_2C/AC) instead of precious metal (Pt, Ru) catalysts, and the yield of EG was remarkably increased to 61% due to a synergistic effect between nickel and W_2C (Degirmenci et al., 2011). W_2C is mainly responsible for converting glucose into EG, and the addition of Ni could not only promote the formation of tungsten carbides but also limit the further hydrogenolysis of glucose to other polyols, thereby promoting the improvement of EG yield. After that, a battery of tungsten-based catalysts such as Ni-WO_3/SBA-15, Ru/WO_3, Raney Ni+H_2WO_4, W_XC/MC, and Ru/AC+H_2WO_4 has been developed to promote the direct production of EG

TABLE 1 | Representative work on the preparation of saccharides and sugar alcohols.

Entry 1	Substrate	Solvent	Catalyst	Temperature (°C)	Time	Yield (%)	References
1	Cellulose	H_2O	AC-Air	180	20 min	Cello-oligosaccharides:54	Chen et al., 2019
2	Cellulose	H_2O	AC-SO_3H	150	24 h	Glucose:40.5	Onda et al., 2008
3	Cellulose	H_2O	Amberlyst-15	150	24 h	Glucose:26.7	Onda et al., 2008
4	Cellulose	H_2O	Pt/γ-Al_2O_3	190	24 h	Sorbitol:25 Mannitol:6	Fukuoka and Dhepe, 2006
5	Cellulose	H_2O	SiO_2-SO_3H	150	10 h	Glucose:56.6	Zhu et al., 2014
6	Cellulose	H_2O	Ru/SiO_2+SiO_2-SO_3H	150	10 h	Sorbitol:43.3 Mannitol:14.7	Zhu et al., 2014
7	Cellulose	H_2O	Ru/SiO_2+SO_3H	150	10 h	Sorbitol:61.2 Mannitol:6.9	Zhu et al., 2014
8	Glucose	H_2O	Ru/SiO_2+SO_3H	150	30 min	Sorbitol:97.5	Zhu et al., 2014
9	Glucose	H_2O	Ru:Ni/MCM-48	120	90 min	Sorbitol:31	Romero et al., 2017
10	Glucose	H_2O	MgO/NbP-500	120	30 min	Fructose:24.6	Gao D. et al., 2019
11	Glucose	H_2O	MgO/ Al_2O_3	120	30 min	Fructose:27.1	Gao D. et al., 2019

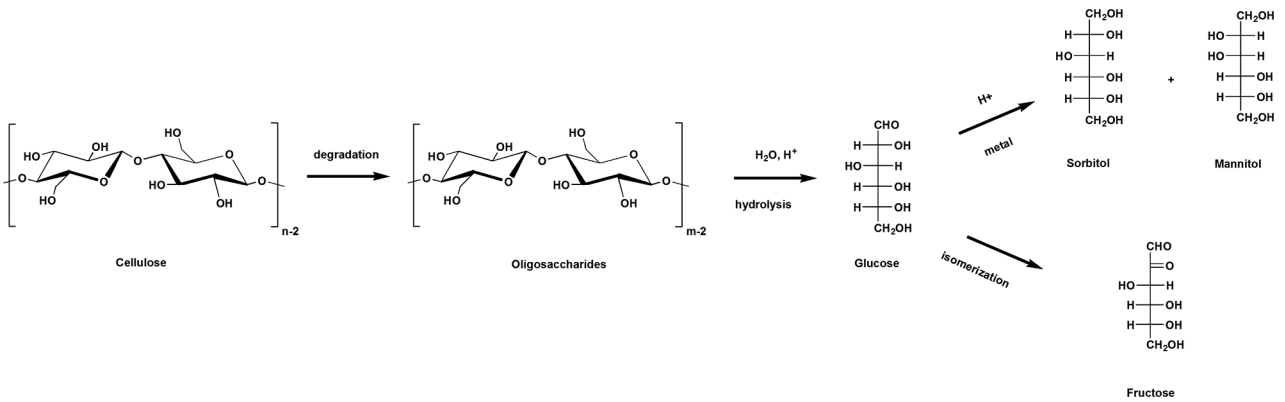

SCHEME 2 | Conversion of cellulose to saccharides and sugar alcohols.

from cellulose with high activity and selectivity (Tai et al., 2013; Wang and Zhang, 2013; Cao et al., 2014; Li N. et al., 2017). The above literature reports a unified reaction mechanism: in the first, water-soluble oligosaccharides and glucose are obtained after the hydrolysis of cellulose in the presence of acid; then, glycolaldehyde is formed with catalysis of tungsten species by fracturing the corresponding C-C bond of oligosaccharides and glucose *via* retro-aldol condensation; finally, glycolaldehyde is catalyzed by a metal catalyst with hydrogenation characteristics to finish the production of target EG.

Ethanol

Besides an ideal additive to gasoline, biomass-derived ethanol can serve not only as a versatile precursor for the production of various chemicals but also as a green solvent that has received considerable attention (Farrell et al., 2006; Subramani and Gangwal, 2008). Traditionally, bio-ethanol is produced *via* the fermentation and distillation processes of pretreated lignocellulosic materials using enzymes and homogeneous acid (Fujita et al., 2004; Himmel et al., 2007; Binder and Raines, 2010). However, the enzymatic process is obviously limited in terms of many technological bottlenecks and economic challenges. For example, because the fermentation generally follows a reaction mechanism including the formation of a pyruvate intermediate and its subsequent decarboxylation, one mole of CO_2 would be simultaneously released when one mole of pyruvate is converted into ethanol, thereby reducing the carbon atom efficiency and resulting in the theoretical yield of bio-ethanol confined to 67 mol% (Kennes et al., 2016). In contrast, the conversion of cellulose to ethanol by a chemical approach remains challenging due to a series of inherently complex reactions including hydrolysis, retro-aldol condensation, and hydrogenation are involved and some other side reactions may be caused by unstable intermediates. Therefore, the providential design of multifunctional and robust catalysts that can regulate all kinds of complex reactions efficiently is paramount. As reported, tungsten-based catalysts and Pt-Cu/SiO_2 single-atom alloy catalyst were successfully applied to the two-step conversion of cellulose to ethanol, methyl glycolate(MG) is easily formed from glycolaldehyde intermediate when the reactions were carried out in methanol solvent, and further hydrogenation is necessary to obtain ethanol after MG hydrogenated to EG (Xu et al., 2017; Yang et al., 2018). Noting that the EG is the precursor of ethanol production and could get a high yield in deionized

water which avoids the use of organic solvent, thereby the process that conversion of cellulose to ethanol is thought highly of in aqueous phase.

Lately, the study about one-pot conversion of cellulose into ethanol catalyzed by a combination of tungstic acid and zirconia-supported Pt nanoparticles (H_2WO_4-Pt/ZrO_2) was presented (Song et al., 2019). As the studies revealed, firstly, *via* the retro-aldol condensation, H_2WO_4 is deemed to be responsible for the breakage of the C-C bond in glucose unit, particularly the C2-C3 bond. Secondly, Pt/ZrO_2 mainly works on the hydrogenation of the C=O bond in glycolaldehyde into EG and the further hydrogenolysis of the C-OH bond in C2 intermediates into ethanol. Lastly, appropriate fractions of Pt^0 and Pt^{2+} on ZrO_2 support impose restrictions on over-hydrogenolysis which are crucial to promote the formation of ethanol. An ethanol yield of 32% and EG yield of 24% at the same time were obtained from cellulose at 523 K in 5 h under 4 MPa H_2 atmosphere with deionized water. Later, a multifunctional Ru-WOx/HZSM-5 catalyst was designed appropriately for one-pot efficient transformation of cellulose to ethanol *via* a series of cascade reactions (Li C. et al., 2019). Characterizations revealed that Ru and WOx nanoparticles were highly dispersed on the surface of HZSM-5 and formed Ru_3W_{17} alloy, which displayed a synergistic catalytic effect along with moderate acidic sites: moderate acid sites are responsible for cellulose hydrolysis, glucose retro-aldol condensation, and EG dehydration, and Ru_3W_{17} alloy sites are responsible for EG hydrogenation to ethanol. Meanwhile, the key retro-aldol condensation reaction could be promoted with the addition of Ru/WOx by suppressing oligomerization led to an increase in the yield of ethanol from 76.8% to 87.5 over 1 wt% cellulose under mild conditions in water. When taking the advantages of Pt/WOx into consideration as the parent catalyst on account of its high efficiency in the selective cleavage of the secondary C-O bond of glycerol to form 1,3-propanediol (Wang et al., 2016; Zhao et al., 2017), another multifunctional catalyst Mo/Pt/WOx was successfully designed to adapt to tandem reactions for one-pot production of ethanol from cellulose (Yang et al., 2019). As expected, Pt/WOx shows a superior activity and selectivity in the critical process of EG to ethanol by the introduction of extra certain content Mo, and the activity and selectivity effected significantly with different sedimentary sequence of Mo and Pt. Finally, constituent content determined catalyst 0.1Mo/2Pt/WOx displayed an idiosyncratic ability for cellulose conversion to ethanol, and experimentally verified that the EG hydrogenolysis to ethanol by breaking the C-O bond is the rate-determining step in the whole tandem catalysis reaction. Similarly, the reaction pathways are consistent with previous reports: EG as a key intermediate can be obtained in the presence of Pt from glycolaldehyde (generated after cellulose hydrolysis under the catalysis of WO_X), and further production of ethanol from EG hydrogenolysis would be proceeded over Mo/Pt/WOx catalyst. Summarizing the above three articles on the direct preparation of ethanol from cellulose, we can know that they have the common point of converting cellulose to the intermediate glycolaldehyde by a tungsten-based catalysts, and then make the conversion of glycolaldehyde to EG under a noble metal with hydrogenation effect, finally, the end product ethanol could be obtained by EG hydrogenolysis, as shown in **Scheme 3b**.

Distinctively, one-pot production of ethanol from cellulose hydrogenolysis using chemo-catalysts Ni@C accompanied by the addition of phosphoric acid (H_3PO_4) in water was reported which demonstrated a different reaction mechanism compared with the conversion path of EG in essence (Liu et al., 2019). As revealed by the experimental results, H_3PO_4 plays the dual roles as acid not only in catalyzing hydrolysis of cellulose to glucose but also in coordinating with glucose to form cyclic di-ester structure (formed *via* dehydration of C-OHs in glucose and P-OHs in H_3PO_4) for activating the corresponding C-C and C-O bonds for further production of ethanol. A variety of catalyst characterizations revealed that Ni was encapsulated by graphene layers, and noted that the fewer the number covering graphene layers, the better the catalytic performance; furthermore, the delocalized π electrons of graphene layers weaken absorption of H atoms on Ni@C surface by creating the electronic negative surface which could facilitate the direct conversion of cellulose to ethanol. Significantly, the result of ^{13}C NMR analysis shows that the generation of ethanol from glucose by the cleavage of C2-C3 and C4-C5 bond as well as the hydroxyl group is removed from the C1 and C6 site in glucose, as shown in **Scheme 3c**. Ni@C catalyst also shows high stability and activity for at least eight runs under optimal conditions (above 60% yield of ethanol at 200°C in 3 h with 40 ml of 0.06 M H_3PO_4 aqueous solution under H_2 atmosphere). In particular, higher ethanol yield (69.1%) in Ni@C-H_3PO_4 catalytic system than theoretical value by glucose fermentation (66.7%) and the prevention of using noble metals provide an opportunity for practical and economical application of direct conversion of cellulose to ethanol. **Table 2** shows the summary of one-pot conversion of cellulose to ethanol.

1,2-Propylene Glycol

In order to increase the yield of 1,2-propylene glycol(1,2-PG) in the process of cellulose conversion, multifunctional catalyst (Ni-W-ZnO/β) was tailored by supporting nickel and tungsten on β-zeolite with addition of ZnO (Gu et al., 2019). Each component of Ni-W-ZnO/β catalyst has its specific role shown below. Due to the abundant acid sites, β-zeolite exhibited a high catalytic performance on the hydrolysis of cellulose to glucose. Further isomerization of glucose to fructose was promoted by addition of ZnO, which is a key step to generate fructose precursor. Ni is effective in the hydrogenation of dihydroxyacetone to acetol and acetol to target 1,2-PG while W facilitates bond cleavage *via* a retro-aldol condensation of fructose to dihydroxyacetone intermediate. As shown in **Scheme 3a**, Ni-W-ZnO/β catalyst shows a high activity and selectivity in the conversion of cellulose to C2/C3 glycols (1,2-PG specially), total yield of EG and 1,2-PG reached 70.1% with 1,2-PG accounting for 51.1%.

Knowing from the above process, hydrogenolysis is the decisive step in the formation of small molecular alcohols, which results in the cleavage of corresponding C-C and C-O bonds by hydrogen and also be regarded as a promising available technology for future biorefinery concepts. Furthermore, how to achieve efficient hydrogenolysis and the exploration of

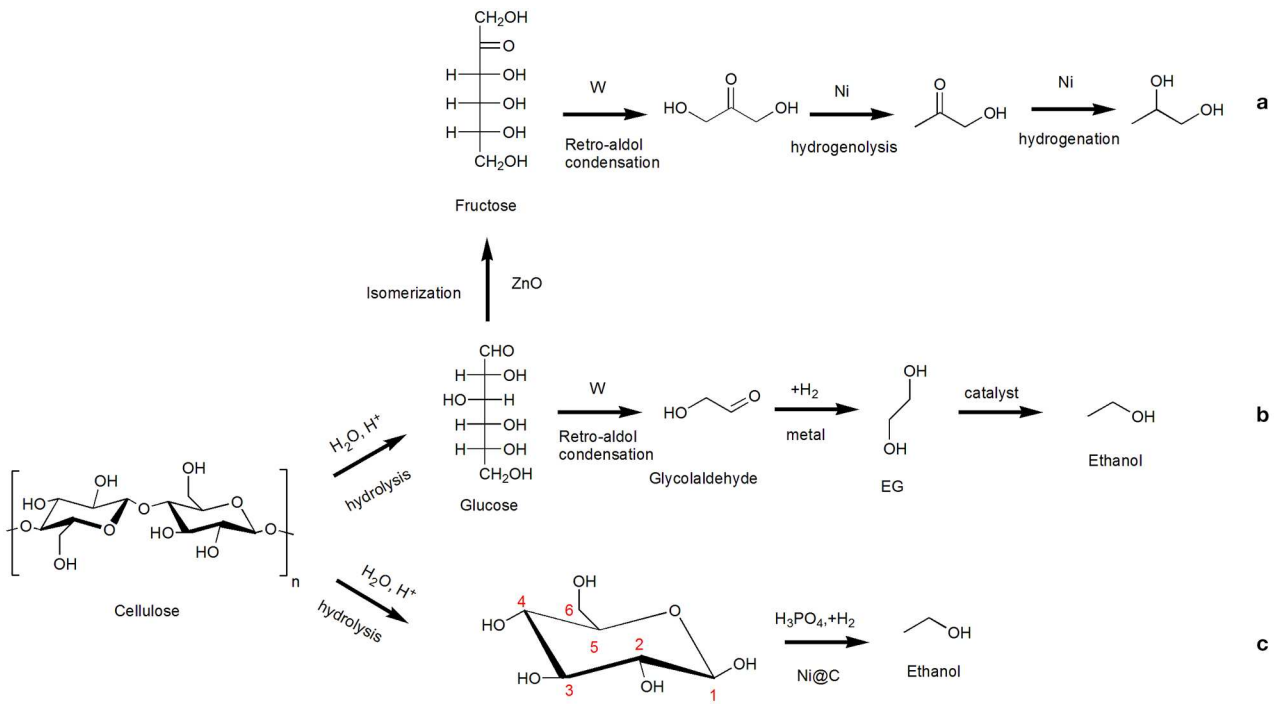

SCHEME 3 | Conversion of cellulose to C2/C3 alcohols.

TABLE 2 | The summary work of one-pot conversion of cellulose to ethanol.

Entry	Catalyst	Cellulose dosage(g)	Solvent	Temperature (K)	Time (h)	Ethanol yield (%)	References
1	0.15 g H_2WO_4-Pt/ZrO_2	0.2	H_2O	523	5	32	Song et al., 2019
2	0.1 g Ru-WOx/HZSM-5	0.1	H_2O	508	10	59	Li C. et al., 2019
3	0.1 g Mo/Pt/WOx	0.15	H_2O	518	2	43.2	Yang et al., 2019
4	0.15 g Ni@C	0.4	H_3PO_4	473	3	69.1	Liu et al., 2019

hydrogenolysis mechanism should be focused on in the future research.

Production of 5-Hydroxymethylfurfural and Its Derivatives

5-Hydroxymethylfurfural

HMF has always been considered as a bridge between renewable biomass resources and platform compounds for its versatile function in terms of obtaining medical drugs, fuel additives, and other bulk chemicals (Körner et al., 2019). It was first reported in 1951 by Newth on the synthesis of HMF from carbohydrates (Newth, 1951), and publications on HMF chemistry have increased significantly in recent years. In the beginning, homogeneous catalysts were favored in the dehydration of fructose to HMF, like HCl (Kuster and Temmink, 1977), oxalic acid (Elhall et al., 1983), H_2SO_4 (Antal et al., 1990), and H_3PO_4 (Tarabanko et al., 2006). With homogeneous catalysts, in order to obtain higher HMF yields, harsh reaction conditions containing higher temperatures and higher pressures are generally required, 50% HMF yields and 95% conversion of fructose could be obtained in the presence of H_2SO_4 under 250°C (Antal et al., 1990). Although the homogeneous catalysts can obtain a certain higher HMF yield, there still exists the problems about difficult separation of homogeneous acid catalysts from the solvent after reaction and the corrosive to the reaction equipment; moreover, the selectivity of the reaction is rather low. Later, related work on HMF synthesis from fructose was published using heterogeneous catalysts in aqueous environment by Carlini et al. When niobium phosphate-based catalysts were applied, quite high selectivity (over 85%) of HMF could be obtained, but only about 30% conversion of fructose were observed in the meantime (Carlini et al., 1999). Cubic zirconium pyrophosphate catalyst (Benvenuti et al., 2000) and vanadyl phosphate catalysts (Carlini et al., 2004) also showed similar reaction patterns, a higher HMF selectivity corresponds to a lower fructose conversion. Generally, large amounts of HMF are unstable in water, its further rehydration to levulinic acid (LA) and formic acid (FA) can be facilitated under acid conditions. More than that, HMF may also be oligomerized or polymerized by itself or with fructose to generate insoluble humins or soluble polymeric by-products, lead to the decrease of

HMF yield, shown as **Scheme 4a**. As a comparative experiment on γ-TiP catalyst has shown, HMF was extracted with an organic solvent—methyl isobutyl ketone (MIBK) when the reaction was halfway through and at the end, the yield of HMF increased apparently from 39 to 67%, although the reaction time was already shortened from 2 to 1 h (Benvenuti et al., 2000). Due to the timely separation of generated HMF from the water solvent, the occurrence of side reactions is reduced, thereby greatly increasing the HMF yield.

When the substrate turns to glucose, the formation of HMF become more complex and difficult attributed to the requirements of Lewis acid for the isomerization of glucose to fructose firstly. In the process of HMF production, Lewis acid sites are prerequisite for the isomerization of glucose into fructose; the lack of Lewis acid sites could make the isomerization rate go down, but excessive Lewis acid sites will result in the formation of undesired by-products and humins, further reduce the HMF selectivity; similarly, Brønsted acid sites are active for dehydration of fructose, the lack of Brønsted acid sites cannot make a full dehydration of fructose to HMF, limiting the generation of HMF, while excessive Brønsted acid sites may suppress the isomerization reaction (Zhang M. et al., 2015; Kreissl et al., 2017; Li X. et al., 2017). Therefore, in order to achieve the cooperative catalytic action for the conversion of glucose to HMF, it is extremely important to find a balance between Lewis acid sites and Brønsted acid sites. In addition to acidic sites, water tolerance is the intrinsic requirement for catalyst when converting glucose to HMF in aqueous phase, thereby niobium-based catalysts have attracted the attention of researchers due to their good water-tolerant property and tunable surface acid density. The acid properties of Lewis acid sites and Brønsted acid sites could be adjusted by controlling the synthesis pH values of porous niobium phosphate catalyst. When $NbPO_4$ catalyst was synthesized at pH = 7, the amounts of Lewis acid and Brønsted acid were balanced and highest 33.6% yield of HMF could be obtained from glucose under optimal reaction conditions in pure water (Zhang M. et al., 2015). According to the literature (Watanabe et al., 2005a,b; Chareonlimkun et al., 2010), more than Lewis acidic sites, basic sites present on metal oxides can also lead to the isomerization of glucose to fructose. Bifunctional catalyst ZrO_2-TiO_2 possesses both basic sites for isomerization and acid sites for dehydration achieved a relatively high HMF yield of 29% in aqueous phase. The result of TPD analysis indicated that ZrO_2 mainly works as an isomerization catalyst to form fructose from glucose, and TiO_2 served as an acidic catalyst mainly responsible for the further dehydration of fructose to HMF.

Direct conversion of cellulose to HMF is more challenging than that from fructose and glucose, since the dissolution of cellulose is required at first in aqueous phase. Therefore, it will be meaningful to find an aqueous solution which could not only hydrolyze cellulose but also promote HMF production. Fortunately, it is reported that cellulose could be dissolved in aqueous $ZnCl_2$ solution with a concentration $\geq$60 wt% by forming a Zn–cellulose complex (Cao et al., 1994, 1995). Moreover, the aqueous $ZnCl_2$ solution also exhibited strong acidity which would be able to facilitate the hydrolysis of cellulose and the dehydration of fructose to HMF, as shown in **Scheme 5**. The Zn^{2+} ions in the concentrated aqueous $ZnCl_2$ solutions can be combined with two adjacent hydroxyl groups on glucose, which may play a same key role like Cr^{2+} in the isomerization of glucose to fructose (Xu and Chen, 1999; Pidko et al., 2010). As high as 30.4% HMF yield can be directly obtained from cellulose in 63 wt% high concentrated $ZnCl_2$ solution (Deng et al., 2012). In a low concentrated solution, since the coordination between H_2O and Zn^{2+} ions is stronger than that between hydroxyl groups and Zn^{2+} ions, there is no excess Zn^{2+} to combine with hydroxyl group, further lead to a lower HMF yield. In short, although aqueous solution achieved a lower yield than organic solvents or ionic liquids in the production of HMF from fructose, glucose, and cellulose, aqueous-phase reaction system has the most available and economic value. Hence, as to researchers, it is very meaningful to seek out novel catalysts to improve both yield and selectivity as far as possible in the conversion of biomass carbohydrates to HMF.

Table 3 shows an overview of published work about HMF production under aqueous conditions.

2,5-Furandicarboxylic Acid

FDCA, obtained after HMF oxidation, is an important monomer in polymer and chemical industry, which can replace petroleum-based terephthalic and isophthalic acids to reduce our dependence on traditional petroleum (Papageorgiou et al., 2016). There are general three intermediate products in the production of FDCA from HMF oxidation, 5-hydroxymethyl-2-furancarboxylic acid (HFCA), 2,5-diformylfuran (DFF), and 5-formyl-2- furancarboxylic acid (FFCA), as shown in **Scheme 4b**. When the aldehyde group on HMF is first selectively oxidized to a carboxyl group, intermediate product HMFCA is obtained. On the contrary, when the hydroxyl group on HMF is first selectively oxidized to an aldehyde group, intermediate product DFF can be obtained. After that, under oxygen conditions, an aldehyde group on DFF can be converted to carboxyl group, and hydroxyl group on HMFCA is oxidized to aldehyde group, both of them could form the other intermediate product 5-formyl-2- furancarboxylic acid (FFCA). FDCA can be obtained after further oxidation of FFCA. Noble metals (like Pt, Pd, and Au) supported by carbon or metal oxides (like Al_2O_3, TiO_2, and CeO_2) have been found to be efficient for the oxidation of HMF to FDCA (Davis et al., 2011; Saha et al., 2013; Li Q. et al., 2019). Several supported Pt, Pd, and Au metal catalyst reactivities were investigated for the oxidation of HMF to FDCA under identical conditions in the aqueous phase of sodium hydroxide (Davis et al., 2011). Pt/C, Pd/C, Au/C, and Au/TiO_2 catalysts were synthesized and applied. In the presence of Pt/C and Pd/C, higher yield of FDCA could be achieved, while mainly intermediate product HMFCA were formed did not continue to be converted to FDCA in the presence of Au/C and Au/TiO_2 under identical conditions (690 kPa O_2, 295 K, 6 h, and 0.3 M NaOH). With the operation of increasing O_2 pressure to 2,000 kPa, reaction time to 22 h, and NaOH concentration to 2.0 M, higher 72% and 80% yield of FDCA can be achieved over Au/C and Au/TiO_2 respectively. The experimental result indicates that Pt and Pd can activate the hydroxyl group of HFCA under a mild condition and lead to the formation of FDCA, whereas Au required higher O_2 pressure

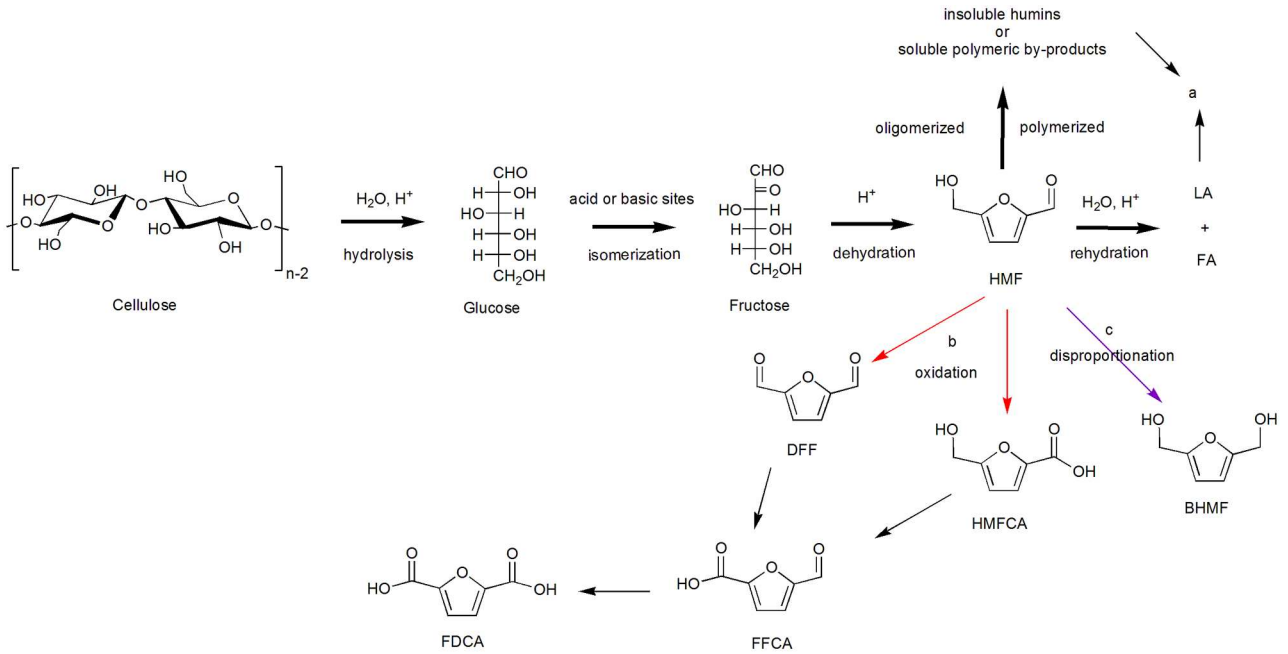

SCHEME 4 | Production of 5-hydroxymethylfurfural (HMF) and its derivatives [mainly 2,5-furandicarboxylic acid (FDCA)].

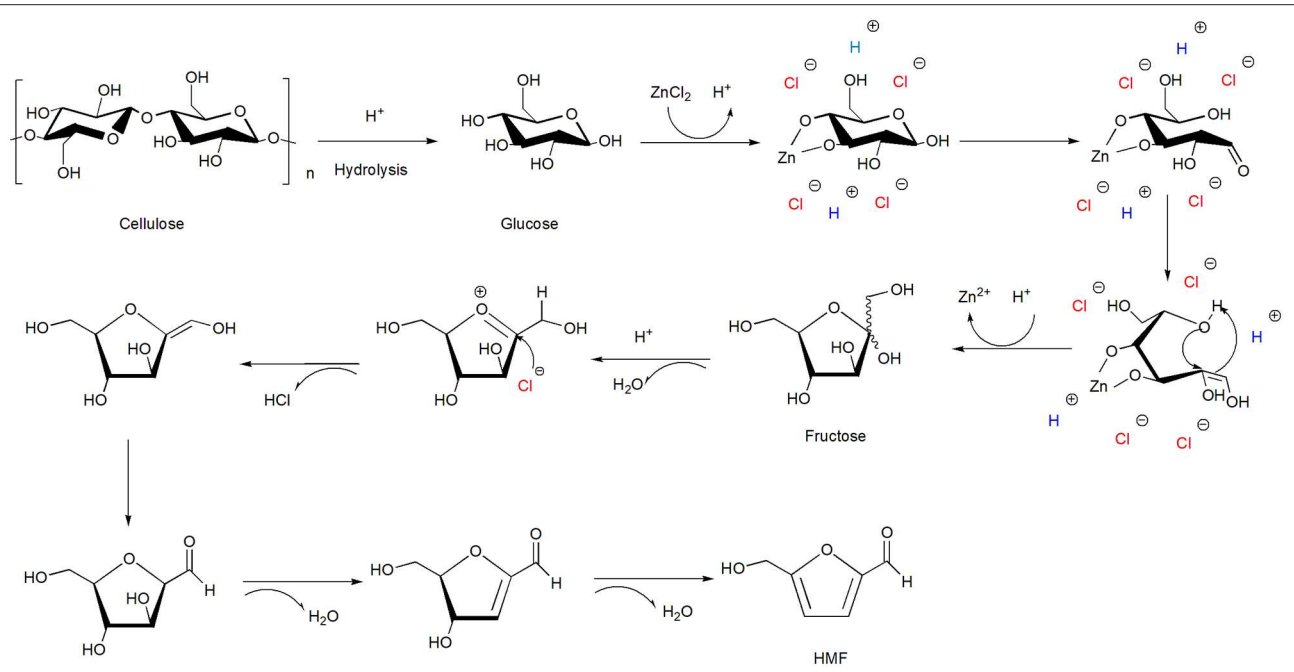

SCHEME 5 | Schematic diagram of 5-hydroxymethylfurfural (HMF) formation from cellulose in the presence of $ZnCl_2$.

and NaOH concentration. The reason can be revealed as the literature reported that a large amount of OH^- is required to activate the hydroxyl group to form aldehyde group intermediate, which can subsequently be oxidized to carboxyl group in the presence of Au catalyst and O_2 (Ketchie et al., 2007). Noting that in the presence of NaOH, undesirable by-products such as 2,5-bis(hydroxymethyl)furan (BHMF) may be formed by disproportionation reaction of HMF. **Scheme 4c**.

According to the previous work in our group, different morphologies of CeO_2 support Au catalysts (Au/CeO_2-rod,

TABLE 3 | Production of 5-hydroxymethylfurfural (HMF) under aqueous conditions.

Entry	Substrate	Catalyst	Temperature (°C)	Time	Yield (%)	Conversion (%)	Selectivity (%)	References
1	Fructose	HCl	90	7 h	43	72	60	Kreissl et al., 2017
2	Fructose	Formic acid	175	45 min	56	56	100	Li X. et al., 2017
3	Fructose	γ-Tip	100	2 h	39	57	69	Benvenuti et al., 2000
4	Fructose	FeVOP	80	1 h	60	71	84	Carlini et al., 2004
5	Glucose	$DyCl_3$	140	2 h	12	30	40	Seri et al., 2001
6	Glucose	TiO_2-ZrO_2	250	5 min	29	44	67	Chareonlimkun et al., 2010
7	Glucose	$MnPO_4$	160	90 min	18	72	25	Xu et al., 2018
8	Glucose	$NbPO_4$	140	60 min	33.6	68.1	49.3	Zhang et al., 2015b
9	Cellulose	$ZnCl_2$+HCl	120	–	30.4	–	–	Deng et al., 2012
10	Cellulose	Bimodal-HZ-5	190	4 h	46	67	69	Li and Yu, 2014

Au/CeO_2-cube and Au/CeO_2-oct) synthesized *via* hydrothermal method and deposition–precipitation exhibited high selectivity of HMF oxidation to FDCA (Li Q. et al., 2019). Combining with experimental results and catalyst characterization, valence of Au and the interfacial acidic properties can be affected by the oxygen vacancies on Au-CeO_2 interface, which determined the catalytic activity. The Au/CeO_2-rod catalysts with the highest oxygen vacancies achieved higher yield of FDCA than Au/CeO_2-cube and Au/CeO_2-oct catalysts in aqueous solution of sodium hydroxide. Further characterization of catalysts shows that Au/CeO_2-rod possesses more interfacial Lewis acidic sites and cationic Au between Au nanoparticles and CeO_2-rod. Hence, we proposed a mechanism of synergistic effect between the interfacial Lewis acid sites, OH^-, and neighboring Au particles, by which the groups (hydroxyl, aldehyde) and molecular O_2 can be activated efficiently, thereby promoting the progress of oxidation reaction, as shown in **Scheme 6**. And **Table 4** exhibits the experimental results about production of FDCA from HMF according to references (Davis et al., 2011; Li Q. et al., 2019).

Although with the addition of mineral base, noble metal catalysts show excellent performance and high yields of FDCA can be achieved, the high costs and produced wastewater may limit their practical application. Therefore, the exploitation of non-noble metal catalysts and greener reaction medium without mineral base or acid should be investigated majorly in the synthesis of FDCA.

Production of Liquid Alkanes *via* Hydrogenolysis and Hydrodeoxygenation

Direct hydrodeoxygenation of cellulose would lead to the formation of gasoline alkanes, mainly pentanes and hexanes. Taking the insoluble property and complex structure of cellulose into consideration, cellulose needs to be first hydrolyzed to soluble hexitol, then pentanes and hexanes would be formed *via* consecutive dehydration, hydrogenation, or hydrogenolysis. Numerous research efforts on hydrogenolysis and hydrodeoxygenation of cellulose to gasoline alkanes have been made (Chen et al., 2013; Liu C. et al., 2014; Liu S. et al., 2014; Beeck et al., 2015; Liu et al., 2015; Venkatakrishnan et al., 2015; Xi et al., 2016).

As shown in **Scheme 7**, reaction pathway *via* HMF: the aldehyde group on HMF is reduced to hydroxyl group leads to the formation of BHMF, and two kinds of intermediate precursor 1-hexanol and 2-hexanol could be obtained. 1-hexanol conversion pathway can be expounded as the following: in the presence of metal catalysts and acid conditions, 1-hexanol can be directly converted to hexane by dehydration and hydrogenation, or fracture of C-O bond under the action of metal sites; on the other hand, pentane could be generated from hexanol *via* the cleavage of C1-C2, meanwhile along with the formation of one molecule CO_2 or methane. Both pentane (mainly) and hexane could be obtained. However, for the conversion of 2-hexanol, reactions are prone to dehydration and hydrogenation of -OH than hydrogenolysis, lead to the generation of hexane. Noting that the conversion route *via* HMF mainly occurs in a reaction solvent containing an organic phase (n-decane, n-dodecane, etc.) or subcritical water (Osaka et al., 2013). There are also some researches on the conversion of cellulose to pentane and hexane in water-organic biphasic system (Chen et al., 2013; Liu S. et al., 2014; Beeck et al., 2015). Therefore, here we mainly introduce some representative transformation of pentanes and hexanes in aqueous phase.

There are generally two pathways of pentanes and hexanes formation in aqueous phase that are proposed from intermediate precursors sorbitol (Chen et al., 2013). As shown in **Scheme 8a**, sorbitol can be obtained from the hydrogenation of glucose after cellulose hydrolysis, which can be directly converted to hexane *via* hydrodeoxygenation under metal-acid catalytic systems; on the other hand, **Scheme 8b**, after dehydration of sorbitol to isosorbide, 1-hexanol can be achieved *via* further hydrogenolysis of isosorbide, pentanes and hexanes(mainly) could also be obtained under metal-acid catalytic systems by fracturing the corresponding C-O and C-C band (Li and Huber, 2010).

It is reported that layered $LiNbMoO_6$ catalysts combined with Ru/C catalyst are conducive to the preparation of liquid alkanes from direct cellulose conversion in low concentration phosphoric acid aqueous solution (Liu S. et al., 2014). In this process, glucose that was obtained after cellulose hydrolysis could be hydrogenated to sorbitol in the presence of Ru/C catalyst, and the formation of isosorbide from sorbitol was inhibited significantly with the addition of layered $LiNbMoO_6$

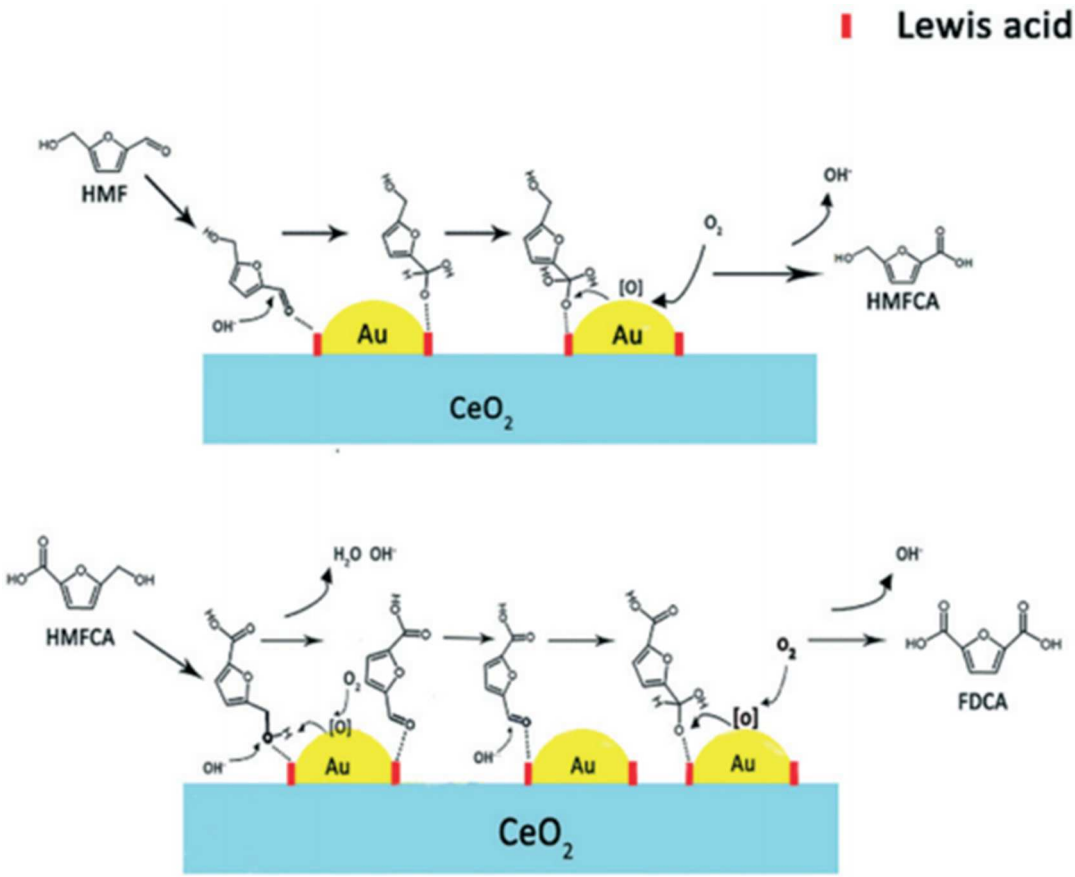

SCHEME 6 | Possible reaction mechanism for oxidation of 5-hydroxymethylfurfural (HMF) to 2,5-furandicarboxylic acid (FDCA). Reprinted with permission from Li C. et al. (2019). Copyright 2019 Royal Society of Chemistry.

catalysts, so that the formation of hexane is promoted efficiently *via* hydrodeoxygenation of sorbitol by combining $LiNbMoO_6$ catalysts and Ru/C catalyst. According to the analysis results of catalysts and experiments, glucose and sorbitol, not isosorbide, are allowed to enter the interlayer pores due to the steric hindrance of the pores between the layered $LiNbMoO_6$ catalyst layers, so the process of converting sorbitol into isosorbide is inhibited, and this mechanism is conducive to the formation of hexane, as shown in **Scheme 9**. Benefit by the unique layer structure of $LiNbMoO_6$ and property of Ru/C, high yield of hexanes (72% C) and pentane (5.9% C) could be obtained directly in low-concentration phosphoric acid aqueous solution by one-pot conversion of cellulose *via* hydrolysis and hydrodeoxygenation.

When isosorbide is formed after the dehydration of sorbitol, the reaction pathway to pentane and hexane production is obviously different from abovementioned, which is hardly converted to alkanes by further hydrodeoxygenation. $Pt/NbOPO_4$ multifunctional catalyst was investigated for alkane production from sorbitol in aqueous solution (Xi et al., 2016), the final product of sorbitol dehydration is isosorbide, also an important intermediate in this process. With following ring opening hydrogenation reactions of isosorbide and two successive hydrogenolysis steps lead to the formation of hexanol, further converted to hexane and pentane *via* C-O band cleavage. In order to have a better understanding of the conversion process, the activation energy of isosorbide hydrogenolysis and sorbitol dehydration was calculated, that is, 72.7 and 147.6 kJ/mol, which are much lower compared to Pt/H-Beta (92 and 171.3 kJ/mol) catalysts. It was also revealed that isosorbide hydrogenolysis is the rate-determining step. Moreover, the strong and high acid amount on $NbOPO_4$ supporter and the promoter effect of component NbO_x on C-O bond cleavage are responsible for sorbitol dehydration and isosorbide hydrogenolysis, respectively. With good catalytic performance of $Pt/NbOPO_4$ catalyst, 55.9% yield of hexane and 4.8% yield of pentane can be achieved from sorbitol under optimal reaction conditions in water phase.

Overall, noble metal catalysts show an efficient and stable catalytic reaction system in the conversion of cellulose to produce alkanes. However, noble metal catalysts cannot be widely used due to its limited availability on earth, which motivated the exploration of alternative non-noble metal catalysts. Ni/HZSM-5 catalyst was investigated by aqueous-phase reforming of sorbitol to bio-gasoline (Zhang et al., 2012). Total 36.4% yield of C5-C6 alkanes can be achieved at 240°C under 4 MPa H_2.

TABLE 4 | Davis et al. (2011) and Li Q. et al. (2019) experimental results about production of 2,5-furandicarboxylic acid (FDCA) from 5-hydroxymethylfurfural (HMF) in aqueous phase.

Entry	Catalyst	Temperature (°C)	Time(h)	Yield (%)	Conversion (%)	Selectivity (%)
1[a]	Pt/C	22	6	79	100	79
2[a]	Pd/C	22	6	71	100	71
3[a]	Au/C (WGC)	22	6	8	100	8
4[a]	Au/C(sol)	22	6	7	100	7
5[a]	Au/TiO_2	22	6	8	100	8
6[b]	Au/C(sol)	22	6	31	100	31
7[b]	Au/TiO_2	22	6	32	100	32
8[b]	Au/C(sol)	22	22	72	100	72
9[b]	Au/TiO_2	22	22	80	100	80
10[c]	Au/CeO_2-rod	130	2.5	87.4	100	87.4
11[c]	Au/CeO_2-cube	130	2.5	19	100	19
12[c]	Au/CeO_2-otc	130	2.5	2	100	2

[a]*Reaction conditions: 0.15 M HMF solution in 0.3 M NaOH, metal:HMF = 6.67 × 10^{-3} mol/mol, P = 690 kPa O_2.*
[b]*Reaction conditions: 0.1 M HMF solution in 2.0 M NaOH, metal:HMF = 8.0 × 10^{-3} mol/mol, P = 2,000 kPa O_2.*
[c]*Reaction conditions: 2.5 h, 130°C, 0.5 MPa O_2, molar ratio of NaOH/HMF = 4, molar ratio of HMF/Au = 400, 0.5 mmol HMF, 20 ml H_2O.*

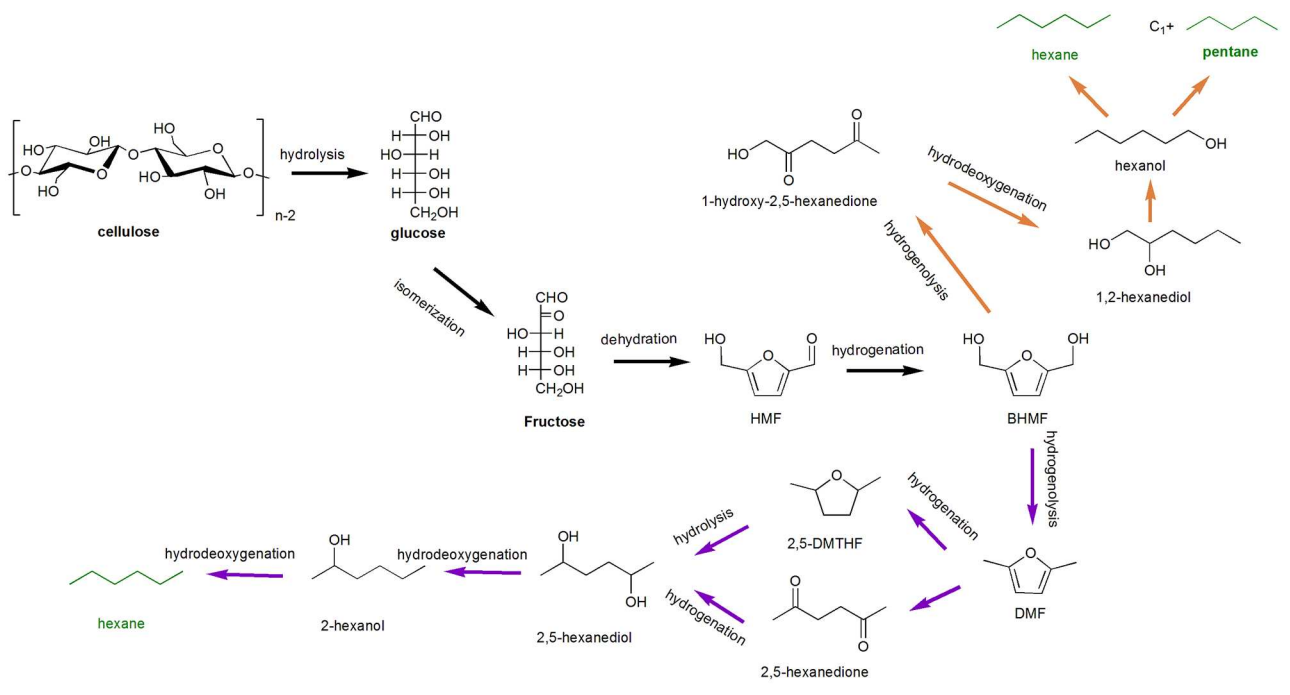

SCHEME 7 | Probable pathway of cellulose conversion to pentane and hexane *via* 5-hydroxymethylfurfural (HMF).

By comparing the characterization analysis results over H_2-TPR/TPD of calcined catalyst at different temperatures (400, 500, 600, and 700°C), the Cat-500 catalyst has the largest H_2 consumption of 1.34 mmol g^{-1} and higher hydrogen desorption, which indicated that decomposed NiO species were reduced completely accompany with the appearance of more Ni active sites on HZSM-5. In addition, the catalyst in lower calcination temperature is not able to provide enough active sites while Ni particles can easily be sintered in higher calcination temperature. Moreover, according to N_2 physical adsorption results, Ni/HZSM-5 catalyst, calcined at 500°C, possess a higher surface area and appropriate amount of macropores. On the one hand, higher surface area means more active sites that could be beneficial to reactions; on the other hand, appropriate amount of macropores could promote the desorption of the target products, so the side reactions (for example, the cleavage of alkanes) could also be suppressed, thereby further enhancing the yield and selectivity of alkanes.

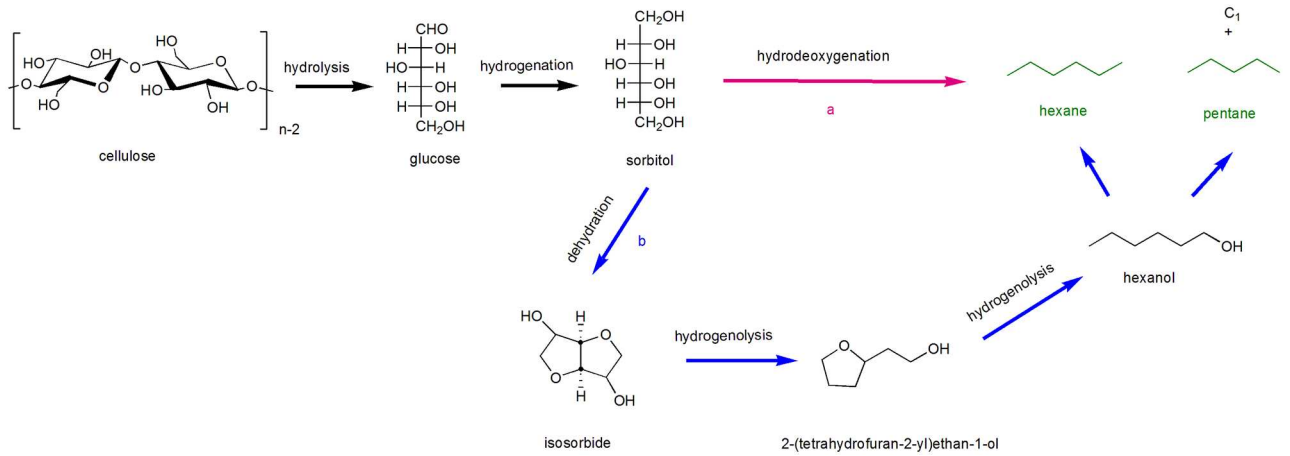

SCHEME 8 | Probable pathway of cellulose conversion to pentane and hexane *via* sorbitol.

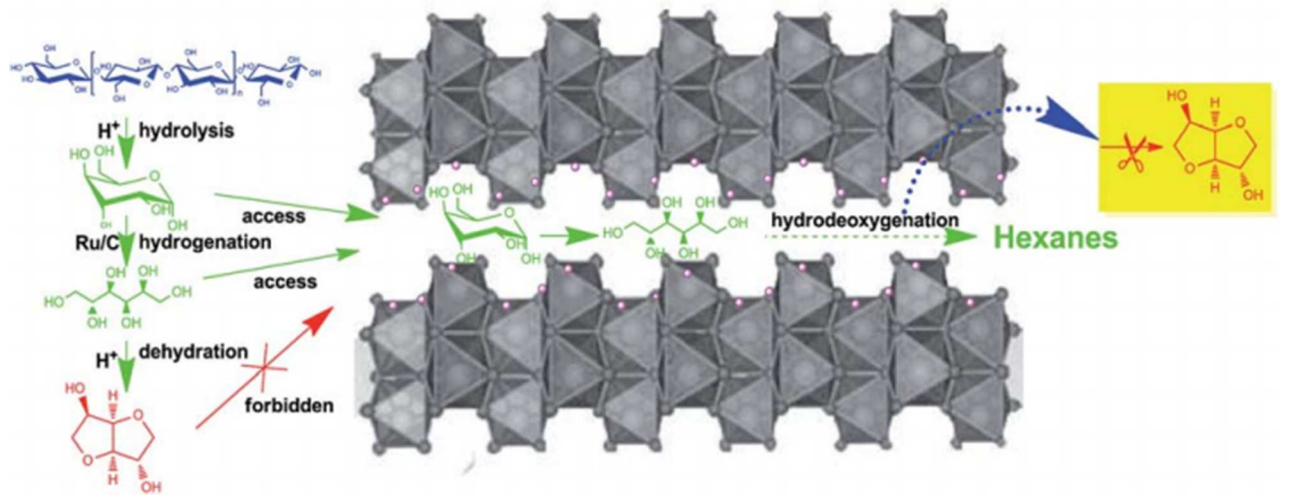

SCHEME 9 | Conversion of cellulose to hexanes over $LiNbMoO_6$ and Ru/C in aqueous phosphoric acid. Reprinted with permission from Liu C. et al. (2014). Copyright 2014 Royal Society of Chemistry.

Table 5 shows the summary work about pentane and hexane preparation *via* different catalysts.

Though a series of multifunctional catalysts are investigated for the production of C5-C6 alkanes, the reaction routes and catalytic mechanism are not clearly enough. Accordingly, the design of catalysts for involved complicated reaction process (hydrolysis, dehydration, hydrogenation, and hydrogenolysis, etc.) should be more targeted and efficient.

ENZYMATIC CONVERSION OF CELLULOSIC MATERIALS AND THE PRODUCTION OF DERIVED GREEN SOLVENTS

As an effective and promising process of cellulose conversion, enzyme treatment methods are thought highly of due to its specificity to the corresponding substrate. Typically, a mixture of several enzymes, cellulase, consists of endo-1-4-β-glucanase, cellobiohydrolase, and β-glucosidase, works synergistically on cellulose hydrolysis process (Nigam, 2013). Firstly, endoglucanse cleaves β-1, 4–glycosidic linkage of D–glucan chains casually in the amorphous regions of cellulose or the surface of microfibrils, so that free chains that contain both reducing and non-reducing ends could be obtained. Then, cellobiose can be achieved while cellobiohydrolase acts on reducing and non-reducing ends. Ultimately, the cellobiose would be converted into glucose by β-glucosidase (Zabed et al., 2016). Moreover, lignocellulosic materials could also be converted by enzymes (Skiba et al., 2016). In the presence of CelloLux-A and BrewZyme BGX industrial enzymes, the hydrolysis of lignocellulosic materials from miscanthus and oat husks was studied. Several monosaccharides including xylose, mannose, glucose, and galactose were obtained after the substrate is treated

TABLE 5 | Summary work about hexanes and pentanes preparation under different catalytic systems in aqueous phase.

Entry	Catalysts	Solvent	Carbon balance (%)	Yield (%)			References
				Hexane	Pentane	Others	
1[a]	Ru/C	H_2O	95.4	1.9	1.1	92.4	Liu S. et al., 2014
2[a]	Ru/C	H_3PO_4	93.6	23.3	12.4	57.9	Liu S. et al., 2014
3[a]	Ru/C+MCM-41	H_3PO_4	93.9	48.6	9.6	35.7	Liu S. et al., 2014
4[a]	Ru/C+HZSM-5	H_3PO_4	93.4	36.6	16.4	40.4	Liu S. et al., 2014
5[a]	Ru/C+γ-Al_2O_3	H_3PO_4	94.5	35.3	14.4	44.8	Liu S. et al., 2014
6[a]	Ru/C+SBA-15	H_3PO_4	95	29.7	13.8	51.5	Liu S. et al., 2014
7[a]	Ru/C+$HNbMoO_6$	H_3PO_4	88.4	65.9	6.9	15.6	Liu S. et al., 2014
8[a]	Ru/C+$LiNbMoO_6$	H_3PO_4	88.6	72	5.9	10.7	Liu S. et al., 2014
9[a]	Ru/C+$LiNbWO_6$	H_3PO_4	84.5	47.7	5.5	31.3	Liu S. et al., 2014
10[b]	Pt/$NbOPO_4$	H_2O	>66	55.9	4.8	>5.3	Xi et al., 2016
11[b]	Pd/$NbOPO_4$	H_2O	>37.7	23.5	5.1	>9.1	Xi et al., 2016
12[b]	Ru/$NbOPO_4$	H_2O	>53.4	8.9	7.8	>36.7	Xi et al., 2016
13[b]	Ir/$NbOPO_4$	H_2O	>58.1	6.1	3.1	>48.9	Xi et al., 2016
14[b]	Rh/$NbOPO_4$	H_2O	>48.5	10.2	15.2	>23.1	Xi et al., 2016
15[c]	Ni/HZSM-5	H_2O	35.3	18.3	4.7	12.3	Zhang et al., 2012
16[d]	Ni/HZSM-5	H_2O	47.6	30	6.4	11.2	Zhang et al., 2012
16[e]	Ni/HZSM-5	H_2O	45	23.7	8.0	13.3	Zhang et al., 2012

[a] *Reaction conditions: 0.8 g microcrystalline cellulose, 0.2 g Ru/C, 230°C, 40 ml solvent, 6 MPa H_2, 24 h, others = C1-C4 alkanes, glucose, cellobiose, sorbitol, sorbitans, isosorbide, 1-hexanol, 1-pentanol, 1,6-hexanediol, ethylene glycol, and propylene glycol.*

[b] *Reaction conditions: 1 g sorbitol, 0.3 g catalysts, 250°C, 20 g H_2O, 4 MPa H_2, 12 h, others = isosorbide (mainly), sorbitan, 2-(tetrahydrofuran-2-yl)ethan-1-ol, and hexanol.*

[c] *Reaction conditions: 0.05 mol sorbitol, 3.0 g catalyst, 240°C, 150 ml deionized water, 3 MPa H_2, others = C1-C4 alkanes.*

[d] *Reaction conditions: 0.05 mol sorbitol, 3.0 g catalyst, 240°C, 150 ml deionized water, 4 MPa H_2, others = C1-C4 alkanes.*

[e] *Reaction conditions: 0.05 mol sorbitol, 3.0 g catalyst, 240°C, 150 ml deionized water, 5 MPa H_2, others = C1-C4 alkanes.*

with enzymes. Expectedly, glucose has the highest yield among those monosaccharides, 75.8 and 53.5% yields can be achieved from miscanthus and oat husks. Surprisingly, bioethanol, a derived green solvent, could be obtained in a high yield with further fermentation after enzymatic hydrolysis.

In addition to bioethanol, levoglucosenone (LGO) and dihydrolevoglucosenone (Cyrene) are also considered as green solvents and building blocks of platform chemicals. LGO is the precursor of synthetic Cyrene that was obtained after cellulose dehydration, which could be subsequently hydrogenated to Cyrene, as shown in **Scheme 10**. Cyrene has the potential in many applications, such as in the field of graphene manufacturing due to its optimal polarity and high viscosity (Salavagione et al., 2017); a replacement for toxic dipolar aprotic solvents, like DMF, NMP, and sulfolane (Camp, 2018); used to synthesize metal-organic framework (Zhang et al., 2016). However, the synthesis of Cyrene mostly used Pd-based catalysts with additional hydrogen. Distinctively, an alkene reductase (OYE 2.6) shows a high performance in the reduction of levoglucosenone to Cyrene (Mouterde et al., 2018), high levoglucosenone conversion of 99 and 99% yield of Cyrene can be achieved by continuous extraction. Furthermore, the formation of side product (1R,2S)-2-hydroxy-6,8-dioxabicyclo [3.2.1] octan-4-one (OH-LGO) is avoided due to the catalytic specificity of alkene reductase (OYE 2.6) and present the best conversion rates.

In view of the high selectivity and activity of the enzyme in the catalytic process, meanwhile meet with the demand of green and sustainable catalytic process, more research should be accounted of in the upcoming development of cellulosic materials conversion.

CONCLUSIONS AND PERSPECTIVES

The transformation of cellulose to oxygenated and hydrocarbon chemicals was reviewed *via* several reaction routes over diverse multifunctional catalysts in aqueous phase. Sugars, alcohols, furfural, furan, and alkane chemicals can be obtained in one or two-step from cellulose conversion, which provide an alternative way to replace traditional fossil fuels with sustainable resources and potential solution for current environment problems. During the conversion process, complex reactions including hydrolysis, dehydration, isomerization, hydrogenolysis, and hydrogenation have high requirements for reaction systems and catalysts. (1) As to reaction solvent, the preferred reaction solvent for efficient conversion of cellulose to the downstream products for practical application is the aqueous phase, which is more available and economical than organic solvents or ionic liquids or other solvents. (2) For reaction conditions, high temperature and added extra gas (H_2, O_2) increased the cost of conversion process and exiting security issues, which would bring a lot of uncertainty for the reaction. (3) When it turns to catalysts, multifunctional catalysts were designed due to the complexity of the various reactions involved in the conversion process, in which different components of the catalysts have unique effects for specific reaction processes, for example, metal components are usual responsible for the hydrogenation, or hydrogenolysis

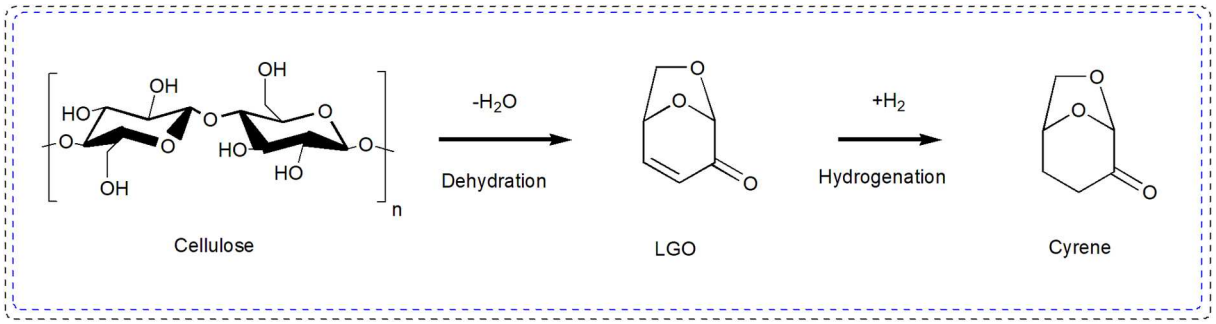

SCHEME 10 | Synthetic route to levoglucosenone (LGO) and Cyrene from cellulose.

of C-O or C-C bonds, or active sites of the reaction. (4) The reaction routes have always been valued in the study of cellulose aqueous-phase transformation, different reaction routes generally correspond to various types of reaction systems over diverse multifunctional catalysts, and the ultimate goal of the study is to achieve a clear understanding of the reaction and reduce the reaction steps as possible for energy-saving purposes. (5) Meet the requirements of green and sustainable catalysis, enzyme catalytic process of cellulosic materials has shown a giant potential for its high selectivity and activity, hence, looking for specific enzymes for specific reactions are of great significance. Overall, the research findings mentioned in this review provide a scientific basis for related subject study, which has broad prospects for future development in biomass conversion.

Although tremendous progresses have been achieved in the conversion of cellulose, there are still a lot of shortcomings and challenges that need to be solved in further study. (1) It can be confirmed that cellulose could be efficiently converted in aqueous phase, but many mineral acids (sulfuric acid, phosphoric acid, hydrochloric acid, etc.) or organic acids (formic acid, acetic acid, fatty acid, etc.) are involved in many aqueous phases, all of these acids has corrosive effects on reaction instruments and may cause water pollution problems, so pure water phase reaction should be the ultimate goal to pursue. (2) The efficient conversion of cellulose under milder conditions should be the focus of researchers. And taking the high oxygen content of cellulose and the presence of water in reaction system into consideration, can oxygen and hydrogen be supplied *in situ* during the reaction process? Those ways can both reduce the energy consumption and expenditure by a large margin. (3) The decisive steps in all kinds of reaction process should be defined in the beginning so that the catalyst can be designed more accurately, and researches on non-noble metals should be reinforced to minimize the use of precious metals in economic aspect. Furthermore, the interaction between different components of the multifunctional catalysts should be clearly understood in order to reduce the occurrence of side reactions and improve the yield of the target products. In particular, the hydrothermal stability and excellent catalytic activity of multifunctional catalysts are the most important things that should be the first to be considered to enable the full utilization of cellulose. (4) The reaction routes are still the key research object of cellulose aqueous phase transformation, the design of catalysts and the comprehension of reaction mechanisms would be a benefit from the premise of a clear reaction route. (5) The high cost, sensitivity to reaction temperature, and pH have become non-negligible factors restricting the application of enzymes in catalytic conversion of biomass. Therefore, further reducing the cost and improving the stability of the enzyme to adapt to various reaction conditions will be focused on in the next research.

AUTHOR CONTRIBUTIONS

HX and QL taking the lead in coordinating the review study and drafting the manuscript. CZ is responsible for obtaining the Scheme permission in the relevant cited references. XH, HW, CZ, SL, and ZX provided professional advice. CC, XZ, and QL participated in the work of manuscript revision. XZ, QL, and LM provided funding support. All authors read and approved the final manuscript.

FUNDING

This work was financially supported by the National Key R&D Program of China (2018YFB1501402), the National Science Foundation of China (51976220 and 51576199), the Natural Science Foundation of Guangdong Province (2017A030308010), the DNL Cooperation Fund, CAS (DNL180302), and the Transformational Technologies for Clean Energy and Demonstration, Strategic Priority Research Program of the Chinese Academy of Sciences (No. XDA21060102).

REFERENCES

Adschiri, T., Hirose, S., Malaluan, R., and Arai, K. (1993). Noncatalytic conversion of cellulose in supercritical and subcritical water. *J. Chem. Eng. Jpn.* 26, 676–680.

Alonso, D. M., Bond, J. Q., and Dumesic, J. A. (2010). Catalytic conversion of biomass to biofuels. *Green Chem.* 12, 1493–1513. doi: 10.1039/c004654j

Alonso, D. M., Wettstein, S. G., and Dumesic, J. A. (2012). Bimetallic catalysts for upgrading of biomass to fuels and

chemicals. *Chem. Soc. Rev*. 41, 8075–8098. doi: 10.1039/c2cs35188a

Amarasekara, A. S., and Reyes, C. D. G. (2019). Brønsted acidic ionic liquid catalyzed one-pot conversion of cellulose to furanic biocrude and identification of the products using LC-MS. *Renew. Energy* 136, 352–357. doi: 10.1016/j.renene.2018.12.108

Antal, M. J. Jr., Mok, W. S., and Richards, G. N. (1990). Mechanism of formation of 5-(hydroxymethyl)-2-furaldehyde from D-fructose and sucrose. *Carbohyd. Res.* 199, 91–109. doi: 10.1016/0008-6215(90)84096-D

Atalla, R. H., and Vanderhart, D. L. (1984). Native cellulose: a composite of two distinct crystalline forms. *Science* 223, 283–285. doi: 10.1126/science.223.4633.283

Beeck, B. O., Dusselier, M., Geboers, J., Holsbeek, J., Morré, E., Oswald, S., et al. (2015). Direct catalytic conversion of cellulose to liquid straight-chain alkanes. *Energy Environ. Sci*. 8, 230–240. doi: 10.1039/C4EE01523A

Benvenuti, F., Carlini, C., Patrono, P., Galletti, A. M. R., Sbrana, G., Massucci, M. A., et al. (2000). Heterogeneous zirconium and titanium catalysts for the selective synthesis of 5-hydroxymethyl-2-furaldehyde from carbohydrates. *Appl. Catal. A Gen*. 193, 147–153. doi: 10.1016/S0926-860X(99)00424-X

Binder, J. B., and Raines, R. T. (2010). Fermentable sugars by chemical hydrolysis of biomass. *Proc. Natl. Acad. Sci. U.S.A*. 107, 4516–4521. doi: 10.1073/pnas.0912073107

Camp, J. E. (2018). Bio-available solvent cyrene: synthesis, derivatization, and applications. *ChemSusChem* 11, 3048–3055. doi: 10.10021/cssc.201801420

Cao, N. J., Xu, Q., Chen, C. S., Gong, C. S., and Chen, L. F. (1994). Cellulose hydrolysis using zinc chloride as a solvent and catalyst. *Appl. Biochem. Biotechnol*. 45, 521–530. doi: 10.1007/BF02941827

Cao, N. J., Xu, Q., and Chen, L. F. (1995). Acid hydrolysis of cellulose in zinc chloride solution. *Appl. Biochem. Biotechnol*. 51:21. doi: 10.1007/bf02933408

Cao, Y., Wang, J., Kang, M., and Zhu, Y. (2014). Efficient synthesis of ethylene glycol from cellulose over Ni-WO_3/SBA-15 catalysts. *J. Mol. Catal. A Chem*. 381, 46–53. doi: 10.1016/j.molcata.2013.10.002

Carlini, C., Giuttari, M., Galletti, A. M. R., Sbrana, G., Armaroli, T., and Busca, G. (1999). Selective saccharides dehydration to 5-hydroxymethyl-2-furaldehyde by heterogeneous niobium catalysts. *Appl. Catal. A Gen*. 183, 295–302. doi: 10.1016/S0926-860X(99)00064-2

Carlini, C., Patrono, P., Galletti, A. M. R., and Sbrana, G. (2004). Heterogeneous catalysts based on vanadyl phosphate for fructose dehydration to 5-hydroxymethyl-2-furaldehyde. *Appl. Catal. A Gen*. 275, 111–118. doi: 10.1016/j.apcata.2004.07.026

Chareonlimkun, A., Champreda, V., Shotipruk, A., and Laosiripojana, N. (2010). Catalytic conversion of sugarcane bagasse, rice husk and corncob in the presence of TiO_2, ZrO_2 and mixed-oxide TiO_2-ZrO_2 under hot compressed water (HCW) condition. *Bioresour. Technol*. 101, 4179–4186. doi: 10.1016/j.biortech.2010.01.037

Charmot, A., Chung, P. W., and Katz, A. (2014). Catalytic hydrolysis of cellulose to glucose using weak-acid surface sites on postsynthetically modified carbon. *ACS Sustain. Chem. Eng*. 2, 2866–2872. doi: 10.1021/sc500669q

Chen, K., Tamura, M., Yuan, Z., Nakagawa, Y., and Tomishige, K. (2013). One-pot conversion of sugar and sugar polyols to n-alkanes without C-C dissociation over the Ir-ReOx/SiO_2 catalyst combined with H-ZSM-5. *ChemSusChem* 6, 613–621. doi: 10.1002/cssc.201200940

Chen, P., Shrotri, A., and Fukuoka, A. (2019). Soluble cello-oligosaccharides produced by carbon-catalyzed hydrolysis of cellulose. *ChemSusChem* 12, 2576–2580. doi: 10.1002/cssc.201900800

Davda, R. R., and Dumesic, J. A. (2004). Renewable hydrogen by aqueous-phase reforming of glucose. *Chem. Commun*. 1, 36–37. doi: 10.1039/B310152E

Davis, S. E., Houk, L. R., Tamargo, E. C., Datye, A. K., and Davis, R. J. (2011). Oxidation of 5-hydroxymethylfurfural over supported Pt, Pd and Au catalysts. *Catal. Today* 160, 55–60. doi: 10.1016/j.cattod.2010.06.004

Degirmenci, V., Uner, D., Cinlar, B., Shanks, B. H., Yilmaz, A., van Santen, R. A., et al. (2011). Sulfated zirconia modified SBA-15 catalysts for cellobiose hydrolysis. *Catal. Lett*. 141, 33–42. doi: 10.1007/s10562-010-0466-1

Delbecq, F., Wang, Y., Muralidhara, A., El Ouardi, K., Marlair, G., and Len, C. (2018). Hydrolysis of hemicellulose and derivatives-A review of recent advances in the production of furfural. *Front. Chem*. 6:146. doi: 10.3389/fchem.2018.00146

Den, W., Sharma, V. K., Lee, M., Nadadur, G., and Varma, R. S. (2018). Lignocellulosic biomass transformations via greener oxidative pretreatment processes: access to energy and value-added chemicals. *Front. Chem*. 6:141. doi: 10.3389/fchem.2018.00141

Deng, T., Cui, X., Qi, Y., Wang, Y., Hou, X., and Zhu, Y. (2012). Conversion of carbohydrates into 5-hydroxymethylfurfural catalyzed by $ZnCl_2$ in water. *Chem. Commun*. 48, 5494–5496. doi: 10.1039/C2CC00122E

Deng, W., Tan, X., Fang, W., Zhang, Q., and Wang, Y. (2009). Conversion of cellulose into sorbitol over carbon nanotube-supported ruthenium catalyst. *Catal. Lett*. 133:167. doi: 10.1007/s10562-009-0136-3

Elhall, T., Martin, J. C., and Descotes, G. (1983). Derivatives of 5-hydroxymethylfurfural I synthesis of DI and terfuran derivatives. *Chem. Inform*. 36:14. doi: 10.1002/chin.198336200

Farrell, A. E., Plevin, R. J., Turner, B. T., Jones, A. D., O'hare, M., and Kammen, D. M. (2006). Ethanol can contribute to energy and environmental goals. *Science* 311, 506–508. doi: 10.1126/science.1121416

Fujita, Y., Ito, J., Ueda, M., Fukuda, H., and Kondo, A. (2004). Synergistic saccharification, and direct fermentation to ethanol, of amorphous cellulose by use of an engineered yeast strain codisplaying three types of cellulolytic enzyme. *Appl. Environ. Microbiol*. 70, 1207–1212. doi: 10.1128/AEM.70.2.1207-1212.2004

Fukuoka, A., and Dhepe, P. L. (2006). Catalytic conversion of cellulose into sugar alcohols. *Angew. Chem. Int. Ed*. 45, 5161–5163. doi: 10.1002/anie.200601921

Gao, D. M., Shen, Y. B., Zhao, B., Liu, Q., Nakanishi, K., Chen, J., et al. (2019). Macroporous niobium phosphate-supported magnesia catalysts for isomerization of glucose-to-fructose. *ACS Sustain. Chem. Eng*. 7, 8512–8521. doi: 10.1021/acssuschemeng.9b00292

Gao, Z., Li, N., Chen, M., and Yi, W. (2019). Comparative study on the pyrolysis of cellulose and its model compounds. *Fuel Proc. Technol*. 193, 131–140. doi: 10.1016/j.fuproc.2019.04.038

Gu, M., Shen, Z., Yang, L., Dong, W., Kong, L., Zhang, W., et al. (2019). Reaction route selection for cellulose hydrogenolysis into C_2/C_3 glycols by ZnO-modified Ni-W/β-zeolite catalysts. *Sci. Rep*. 9, 1–10. doi: 10.1038/s41598-019-48103-6

Gunther, W. R., Wang, Y., Ji, Y., Michaelis, V. K., Hunt, S. T., Griffin, R. G., et al. (2012). Sn-Beta zeolites with borate salts catalyse the epimerization of carbohydrates via an intramolecular carbon shift. *Nat. Commun*. 3:1109. doi: 10.1038/ncomms2122

Han, J. W., and Lee, H. (2012). Direct conversion of cellulose into sorbitol using dual-functionalized catalysts in neutral aqueous solution. *Catal. Commun*. 19, 115–118. doi: 10.1016/j.catcom.2011.12.032

Himmel, M. E., Ding, S. Y., Johnson, D. K., Adney, W. S., Nimlos, M. R., Brady, J. W., et al. (2007). Biomass recalcitrance: engineering plants and enzymes for biofuels production. *Science* 315, 804–807. doi: 10.1126/science.1137016

Huber, G. W., Shabaker, J. W., and Dumesic, J. A. (2003). Raney Ni-Sn catalyst for H_2 production from biomass-derived hydrocarbons. *Science* 300, 2075–2077. doi: 10.1126/science.1085597

Ji, N., Zhang, T., Zheng, M., Wang, A., Wang, H., Wang, X., et al. (2008). Direct catalytic conversion of cellulose into ethylene glycol using nickel-promoted tungsten carbide catalysts. *Angew. Chem. Int. Ed*. 47, 8510–8513. doi: 10.1002/anie.200803233

Jing, Y., Guo, Y., Xia, Q., Liu, X., and Wang, Y. (2019). Catalytic production of value-added chemicals and liquid fuels from lignocellulosic biomass. *Chem* 5, 2520–2546. doi: 10.1016/j.chempr.2019.05.022

Jun, S., Joo, S. H., Ryoo, R., Kruk, M., Jaroniec, M., Liu, Z., et al. (2000). Synthesis of new, nanoporous carbon with hexagonally ordered mesostructure. *J. Am. Chem. Soc*. 122, 10712–10713. doi: 10.1021/ja002261e

Kennes, D., Abubackar, H. N., Diaz, M., Veiga, M. C., and Kennes, C. (2016). Bioethanol production from biomass: carbohydrate vs syngas fermentation. *J. Chem. Technol. Biotechnol*. 91, 304–317. doi: 10.1002/jctb.4842

Ketchie, W. C., Murayama, M., and Davis, R. J. (2007). Promotional effect of hydroxyl on the aqueous phase oxidation of carbon monoxide and glycerol over supported Au catalysts. *Top. Catal*. 44, 307–317. doi: 10.1007/s11244-007-0304-x

Kim, K. H., and Hong, J. (2001). Supercritical CO_2 pretreatment of lignocellulose enhances enzymatic cellulose hydrolysis. *Bioresour. Technol*. 77, 139–144. doi: 10.1016/S0960-8524(00)00147-4

Kitano, M., Yamaguchi, D., Suganuma, S., Nakajima, K., Kato, H., Hayashi, S., et al. (2009). Adsorption-enhanced hydrolysis of β-1, 4-glucan on graphene-based amorphous carbon bearing SO_3H, COOH, and OH groups. *Langmuir* 25, 5068–5075. doi: 10.1021/la8040506

Kobayashi, H., Komanoya, T., Hara, K., and Fukuoka, A. (2010). Water-tolerant mesoporous-carbon-supported ruthenium catalysts for the hydrolysis of cellulose to glucose. *ChemSusChem* 3, 440–443. doi: 10.1002/cssc.200900296

Kobayashi, H., Yabushita, M., Hasegawa, J. Y., and Fukuoka, A. (2015). Synergy of vicinal oxygenated groups of catalysts for hydrolysis of cellulosic molecules. *J. Phys. Chem. C* 119, 20993–20999. doi: 10.1021/acs.jpcc.5b06476

Kobayashi, H., Yabushita, M., Komanoya, T., Hara, K., Fujita, I., and Fukuoka, A. (2013). High-yielding one-pot synthesis of glucose from cellulose using simple activated carbons and trace hydrochloric acid. *ACS Catal.* 3, 581–587. doi: 10.1021/cs300845f

Körner, S., Albert, J., and Held, C. (2019). Catalytic low-temperature dehydration of fructose to 5-hydroxymethylfurfural using acidic deep eutectic solvents and polyoxometalate catalysts. *Front. Chem.* 7:661. doi: 10.3389/fchem.2019.00661

Kreissl, H. T., Li, M. M., Peng, Y. K., Nakagawa, K., Hooper, T. J., Hanna, J. V., et al. (2017). Structural studies of bulk to nanosize niobium oxides with correlation to their acidity. *J. Am. Chem. Soc.* 139, 12670–12680. doi: 10.1021/jacs.7b06856

Kuster, B. F., and Temmink, H. M. (1977). The influence of pH and weak-acid anions on the dehydration of D-fructose. *Carbohydr. Res.* 54, 185–191. doi: 10.1016/S0008-6215(00)84808-9

Lee, H. S., and Hong, J. (2000). Kinetics of glucose isomerization to fructose by immobilized glucose isomerase: anomeric reactivity of D-glucose in kinetic model. *J. Biotechnol.* 84, 145–153. doi: 10.1023/B:MCBI.0000049152.06259.4b

Li, C., Wang, Q., and Zhao, Z. K. (2008). Acid in ionic liquid: An efficient system for hydrolysis of lignocellulose. *Green Chem.* 10, 177–182. doi: 10.1039/B711512A

Li, C., Xu, G., Wang, C., Ma, L., Qiao, Y., Zhang, Y., et al. (2019). One-pot chemocatalytic transformation of cellulose to ethanol over Ru-WOx/HZSM-5. *Green Chem.* 21, 2234–2239. doi: 10.1039/C9GC00719A

Li, C., and Zhao, Z. K. (2007). Efficient acid-catalyzed hydrolysis of cellulose in ionic liquid. *Adv. Synth. Catal.* 349, 1847–1850. doi: 10.1002/adsc.200700259

Li, N., and Huber, G. W. (2010). Aqueous-phase hydrodeoxygenation of sorbitol with Pt/SiO_2-Al_2O_3: Identification of reaction intermediates. *J. Catal.* 270, 48–59. doi: 10.1016/j.jcat.2009.12.006

Li, N., Zheng, Y., Wei, L., Teng, H., and Zhou, J. (2017). Metal nanoparticles supported on WO3 nanosheets for highly selective hydrogenolysis of cellulose to ethylene glycol. *Green Chem.* 19, 682–691. doi: 10.1039/C6GC01327A

Li, Q., Wang, H., Tian, Z., Weng, Y., Wang, C., Ma, J., et al. (2019). Selective oxidation of 5-hydroxymethylfurfural to 2,5-furandicarboxylic acid over Au/CeO_2 catalysts: the morphology effect of CeO_2. *Catal. Sci. Technol.* 9, 1570–1580. doi: 10.1039/C9CY00211A

Li, W., Zhang, T., Xin, H., Su, M., Ma, L., Jameel, H., et al. (2017). *p*-Hydroxybenzenesulfonic acid-formaldehyde solid acid resin for the conversion of fructose and glucose to 5-hydroxymethylfurfural. *RSC Adv.* 7, 27682–27688. doi: 10.1039/C7RA03155F

Li, X., Peng, K., Liu, X., Xia, Q., and Wang, Y. (2017). Comprehensive understanding of the role of Brønsted and Lewis acid sites in glucose conversion into 5-hydromethylfurfural. *ChemCatChem* 9, 2739–2746. doi: 10.1002/cctc.201601203

Li, X., Zhang, Y., Xia, Q., Liu, X., Peng, K., Yang, S., et al. (2018). Acid-free conversion of cellulose to 5-hydroxymethylfurfural catalyzed by hot seawater. *Ind. Eng. Chem. Res.* 57, 3545–3553. doi: 10.1021/acs.iecr.8b00443

Li, Y., and Yu, J. (2014). New stories of zeolite structures: their descriptions, determinations, predictions, and evaluations. *Chem. Rev.* 114, 7268–7316. doi: 10.1021/cr500010r

Li, Z., Liu, Y., Liu, C., Wu, S., and Wei, W. (2019). Direct conversion of cellulose into sorbitol catalyzed by a bifunctional catalyst. *Bioresour. Technol.* 274, 190–197. doi: 10.1016/j.biortech.2018.11.089

Liebert, T., Seifert, M., and Heinze, T. (2008). Efficient method for the preparation of pure, water-soluble cellodextrines. *Macromol. Symp.* 262, 140–149. doi: 10.1002/masy.200850214

Liu, C., Carraher, J. M., Swedberg, J. L., Herndon, C. R., Fleitman, C. N., and Tessonnier, J. P. (2014). Selective base-catalyzed isomerization of glucose to fructose. *ACS Catal.* 4, 4295–4298. doi: 10.1021/cs501197w

Liu, Q., Wang, H., Xin, H., Wang, C., Yan, L., Wang, Y., et al. (2019). Selective cellulose hydrogenolysis to ethanol using Ni@C combined with phosphoric acid catalysts. *ChemSusChem* 12, 3977–3987. doi: 10.1002/cssc.201901110

Liu, S., Tamura, M., Nakagawa, Y., and Tomishige, K. (2014). One-pot conversion of cellulose into n-hexane over the $Ir\text{-}ReOx/SiO_2$ catalyst combined with HZSM-5. *ACS Sustain. Chem. Eng.* 2, 1819–1827. doi: 10.1021/sc5001463

Liu, Y., Chen, L., Wang, T., Zhang, X., Long, J., Zhang, Q., et al. (2015). High yield of renewable hexanes by direct hydrolysis-hydrodeoxygenation of cellulose in an aqueous phase catalytic system. *RSC Adv.* 5, 11649–11657. doi: 10.1039/C4RA14304C

Luo, C., Wang, S., and Liu, H. (2007). Cellulose conversion into polyols catalyzed by reversibly formed acids and supported ruthenium clusters in hot water. *Angew. Chem. Int. Ed.* 46, 7636–7639. doi: 10.1002/anie.200702661

Mariscal, R., Maireles-Torres, P., Ojeda, M., Sádaba, I., and López Granados, M. (2016). Furfural: a renewable and versatile platform molecule for the synthesis of chemicals and fuels. *Energy Environ. Sci.* 9, 1144–1189. doi: 10.1039/C5EE02666K

Martin-Mingot, A., Vigier, K. D. O., Jérôme, F., and Thibaudeau, S. (2012). High efficiency of superacid HF-SbF 5 for the selective decrystallization-depolymerization of cellulose to glucose. *Org. Biomol. Chem.* 10, 2521–2524. doi: 10.1039/c2ob07143f

Mayes, H. B., Nolte, M. W., Beckham, G. T., Shanks, B. H., and Broadbelt, L. J. (2014). The alpha-bet (a) of glucose pyrolysis: computational and experimental investigations of 5-hydroxymethylfurfural and levoglucosan formation reveal implications for cellulose pyrolysis. *ACS Sustain. Chem. Eng.* 2, 1461–1473. doi: 10.1021/sc500113m

Mellmer, M. A., Martin Alonso, D. M., Luterbacher, J. S., Gallo, J. M. R., and Dumesic, J. A. (2014a). Effects of gamma-valerolactone in hydrolysis of lignocellulosic biomass to monosaccharides. *Green Chem.* 16, 4659–4662. doi: 10.1039/C4GC01768D

Mellmer, M. A., Sanpitakseree, C., Demir, B., Bai, P., Ma, K. W., Neurock, M., et al. (2018). Solvent-enabled control of reactivity for liquid-phase reactions of biomass derived compounds. *Nat. Catal.* 1, 199–207. doi: 10.1038/s41929-018-0027-3

Mellmer, M. A., Sener, C., Gallo, J. M. R., Luterbacher, J. S., Alonso, D. M., and Dumesic, J. A. (2014b). Solvent effects in acid-catalyzed biomass conversion reactions. *Angew. Chem. Int. Ed.* 53, 11872–11875. doi: 10.1002/anie.201408359

Moliner, M., Román-Leshkov, Y., and Davis, M. E. (2010). Tin-containing zeolites are highly active catalysts for the isomerization of glucose in water. *Proc. Natl. Acad. Sci. U.S.A.* 107, 6164–6168. doi: 10.1073/pnas.1002358107

Mouterde, L. M., Allais, F., and Stewart, J. D. (2018). Enzymatic reduction of levoglucosenone by an alkene reductase (OYE 2.6): a sustainable metal-and dihydrogen-free access to the bio-based solvent Cyrene®. *Green Chem.* 20, 5528–5532. doi: 10.1039/C8GC03146K

Newth, F. H. (1951). The formation of furan compounds from hexoses. *Adv. Carbohydr. Chem.* 6, 83–106. doi: 10.1016/S1876-0813(08)60032-9

Nigam, P. S. (2013). Microbial enzymes with special characteristics for biotechnological applications. *Biomolecules,* 3, 597–611. doi: 10.3390/biom3030597

Onda, A., Ochi, T., and Yanagisawa, K. (2008). Selective hydrolysis of cellulose into glucose over solid acid catalysts. *Green Chem.* 10, 1033–1037. doi: 10.1039/b808471h

Oozeerally, R., Burnett, D. L., Chamberlain, T. W., Walton, R. I., and Degirmenci, V. (2018). Exceptionally efficient and recyclable heterogeneous metal-organic framework catalyst for glucose isomerization in water. *ChemCatChem* 10, 706–709. doi: 10.1002/cctc.201701825

Osaka, Y., Ikeda, Y., Hashizume, D., and Iwamoto, M. (2013). Direct hydrodeoxygenation of cellulose and xylan to lower alkanes on ruthenium catalysts in subcritical water. *Biomass Bioenergy* 56, 1–7. doi: 10.1016/j.biombioe.2013.04.012

Paine, J. B. III, Pithawalla, Y. B., Naworal, J. D., and Thomas, C. E. Jr. (2007). Carbohydrate pyrolysis mechanisms from isotopic labeling: part 1: the pyrolysis of glycerin: discovery of competing fragmentation mechanisms affording acetaldehyde and formaldehyde and the implications for carbohydrate pyrolysis. *J. Anal. Appl. Pyrolysis* 80, 297–311. doi: 10.1016/j.jaap.2007.03.007

Pang, J., Sun, J., Zheng, M., Li, H., Wang, Y., and Zhang, T. (2019). Transition metal carbide catalysts for biomass conversion: a review. *Appl. Catal. B Environ.* 254, 510–522. doi: 10.1016/j.apcatb.2019.05.034

Pang, J., Wang, A., Zheng, M., Zhang, Y., Huang, Y., Chen, X., et al. (2012). Catalytic conversion of cellulose to hexitols with mesoporous carbon supported Ni-based bimetallic catalysts. *Green Chem*. 14, 614–617. doi: 10.1039/C2GC16364K

Papageorgiou, G. Z., Papageorgiou, D. G., Terzopoulou, Z., and Bikiaris, D. N. (2016). Production of bio-based 2,5-furan dicarboxylate polyesters: recent progress and critical aspects in their synthesis and thermal properties. *Eur. Polym. J*. 83, 202–229. doi: 10.1016/j.eurpolymj.2016.08.004

Patwardhan, P. R., Satrio, J. A., Brown, R. C., and Shanks, B. H. (2009). Product distribution from fast pyrolysis of glucose-based carbohydrates. *J. Anal. Appl. Pyrol.* 86, 323–330. doi: 10.1016/j.jaap.2009.08.007

Pidko, E. A., Degirmenci, V., van Santen, R. A., and Hensen, E. J. (2010). Glucose activation by transient Cr^{2+} dimers. *Angew. Chem. Int. Ed*. 49, 2530–2534. doi: 10.1002/anie.201000250

Ribeiro, L. S., Delgado, J. J., Órfão, J. J., and Pereira, M. F. R. (2017). Carbon supported Ru-Ni bimetallic catalysts for the enhanced one-pot conversion of cellulose to sorbitol. *Appl. Catal. B Environ*. 217, 265–274. doi: 10.1016/j.apcatb.2017.04.078

Rinaldi, R., and Schüth, F. (2009). Design of solid catalysts for the conversion of biomass. *Energy Environ. Sci*. 2, 610–626. doi: 10.1039/b902668a

Romero, A., Cantero, D. A., Nieto-Márquez, A., Martínez, C., Alonso, E., and Cocero, M. J. (2016). Supercritical water hydrolysis of cellulosic biomass as effective pretreatment to catalytic production of hexitols and ethylene glycol over Ru/MCM-48. *Green Chem*. 18, 4051–4062. doi: 10.1039/C6GC00374E

Romero, A., Nieto-Márquez, A., and Alonso, E. (2017). Bimetallic Ru:Ni/MCM-48 catalysts for the effective hydrogenation of d-glucose into sorbitol. *Appl. Catal. A Gen*. 529, 49–59. doi: 10.1016/j.apcata.2016.10.018

Saha, B., Gupta, D., Abu-Omar, M. M., Modak, A., and Bhaumik, A. (2013). Porphyrin-based porous organic polymer-supported iron (III) catalyst for efficient aerobic oxidation of 5-hydroxymethyl-furfural into 2,5-furandicarboxylic acid. *J. Catal*. 299, 316–320. doi: 10.1016/j.jcat.2012.12.024

Salavagione, H. J., Sherwood, J., Budarin, V. L., Ellis, G. J., Clark, J. H., and Shuttleworth, P. S. (2017). Identification of high performance solvents for the sustainable processing of graphene. *Green Chem.* 19, 2550–2560. doi: 10.10391/C7GC00112F

Sankar, M., Dimitratos, N., Miedziak, P. J., Wells, P. P., Kiely, C. J., and Hutchings, G. J. (2012). Designing bimetallic catalysts for a green and sustainable future. *Chem. Soc. Rev*. 41, 8099–8139. doi: 10.1039/c2cs35296f

Seri, K. I., Inoue, Y., and Ishida, H. (2001). Catalytic activity of lanthanide (III) ions for the dehydration of hexose to 5-hydroxymethyl-2-furaldehyde in water. *Bull. Chem. Soc. Jpn*. 74, 1145–1150. doi: 10.1246/bcsj.74.1145

Shuai, L., and Luterbacher, J. (2016). Organic solvent effects in biomass conversion reactions. *ChemSusChem* 9, 133–155. doi: 10.1002/cssc.201501683

Singh, R., Krishna, B. B., Mishra, G., Kumar, J., and Bhaskar, T. (2016). Strategies for selection of thermo-chemical processes for the valorisation of biomass. *Renew. Energy* 98, 226–237. doi: 10.1016/j.renene.2016.03.023

Skiba, E. A., Budaeva, V. V., Baibakova, O. V., Udoratina, E. V., Shakhmatov, E. G., Shcherbakova, T. P., et al. (2016). Enzymatic hydrolysis of lignocellulosic materials in aqueous media and the subsequent microbiological synthesis of bioethanol. *Catal. Indus.* 8, 168–175. doi: 10.1134/S2070050416020100

Song, H., Wang, P., Li, S., Deng, W., Li, Y., Zhang, Q., et al. (2019). Direct conversion of cellulose into ethanol catalysed by a combination of tungstic acid and zirconia-supported Pt nanoparticles. *Chem. Commun*. 55, 4303–4306. doi: 10.1039/C9CC00619B

Subramani, V., and Gangwal, S. K. (2008). A review of recent literature to search for an efficient catalytic process for the conversion of syngas to ethanol. *Energy Fuels* 22, 814–839. doi: 10.1021/ef700411x

Tai, Z., Zhang, J., Wang, A., Pang, J., Zheng, M., and Zhang, T. (2013). Catalytic conversion of cellulose to ethylene glycol over a low-cost binary catalyst of Raney Ni and tungstic acid. *ChemSusChem* 6, 652–658. doi: 10.1002/cssc.201200842

Tanase, T., Takei, T., Hidai, M., and Yano, S. (2001). Substrate-dependent chemoselective aldose-aldose and aldose-ketose isomerizations of carbohydrates promoted by a combination of calcium ion and monoamines. *Carbohydr. Res*. 333, 303–312. doi: 10.1016/S0008-6215(01)00156-2

Tarabanko, V., Chernyak, M. Y., Nepomnyashchiy, I., and Smirnova, M. A. (2006). High temperature 5-hydroxymethylfurfural synthesis in a flow reactor. *Chem. Sustain. Dev*. 14, 49–53.

Van Putten, R. J., Van Der Waal, J. C., De Jong, E. D., Rasrendra, C. B., Heeres, H. J., and de Vries, J. G. (2013). Hydroxymethylfurfural, a versatile platform chemical made from renewable resources. *Chem. Rev*. 113, 1499–1597. doi: 10.1021/cr300182k

Venkatakrishnan, V. K., Delgass, W. N., Ribeiro, F. H., and Agrawal, R. (2015). Oxygen removal from intact biomass to produce liquid fuel range hydrocarbons via fast-hydropyrolysis and vapor-phase catalytic hydrodeoxygenation. *Green Chem*. 17, 178–183. doi: 10.1039/C4GC01746C

Wang, A., and Zhang, T. (2013). One-pot conversion of cellulose to ethylene glycol with multifunctional tungsten-based catalysts. *Acc. Chem. Res*. 46, 1377–1386. doi: 10.1021/ar3002156

Wang, H., Zhu, C., Liu, Q., Tan, J., Wang, C., Liang, Z., et al. (2019). Selective conversion of cellulose to hydroxyacetone and 1-hydroxy-2-butanone with Sn-Ni bimetallic catalysts. *ChemSusChem* 12, 2154–2160. doi: 10.1002/cssc.201900172

Wang, J., Ren, J., Liu, X., Xi, J., Xia, Q., Zu, Y., et al. (2012). Direct conversion of carbohydrates to 5-hydroxymethylfurfural using sn-mont catalyst. *Green Chem*. 14, 2506–2512. doi: 10.1039/C2GC35699F

Wang, J., Xi, J., and Wang, Y. (2015). Recent advances in the catalytic production of glucose from lignocellulosic biomass. *Green Chem*. 17, 737–751. doi: 10.1039/C4GC02034K

Wang, J., Zhao, X., Lei, N., Li, L., Zhang, L., Xu, S., et al. (2016). Hydrogenolysis of glycerol to 1,3-propanediol under low hydrogen pressure over WOx-Supported single/pseudo-single atom Pt catalyst. *ChemSusChem* 9, 784–790. doi: 10.1002/cssc.201501506

Watanabe, M., Aizawa, Y., Iida, T., Aida, T. M., Levy, C., Sue, K., et al. (2005a). Glucose reactions with acid and base catalysts in hot compressed water at 473 K. *Carbohydr. Res*. 340, 1925–1930. doi: 10.1016/j.carres.2005.06.017

Watanabe, M., Aizawa, Y., Iida, T., Nishimura, R., and Inomata, H. (2005b). Catalytic glucose and fructose conversions with TiO_2 and ZrO_2 in water at 473 K: relationship between reactivity and acid-base property determined by TPD measurement. *Appl. Catal. A Gen*. 295, 150–156. doi: 10.1016/j.apcata.2005.08.007

Xi, J., Xia, Q., Shao, Y., Ding, D., Yang, P., Liu, X., et al. (2016). Production of hexane from sorbitol in aqueous medium over $Pt/NbOPO_4$ catalyst. *Appl. Catal. B Environ*. 181, 699–706. doi: 10.1016/j.apcatb.2015.08.052

Xin, H., Zhang, T., Li, W., Su, M., Li, S., Shao, Q., et al. (2017). Dehydration of glucose to 5-hydroxymethylfurfural and 5-ethoxymethylfurfural by combining Lewis and Brønsted acid. *RSC Adv*. 7, 41546–41551. doi: 10.1039/C7RA07684C

Xin, S., Yang, H., Chen, Y., Yang, M., Chen, L., Wang, X., et al. (2015). Chemical structure evolution of char during the pyrolysis of cellulose. *J. Anal. Appl. Pyrol.* 116, 263–271. doi: 10.1016/j.jaap.2015.09.002

Xu, G., Wang, A., Pang, J., Zhao, X., Xu, J., Lei, N., et al. (2017). Chemocatalytic conversion of cellulosic biomass to methyl glycolate, ethylene glycol, and ethanol. *ChemSusChem* 10, 1390–1394. doi: 10.1002/cssc.201601714

Xu, Q., and Chen, L. F. (1999). Ultraviolet spectra and structure of zinc-cellulose complexes in zinc chloride solution. *J. Appl. Polym. Sci*. 71, 1441–1446. doi: 10.1002/(SICI)1097-4628(19990228)71:93.0.CO;2-G

Xu, S., Pan, D., Li, W., Shen, P., Wu, Y., Song, X., et al. (2018). Direct conversion of biomass-derived carbohydrates to 5-hydroxymethylfurfural using an efficient and inexpensive manganese phosphate catalyst. *Fuel Proc. Technol*. 181, 199–206. doi: 10.1016/j.fuproc.2018.09.027

Yabushita, M., Kobayashi, H., Hasegawa, J. Y., Hara, K., and Fukuoka, A. (2014). Entropically favored adsorption of cellulosic molecules onto carbon materials through hydrophobic functionalities. *ChemSusChem* 7, 1443–1450. doi: 10.1002/cssc.201301296

Yamaguchi, D., Kitano, M., Suganuma, S., Nakajima, K., Kato, H., and Hara, M. (2009). Hydrolysis of cellulose by a solid acid catalyst under optimal reaction conditions. *J. Physical Chem. C* 113, 3181–3188. doi: 10.1021/jp808676d

Yang, C., Miao, Z., Zhang, F., Li, L., Liu, Y., Wang, A., et al. (2018). Hydrogenolysis of methyl glycolate to ethanol over a $Pt\text{-}Cu/SiO_2$ single-atom alloy catalyst: a further step from cellulose to ethanol. *Green Chem*. 20, 2142–2150. doi: 10.1039/C8GC00309B

Yang, M., Qi, H., Liu, F., Ren, Y., Pan, X., Zhang, L., et al. (2019). One-pot production of cellulosic ethanol via Tandem catalysis over a multifunctional Mo/Pt/WOx catalyst. *Joule* 3. 1937–1948. doi: 10.1016/j.joule.2019.05.020

Yu, Y., Liu, D., and Wu, H. (2012). Characterization of water-soluble intermediates from slow pyrolysis of cellulose at low temperatures. *Energy Fuels* 26, 7331–7339. doi: 10.1021/ef3013097

Zabed, H., Sahu, J. N., Boyce, A. N., and Faruq, G. (2016). Fuel ethanol production from lignocellulosic biomass: an overview on feedstocks and technological approaches. *Renew. Sustain. Energy Rev.* 66, 751–774. doi: 10.1016/j.rser.2016.08.038

Zavrel, M., Bross, D., Funke, M., Büchs, J., and Spiess, A. C. (2009). High-throughput screening for ionic liquids dissolving (ligno-) cellulose. *Bioresour. Technol.* 100, 2580–2587. doi: 10.1016/j.biortech.2008.11.052

Zhang, H., Wu, J., Zhang, J., and He, J. (2005). 1-Allyl-3-methylimidazolium chloride room temperature ionic liquid: a new and powerful nonderivatizing solvent for cellulose. *Macromolecules* 38, 8272–8277. doi: 10.1021/ma0505676

Zhang, J., White, G. B., Ryan, M. D., Hunt, A. J., and Katz, M. J. (2016). Dihydrolevoglucosenone (Cyrene) as a green alternative to N, N-dimethylformamide (DMF) in MOF synthesis. *ACS Sustain. Chem. Eng.* 4, 7186–7192. doi: 10.1021/acssuschemeng.6b02115

Zhang, M., Geng, Z., and Yu, Y. (2015). Density functional theory (DFT) study on the pyrolysis of cellulose: the pyran ring breaking mechanism. *Comput. Theor. Chem*. 1067, 13–23. doi: 10.1016/j.comptc.2015.05.001

Zhang, Q., Wang, T., Li, B., Jiang, T., Ma, L., Zhang, X., et al. (2012). Aqueous phase reforming of sorbitol to bio-gasoline over Ni/HZSM-5 catalysts. *Appl. Energy* 97, 509–513. doi: 10.1016/j.apenergy.2011.12.044

Zhang, T., Fan, W., Li, W., Xu, Z., Xin, H., Su, M., et al. (2017). One-pot conversion of carbohydrates into 5-(Hydroxymethyl) furfural using heterogeneous Lewis-acid and Brønsted-acid catalysts. *Energy Technol*. 5, 747–755. doi: 10.1002/ente.201600492

Zhang, T., Li, W., Xin, H., Jin, L., and Liu, Q. (2019). Production of HMF from glucose using an Al^{3+}-promoted acidic phenol-formaldehyde resin catalyst. *Catal. Commun*. 124, 56–61. doi: 10.1016/j.catcom.2019.03.001

Zhang, Y., Liu, C., and Chen, X. (2015a). Unveiling the initial pyrolytic mechanisms of cellulose by DFT study. *J. Anal. Appl. Pyrolysis* 113, 621–629. doi: 10.1016/j.jaap.2015.04.010

Zhang, Y., Wang, J., Li, X., Liu, X., Xia, Y., Hu, B., et al. (2015b). Direct conversion of biomass-derived carbohydrates to 5-hydroxymethylfurural over water-tolerant niobium-based catalysts. *Fuel* 139, 301–307. doi: 10.1016/j.fuel.2014.08.047

Zhang, Z., Song, J., and Han, B. (2017). Catalytic transformation of lignocellulose into chemicals and fuel products in ionic liquids. *Chem. Rev*. 117, 6834–6880. doi: 10.1021/acs.chemrev.6b00457

Zhao, X., Wang, J., Chen, C., Huang, Y., Wang, A., and Zhang, T. (2014). Graphene oxide for cellulose hydrolysis: how it works as a highly active catalyst?. *Chem. Commun*. 50, 3439–3442. doi: 10.1039/C3CC49634A

Zhao, X., Wang, J., Yang, M., Lei, N., Li, L., Hou, B., et al. (2017). Selective hydrogenolysis of glycerol to 1,3-Propanediol: manipulating the frustrated Lewis pairs by introducing gold to Pt/WOx. *ChemSusChem* 10, 819–824. doi: 10.1002/cssc.201601503

Zhu, W., Yang, H., Chen, J., Chen, C., Guo, L., Gan, H., et al. (2014). Efficient hydrogenolysis of cellulose into sorbitol catalyzed by a bifunctional catalyst. *Green Chem*. 16, 1534–1542. doi: 10.1039/C3GC41917G

Conflict of Interest: The authors declare that the research was conducted in the absence of any commercial or financial relationships that could be construed as a potential conflict of interest.

frontiers in Chemistry

ORIGINAL RESEARCH
published: 31 July 2020
doi: 10.3389/fchem.2020.00587

Enzymatic Hydrolysis of Sugarcane Bagasse in Aqueous Two-Phase Systems (ATPS): Exploration and Conceptual Process Design

Bianca Consorti Bussamra[1,2], *Paulus Meerman*[1], *Vidhvath Viswanathan*[1], *Solange I. Mussatto*[3], *Aline Carvalho da Costa*[2], *Luuk van der Wielen*[1,4] *and Marcel Ottens*[1]*

[1] Department of Biotechnology, Delft University of Technology, Delft, Netherlands, [2] Development of Processes and Products (DDPP), University of Campinas, Campinas, Brazil, [3] Novo Nordisk Foundation Center for Biosustainability, Technical University of Denmark, Kongens Lyngby, Denmark, [4] Bernal Institute, University of Limerick, Limerick, Ireland

The enzymatic conversion of lignocellulosic material to sugars can provide a carbon source for the production of energy (fuels) and a wide range of renewable products. However, the efficiency of this conversion is impaired due to product (sugar) inhibition. Even though several studies investigate how to overcome this challenge, concepts on the process to conduct the hydrolysis are still scarce in literature. Aqueous two-phase systems (ATPS) can be applied to design an extractive reaction due to their capacity to partition solutes to different phases in such a system. This work presents strategies on how to conduct extractive enzymatic hydrolysis in ATPS and how to explore the experimental results in order to design a feasible process. While only a limited number of ATPS was explored, the methods and strategies described could easily be applied to any further ATPS to be explored. We studied two promising ATPS as a subset of a previously high throughput screened large set of ATPS, providing two configurations of processes having the reaction in either the top phase or in the bottom phase. Enzymatic hydrolysis in these ATPS was performed to evaluate the partitioning of the substrate and the influence of solute partitioning on conversion. Because ATPS are able to partition inhibitors (sugar) between the phases, the conversion rate can be maintained. However, phase forming components should be selected to preserve the enzymatic activity. The experimental results presented here contribute to a feasible ATPS-based conceptual process design for the enzymatic conversion of lignocellulosic material.

Keywords: sugarcane bagasse, product inhibition, enzymatic hydrolysis, extractive process, aqueous two-phase systems (ATPS)

OPEN ACCESS

Edited by:
Dmitry Yu. Murzin,
Åbo Akademi University, Finland

Reviewed by:
Alankar Vaidya,
Forest Research Institute of New Zealand (Trading as Scion), New Zealand
Pau Loke Show,
University of Nottingham, United Kingdom

***Correspondence:**
Marcel Ottens
m.ottens@tudelft.nl

Specialty section:
This article was submitted to Green and Sustainable Chemistry, a section of the journal Frontiers in Chemistry

Received: *20 December 2019*
Accepted: *08 June 2020*
Published: *31 July 2020*

Citation:
Bussamra BC, Meerman P, Viswanathan V, Mussatto SI, Carvalho da Costa A, van der Wielen L and Ottens M (2020) Enzymatic Hydrolysis of Sugarcane Bagasse in Aqueous Two-Phase Systems (ATPS): Exploration and Conceptual Process Design. Front. Chem. 8:587. doi: 10.3389/fchem.2020.00587

INTRODUCTION

The search for alternatives to replace fossil fuels by renewable energy has been seen as a major necessity in modern times (Passoth and Sandgren, 2019). In order to reach the requirements established by the Paris Agreement in 2017, net zero greenhouse gases emission must be achieved by 2050 (Pye et al., 2017). Sun, wind, and lignocellulosic residues can be sources of renewable energy (Goldemberg and Teixeira Coelho, 2004). However, unlike wind and solar energy, biomass (lignocellulosic residues) can provide a carbon source not only for energy

(fuel) production, but also for the production of a wide range of renewable products (Straathof, 2014). Sugarcane bagasse is the most abundant lignocellulosic residue in Brazilian agriculture. Among the 1.8 billion tons of sugarcane processed annually in the world, Brazil is the first producer, holding 41% of the world production. This amount yields ∼105 million tons of the residue (sugarcane bagasse) per year (UN Food and Agriculture Organization, 2017).

The enzymatic conversion of sugarcane bagasse to obtain monomers of glucose usually presents a limited efficiency as a consequence of several factors such as the cellulose crystallinity, product inhibition, and enzyme degradation (Gupta et al., 2016). There are several research lines cooperating to improve the utilization of lignocellulose as a raw material to the production of biofuel and chemicals. Pre-treatment of the biomass is necessary to expose the cellulose component to the cellulases. In order to establish a good balance between the decrease of the biomass recalcitrance to enzymatic hydrolysis and disadvantages of each pre-treatment, several types of processes have been investigated: physicochemical, chemical using acids and alkalis, and solvent extraction (Liu et al., 2019). Biological pre-treatments have been proposed as an alternative to chemical ones, mainly because of the reduction of toxic compounds and fermentation inhibitors generation (Sindhu et al., 2016), and improvement in the subsequent enzymatic hydrolysis (Vaidya and Singh, 2012; Singh et al., 2016). The inhibition on cell growth and metabolism, which leads to reduction of product of interest formation in fermentation, can be caused by substances present in the plant composition or released during pre-treatment and/or hydrolysis processes. Among many strategies to mitigate this product-induced inhibition of microbes, studies highlight the use of stabilizing substances and conditions, stream selection, and product removal (Cray et al., 2015). In the spectrum of the biocatalysis, the enzyme degradation can be related, for instance, to chemical reaction with lignin (Newman et al., 2013). The development of new biocatalysts, such as accessory enzymes, and use of additives (Donaldson et al., 2014; Vaidya et al., 2014; Fahmy et al., 2019) have been identified as potential fields to promote more efficient and tolerant enzymatic reactions. Moreover, the synergy of fungal enzymes and the design of rational cocktails have provided improved hydrolysis performance (Bussamra et al., 2015; Cameron et al., 2015; Gupta et al., 2016). However, few studies question the conventional process to conduct the enzymatic hydrolysis of cellulose to monomers, e.g., the optimization of reaction conditions, reactor design, enzyme recycling, and recovery strategies. The main drawback regarding the enzymatic hydrolysis is the product inhibition of the enzymes (Bezerra and Dias, 2005; Gupta et al., 2016). In other words, the higher the glucose concentration, the less efficient the process is. By addressing this need, a more efficient enzymatic hydrolysis could be performed, reducing the costs of the process, enhancing the yield, and contributing to establish biomass as feedstock for the production of renewables.

In order to overcome the challenge of product inhibition during enzymatic hydrolysis, some solutions have been suggested in literature, including: simultaneous saccharification and fermentation (SSF) (Mohagheghi et al., 1992), development of glucose tolerant enzymes (Cao et al., 2015), partial cellulose hydrolysis (direct use of lignocellulose-derived sugars by the microorganisms) (Chen, 2015), and *in situ* product removal (Hahn-Hägerdal et al., 1981; Yang et al., 2011). Extractive processes such as SSF indicates a positive effect on cellulose hydrolysis because the inhibition by ethanol is less harmful to enzymes than the one caused by cellobiose (Bezerra and Dias, 2005). However, ethanol inhibition still exposes a potential problem in the SSF (Wu and Lee, 1997). In order to remove the inhibitor, ATPS can be applied as a strategy to separate the product and the enzymes. ATPS are formed by two immiscible components dissolved in water (Benavides et al., 2011). These components, named as phase forming components (PFC), can be polymers, salts (Van Sonsbeek et al., 1993), or ionic liquids (Freire et al., 2012). Above a critical concentration of the PFC, the system presents two phases in which molecules (solutes) can be unevenly partitioned in accordance to the system composition (Baskir et al., 1989).

Even though extractive processes based on *in situ* product removal have been extensively applied to enzymatic reactions (Ferreira et al., 2018) and/or fermentation (Hahn-Hägerdal et al., 1981; Kulkarni et al., 1999), to the extent of our knowledge, enzymatic hydrolysis in biphasic systems composed by salt-polymer is still rarely reported. This work aims to unlock the potential of a novel and extractive process to conduct the enzymatic hydrolysis of lignocellulosic materials. In this study, we evaluated the efficiency of performing the extractive reaction by ATPS composed by polyethylene glycol and the salts potassium citrate and magnesium sulfate. In the referred systems, glucose and the reactive phase (bagasse and enzymes) can be separated to prevent product (glucose) inhibition. Moreover, we showed how experimental results at lab scale and parameters of the process are interconnected, providing information on technical conditions to further design a new industrial process for lignocellulosic conversion.

METHODS

Research Design

In this work, the enzymatic hydrolysis of sugarcane bagasse in ATPS was explored and two processes were designed. According to the partitioning of bagasse and solutes in the phases, the reaction and extractive phases can alter. Based on that, two approaches were discussed: hydrolysis occurring in the bottom phase (**Figure 1A**) and in the top phase (**Figure 1B**). The process design for each approach was developed according to experimental data and literature evidences. However, the quantitative evaluation of each unit of operation is out of the scope of this work.

Experimental data provided information for the design of ATPS reactor and ultrafiltration unit operations. The linkage between the experimental results and their usage into the process design is presented in **Table 1**. The strategy suggested for sugar recovery was based on literature evidence. The findings regarding the behavior of sugarcane bagasse hydrolysis in ATPS, connected to the potential of system components recycle, yielded insights on how feasible this extractive conversion could be.

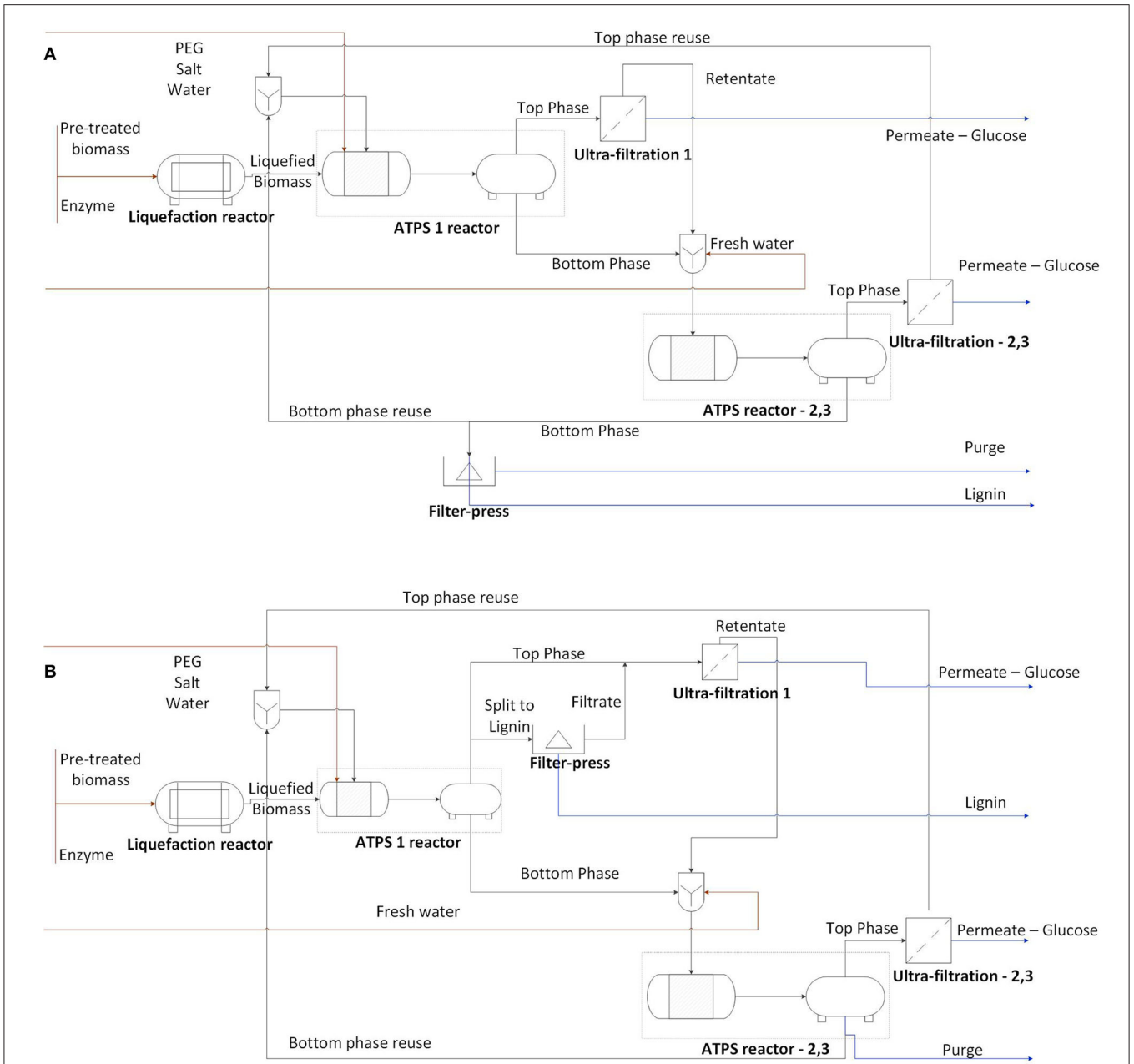

FIGURE 1 | Conceptual process design for **(A)** hydrolysis in bottom phase (schematic representation of an ATPS process for magnesium sulfate and PEG 6000) or **(B)** hydrolysis in top phase (schematic representation of an ATPS process for potassium citrate and PEG 6000). The numbers represent the how many cycles each unit of operation operates, which can vary for each ATPS and desired efficiency and recovery of the process. Considering an ATPS step with both mixing and separation compartments, two vessels are presented per ATPS unit operation.

The conversion of lignocellulosic biomass into sugars was catalyzed by the enzymes presented in the commercial cocktail Cellic CTec 2 (Novozymes, Bagsværd, Denmark). In order to create the extractive environment, ATPS formed by polymer and salts were applied to conduct the reaction. In the explorative investigation of ATPS applied to lignocellulosic conversion, topics such as the adsorption of phase forming components to the bagasse fibers and the influence of enzyme load on the hydrolysis were approached. Sequentially, the potential of recycling the enzymes in a continuous process was evaluated according to the distribution of specific enzymes among the phases and the adsorption of specific enzymatic activities to the bagasse. To complete the definition of parameters to further design the extractive process, the continuous recovery of sugar (glucose) from the system was theoretically analyzed.

Materials

The Brazilian Biorenewables National Laboratory (LNBR) provided the sugarcane bagasse: hydrothermally pre-treated (at 190°C, 10 min) followed by delignification (at 100°C, 1 h, and 1% NaOH). Although the presence of lignin does not influence the decrease in conversion with increasing solid loads (Modenbach and Nokes, 2013), this bagasse treatment was selected due to the fact that lignin could interfere in the enzyme performance and, consequently, in the product inhibition study. The bagasse, composed of 79.2% ± 0.9 cellulose, 2.6% ± 0.1 hemicellulose, 12.6% ± 0.3 lignin, and 6.2% ± 0.2 ash [composition determination as defined by Sluiter et al. (2016)], presented a wet basis humidity of 7.6% and was milled at 0.08 mm mesh. The milling process occurred at the speed of 104 rotations per minute (RPM) (Fritsch, Pulverisette 14).

Polyethylene glycol (PEG) with molar mass 2000 g/mol (PEG 2000) and 4000 g/mol (PEG 4000) were purchased from Merck (Darmstad, Germany). PEG 6000 (6000 g/mol) and magnesium sulfate heptahydrate ($MgSO_4 \cdot 7H_2O$) were acquired from J.T. Baker (Fisher, New Jersey, USA). Sodium carbonate (Na_2CO_3) and 3,5-Dinitrosalicylic acid (DNS), both used for enzymatic activities assays, anhydrous glucose, and potassium citrate tribasic monohydrate ($K_3C_6H_5O_7 \cdot H_2O$) were supplied by Sigma Aldrich (Taufkirchen, Germany). The pH was adjusted by adding sodium hydroxide (4 M) or hydrogen chloride, both purchased from Merck. Citrate buffer 50 mM was prepared according to Adney and Baker (2008).

Stock solutions were prepared by dissolving the respective PEG molecular weight or salt in double distilled deionized water (Milli-Q water), in order to obtain the following stock solutions: 38% w/w PEG 2000, 40% w/w PEG 4000, 39% w/w PEG 6000, and 40% w/w magnesium sulfate or potassium citrate solutions.

TABLE 1 | Experiments performed to enable a reasonable process design parameters definition.

Experiment	Type of parameter to be defined and the respective unit operation in the process design
Salt type and polymer molecular weight influence on bagasse partition	ATPS reactor: reaction phase (top or bottom)
Density of PFC before and after their adsorption to bagasse	ATPS reactor: addition mode of PFC to the bagasse
Enzymatic load influence on the concentration of free enzymes (not adsorbed) on conventional hydrolysis (kinetics) and specific enzymatic activities in the supernatant	Ultrafiltration: feasibility to recycle enzymes in terms of available amount of free proteins
TLL (tie line length), salt type and polymer molecular weight influence on the partitioning of proteins and sugars (K_s/K_p)	ATPS reactor: concentration of PFC in reaction
TLL and time of ATPS hydrolysis (kinetics) influence on sugar release	ATPS reactor: concentration of PFC and residence time of reaction
Rate of enzymatic hydrolysis (conventional and ATPS)	ATPS reactor: feed (flow) rate of substrate in order to maintain constant water-insoluble substrate (WIS) in a continuous operation mode and to achieve the desired yield
Binodal curves and tie lines data	ATPS reactor: estimation of outlet concentrations of top and bottom phases given an inlet composition of ATPS
Partitioning of specific enzymatic classes in ATPS (top and bottom)	Ultrafiltration: feasibility to recycle enzymes in terms of enrichment of one specific enzymatic class in continuous operation

ATPS Formation (Equilibrium and Separation)

The selection of ATPS composition (salt type and polymer molecular weight) and concentration (tie line length–TLL) were based on data previously published by Bussamra et al. (2019). The ATPS, respective TLL, and experiment to which they were applied and motivation are presented in **Table 2**.

The ATPS 1–5 were evaluated for the partitioning of glucose and proteins at a fixed concentration of each solute and without the presence of substrate. Because ATPS 6 was not favorable to conduct hydrolysis, the partitioning of solutes was not evaluated at this composition. Systems were formed by addition of the required amount of PEG and salt stock solutions to an aqueous solution of 5 mL total volume. Sugar stock solution (800 g/L, prepared in Milli-Q water) was added to a

TABLE 2 | Connection of the selected ATPS to respective application in experiments.

System	Phase forming components	TLL (%)	Experiment	Motivation
ATPS 1	Potassium citrate and PEG 2000	12.8	Glucose and protein partition	Low TLL, less inhibition of enzymes by PFC. Less viscous system compared to PEG 6000.
ATPS 2	Potassium citrate and PEG 6000	15.3	Glucose and protein partition; Hydrolysis kinetics	Lowest TLL reported by Bussamra et al. (2019) for this system composition. Enzymes could be more active compared to ATPS 3.
ATPS 3	Potassium citrate and PEG 6000	23.7	Glucose and protein partition	High precipitation of proteins.
ATPS 4	Magnesium sulfate and PEG 2000	20.5	Glucose and protein partition	High K_{sugar}. Enzymes could be more active compared to ATPS 5 (ATPS 4 is less concentrated and less viscous).
ATPS 5	Magnesium sulfate and PEG 6000	30.5	Glucose and protein partition; Hydrolysis kinetics	High sugar selectivity ($K_{sugar}/K_{protein}$).
ATPS 6	Potassium citrate and PEG 6000	34.2	Liquefaction following hydrolysis	Lowest TLL to provide high $K_{protein}$ (Bussamra et al., 2019).

final concentration of 90 g/L in the system. The volume of enzymes (29.5 μL) was calculated considering a hypothetical solid load of 10% WIS and an enzyme load of 10 FPU/g bagasse. This amount of enzymatic cocktail corresponded to a protein concentration of ∼0.92 mg/mL. The systems were incubated for 1 h at 50°C and 250 rpm in orbital shaker. Phase separation was promoted by centrifugation at 4,000 rpm, 40°C for 30 min (Eppendorf 5810R Multipurpose Centrifuge®). Top phase was withdrawn using an automatic pipet and bottom phase via 2 mL syringe coupled with appropriated needle. All systems were prepared in duplicates. The partition coefficient in a two-phase system was determined as the ratio of solute concentration in the top phase to that in the bottom phase (Li et al., 2002).

Adsorption of Phase-Forming Components to Sugarcane Bagasse

Predetermined amounts of bagasse (5% WIS) were emerged for 3 h at 250 rpm and 50°C in four different solutions of phase-forming components (final volume 15 mL): magnesium sulfate (40% w/w), potassium citrate (40% w/w), PEG4000 (40% w/w), and Milli-Q water. Subsequently, the samples were centrifuged at 1300 rpm, 40°C for 30 min (Eppendorf 5810R Multipurpose Centrifuge®). The bagasse was separated from the supernatant and the wet basis humidity was determined using a moisture balance (Sartorius Ma35). The density of both the stock solutions of phase forming components and the supernatant liquids, measured using a pycnometer, was 5.113 cm^3 (Blaubrand, Germany). The comparison in density of both solutions (stock and supernatant) indicates whether there is a preferential adsorption of phase forming components to sugarcane bagasse in relation to water (for instance, a less concentrated supernatant illustrates a preferential adsorption of the phase-forming component to the substrate).

Conventional and ATPS Enzymatic Hydrolysis

Conventional hydrolysis occurs in the presence of citrate buffer 50 mM, pH 4.8, with 0.02% sodium azide. The conventional hydrolysis kinetics at solid load 10% WIS were performed at enzyme loads 10, 20, and 40 FPU/g bagasse at a reaction volume of 30 mL. Samples from conventional hydrolysis were centrifuged at 4,000 rpm, 4°C, for 10 min (Eppendorf 5810R Multipurpose Centrifuge®). Supernatants were collected for both protein and glucose quantifications. Conversion of biomass (x) was calculated according to the following formula, taking into account the amount of soluble sugars in the liquid phase after hydrolysis (S_g, in glucose equivalent concentration; V_H, the volume of the solution where the hydrolysis was performed; and the correction factor for hydration 0.9, in order to correct for the water molecule added upon hydrolysis [Selig et al., 2008]), and the initial amount of glucose equivalent in the solid cellulose sample before hydrolysis (W, the weight of dry lignocellulosic sample, and F_g, the fraction of cellulose in the lignocellulosic sample):

$$x = \left(\frac{S_g \cdot V_H}{W_{dry\ bagasse} \cdot F_g} \right) \cdot 0.9 \cdot 100\% \quad (1)$$

ATPS hydrolysis was conducted at ATPS 2 and 5, as presented in **Table 2**. The phase-forming components (Milli-Q water and salt and PEG stock solutions) were mixed to achieve a volume ratio of 1:1, in a reaction volume of 15 mL according to the respective TLL. The bagasse was added to the system under agitation at a solid load of 10% WIS. Lastly, sodium azide and enzyme were added to a load 0.02% and 20 FPU/g bagasse, respectively. For each time evaluated, a unique system in duplicate was prepared once the withdrawal of top and bottom phases requires the discontinuation of the reaction and centrifugation of the system. The centrifugation occurred for 30 min, at 4,000 rpm and 40°C (Eppendorf 5810R Multipurpose Centrifuge®). All hydrolysis reactions were performed at 50°C and 250 rpm in orbital shaker.

Liquefaction Followed by Hydrolysis

For the hydrolysis following the liquefaction, the ATPS were formed by the addition of 9.9 mL of salt (potassium citrate 40% w/w) and 10.1 mL of polymer (PEG 6000 39% w/w) to 6 mL of liquefied bagasse (20% WIS and 10 FPU/g bagasse, for solid load and enzyme load, respectively, in citrate buffer 50 mM pH 4.8, hydrolyzed for 24 h). Considering the liquefied bagasse volume being the solvent of the ATPS, the hydrolysis was performed at the TLL 34.2% and volume ratio of 1. However, the ATPS was more concentrated because part of the liquefied volume was occupied by cellulose, lignin, ash, and already released sugars. For comparison with a conventional system, 20 mL of buffer (citrate 50 mM pH 4.8) was added to 6 mL of liquefied bagasse.

Enzymatic Activities

An international unit of enzymatic activity is defined as the amount of enzyme required to produce 1 μmol of product per minute. 1 mM p-nitrophenyl-β-D-glucopyranoside (p-NPG), 1 mM p-nitrophenyl-β-D-xylopyranoside, and 4 mM p-nitrophenyl-β-D-cellobioside (p-NPC) (Sigma–Aldrich, St. Louis, EUA) were the substrates for the activity determining reaction for β-glucosidase, β-xylosidase and cellobiohydrolase, respectively. After 10 min for β-glucosidase and β-xylosidase and 30 min for cellobiohydrolase activity measurement at 50°C, the reactions (comprised of 80 μL of the substrate and 20 μL of the enzyme) were stopped by addition of 1 mol/L sodium carbonate. Absorbance at 400 nm was used to estimate p-NP concentration release (Bussamra et al., 2015).

The total cellulose activity measured according to the filter paper units (FPU) was performed by reducing the NREL methods (Adney and Baker, 2008) 10 times. The sugar release was quantified following the methods suggested by Miller (1959).

Sugar and Protein Quantification

Sugar and protein present in top and bottom phases were measured according to methodology described by Bussamra

et al. (2019). Sugar quantification followed the Megazyme Glucose Reagent assay (Megazyme, Wicklow, Ireland), and no adaptation was needed to ATPS samples. Hydrolysis samples for glucose measurement were boiled for 5 min and 99°C after collected (Eppendorf Thermomixer® C.), in order to deactivate the enzymes. The protocol used for protein quantification, based on Bradford (1976) method and performed using the Coomassie Protein Assay Reagent (Thermo Scientific, USA), required adaptation for ATPS samples, explained in detail in the cited reference (Bussamra et al., 2019). The solute concentrations in g/L were defined per volume of the respective phase being measured.

The uncertainties of the all measurements calculated by calibration curves were estimated according to Barwick (2003), and the errors were propagated accordingly.

SDS-PAGE Electrophoresis

For the analysis of specific enzymes partition in ATPS, the bottom phase of ATPS 2 (**Table 2**) was evaluated in SDS-PAGE electrophoresis. To prevent interference of salt and PEG in the method, the bottom phase had the phase formation exchanged by Milli-Q water using a 10.000 MWCO Amicon® Ultra Centrifugal Filters as described by the supplier. Retentate of this operation (protein enriched) was dissolved in Milli-Q water. Top phase could not be evaluated through this method because the 10.000 MWCO membrane was clotted with the high concentration of PEG 6000 in that phase. The samples were diluted ¾ times in NuPAGE™ LDS Sample Buffer (4X) (ThermoFisher Scientific, USA), and this mixture was heated at 70°C for 10 min. 12% (w/v) Bis-Tris polyacrylamide gel (NuPAGE™, 1.0 mm, 12-well) (ThermoFisher Scientific, USA) was loaded with 10 μL prepared samples and stained by GelCode™ Blue Safe Protein Stain (ThermoFisher Scientific, USA). Mark12™ Unstained Standard (ThermoFisher Scientific, USA) was used as molecular weight ladder consisting on the following sizes: 200, 116.3, 97.4, 66.3, 55.4, 36.5, 31, 21.5, 14.4, 6, 3.5, and 2.5 kDa. The protein concentration of the bottom phase sample preparation was 0.39 ± 0.02 mg/mL. The maximum protein load in the band was 0.5 μg.

Theoretical Sequential Partitioning of Sugar and Recovery

The sequential partitioning of sugar in different stages (continuous process) was modeled based on the mass balance of the components in each stage and according to the equilibrium dictated by the partition coefficients for sugar and enzyme in the ATPS and the concentration factor for the ultra-filtration unit. An initial volume ratio of 1 was assumed for equal volume between the top and bottom phases. According to the partition coefficient and volume ratio, the top and bottom phase concentrations and volume ratio were estimated for each stage (cycle).

The concentration factor determined the permeate and retentate concentrations and flow rates. The permeate was assumed to leave the system as glucose, while the retentate was diluted to the original (top) phase volume and recycled back to the ATPS. Thus, in each stage, the concentration of sugar in the retentate was diluted. The calculation was repeated for each stage under the same assumptions. At the simulation presented here, the two different partition coefficients of sugar were assessed (1.5 and 0.71), considering the same concentration factors of 1.5. The result was assessed in terms of sugar recoveries after the ultrafiltration unit operation.

RESULTS

The evidence from experiments can guide the definition of parameters to design an extractive process to relieve product inhibition. **Table 1** contains the defined process design parameters and the correspondent type of experimental data to substantiate the decision-making. The partitioning of components in ATPS depends on the system composition (Benavides et al., 2011), and determines the strategy to recycle system components and recover products. Here, we presented pre-selected ATPS capable to provide different partition coefficients of sugar and enzymes, and how the phase forming components can influence the partitioning of lignocellulosic biomass. The influence of protein load, enzyme adsorption on bagasse, and partition of specific enzymatic activities in conventional hydrolysis brought insight on the design of the ultrafiltration unit operation regarding the recycle of enzymes.

Selection of ATPS Based on Partition Coefficients of Solutes

The pre-selected systems were previously indicated by Bussamra et al. (2019) as potential ATPS to separate sugar and enzymes. At this work, five systems, described in **Table 2**, were reproduced to have their partition coefficient measured at higher scale (5 mL). In the design of a process, more important than the partition coefficient itself is the relation between the partition coefficient of solutes aimed to be separated. The relative partitioning of these solutes represents how efficient their separation is among the phases. In all the systems, the partition coefficients of sugar were higher than for proteins.

The strategy designed to recover the product (sugar) in this process, regardless of which phase the bagasse partitions to, suggests the sequential partitioning of sugar to the top phase and the recovery occurring in that phase. Thus, ATPS 2 and ATPS 5 seemed to be the most efficient for that purpose due to the high selectivity for sugar $K_{sugar}/K_{protein}$ (**Table 3**).

TABLE 3 | Relative partitioning of sugar and protein in five different ATPS (systems defined in **Table 2**).

System	K_{sugar}	$K_{sugar}/K_{protein}$
ATPS 1	0.6	1.6
ATPS 2	0.6	2.4
ATPS 3	0.5	2.2
ATPS 4	0.7	1.7
ATPS 5	0.5	5.4

Exploratory Investigation of ATPS Applied to Lignocellulosic Hydrolysis

Preliminary investigation on influence of parameters inherent to ATPS (e.g., phase forming components adsorption on the bagasse fibers) is of paramount importance to set up coherent hydrolysis experiments.

The phase-forming components influence the bagasse partition in ATPS. After hydrolysis, the systems composed by potassium citrate favored the lignocellulose partition to the top phase, while systems containing magnesium sulfate triggered the partition to the bottom phase (visual inspection of the systems). **Figure 1** presents scenarios where the choice of phase forming components determines whether the reactive phase (phase containing the bagasse) is the top or the bottom phase. The PEG molecular weight was closely related to the partition of the bagasse, being a contributor to increasing the partition of bagasse to the top phase. Moreover, bagasse presented a non-selective adsorption of phase forming components. Consequently, the bagasse adsorption of phase forming components does not influence the system composition.

The cellulolytic enzymes adsorb to the substrate and consequently partition according to the substrate-enriched phase in the system (Tjerneld et al., 1985). Due to that, the partition of bagasse in ATPS determines in which phase the reaction occurs, and this is closely related to the selection of operation units in the process design to further recover the product and recycle the phase components. Beyond the fact that enzymes were in very diluted amount in the system, they were mostly adsorbed to the bagasse after 3 h reaction in conventional hydrolysis (**Figure 2**). For instance, 70% of the proteins adsorbed to the bagasse in the first 3 h for the enzyme load of 20 FPU/g bagasse. Interestingly, protein desorption did not follow the glucose release profile in conventional hydrolysis at 10% WIS, regardless the enzyme load (10, 20, or 40 FPU/ bagasse) (**Figure 2**).

The two specific activities tested in the commercial cocktail presented similar adsorption to sugarcane bagasse, and this non-selective adsorption did not change according to the enzyme load. Both β-glucosidase and cellobiohydrolase presented <5% of enzymatic activity in the supernatant (not adsorbed) after 3 h hydrolysis, except for cellobiohydrolase at enzyme load of 40 FPU/g bagasse, which presented ∼10% of that activity in the supernatant up to 6 h hydrolysis (**Figure 3**). We can assume that this reduction of measured enzymatic activity is not solely a consequence of protein deactivation because the non-adsorbed protein also reduced considerably after 3 h reaction (**Figure 2**).

Considering the protein adsorption and conversion profile of the three enzyme loads evaluated, the one at 20 FPU/g bagasse presented similar protein adsorption (in percentage to the total protein added) in comparison with the higher enzyme load for the same solid load (10% WIS). This fact indicates that the biomass could still adsorb proteins when the enzyme load increased from 20 to 40 FPU/g. However, the balance between adsorbed (∼70%) and free enzymes was achieved and maintained from 20 FPU/g bagasse enzyme load—higher enzyme loads stills presents ∼70% of adsorbed enzymes. On the other hand, the percentage of free cellobiohydrolases increased with the increase of enzyme load (20–40 FPU/g bagasse), indicating that there was an excess of this enzyme class in the reaction—celobiohydrolases are processive enzymes and should be adsorbed to the fibers to provide catalytic function once they slide along the cellulose chain to the next cleavage site as the product is released (Gupta et al., 2016). Moreover, considering the increase in conversion (∼12%) when comparing the enzyme load at 20–40 FPU/g and the cost of the enzymes, the gain in hydrolysis seems not

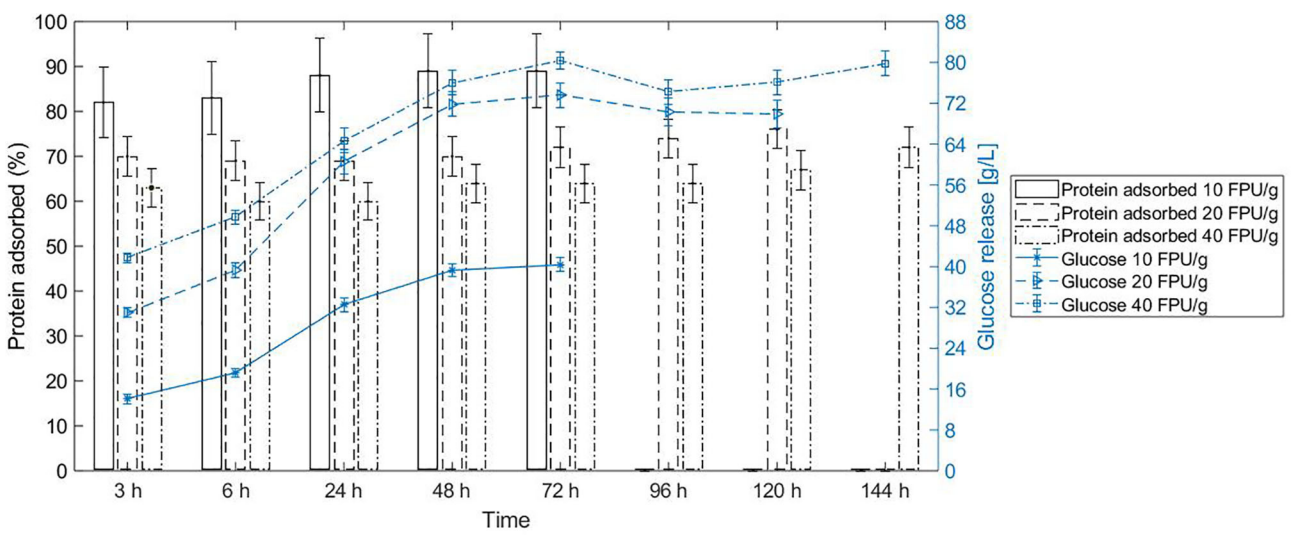

FIGURE 2 | Protein adsorption/desorption does not follow the glucose release in conventional hydrolysis at 10% WIS (solid load), at different enzyme loads of 10 FPU/g bagasse, 20 FPU/g bagasse, and 40 FPU/g bagasse. The bars represent the protein adsorbed (left y axis), and the curve shows the glucose release (right y axis). The conversion of reaction at each enzyme load achieved 47% ± 1.5, 79.4% ± 3.2, and 88.7% ± 2.7, respectively.

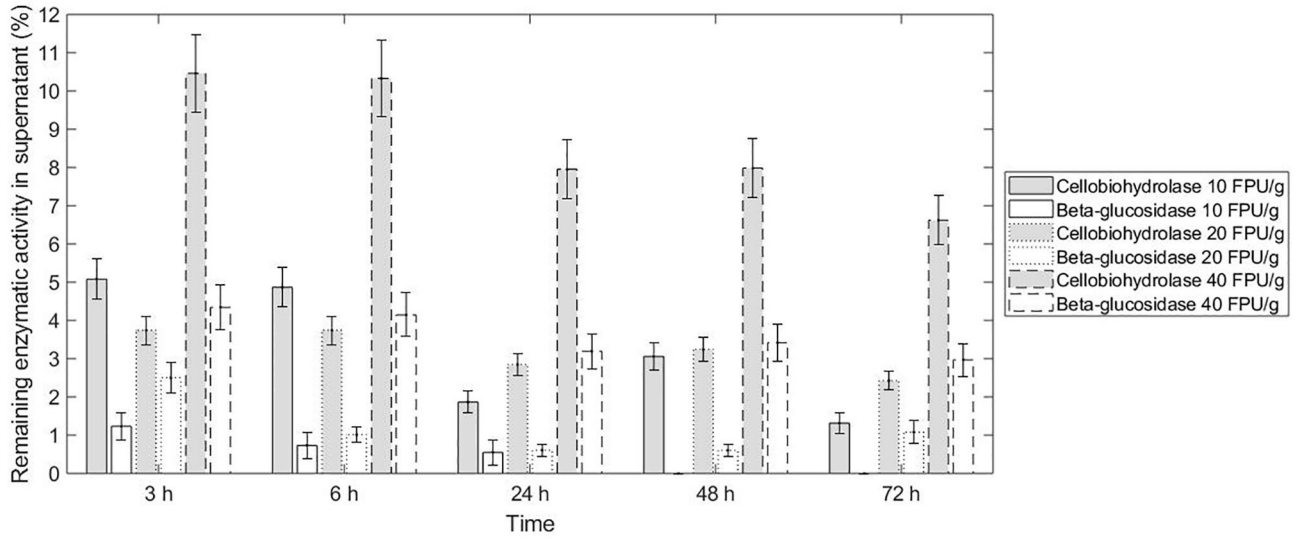

FIGURE 3 | Selective adsorption of enzymes to the sugarcane bagasse during the conventional hydrolysis reaction at 10% WIS (solid load), at different enzyme loads of 10 FPU/g bagasse, 20 FPU/g bagasse, and 40 FPU/g bagasse. The remaining enzymatic activity corresponds to the percentage of activity quantified in the supernatant in relation to the theoretical activity in case of no enzymatic adsorption. The total theoretical activities of cellobiohydrolase and β-glucosidase are, respectively, 1.7 ± 0.2 and 3.9 ± 0.5 (enzyme load 10 FPU/g bagasse), 4.1 ± 0.4 and 9.2 ± 1.2 (enzyme load 20 FPU/g bagasse), and 8.3 ± 0.8 and 18.4 ± 2.4 (enzyme load 40 FPU/g bagasse).

defensible. Then, the enzyme load of 20 FPU/g bagasse was chosen to conduct the ATPS hydrolysis.

Comparison Between Conventional and ATPS Hydrolysis of Lignocellulosic Material

The sugar released in bottom phase of ATPS composed by potassium citrate-PEG 6000 reached the same concentration as the conventional hydrolysis (**Figure 4**). Because of the uneven partition of sugars in the ATPSs composed by potassium citrate-PEG 6000 (TLL 15.3%) and magnesium sulfate-PEG 6000 (TLL 30.5%), the concentration of sugars during enzymatic hydrolysis contributed to different reaction rates in each phase of the system. For both ATPS studied, the partition coefficient of sugars was smaller than 1 (higher concentration of sugars in bottom phase). For the ATPS hydrolysis, the reaction did not discontinue after 48 h (**Figure 4**). In conventional hydrolysis, the sugar release ceased after 48 h reaction.

When the system reaction was composed of liquefied substrate (sugarcane bagasse hydrolyzed for 24 h at conventional hydrolysis), no extra glucose was released for both conventional and ATPS hydrolysis (**Figure 5A**).

Potential of Enzyme Recycling and Sugar Recovery in ATPS

Enzymes contribute in a great extent to the costs and to the conversion efficiency of a continuous process of hydrolysis (Torres, 2016). In the process configuration applied to the potassium citrate system (**Figure 1B**), in which top phase is the reactive phase, the free enzymes can be recovered in an ultrafiltration step. This operation unit also intends to recycle phase forming components (PEG) and recover the product (sugar). However, the partition of specific enzymes of the cocktail should be even among the phases or the entire cocktail should be one-sided partitioned to avoid the enrichment of the enzymatic cocktail with a specific activity (class of protein) in a continuous process with recycling. The ATPS 2 (potassium citrate and PEG 6000, TLL 15.3%) accomplished these requirements since all bands of proteins identified in the enzymatic cocktail (lane 2) were also present in the bottom phase (lane 3) (**Figure 6**).

For both process alternatives, the final product (glucose) is suggested to be recovered from the polymer enriched-phase. The recovery of sugar from salt enriched-phase is rarely reported in literature. On the other hand, the separation of glucose and polymer is widely acquired through ultrafiltration. Even though some systems separate glucose preferably to the bottom phase (salt enriched-phase), the recovery from the top phase is possible through the repartitioning of the sugar-enriched bottom phase to a new sugar-depleted top phase. Evidently, the higher the partition coefficient of glucose in the system, the lower the number of cycles to achieve the desirable concentration of sugar in the end stream of the process. The efficiency of this strategy was assessed theoretically. A recovery of 0.65 kg/kg glucose was achieved through a sequential partition of glucose to the top phase for an ATPS presenting K_{sugar} of 0.71 after six cycles. If the K_{sugar} increased to 1.5, 0.67 kg/kg recovery would be achieved after four cycles (**Figure 7**).

DISCUSSION

This section discusses how the experimental results assisted the definition of parameters to a future process design. Moreover, the

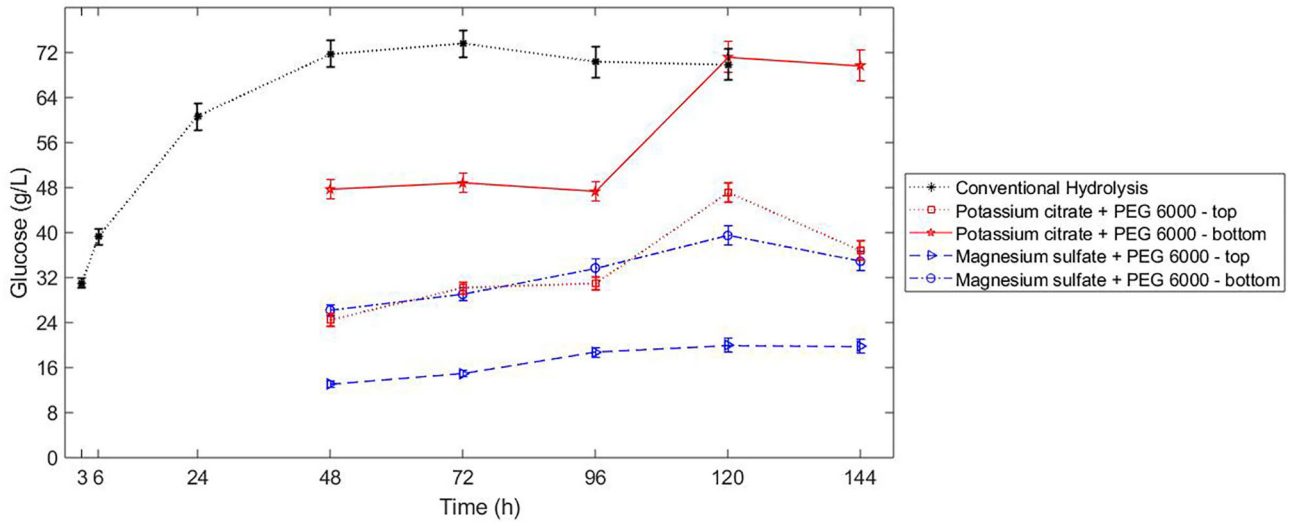

FIGURE 4 | Kinetics of conventional hydrolysis of hydrothermal sugarcane (10% WIS, 20 FPU/g bagasse) bagasse vs. ATPS hydrolysis (10% WIS, 20 FPU/g bagasse), without previous liquefaction of the sugarcane bagasse.

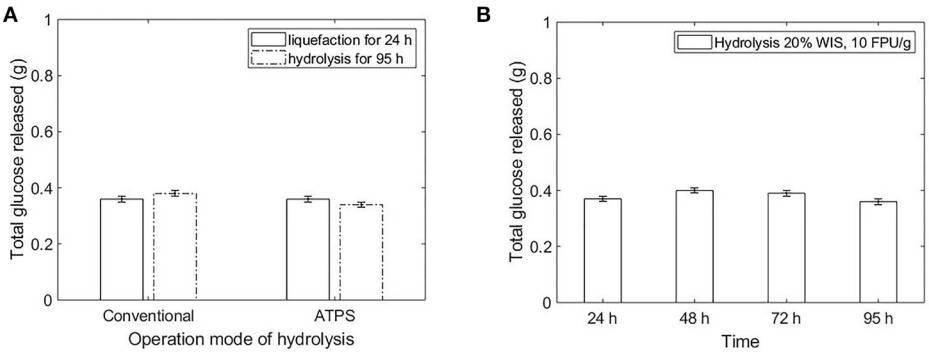

FIGURE 5 | (A) Comparison in sugar release after liquefaction for 24 h (20% WIS solid load and 10 FPU/g bagasse enzyme load) followed by hydrolysis (total reaction of 95 h), for conventional and ATPS operation modes. **(B)** Conventional hydrolysis of sugarcane bagasse (20% WIS solid load and 10 FPU/g bagasse enzyme load)—prolongation of the liquefaction up to 95 h (conversion of 34.5% ± 1). The glucose release was presented in total grams in the reaction, in order to compare systems with different volumes.

discussion also indicates the suitability of conducting enzymatic hydrolysis in ATPS.

ATPS and Enzymatic Hydrolysis of Sugarcane Bagasse

In order to operate lignocellulosic hydrolysis in ATPS, the system formation and equilibrium, influence of viscosity on mixing, and analytical techniques are of paramount importance to a proper reaction conduction and quantification. Even though we showed that the bagasse has non-selective adsorption toward the phase forming components in comparison to water, we suggest the addition of bagasse to the heterogeneous solution under mixing, providing contact to all components at the same time.

During the hydrolysis, the cleavage of specific sites of the polymer chain can affect its hydrophobicity, and consequently its partition in the system. This statement can be supported by the work of Fu et al. (2019), who suggested a method to quantify hydrophobicity based on the partition of natural organic matter on ATPS composed by PEG and potassium citrate. Additionally, the density of the substrate decreases during the hydrolysis, diminishing the gravity force in favor of setting down the substrate components, which might also explain the different bagasse partitioning before and after hydrolysis.

The increase of viscosity due to high solid load can impact the mixing and consequently the efficiency of the reaction (Rosgaard et al., 2007). When operating in ATPS, the concentration of phase-forming components, specially the polymer, becomes a great contributor to increase viscosity. Then, the solid load cannot be considered as a unique factor to the mass transfer limitation (set at a maximum of 20% WIS to ATPS hydrolysis by this work). Another limitation of ATPS application relies on the analytical techniques to quantify proteins (González-González

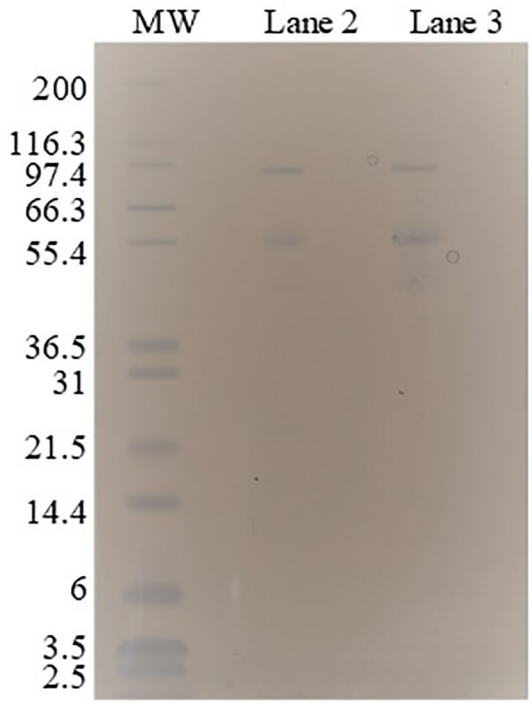

FIGURE 6 | SDS–PAGE electrophoresis of enzymatic cocktail (lane 2) and bottom phase (lane 3) after partition in the ATPS 2 (potassium citrate and PEG 6000, TLL 15.3%). Molecular weights (*MW*), in kDa, in decreasing order (lane 1): 200, 116.3, 97.4, 66.3, 55.4, 36.5, 31, 21.5, 14.4, 6, 3.5, and 2.5.

et al., 2011; Silvério et al., 2012; Glyk et al., 2015). Some strategies have already been suggested in literature using conventional methods of quantification (Bussamra et al., 2019).

Although ATPS seem to maintain the conversion rate due to the inhibitor partition in the system, the ATPS should provide a proper environment to preserve the enzymatic activity. The performance of the enzymes when incubated in the salts potassium citrate (10% w/w pH 5) and magnesium sulfate (10% w/w pH 5) was reduced ∼50% in relation to the enzymatic activity in optimum conditions (conventional hydrolysis—citrate buffer 50 mM) (Bussamra et al., 2019). Although temperature can be easily controlled to operate in the optimum for the enzymes, pH is an important factor when dealing with ATPS since the different salts present different properties under pH variation, which can also impact the enzymatic activity. Therefore, an ATPS composed by harmless phase forming components to the enzymes would provide the environment to both preserve the enzymatic activity and overcome product inhibition (through sugar extraction to the opposite phase of the reaction). Alternative phase-forming components can provide optimal environment to the catalytic activity, such as ionic liquids (Ferreira et al., 2018).

Conventional vs. ATPS Hydrolysis

Even though the product inhibition was not identified as a cause to decrease cellulose hydrolysis by Bommarius et al. (2008), other authors have refereed to product inhibition as the main factor to decrease the conversion rate at high conversions (Xiao et al., 2004; Bezerra and Dias, 2005). A previous study has identified the advantage to remove inhibitor (sugar) from the reaction in order to maintain the conversion rate (Yang et al., 2011). Here, the stagnation in sugar release after dilution of the 24 h liquefied bagasse indicates that sugar concentration is not the only factor contributing to the product inhibition in enzymatic hydrolysis (**Figure 5B**). Considering that 90% of the enzymes were already adsorbed to the fibers at 24 h of reaction at the enzyme load of 10 FPU/g bagasse, the reaction did not stop because of enzyme dilution and consequent inaccessibility to the fibers. Diluting the reaction system without the removal of products kept the inhibitor-to-enzyme ratio constant. Xiao et al. (2004) showed that the decrease of this ratio is crucial to overcome product inhibition. To a certain extent, the ATPS also decrease this ratio in one of the phase system, partitioning the sugar between the top and bottom. Moreover, the cellulose chain could be inaccessible after 24 h due to the increased proportion of highly-recalcitrant region of the fibers (crystalline cellulose), since amorphous regions are hydrolyzed first.

Although the mechanism of cellulase binding on lignocellulosic biomass (substrate-enzyme interaction) is not completely understood, some models can elucidate factors affecting the enzyme rates and activities (Bansal et al., 2009). Cellobiose, released during the cleavage of the bagasse chain during hydrolysis, is a non-competitive inhibitor to cellulases (Bezerra and Dias, 2005). However, some studies classify cellobiose as a secondary inhibitor once the high glucose concentration (mainly inhibitor) leads to the accumulation of cellobiose. The degree of inhibition caused by glucose is also more pronounced to cellulase mixture than to isolated β-glucosidase (Xiao et al., 2004). The reported nature and degree of glucose inhibition might be a likely cause associated with the decrease in conversion rate after 24 h conventional hydrolysis at solid load of 10% WIS and enzyme load of 10 FPU/g bagasse (**Figure 2**).

In the potassium citrate-PEG 6000 ATPS hydrolysis, the cellulose conversion increased in 51.5% from 96 to 120 h, whereas the conventional hydrolysis did not present any sugar release in the same period. However, similar conversion increase (54%) already happened from 6 to 24 h in conventional hydrolysis. A similar glucan conversion achieved at different times has been demonstrated when the substrate presents change in crystallinity (Gao et al., 2013). The phase forming components could influence the exposure of the amorphous part of the cellulose, as well as reducing the hydrophobicity of the cellulose surfaces, impairing the enzymes binding to the substrate. Moreover, decreasing rates of hydrolysis with high degrees of conversion have been associated to the jamming effect, which is the interference of adjacent enzymes adsorbed on cellulose surface at high protein concentration (Bommarius et al., 2008). Protein degradation could also trigger the discontinuation of the enzymatic conversion (Bansal et al., 2009).

Even though the sugar released in bottom phase during the hydrolysis conducted in ATPS composed by potassium citrate-PEG 6000 (TLL 15.3%) was similar to the sugar released

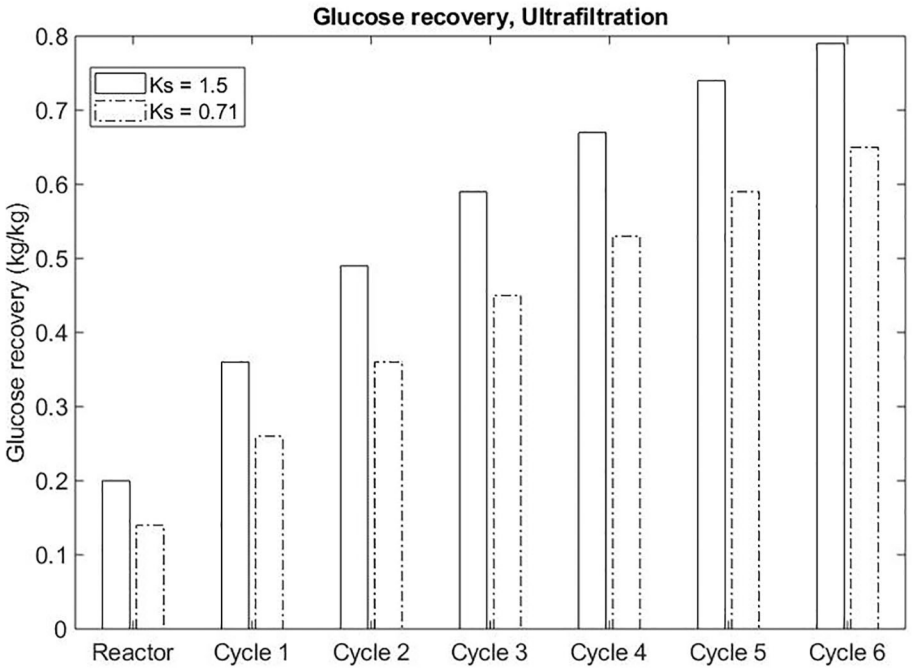

FIGURE 7 | Sequential ATPS formation to recover sugar in the ultrafiltration unit of operation.

in conventional hydrolysis, some peculiarities of the different approaches can benefit the implementation of the ATPS conversion. In ATPS, the inhibitor is partitioned in the system and the maintenance of the enzymatic activity after 48 h reaction for ATPS hydrolysis can be an indication that sugar in being removed from the reactive phase. However, the partitioning of sugar and consequent preservation of the reaction rate could also imply a delay in achieving the inhibitory concentration of products in the respective phase.

In both approaches (**Figure 1**), glucose and protein partition predominantly to the bottom phase. Even though the selectivity for sugars was higher in ATPS 5 (**Table 3**), the sugar release in that system was lower in comparison to ATPS 2 (**Figure 4**). This can be explained by the reactive phase (bottom phase, due to bagasse partition) presenting the higher concentration of inhibitor (glucose) among the phases. Moreover, ATPS 2, composed of potassium citrate, could better maintain the optimal catalytic pH than ATPS 5.

The TLL influences directly the hydrolysis performance once the high concentrated systems can decrease the enzymatic performance and limit the mass transfer of the system. On the other hand, low TLL does not present a satisfactory difference between the partition coefficients of sugar and proteins. To overcome this issue, a liquefaction of the bagasse in buffer (conventional hydrolysis) prior to ATPS formation would promote the adsorption of the enzymes to the bagasse and the conversion at high initial rates. After the ATPS formation, the sugar concentration would partition in the system and the reaction rate would be maintained until the achievement of the inhibitory concentration of products in one of the phases. The mass transfer limitation should be smaller in this mode of operation, once the substrate would be partially hydrolyzed when the ATPS are formed. Moreover, the conventional and mild environment used to liquefy the bagasse would prevent the enzymatic activity reduction due to salt contact (present in ATPS) in the beginning of the reaction. Surprisingly, the liquefaction for 24 h followed by hydrolysis did not contribute to the maintenance of the conversion rate (**Figure 5**). After 24 h liquefaction (conventional hydrolysis at 20% WIS solid load and 10 FPU/g bagasse enzyme load), the enzymes were already inhibited (**Figure 5B**). In order to take advantages of both conventional and ATPS hydrolysis, the liquefaction should provide conversion at high initial rates and the ATPS formation should enable a high total sugar release due to the partition of product to other phase. Then, a liquefaction of the bagasse for 6 h prior to hydrolysis in ATPS would provide both benefits. Moreover, a higher initial rate could be achieved by increasing the enzyme load to 20 FPU/g bagasse (**Figure 2**). The liquefaction before the ATPS formation also overcomes the challenge of fitting the volume of bagasse in the volume of the reactive phase, since the substrate will be partially converted and the solid load decreased when biphasic system is formed.

Recycle and Recovery of System Components

The strategy designed to recuperate the product (sugar) in this process suggests the sequential partition of sugar to the top phase and the recovery occurring in that phase (PEG-enriched phase) after ultrafiltration. Theoretically, the

permeate stream containing the product also presents soluble lignin and salt in the same concentration of the salt in top phase. The recovery of sugar could be improved by an ATPS presenting higher partition coefficient of glucose and by strategies to remove salts in accordance to the application of product stream.

In the system configuration of top phase as reactive phase, the ultrafiltration operation unit also grants the recycle of PEG and enzymes back to the process. However, enzymes do not desorb from bagasse after maximum conversion is achieved in conventional hydrolysis (**Figure 2**), impairing their recycle to the system reaction as free enzymes. A similar high binding capacity of around 85% of the cellulolytic enzymes has been reported by Gao et al. (2013). This irreversible cellulose binding was observed for hydrolysis involving lignocellulosic substrates, contrarily for amorphous cellulose hydrolysis, in which the substrate favors the desorption after depletion of substrate (Gao et al., 2013). However, due to the extensive solubilization of cellulose and hemicellulose, the irreversible binding of cellulose is mostly related to the presence of lignin. Moreover, the binding capacity of the enzymes does not indicate an improved cellulose conversion since the enzymes can be non-productively bound to the substrate (Gao et al., 2013). The recycle of enzymes from the supernatant has already been demonstrated to succeed at industrial conditions (high solid load and low enzyme dosage) for wheat straw substrate hydrolysis (Haven et al., 2015). This recycling strategy is restricted to the enzymatic stability of the recovered enzymes. Improved conditions for enzyme stability can enhance the potential of recycling free/desorbed enzymes (Haven et al., 2015). In a continuous system, the free enzymes are constantly removed from the reaction. The removal of desorbed/free enzymes does not impact significantly the rate and extent of the hydrolysis (Hu et al., 2018). However, it is important that the recycle occurs after the equilibrium in enzymatic adsorption is achieved.

Considering the reactive phase as the bottom phase, the enzymes are recycled back to the system adsorbed to the unconverted biomass. The recycle of enzymes associated with insoluble solids has already been proven as an effective method to decrease enzyme usage when operating hydrolysis in several rounds (Weiss et al., 2013). The bound enzymes are capable of hydrolyzing cellulose from fresh substrate. Moreover, the solid recycle method increases the contact time between catalyst and substrate, and enables unreacted substrate to return to the reaction. Increasing the amount of solid fraction recycled also increases the glucose release. However, the recycle of solids leads to increased lignin in the solid composition and increased total solid concentration, which requires higher tank size and a process able to deal with higher solids concentration and volumes. Thus, the process should be balanced between recycling enzyme activity and increased operating solids concentration. This method of recycling enzymes requires complementation of fresh enzymes at each recycle round once there are losses of enzymes in the liquid fraction and non-productive binding to lignin (Weiss et al., 2013).

TABLE 4 | Information to be retrieved from experiments to provide empirical basis to a reliable definition of parameters to the process design.

Information substantiated by experiments	Type of parameters to be defined in the process design
Partition of specific enzymatic classes after ultrafiltration (retentate and permeate)	Feasibility to recycle enzymes in terms of enrichment of one specific enzymatic class in continuous operation
Enzymatic activity in the ultrafiltration unit (feed and retentate). Model: potassium citrate-based ATPS	Feasibility to recycle enzymes in terms of recovery efficiency (retention coefficient for the process design)
PEG concentration in the ultrafiltration unit (feed and retentate). Model: potassium citrate-based ATPS	Feasibility to recycle PEG (concentration factor for the process design)
Partition of glucose in ATPS (top and bottom) after ultrafiltration, in which retentate composes the next top phase for the repartition of glucose in ATPS	Number of ATPS cycles to repartition glucose and achieve the desired sugar recovery
Thermodynamic model to predict phase separation and partition of solutes in ATPS	Contribution to a reliable calculation of phase composition and partition coefficient of solutes at different TLL (after recycle of PFCs)

Parameter Definition to a Process Design and Technical Challenges

Here, we bring an overview of parameter definition when designing the extractive process to relieve product inhibition based on ATPS. In addition to the process definition provided by the experimental data, we indicate other aspects of the process design that could be benefited by additional experiments (summarized in **Table 4**).

Because the phase-forming components can influence the partition of the bagasse in the system, polymer and salts can be chosen in order to promote the reactive phase (enriched in substrate and adsorbed enzymes) apart from the glucose-enriched phase. Moreover, the selection of phase forming components and concentration (TLL) should also be based on the capacity of maintaining the enzymatic activity of cellulases. The appropriate choice of components determines the efficiency of the ATPS-based hydrolysis. As presented in **Figure 1**, the ATPS reactor has a separate vessel for phase separation. At this stage, the bagasse is partially hydrolyzed and the process design is not affected by the different partitioning of bagasse observed before and after hydrolysis.

In a continuous process involving ATPS, the recycling of components requires more attention than monophasic systems (conventional hydrolysis) since the recycled stream might not contain the same composition of phase forming components as the initial one (the TLL can alter at each cycle) depending on the recycled, purged, and fresh streams of system components. In order to estimate the outlet concentrations of top and bottom phases, given the new inlet composition of the ATPS, phase diagrams previously reported by Bussamra et al. (2019) were used. To automatically predict the new phase compositions partition coefficients, a thermodynamic model should be

developed and implemented on the design calculation. Different compositions of top phase can affect the repartitioning of sugar. Giving the experimentally determined partition coefficient of this solute in the corresponding system composition, the authentic number of cycles to repartition glucose and achieve the desired sugar recovery can be empirically determined in order to model a reliable recovery operation.

Although the conventional hydrolysis does not indicate a desorption of enzymes after the reaction, PEG has been demonstrated to favor enzyme adsorption on the surface of the biomass, preventing the binding to the lignin (Malmsten and Van Alstine, 1996; Haven and Jørgensen, 2013). This feature of the ATPS could promote the recycle of enzymes and validate the hydrolysis model proposed by Stickel et al. (2018), in which the concentration of free enzymes increases with the decrease of substrate (glucan). Moreover, the non-selective partition and adsorption of the different enzymatic activities tested suggest a constant recycled cocktail composition. In the dextran-PEG 20000 system reported by Tjerneld et al. (1985), all the cellulolytic enzymes partitioned to the bottom phase, not affecting the continuous process of cellulose conversion in ATPS (Tjerneld et al., 1991). The paradigm that β-glucosidase (from Cellic CTec 2) would not adsorb to the substrate or only adsorb to a min or extent had already been broken by Haven and Jørgensen (2013). Some preferential adsorption of enzymatic classes has been observed for the cocktail Cellic CTec 3, in which cellobiohydrolase presented a higher binding affinity toward the substrate than endoglucanase (Hu et al., 2018). The preferential adsorption can be connected to the required enzymatic classes to hydrolyze a specific substrate composition. However, the recycled stream of the enzymes is an outcome not only from the ATPS separation reactor, but also from the ultrafiltration operation unit. Based on that, the evaluation of the partition of specific enzymatic classes on retentate and permeate from ultrafiltration should also be considered. Consequently, the recovery efficiency should be assessed in terms of maintenance of enzymatic activity after ultrafiltration (retentate stream), and considering the number of ultrafiltration cycles needed to repartition glucose and obtain the desirable recovery of this product. When assessing the enzymatic activity of the retentate to be recycled to the system, it is also important to regard the theoretical loss of enzymes in the permeate and purge streams (Stickel et al., 2018).

Combining the empirical information reported in this work (**Table 1**) with literature evidence, a qualitative process was designed to conduct enzymatic hydrolysis in ATPS. Moreover, the kinetic data on conventional and ATPS enzymatic hydrolysis generated here can improve the fundamental understanding of variables regarding the enzymes and substrate. A more detailed and phenomenological understanding of the hydrolysis process can give insights on kinetic models and/or validate existent ones (Bansal et al., 2009). In conclusion, the set of information acquired so far indicates that the ATPS hydrolysis could be reasonable modeled under such considerations.

CONCLUSION

This study demonstrated the suitability of conducting the enzymatic hydrolysis of lignocellulosic materials in aqueous two-phase systems (ATPS). This extractive technique, when applied to enzymatic conversions in the presence of solid substrate, presents peculiarities regarding the enzymatic activity performance and the partition of the substrate in dependence on the system composition. In the ATPS enzymatic hydrolysis, the reactive phase is determined by the substrate enriched-phase since the majority of the enzymes adsorbs to the fibers. The process design for such application involves a liquefaction of the bagasse prior to the ATPS hydrolysis. Because the proteins do not desorb from the fibers along the hydrolysis, the approach considering the recycle of enzymes when adsorbed to the substrate is more appropriate. Experimental studies on the ultrafiltration unit operation would substantiate the assumptions regarding the feasibility to recycle not adsorbed enzymes and phase forming components, and to recover the product. Based on the data acquired and literature evidence, this work provides valuable information (technical conditions) to a future quantitative evaluation of the processes.

DATA AVAILABILITY STATEMENT

All datasets generated for this study are included in the article.

AUTHOR CONTRIBUTIONS

BB wrote the manuscript, participated in the design of the experiments, experiments performance, data analysis, and data interpretation. PM performed some of the experiments reported at this work, participated on the design of the experiments and discussion about the experimental results. VV contributed to the conceptual process design, defining the theoretical bases for the process design, producing the modeling results, and writing of Topic 11 in Methods. SM supervised the work, provided close revision of the results along the data generation, and assisted on data discussion. AC and LW supervised the work, contributed to the scope of the work and to the revision of the manuscript. MO supervised the work, contributed to the scope of the work, to the close discussion on each experimental data obtained, and to the revision of the manuscript. All authors contributed to the article and approved the submitted version.

FUNDING

This work was financially supported by the Foundation for Research of State of Sao Paulo, Brazil [grant numbers 2015/20630-4, 2016/04749-4, 2016/06142-0, and BEPE 2016/21951-1] and the BE-Basic Foundation, The Netherlands. This research was carried out during a Dual Degree Ph.D. program under agreement between UNICAMP and TU Delft.

REFERENCES

Adney, B., and Baker, J. (2008). *Measurement of Cellulase Activities. Laboratory Analytical Procedure (LAP) Issue Date : 08/12/1996*. Technical Report. National Renewable Energy Laboratory.

Bansal, P., Hall, M., Realff, M. J., Lee, J. H., and Bommarius, A. S. (2009). Modeling cellulase kinetics on lignocellulosic substrates. *Biotechnol. Adv.* 27, 833–848. doi: 10.1016/j.biotechadv.2009.06.005

Barwick, V. (2003). *Preparation of Calibration Curves. A Guide to Best Practice*. Available online at: http://www.lgcgroup.com/our-science/national-measurement-laboratory/publications-and-resources/good-practice-guides/preparation-of-calibration-curves-a-guide-to-best/ (accessed November 16, 2017).

Baskir, J. N., Hatton, T. A., and Suter, U. W. (1989). Protein partitioning in two-phase aqueous polymer systems. *Biotechnol. Bioeng.* 34, 541–558. doi: 10.1002/bit.260340414

Benavides, J., Rito-Palomares, M., and Asenjo, J. A. (2011). *Aqueous Two-Phase Systems, 2nd Edn*. Amsterdam: Elsevier B.V. doi: 10.1016/B978-0-08-088504-9.00124-0

Bezerra, R. M. F., and Dias, A. A. (2005). Enzymatic kinetic of cellulose hydrolysis: inhibition by ethanol and cellobiose. *Appl. Biochem. Biotechnol.* 126, 49–59. doi: 10.1007/s12010-005-0005-5

Bommarius, A. S., Katona, A., Cheben, S. E., Patel, A. S., Ragauskas, A. J., Knudson, K., et al. (2008). Cellulase kinetics as a function of cellulose pretreatment. *Metab. Eng.* 10, 370–381. doi: 10.1016/j.ymben.2008.06.008

Bradford, M. M. (1976). A rapid and sensitive method for the quantitation of microgram quantities of protein utilizing the principle of protein-dye binding. *Anal. Biochem.* 72, 248–254. doi: 10.1016/0003-2697(76)90527-3

Bussamra, B. C., Castro Gomes, J., Freitas, S., Mussatto, S. I., Carvalho da Costa, A., van der Wielen, L., et al. (2019). A robotic platform to screen aqueous two-phase systems for overcoming inhibition in enzymatic reactions. *Bioresour. Technol.* 280, 37–50. doi: 10.1016/j.biortech.2019.01.136

Bussamra, B. C., Freitas, S., and da Costa, A. C. (2015). Improvement on sugar cane bagasse hydrolysis using enzymatic mixture designed cocktail. *Bioresour. Technol.* 187, 173–181. doi: 10.1016/j.biortech.2015.03.117

Cameron, H., Campion, S. H., Singh, T., and Vaidya, A. A. (2015). Improved saccharification of steam-exploded *Pinus radiata* on supplementing crude extract of *Penicillium* sp. *3 Biotech* 5, 221–225. doi: 10.1007/s13205-014-0212-2

Cao, L. C., Wang, Z. J., Ren, G. H., Kong, W., Li, L., Xie, W., et al. (2015). Engineering a novel glucose-tolerant β-glucosidase as supplementation to enhance the hydrolysis of sugarcane bagasse at high glucose concentration. *Biotechnol. Biofuels* 8:202. doi: 10.1186/s13068-015-0383-z

Chen, R. (2015). A paradigm shift in biomass technology from complete to partial cellulose hydrolysis: lessons learned from nature. *Bioengineered* 6, 69–72. doi: 10.1080/21655979.2014.1004019

Cray, J. A., Stevenson, A., Ball, P., Bankar, S. B., Eleutherio, E. C. A., Ezeji, T. C., et al. (2015). Chaotropicity: a key factor in product tolerance of biofuel-producing microorganisms. *Curr. Opin. Biotechnol.* 33, 228–259. doi: 10.1016/j.copbio.2015.02.010

Donaldson, L. A., Newman, R. H., and Vaidya, A. (2014). Nanoscale interactions of polyethylene glycol with thermo-mechanically pre-treated *Pinus radiata* biofuel substrate. *Biotechnol. Bioeng.* 111, 719–725. doi: 10.1002/bit.25138

Fahmy, M., Sohel, M. I., Vaidya, A. A., Jack, M. W., and Suckling, I. D. (2019). Does sugar yield drive lignocellulosic sugar cost? Case study for enzymatic hydrolysis of softwood with added polyethylene glycol. *Process Biochem.* 80, 103–111. doi: 10.1016/j.procbio.2019.02.004

Ferreira, A. M., Passos, H., Okafuji, A., Tavares, A. P. M., Ohno, H., Freire, M. G., et al. (2018). An integrated process for enzymatic catalysis allowing product recovery and enzyme reuse by applying thermoreversible aqueous biphasic systems. *Green Chem.* 20, 1218–1223. doi: 10.1039/C7GC03880A

Freire, M. G., Cláudio, A. F. M., Araújo, J. M. M., Coutinho, J., a,. P., Marrucho, I. M., et al. (2012). Aqueous biphasic systems: a boost brought about by using ionic liquids. *Chem. Soc. Rev.* 41:4966. doi: 10.1039/c2cs35151j

Fu, H., Liu, K., Alvarez, P. J. J., Yin, D., Qu, X., and Zhu, D. (2019). Chemosphere quantifying hydrophobicity of natural organic matter using partition coefficients in aqueous two-phase systems. *Chemosphere* 218, 922–929. doi: 10.1016/j.chemosphere.2018.11.183

Gao, D., Chundawat, S. P. S., Sethi, A., Balan, V., Gnanakaran, S., and Dale, B. E. (2013). Increased enzyme binding to substrate is not necessary for more efficient cellulose hydrolysis. *Proc. Natl. Acad. Sci. U.S.A.* 110, 10922–10927. doi: 10.1073/pnas.1213426110

Glyk, A., Heinisch, S. L., Scheper, T., and Beutel, S. (2015). Comparison of colorimetric methods for the quantification of model proteins in aqueous two-phase systems. *Anal. Biochem.* 477, 35–37. doi: 10.1016/j.ab.2015.02.007

Goldemberg, J., and Teixeira Coelho, S. (2004). Renewable energy - traditional biomass vs. modern biomass. *Energy Policy* 32, 711–714. doi: 10.1016/S0301-4215(02)00340-3

González-González, M., Mayolo-Deloisa, K., Rito-Palomares, M., and Winkler, R. (2011). Colorimetric protein quantification in aqueous two-phase systems. *Process Biochem.* 46, 413–417. doi: 10.1016/j.procbio.2010.08.026

Gupta, V. K., Kubicek, C. P., Berrin, J. G., Wilson, D. W., Couturier, M., Berlin, A., et al. (2016). Fungal enzymes for bio-products from sustainable and waste biomass. *Trends Biochem. Sci.* 41, 633–645. doi: 10.1016/j.tibs.2016.04.006

Hahn-Hägerdal, B., Mattiasson, B., and Albertsson, P. Å. (1981). Extractive bioconversion in aqueous two-phase systems. A model study on the conversion of cellulose to ethanol. *Biotechnol. Lett.* 3, 53–58. doi: 10.1007/BF00145110

Haven, M. Ø., and Jørgensen, H. (2013). Adsorption of β-glucosidases in two commercial preparations onto pretreated biomass and lignin. *Biotechnol. Biofuels* 6, 1–14. doi: 10.1186/1754-6834-6-165

Haven, M. Ø., Lindedam, J., Jeppesen, M. D., Elleskov, M., Rodrigues, A. C., Gama, M., et al. (2015). Continuous recycling of enzymes during production of lignocellulosic bioethanol in demonstration scale. *Appl. Energy* 159, 188–195. doi: 10.1016/j.apenergy.2015.08.062

Hu, J., Mok, Y. K., and Saddler, J. N. (2018). Can we reduce the cellulase enzyme loading required to achieve efficient lignocellulose deconstruction by only using the initially absorbed enzymes? *ACS Sustain. Chem. Eng.* 6, 6233–6239. doi: 10.1021/acssuschemeng.8b00004

Kulkarni, N., Vaidya, A., and Rao, M. (1999). Extractive cultivation of recombinant *Escherichia coli* using aqueous two phase systems for production and separation of extracellular xylanase. *Biochem. Biophys. Res. Commun.* 255, 274–278. doi: 10.1006/bbrc.1998.9912

Li, M., Kim, J. W., and Peeples, T. L. (2002). Amylase partitioning and extractive bioconversion of starch using thermoseparating aqueous two-phase systems. *J. Biotechnol.* 93, 15–26. doi: 10.1016/S0168-1656(01)00382-0

Liu, C. G., Xiao, Y., Xia, X. X., Zhao, X. Q., Peng, L., Srinophakun, P., et al. (2019). Cellulosic ethanol production: progress, challenges and strategies for solutions. *Biotechnol. Adv.* 37, 491–504. doi: 10.1016/j.biotechadv.2019.03.002

Malmsten, M., and Van Alstine, J. M. (1996). Adsorption of poly(ethylene glycol) amphiphiles to form coatings which inhibit protein adsorption. *J. Colloid Interface Sci.* 177, 502–512. doi: 10.1006/jcis.1996.0064

Miller, G. L. (1959). Use of dinitrosalicylic acid reagent for determination of reducing sugar. *Anal. Chem.* 31, 426–428. doi: 10.1021/ac60147a030

Modenbach, A. A., and Nokes, S. E. (2013). Enzymatic hydrolysis of biomass at high-solids loadings - a review. *Biomass Bioenergy* 56, 526–544. doi: 10.1016/j.biombioe.2013.05.031

Mohagheghi, A., Tucker, M., Grohmann, K., and Wyman, C. (1992). High solids simultaneous saccharification and fermentation of pretreated wheat straw to ethanol. *Appl. Biochem. Biotechnol. Part A Enzym. Eng. Biotechnol.* 33, 67–81. doi: 10.1007/BF02950778

Newman, R. H., Vaidya, A. A., and Campion, S. H. (2013). A mathematical model for the inhibitory effects of lignin in enzymatic hydrolysis of lignocellulosics. *Bioresour. Technol.* 130, 757–762. doi: 10.1016/j.biortech.2012.12.122

Passoth, V., and Sandgren, M. (2019). Biofuel production from straw hydrolysates: current achievements and perspectives. *Appl. Microbiol. Biotechnol.* 103, 5105–5116. doi: 10.1007/s00253-019-09863-3

Pye, S., Li, F. G. N., Price, J., and Fais, B. (2017). Achieving net-zero emissions through the reframing of UK national targets in the post-Paris agreement era. *Nat. Energy* 2, 1–8. doi: 10.1038/nenergy.2017.24

Rosgaard, L., Andric, P., Dam-Johansen, K., Pedersen, S., and Meyer, A. S. (2007). Effects of substrate loading on enzymatic hydrolysis and viscosity of pretreated barley straw. *Appl. Biochem. Biotechnol.* 143, 27–40. doi: 10.1007/s12010-007-0028-1

Selig, M., Weiss, N., and Ji, Y. (2008). Enzymatic saccharification of lignocellulosic biomass. *Natl. Renew. Energy Lab.* 1–5.

Silvério, S. C., Moreira, S., Milagres, A. M. F., Macedo, E. A., Teixeira, J. A., and Mussatto, S. I. (2012). Interference of some aqueous two-phase system phase-forming components in protein determination by the Bradford method. *Anal. Biochem.* 421, 719–724. doi: 10.1016/j.ab.2011.12.020

Sindhu, R., Binod, P., and Pandey, A. (2016). Biological pretreatment of lignocellulosic biomass - an overview. *Bioresour. Technol.* 199, 76–82. doi: 10.1016/j.biortech.2015.08.030

Singh, T., Vaidya, A. A., Donaldson, L. A., and Singh, A. P. (2016). Improvement in the enzymatic hydrolysis of biofuel substrate by a combined thermochemical and fungal pretreatment. *Wood Sci. Technol.* 50, 1003–1014. doi: 10.1007/s00226-016-0838-9

Sluiter, J. B., Chum, H., Gomes, A. C., Tavares, R. P. A., Azevedo, V., Pimenta, M. T. B., et al. (2016). Evaluation of Brazilian sugarcane bagasse characterization: an interlaboratory comparison study. *J. AOAC Int.* 99, 579–585. doi: 10.5740/jaoacint.15-0063

Stickel, J. J., Adhikari, B., Sievers, D. A., and Pellegrino, J. (2018). Continuous enzymatic hydrolysis of lignocellulosic biomass in a membrane-reactor system. *J. Chem. Technol. Biotechnol.* 93, 2181–2190. doi: 10.1002/jctb.5559

Straathof, A. J. J. (2014). Transformation of biomass into commodity chemicals using enzymes or cells. *Chem. Rev.* 114, 1871–1908. doi: 10.1021/cr400309c

Tjerneld, F., Persson, I., Albertsson, P.-Å., and Hahn-Hägerdal, B. (1985). Enzymatic hydrolysis of cellulose in aqueous two-phase systems. I. partition of cellulases from *Trichoderma reesei*. *Biotechnol. Bioeng.* 27, 1036–1043. doi: 10.1002/bit.260270715

Tjerneld, F., Persson, I., and Lee, J. M. (1991). Enzymatic cellulose hydrolysis in an attrition bioreactor combined with an aqueous two-phase system. *Biotechnol. Bioeng.* 37, 876–882. doi: 10.1002/bit.260370912

Torres, G. B. (2016). *Decision Making at Early Design Stages: Economic Risk Analysis of Add-On Processes to Existing Sugarcane Biorefineries*. Available online at: http://repositorio.unicamp.br/jspui/handle/REPOSIP/304789 (accessed July 16, 2020).

UN Food and Agriculture Organization, C. S. D. (FAOSTAT) (2017). *Sugarcane Production in 2017, Crops/Regions/World/ Production*. Available online at: http://www.fao.org/faostat/en/#data/QC (accessed December 2, 2019).

Vaidya, A., and Singh, T. (2012). Pre-treatment of *Pinus radiata* substrates by basidiomycetes fungi to enhance enzymatic hydrolysis. *Biotechnol. Lett.* 34, 1263–1267. doi: 10.1007/s10529-012-0894-7

Vaidya, A. A., Newman, R. H., Campion, S. H., and Suckling, I. D. (2014). Strength of adsorption of polyethylene glycol on pretreated *Pinus radiata* wood and consequences for enzymatic saccharification. *Biomass Bioenergy* 70, 339–346. doi: 10.1016/j.biombioe.2014.08.024

Van Sonsbeek, H. M., Beeftink, H. H., and Tramper, J. (1993). Two-liquid-phase bioreactors. *Enzyme Microb. Technol.* 15, 722–9. doi: 10.1016/0141-0229(93)90001-I

Weiss, N., Börjesson, J., Pedersen, L. S., and Meyer, A. S. (2013). Enzymatic lignocellulose hydrolysis: improved cellulase productivity by insoluble solids recycling. *Biotechnol. Biofuels* 6:5. doi: 10.1186/1754-6834-6-5

Wu, Z., and Lee, Y. Y. (1997). Inhibition of the enzymatic hydrolysis of cellulose by ethanol. *Biotechnol. Lett.* 19, 977–979. doi: 10.1023/A:1018487015129

Xiao, Z., Zhang, X., Gregg, D. J., and Saddler, J. N. (2004). Effects of sugar inhibition on cellulases and β-glucosidase during enzymatic hydrolysis of softwood substrates. *Appl. Biochem. Biotechnol.* 115, 1115–1126. doi: 10.1385/ABAB:115:1-3:1115

Yang, J., Zhang, X., Yong, Q., and Yu, S. (2011). Three-stage enzymatic hydrolysis of steam-exploded corn stover at high substrate concentration. *Bioresour. Technol.* 102, 4905–4908. doi: 10.1016/j.biortech.2010.12.047

Conflict of Interest: The authors declare that the research was conducted in the absence of any commercial or financial relationships that could be construed as a potential conflict of interest.

frontiers in Chemistry

ORIGINAL RESEARCH
published: 25 November 2020
doi: 10.3389/fchem.2020.525277

In situ Generated Ru(0)-HRO@Na-β From Hydrous Ruthenium Oxide (HRO)/Na-β: An Energy-Efficient Catalyst for Selective Hydrogenation of Sugars

Sreedhar Gundekari[1,2,3], *Heena Desai*[1], *Krishnan Ravi*[1,2], *Joyee Mitra*[1,2] *and Kannan Srinivasan*[1,2]*

[1] Inorganic Materials and Catalysis Division, CSIR-Central Salt and Marine Chemicals Research Institute, Council of Scientific and Industrial Research (CSIR), Bhavnagar, India, [2] Academy of Scientific and Innovative Research, Council of Scientific and Industrial Research (CSIR)-Central Salt and Marine Chemicals Research Institute, Bhavnagar, India, [3] Thermo-Chemical Conversion Division, Sardar Patel Renewable Energy Research Institute (SPRERI), Anand, India

OPEN ACCESS

Edited by:
Georgios Papadogianakis, National and Kapodistrian University of Athens, Greece

Reviewed by:
Qiying Liu, Guangzhou Institute of Energy Conversion (CAS), China
Venugopal Akula, Indian Institute of Chemical Technology (CSIR), India
Jyri-Pekka Tuomo Mikkola, Åbo Akademi University, Finland
Narendra Kumar, Åbo Akademi University, Finland

***Correspondence:**
Kannan Srinivasan
skannan@csmcri.res.in;
kanhem1@yahoo.com

Specialty section:
This article was submitted to Catalysis and Photocatalysis, a section of the journal Frontiers in Chemistry

Received: 10 January 2020
Accepted: 13 October 2020
Published: 25 November 2020

Citation:
Gundekari S, Desai H, Ravi K, Mitra J and Srinivasan K (2020) In situ Generated Ru(0)-HRO@Na-β From Hydrous Ruthenium Oxide (HRO)/Na-β: An Energy-Efficient Catalyst for Selective Hydrogenation of Sugars. Front. Chem. 8:525277. doi: 10.3389/fchem.2020.525277

A green process for the hydrogenation of sugars to sugar alcohols was designed in aqueous medium using hydrous ruthenium oxide (HRO) as a pre-catalyst supported on Na-β zeolite. Under optimized reaction conditions, sugars such as xylose, glucose, and mannose converted completely to the corresponding sugar alcohols xylitol, sorbitol, and mannitol with 100% selectivity. The pre-catalyst (HRO) is converted *in situ* to active Ru(0) species during the reaction under H_2, which is responsible for the hydrogenation. The catalyst was recyclable up to five cycles with no loss in activity. The reduction of HRO to the active Ru(0) species is dependent on the reaction temperature and H_2 pressure. Ru(0) formation increased and consequently an increased hydrogenation of sugars was observed with an increase in reaction temperature and hydrogen pressure. Further, *in situ* generation of Ru(0) from HRO was assessed in different solvents such as water, methanol, and tetrahydrofuran; aqueous medium was found to be the most efficient in reducing HRO. This work further demonstrates the use of supported HRO as an efficient pre-catalyst for biomass-based hydrogenation reactions.

Keywords: sugars, sugar alcohol, hydrogenation, hydrous ruthenium oxide, *in situ* reduction, recyclable catalyst

INTRODUCTION

Lignocellulosic biomass is an important raw material for the production of fuels, polymer, and chemical intermediates. Biomass is renewable, unlike fossil resources, and its conversion maintains the CO_2 level in the atmosphere. Their usage is also beneficial to the rural economy (Werpy et al., 2004; Climent et al., 2011b; Serrano-Ruiz et al., 2011; Vennestrøm et al., 2011; Melero et al., 2012). The Department of Energy (DOE) and universities of Europe listed important building blocks from such lignocellulosic biomass that includes polyols in addition to carboxylic acids, phenolic, and furan compounds (Lange et al., 2012; Kelkar et al., 2014; Sheldon, 2014; Teong et al., 2014). Sugars derived from cellulose and hemicellulose of lignocellulosic biomass are used for the preparation of sugar alcohols by selective hydrogenation, and several industries worldwide are interested in this conversion. The global consumption of sugar alcohols is estimated to be 1.6 million metric tons in

2017 and is projected to reach 1.9 million metric tons by 2022 at a CAGR of 3.4% (Climent et al., 2011a; Luterbacher et al., 2014).

Sugar alcohols such as sorbitol, xylitol, and mannitol are commonly available low-calorie sweeteners and are used in various industries like food, cosmetics, and pharmaceuticals. The sugar alcohols are non-toxic, non-carcinogenic, and non-hygroscopic. Thus, these could be safely consumed by diabetic patients (Grembecka, 2015). Moreover, sorbitol is the starting material for the production of ascorbic acid (vitamin C) and also is a precursor for hexane fuel (Corma et al., 2007; Alonso et al., 2012). Aside from their widespread use as sweeteners, the sorbitol-derived isosorbide and anhydro-sugars are industrially relevant as precursors for the preparation of PET like polymers such as polyethylene isosorbide terephthalates. The xylitol-derived xylaric, xylonic acid, and the mixture of hydroxyl furans can open up new opportunities in polymer preparation. The specific hydrogenolysis (C-C and C-O) of sorbitol and xylitol results in polyols like propylene glycol, ethylene glycol, and glycerol (**Supplementary Figure 1**). Controlled hydrogenolysis of sugar alcohols results in lactic acid, which is largely used in polylactate production (Bozell and Petersen, 2010; Gallezot, 2012; Kobayashi and Fukuoka, 2013; Isikgor and Becer, 2015; Zada et al., 2017).

The hydrogenation of sugars to sugar alcohols has been extensively studied with homogeneous and heterogeneous catalysts, among which heterogeneous Ni- and Ru-based catalysts are found to be more effective (Corma et al., 2007; Alonso et al., 2012; Chatterjee et al., 2015; Zhang et al., 2016; Zada et al., 2017). This hydrogenation is industrially practiced mainly with a Raney® Ni catalyst under aqueous basic medium and encounters a problem of Ni leaching. Many elements have been incorporated in Raney® Ni to improve the stability and enhance the catalytic activity (Wisniak et al., 1974; Chao and Huibers, 1982). Mo-, P-, Cr-, and Fe-promoted Raney® Ni catalyst showed lesser deactivation for the conversion of glucose to sorbitol and xylose to xylitol (Li et al., 2000; Mikkola et al., 2000; Kusserow et al., 2003). Ni–B/SiO_2 amorphous catalyst (prepared by chemical reduction with KBH_4) rendered a good conversion of glucose as compared to conventional Raney® Ni (Li et al., 2002). Morales et al. discussed a mixed metal oxide catalyst $La_{1-x}Ce_xAl_{0.18}Ni_{0.82}O_3$ ($x = 0.0, 0.1, 0.5, 0.7$) for xylose-to-xylitol conversion at 100°C, 25 bar H_2 for 5 h and achieved 100% conversion with moderate selectivity (Morales et al., 2016).

To counter the leaching issues with Ni catalysts, Ru-based catalysts have also been employed for this hydrogenation. The supported Ru catalysts show good catalytic activity, product selectivity, and stability as compared with Ni-based catalysts. Guo et al. reported an ultrafine Ru-B amorphous alloy catalyst for the conversion of glucose to sorbitol. This catalyst was shown to be more active than crystallized Ru-B and Ru powder catalysts (Guo et al., 2003). Ru catalysts employed mainly two supports [i.e., carbon (different forms: activated, foam, and nanotubes) and γ-Al_2O_3 under batch and continuous modes at 110–130°C and 20–40 bar H_2 to yield 95–98% of the desired sugar alcohols (Arena, 1992; Hoffer et al., 2003; Eisenbeis et al., 2009; Sifontes Herrera et al., 2011; Aho et al., 2015; Pham et al., 2016)].

A Ru/NiO-TiO_2 catalyst reported by Hwang's group resulted in 96% conversion of glucose with 98% selectivity of sorbitol at 120°C, 55 bar H_2 for 2 h. Complete conversion of mannose with >90% selectivity of mannitol in 4 h and >99% conversion of xylose with >99% selectivity for xylitol in 2 h was also reported (Mishra et al., 2012; Yadav et al., 2012; Mishra and Hwang, 2013). The same research group reported Ru/H-Y zeolite (prepared by $NaBH_4$ reduction in ethanol under N_2) catalyst for sugar hydrogenation showing 98% conversion of xylose and 98% selectivity for xylitol and >98% selectivity of sorbitol with the quantitative conversion of glucose under 55 bar of H_2 at 120°C for 2–3 h (Mishra et al., 2013, 2014). Ru supported on amine functionalized nanoporous polymer (AFPS) was effective in converting glucose to sorbitol with 98% selectivity at 100°C, 55 bar H_2 for 2 h (Dabbawala et al., 2016). However, in all these reports, a very high hydrogen pressure was required to enable such high yields.

The Mu group reported Ru/ZSM-5 (obtained from H_2 reduction) as catalyst for hydrogenation of glucose to sorbitol in 2 h with 99% conversion and selectivity at 120°C, under 40 bar H_2 (Guo et al., 2014). Zhang et al. screened several catalysts for glucose hydrogenation to sorbitol, including Ru/MCM-41, Pd/C, Ru/C, and Raney® Ni. Among these, the Ru/MCM-41 (obtained from formaldehyde reduction process) catalyst showed highest catalytic activity (complete conversion with >80% selectivity) at 120°C, 30 bar H_2 for 2 h. However, a decrease in the catalytic activity was observed in subsequent reaction cycles (Zhang et al., 2011). The Shiju group employed Ru on TiO_2 (calcined at 800–900°C) for the complete conversion of xylose to xylitol with 98% yield at 120°C and 20 bar H_2 (Hernandez-Mejia et al., 2016).

Generally, the catalysts used for this hydrogenation are reduced metals that require a pre-reduction step before reaction. The step involves additional energy (electricity, H_2, and manpower) and time, and is often more energy-intensive compared to the catalytic reaction. To minimize the energy requirements for the synthesis of active catalysts used in hydrogenation and hydrodeoxygenation reactions, our group has been working on the *in situ* generated catalysts. Hydrous ruthenium oxide (HRO) is one such efficient pre-catalyst wherein the catalytically active Ru(0) species is generated *in situ* under mild reaction conditions in an aqueous medium that drives the reaction (Gundekari and Srinivasan, 2019). In the present work, HRO is discussed as the pre-catalyst for the hydrogenation of sugar to sugar alcohols. A comparison of the performance of our *in situ* generated catalyst with the reported catalytic systems have been summarized in the **Supplementary Table 1**.

Abbreviations: HRO, Hydrous ruthenium oxide; Ru-HRO, *In situ* generated Ru along with HRO (general denotation); Ru-HRO-1, *In situ* generated Ru along with HRO (after 1st cycle using HRO catalyst precursor); Ru-HRO-2, *In situ* generated Ru along with HRO (after 2nd cycle using Ru-HRO-1); HRO/Na-β, HRO supported Na-β (catalyst precursor); Ru-HRO@Na-β, *In situ* generated Ru along with HRO on Na-β (general denotation); Ru-HRO@Na-β-1, *In situ* generated Ru along with HRO on Na-β (after 1st cycle using HRO/Na-β catalyst precursor); Ru-HRO@Na-β-2, *In situ* generated Ru along with HRO on Na-β (after 2nd cycle using Ru-HRO@Na-β-1); Ru-RuO_2-1, *In situ* generated Ru along with RuO_2 (after 1st cycle using RuO_2 catalyst precursor).

EXPERIMENTAL

Materials and Methods

Sorbitol (≥98%), xylitol (≥99%), mannose (99%), and $RuCl_3.xH_2O$ were purchased from Sigma-Aldrich. Xylose (98%), mannitol (99%), and RuO_2 were procured from Alfa Aesar. The Na-β zeolite was purchased from Zeochem, Switzerland. Glucose, metal salts, and hydrogen (>99.99% purity) were purchased from local vendors in India.

Catalyst Preparation

Hydrous Ruthenium Oxide (HRO)

HRO catalyst was prepared by a simple precipitation method: a solution 0.001 M of $RuCl_3$ was added to the appropriate amount of $CaCO_3$ aqueous solution and allowed to stand for 1 h without any stirring and heating. pH 7–8 was maintained during the reaction. The obtained precipitate was washed several times with water for the removal of chloride ions (confirmed with $AgNO_3$ solution) and dried for 3 h at 100°C.

HRO/Na-β

HRO supported on Na-β zeolite was prepared by simultaneous precipitation of HRO and its impregnation on Na-β zeolite. The 0.001 M of $RuCl_3$ solution is mixed with the appropriate amount of aqueous $CaCO_3$ solution and the desired amount of zeolite, with pH maintained at ∼7–8. The resulting mixture was stirred up to 12 h at room temperature; the obtained precipitate was washed with water and dried for 3 h at 100°C.

Procedure for Catalytic Hydrogenation of Sugars

The reactions were carried out in a stainless steel (SS-316) high-pressure 100-ml reactor (Amar Equipment PVT. LTD. India), equipped with an electrically heated jacket with a mechanical stirrer. The reactor was loaded with the catalyst and the substrate (sugars) dissolved in water, purged with N_2 three times before pressurizing with a fixed amount of H_2, and the reaction was carried out at desired temperatures and time duration. After completion of the reaction, the reactor was cooled to room temperature and the excess H_2 was released. The catalyst was separated by simple centrifugation and used for the next cycle without any pretreatment.

Product Analysis

The quantitative analysis of product mixture was done by using the Shimadzu Ultra-High Performance Liquid Chromatography (UHPLC) system equipped with low-temperature evaporative light scattering detector (ELSD-LTII) using a Supelcogel-610H column. The mobile phase was distilled H_2O with a flow rate of 0.5 ml min^{-1}, and the column oven was set at 40°C.

Catalyst Characterization

PXRD measurement was carried out in a Philips X'Pert MPD system using Cu Kα radiation (λ = 1.5406 Å). The operating voltage and current were 40 kV and 30 mA, respectively. A step size of 0.04° with a step time of 2 s was used for data collection. The data were processed using the Philips X'Pert (version 2.2e) software. Identification of the crystalline phases was made by comparison with the JCPDS files.

Thermogravimetric analysis (TGA) was carried out in Mettler-Toledo (TGA/SDTA 851^e) and the data were processed using Star^e software, in air at a flow rate of 60 ml/min and at a heating rate of 10°C/min in the temperature range 50–900°C.

Transmission electron microscope (TEM) images were obtained with a JEOL JEM-2100 microscope with an acceleration voltage of 200 kV using carbon-coated 200 mesh copper/gold grids. The samples were ultrasonically dispersed in ethanol for 5 min and deposited onto carbon film using capillary and dried in air for 30 min.

The surface morphology studies were done with a scanning electron microscope (JEOL series JSM-7100F) equipped with Oxford instruments energy-dispersive X-ray spectrometer (EDX) facility. The samples were coated with gold using sputter coating before analysis to avoid charging effects during recording. Analyses were carried out with an accelerating voltage of 15 kV and a working distance of 10 mm, with magnification values in-between 500× and 15,000×.

The acidity of HRO/Na-β was analyzed through pyridine adsorption and monitored using Fourier-transformed infrared (py-FTIR) spectroscopic technique. For py-FTIR analysis, the sample was initially oven-dried at 100°C for 3 h. To the oven-dried sample (50 mg), 0.1 ml of pyridine was admixed directly. The physisorbed pyridine present in the sample was dried in the oven at 120°C for 1 h to remove it. Further, the sample is cooled to room temperature, the spectra were recorded with a nominal resolution of 4 cm^{-1} in the spectral range of 400–4,000 cm^{-1} using a KBr background, and 15 scans were accumulated for spectrum.

Elemental chemical analyses of the samples were determined using inductively coupled plasma emission spectrometry (ICPOES; Perkin Elmer, OES, Optical 2000 DV). The samples were digested in a minimum amount of concentrated HNO_3 and H_2SO_4 further diluted using milli Q water <10 ppm and analyzed.

Specific surface area and pore size analysis of the samples were measured by nitrogen adsorption at −196°C using a sorptometer (ASAP-2020, Micromeritics). The samples were degassed under vacuum at 80°C for 90 min prior to measurements in order to expel the interlayer water molecules. The BET-specific surface area was calculated by using the standard Brunauer, Emmett, and Teller method on the basis of adsorption data.

RESULTS AND DISCUSSIONS

Studies of Catalyst Screening and Reaction Optimization Parameters for Hydrogenation of Xylose to Xylitol

HRO pre-catalyst was synthesized to demonstrate selective hydrogenation of sugars (xylose, glucose, and mannose) to sugar alcohols (xylitol, sorbitol, and mannitol) catalyzed by *in situ* generated Ru(0) active species. An initial blank experiment on xylose hydrogenation was conducted at 120°C, 30 bar H_2 for 1 h, in absence of catalyst; no reaction was noted (**Table 1**, entry 1).

TABLE 1 | Catalyst screening and optimization reaction condition for the hydrogenation of xylose to xylitol[a].

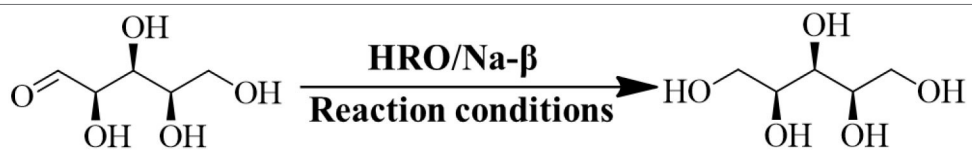

Entry	Catalyst/Pre-catalyst	Catalyst/Pre-catalyst (mg)	Temp (°C)	Pressure in bar (H_2)	Time (min)	Conv. (%)
1	Blank	-	120	30	60	n.o
2	5% Ru/C	50	120	30	60	99
3	HRO/Na-β	50	120	30	60	100
4	HRO/Na-β	50	100	30	60	100
5	HRO/Na-β	50	80	30	60	100
6	HRO/Na-β	50	60	30	60	80
7	HRO/Na-β	50	80	20	60	100
8	HRO/Na-β	50	80	10	60	60
9	HRO/Na-β	50	80	20	30	100
10	HRO	2.5	80	20	30	85
11	RuO_2	2.5	80	20	30	30
12[b]	HRO	2.5	80	20	30	8
13	Ru-HRO-1	2.5	80	20	30	84
14[c]	HRO/Na-β	250	80	50	100	>99
15[d]	HRO/Na-β	500	80	50	68	99
16[e]	HRO/Na-β	1000 (1 g)	80	50	47	99
17[e]	Ru-HRO@Na-β[f]	950	80	50	26	99

[a] *Reaction conditions: 1 g of xylose in 40 ml of H_2O, 50 mg of HRO/Na-β pre-catalyst (5 wt% of Ru), 60–120°C, 10–30 bar H_2, 30–60 min.*
[b] *1 g of xylose in 40 ml of methanol.*
[c] *5 g of xylose in 40 ml of H_2O.*
[d] *10 g of xylose in 40 ml of H_2O.*
[e] *15 g of xylose in 40 ml of H_2O.*
[f] *Recovered catalyst from entry 16; n.o, Not observed.*

During catalyst screening, 5% Ru/C showed 100% conversion of xylose with 99% yield of xylitol (**Table 1**, entry 2). Then, we checked the catalytic efficiency of our Na-β zeolite supported HRO material (HRO/Na-β) and it showed conversion and yield similar to 5% Ru/C catalyst (**Table 1**, entry 3). The energy-efficient preparation of *in situ* generated Ru-HRO@Na-β catalyst (explained in the catalyst characterization) from HRO/Na-β during reaction was interesting to us. Hence, we have explored this material for the hydrogenation of various sugars to sugar alcohols. In all the hydrogenation reactions, we have observed 100% selectivity of the desired sugar alcohols, and thus only the conversions (%) of reactants (sugars) are mentioned in the subsequent sections.

Reaction parameters such as temperature, hydrogen pressure, and reaction time were varied using HRO/Na-β as the catalyst precursor in order to identify a mild reaction condition for the hydrogenation of sugars. Xylose hydrogenation is studied for optimization of reaction conditions. The temperature was decreased from 120 to 60°C by steps of 20°C at 30 bar H_2 for 1 h using 5 wt% of HRO/Na-β (50 mg) (**Table 1**, entries 3–6). Complete conversion of xylose was observed at 120, 100, and 80°C, and a decreased conversion to 80% was observed on further reducing the temperature to 60°C. Thus, the temperature was fixed at 80°C for subsequent reactions. H_2 pressure was varied from 30 to 10 bar by a factor of 10 at 80°C for 1 h, and it was observed that 20 bar H_2 was sufficient for the complete conversion of xylose. Ten bar H_2 showed a decrease in conversion of xylose to 77%; thus, the H_2 pressure was fixed at 20 bar (**Table 1**, entries 5, 7, and 8). After having optimized the temperature (80°C) and pressure (20 bar H_2), the reaction time was decreased from 60 to 30 min. Complete conversion of xylose to xylitol was observed even after 30 min of reaction (**Table 1**, entry 7 and 9).

The xylose hydrogenation was also conducted with un-supported HRO at optimized reaction conditions. After the reaction, the obtained material, named Ru-HRO-1 [HRO is not completely converted to Ru(0)], showed 85% conversion of xylose (**Table 1**, entry 10). The supported HRO on Na-β-zeolite (HRO/Na-β) showed 100% conversion, implying that the support is playing a positive role to improve the catalytic activity of Ru-HRO-1. Ru(0) sites are well-dispersed in the support and hence easily accessible to the substrate molecules. This was confirmed

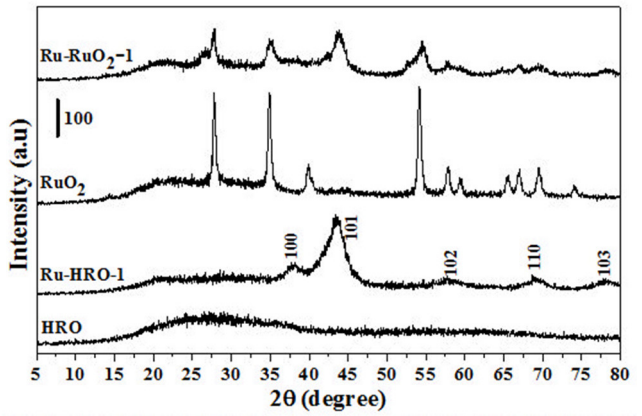

FIGURE 1 | PXRD of materials before (HRO and RuO_2) and after reaction (Ru-HRO-1: Recovered material from **Table 1**, entry 10 and Ru-RuO_2-1: Recovered material from **Table 1**, entry 11).

from TEM analysis (**Figure 8D**). In case of un-supported Ru-HRO, Ru particles are agglomerated (**Figure 8B**), effectively reducing the available active sites and hence conversion observed in this case was less when compared with supported Ru-HRO. In addition, the supported catalyst is easy to remove after the reaction as compared to Ru-HRO-1. Xylose hydrogenation was also conducted with RuO_2 and resulted in a decrease in conversion (30%) as compared with the HRO material (**Table 1**, entries 10 and 11). Under the reaction conditions, the RuO_2 generates a smaller number of Ru(0) active catalytic species compared to HRO, which is demonstrated by PXRD (**Figure 1**). The PXRD of Ru-HRO-1 (recovered material from **Table 1**, entry 10) showed a high-intensity peak of Ru(0) at 43°, which was less in Ru-RuO_2-1 (recovered material from **Table 1**, entry 11). TPR analysis revealed that HRO reduction started at a lower temperature (135°C) compared to RuO_2 (250°C) (Gundekari and Srinivasan, 2019). Using HRO, reaction conducted in the presence of methanol as solvent showed only 8% conversion of xylose with 100% selectivity for xylitol (**Table 1**, entry 12). Compared to aqueous medium, the organic solvents proved to be less effective for the conversion of HRO to active Ru(0). The detailed explanation of the effect of solvents in the conversion HRO to Ru (0) is mentioned in section Catalyst Characterization. The catalytic activity was successfully demonstrated at a 5-g scale of xylose, and >99% conversion of xylose was achieved without compromising the selectivity of xylitol under the optimized reaction conditions (**Table 1**, entry 14). The concentration of xylitol was further increased to 10 g (25 wt%) and 15 g (37.5 wt%) scale, and a decrease in the conversion [i.e., 68 and 47% (**Table 1**, entry 15 and 16), was observed]. The decrease in the catalytic activity is due to the decrease in the Ru wt% in the catalyst. The product mixture in the case of the 10- and 15-g scale turned light green in color from a colorless solution, which is presumably due to the leaching of Ru metal from zeolitic support.

TABLE 2 | Optimization of reaction condition for glucose and mannose hydrogenation to sorbitol and mannitol using HRO/Na-β pre-catalyst[a].

S. No	Temp. (°C)	H_2 pressure in bar	Time (min)	Conv. (%)
1[b]	80	20	30	85
2[b]	100	20	30	92
3[b]	100	20	45	100
4[c]	100	20	45	100

[a] *Reaction conditions: 1 g of carbohydrate in 40 ml of H_2O, 50 mg of HRO/Na-β pre-catalyst (5 wt%).*
[b] *Glucose.*
[c] *Mannose.*

Optimization of Reaction Conditions for Hydrogenation of C_6-Sugars (Glucose and Mannose) to Sugar Alcohols (Sorbitol and Mannitol) Using HRO/Na-β Pre-catalyst

The optimized reaction condition for the conversion of xylose to xylitol is 80°C, 20 bar H_2 for 30 min. Hydrogenation of glucose was attempted under this reaction condition; 85% conversion was observed for glucose (**Table 2**, entry 1). The decrease in conversion may be attributed to the difference in the size of the molecule from xylose to glucose. Actually, the Ru particles formed via *in situ* reduction of HRO are very small (average particle size ∼ 1–2 nm; **Figure 8**). Some of the finer Ru particles deposit on the pores (0.67 nm) of β-zeolite support (Hao et al., 2018). The Stokes diameter of xylose is 0.64 nm, which can easily enter β-zeolite pores and interact with the ultrafine Ru particles. Owing to the highly active nature of these Ru particles, the hydrogenation of xylose was accelerated (Sjoman et al., 2007; Roli et al., 2016). The Stokes diameter of glucose is 0.73 nm; it cannot go inside the pores of β-zeolite and does not interact with such ultrafine Ru particles, which may be the reason for the activity difference in xylose and glucose (Sjoman et al., 2007; Roli et al., 2016). To improve the conversion of glucose, the reaction parameters were modified (temperature increased from 80 to 100°C and reaction time enhanced from 30 min to 45 min). Under these reaction conditions (100°C, 20 bar H_2 for 45 min), glucose was completely converted to sorbitol (**Table 2**, entries 2 and 3). Similar conversion and selectivity were also observed for mannose hydrogenation to mannitol (**Table 2**, entry 4).

The catalytic activity is dependent on the reaction temperature and pressure (H_2). An increase in these parameters increases the reduction capacity of HRO due to an increased conversion to Ru(0), which is the active species for hydrogenation. Increasing reaction temperature from 100 to 200°C and pressure (H_2) from 20 to 40 bar completed the conversion of glucose to sorbitol within 10 min of time (**Supplementary Table 3**, entries 1–3). Increase in the reduction of HRO on changing the parameters was supported from various physicochemical techniques, and discussed in the catalyst characterization section.

Recyclability of Ru-HRO@Na-β Catalyst for Xylose Conversion to Xylitol

The recyclability of a catalyst is attractive for bulk chemical synthetic industrial applications. After the xylose-to-xylitol

conversion (**Supplementary Table 2**, entry 1), the catalyst was removed from the product mixture by simple centrifugation, washed with deionized water, and further used for the next cycle under our optimized reaction conditions. The observed catalytic activity was comparable to the fresh catalyst (**Supplementary Table 2**, entry 2). The same procedure was followed for four more reaction cycles, and similar catalytic activity [i.e., 98–99% conversion of xylose with 100% selectivity (**Supplementary Table 2**, entries 3–6), was observed]. The ICP analysis showed the leaching of a negligible amount of Ru metal into the aqueous product mixture after these reaction cycles. At a higher concentration of the sugar solution, the recyclability of the catalyst is poor because of significant amount of Ru metal leaching from the support. We observed only 26% of conversion in the second cycle of the 15-g scale where the conversion was 47% in the fresh cycle (**Table 1**, entries 16 and 17).

Catalyst Characterization

HRO consists of Ru in multiple oxidation states, and the material acts as a pre-catalyst (catalyst precursor). Under hydrogen environment at elevated temperatures, HRO *in situ* generates Ru(0) nanoparticles, which is the active catalytic species. *In situ* formation of Ru(0) from HRO is studied by various analytical tools. The PXRD of HRO did not show any diffraction peaks attesting to its amorphous nature. After the reaction (**Table 1**, entry 10), the obtained material (Ru-HRO-1) showed diffraction peaks at 2θ of 38.3, 41.9, 43.7, 58.3, 69.4, and 78.4, corresponding to (100), (002), (101), (102), (110), and (103) planes of the hexagonal close-packed (hcp) Ru metal, respectively (ICDD-JCPDS card No. 06-0663) (**Figure 1**). The Na-β support shows diffraction peaks at 7.2, 21.4, 22.4, 25.2, 27.0, 28.7, and 29.5, which were characteristic peaks of this zeolite. Similar peaks were observed after impregnation of HRO, which indicate that the HRO impregnation did not affect the crystallinity of the zeolite. Na-β zeolite support retained its crystallinity even after the reaction. HRO was converted to Ru(0), as was depicted from the new peak at 43°, corresponding to Ru(0) (**Figure 2**).

A set of reactions were conducted for 10 min in aqueous medium at different temperatures to understand the reduction of HRO (**Figures 3**, **4**). The reduction of HRO to Ru(0) critically depends on the temperature and H_2 pressure. The reduction is dependent on the temperature and H_2 pressure; increasing these parameters increased the reduction efficiency. The PXRD profile of the obtained Ru-HRO-1 material from HRO at different temperatures (50, 100, 150, and 200°C) was monitored in **Figure 3** (the materials denoted as Ru-HRO-1-T50, Ru-HRO-1-T100, Ru-HRO-1-T150, and Ru-HRO-1-T200) which reveals an increase in the intensity of Ru(0) peak with the increase in reaction temperature. When the H_2 pressure was increased from 20 to 40 bar, we observed a similar increase in the intensity of Ru(0) peak (**Figure 4**) and materials are denoted as Ru-HRO-1-P20 and Ru-HRO-1-P40.

TGA of materials are shown in **Figure 5**. The weight loss of HRO (22%) was observed in the temperature range of 50 to

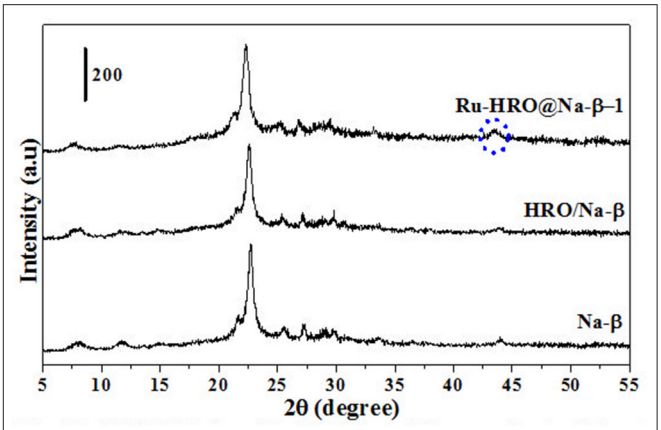

FIGURE 2 | PXRD of Na-β, HRO/Na-β, and Ru-HRO/Na-β-1 (Recovered material from **Supplementary Table 2**, entry 1).

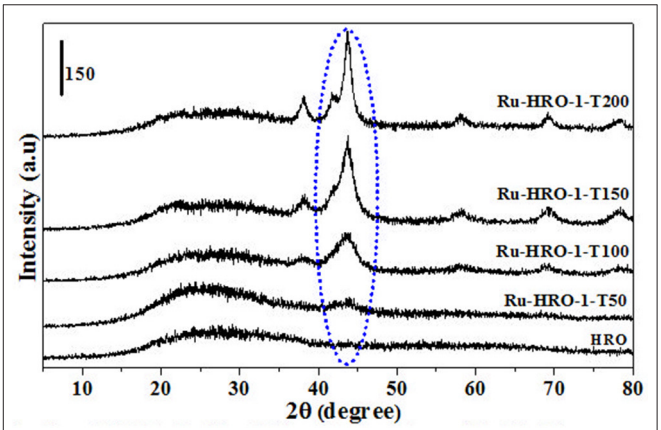

FIGURE 3 | Reduction of HRO to Ru(0) at different temparatures (50–200°C). Reaction conditions: 25 mg of HRO in 40 mL of H_2O, 20 bar H_2, 10 min.

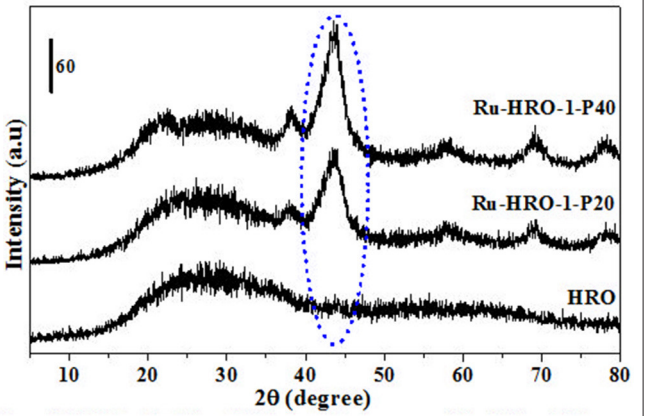

FIGURE 4 | Reduction of HRO to Ru(0) at different H_2 pressure (20–40 bar H_2). Reaction conditions: 25 mg of HRO in 40 mL of H_2O, 100°C, 10 min.

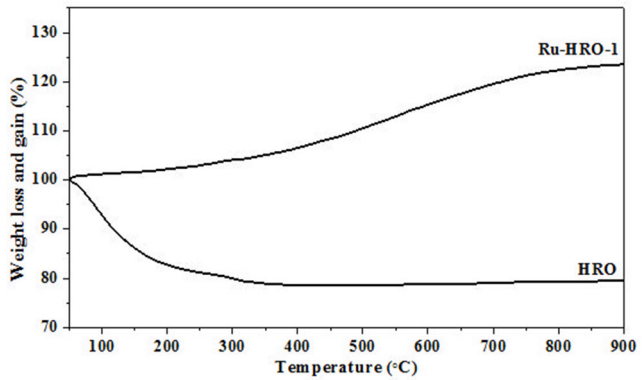

FIGURE 5 | TGA of HRO and Ru-HRO-1 (Recovered material from **Supplementary Table 3**, entry 2).

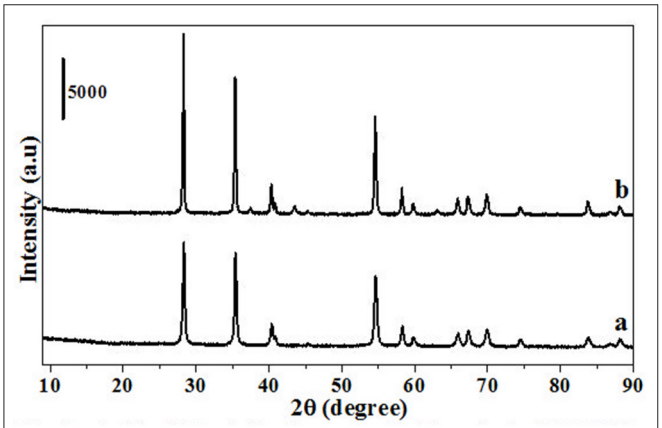

FIGURE 6 | PXRD of materials obtained after thermogravimetric analysis. **(a)** HRO **(b)** Ru-HRO-1.

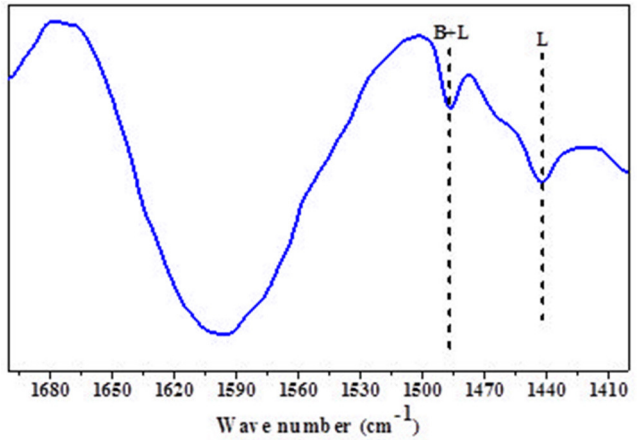

FIGURE 7 | py-FTIR of the catalyst precursor HRO/Na-β.

350°C. The weight loss at the temperature range 50 to <200°C is consistent with the loss of physisorbed H_2O molecules on the HRO and >200 to 350°C temperature range is attributed to strongly held H_2O molecules in HRO. After TGA, the obtained material is crystalline RuO_2, which is confirmed by PXRD, due to the presence of intense peaks corresponding to 110, 101, 200, 211, 220, 002, 310, 112, 301, and 201 planes of tetragonal RuO_2 (JCPDS card no. 21-1172). This implies that the presence of strongly held H_2O molecules results in the amorphous nature of HRO (**Figure 6a**). On the other hand, at 200°C (**Figure 3**), Ru(0) was generated from HRO during the reaction. The material obtained after the reaction showed a weight gain (23%) in TGA gradually from 50 to 900°C. In the presence of air atmosphere, the Ru(0) particles generated in the course of the reaction forms the RuO_2 under TGA conditions, and it was the reason for the observed weight gain (**Figure 6b**). The experiment also supported the *in situ* formation of Ru(0) from HRO during the reaction.

Mishra et al. disclosed that mild acidity of support (zeolites) increases the selectivity of sugar hydrogenated product (Mishra et al., 2014). The py-FTIR of the catalyst precursor (HRO/Na-β) shows a peak between 1,490 and 1,480 cm^{-1}, corresponding to a mixture of Brönsted and Lewis acidic sites. Another peak observed at 1,450–1,435 cm^{-1} identifies the Lewis acidic sites (**Figure 7**).

The TEM images of Ru in HRO particles showed agglomeration. After the reaction, the obtained material (here, Ru-HRO-2; recovered material from **Table 1**, entry 13) showed a decrease in agglomeration, which might be due to a cleavage of Ru-O-Ru linkages while forming Ru(0) from HRO (**Figures 8A,B**). A similar observation was found in SEM analysis also; HRO consists of bulk clusters on the grid, but in the case of Ru-HRO-2 (recovered from **Table 1**, entry 13), a decrease in the clusters concomitant to an increase in individual particles were observed (**Figures 9A,B**). SEM-EDX is shown in **Supplementary Figures 2A,B**. HRO consists of 50% of oxygen and the remaining is Ru. A decrease in the oxygen content was observed for Ru-HRO-2 (recovered material from **Table 1**, entry 13) up to 29%. The oxygen and water molecules in HRO were removed at elevated temperatures under reductive environment of our reaction conditions resulting in Ru(0). It was also confirmed that the entire HRO is not reduced in a single reaction cycle and the Ru(0) amount increases with successive reaction cycles. The TEM images of HRO supported on Na-β showed that the HRO clusters were well-dispersed on the support and the Ru-HRO@Na-β-2 (recovered material from **Supplementary Table 2**, entry 2) showed some divided particles ascribed to Ru(0) along with some clusters attributed to the un-converted HRO (**Figures 8C,D**).

The BET-specific surface area of the HRO was measured as 94 m^2/g. The nitrogen adsorption isotherms for HRO showed a characteristic type-IV isotherm that was attributed to the capillary condensation of pores with H1-type hysteresis according to IUPAC classification (**Figure 10**) (Luxton et al., 2011). After the reaction (**Table 1**, entry 10), the obtained material/*in situ* catalyst Ru-HRO-1 showed 60 m^2/g and retained type-IV isotherm with H1-type hysteresis. We presume that the

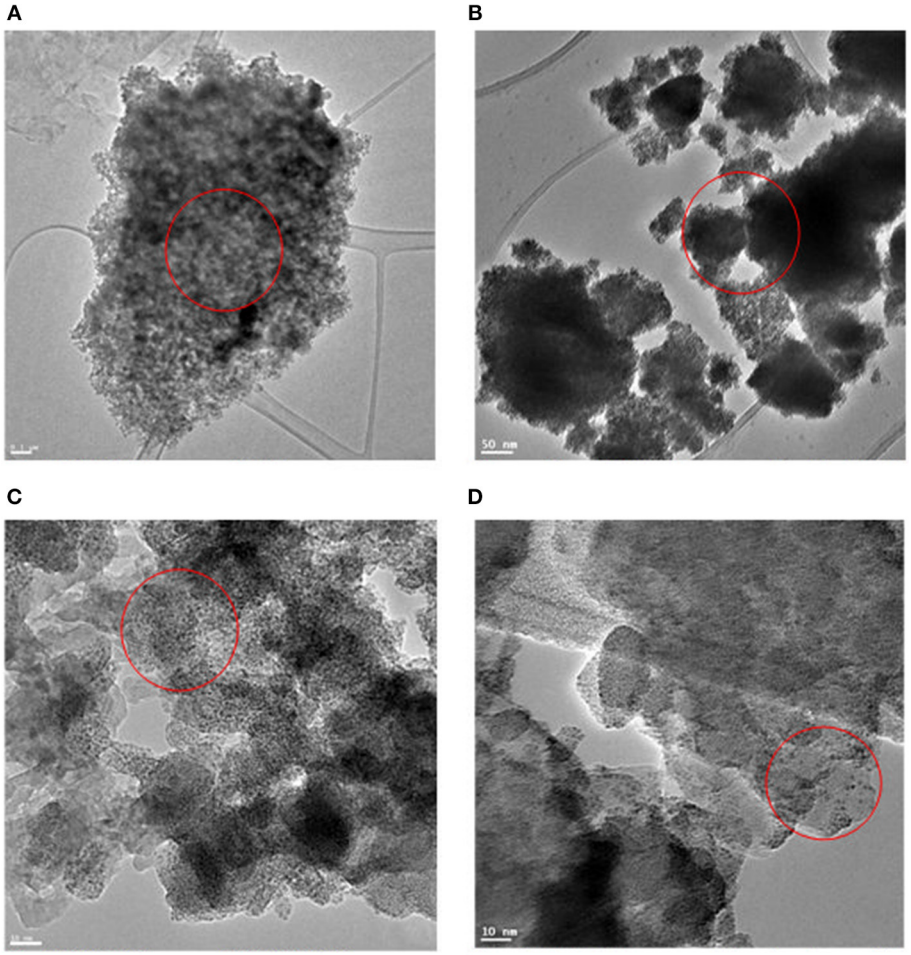

FIGURE 8 | TEM image of materials. **(A)** TEM image of HRO. **(B)** TEM image of Ru-HRO-2 (Recovered material from **Table 1**, entry 13). **(C)** TEM image of HRO/Na-β. **(D)** TEM image of *in situ* formed Ru-HRO@Na-β-2 (Recovered material from **Supplementary Table 2**, entry 2).

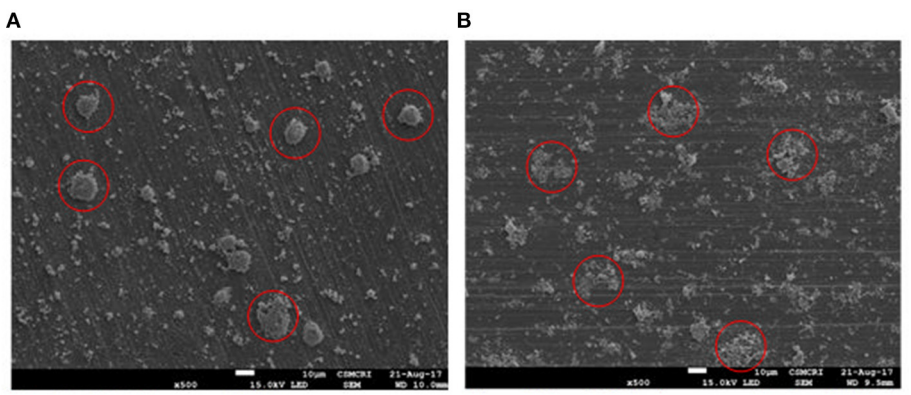

FIGURE 9 | SEM image of materials. **(A)** SEM image of HRO. **(B)** SEM image of Ru-HRO-2 (Recovered material from **Table 1**, entry 13).

surface area comes from the existence of HRO in the material. Under the reaction conditions, some of the HRO converts to Ru(0) and thereby reduces the amount of HRO, causing a decrease in the surface area. The surface area and type-IV isotherm observed after the reaction was due to the unconverted HRO in the Ru-HRO-1 catalyst (**Figure 10**). According to our

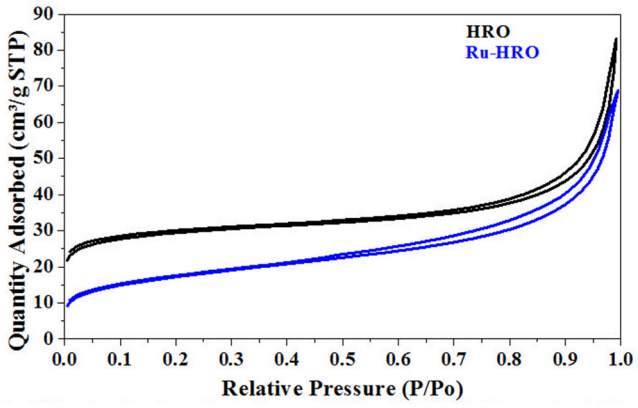

FIGURE 10 | N_2 absorption-desorption isotherms of HRO and Ru-HRO-1 (Recovered material from **Table 1**, entry 10).

previous work, HRO has Ru in +6 and +3 oxidation states. The *in situ* generated Ru-HRO catalyst exhibited (0) and +4 oxidation states, which means during the reaction under H_2, the +6 is transformed to +4 and +4 is transformed to (0) (Gundekari and Srinivasan, 2019).

The reduction behavior of HRO was studied by conducting a set of reactions mentioned in **Table 3** and materials obtained after the reaction were characterized using PXRD (**Figure 11a** belongs to HRO). The reduction of HRO to Ru(0) was observed in the presence of H_2O in the medium and H_2 environment (**Table 3**, entry 1; **Figure 11b**). Aqueous medium in the absence of H_2 did not promote HRO reduction, indicating that H_2O was not participating the reduction of HRO. Thus, the H_2 consumed for this conversion (HRO to Ru-HRO) is obtained from the molecular H_2 only (**Table 3**, entry 2; **Figure 11c**). The reaction conducted with only H_2 in the absence of H_2O and/or any medium showed less Ru(0) in the obtained material as compared with **Table 3**, entry 1. This result indicates that water facilitates the reaction by increasing the availability of H_2 to HRO (**Table 3**, entry 3; **Figure 11d**). In the presence of H_2, other solvents such as methanol and tetrahydrofuran (THF) showed much less conversion of HRO to Ru(0) (**Table 3**, entries 4 and 5; **Figures 11e,f**) as compared with aqueous medium and solvent-free conditions (**Table 3**, entry 3). From the above set of experiments, the suitability of water as the reaction medium for conducting hydrogenation reactions in the presence of HRO as the pre-catalyst was ascertained.

Reaction Mechanism

The proposed mechanism of reduction of sugar alcohols is depicted in **Supplementary Figure 3** considering the reaction conditions employed. Initially, under a hydrogen environment, a certain amount of HRO is converted to Ru(0), which is the active species for the hydrogenation. The hydrogen molecules are adsorbed on the surface of the *in situ* generated Ru(0) and form metal–hydrogen bonds. The sugar molecules adsorbed on the surface and in close proximity of Ru-H bonds undergo hydrogenation of the carbonyl group of the sugar molecule (HC=O) to alcohol, thereby forming the corresponding sugar alcohol (CH-OH). The alcohols once formed are desorbed from the surface. Subsequently, Ru(0) metal (freshly formed from HRO or used species for hydrogenation) interacts with the available hydrogen and the reaction continues thereafter as indicated above until the complete conversion of sugar molecules to sugar alcohols.

TABLE 3 | Reduction behavior of HRO.

Entry	H_2 source	Solvent	PXRD
1	H_2	H_2O	**Figure 11b**
2	-	H_2O	**Figure 11c**
3	H_2	-	**Figure 11c**
4	H_2	THF	**Figure 11e**
5	H_2	Methanol	**Figure 11f**

Reaction conditions: 25 mg of HRO material, 40 ml of solvent, 100°C, 20 bar H_2, 30 min.

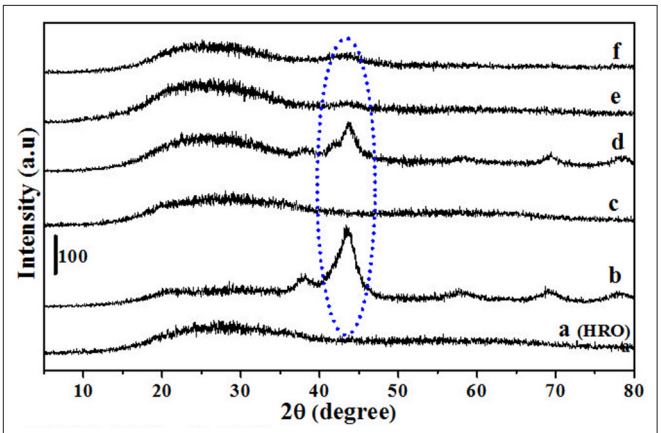

FIGURE 11 | PXRD of **(a)** HRO Ru-HRO-1. The denotation of **(b–f)** mentioned in **Table 3**.

CONCLUSION

We have successfully demonstrated the selective hydrogenation of sugars (xylose, glucose, and mannose) to corresponding sugar alcohols (xylitol, sorbitol, and mannitol) with 100% yields using HRO/Na-β pre-catalyst under optimized reaction conditions (80–100°C, 20 bar H_2, 30–45 min). *In situ* formation of Ru(0) from HRO during the reaction is characterized by several physico-chemical techniques. Control experiments support the idea that the reduction reaction under aqueous condition is efficient and beneficial for the conversion of HRO to Ru(0) as compared to organic solvents such as methanol and THF. The present catalytic method has the advantage of minimizing the energy and H_2 consumption of the overall process by avoiding external reduction (generally used in the conventional catalytic processes). Moreover, the *in situ* generation of catalyst

precludes the need for co-catalysts and additives and has good recyclability.

DATA AVAILABILITY STATEMENT

All datasets generated for this study are included in the article/**Supplementary Material**.

AUTHOR CONTRIBUTIONS

SG: designed and worked for the manuscript. HD, KR, and JM: helped in optimization and characterization studies and proof-editing of the manuscript. KS: overall supervision of the work and in writing the manuscript. All authors contributed to the article and approved the submitted version.

ACKNOWLEDGMENTS

CSIR-CSMCRI Communication No. 146/2019. SG thanks CSIR, New Delhi, for a Senior Research Fellowship. The authors thank CSIR, New Delhi for financial support under the projects MLP-0028, CSC-0123, and DST, India under IFA-13/CH 129 (DST-INSPIRE Faculty Award). The authors thank the Analytical Division and Centralized Instrumental Facilities of this institute for analytical support.

SUPPLEMENTARY MATERIAL

The Supplementary Material for this article can be found online at: https://www.frontiersin.org/articles/10.3389/fchem.2020.525277/full#supplementary-material

REFERENCES

Aho, A., Roggan, S., Eranen, K., Salmi, T., and Murzin, D. Y. (2015). Continuous hydrogenation of glucose with ruthenium on carbon nanotube catalysts. *Catal. Sci. Technol.* 5, 953–959. doi: 10.1039/C4CY01088D

Alonso, D. M., Wettstein, S. G., and Dumesic, J. A. (2012). Bimetallic catalysts for upgrading of biomass to fuels and chemicals. *Chem. Soc. Rev.* 41, 8075–8098. doi: 10.1039/c2cs35188a

Arena, B. J. (1992). Deactivation of ruthenium catalysts in continuous glucose hydrogenation. *Appl. Catal. A Gen.* 87, 219–229. doi: 10.1016/0926-860X(92)80057-J

Bozell, J. J., and Petersen, G. R. (2010). Technology development for the production of biobased products from biorefinery carbohydrates-the US Department of Energy's "Top 10" revisited. *Green Chem.* 12, 539–554. doi: 10.1039/b922014c

Chao, J. C., and Huibers, D. T. A. (1982). Catalytic hydrogenation of glucose to produce sorbitol. US Patent No. 4322569

Chatterjee, C., Pong, F., and Sen, A. (2015). Chemical conversion pathways for carbohydrates. *Green Chem.* 17, 40–71. doi: 10.1039/C4GC01062K

Climent, M. J., Corma, A., and Iborra, S. (2011a). Converting carbohydrates to bulk chemicals and fine chemicals over heterogeneous catalysts. *Green Chem.* 13, 520–540. doi: 10.1039/c0gc00639d

Climent, M. J., Corma, A., and Iborra, S. (2011b). Heterogeneous catalysts for the one-pot synthesis of chemicals and fine chemicals. *Chem. Rev.* 111, 1072–1133. doi: 10.1021/cr1002084

Corma, A., Iborra, S., and Velty, A. (2007). Chemical routes for the transformation of biomass into chemicals. *Chem. Rev.* 107, 2411–2502. doi: 10.1021/cr050989d

Dabbawala, A. A., Mishra, D. K., and Hwang, J.-S. (2016). Selective hydrogenation of D-glucose using amine functionalized nanoporous polymer supported Ru nanoparticles based catalyst. *Catal. Today* 265, 163–173. doi: 10.1016/j.cattod.2015.09.045

Eisenbeis, C., Guettel, R., Kunz, U., and Turek, T. (2009). Monolith loop reactor for hydrogenation of glucose. *Catal. Today* 147(Suppl), S342–S346. doi: 10.1016/j.cattod.2009.07.019

Gallezot, P. (2012). Conversion of biomass to selected chemical products. *Chem. Soc. Rev.* 41, 1538–1558. doi: 10.1039/C1CS15147A

Grembecka, M. (2015). Sugar alcohols—their role in the modern world of sweeteners: a review. *Eur. Food Res. Technol.* 241, 1–14. doi: 10.1007/s00217-015-2437-7

Gundekari, S., and Srinivasan, K. (2019). Hydrous ruthenium oxide: a new generation remarkable catalyst precursor for energy efficient and sustainable production of γ-valerolactone from levulinic acid in aqueous medium. *Appl. Catal. A Gen.* 569, 117–125. doi: 10.1016/j.apcata.2018.10.018

Guo, H., Li, H., Zhu, J., Ye, W., Qiao, M., and Dai, W. (2003). Liquid phase glucose hydrogenation to d-glucitol over an ultrafine Ru-B amorphous alloy catalyst. *J. Mol. Catal. A Chem.* 200, 213–221. doi: 10.1016/S1381-1169(03)00008-6

Guo, X., Wang, X., Guan, J., Chen, X., Qin, Z., Mu, X., et al. (2014). Selective hydrogenation of D-glucose to D-sorbitol over Ru/ZSM-5 catalysts. *Chinese J. Catal.* 35, 733–740. doi: 10.1016/S1872-2067(14)60077-2

Hao, W., Zhang, W., Guo, Z., Ma, J., and Li, R. (2018). Mesoporous beta zeolite catalysts for benzylation of naphthalene: effect of pore structure and acidity. *Catalysts* 8:504. doi: 10.3390/catal8110504

Hernandez-Mejia, C., Gnanakumar, E. S., Olivos-Suarez, A., Gascon, J., Greer, H. F., Zhou, W., et al. (2016). Ru/TiO_2-catalysed hydrogenation of xylose: the role of the crystal structure of the support. *Catal. Sci. Technol.* 6, 577–582. doi: 10.1039/C5CY01005E

Hoffer, B. W., Crezee, E., Mooijman, P. R. M., Van Langeveld, A. D., Kapteijn, F., and Moulijn, J. A. (2003). Carbon supported Ru catalysts as promising alternative for Raney®-type Ni in the selective hydrogenation of d-glucose. *Catal. Today* 79–80, 35–41. doi: 10.1016/S0920-5861(03)00040-3

Isikgor, F. H., and Becer, C. R. (2015). Lignocellulosic biomass: a sustainable platform for the production of bio-based chemicals and polymers. *Polym. Chem.* 6, 4497–4559. doi: 10.1039/C5PY00263J

Kelkar, S., Saffron, C. M., Li, Z., Kim, S.-S., Pinnavaia, T. J., Miller, D. J., et al. (2014). Aromatics from biomass pyrolysis vapour using a bifunctional mesoporous catalyst. *Green Chem.* 16, 803–812. doi: 10.1039/C3GC41350K

Kobayashi, H., and Fukuoka, A. (2013). Synthesis and utilisation of sugar compounds derived from lignocellulosic biomass. *Green Chem.* 15, 1740–1763. doi: 10.1039/c3gc00060e

Kusserow, B., Schimpf, S., and Claus, P. (2003). Hydrogenation of glucose to sorbitol over nickel and ruthenium catalysts. *Adv. Synth. Catal.* 345, 289–299. doi: 10.1002/adsc.200390024

Lange, J.-P., Van Der Heide, E., Van Buijtenen, J., and Price, R. (2012). Furfural—a promising platform for lignocellulosic biofuels. *ChemSusChem* 5, 150–166. doi: 10.1002/cssc.201100648

Li, H., Li, H., and Deng, J.-F. (2002). Glucose hydrogenation over Ni–B/SiO_2 amorphous alloy catalyst and the promoting effect of metal dopants. *Catal. Today* 74, 53–63. doi: 10.1016/S0920-5861(01)00530-2

Li, H., Wang, W., and Fa Deng, J. (2000). Glucose hydrogenation to sorbitol over a skeletal Ni-P amorphous alloy catalyst (Raney® Ni-P). *J. Catal.* 191, 257–260. doi: 10.1006/jcat.1999.2792

Luterbacher, J. S., Alonso, D. M., and Dumesic, J. A. (2014). Targeted chemical upgrading of lignocellulosic biomass to platform molecules. *Green Chem.* 16, 4816–4838. doi: 10.1039/C4GC01160K

Luxton, T. P., Eick, M. J., and Scheckel, K. G. (2011). Characterization and dissolution properties of ruthenium oxides. *J. Colloid Interf. Sci.* 359, 30–39. doi: 10.1016/j.jcis.2011.03.075

Melero, J. A., Iglesias, J., and Garcia, A. (2012). Biomass as renewable feedstock in standard refinery units. Feasibility, opportunities and challenges. *Energy Environ. Sci.* 5, 7393–7420. doi: 10.1039/c2ee21231e

Mikkola, J.-P., Vainio, H., Salmi, T., Sjöholm, R., Ollonqvist, T., and Väyrynen, J. (2000). Deactivation kinetics of Mo-supported Raney® Ni catalyst in

the hydrogenation of xylose to xylitol. *Appl. Catal. A Gen.* 196, 143–155. doi: 10.1016/S0926-860X(99)00453-6

Mishra, D. K., Dabbawala, A. A., and Hwang, J.-S. (2013). Ruthenium nanoparticles supported on zeolite Y as an efficient catalyst for selective hydrogenation of xylose to xylitol. *J. Mol. Catal. A Chemical*. 376, 63–70. doi: 10.1016/j.molcata.2013.04.011

Mishra, D. K., Dabbawala, A. A., Park, J. J., Jhung, S. H., and Hwang, J.-S. (2014). Selective hydrogenation of d-glucose to d-sorbitol over HY zeolite supported ruthenium nanoparticles catalysts. *Catal. Today* 232, 99–107. doi: 10.1016/j.cattod.2013.10.018

Mishra, D. K., and Hwang, J.-S. (2013). Selective hydrogenation of d-mannose to d-mannitol using NiO-modified TiO_2 (NiO-TiO_2) supported ruthenium catalyst. *Appl. Catal. A: Gen.* 453, 13–19. doi: 10.1016/j.apcata.2012.11.042

Mishra, D. K., Lee, J.-M., Chang, J.-S., and Hwang, J.-S. (2012). Liquid phase hydrogenation of d-glucose to d-sorbitol over the catalyst (Ru/NiO–TiO_2) of ruthenium on a NiO-modified TiO_2 support. *Catal. Today* 185, 104–108. doi: 10.1016/j.cattod.2011.11.020

Morales, R., Campos, C. H., Fierro, J. L. G., Fraga, M. A., and Pecchi, G. (2016). Perovskite as nickel catalyst precursor - impact on catalyst stability on xylose aqueous-phase hydrogenation. *RSC Adv.* 6, 67817–67826. doi: 10.1039/C6RA13395A

Pham, T. N., Samikannu, A., Rautio, A.-R., Juhasz, K. L., Konya, Z., Wärn,å, J., et al. (2016). Catalytic hydrogenation of d-Xylose Over Ru decorated carbon foam catalyst in a SpinChem® Rotating Bed Reactor. *Top. Catal.* 59, 1165–1177. doi: 10.1007/s11244-016-0637-4

Roli, N. F. M., Yussof, H. W., Seman, M. N. A., Saufi, S. M., and Mohammad, A. W. (2016). Separating xylose from glucose using spiral wound nanofiltration membrane: effect of cross-flow parameters on sugar rejection. *IOP Conf. Ser. Mater. Sci. Eng.* 162:012035. doi: 10.1088/1757-899X/162/1/012035

Serrano-Ruiz, J. C., Luque, R., and Sepulveda-Escribano, A. (2011). Transformations of biomass-derived platform molecules: from high added-value chemicals to fuels via aqueous-phase processing. *Chem. Soc. Rev.* 40, 5266–5281. doi: 10.1039/c1cs 15131b

Sheldon, R. A. (2014). Green and sustainable manufacture of chemicals from biomass: state of the art. *Green Chem.* 16, 950–963. doi: 10.1039/C3GC41935E

Sifontes Herrera, V. A., Oladele, O., Kordás, K., Eränen, K., Mikkola, J.-P., Murzin, D. Y., et al. (2011). Sugar hydrogenation over a Ru/C catalyst. *J. Chem. Technol. Biotechnol.* 86, 658–668. doi: 10.1002/jctb.2565

Sjoman, E., Manttari, M., Nystrom, M., Koivikko, H., and Heikkila, H. (2007). Separation of xylose from glucose by nanofiltration from concentrated monosaccharide solutions. *J. Membrane Sci.* 292, 106–115. doi: 10.1016/j.memsci.2007.01.019

Teong, S. P., Yi, G., and Zhang, Y. (2014). Hydroxymethylfurfural production from bioresources: past, present and future. *Green Chem.* 16, 2015–2026. doi: 10.1039/c3gc42018c

Vennestrøm, P. N. R., Osmundsen, C. M., Christensen, C. H., and Taarning, E. (2011). Beyond petrochemicals: the renewable chemicals industry. *Angew. Chem. Int. Ed.* 50, 10502–10509. doi: 10.1002/anie.201102117

Werpy, T., Petersen, G., Aden, A., Bozell, J., Holladay, J., White, J., et al. (2004). *Top value added chemicals from biomass volume I-results of screening for potential candidates from sugars and synthesis gas*. Pacific Northwest National Laboratory (PNNL), and National Renewable Energy Laboratory (NREL), U.S. Department of Energy (DOE) report, Tennessee, USA. doi: 10.2172/15008859

Wisniak, J., Hershkowitz, M., Leibowitz, R., and Stein, S. (1974). Hydrogenation of xylose to xylitol. *Ind. Eng. Chem. Prod. Res. Develop.* 13, 75–79. doi: 10.1021/i360049a015

Yadav, M., Mishra, D. K., and Hwang, J.-S. (2012). Catalytic hydrogenation of xylose to xylitol using ruthenium catalyst on NiO modified TiO_2 support. *Appl. Catal. A: Gen.* 425–426, 110–116. doi: 10.1016/j.apcata.2012.03.007

Zada, B., Chen, M. Y., Chen, C. B., Yan, L., Xu, Q., Li, W. Z., et al. (2017). Recent advances in catalytic production of sugar alcohols and their applications. *Sci. China Chem.* 60, 853–869. doi: 10.1007/s11426-017-9067-1

Zhang, J., Lin, L., Zhang, J., and Shi, J. (2011). Efficient conversion of D-glucose into D-sorbitol over MCM-41 supported Ru catalyst prepared by a formaldehyde reduction process. *Carbohydr. Res.* 346, 1327–1332. doi: 10.1016/j.carres.2011.04.037

Zhang, X. G., Wilson, K., and Lee, A. F. (2016). Heterogeneously catalyzed hydrothermal processing of C_5-C_6 sugars. *Chem. Rev.* 116, 12328–12368. doi: 10.1021/acs.chemrev.6b00311

Conflict of Interest: The authors declare that the research was conducted in the absence of any commercial or financial relationships that could be construed as a potential conflict of interest.

Advantages of publishing in Frontiers

OPEN ACCESS
Articles are free to read for greatest visibility and readership

FAST PUBLICATION
Around 90 days from submission to decision

HIGH QUALITY PEER-REVIEW
Rigorous, collaborative, and constructive peer-review

TRANSPARENT PEER-REVIEW
Editors and reviewers acknowledged by name on published articles

Frontiers
Avenue du Tribunal-Fédéral 34
1005 Lausanne | Switzerland

Visit us: www.frontiersin.org
Contact us: frontiersin.org/about/contact

REPRODUCIBILITY OF RESEARCH
Support open data and methods to enhance research reproducibility

DIGITAL PUBLISHING
Articles designed for optimal readership across devices

FOLLOW US
@frontiersin

IMPACT METRICS
Advanced article metrics track visibility across digital media

EXTENSIVE PROMOTION
Marketing and promotion of impactful research

LOOP RESEARCH NETWORK
Our network increases your article's readership